

UNCLASSIFIED

AD NUMBER
AD385595
NEW LIMITATION CHANGE
TO Approved for public release, distribution unlimited
FROM Distribution authorized to DoD only; Administrative/Operational Use; SEP 1967. Other requests shall be referred to Army Aviation Materiel Labs., Fort Eustis, VA.
AUTHORITY
USAAML ltr, 17 Oct 1968

THIS PAGE IS UNCLASSIFIED

UNCLASSIFIED

AD

USAAVLADS TECHNICAL REPORT 67-47 ✓

DESIGN AND DEVELOPMENT OF SMALL, SINGLE-STAGE
CENTRIFUGAL COMPRESSOR (U)

By

A. D. Welliver

J. Acurio

September 1967

U. S. ARMY AVIATION MATERIEL LABORATORIES
FORT EUSTIS, VIRGINIA

CONTRACT DA 44-177-AMC-173(T) ✓

✓ THE BOEING COMPANY
SEATTLE, WASHINGTON

Downgraded from SECRET to UNCLASSIFIED
and will appear in TAD 67-5 dated
1 March 1969 (cited in letter from DDC-TS
dated 10 January 1969)

Fred J. Alante
Fred J. Alante

FPS 14 January 1969

In addition to security requirements which
apply to this document and must be met,
each transmittal outside the Department of
Defense must have prior approval of U.S.
Army Aviation Materiel Laboratories,
Fort Eustis, Virginia 23604

Violating
State
or Laws
or Mission

It is prohibited in any manner to an
unauthorized person is prohibited by law.



UNCLASSIFIED

of 86 Copies

AD 385595

FILE COPY

Disclaimers

The findings in this report are not to be construed as an official Department of the Army position unless so designated by other authorized documents.

When Government drawings, specifications, or other data are used for any purpose other than in connection with a definitely related Government procurement operation, the United States Government thereby incurs no responsibility nor any obligation whatsoever; and the fact that the Government may have formulated, furnished, or in any way supplied the said drawings, specifications, or other data is not to be regarded by implication or otherwise as in any manner licensing the holder or any other person or corporation, or conveying any rights or permission, to manufacture, use, or sell any patented invention that may in any way be related thereto.

Trade names cited in this report do not constitute an official endorsement or approval of the use of such commercial hardware or software.

Disposition Instructions

When this report is no longer needed, Department of the Army organizations will destroy it in accordance with the procedures given in AR 580-5.

62-001-10

CPSTI	WHITE SECTION	<input type="checkbox"/>
COE	BUFF SECTION	<input checked="" type="checkbox"/>
UNANNOUNCED		<input type="checkbox"/>
STIFICATION		

DESCRIPTION/AVAILABILITY CODES

DIST.	AVAIL.	DD/M	SPECIAL
4			

UNCLASSIFIED



DEPARTMENT OF THE ARMY
U. S. ARMY AVIATION MATERIEL LABORATORIES
FORT EUSTIS, VIRGINIA 23604

- (U) This report has been reviewed by the U. S. Army Aviation Materiel Laboratories and is considered to be technically sound.
- (U) The work was performed under the terms of Contract DA 44-177-AMC-173(T) and consists of the design and demonstration of a small, single-stage centrifugal compressor based on technology derived in the first part of the program reported under "Element Design and Development of Small Centrifugal Compressor", USAAVLABS Technical Report 67-30.
- (U) The objective of this research was to advance single-stage centrifugal compressor technology to a pressure ratio of 10:1 and an efficiency of 80 percent and to the point to where sufficient design data are available to permit an engine designer to incorporate this compressor concept into an actual engine.
- (U) Although the performance objectives were not fully demonstrated, no fundamental aerodynamic reasons were found which would preclude attainment of the objectives in subsequent research programs.

MISSING PAGE NUMBERS ARE BLANK

UNCLASSIFIED

UNCLASSIFIED

1475

Task UM121401D14413

Contract DA 44-177-AMC-173(T)

USAAVLABS Technical Report 67-47

September 1967

TR-67-47

151

DESIGN AND DEVELOPMENT OF SMALL, SINGLE-STAGE
CENTRIFUGAL COMPRESSOR (U)

Final Report

D4-3434

by

A. D. Welliver

E. Acurio

Prepared by

The Boeing Company
Seattle, Washington

for

U. S. ARMY AVIATION MATERIEL LABORATORIES

FORT EUSTIS, VIRGINIA

UNCLASSIFIED

In addition to security requirements which apply to this document and must be met, each transmittal outside the Department of Defense must have prior approval of U. S. Army Aviation Materiel Laboratories, Fort Eustis, Virginia 23604.

This material contains information affecting the national defense of the United States within the meaning of the Espionage Laws (18 U. S. C. 793 and 794), the transmission or revelation of which in any manner to an unauthorized person is prohibited by law.

UNCLASSIFIED

CONFIDENTIAL

The Summary, Sections 8.0 and 9.0 are classified ~~Confidential~~ in their entirety. Sections 2.0, 6.0 and 7.0 are classified ~~Confidential~~ when compiled in a complete section. Individual pages are unclassified when separated from the section.

CONFIDENTIAL

CONFIDENTIAL

UNCLASSIFIED

(C) SUMMARY (U)

The research program discussed in this report was conducted for the U. S. Army Aviation Materiel Laboratories. The purpose of the work was to define, by analysis and experimental evaluation, the design criteria and performance characteristics of the high-pressure-ratio single-stage centrifugal compressor. The overall performance target was a pressure ratio of 10:1 at an adiabatic efficiency of 80 percent at an airflow of 2 pounds per second. The research was expected to lead to development of advanced technologies applicable to small gas turbine engines. The potential advances identified were:

- 1) Doubling of current power to weight ratio.
- 2) Reducing full and part load fuel consumption.
- 3) Minimizing cost per horsepower.

To illustrate the advances possible, two types of thermodynamic cycles (simple and regenerative) were studied. It was shown that a compressor meeting the above targets would provide an opportunity for reducing specific fuel consumptions to 0.49 pound per horsepower per hour (simple cycle) and 0.38 pound per horsepower per hour (regenerative).

RESEARCH COMPONENTS

Studies of compressor designs by the contractor in the pressure ratio range of 3.5:1 to 7:1 formed the background for initial work in this program.

Principal areas of investigation were directed toward

- 1) Minimizing the effect of transonic flow conditions at the inducer and diffuser entrance, including the evaluation of inducer hub-to-tip diameter ratio.
- 2) Establishing methods to provide operating range at high-pressure ratio.
- 3) Establishing flow models for the impeller and diffuser to identify losses throughout the compressor and to determine improved techniques for future compressor design. The results of the above effort are presented in Reference 1.

At the completion of the effort described in Reference 1, the goal of 10:1 pressure ratio at 80-percent adiabatic efficiency still appeared to be possible. A new impeller and diffuser were designed and tested to evaluate the concepts reported in Reference 1 and to provide additional information where necessary to meet the target. The new impeller and diffuser were designated RF-2 and V1 respectively.

UNCLASSIFIED

UNCLASSIFIED

The RF-2 impeller was designed to provide a total-to-total pressure ratio of approximately 12.2:1 at an impeller-tip speed of about 2000 fps. The absolute Mach number leaving the impeller was 1.27. The inducer hub-to-tip diameter ratio was 0.45 with a maximum inlet relative Mach number of 0.86 at 50,000 rpm. The impeller tip had a diameter of approximately 9.2 inches, was similar in size to the workhorse impeller, and was designed with 18 blades.

The investigations reported in Reference 1 had shown that a major loss in the centrifugal impeller resulted from the impeller-exit mixing process. Other losses were due to the blade-shroud clearance and friction from all wetted surfaces. The impeller-exit mixing loss was related to the exit wake-to-jet width ratio. This ratio was a function of the amount of relative diffusion accomplished in the inducer passage prior to flow separation on the suction surface. As the impeller-exit jet width was increased, the exit mixing losses were reduced. It was further shown that the inducer entrance design had a large influence on the separation point. The inducer for the RF-2 impeller was designed with a low inlet relative Mach number. The inducer blade leading-edge shape was designed to minimize the overvelocity on the suction surface. An airfoil parameter κ was used to evaluate the inducer nose shape. Based on this analysis, impeller performance was expected to be better than the performance of the three impellers discussed in Reference 1. The inducer also had a more axial flow path than previous impeller designs to reduce the blade-to-blade Coriolis forces which have an adverse effect on the suction-surface boundary layer.

The V1 diffuser was a vane-island type designed to match the impeller discharge Mach number of 1.27. The diffuser was designed with 10 channels and a 10° asymmetrical divergence angle. The vane leading edge was set at an impeller diameter ratio of 1.06. The design throat Mach number was approximately 0.95, and a throat blockage of 0.92 was expected.

During the experimental program reported in Reference 1, it was found that performance of a vane-island diffuser was dependent on channel entrance Mach number and throat blockage. Best performance was obtained with a low entry-shock Mach number (Mach number ≈ 1.05) which resulted in low throat blockage and a high subsonic throat Mach number (Mach number ≈ 0.95).

IMPELLER TESTS

Tests of the RF-2 impeller showed that the pressure ratio based on the total-pressure measurements at the impeller tip was near 11.2:1. Data analysis indicated that the test slip factor was 4 percent lower than expected and that the temperature-rise factor was 0.96, as expected. The predicted impeller pressure ratio based on the measured slip factor showed agreement with test data within 1 percent. Investigation of the effects of the wake-jet flow on the probe cast some doubt on the validity of the total-pressure measurements. Comparison of the

UNCLASSIFIED

UNCLASSIFIED

measured total pressure at the diffuser throat showed that the pressure from the RF-2 impeller was about 1/2 atmosphere higher than the pressure from the work-horse impeller. Static-pressure rise, measured along the impeller shroud, at an airflow of 1.98 pounds per second agreed with the design pressure rise up to the predicted separation point. This agreement of analysis and test data suggested that the impeller was operating close to the design target.

The RF-2 impeller was tested with two modifications. First, the inducer leading edge was modified from a radial to a swept-back configuration. This modification gave further evidence that the inducer was not separated near the leading edge due to high Mach number effects. A reduction in impeller-tip width to decrease exit mixing loss was investigated. An efficiency gain of 3 percent demonstrated the large influence of jet-wake-width ratio at the impeller exit on overall performance.

DIFFUSER TESTS

The V1 diffuser was tested with the RF-2 impeller. Data analysis showed that the diffuser-channel static-pressure recovery was less than expected and that the throat blockage was greater than expected. Airflow range up to 16 percent was demonstrated.

Further investigation showed that the aspect ratio of the diffuser throat had an effect on the channel blockage and static-pressure recovery. Trends of performance changes with aspect ratio were developed and confirmed by test.

It was shown that boundary-layer bleed at the diffuser throat was an effective way to increase static-pressure recovery and overall compressor performance. The effect of the boundary-layer bleed was related to the lambda shock on the pressure surface near the vane leading edge. Diffuser-channel separation, caused by the lambda shock, was delayed by the bleed.

OVERALL COMPRESSOR PERFORMANCE

The maximum compressor pressure ratio (total to static) measured was 10.6:1. Airflow range up to 16 percent was demonstrated at compressor pressure ratios between 9.0 and 10.0:1. Compressor adiabatic efficiency of 72.5 percent was nearly constant at all compressor speeds.

No fundamental aerodynamic reasons were found during this program which would prevent attainment of the program goals ($P/P = 10.0:1$ @ $\eta = 80$ percent) for a single-stage centrifugal compressor. Further understanding is necessary to reduce the diffuser-throat boundary-layer blockage, the recirculation occurring at the impeller tip, and the large impeller-exit mixing losses resulting from early separation of the flow from the inducer blading. A description of the recommended research and development effort is presented in Section 9.0.

V

UNCLASSIFIED

UNCLASSIFIED

Appendix I

A discussion of the procedures and results of the stress and vibration analyses is presented for the RF-2 impeller components. The temperature distribution, Campbell diagram, natural-frequency calculations, and stress calculations are included.

Appendix II

Appendix II covers the design modifications to the diffuser test rig required to accommodate the 2-piece impeller configuration. It provides information relative to the methods used and the mechanical areas investigated. This appendix is intended to supplement the discussions given in Section 2.4 in the body of this report.

Appendix III

Appendix III contains the static-pressure measurements on the side walls of the diffuser in the vaneless space, the semivaneless space and the channels for the 10-vane-island diffuser configurations that were tested.

UNCLASSIFIED

(U) CONTENTS

	<u>Page</u>
SUMMARY	iii
LIST OF ILLUSTRATIONS	ix
LIST OF TABLES	xx
LIST OF SYMBOLS	xxi
1.0 INTRODUCTION	1
1.1 Objectives	1
1.2 Previous Results	1
1.3 Research Approach	4
2.0 DESIGN ANALYSIS	5
2.1 Summary of Technologies	5
2.2 Impeller Design	7
2.3 Diffuser Design	20
2.4 Mechanical Design	22
3.0 FABRICATION OF RESEARCH COMPONENTS	37
3.1 Impeller	37
3.2 Test Section	46
4.0 INSTRUMENTATION	53
4.1 Pressure-Measurement Instrumentation	53
4.2 Temperature-Measurement Probes	53
4.3 Tip-Clearance Measurement	56
5.0 TEST EQUIPMENT AND PROCEDURES	57
5.1 Compressor Test Rig	57
5.2 Aerodynamic-Performance Instrumentation	60
5.3 Performance Data Acquisition	72
6.0 TEST RESULTS	77
6.1 Impeller	77
6.2 Diffusers	196

(U) CONTENTS (Continued)

	<u>Page</u>
7.0 EVALUATION OF TEST RESULTS	247
7.1 Impeller Tests	247
7.2 Diffuser	267
7.3 Overall Compressor	295
8.0 CONCLUSIONS	297
9.0 RECOMMENDATIONS	299
9.1 Inducer Investigation	299
9.2 Impeller-Exit Mixing Loss Analysis	299
9.3 Diffuser	300
9.4 Cascade Diffuser	300
REFERENCES	301
APPENDIXES	302
I IMPELLER STRESS AND VIBRATION ANALYSIS	302
II MECHANICAL DESIGN ANALYSIS	315
III DIFFUSER TEST DATA	326
DISTRIBUTION	421

(U) ILLUSTRATIONS

<u>Figure</u>		<u>Page</u>
1	Pressure Ratio Versus Airflow, Workhorse Impeller	2
2	Pressure Ratio Versus Airflow, DI-1 Diffuser (Comparison at 1.06 and 1.10 Radius Ratio)	3
3	Design Inlet Vector Diagrams Based on Unblocked Flow Area, RF-2	8
4	Design Inlet Vector Diagrams Based on Blocked Flow Area, RF-2 .	9
5	Comparison of the Blade Turning Schedules at the RMS Radius for the RF-1 and RF-2 Impellers	10
6	Blade Surface Velocities for Hub Streamtube of RF-2 Impeller (Design Speed)	11
7	Blade Surface Velocities for RMS Streamtube of RF-2 Impeller (Design Speed)	13
8	Blade Surface Velocities for Tip Streamtube of RF-2 Impeller (Design Speed)	14
9	Comparison of Inducer-Blade Blockage for RF-1 and RF-2	15
10	Predicted Static-Pressure Rise Along the Inducer Shroud	15
11	Design Exit Velocity Diagrams for RF-2 Impeller	16
12	Inducer Blade Sections	17
13	Inlet Blade Shape	19
14	Diffuser-Vane Geometry	21
15	Aerodynamic Design Information	23
16	Two-Piece Impeller	25
17	Predicted Impeller Disk Stress Distribution Before Proof-Spin . .	26
18	Predicted Impeller Deflection Before Proof-Spin	27
19	Section View of Test Section	29
20	Front Cover and Inlet	30
21	Test-Section Bolt Pattern	32
22	Campbell Diagram Used for Diffuser Selection	33
23	Schlieren Window Installation	34

(U) ILLUSTRATIONS (Continued)

<u>Figure</u>		<u>Page</u>
24	Typical Probe Installation	35
25	Impeller Component Machining	38
26	Hand-Working of Inducer Leading Edge	39
27	Completed Inducer Section	39
28	Completed Radial Section	40
29	Radial Section on Optical Comparator for Inspection	40
30	Impeller Assembly Method (Shown Twice Actual Size)	42
31	Impeller Components During Assembly	43
32	Impeller Blade Blending	43
33	Joint Between Inducer and Radial Sections	44
34	Inducer Test Modification	45
35	Front Cover Assembly	47
36	Backplate	48
37	Collector	49
38	Inlet	50
39	Vane-Islands Installed on Backplate	51
40	Total-Pressure Rake	54
41	Static-Pressure Taps in Diffuser Backplate	55
42	Digital-Data System	55
43	Compressor Test Rig Cell Installation	58
44	Front View of Compressor Installation	58
45	Impeller-Tip Clearance Probes Installed in Front Cover	59
46	Impeller-Tip-to-Shroud Clearance Versus Rotor Speed	59
47	Compressor and Turbodriven Housing Vibration	61
48	Instrumentation Locations	63
49	Diffuser Frontplate Static-Pressure Tap Locations	65
50	Diffuser Backplate Static-Pressure Tap Locations	67

(U) ILLUSTRATIONS (Continued)

<u>Figure</u>		<u>Page</u>
51	Static-Pressure Taps in Diffuser	69
52	Total-Pressure Rake Installation	70
53	Total-Pressure Rake in Diffuser Throat	71
54	Total-Pressure Rakes and Plugs	71
55	Inducer Leading-Edge Modification	80
56	Reduced Blade Width Modification	80
57	Performance of RF-2 Impeller with Reduced Blade Width	82
58	Pressure Ratio Versus Airflow	83
59	Pressure Ratio Versus Airflow	84
60	Pressure Ratio Versus Airflow	85
61	Pressure Ratio of RF-2 Impeller at Design Speed	86
62	Impeller-Tip Total-Temperature Survey, RF-2	87
63	Impeller-Tip Total-Temperature Survey, RF-2	88
64	Impeller-Tip Total-Temperature Survey, RF-2	89
65	Impeller-Tip Total-Pressure Survey, RF-2	90
66	Impeller-Tip Total-Pressure Survey, RF-2	91
67	Impeller-Tip Total-Pressure Survey, RF-2	92
68	Impeller-Tip Total-Pressure Survey, RF-2	93
69	Impeller-Tip Total-Pressure Survey, RF-2	94
70	Impeller-Tip Total-Pressure Survey, RF-2	95
71	Impeller-Tip Total-Pressure Survey, RF-2	96
72	Impeller-Tip Total-Pressure Survey, RF-2	97
73	Impeller-Tip Total-Pressure Survey, RF-2	98
74	Impeller-Tip Total-Pressure Survey, RF-2	99
75	Impeller-Tip Total-Pressure Survey, RF-2	100
76	Impeller-Tip Total-Pressure Survey, RF-2	101
77	Impeller-Tip Total-Pressure Survey, RF-2	102

(U) ILLUSTRATIONS (Continued)

<u>Figure</u>		<u>Page</u>
78	Impeller-Tip Total-Pressure Survey, RF-2	103
79	Impeller-Tip Total-Pressure Survey, RF-2	104
80	Impeller-Tip Total-Pressure Survey, RF-2	105
81	Impeller-Tip Total-Pressure Survey, RF-2	106
82	Impeller-Tip Total-Pressure Survey, RF-2	107
83	Impeller-Tip Total-Pressure Survey, RF-2	108
84	Impeller-Tip Total-Pressure Survey, RF-2	109
85	Impeller-Tip Total-Pressure Survey, RF-2	110
86	Impeller-Tip Total-Pressure Survey, RF-2	111
87	Impeller-Tip Total-Pressure Survey, RF-2	112
88	Impeller-Tip Total-Pressure Survey, RF-2	113
89	Impeller-Tip Total-Pressure Survey, RF-2	114
90	Impeller-Tip Flow-Angle Survey, RF-2	115
91	Impeller-Tip Flow-Angle Survey, RF-2	116
92	Impeller-Tip Flow-Angle Survey, RF-2	117
93	Inlet Duct Hub Static Pressures, RF-2	119
94	Inlet Duct and Inducer Shroud Static Pressures, RF-2	121
95	Inlet Duct and Inducer Shroud Static Pressures, RF-2	122
96	Inlet Duct and Inducer Shroud Static Pressures, RF-2	123
97	Inlet Duct and Inducer Shroud Static Pressures, RF-2	124
98	Inlet Duct and Inducer Shroud Static Pressures, RF-2	125
99	Inlet Duct and Inducer Shroud Static Pressures, RF-2	126
100	Inlet Duct and Inducer Shroud Static Pressures, RF-2	127
101	Inlet Duct and Inducer Shroud Static Pressures, RF-2	128
102	Inlet Duct and Inducer Shroud Static Pressures, RF-2	129
103	Inlet Duct and Inducer Shroud Static Pressure, RF-2	130
104	Static Pressure Along the Shroud, RF-2	131

(U) ILLUSTRATIONS (Continued)

<u>Figure</u>		<u>Page</u>
105	Static Pressure Along the Shroud, RF-2	132
106	Static Pressure Along the Shroud, RF-2	133
107	Static Pressure Along the Shroud, RF-2	134
108	Static Pressure Along the Shroud, RF-2	135
109	Static Pressure Along the Shroud, RF-2	136
110	Static Pressure Along the Shroud, RF-2	137
111	Static Pressure Along the Shroud, RF-2	138
112	Static Pressure Along the Shroud, RF-2	139
113	Circumferential Variation of Impeller-Exit Static Pressure	140
114	Circumferential Variation of Impeller-Exit Static Pressure	141
115	Circumferential Variation of Impeller-Exit Static Pressure	142
116	Circumferential Variation of Impeller-Exit Static Pressure	143
117	Circumferential Variation of Impeller-Exit Static Pressure	144
118	Circumferential Variation of Impeller-Exit Static Pressure	145
119	Circumferential Variation of Impeller-Exit Static Pressure	146
120	Circumferential Variation of Impeller-Exit Static Pressure	147
121	Circumferential Variation of Impeller-Exit Static Pressure	148
122	Circumferential Variation of Impeller-Exit Static Pressure	149
123	Circumferential Variation of Impeller-Exit Static Pressure	150
124	Circumferential Variation of Impeller-Exit Static Pressure	151
125	Circumferential Variation of Impeller-Exit Static Pressure	152
126	Circumferential Variation of Impeller-Exit Static Pressure	153
127	Circumferential Variation of Impeller-Exit Static Pressure	154
128	Circumferential Variation of Impeller-Exit Static Pressure	155
129	Circumferential Variation of Impeller-Exit Static Pressure	156
130	Circumferential Variation of Impeller-Exit Static Pressure	157
131	Circumferential Variation of Impeller-Exit Static Pressure	158

(U) ILLUSTRATIONS (Continued)

<u>Figure</u>		<u>Page</u>
132	Circumferential Variation of Impeller-Exit Static Pressure	159
133	Circumferential Variation of Impeller-Exit Static Pressure	160
134	Circumferential Variation of Impeller-Exit Static Pressure	161
135	Circumferential Variation of Impeller-Exit Static Pressure	162
136	Impeller-Exit Mach Number Survey, RF-2.	163
137	Impeller-Exit Mach Number Survey, RF-2.	165
138	Inlet Vector Diagrams, RF-2.	167
139	Inlet Vector Diagrams, RF-2.	168
140	Inlet Vector Diagrams, RF-2.	169
141	Inlet Vector Diagrams, RF-2.	170
142	Inlet Vector Diagrams, RF-2.	171
143	Inlet Vector Diagrams, RF-2.	172
144	Inlet Vector Diagrams, RF-2.	173
145	Inlet Vector Diagrams, RF-2.	174
146	Inlet Vector Diagrams, RF-2.	175
147	Exit Vector Diagrams at 1.028 Radius Ratio, RF-2	177
148	Exit Vector Diagrams at 1.028 Radius Ratio, RF-2	179
149	Exit Vector Diagrams at 1.028 Radius Ratio, RF-2	181
150	Inducer Incidence, RF-2	183
151	Inducer Incidence, RF-2	185
152	Variation of Inducer Incidence with Airflow, RF-2	187
153	Variation of Slip Factor Across Impeller Tip, RF-2.	188
154	Variation of Average Slip Factor with Rotational Speed for RF-2 Impeller with Reduced Blade Width	189
155	Average Slip Factor at Design Speed, RF-2	190
156	Variation of Temperature-Rise Factor Across Impeller Tip, RF-2	191

(U) ILLUSTRATIONS (Continued)

<u>Figure</u>		<u>Page</u>
157	Variation of Average Temperature-Rise Factor with Rotational Speed for RF-2 Impeller with Reduced Blade Width	193
158	Average Temperature-Rise Factor at Design Speed, RF-2	194
159	Inlet Blockage Factor Versus Airflow, RF-2.	195
160	V1 Diffuser Vane Modifications	201
161	V1 Diffuser Vane Modifications	201
162	V1 Diffuser Vane Modifications	202
163	V1 Diffuser Vane Modifications	202
164	V2 Diffuser Vane and Modifications	203
165	Pressure Ratio Versus Airflow	206
166	Pressure Ratio Versus Airflow	207
167	Pressure Ratio Versus Airflow	209
168	Pressure Ratio Versus Airflow	211
169	Pressure Ratio Versus Airflow	212
170	Pressure Ratio Versus Airflow	213
171	Pressure Ratio Versus Airflow	214
172	Pressure Ratio Versus Airflow	215
173	Pressure Ratio Versus Airflow	217
174	Pressure Ratio Versus Airflow	219
175	Pressure Ratio Versus Airflow	220
176	Pressure Ratio Versus Airflow	221
177	Static-Pressure Variation in Diffuser	222
178	Static-Pressure Variation in Diffuser	223
179	Static-Pressure Variation in Diffuser	224
180	Static-Pressure Variation in Diffuser	225
181	Static-Pressure Variation in Diffuser	226
182	Static-Pressure Variation in Diffuser	227
183	Static-Pressure Variation in Diffuser	228

(U) ILLUSTRATIONS (Continued)

<u>Figure</u>		<u>Page</u>
184	Static-Pressure Variation in Diffuser	229
185	Static-Pressure Variation in Diffuser	230
186	Static-Pressure Variation in Diffuser	231
187	Static-Pressure Variation in Diffuser	232
188	Static-Pressure Variation in Diffuser	233
189	Static-Pressure Variation in Diffuser	234
190	Static-Pressure Variation in Diffuser	235
191	Static-Pressure Variation in Diffuser	236
192	Static-Pressure Variation in Diffuser	237
193	Static-Pressure Variation in Diffuser	238
194	Static-Pressure Variation in Diffuser	239
195	Static-Pressure Variation in Diffuser	240
196	Temperature Rise Versus Airflow	241
197	Diffuser-Throat Total Pressure Versus Width	243
198	Diffuser-Throat Total Pressure Versus Width	245
199	Variation of Performance with Incidence, RF-2	249
200	Impeller Core and Throat Total Pressure Versus Airflow, RF-2 . .	252
201	Comparison of Impeller-Exit Total Pressure, RF-2	253
202	Front-Cover Modification	254
203	Difference Between Temperature-Rise Factor and Slip Factor, RF-2.	256
204	Assumed Relationship Between the Inducer Operating Line and the Separation-Effects Boundary	257
205	Incidence Changes Due to Sweep and Cutback, RF-2.	259
206	Assumed Relationship Between the Inducer Operating Line and the Separation-Effects Boundary	259
207	Assumed Relationship Between the Inducer Operating Line and the Separation-Effects Boundary	260
208	Jet-Wake Flow Model	263

(U) ILLUSTRATIONS (Continued)

<u>Figure</u>		<u>Page</u>
209	Variation of Slip Factor with the Ratio of Wake Width to Blade Pitch, RF-2	264
210	Centerline Total Pressures at the Diffuser-Throat Entrance for Tests 3310A and 3353D	266
211	Comparison of Pressure Recovery for Compressor Channel with 2-Dimensional Diffuser Data	272
212	Throat Blockage Factor Versus Mach Number Ahead of Shock . .	273
213	Diffuser-Throat Total Pressure Versus Airflow	275
214	Calculated Diffuser-Throat Total Pressure	276
215	Calculated Diffuser-Throat Total Pressure Versus Airflow	277
216	Comparison of Measured and Calculated Throat Total Pressure . .	278
217	Comparison of Static Pressure Along Shroud for 3 Tests, RF-2 . .	280
218	Comparison of Pressure Recovery for Compressor Channel with 2-Dimensional Diffuser Data	281
219	Throat Blockage Factor Versus Mach Number Ahead of Shock . .	282
220	Cross Section of Diffuser-Throat Core Flow and Boundary Layer .	284
221	Sketch of Diffuser with 0.032-Inch Bleed Port	284
222	Comparison of Static-Pressure Recovery for Bleed and Non-Bleed Diffuser Tests	285
223	Sketch of Diffuser Showing Location of Second Bleed Port	286
224	Pressure Ratio Versus Airflow	287
225	Comparison of Temperature Rise for Bleed and Non-Bleed Tests .	288
226	Sketch of Lambda Shock Relative to Bleed Ports	289
227	DI-1 Channel Pressures at 2:1 Area Ratio	290
228	Diffuser-Throat Total-Pressure Profile	291
229	Comparison of Blockage Factor Versus Airflow for Various Diffuser Depths	292
230	Blockage Versus Aspect Ratio	294
231	Static-Pressure Recovery Versus Aspect Ratio	294

(U) ILLUSTRATIONS (Continued)

<u>Figure</u>		<u>Page</u>
232	Suggested Trend of Static-Pressure Recovery Versus Aspect Ratio	295
233	Coordinate System for Triaxial-Stress and Deflection Analysis . .	303
234	Disk and Blade Profile of RF-2 Impeller	304
235	Temperature Distribution of RF-2 Inducer-Impeller	305
236	Natural Frequencies of RF-2 Inducer Blades	306
237	Natural Frequencies of RF-2 Impeller Blades	307
238	Campbell Diagram for RF-2	308
239	Blade Stress Calculations for RF-2	309
240	RF-2 Impeller-Blade Force, Weight, and Inertia	310
241	Blade-Root Stress, Temperature, and Safety Factor for RF-2 . .	311
242	Disk Calculations for RF-2 Impeller	312
243	Predicted Impeller Disk Stress Distribution Before Proof-Spin . .	313
244	Predicted Impeller Deflection Before Proof-Spin	314
245	Bearing Stiffness Versus Rotor Speed	317
246	Shaft Mode Shapes	318
247	Collector Configuration for Stress Calculations	320
248	Diffuser Backplate Configuration for Deflection Calculation . . .	321
249	Relative Positions of Lines 3, 5 and 7 on Speed Lines of a Compressor Map	327
250	Locations of Static-Pressure Taps with Respect to V1, V1-1, V1-2 and V1-3 Diffuser Vanes	341
251	Locations of Static-Pressure Taps with Respect to V1-4 Diffuser Vanes	347
252	Locations of Static-Pressure Taps with Respect to V1-5 Diffuser Vanes	353
253	Locations of Static-Pressure Taps with Respect to V1-6 Diffuser Vanes	359
254	Locations of Static-Pressure Taps with Respect to V1-7 Diffuser Vanes	365

(U) ILLUSTRATIONS (Continued)

<u>Figure</u>		<u>Page</u>
255	Locations of Static-Pressure Taps with Respect to V1-8 Diffuser Vanes	371
256	Locations of Static-Pressure Taps with Respect to V1-9 Diffuser Vanes	377
257	Locations of Static-Pressure Taps with Respect to V1-10 Diffuser Vanes	389
258	Locations of Static-Pressure Taps with Respect to V1-11 and V1-12 Diffuser Vanes	401
259	Locations of Static-Pressure Taps with Respect to V2 Diffuser Vanes	409
260	Locations of Static-Pressure Taps with Respect to V2-1 Diffuser Vanes	413
261	Locations of Static-Pressure Taps with Respect to V2-2 Diffuser Vanes	419

(U) TABLES

<u>Table</u>		<u>Page</u>
I	Inducer Diffusion Factors	12
II	Inducer-Entrance Blade Shape (κ Factor)	18
III	Design Parameters for V1 Diffuser	22
IV	Diffuser-Vane Configurations	73
V	Impeller Tests	78
VI	Diffuser Tests	197

(U) SYMBOLS

A	area (in. ²)
A _{td}	cross-sectional area of impeller disk (in. ²)
A*	area at station where the Mach number is unity (in. ²)
A/A*	isentropic area ratio
AR	aspect ratio, AR = b/W
a	acoustic velocity (fps),

$$a = \sqrt{\gamma g R T_s}$$

radius to center of collector cross section (in.), or radius to diffuser-plate bolt circle (in.)

B	blockage,
---	-----------

$$B = 1 - \frac{A_{\text{flow}}}{A_{\text{geometric}}}$$

b	impeller - tip blade width (in.), diffuser passage depth (in.), radius of collector cross section (in.), or inner radius of diffuser back-plate (in.)
---	---

C _p	static pressure recovery,
----------------	---------------------------

$$C_p = \frac{P_{\text{coll}} - P_{s_y}}{P_{T_y} - P_{s_y}}$$

D	diameter (in.) or diameter of diffuser-plate bolt circle (in.)
ΔD _{al}	diametral growth of aluminum (in.)
ΔD _{st}	diametral growth of steel (in.)
DI	diffuser island
d	diameter (in.)
E	modulus of elasticity (psi)
E _{al}	modulus of elasticity of aluminum (psi)
E _{st}	modulus of elasticity of steel (psi)

(U) SYMBOLS (Continued)

F	bolt force (lb)
F _{fu}	failure force based on ultimate stress (lb)
F _{fy}	failure force based on yield stress (lb)
F _{sr}	calculated blade pull (lb)
F _{td}	total disk force (lb)
F _{ts}	total blade force (lb)
F _{tw}	total wheel force (lb)
F'	blade radial force per inch of axial length (lb/in.)
g	gravitational constant (32.17 ft/sec ²)
h	passage width (in.) or specific enthalpy (Btu/lb)
h _{al}	thickness of aluminum liner at steel-aluminum interface (in.)
h _{st}	thickness of steel front cover at steel-aluminum interface (in.)
I _{ts}	total blade mass moment of inertia (lb-in.-sec ²)
I _{tw}	total wheel mass moment of inertia (lb-in.-sec ²)
I'	blade mass moment of inertia per inch of axial length (lb-in.-sec ² /in.)
i	incidence angle (degrees)
J	mechanical equivalent of heat $\left(\frac{778 \text{ ft-lb}}{\text{Btu}}\right)$
K	spring rate (lb/in.)
L	flow path length (ft or in.)
M	Mach number
MF	mixed flow
m	meridional distance (in.) or material specific volume, $m = 1/\gamma$ (ft ³ /lb)
N	rotational speed (rpm)
n	number of blades
P	static pressure (psia or in. Hg) or separating force for diffuser plates (lb)
P _{coll}	static pressure in collector (psia or in. Hg)

(U) SYMBOLS (Continued)

P_s	static pressure (psia or in. Hg)
P_t, P_T	total pressure (psia or in. Hg)
P/P	pressure ratio
p	internal pressure on diffuser plates (psig)
R	radius (in.) or gas constant for air $\left(\frac{53.3 \text{ ft-lb}}{\text{lb-}^\circ\text{F}}\right)$
RF	radial flow
RMS	root mean square
R/R	radius ratio
r	radius (in.)
r_r	root radius (in.)
r_t	tip radius (in.)
r_1	inner radius of diffuser plates (in.)
r_2	outer radius of diffuser plates (in.)
S	circumferential distance (in.)
S_{as}	allowable stress (psi)
S_c	calculated blade-root stress (psi)
S_{M-H}	Mises - Hencky stress (psi)
S_o	circumferential distance between adjacent vane tips (in.)
S_{root}	local blade-root stress (psi)
S_{tan}	average tangential disk stress (psi)
SF	slip factor,

$$SF = \frac{V_{T_4}}{U_4}$$

T	metal temperature ($^\circ\text{F}$)
T_n	bearing stiffness (lb/sec/in.)
T_s	absolute static temperature ($^\circ\text{R}$)
T_t	absolute total temperature ($^\circ\text{R}$)

(U) SYMBOLS (Continued)

ΔT	temperature difference ($^{\circ}F$)
TRF	temperature-rise factor,
$TRF = \Delta h_t / (U_4^2 / gJ)$	
t	blade thickness (in.) or collector wall thickness (in.)
t_r	blade thickness at the root (in.)
t_t	blade thickness at the tip (in.)
U	impeller peripheral velocity (fps)
V	velocity (fps) or vane island
V_T	tangential component of velocity (fps)
W	airflow (lb/sec), diffuser height (in.), internal pressure on diffuser backplate (psig)
W_a	airflow (lb/sec)
W_{ts}	total blade weight (lb)
W_{tw}	total wheel weight (lb)
W'	weight of blade per inch of axial length (lb/in.)
X	force per unit area due to interference (psi)
y_{max}	maximum axial deflection of diffuser backplate (in.)
Z	number of impeller blades or axial distance (in.)
Z_{eq}	equivalent number of impeller blades
α	angle (degrees) or ratio of the backplate inner radius to the outer radius, $\alpha = b/a$
α_{al}	coefficient of thermal expansion for aluminum (in./in. - $^{\circ}F$)
α_{st}	coefficient of thermal expansion for steel (in./in. - $^{\circ}F$)
α_1	angle between impeller-inlet absolute vector and meridional plane (degrees)
α_2	angle between impeller-inlet relative vector and meridional plane (degrees)
α_3	angle between impeller-exit relative vector and meridional plane (degrees)

(U) SYMBOLS (Continued)

α_4	angle between impeller-exit absolute vector and meridional plane (degrees)
β_{B2}	angle between impeller vane and meridional plane (degrees)
γ	ratio of specific heats, $\gamma = C_p / C_v \quad \text{or material density (lb/in.}^3\text{)}$
δ	<u>measured ambient pressure (in. Hg)</u> 29.92 in. Hg
δ^*	boundary-layer displacement thickness (in.)
ϵ	ratio of wake width to blade pitch at impeller exit
η	adiabatic efficiency (percent)
η_s	safety factor based on allowable stress
η_u	safety factor based on ultimate stress
η_y	safety factor based on yield stress
θ	channel-diffuser angle (degrees) or <u>measured ambient temperature (°R)</u> 519.7 °R
κ	airfoil nose-shape parameter
λ	tangent of the angle between the bulk-mean absolute flow vector and the meridional plane at the impeller exit
ρ	density of air (lb _m /ft ³)
σ	bolt stress (psi)
σ_A	skin stress (psi)
σ_r	radial normal stress (psi)
σ_x	axial normal stress (psi)
σ_θ	tangential normal stress (psi)
τ_{xr}	shear stress in the x-r plane (psi)
ϕ	blockage factor, $\phi = 1 - B$
χ	airfoil suction-surface parameter
ω	impeller angular velocity (rad/sec)

(U) SYMBOLS (Continued)

SUBSCRIPTS:

a	absolute
H	hub
T, t	total or tip
t - a	time averaged
x	condition ahead of normal shock
y	condition behind normal shock
1	impeller-inlet absolute vector
2	impeller-inlet relative vector
3	impeller-exit relative vector
4	impeller-exit absolute vector
∞	undisturbed approach flow

1.0 (U) INTRODUCTION

The studies of design techniques and the evaluation of test results presented in Reference 1 provided a basis for advancing the technology of high-pressure-ratio centrifugal compressors. From this work, in which impellers and diffusers were studied separately, a new complete compressor was designed for evaluation as a combined system. The design target remained at 10:1 pressure ratio and 80-percent adiabatic efficiency, as projected at the initiation of the program. This new impeller-diffuser combination was designed in August 1966, and all testing was completed in February 1967. The plan was to demonstrate the principles developed in the basic impeller and diffuser studies and to identify advantageous follow-on work for future research.

1.1 OBJECTIVES

The objectives of this portion of the Army compressor research program were to apply the theories of flow mechanics documented in Section 7.0 of Reference 1, and to confirm the revised design approach by test and evaluation of a complete compressor unit. The new configuration consisted of a 2-piece impeller and a 10-channel diffuser. The compressor test rig formerly used to test the vane-island and cascade diffuser elements was modified to adapt the new components. Design airflow was 2.0 pounds per second at a rotor speed of 50,000 rpm.

1.2 PREVIOUS RESULTS

Development of high-pressure-ratio (10:1) centrifugal compressor technology for small-gas-turbine applications was started by the contractor for the U. S. Army in May 1964. This effort was an extension of earlier company-sponsored research in the pressure-ratio range of 6:1 to 7:1 and led to the development of mathematical impeller and diffuser flow models. These mathematical flow models were continually revised as new data became available from these component tests. In addition, new loss analyses were devised through an iterative process of systematically updating the flow models. Results of the studies showed that

- 1) The major loss in the impeller was a result of exit mixing of the jet and wake, caused by large separation in the early portion of the inducer.
- 2) Other impeller-flow-path losses (clearance and friction) are small by comparison and account for less than 4 percent of the total pressure loss.
- 3) The major portion of diffuser pressure recovery occurs in the diverging channel.
- 4) The largest total pressure loss occurs in the vaneless and semivaneless spaces with little diffusion.

Of the configurations tested, the best impeller was a radial-flow type used to test diffuser elements; the best diffuser was an 8-vane-island type. The results obtained from the basic studies are shown in Figures 1 and 2. From these results, it was established that there was no technical barrier preventing the achievement of single-stage pressure ratios in excess of 10:1. However, it was shown that high adiabatic efficiency (80 percent) depended principally on:

- 1) Minimizing impeller-exit mixing losses.
- 2) Shock strength and location ahead of and in the diffuser throat.
- 3) Matching of the impeller and the diffuser to produce optimum performance.

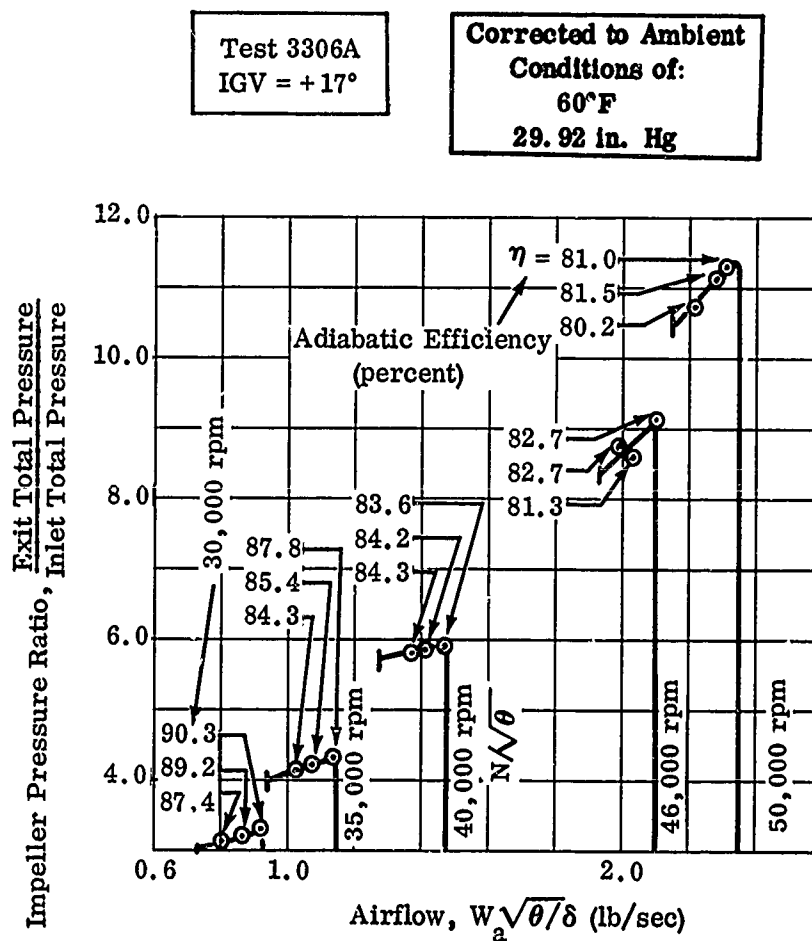


Figure 1. Pressure Ratio Versus Airflow, Workhorse Impeller.

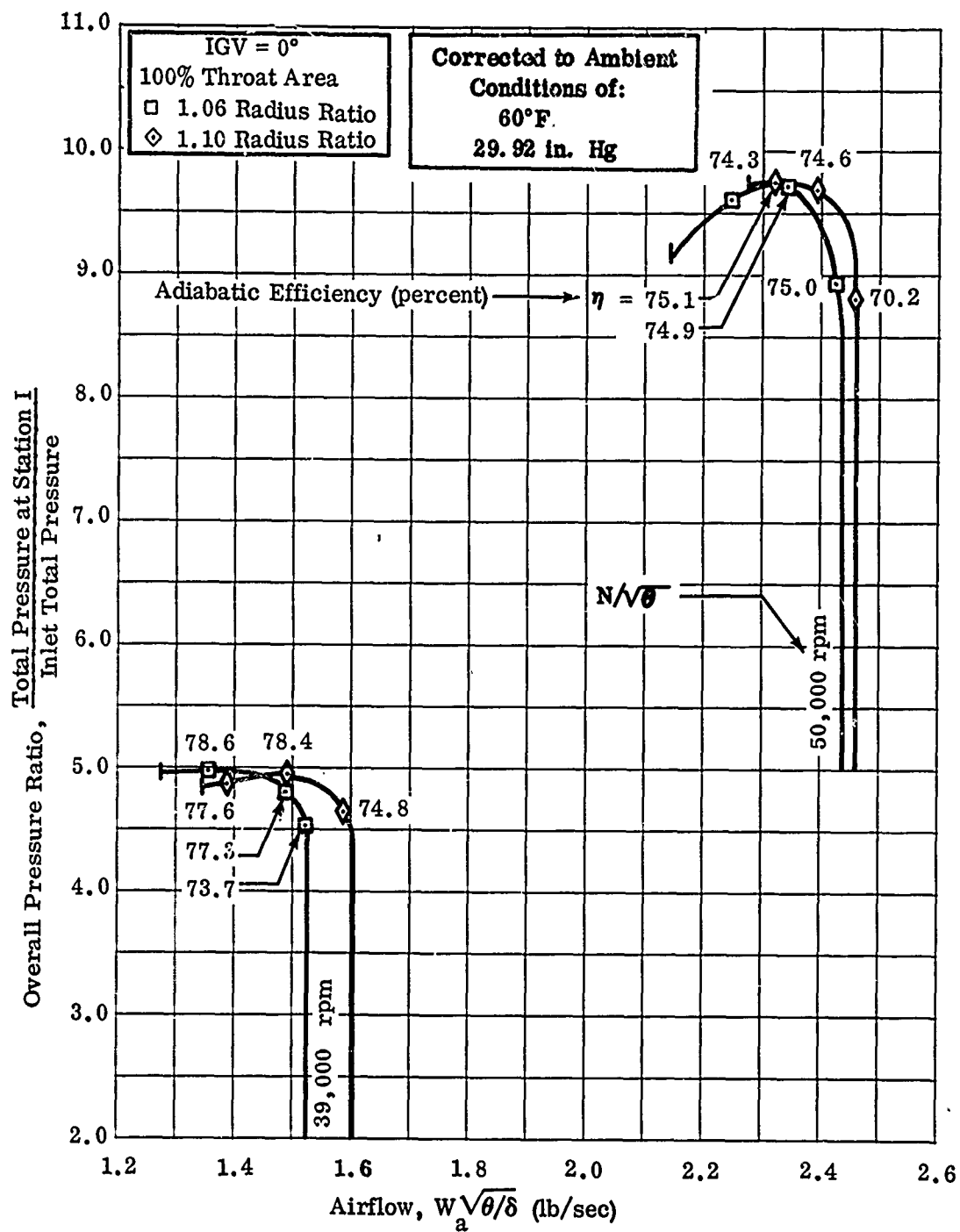


Figure 2. Pressure Ratio Versus Airflow, DI-1 Diffuser
(Comparison at 1.06 and 1.10 Radius Ratio).

1.3 RESEARCH APPROACH

From the previous results, areas requiring significant technical advances were identified for both impeller and diffuser designs. Investigations of high-pressure-ratio centrifugal compressors included:

- 1) Minimizing the effects of transonic flow conditions at the inducer and the diffuser entrance.
- 2) Determining the influence of inducer hub-to-tip diameter and its effects on inducer and impeller performance.
- 3) Establishing methods to provide adequate operating range at high-pressure ratios.

The earlier impeller and diffuser elements were designed to provide the technology required to reach a 10:1 pressure ratio at 80-percent efficiency. These first elements were tested and evaluated concurrently to define the physical dimensions and flow dynamics of components. From this performance evaluation, a new, complete compressor was designed to reach the specified performance levels. The new design included consideration of the effects of early flow separation in the inducer on exit mixing losses in the impeller. In addition, studies were directed toward defining a diffuser configuration that would achieve the best balance between pressure recovery and the flow range.

The plan was as follows:

- 1) Use a 2-piece inducer-impeller in which all of the tangential turning would be accomplished in the inducer before turning to the radial direction in the impeller. The configuration, based on airfoil theories presented in Section 7.0 of Reference 1, was expected to delay early separation and minimize Coriolis effects.
- 2) Use a short throat (1/8 inch) in the diffuser to avoid reacceleration of the flow to Mach 1.0 at the entrance to the diverging section. From the previous tests, it was expected that both range and pressure recovery could be optimized with 8 to 16 channels at a radius ratio of about 1.06.
- 3) Match the impeller-diffuser combination by establishing the performance of each component through test evaluations. Modify the components as necessary to improve the overall match.
- 4) Identify areas of further detailed research for possible continuation or extension of this work by other investigators.

CONFIDENTIAL

2.0 (C) DESIGN ANALYSIS (U)

Early in this program, diffusers and impellers were investigated to determine new technologies necessary for attaining high-pressure ratio (10:1) in the single-stage centrifugal compressor. Tests which followed these initial studies led to new understanding of compressor fluid-flow characteristics, and the new information was combined with available knowledge to design the new impeller and diffuser discussed in this section. Based on these investigations, the goal of the new compressor was kept as originally set, 10:1 pressure ratio at an adiabatic efficiency of 80 percent.

2.1 SUMMARY OF TECHNOLOGIES

Detailed results of the impeller and diffuser investigations conducted earlier in the program are presented in Section 7.0 of Reference 1. A summary of the technologies resulting from this work is presented herein.

2.1.1 Impeller

For the inducer design, it was determined that inlet relative Mach number should be less than previously used for the MF-1, RF-1, and workhorse impellers to avoid high overvelocities at the suction surface of the leading edge. To achieve this objective, it is desirable to maintain low blockage at a minimum inducer hub-to-tip diameter ratio, which can be determined from mechanical design considerations. In addition, proper balance must be established among design incidence, inducer loading, and impeller work requirement. Tests showed the importance of not forcing the inducer to operate at a high incidence when the inlet relative Mach number is in the high subsonic range (0.7-0.9). Low incidence (+1 degree) will keep the compressibility effects and the strength of the resultant shock at a minimum.

The dependence of slip factor on the number of blades was shown; i.e., for a given impeller diameter and rotational speed, an increase in the number of blades results in an increase in slip factor. A modified form of Eckert's equation was developed for high-pressure-ratio impellers,

where:

$$\text{Predicted Slip Factor} = (\text{Slip Factor})_{\text{Eckert}} + (0.02 \text{ to } 0.03) \quad (1)$$

The increase over Eckert's slip factor is empirical and is based on the results of the three impellers (MF-1, RF-1, and workhorse), which showed values that were from 0.02 to 0.03 higher than originally predicted.

CONFIDENTIAL

CONFIDENTIAL

The impeller investigations showed that performance was dependent on the point of separation in the blade passage. It was determined that delayed separation would reduce the impeller-exit-wake width and thus reduce the impeller-exit mixing loss, which is a large part of the total loss. In addition, consideration was given to the effects of the Coriolis forces on the impeller performance. In the high-pressure-ratio impeller, where separation can take place in the inducer, presence of the Coriolis force can result in low-energy fluid being deposited on the suction surface from the pressure surface. The component of this Coriolis force in the blade-to-blade direction is proportional to the product of the rotational speed and the radial component of the through-flow velocity. The direction of this force is from the pressure surface to the suction surface, reducing the amount of flow deceleration which can take place prior to separation. Because of difficulties arising from this force and the necessity to minimize its influence, the inducer should be designed to complete the tangential turning prior to turning to the radial direction (essentially an axial inducer). The design technique was modified and it was indicated that the inducer leading-edge region should be designed using the methods of Schlichting, in conjunction with Pearcey's κ parameter, to determine the configuration which produces the minimum overvelocity while showing the least tendency to be adversely affected by shock-induced separation (Section 7.2 of Reference 1).

Performance of the impeller can be estimated by determining losses from friction, clearance, and exit mixing (Section 7.1.7 of Reference 1). As part of the loss analysis, it is necessary to establish the point of separation in the blade passage. Limits for deceleration of the relative flow along the suction surface can be determined using boundary-layer calculations, and the solution of turbulent boundary-layer flows is accomplished through the use of approximate methods presented in Section 7.1.9 of Reference 1.

2.1.2 Diffuser

The diffuser investigation showed that the major static-pressure rise through the diffuser occurred in the diverging channel and that the channel-static-pressure recovery was dependent on throat-entrance blockage and Mach number. Tests showed that shock strength in the channel-throat straight section, and therefore boundary-layer blockage, was dependent on the throat length and geometrical throat area. The entrance subsonic Mach number accelerated through the throat straight section in accordance with Fanno line calculations. If the throat was long enough with respect to the entrance subsonic Mach number, the flow at the throat exit was sonic. It was found that flow at this condition could undergo supersonic acceleration into the diffuser channel and be accompanied by a shock. At upstream shock Mach numbers above 1.1 to 1.2, the channel performance deteriorated rapidly.

Single-channel-diffuser tests were conducted to determine the effects of throat-entrance Mach number on channel-static-pressure recovery. It was found that no critical subsonic Mach number existed for 2-dimensional channel diffusers,

CONFIDENTIAL

contrary to indications in the literature. Channel performance was nearly constant up to throat Mach numbers of 1.0. At critical pressure ratios, flow values equivalent to throat Mach numbers of 1.0, a shock occurred in the channel. Static-pressure recovery again deteriorated rapidly above upstream Mach numbers of 1.1 to 1.2. Detailed discussions of the single-channel diffuser tests and a literature search relative to critical throat Mach number of diffusers are presented in Appendixes XI and XII of Reference 1.

The single-channel diffuser tests, combined with the compressor rig tests, showed that best channel performance was obtained with a divergence angle of 10 degrees for a low-aspect-ratio diffuser ($AR = 0.25$). In addition to the necessary low aspect ratio, diffusers designed in this program required minimum throat blockage for best performance. Therefore, the diffuser should be designed with a low channel-entrance Mach number to avoid large growth in the boundary layer across the entry shock; otherwise, predictions of throat blockage will not be correct. The vaneless-space diameter ratio was determined from considerations of impeller-exit flow conditions. It was found that the vanes should be placed close to the impeller tip, but outside of the impeller-exit-wake mixing zone ($R/R \approx 1.05$). A discussion of vane radius ratio is presented in Section 7.2 of Reference 1.

2.2 IMPELLER DESIGN

The new impeller, designated as RF-2, was designed with the lowest inlet relative Mach number of any of the configurations investigated in the program. The Mach number selected for the inducer tip was 0.86, when based on a blockage factor of 1.0. This lower Mach number was chosen to avoid supersonic overvelocities at the inducer leading edge and to minimize the likelihood of early separation. The inducer was sized for a hub-to-tip-diameter ratio of 0.447 with an inlet absolute Mach number (axial) of 0.46 (based on unblocked flow). Velocity diagrams for these conditions are given in Figures 3 and 4, and represent design conditions at the tip, RMS, and hub. The relations between airflow continuity and the vector diagram (as discussed in Section 2.2.1 of Reference 1) were used to determine inducer-tip diameter (3.60 inches). The rotor speed was established as 50,000 rpm to permit use of the existing workhorse-impeller test rig. Detailed discussion of this rig was presented in Section 2.4 of Reference 1. A comparison of blade-turning schedule for the new impeller and RF-1 is shown in Figure 5. Note that the turning rate, and therefore blade loading, is considerably less near the leading edge for the new design.

The methods given in Appendix I of Reference 1 were used to establish inducer radial equilibrium and impeller-blade-surface velocities. Factors considered in minimizing the peak overvelocity on the suction surface of the inducer blade near the leading edge also were given in Reference 1 (Section 7.0). Velocity distributions for the blade surface and mid-channel flows are presented in Figures 6,

CONFIDENTIAL

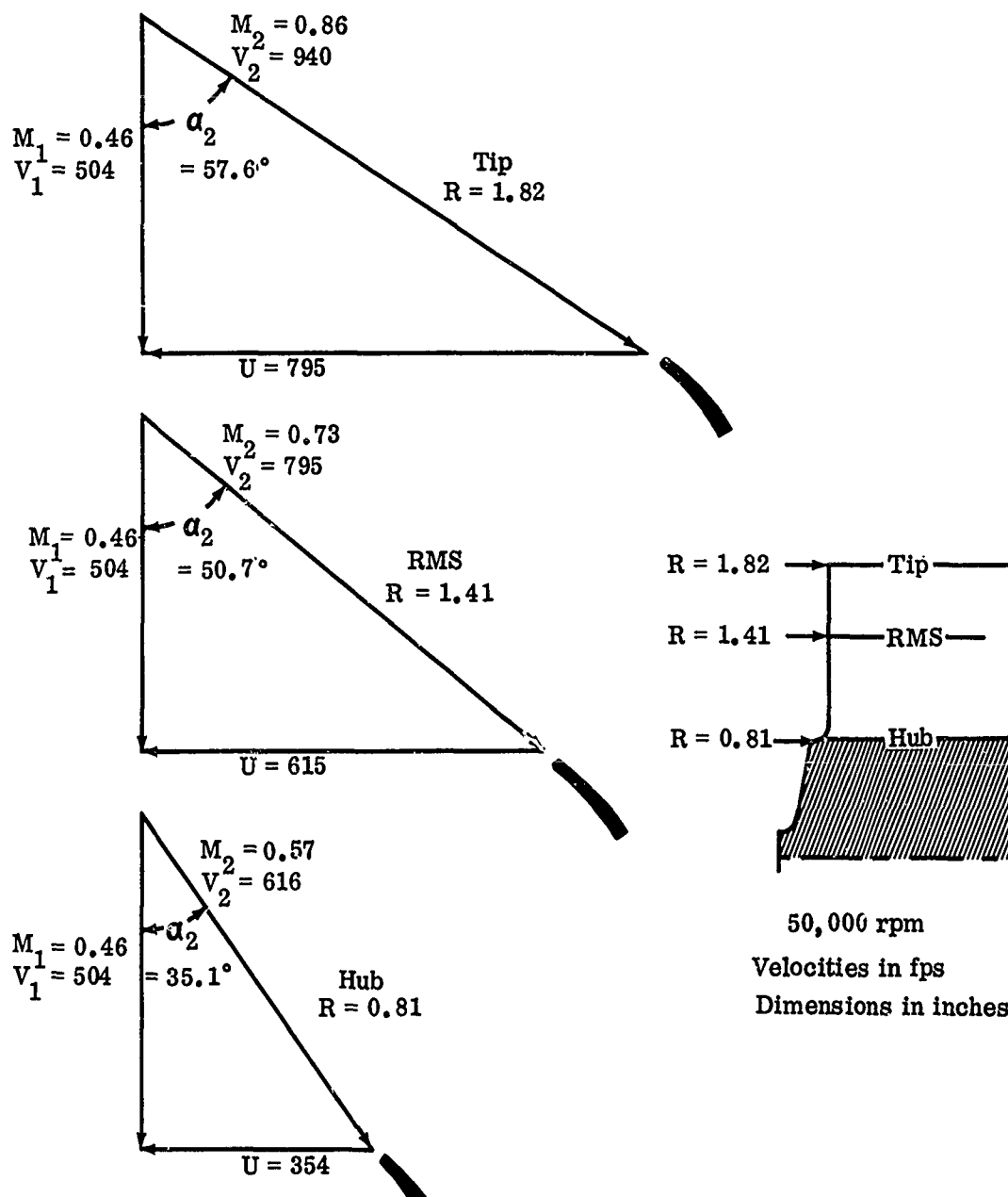


Figure 3. Design Inlet Vector Diagrams Based on Unblocked Flow Area, RF-2.

CONFIDENTIAL

CONFIDENTIAL

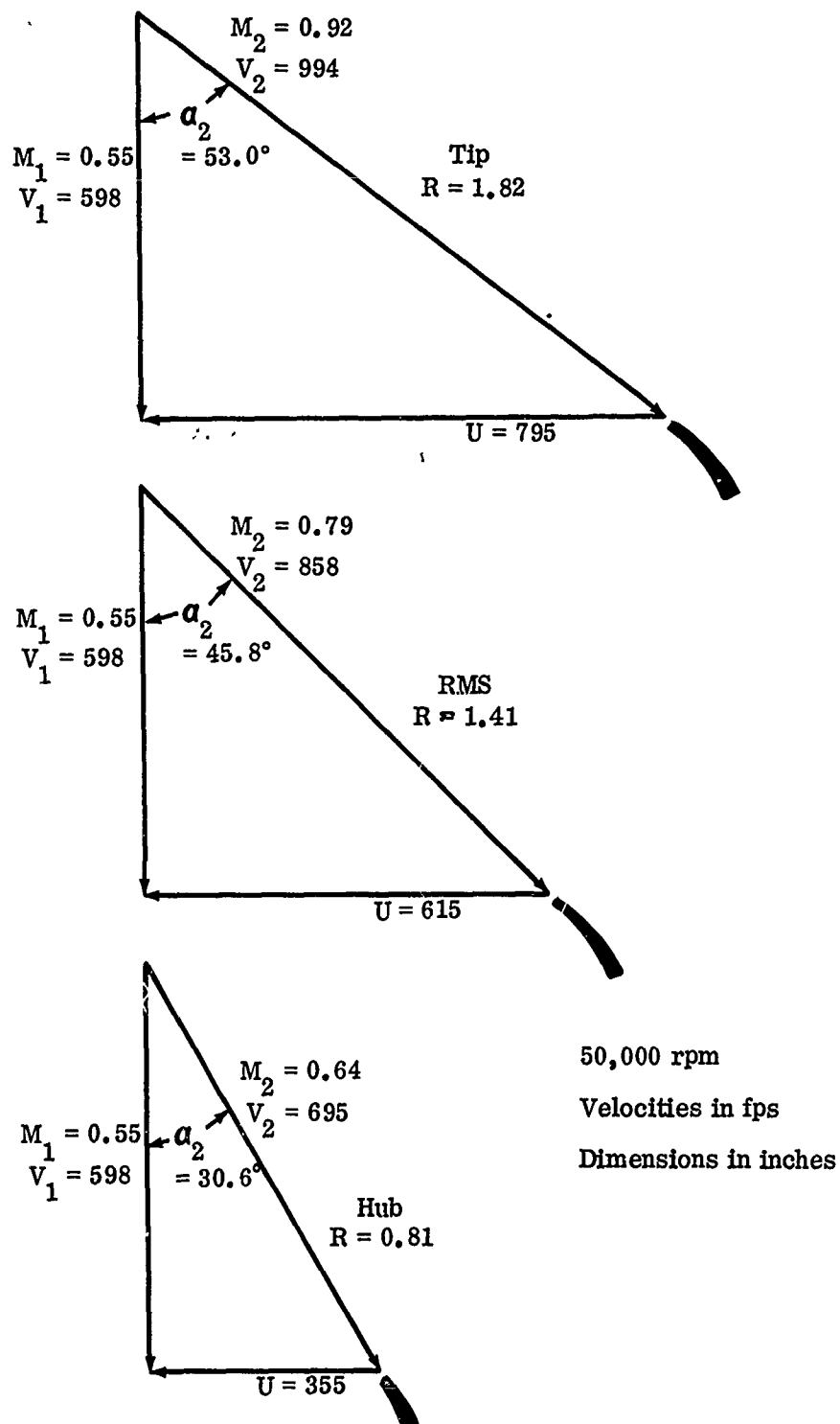


Figure 4. Design Inlet Vector Diagrams Based on Blocked Flow Area, RF-2.

CONFIDENTIAL

CONFIDENTIAL

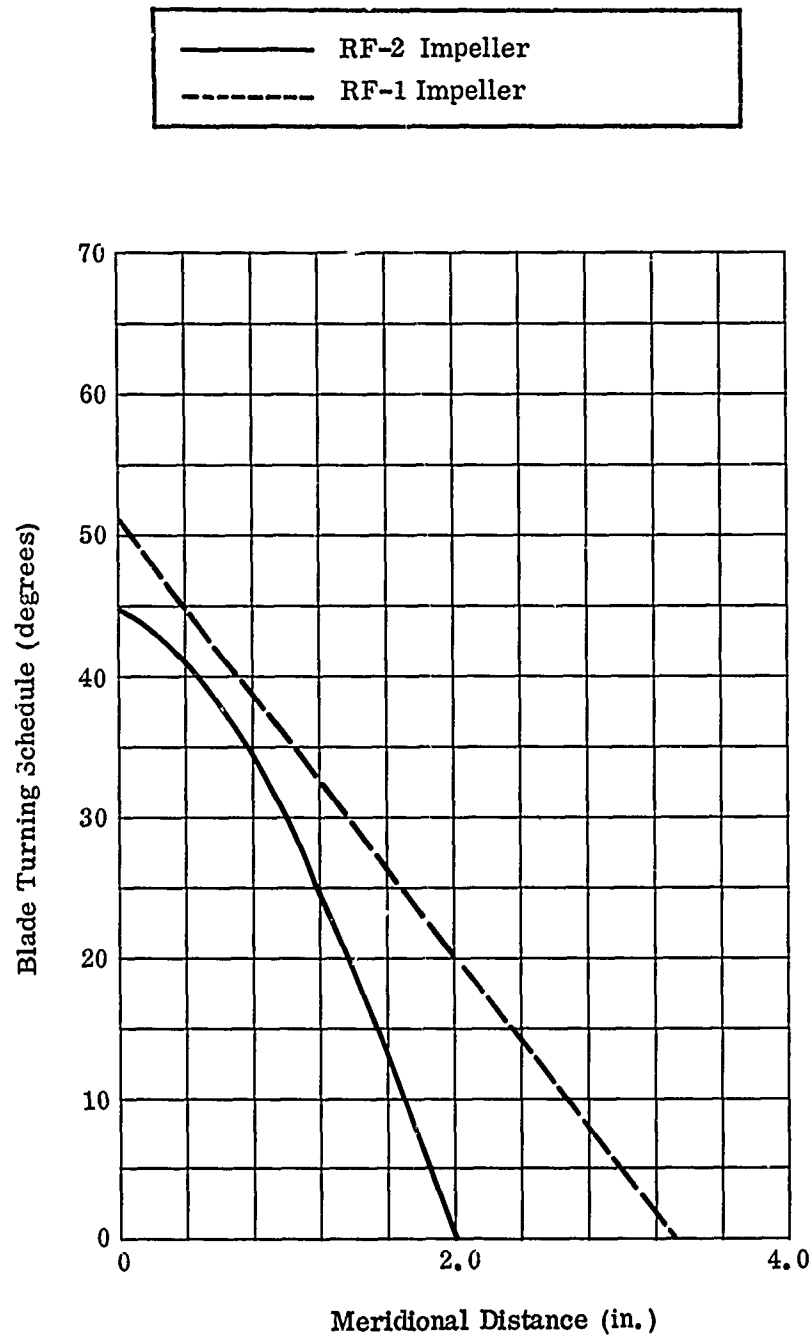


Figure 5. Comparison of the Blade Turning Schedules at the RMS Radius for the RF-1 and RF-2 Impellers.

CONFIDENTIAL

CONFIDENTIAL

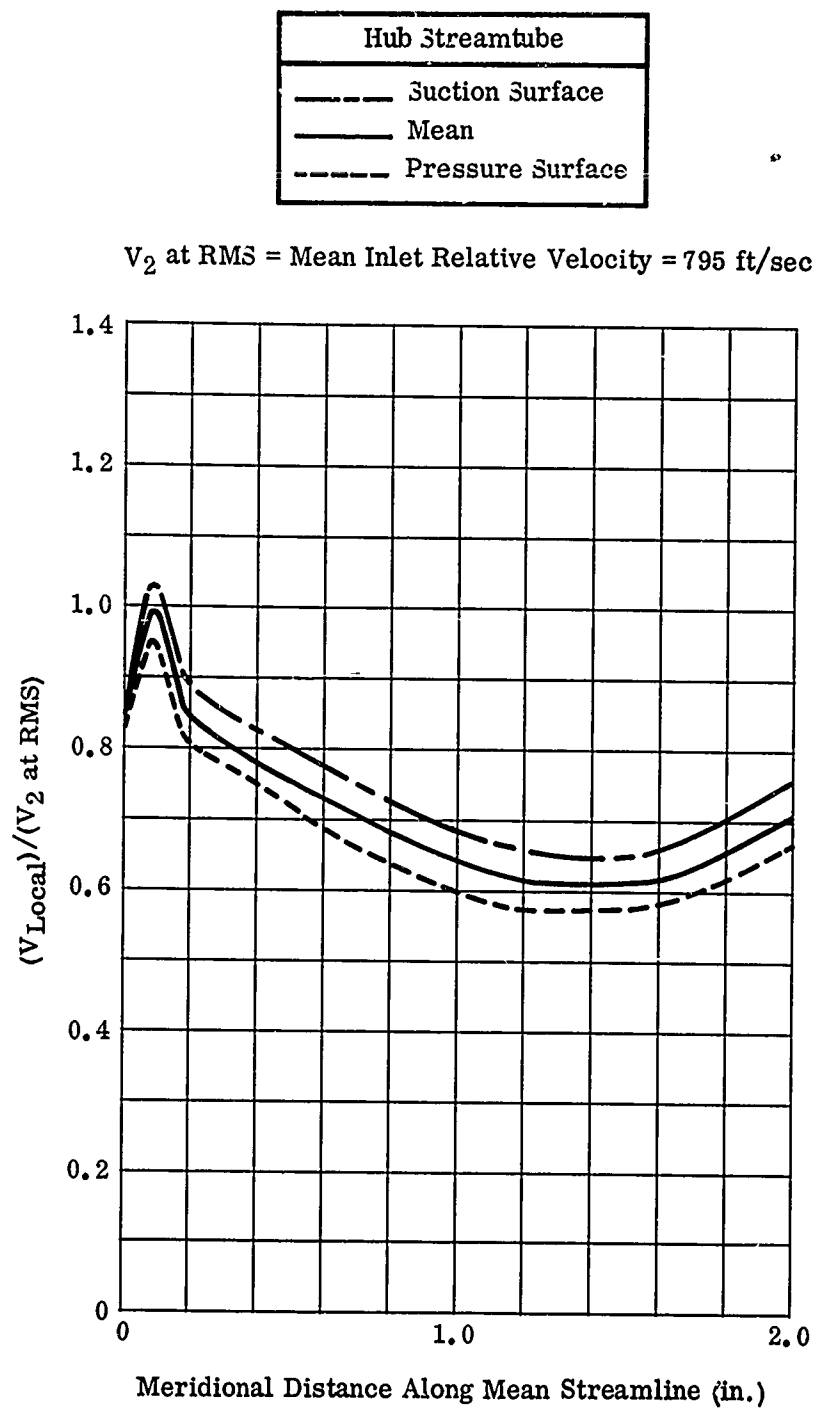


Figure 6. Blade Surface Velocities for Hub Streamtube of RF-2 Impeller (Design Speed).

CONFIDENTIAL

7, and 8 for the mean radii of the hub, RMS, and tip streamtubes, respectively (3 of the 5 streamtubes calculated). No radial-equilibrium analysis was made for the radial portion of the impeller because velocity distributions indicated that the flow will separate from the suction surface near the exit of the inducer; analyses of these separated flows were impractical and beyond the scope of presently available analytical tools.

Blade blockage predictions for the impeller design are shown in Figure 9. The blade width* at the tip of the new impeller was 0.180 inch, compared to 0.250 inch for the workhorse impeller. The smaller blade width was necessitated because the design airflow was reduced from 2.43 pounds per second for the workhorse impeller to 2.0 pounds per second for the new design, and the design speed (and therefore impeller-tip diameter) was the same as that for the workhorse. The blade-tip width was reduced to obtain low impeller-exit mixing loss (a function of wake-to-jet width). It was expected that the 0.180-inch width would result in a smaller wake-to-jet-width ratio (ϵ) than the workhorse impeller. Data used to predict the change in mixing loss are presented in Section 7.0 of Reference 1.

As in previous analyses, the normal static-pressure gradients through the blade-passage area of the inducer were determined from the radial-equilibrium program. These gradients were used to estimate static-pressure rise along the shroud of the inducer, as shown in Figure 10. In the earlier tests, similar predictions were used to evaluate impeller performance; static pressure along the shroud was used to indicate separation points in the inducer. It was determined that these measurements were critical to assessing overall impeller performance. Rotor loading (diffusion factor) for the inducer, using the velocities based on unseparated flow, is shown in Table I.

TABLE I	
INDUCER DIFFUSION FACTORS	
Streamtube	Diffusion Factor
Hub	0.191
RMS	0.341
Tip	0.596

Overall impeller efficiency and pressure ratio were predicted as 84.6 percent and 12.1:1, based on estimates of friction, clearance, and exit mixing losses. A discussion of loss calculations is presented in Section 7.1 of Reference 1. The one-dimensional, impeller-exit vector diagram is presented in Figure 11.

*Referred to as blade "height" in Reference 1.

CONFIDENTIAL

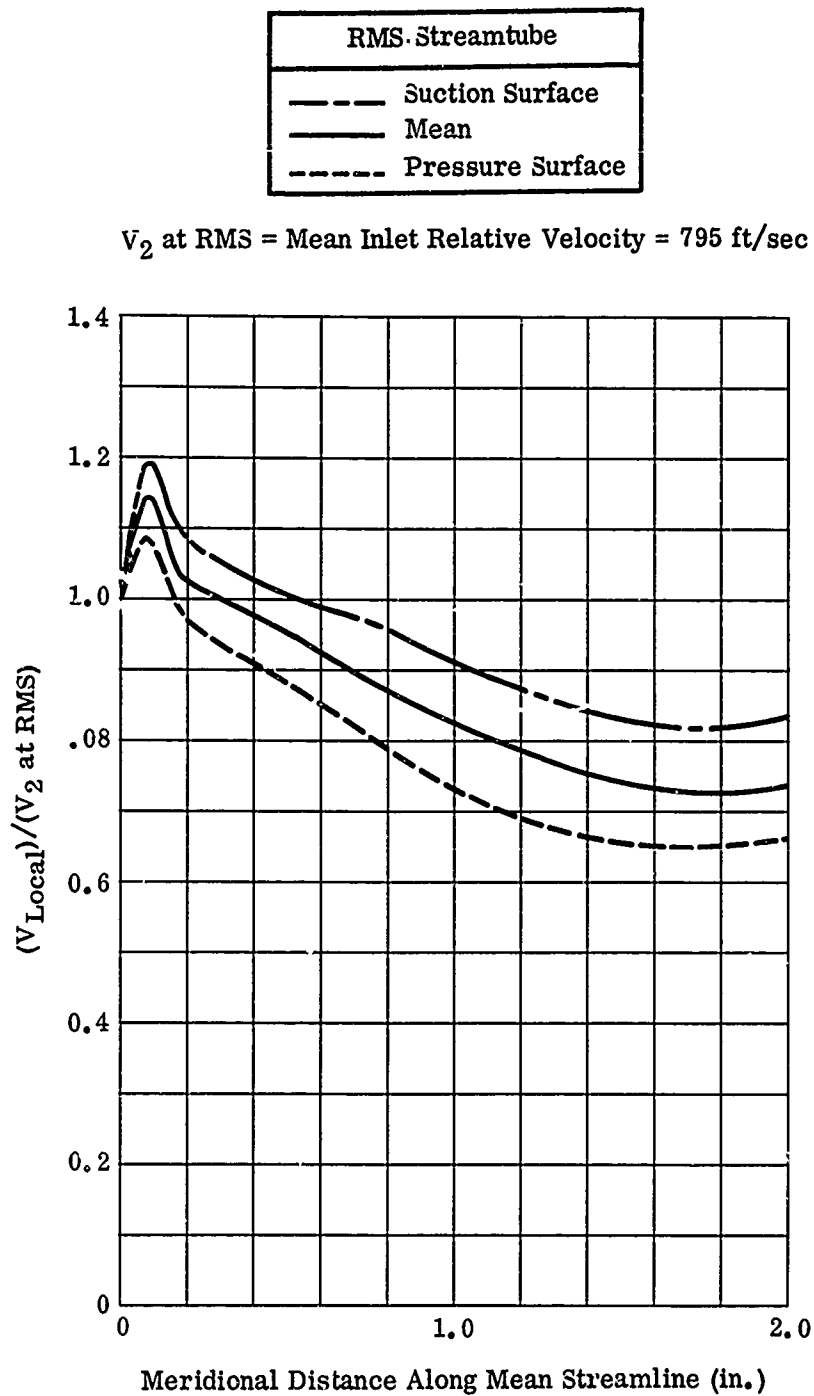


Figure 7. Blade Surface Velocities for RMS Streamtube of RF-2 Impeller (Design Speed).

CONFIDENTIAL

CONFIDENTIAL

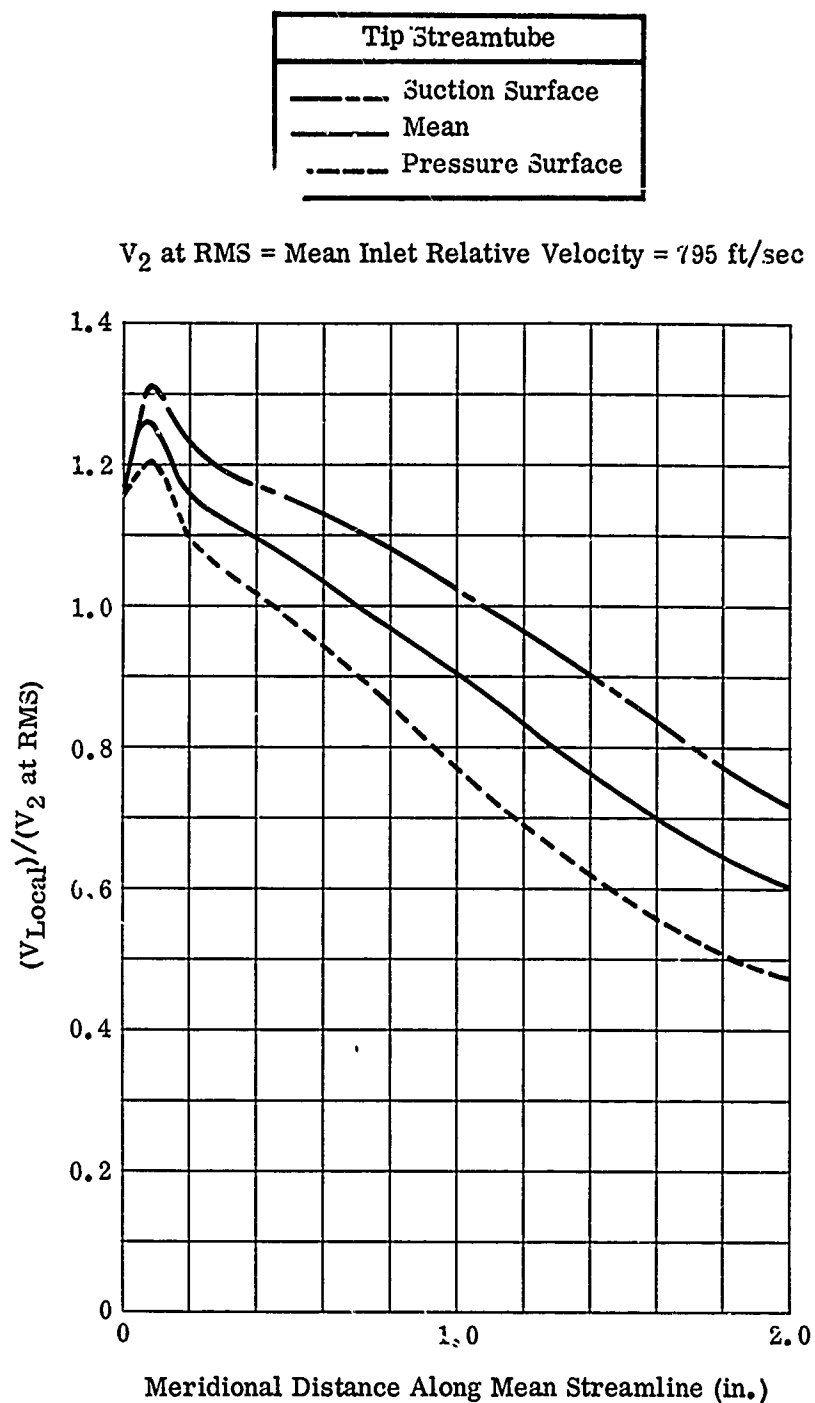


Figure 8. Blade Surface Velocities for Tip Streamtube of RF-2 Impeller (Design Speed).

CONFIDENTIAL

CONFIDENTIAL

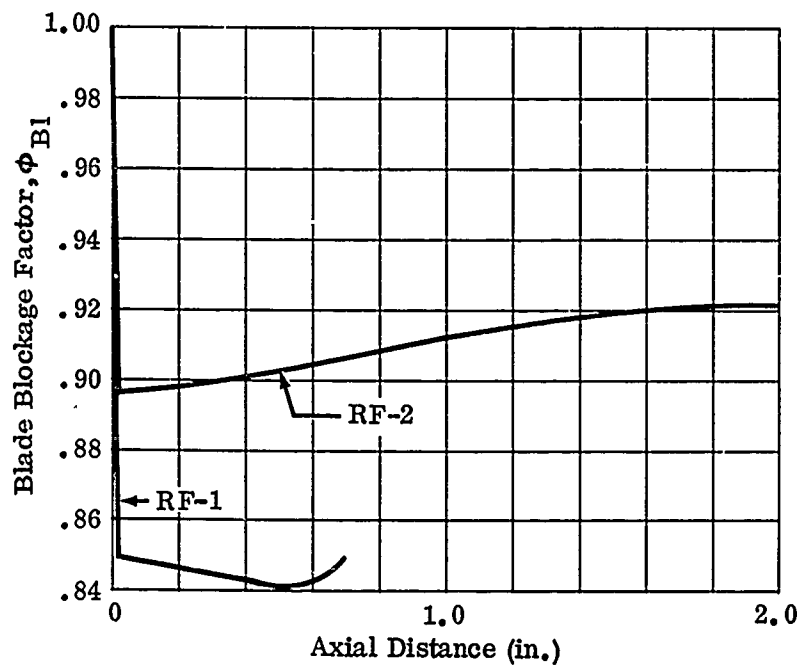


Figure 9. Comparison of Inducer-Blade Blockage for RF-1 and RF-2.

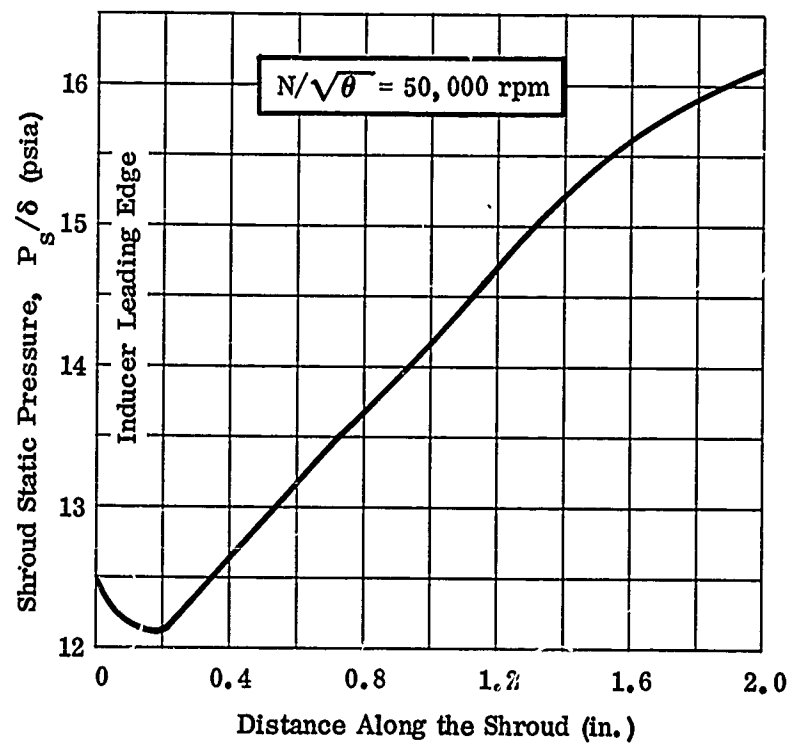
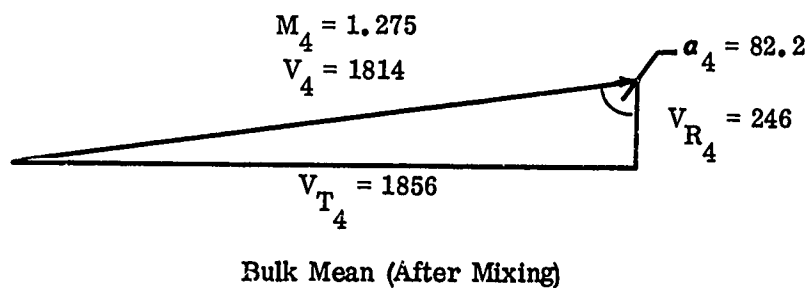
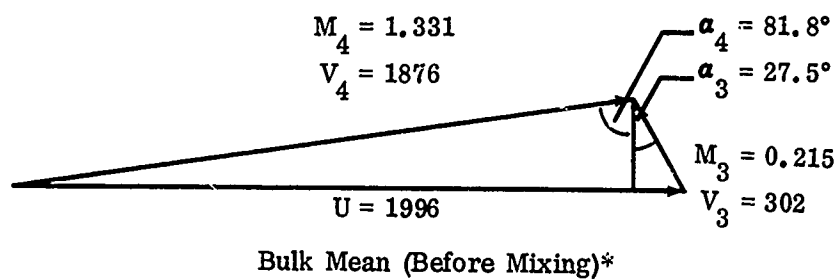
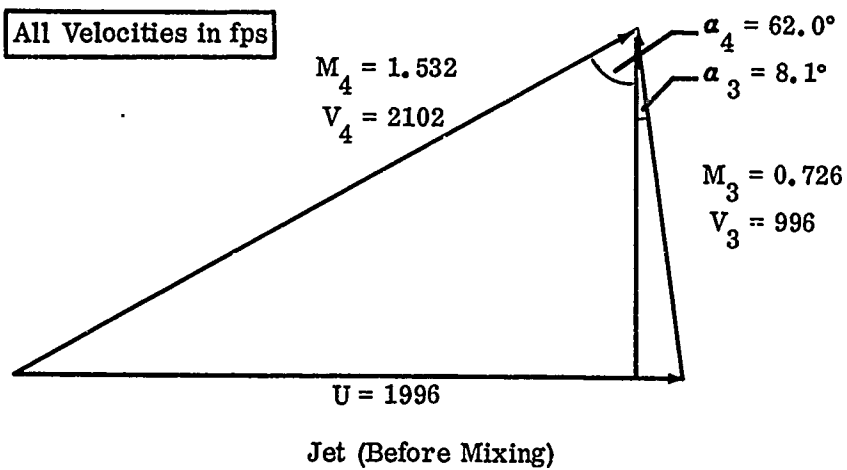


Figure 10. Predicted Static-Pressure Rise Along the Inducer Shroud.

CONFIDENTIAL

CONFIDENTIAL



* Used in exit mixing loss analysis

Figure 11. Design Exit Velocity Diagrams for RF-2 Impeller.

CONFIDENTIAL

CONFIDENTIAL

In addition to the lightly loaded leading-edge region, several other concepts were incorporated in the RF-2 design which were different from those used in the previous impellers described in Reference 1. The first is that all of the tangential turning in RF-2 is accomplished prior to turning the flow to the radial direction, instead of combining the 2 turns as with RF-1, MF-1, and the workhorse. This change brought the inducer closer to an axial-rotor design in concept and eliminated the blade-to-blade component of the Coriolis force. Elimination of the radial-velocity components in the inducer section, where the blade loading is highest due to the tangential turning, can be expected to delay separation and result in a performance improvement (as shown by the loss analysis presented in Section 7.2 of Reference 1).

The second change in design concept was applied to the inducer-entrance region, where the pressure surface, rather than the camber line, was aligned with the incoming-flow direction. The zero incidence with respect to the pressure surface was based on the blocked-flow area. Resulting velocity diagrams are shown in Figure 4. In addition, the pressure surface was designed as a radial-driving face for the full-blade height (see Figure 12).

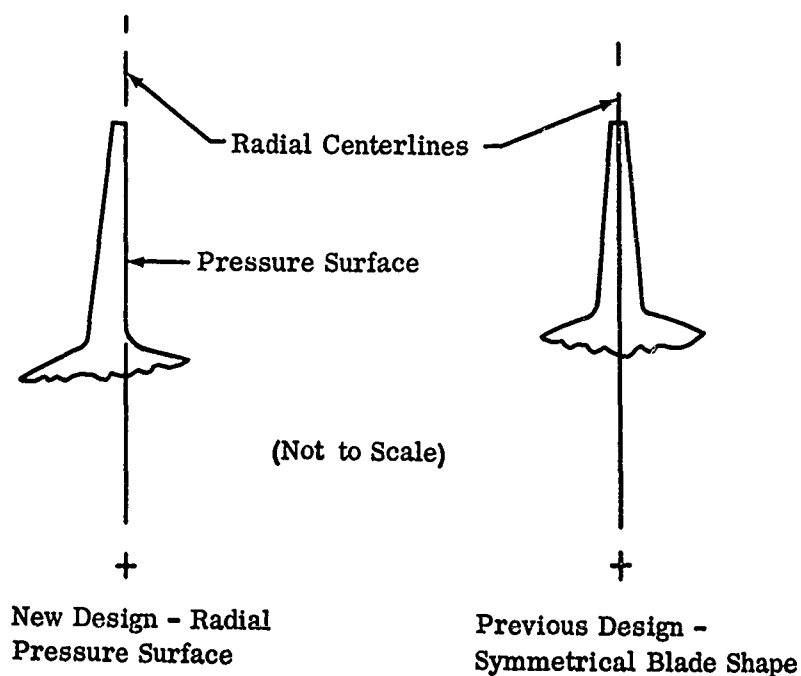


Figure 12. Inducer Blade Sections.

CONFIDENTIAL

A third change for RF-2 was to design constant-thickness profiles rather than the double-circular-arc profiles used in the previous designs (blade sections projected in cylindrical surfaces with the centerline for their axis). Removal of material from the suction surfaces only, which results in a sharp turning of the camber line in the leading-edge region, was expected to align the local mean camber line with the unblocked approach vector at Point A, as shown in Figure 13.

The flow at Point B (Figure 13) was expected to be parallel to the blades, having turned through the incidence angle, i . This flow-angle change was believed to be necessary to compensate for the blade blockage. By constructing the pressure surface radially and aligning it with the blocked vector, the change in the mean-camber-line angle can be accommodated; removal of material from the suction surface at the leading edge was expected to provide the necessary guidance for the incoming air to reduce the previously noted overvelocities.

In Section 7.1 of Reference 1, a detailed discussion was presented showing the analysis of aircraft wings by Pearcey (Reference 2) as applied to the inducer-leading-edge-flow solution. Further study of the analogy during the design of the new impeller led to revision of the κ factor for application to inducer blades. A comparison of κ factors for the new design and the workhorse and RF-1 impellers is shown in Table II.

TABLE II		
INDUCER-ENTRANCE BLADE SHAPE (κ FACTOR)		
Impeller	RMS Radius κ	Tip Radius κ
New Design (RF-2)	0.056	0.097
Workhorse	0.044	0.095
RF-1	0.500*	0.424
*Approximate		

A detailed discussion of the κ -factor analysis is presented in Section 7.0 of Reference 1 and will not be repeated here. However, it should be noted that a low κ value results in the best blade shape for delayed separation. The comparison in Table II also shows that the new inducer was designed with a κ factor close to the workhorse impeller, which had shown the best performance in previous tests.

CONFIDENTIAL

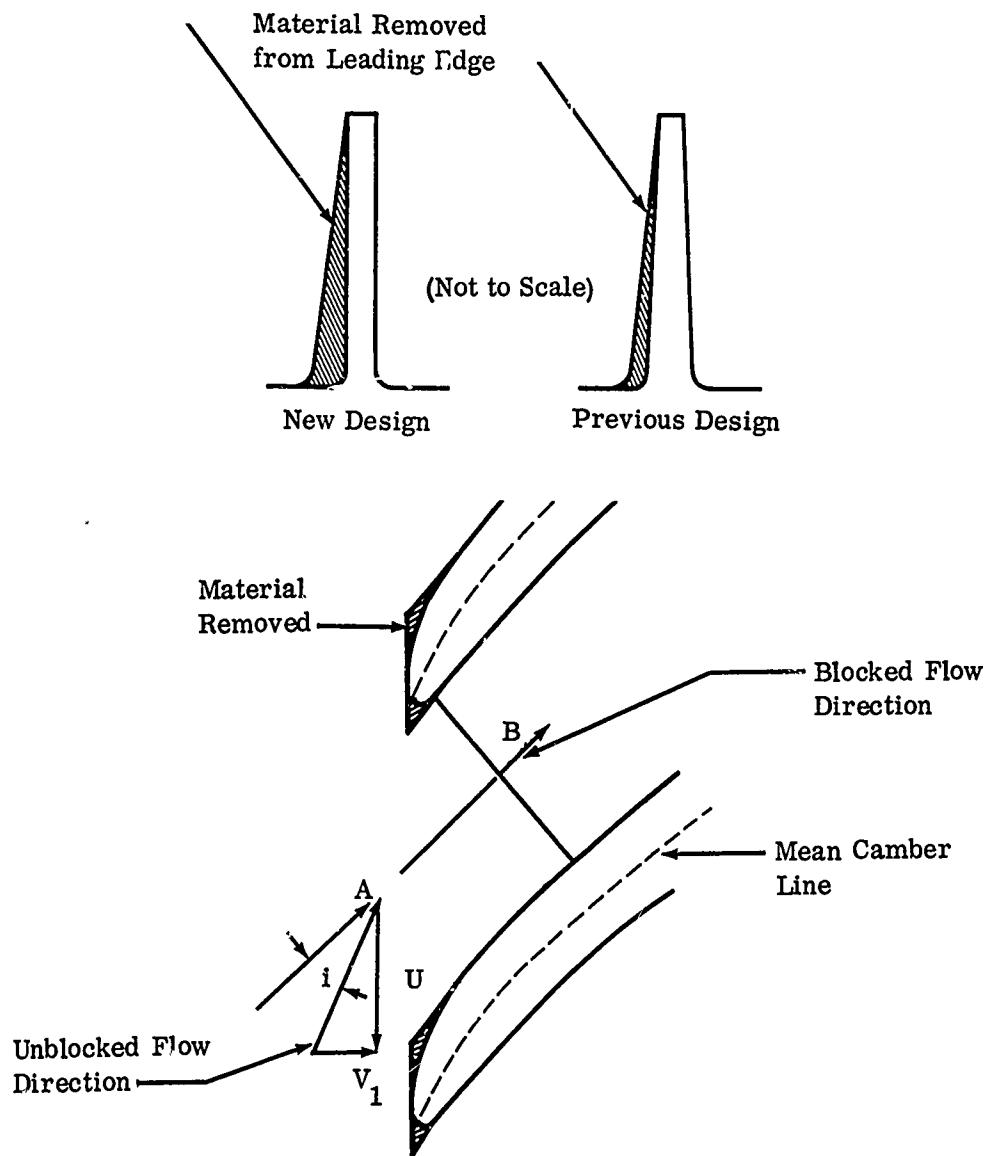


Figure 13. Inlet Blade Shape.

The analysis given in Reference 1 also illustrated the validity of the approach for selecting nose shapes. Because small changes in the nose design can affect the κ value, analysis of the test results of the new impeller will be aimed at establishing whether a further reduction in κ factor is desirable in future research to achieve best impeller performance.

CONFIDENTIAL

2.3 DIFFUSER DESIGN

During the experimental program presented in Reference 1, it was found that the performance of a vane-island diffuser was dependent on channel-entrance Mach number and throat blockage. It was also shown through experiment that best performance was obtained with a low entry-shock Mach number ($M \approx 1.05$ ahead of the vane leading edge) which resulted in low throat blockage and a high subsonic throat Mach number ($M \approx 0.95$). Best performance was also obtained when the straight section of the diffuser throat was short enough to prevent acceleration of the flow to Mach 1.0 at the throat exit, a condition which was shown to produce supersonic flow in the diverging channel. Diffuser DI-1-2 (Section 7.3 of Reference 1) demonstrated the best performance trend and was used as a model for design of the new configuration, which had a throat length of 1/8 inch.

The number of vanes chosen for the new design was based on mechanical design considerations. As discussed in Section 2.4, the predicted Campbell diagram for the impeller indicated that 10 vanes would avoid exciting the rotor at an order and frequency corresponding to design speed. It was shown from the previous tests (using 8, 12, and 16 vanes) that within the range studied, the number of vanes had no influence on performance (see Section 7.0 of Reference 1).

The divergence angle was selected as 10 degrees, typical of the best diffusers run in the earlier test series. The single-channel data presented in Appendix XII of Reference 1 also showed that peak performance was obtained at 10-degree-divergence angles for aspect ratios near the new design.

The throat area was determined from airflow continuity as shown in Section 2.3 of Reference 1. The design throat Mach number (0.95) was about the same as that for DI-1-2. It was expected that the entry shock just ahead of the throat would correspond to a Mach number of 1.05. A low blockage of 0.92 also was expected, as shown by the analysis presented in Section 7.3 of Reference 1. However, it was recognized that further investigation of the influence of aspect ratio on blockage was necessary to establish performance potential of possible throat geometries. From the studies presented in Reference 1, it was shown that boundary layer on the blade-suction surface was bled by secondary flow. Therefore, the throat blockage resulted primarily from the side-wall boundary layer. For a given throat area, reducing the aspect ratio exposes an increased percentage of the perimeter to side-wall effects. If the boundary-layer thickness is a function of the flow-path length (assuming that growth through the 1.05 entry shock is small), the blockage will increase with a reduced aspect ratio at a given entry-shock Mach number. The aspect ratio of the new diffuser (0.41) was the lowest designed thus far in the program. This reduced aspect ratio was necessary to match the new impeller-blade-tip width ($b = 0.180$ inch), as shown in Section 2.2.

CONFIDENTIAL

Therefore, the possibility existed that throat blockage might be higher than the predicted value, which would result in lower than design performance. It was planned to test several diffuser modifications, if necessary, to evaluate these effects. However, based on the design throat blockage, channel-static-pressure recovery was expected to be 0.62 with an overall diffuser-total-pressure recovery of 0.82.

The geometry of the new design is shown in Figure 14. Design parameters selected are listed in Table III. The figure shows that the channel was designed with all of the 10-degree divergence on the pressure surface, as were the best diffusers tested earlier in the program. It was planned that modifications to this geometry be made (depending on test results) to investigate further the effects of channel symmetry on performance.

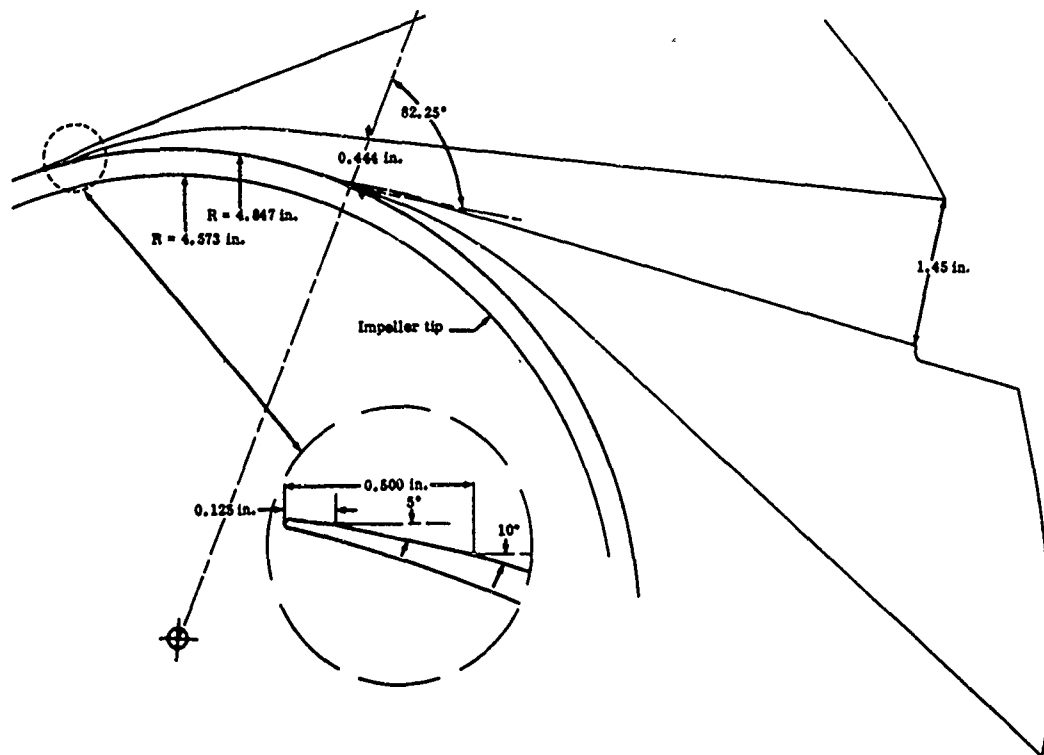


Figure 14. Diffuser-Vane Geometry.

CONFIDENTIAL

TABLE III			
DESIGN PARAMETERS FOR V1 DIFFUSER			
Number of Vanes	10	Throat Length	0.125 in.
Throat Mach Number	0.95	Channel Divergence Angle	10 deg
Blockage Factor	0.92	Area Ratio	3.3
Throat Height	0.444 in.	Vane Angle	82.2 deg
Passage Depth	0.180 in.	Wedge Angle	7.0 deg

2.4 MECHANICAL DESIGN

This section discusses the mechanical design and requirements of the impeller, diffuser, and test section used in aerodynamic testing. These components were designed for use with the diffuser test rig described in Reference 1. The impeller was a 2-piece, radial-flow design and was adapted to the existing workhorse-impeller shaft. A 10-channel, vane-island diffuser was selected for the new test section.

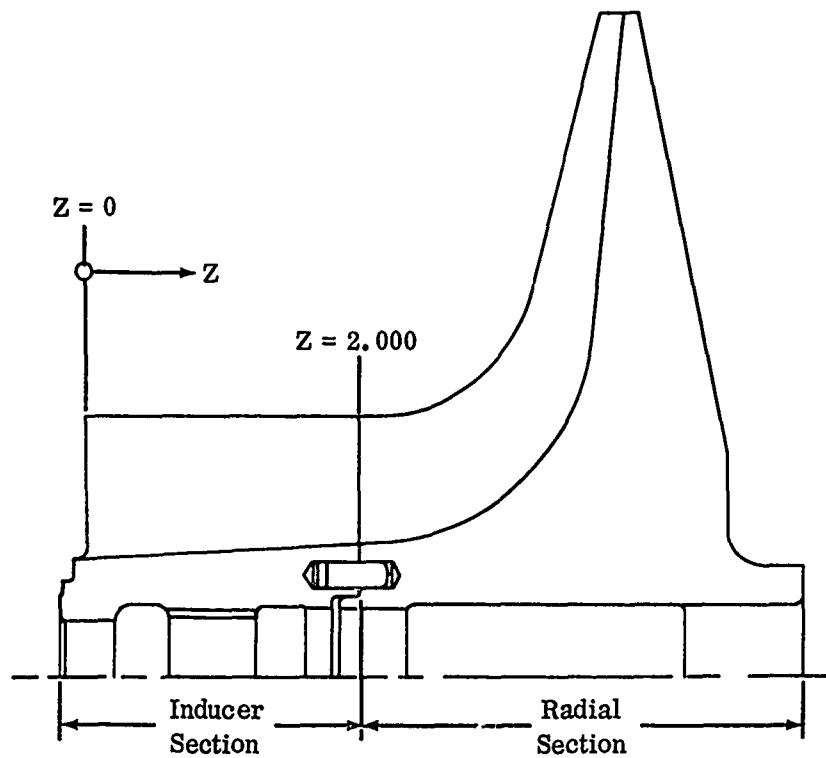
2.4.1 Impeller

Figure 15 shows the final design information relative to the impeller size and blade configuration. The mechanical design requirements for the impellers described in Section 2.4 of Reference 1 were applied to this impeller, with the exception of a closer, 0.015-inch, blade-to-shroud clearance goal. In addition, the impeller was a 2-piece design, with the tangential turning completed in the inducer section and with radial turning done in the impeller (radial) section. A radial-driving face was designed for blades in the inducer section, whereas blades in the remainder of the impeller were symmetrical, consistent with maintaining a desirable distribution of centrifugal loads in regions of highest blade stresses. The inducer section was mated with the radial section, as shown in Figure 16; 2 pins were used to maintain blade alignment and transmit driving torque from the inducer section to the radial section.

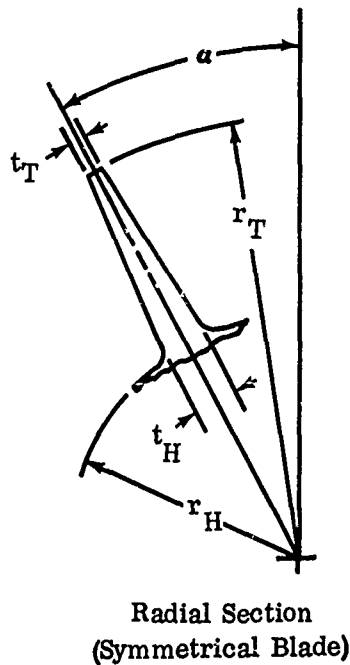
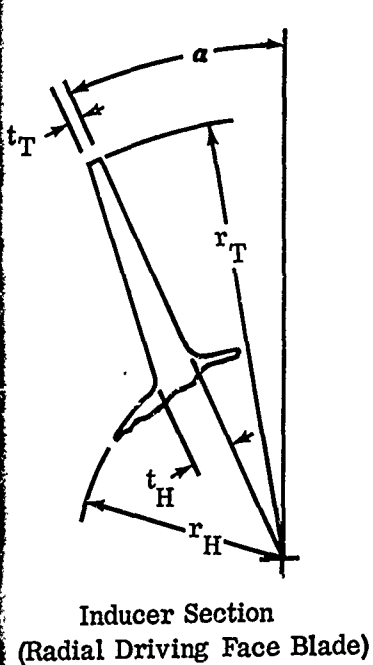
The 2-piece design allowed use of available titanium forgings. In addition, the separate inducer with all of the turning in 1 section reduced machining time by comparison with the previous designs described in Reference 1. The transition (or blending) of the blades from the inducer to the symmetrical-blade radial section was accomplished by hand working (see Section 3.0).

Two bore-pilot surfaces were used, 1 at the aft hub (in the radial section) and 1 at the joint between the 2 sections (Figure 16) to match the existing shaft pilots.

CONFIDENTIAL



Design Speed: 50,000 rpm
 Number of Blades: 18
 Tip Diameter: 9.12 in.
 Overall Length: 5.48 in.



Distance Z (in.)	Turning Angle α (degrees)
0	0
0.120	4.78
0.300	11.60
0.500	18.59
0.700	24.87
0.900	30.32
1.100	34.88
1.300	38.53
1.500	41.27
1.700	43.10
1.900	44.03
2.000	44.15
2.430	44.80
2.860	44.80
3.290	44.80
3.720	44.80

Figure 15. Aerodynamic Design Information.

CONFIDENTIAL

Design Speed: 50,000 rpm
 Number of Blades: 18
 Tip Diameter: 9.12 in.
 Overall Length: 5.48 in.

Blade Geometry

Distance Z (in.)	Turning Angle α (degrees)	Radius r_H (in.)	Radius r_T (in.)	Thickness t_H (in.)	Thickness t_T (in.)
0	0	0.813	1.800	0.063	0.045
0.120	4.78	0.819	1.800	0.063	0.044
0.300	11.60	0.829	1.800	0.062	0.043
0.500	18.59	0.839	1.800	0.061	0.041
0.700	24.87	0.850	1.800	0.060	0.039
0.900	30.32	0.860	1.800	0.059	0.037
1.100	34.88	0.871	1.800	0.058	0.035
1.300	38.53	0.881	1.800	0.057	0.033
1.500	41.27	0.892	1.800	0.056	0.032
1.700	43.10	0.902	1.800	0.055	0.031
1.900	44.03	0.913	1.800	0.055	0.030
2.000	44.15	0.918	1.800	0.055	0.030
2.430	44.80	0.958	1.839	0.055	0.030
2.860	44.80	1.108	2.051	0.055	0.030
3.290	44.80	1.431	2.711	0.055	0.030
3.720	44.80	2.313	4.316	0.055	0.030

CONFIDENTIAL

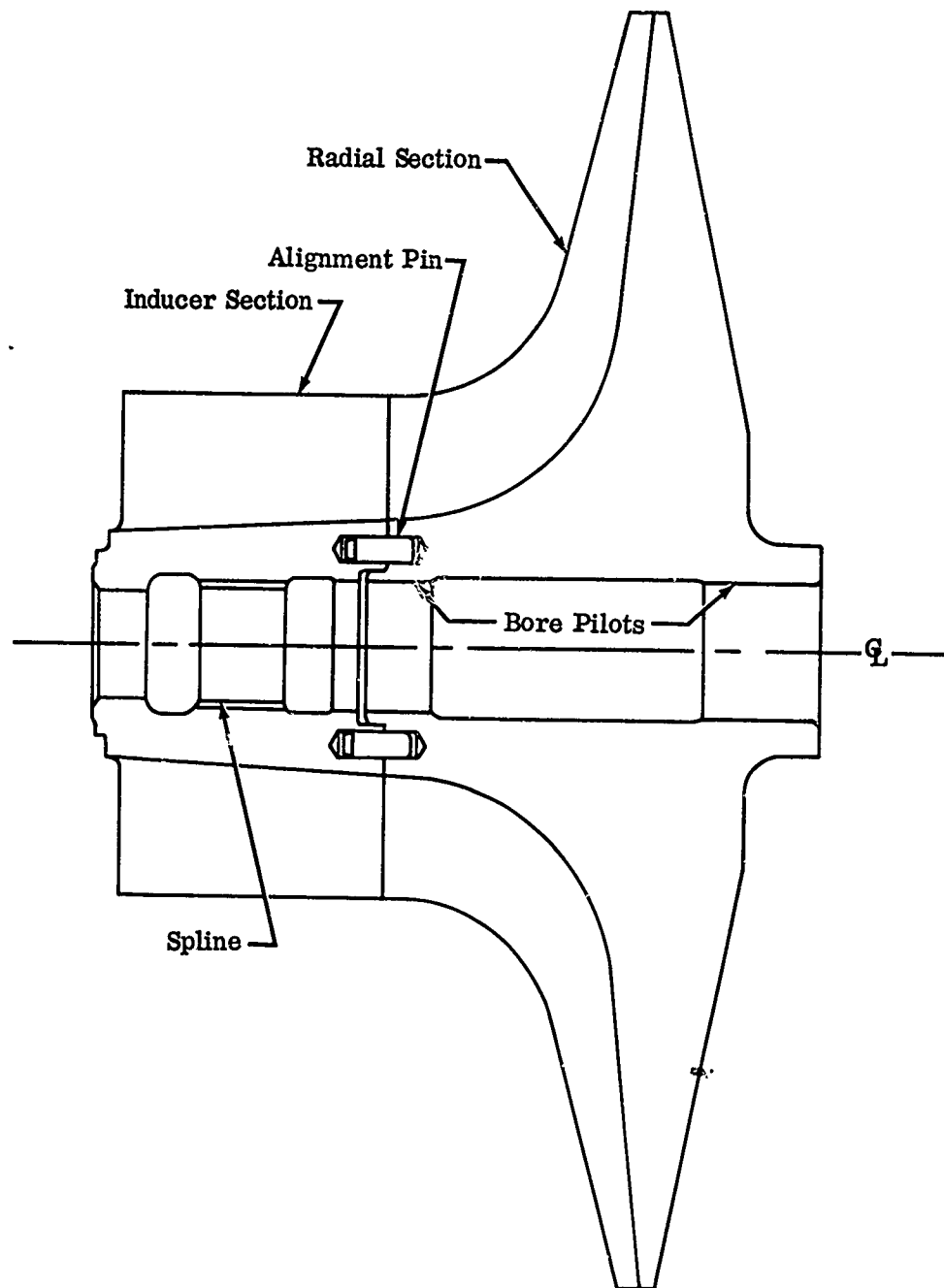


Figure 16. Two-Piece Impeller.

CONFIDENTIAL

Material Selection

Because this impeller was designed to operate at the same tip speed and temperature conditions as the previous configurations, the same requirements applied. Based on the successful use of titanium for high-speed impellers earlier in the program, 6Al-4V was again selected. Other materials were considered for the inducer, but the titanium alloy was found to provide the best balance of properties.

Impeller Stress

The same general stress analysis procedure given in Section 2.4 of Reference 1 was applied to this impeller, including blade and disk stresses and blade vibratory stresses. However, disk stresses were calculated using a new contractor developed program that determined the stress distribution and deflection of the disk resulting from centrifugal and thermal loading (Figures 17 and 18). The advantages

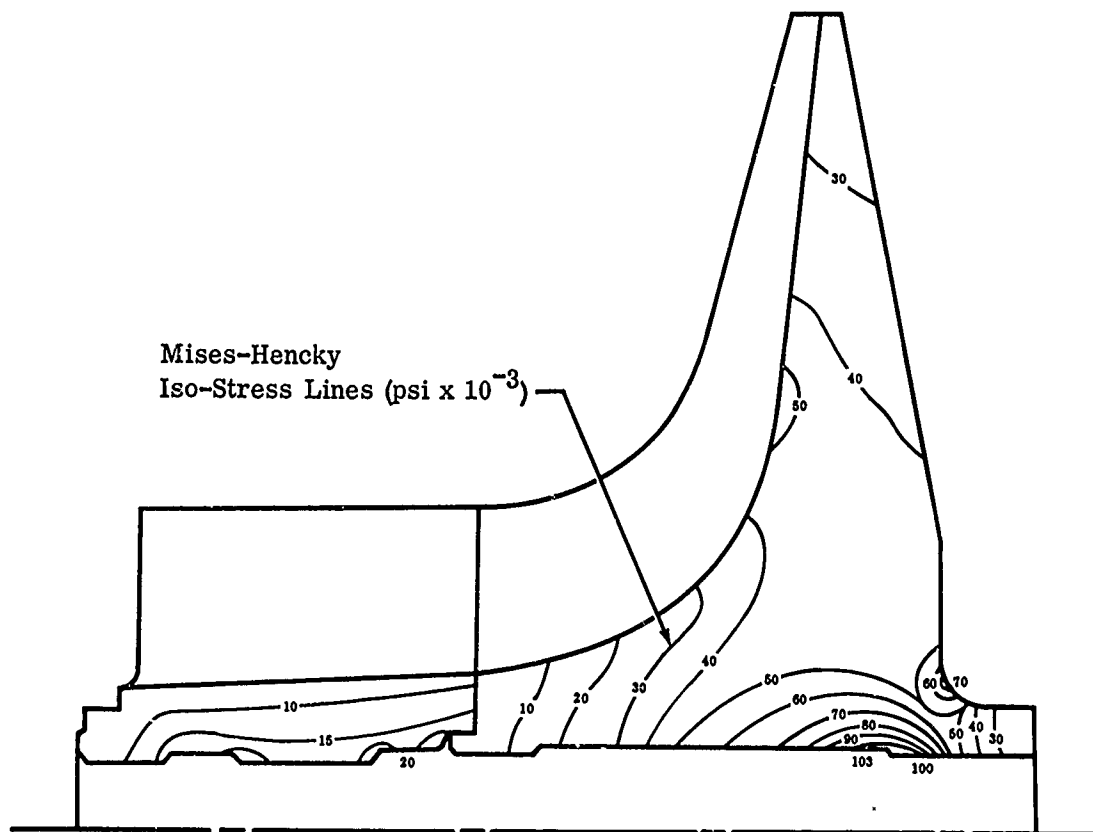
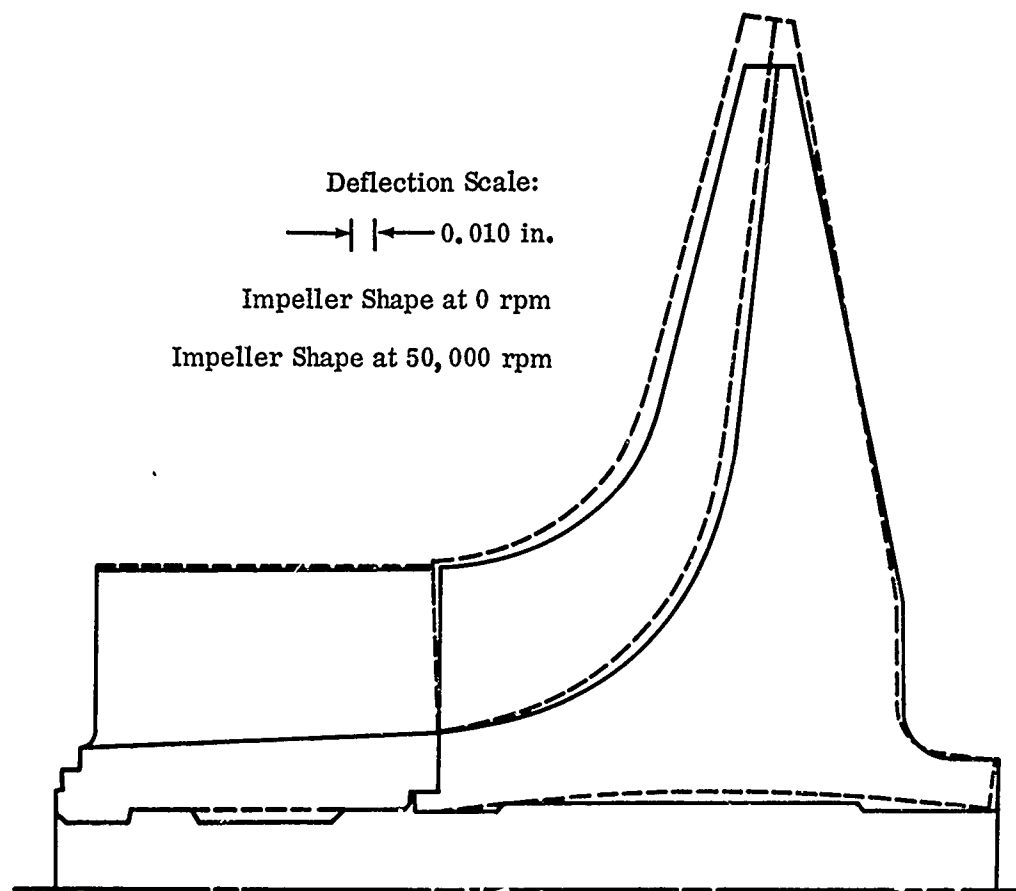


Figure 17. Predicted Impeller Disk Stress Distribution Before Proof-Spin.

CONFIDENTIAL



a. Impeller Deflection



b. Bore Deflection

Figure 18. Predicted Impeller Deflection Before Proof-Spin.

CONFIDENTIAL

CONFIDENTIAL

over previous methods, which determined average tangential stress, were that the hub extension lengths and impeller growth could be more accurately defined. Further, local high-stress areas were determined, as shown in Figure 17. A new definition of disk safety factors was required for this method because actual point-values of stress were used, rather than an average stress value. However, residual compressive stresses introduced during the proof spin of the impeller redistributed and lowered the stresses from the calculated values. Therefore, the disk safety factor, when calculated using the previous method presented in Section 2.4 of Reference 1, was found to be 1.75, well above the 1.25 required minimum. The blade-root safety factor was 1.21, slightly below the 1.25 recommended minimum, but was considered adequate for experimental test hardware. All safety factors were based on 0.2-percent minimum yield.

The complete stress analysis and results, including blade-root stress distribution and blade-vibration-frequency spectrum, are presented in Appendix I.

2.4.2 Test Section

In addition to the impeller, the test section consisted of the inlet, impeller shroud, diffuser, and collector (Figure 19). Primary test section design considerations were to minimize mechanical and thermal distortions and to simplify installation of instrumentation equipment for quicker changes during testing.

Component Design

The front cover plate, which formed the impeller shroud and front diffuser wall, was made up of 2 parts — an aluminum liner and a mild steel frontplate with 10 stiffening webs. The backplate was also mild steel (with 10 webs), and formed the rear diffuser wall and the structural base for the test section by attaching to the rotor housing. A minimum diffuser-wall thickness of 0.35 inch was specified for the frontplate and backplate to accommodate the instrumentation required for testing. An aluminum inlet was attached to the front cover with the inner-hub fairing supported by three airfoil-shaped struts (Figure 20). The collector used on the diffuser rig described in Reference 1 was used with this design (see Section 3.0).

Aluminum was used where the temperature would not exceed 450°F to facilitate fabrication and reduce weight. In addition, the aluminum liner provided an abradable surface in the inducer area to permit close clearances without risking blade damage. Mild steel was selected for the frontplate and backplate because it offered the best balance of thermal characteristics, machineability, and availability. The maximum compressive load due to thermal expansion between the liner and frontplate was calculated to be 700 psi, far below the allowable 25,500 psi for aluminum. Appendix II contains the test section design analysis.

CONFIDENTIAL

CONFIDENTIAL

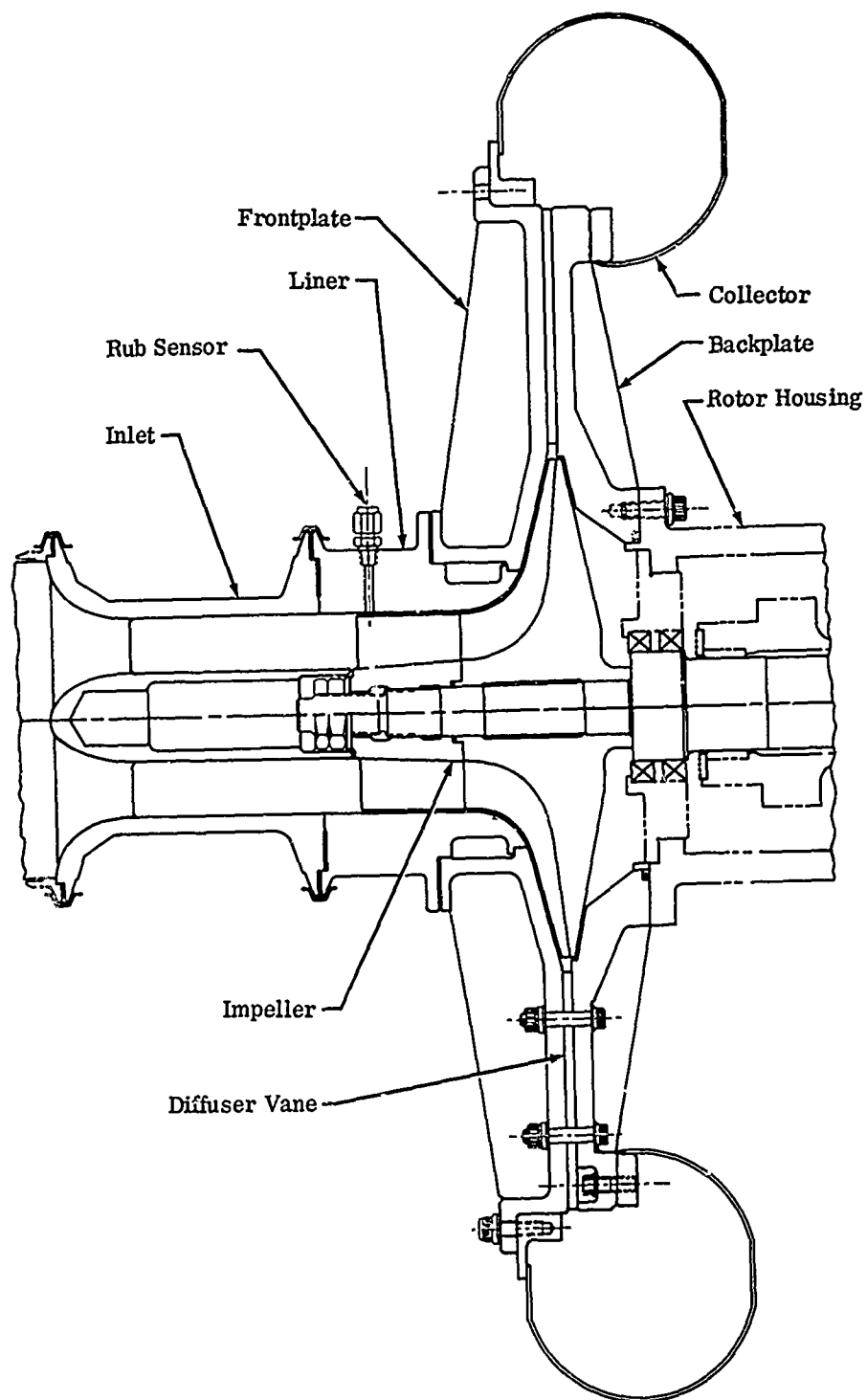


Figure 19. Section View of Test Section.

CONFIDENTIAL

CONFIDENTIAL

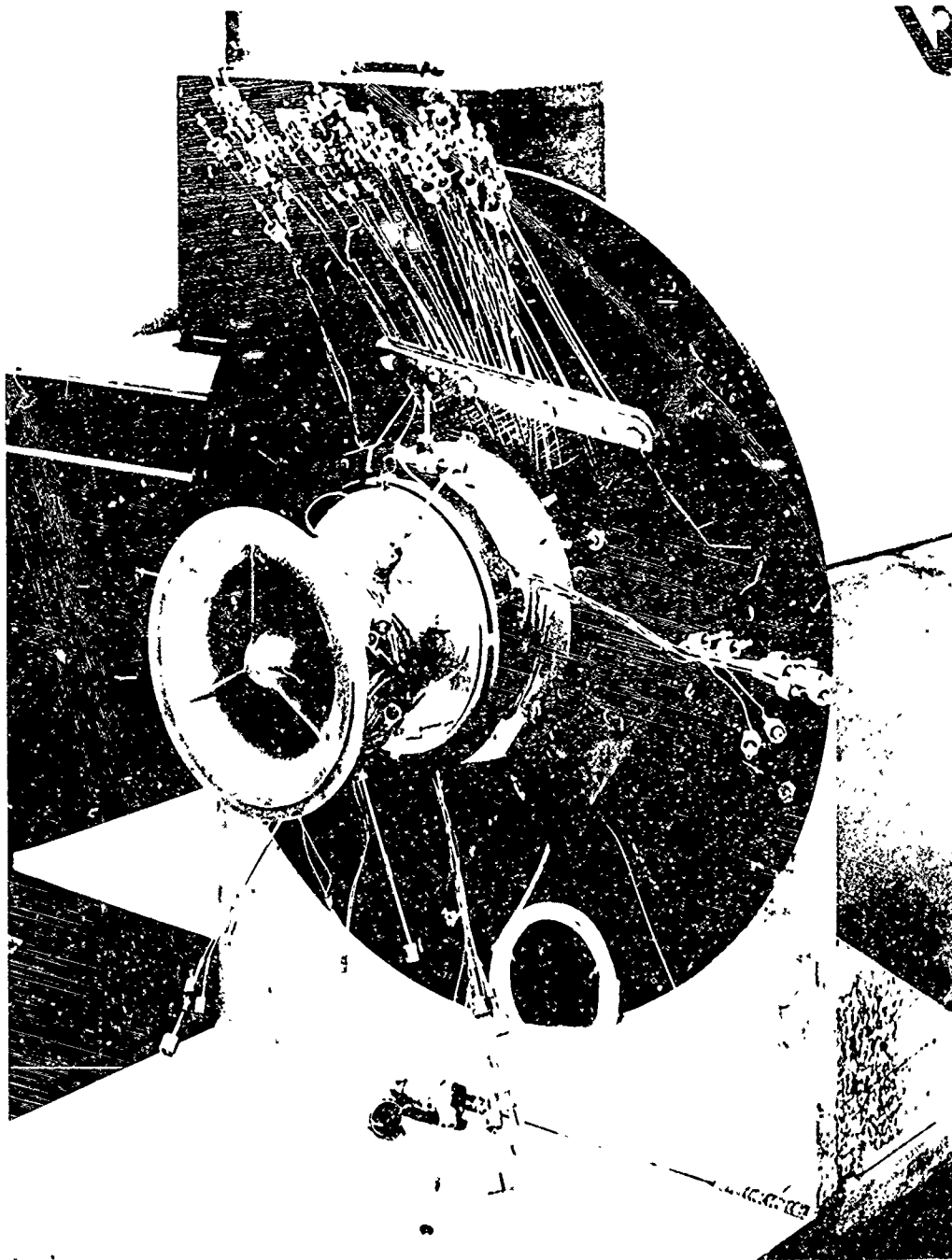


Figure 20. Front Cover and Inlet.

CONFIDENTIAL

Diffuser vane-island design was similar to that of Reference 1, except there were no provisions for changing the diameter-ratio or throat-area settings. As in the previous tests, the vanes were located on the backplate with 2 pins and were clamped between the diffuser walls; however, because vane position would not be changed between tests, additional bolts could be located on this rig (Figure 21) to provide maximum restraint against thermal distortion of components, maintaining a tight seal between the vane sides and diffuser walls and permitting the 0.015-inch impeller-shroud goal to be met. Selection of 10 vanes for the diffuser was based on the Campbell diagram (Figure 22), which shows that impeller-blade natural-frequency excitations (circled points) would be at 60,000 rpm and below 40,000 rpm; 8 or 12 vanes would produce excitations just below or at the design speed.

The impeller-shroud clearance goal of 0.015 inch was planned using an eddy-current probe that continuously displayed the actual clearance within 10 percent. Details of this probe are discussed in Appendix VII of Reference 1.

Provisions for schlieren windows in the frontplate and backplate were considered, although they were not used. The windows were designed to be held in a separate frame by spring clips to minimize window distortion, and the frame was designed to attach to the plate with adjustable mounts, permitting alignment of the window inner surface with the diffuser wall (Figure 23). Hand working of the cutout in the plate to actual window dimensions was planned to minimize discontinuities in the diffuser wall. A metal (Inconel X) diaphragm seal was designed for installation between the plate and frame, with asbestos gasket material between the Vycor* windows and the frame.

Provisions for Instrumentation

Special installation mounts for total-temperature and total-pressure probes were designed to permit removal or replacement without disassembly of the rig. To achieve proper probe alignment, adapters were individually mated and keyed with instrumentation bosses (Figure 24), which were welded in place during the fabrication stage. In addition, blank plugs were made to replace the adapters for testing without probes. These probes and other instrumentation used are discussed in Section 4.0.

Rotor System

As previously mentioned, the new test section used the rotor system of the diffuser rig, including the same shaft, bearings, and housing, and was driven by the same turbodrives unit. No modifications were necessary to accommodate the

*Trademark, Corning Glass Works, Corning, New York.

CONFIDENTIAL

new test section, but an analysis of the rotor with the new impeller was made to predict the dynamic characteristics (Appendix II). The same computer-input data as those for the previous rotor system were used, with changes corresponding to differences between the impellers. The third critical speed was calculated to be approximately 100 rpm higher than the previous rotor and was considered an insignificant change.

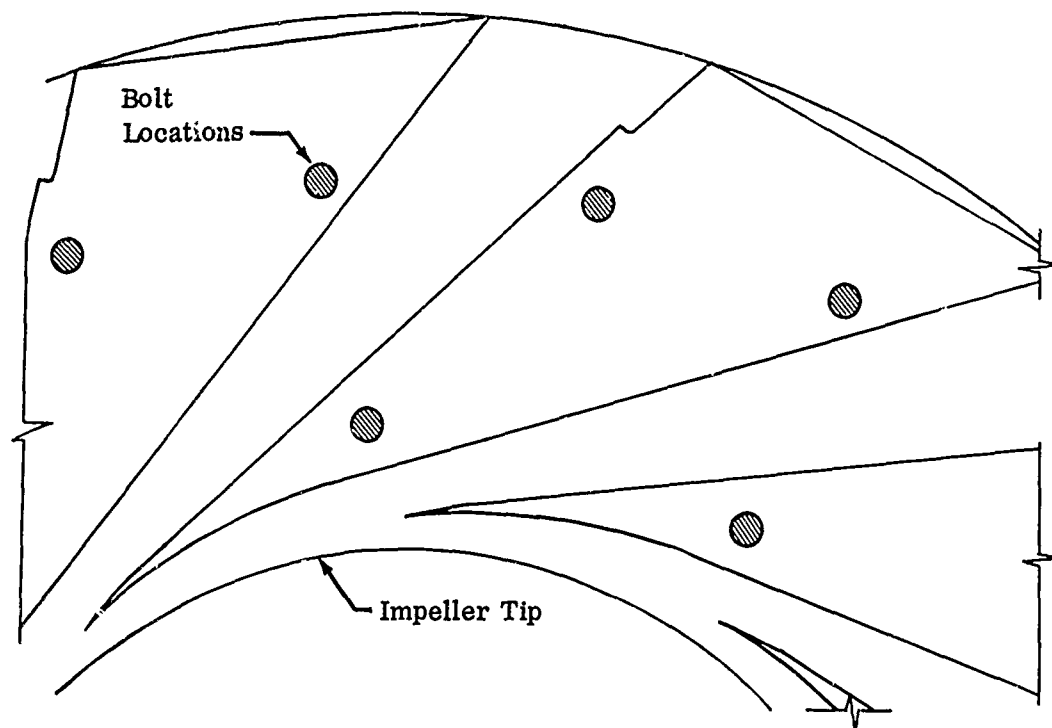


Figure 21. Test-Section Bolt Pattern.

CONFIDENTIAL

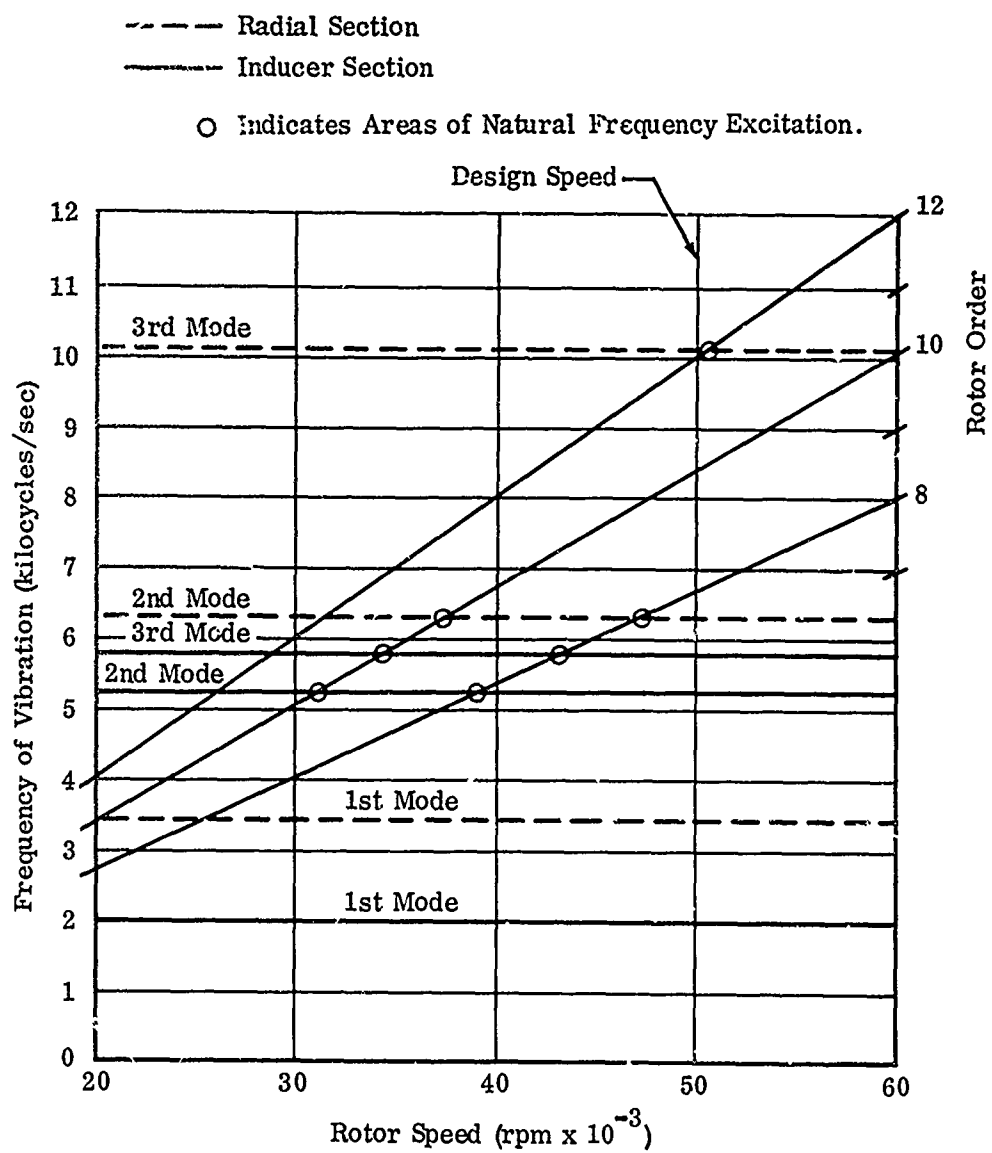


Figure 22. Campbell Diagram Used for Diffuser Selection.

CONFIDENTIAL

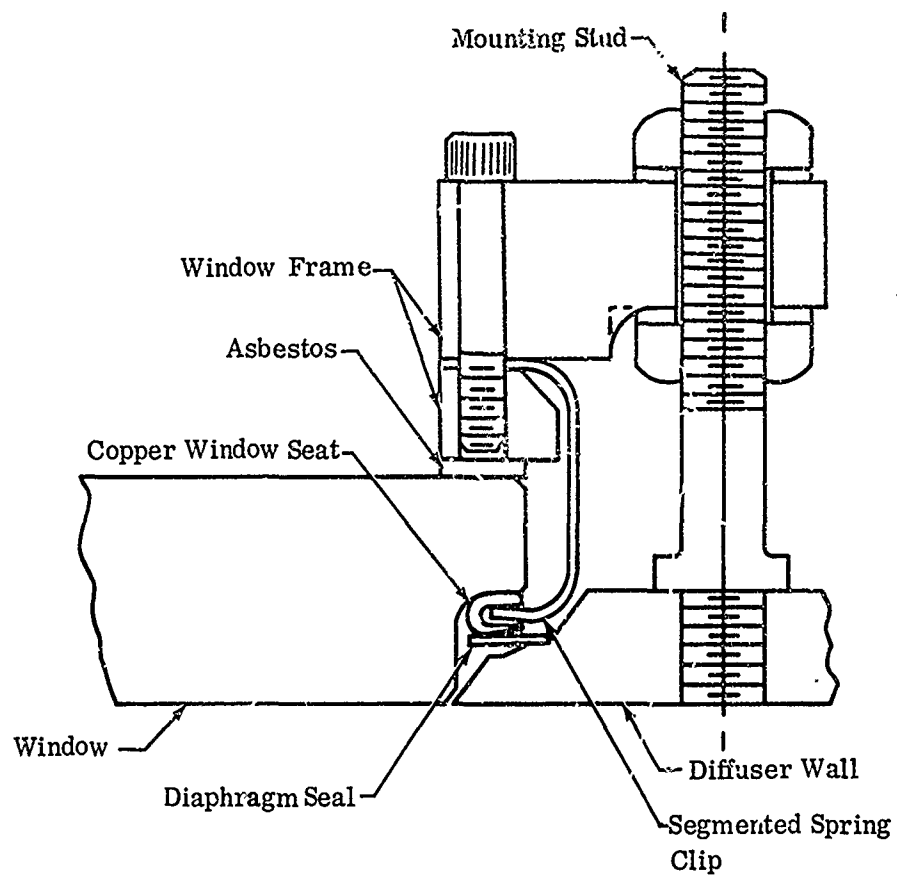


Figure 23. Schlieren Window Installation.

CONFIDENTIAL

CONFIDENTIAL

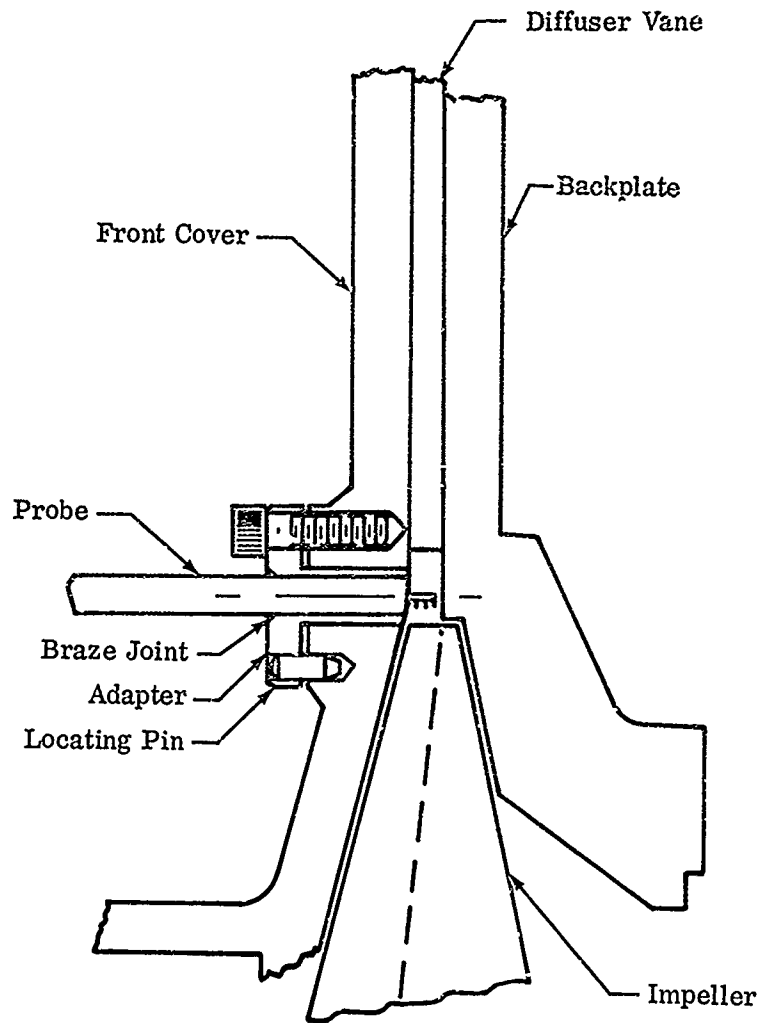


Figure 24. Typical Probe Installation.

CONFIDENTIAL

3.0 (U) FABRICATION OF RESEARCH COMPONENTS

Fabrication of the components necessary for conducting compressor tests included the machining, inspection, and assembly operations. Because the impeller fabrication process was independent of the other test section components, it is discussed separately and includes the proof-spin and balancing procedures. In addition to the initial fabrication efforts, component modifications made during the test program are discussed.

3.1 IMPELLER

Components for 2 impeller assemblies, each consisting of an inducer section and a radial section, were fabricated from 6 Al-4V titanium forgings by an outside vendor; on-site inspection was made by the contractor's quality control personnel.

Additional work required to complete the impeller — including proof-spin, mating (component fitting and blade surface blending), finish boring, splining, and balancing — was performed at the contractor's facilities. One impeller was completed, and a second set of components was retained as a spare.

3.1.1 Impeller-Component Fabrication

The impeller components were fabricated in the same manner as reported in Section 3.0 of Reference 1, except that previous impellers were machined in one piece. Figure 25 shows the parts during the cavity-milling step, and Figure 26 shows the hand-working of the inducer leading edge. The completed inducer and radial sections are shown in Figures 27 and 28 respectively. Machining tolerances were as specified in Reference 1.

Blending of the blades between the 2 components after assembly was planned to ensure proper alignment and surface continuity, as described in Section 3.1.4. For this reason, excess blade thickness for later hand-working was provided at the entrance to the radial section, where the transition between the radial-driving face blades and the symmetrical blades was made.

3.1.2 Inspection

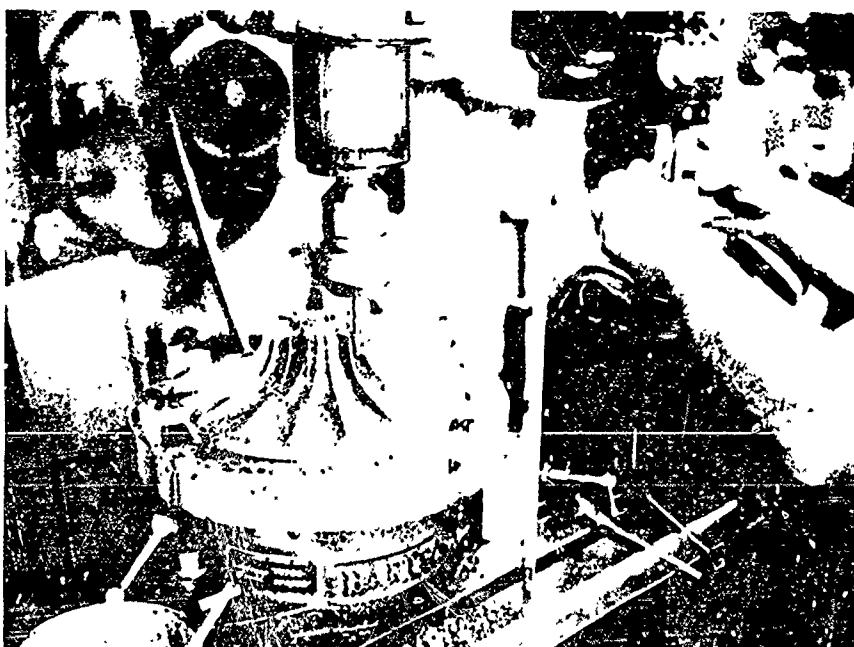
The inspection procedure for this impeller was the same as that described in Reference 1. Figure 29 shows the radial section mounted on the optical comparator, ready for inspection.

3.1.3 Proof-Spinning

The radial section was proof spun to 66,000 rpm in the same manner as the impellers of Reference 1; however, proof-spinning of the inducer section was



a. Inducer Section



b. Radial Section

Figure 25. Impeller Component Machining.

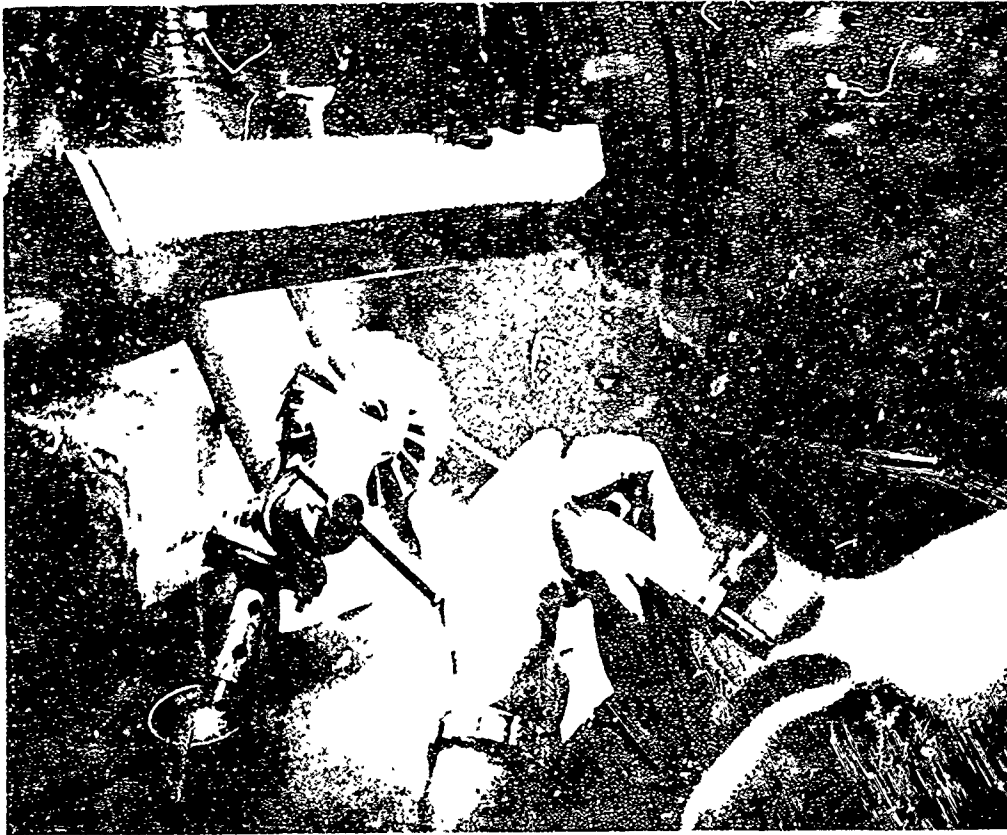


Figure 26. Hand-Working of Inducer Leading Edge.

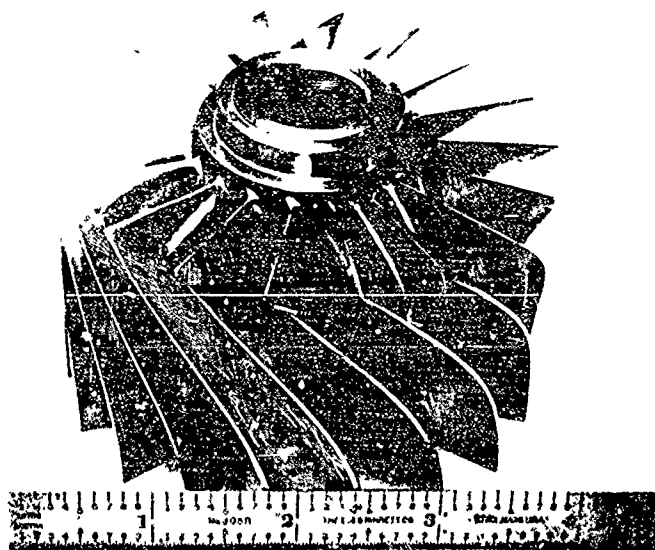


Figure 27. Completed Inducer Section.

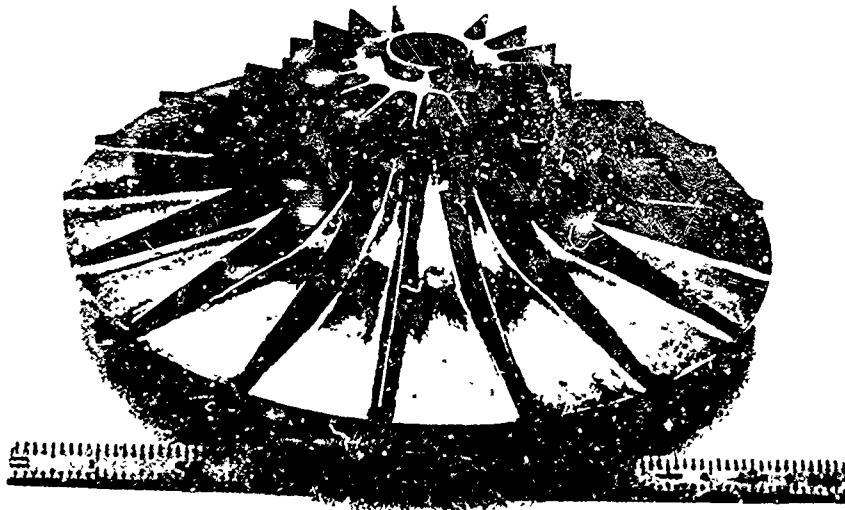


Figure 28. Completed Radial Section.

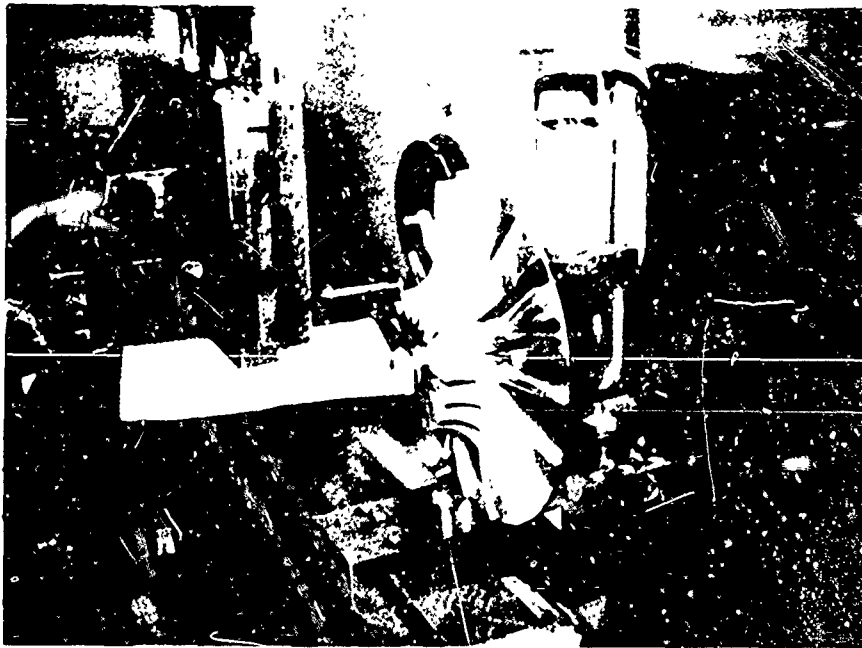


Figure 29. Radial Section on Optical Comparator for Inspection.

not necessary because of the known low stress level that would be encountered during operation.

3.1.4 Assembly and Blade-Blending

Figure 30 shows the method of impeller assembly. The alignment shoulder on the radial section and the mating counterbore in the inducer section were machined for a light interference fit, with concentricities held within 0.0005 inch. The two 3/16-inch-diameter pins, which fixed the blade alignment and transmitted torque between the 2 sections, were medium force-fitted into the inducer section and light press-fitted into the radial section. Holes for the pins were machined on a precision jig-bore machine, and were closely coordinated to provide the alignment necessary for proper assembly. Disassembly required a special tool designed to force the components apart. Figure 31 shows the impeller being assembled.

Figure 32 shows the area in which the blade-bending was accomplished and the excess material on the radial-section blade. The maximum blade mismatch allowed on the finished part was 0.001 inch; work was performed with a small high-speed grinder, similar to the one shown in Figure 26. The finished joint is shown in Figure 33.

3.1.5 Boring, Splining, and Balancing

These operations were performed to the same specifications as those described in Reference 1. The final bores were precision ground in 1 operation with the impeller assembled to ensure concentricity between the adjacent bores in the 2 components. However, the spline was shaped in the inducer with the parts disassembled.

Dynamic balancing was done in 4 steps: (1) the inducer section alone, (2) the radial section alone, (3) with the 2 components assembled on a precision arbor (as a reference check), and (4) with the components assembled and installed on the shaft. These steps were taken to eliminate possible opposing imbalances between the components, which could produce undesirable rotor dynamics. The maximum allowable imbalance was 0.005 ounce-inch.

3.1.6 Test Modifications

The impeller was modified in 2 steps: first, the inducer tip was cut back; then the radial-section blade width was reduced by 0.045 inch. Figure 34 shows the reworked inducer. Hand-working of the inducer leading edges was required to restore the proper blade shape. In both cases the spaces between the blades were filled with a low-temperature melting-point material to prevent possible vibration damage to the blades during machining.

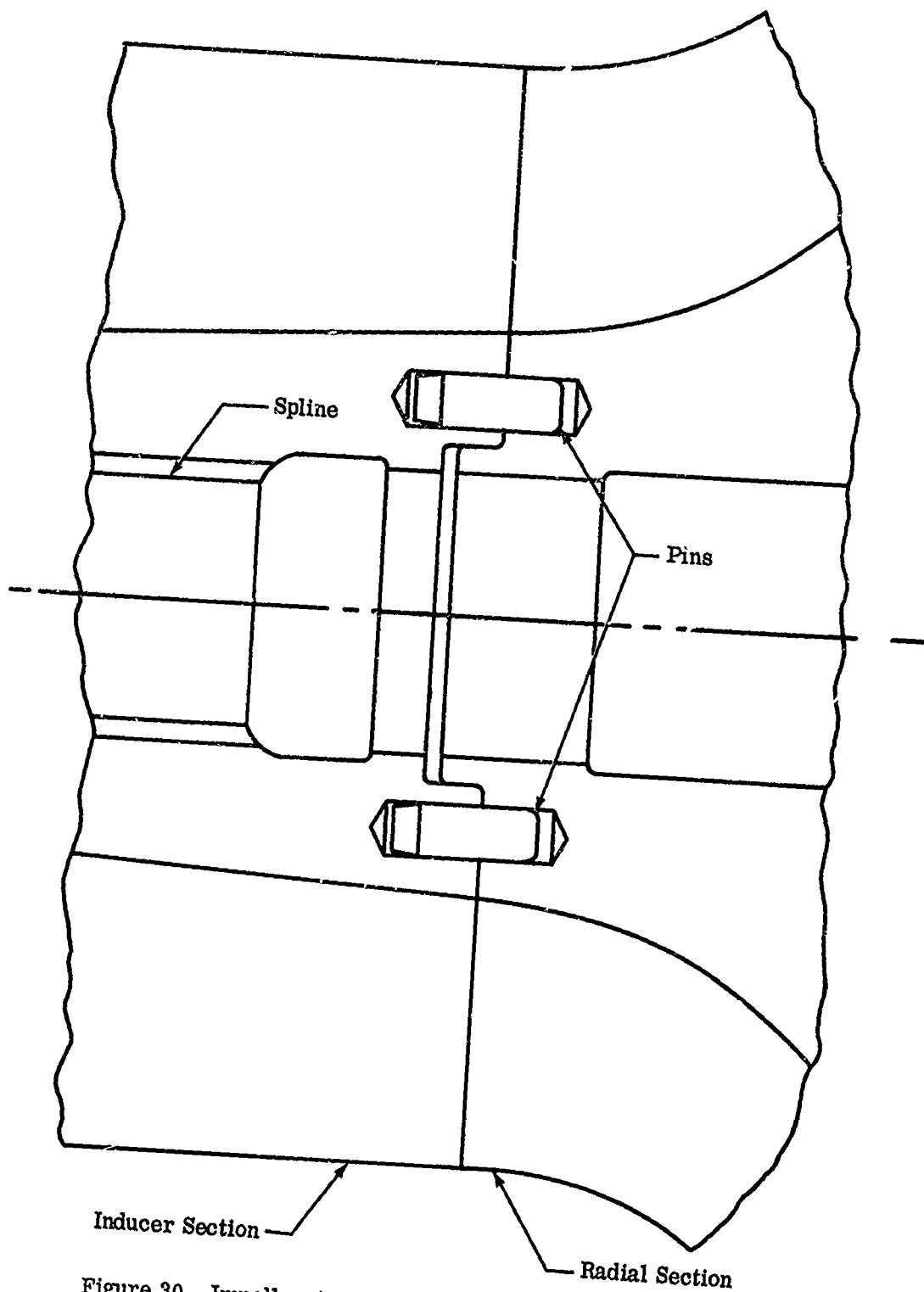


Figure 30. Impeller Assembly Method (Shown Twice Actual Size).

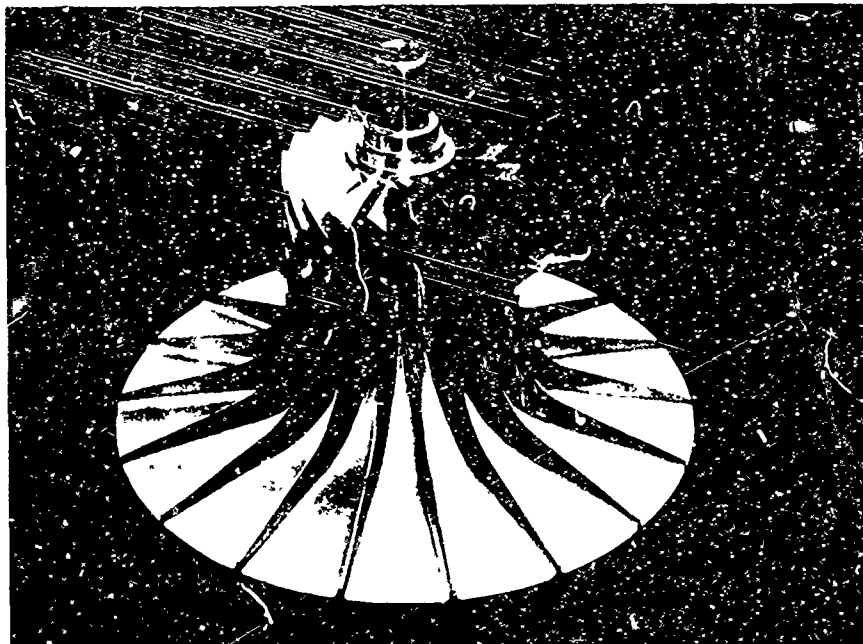


Figure 31. Impeller Components During Assembly.

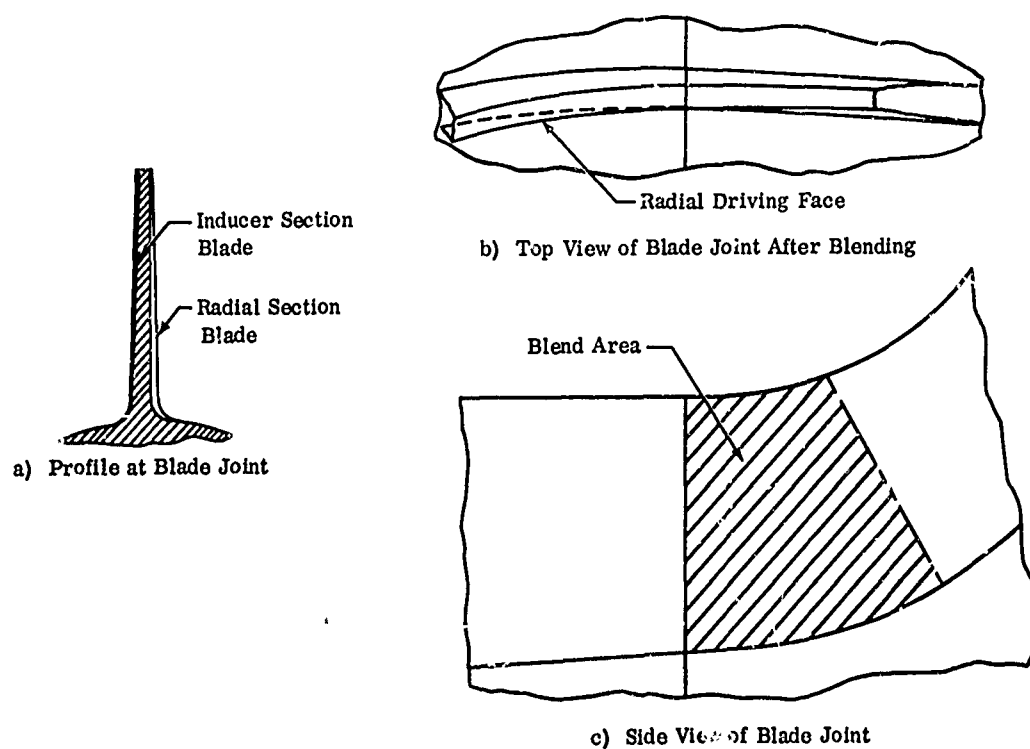


Figure 32. Impeller Blade Blending.



Figure 33. Joint Between Inducer and Radial Sections.



Figure 34. Inducer Test Modification.

3.2 TEST SECTION

Fabrication of the components described in Section 2.4.2 is discussed here, along with modifications of the front cover and diffuser vanes required for additional aerodynamic testing.

3.2.1 Front Cover

The aluminum liner and mild steel frontplate, which made up the front cover assembly (Figure 35), were machined separately with excess material left on the contoured shroud surface for machining with the 2 parts assembled. The frontplate was 1 piece, except for the ten 0.25-inch-thick webs that were welded in place on the roughed-out plate. The special instrumentation bosses were also welded in place at this time. Stress relieving before and after welding kept warpage to a minimum.

Shroud contour was held within 0.003 inch of the basic contour and was inspected on an optical comparator. Concentricity to the overall rig assembly was held within 0.0003 inch; noncritical surfaces were fabricated to a ± 0.010 -inch tolerance, but mating surfaces were held parallel and normal to the centerline within 0.001 inch; the diffuser wall was held flat within 0.001 inch. The front cover was modified during the test program by removing 0.020 inch from the diffuser-wall surface to accommodate thicker vanes while maintaining the same impeller-shroud clearance.

3.2.2 Backplate

Construction of the backplate (Figure 36) was similar to that of the frontplate, including 10 webs welded in place on the rough-machined part. Tolerances were consistent with those for the frontplate.

3.2.3 Collector

The diffuser rig collector was modified for use on this rig by changing the backplate flange, as shown in Figure 37.

3.2.4 Inlet

Fabrication of this inlet (Figure 38) was the same as that described in Section 3.2.4 of Reference 1.

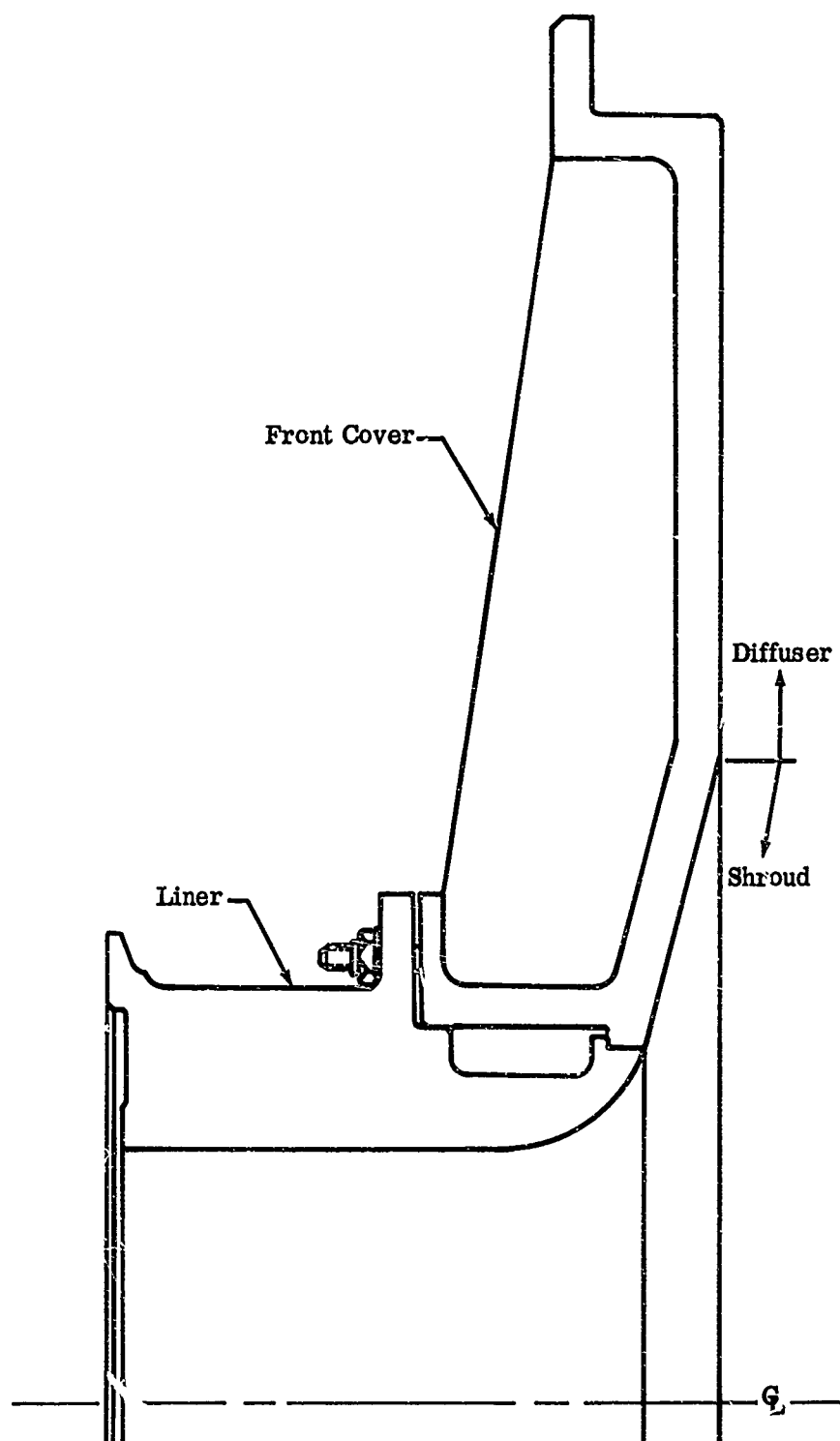


Figure 35. Front Cover Assembly.

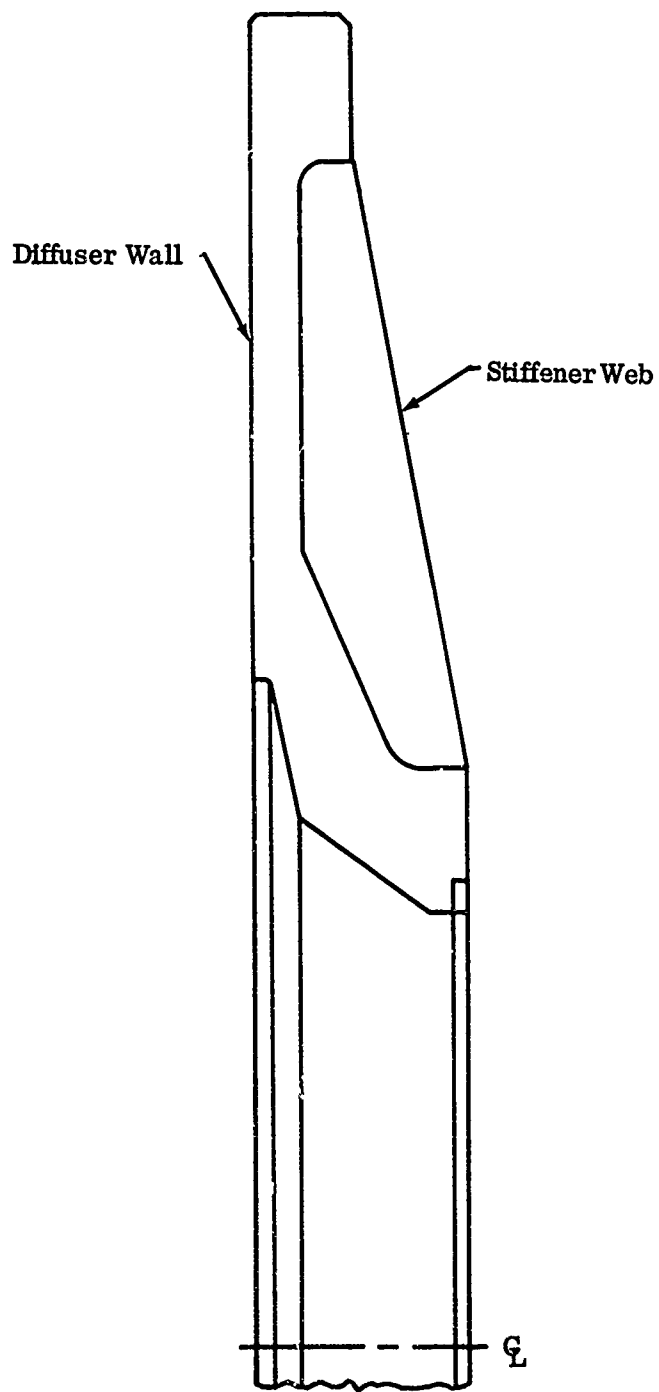


Figure 36. Backplate.

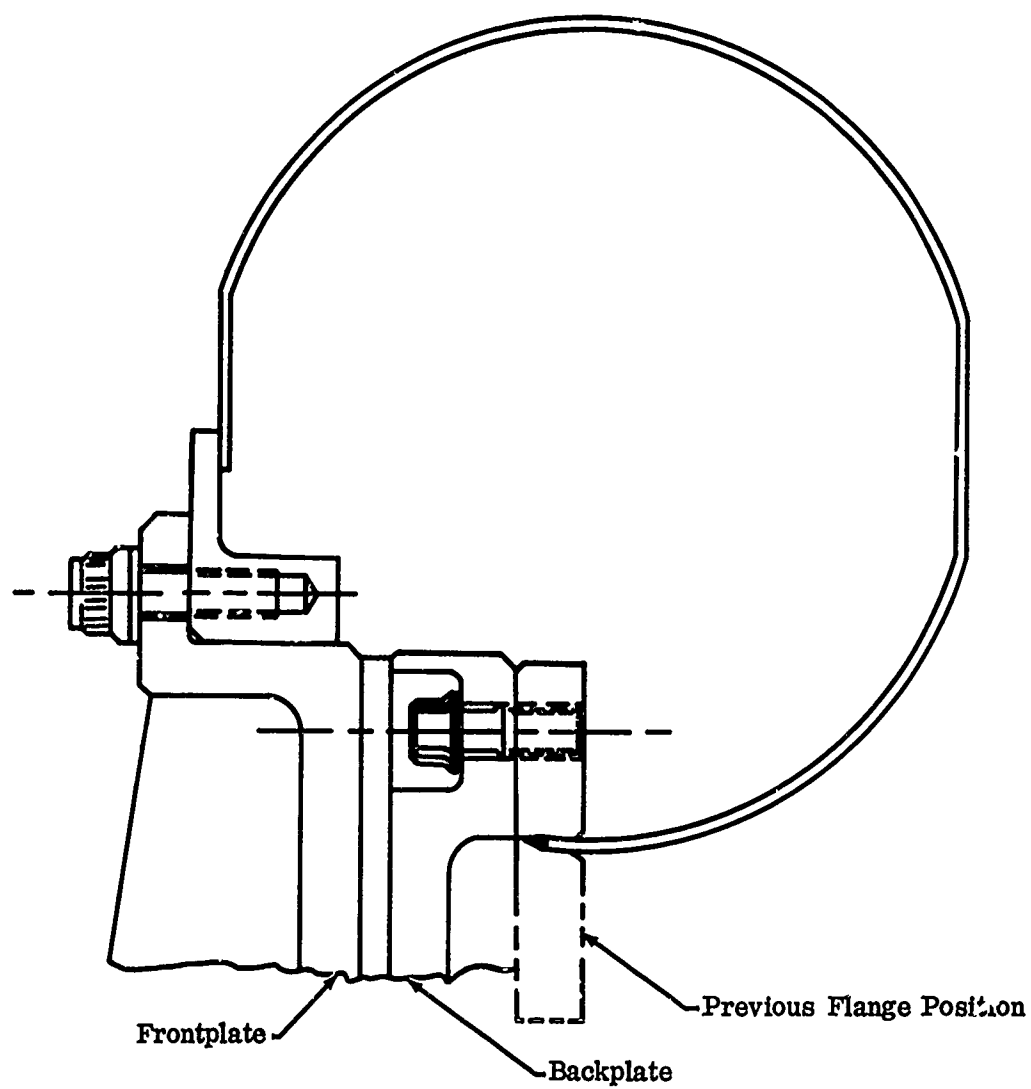


Figure 37. Collector.

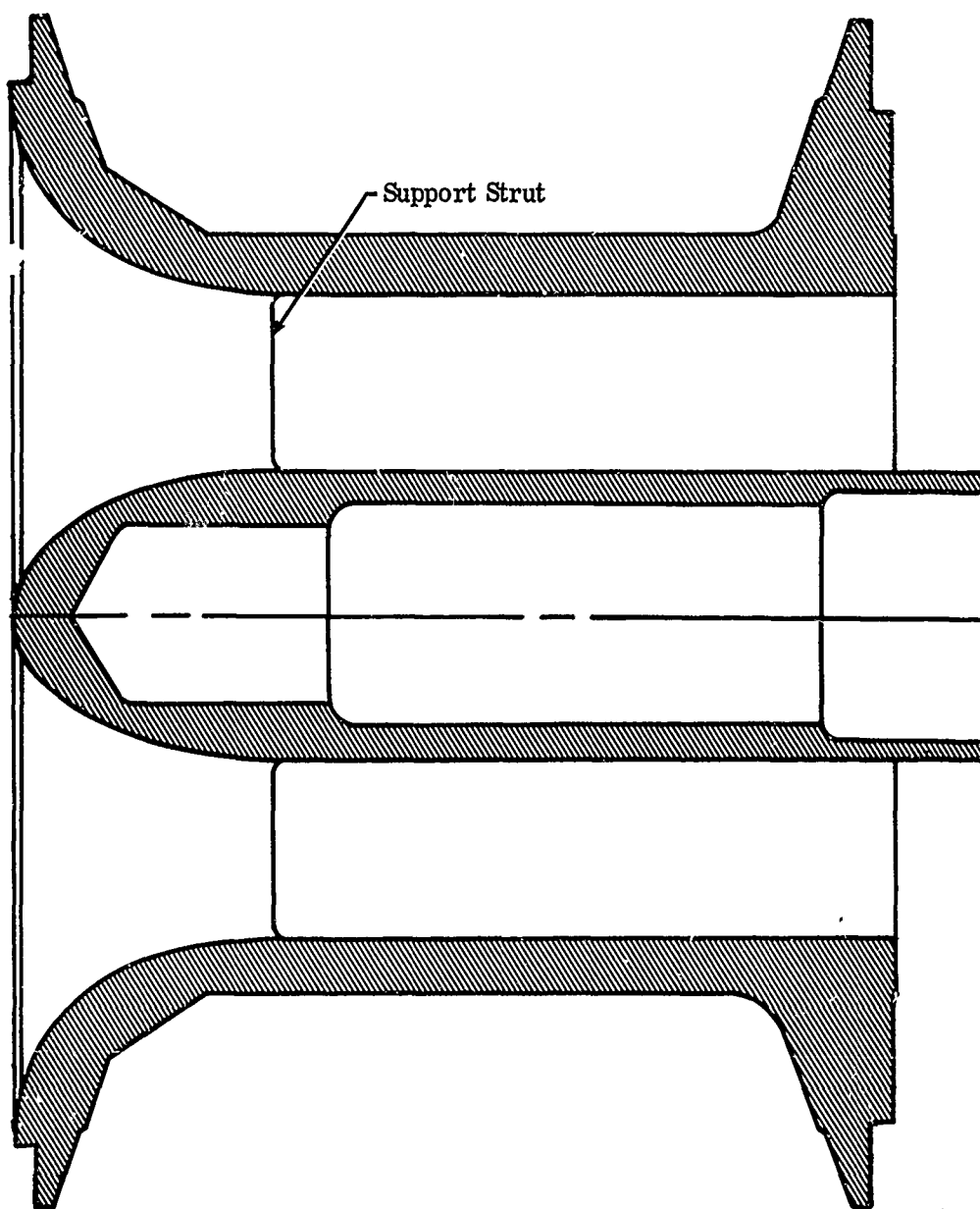


Figure 38. Inlet.

3.2.5 Vane-Islands

One set of 10 vanes was fabricated and installed on the backplate (shown in Figure 39). Precision tooling holes were drilled in vane blanks that were rough-cut from flat-ground low-carbon steel, after which the vanes were ground to the finish dimensions in tooling fixtures. One fixture was used to machine the large radius on the suction surface, and another was used to machine the straight surfaces by locating the surface to be ground parallel to the cutting plane. All vanes were held together in the fixtures to provide maximum uniformity. The machining tolerance was ± 0.001 inch.

Several modifications were made to the vanes during the test program; either a regrind of certain surfaces was required, wedges were added to the pressure surface downstream of the throat to change the divergence angle, or both. The regrinds were accomplished by changing the tooling fixtures; the wedges, machined from the same material, were either pinned in place (the smaller wedges) or electron-beam welded. Electron-beam welding was used because it provided a positive means of attachment with the least risk of vane warpage.

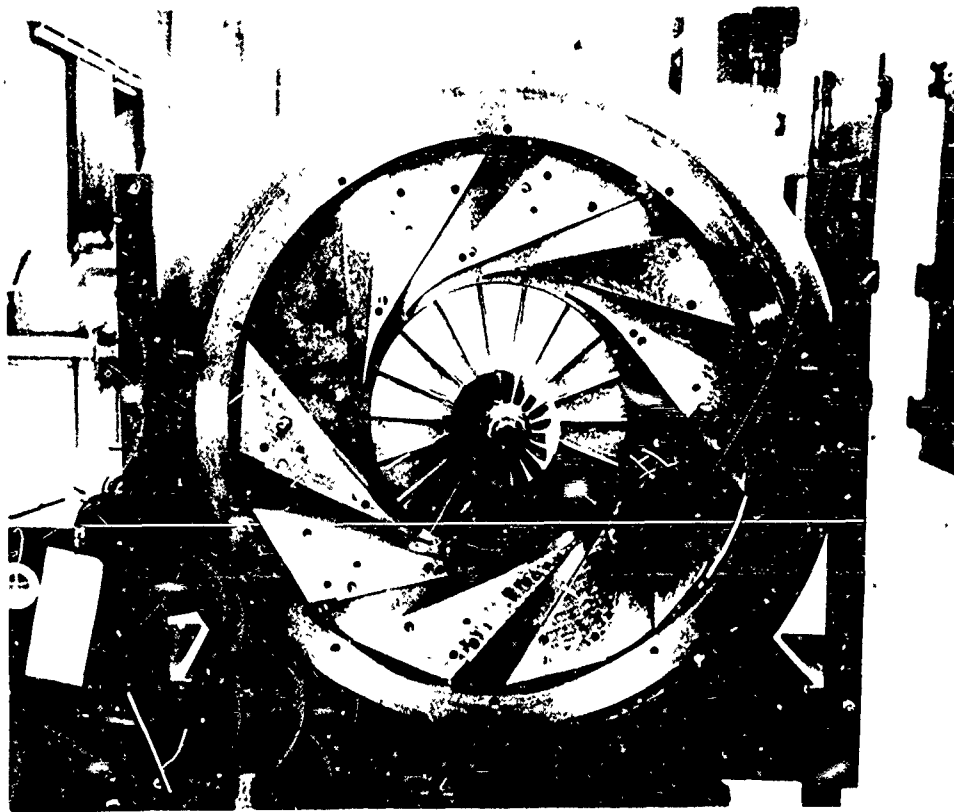


Figure 39. Vane-Islands Installed on Backplate.

4.0 (U) INSTRUMENTATION

Items of instrumentation used in measuring the various impeller-shroud pressures, diffuser pressures, and impeller-discharge temperature are described in the following sections. The basic probes are discussed in Section 4.0 of Reference 1. Applicable modifications are discussed in this section.

4.1 PRESSURE-MEASUREMENT INSTRUMENTATION

As in the earlier portion of the program, total-pressure rakes (3 probes each) were designed to measure discharge profiles across the impeller tip (Figure 40). A yaw-pressure probe was also installed at the impeller tip to measure flow angle and total pressure.

As in previous test configurations, static-pressure taps had 0.018-inch-diameter holes with sharp corners. Figure 41 shows the static-pressure taps in a back-plate of the diffuser rig with a 10-vane-island diffuser.

The digital-data-acquisition system was modified to measure and record temperature as well as pressure data. The system had the capability of handling up to 184 pressure inputs and 50 temperature inputs. The system (Figure 42) consisted of eight 24-channel cutoff valves; a storage volume for each pressure; four 48-channel scanner valves which were used to port the stored pressure to 4 pressure transducers; a thermocouple reference oven; and a digital-data system. Included in the digital-data system were an integrating digital voltmeter, a magnetic recorder, and a paper-tape printer.

When each data point was recorded, the pressures were trapped in the storage volumes by the cutoff valves. The system then immediately scanned the temperatures and digitized and recorded the information on the magnetic tape and the printed paper tape. The trapped pressures were then sequentially ported by the scanner valves to the 4 pressure transducers. The signals from the pressure transducers were digitized by the digital voltmeter and recorded on both the magnetic and printed paper tapes. Temperatures were scanned at a rate of 10 per second and pressures were scanned at a rate of 7 per second. After all pressures and temperatures were recorded, the cutoff valves were opened and the system was ready for the next data point.

The data recorded by the system on computer-compatible magnetic tape were converted to engineering units by a digital computer.

4.2 TEMPERATURE-MEASUREMENT PROBES

Probes to measure air temperature just outside of the impeller tip were selected for minimum size and high accuracy. Each was made as small as possible to

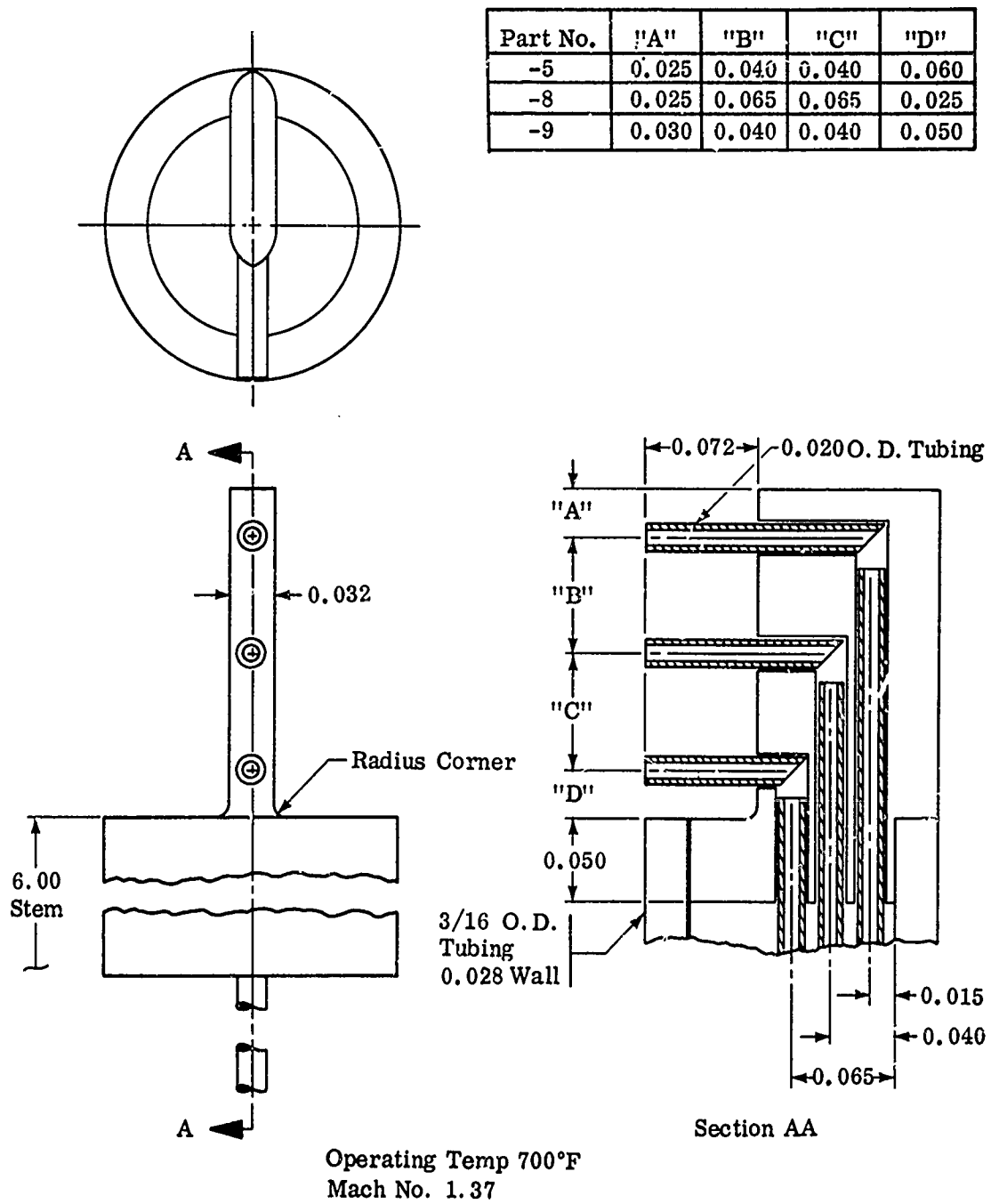


Figure 40. Total-Pressure Rake.

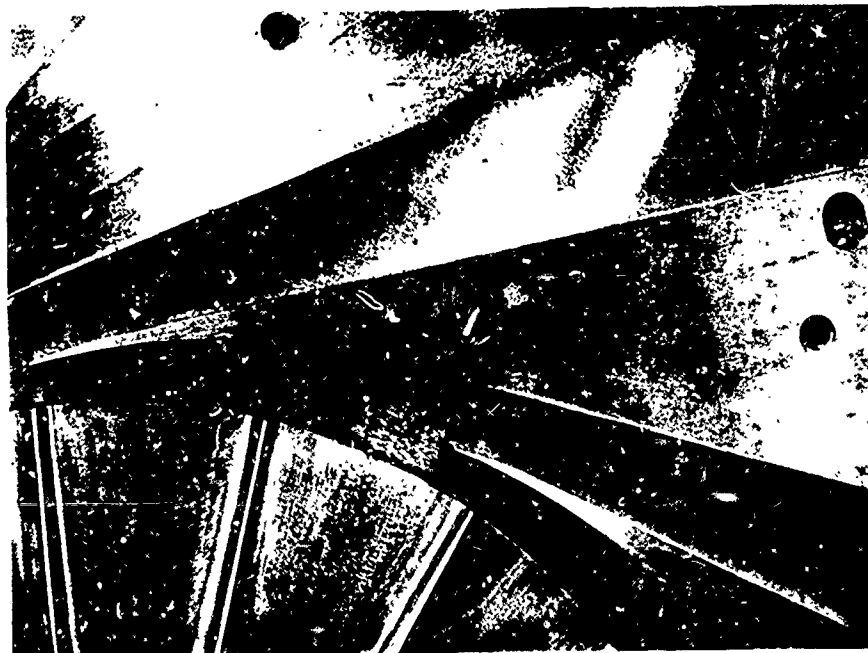


Figure 41. Static-Pressure Taps in Diffuser Backplate.

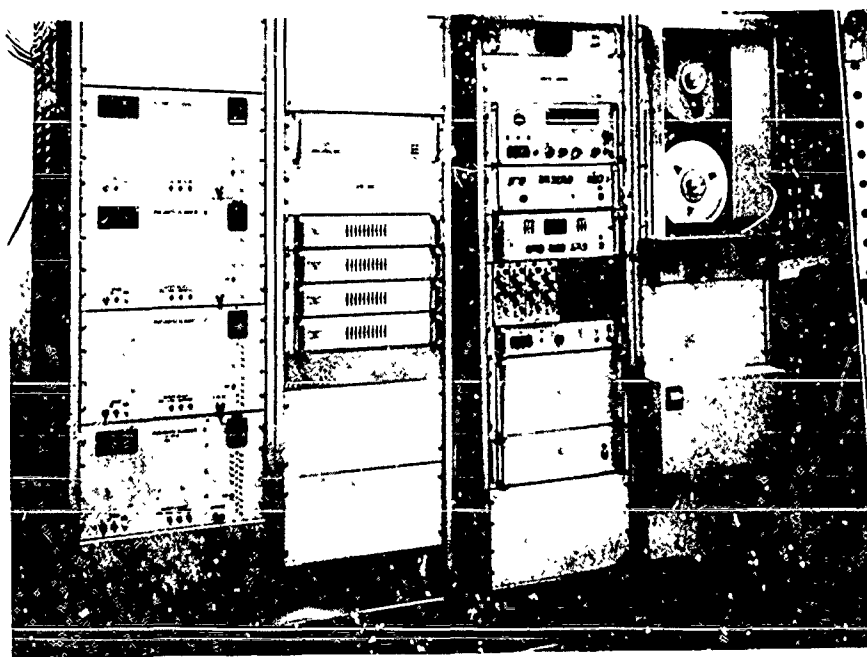


Figure 42. Digital-Data System.

minimize airflow disturbance, as a result of earlier studies presented in Section 4.0 and Appendix VII of Reference 1.

4.3 TIP-CLEARANCE MEASUREMENT

Impeller blade tip-to-shroud running clearance was measured with an eddy-current clearance detection system. An evaluation and a detailed description of this system are presented in Appendix VIII of Reference 1.

An initial calibration was performed on a layout drilling machine in a manner similar to that described previously. A point was checked during rig operation utilizing a fixed rub sensor set at 0.030-inch clearance.

5.0 (U) TEST EQUIPMENT AND PROCEDURES

Test equipment and procedures used for the compressor investigations were similar to those described in Section 5.0 of Reference 1. Performance tests were conducted at the same test site and with the same bearing-rotor system and turbodriven unit as those used for the earlier diffuser tests. Variations in procedures previously reported are discussed in the following text.

5.1 COMPRESSOR TEST RIG

The compressor test rig installation in the test cell is shown in Figures 43 and 44. Figure 43 is an overall view of the compressor and turbodriven unit, and Figure 44 shows a front view of the compressor. Static-pressure taps and impeller-clearance-detector probes were installed as shown.

The new compressor test section was designed to adapt to the existing diffuser test rotor system. The compressor-component assembly tested is described in Section 2.0.

One impeller was used for all compressor performance tests. A backup impeller was fabricated as a spare but was not used. The test impeller was proof spun using the equipment described in Appendix IV of Reference 1.

Two 10-channel diffuser configurations were tested, V1 and V2. Vane designs are described in Sections 2.0, 6.0, and 7.0. The test results of various impeller and diffuser-vane modifications are presented in Section 6.0. A total of 42 compressor performance tests were conducted.

Mechanical checkout of the compressor test section was accomplished as planned and without difficulty. The impeller-tip clearance probe was used to monitor and establish design-speed operating clearance. Figure 45 shows the installation of the clearance probe in the shroud near the impeller-tip radius. Also shown are the minimum clearance probes (stationary type set at 0.007-inch depth). Impeller contact with the probes at this depth did not occur during the tests.

A check of impeller running clearance, as indicated by the clearance-measuring probe, was performed by extending the minimum clearance (stationary) probe to a depth of 0.030 inch and increasing speed until contact with this probe was made. The clearance-measuring probe and the stationary probe indicated the same clearance at 46,000 rpm during a checkout test, and the reliability of the measuring system was confirmed. Figure 46 is a typical impeller-tip-to-shroud clearance plot obtained during tests. The decrease in tip clearance with an increase in speed was primarily attributed to a small deflection of the impeller under the influence of centrifugal load. Thermal distortion of the shroud was considered to be insignificant.

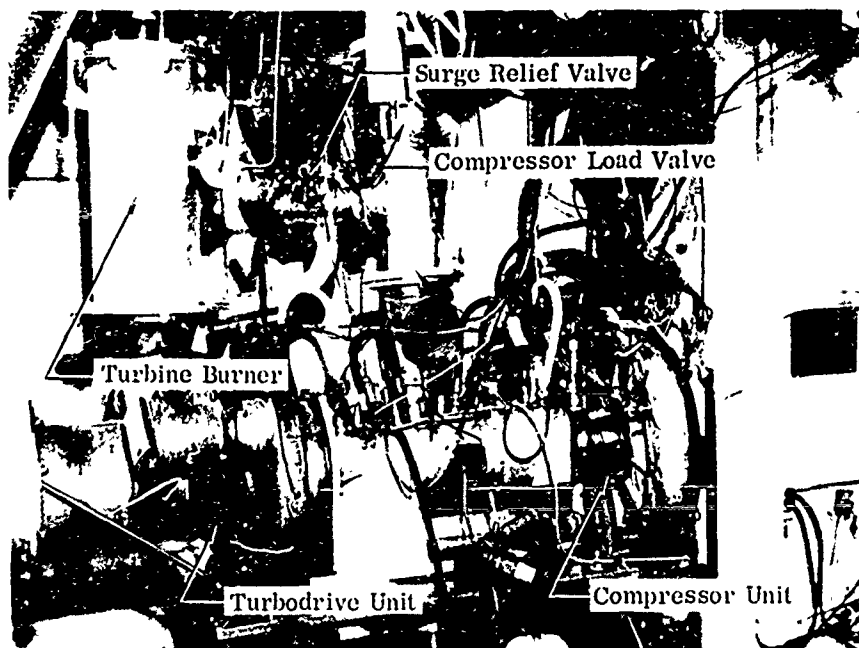


Figure 43. Compressor Test Rig Cell Installation.

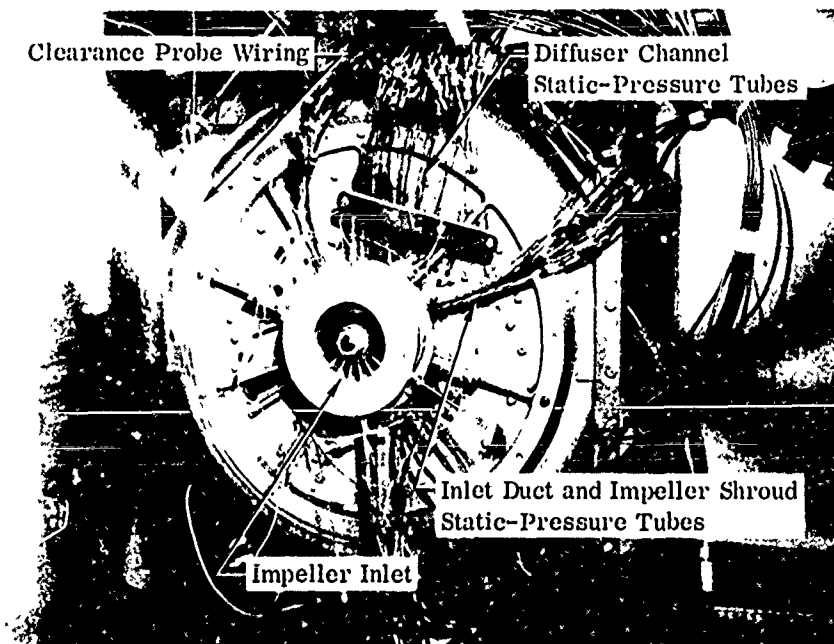


Figure 44. Front View of Compressor Installation.

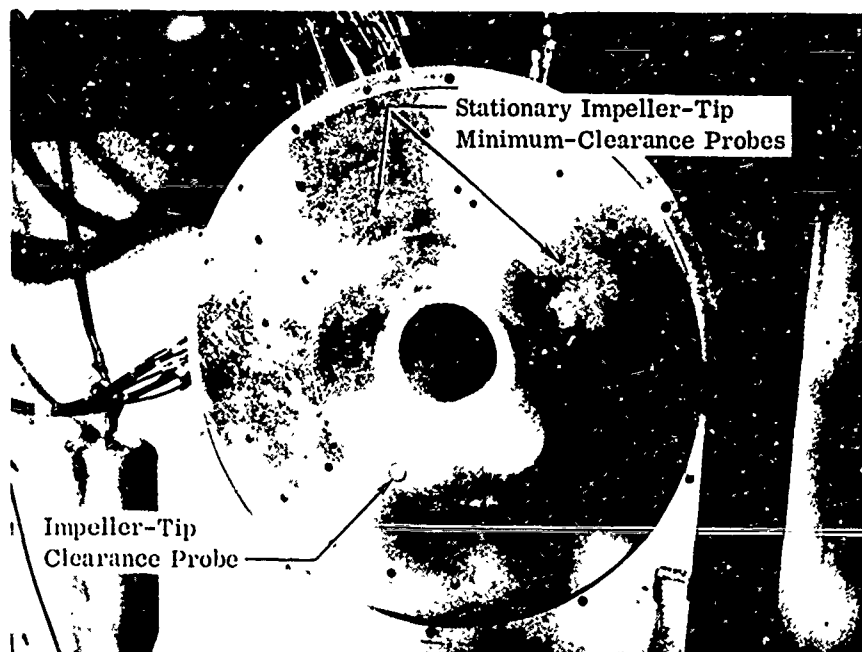


Figure 45. Impeller-Tip Clearance Probes Installed in Front Cover.

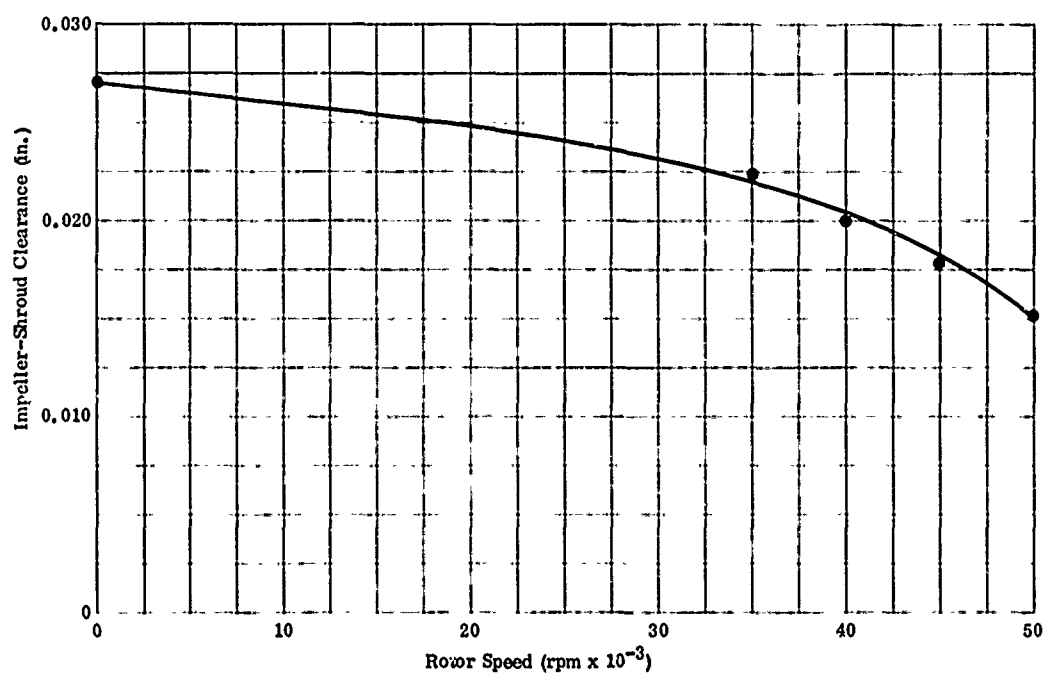


Figure 46. Impeller-Tip-to-Shroud Clearance Versus Rotor Speed.

Compressor vibration-acceleration was scanned in the range of 200 to 20,000 cycles per second at speeds of 20,000 through 50,000 rpm in 5000-rpm increments during the initial checkout test. Peak vibration corresponding to third shaft-critical speed occurred at 45,500 rpm. Figure 47 is a plot of compressor and turbodrive housing vibration-acceleration throughout the operational speed range. Recorded vibration was within the previously established operating limits, as described in Table XIII of Reference 1.

5.2 AERODYNAMIC-PERFORMANCE INSTRUMENTATION

Instrumentation used in the compressor performance analysis included static-pressure taps in the inlet duct, shroud, diffuser-channel front and backplates, and the collector. Total-pressure probes were installed at the compressor inlet, at the impeller exit, and at three locations across the diffuser throat. Total-pressure Kiel probes, 3-probe rakes, and yaw probes as described in Section 4.0 of Reference 1 were used for these tests. Compressor-inlet and collector-air temperatures were obtained with the same type bare-wire, iron-constantan thermocouple previously used. Compressor test section instrumentation is shown in Figures 48, 49, and 50.

Static-pressure wall taps (0.030 inch diameter) were machined in the front and rear diffuser plates, impeller shroud, and inlet duct. Figure 51 shows the backplate static-pressure taps in the semivaneless space and diffuser passage. A similar set of static taps was machined in the diffuser frontplate. Installation of the static-pressure tubes in the plates was accomplished with copper swage fittings as in the previous test configuration.

Compressor-inlet total pressure was obtained with 3 Kiel probes installed at different depths in the inlet duct. Installation of an impeller-discharge 3-probe rake (P_{R1}) in the shroud is shown in Figure 52. The diffuser-throat total-pressure rake (P_{R4}) is shown in Figure 53. These 2 rakes are shown removed from the shroud in Figure 54. As shown, the probe body was brazed into a dowel-positioned adapter, which was easily and quickly installed or removed without the need for visual setting of the probe. When the rakes were not in use, the bore was plugged with a blank adapter, also shown in Figure 54. Impeller-exit flow angle, total pressure, and temperature were obtained by the same procedure and with the same type of probes as those described in Sections 4.0 and 5.0 of Reference 1. The miniature-type total-temperature probe was used for these tests.

Compressor airflow was measured with a Boeing-built 5.46-inch diameter A.S.M.E. flow nozzle. The flow nozzle inlet configuration, plenum chamber and method of measurement were identical to those reported previously.

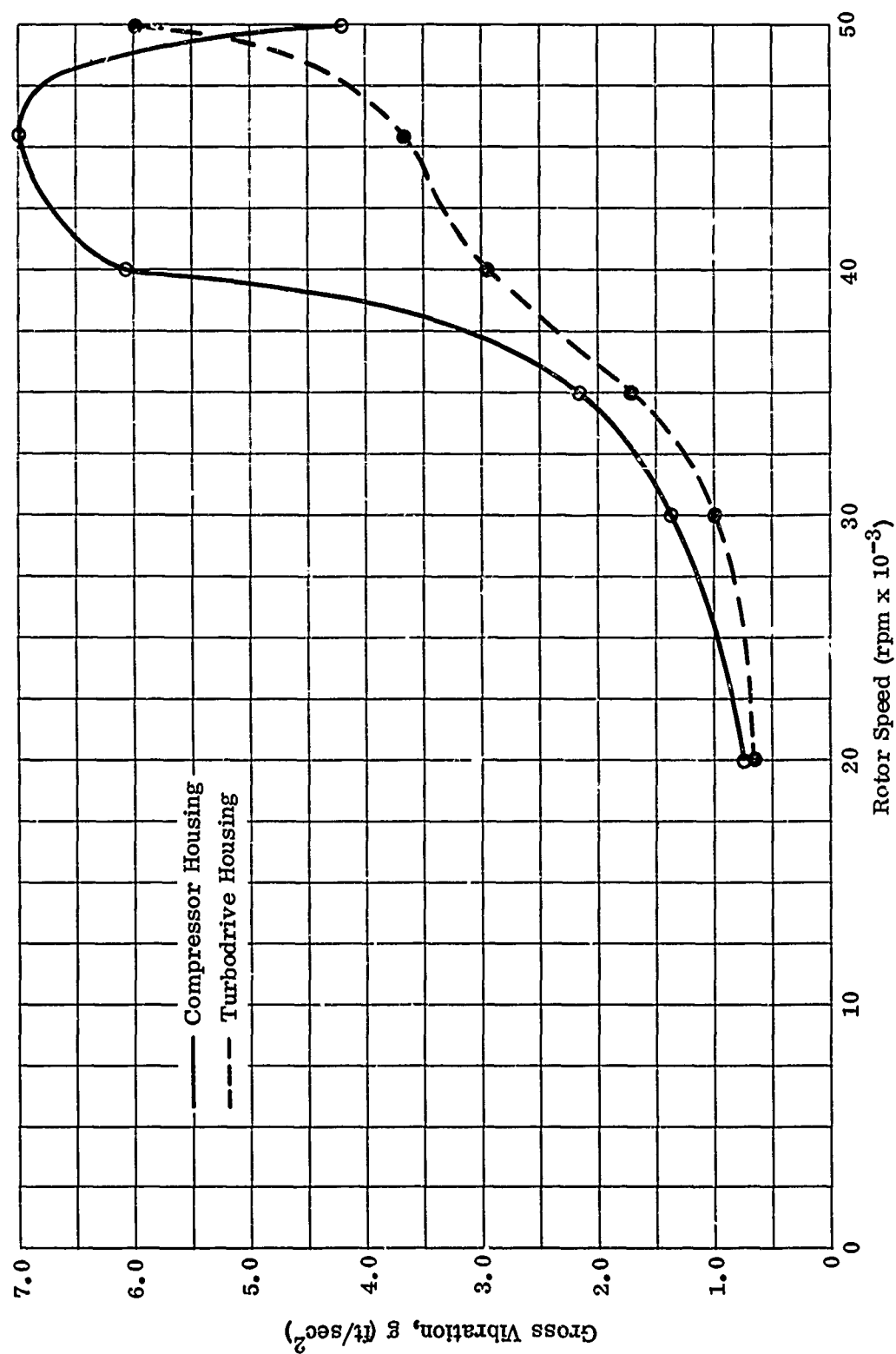


Figure 47. Compressor and Turbodriven Housing Vibration.

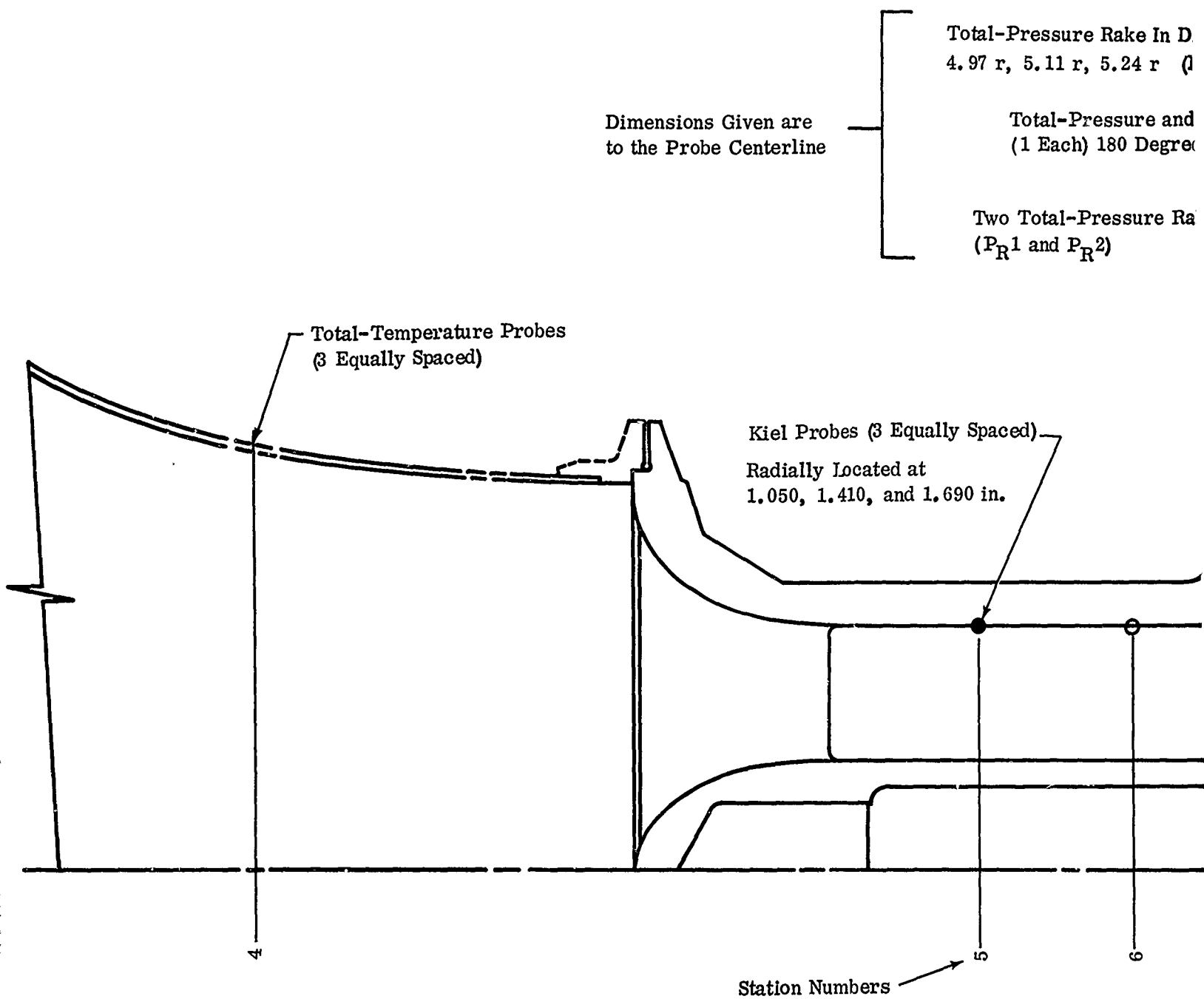


Figure 48. Instrumentation Locations.

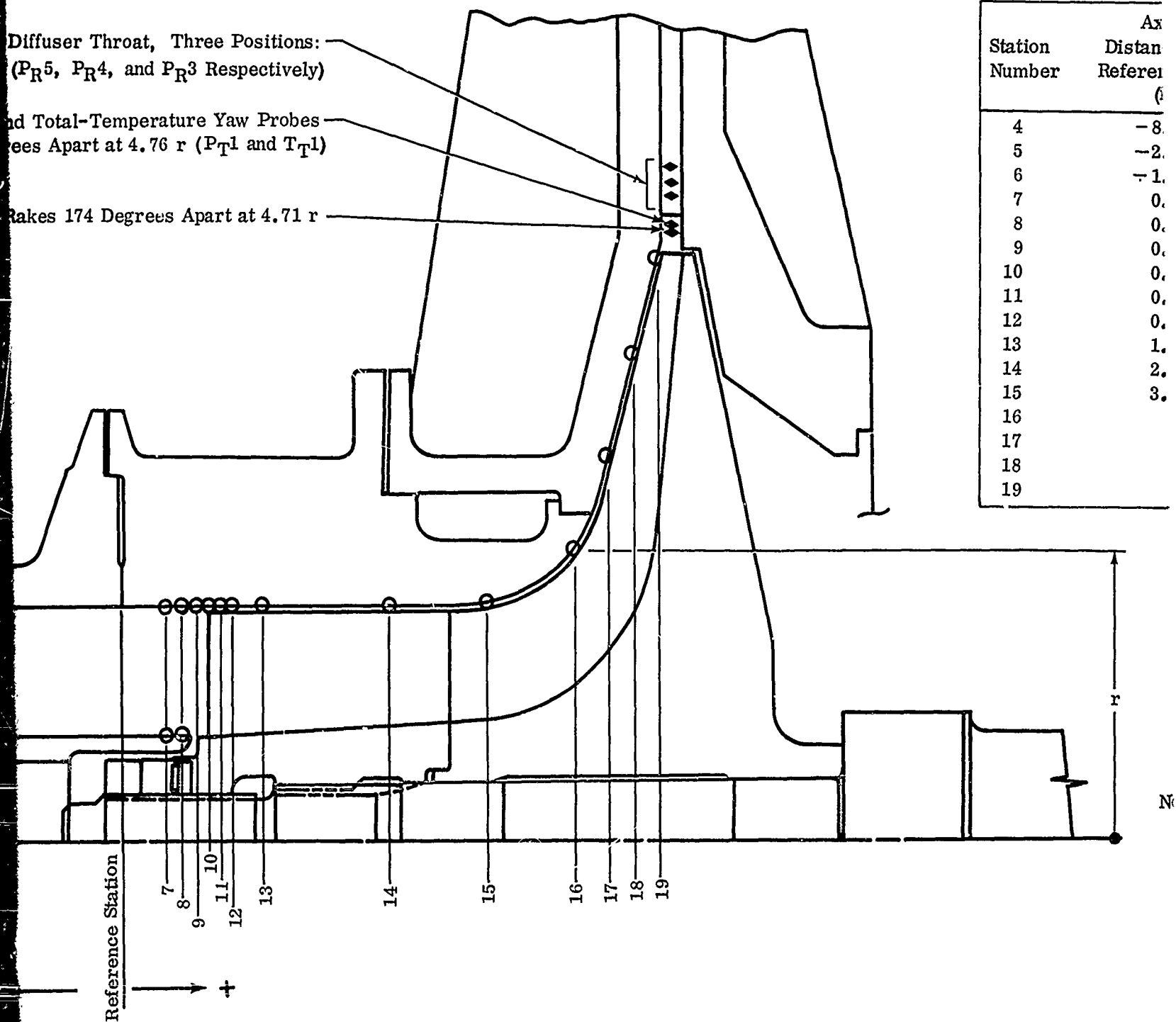
Instrument

**Diffuser Throat, Three Positions:
(P_{R5} , P_{R4} , and P_{R3} Respectively)**

and Total-Temperature Yaw Probes
Feet Apart at 4.76 r (P_{T1} and T_{T1})

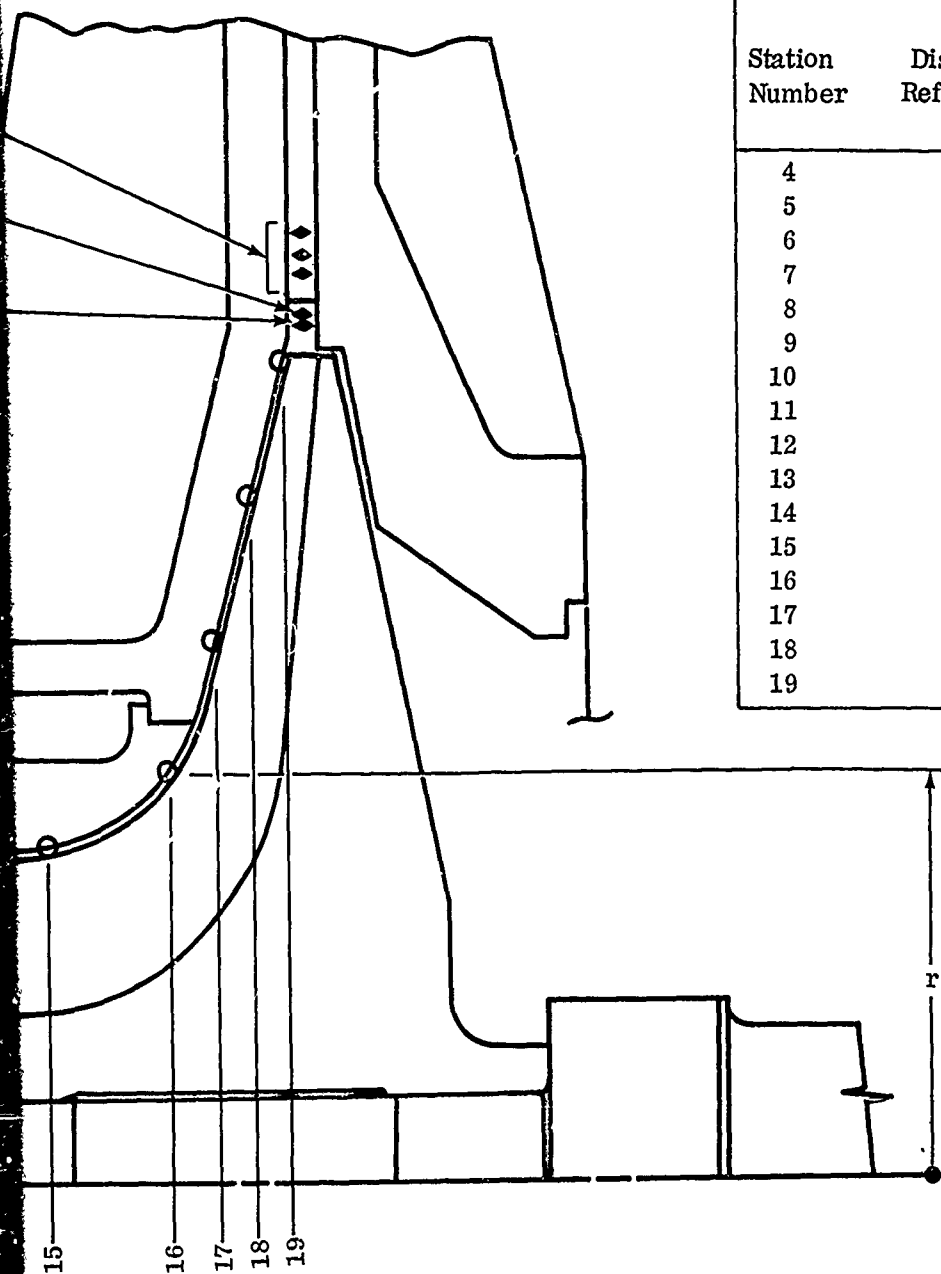
Rakes 174 Degrees Apart at 4.71 r

Station Number	Ax Distan Referen (ft)
4	-8
5	-2
6	-1
7	0
8	0
9	0
10	0
11	0
12	0
13	1
14	2
15	3
16	
17	
18	
19	



Instrumentation Stations

Station Number	Axial Distance From Reference Station (in.)	Radial Distance From Centerline, r (in.)
4	-8.18	
5	-2.50	
6	-1.28	
7	0.37	
8	0.52	
9	0.62	
10	0.72	
11	0.82	
12	0.92	
13	1.17	
14	2.22	
15	3.04	
16		2.52
17		3.00
18		3.80
19		4.71



○ Indicates Static-Pressure Taps; 3 Equally Spaced At Each Station Indicated

Note: Collector Pressure and Temperature Probes Not Shown

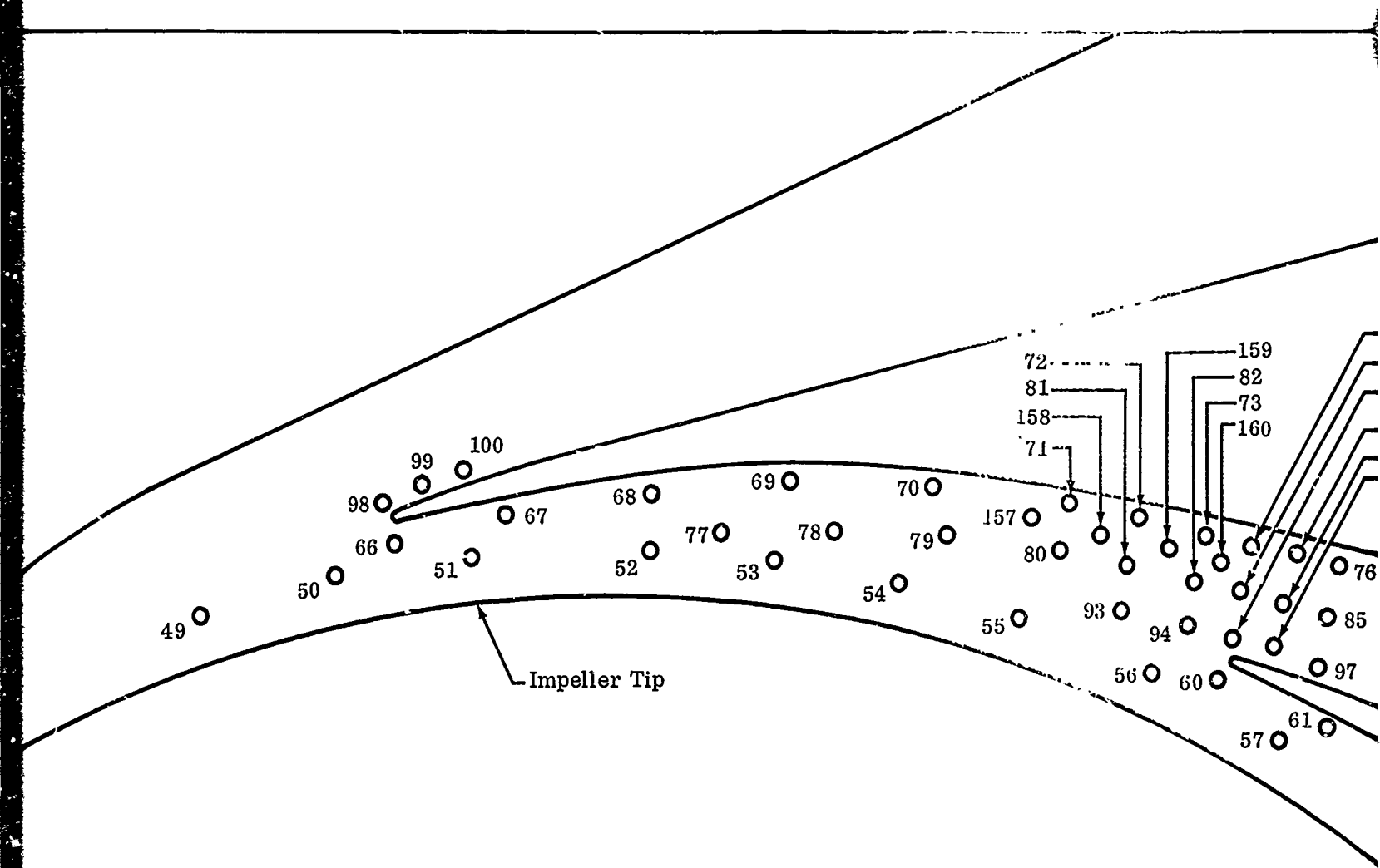
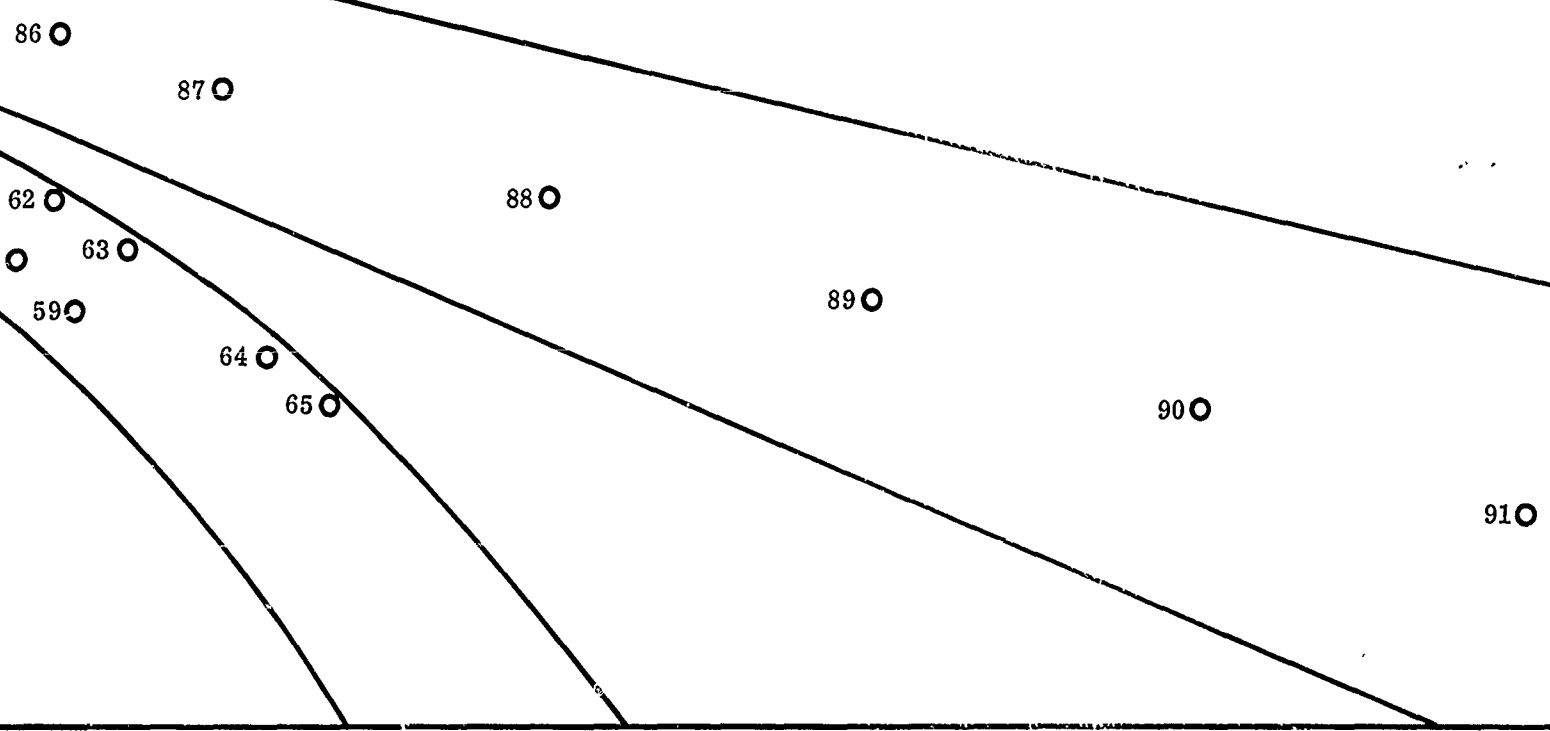


Figure 49. Diffuser Frontplate Static-Pressure Tap Locations.

-74
-83
-95
-75
-84
-96

3



88 ○

89 ○

90 ○

91 ○

92 ○

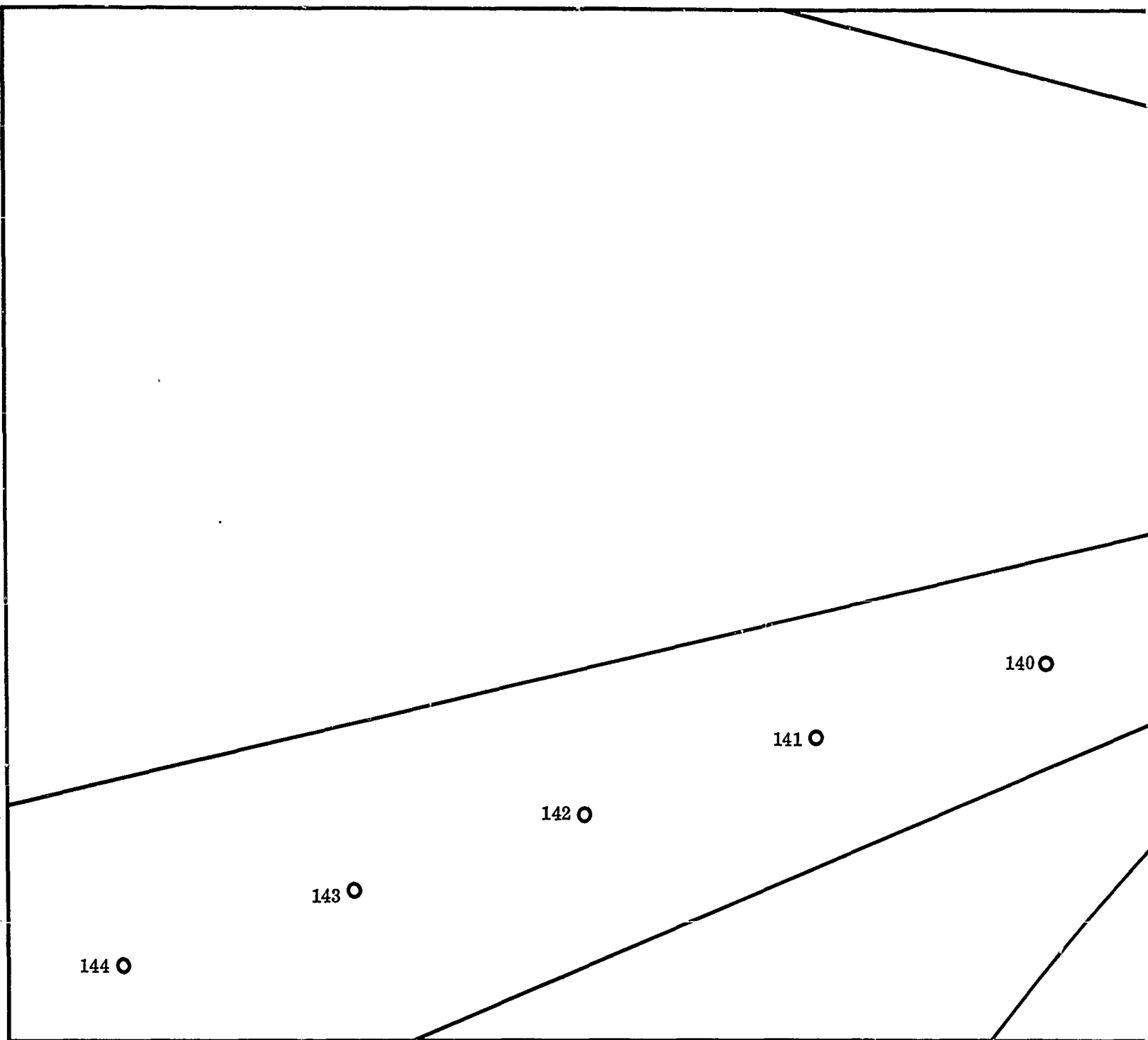
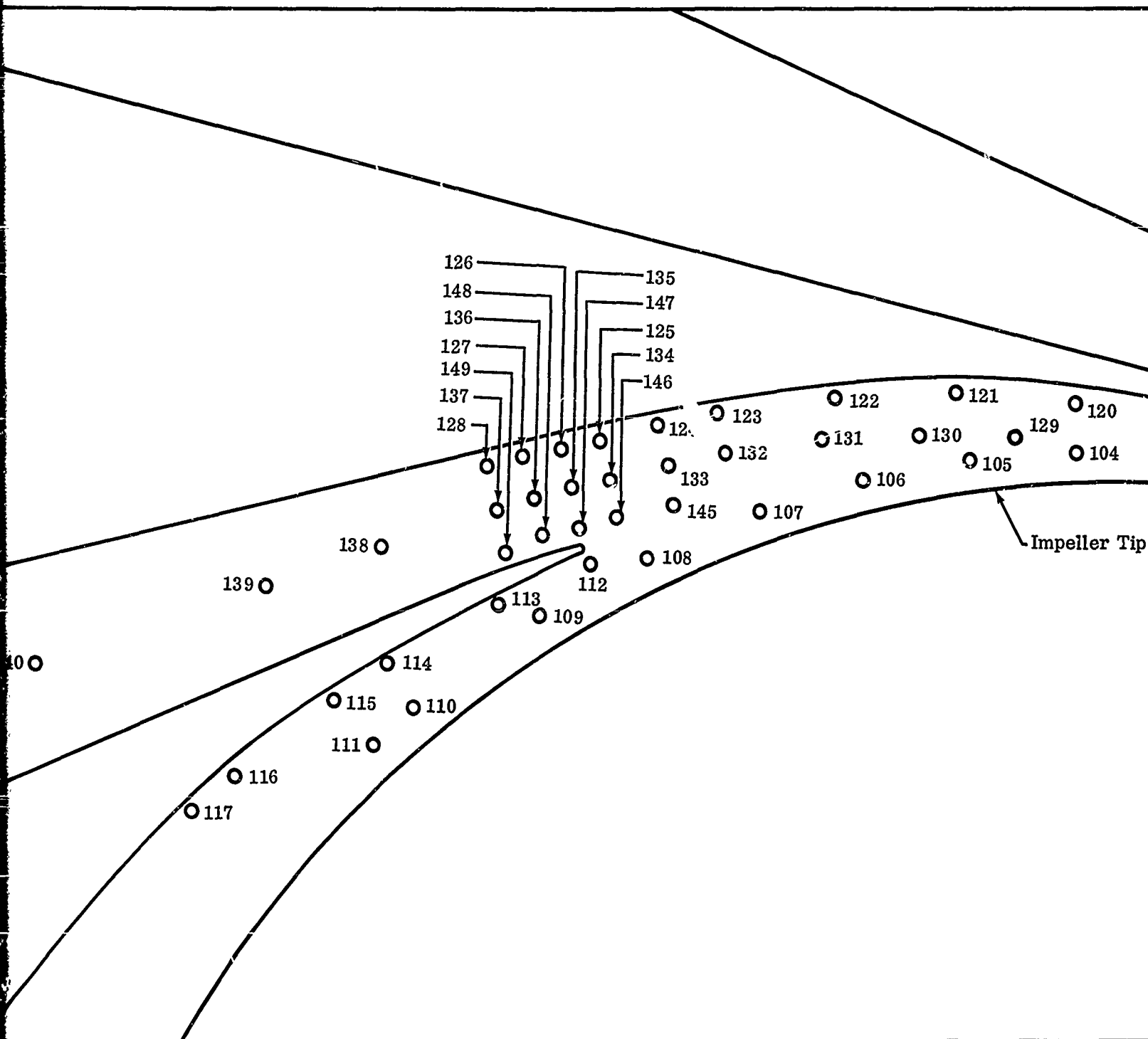
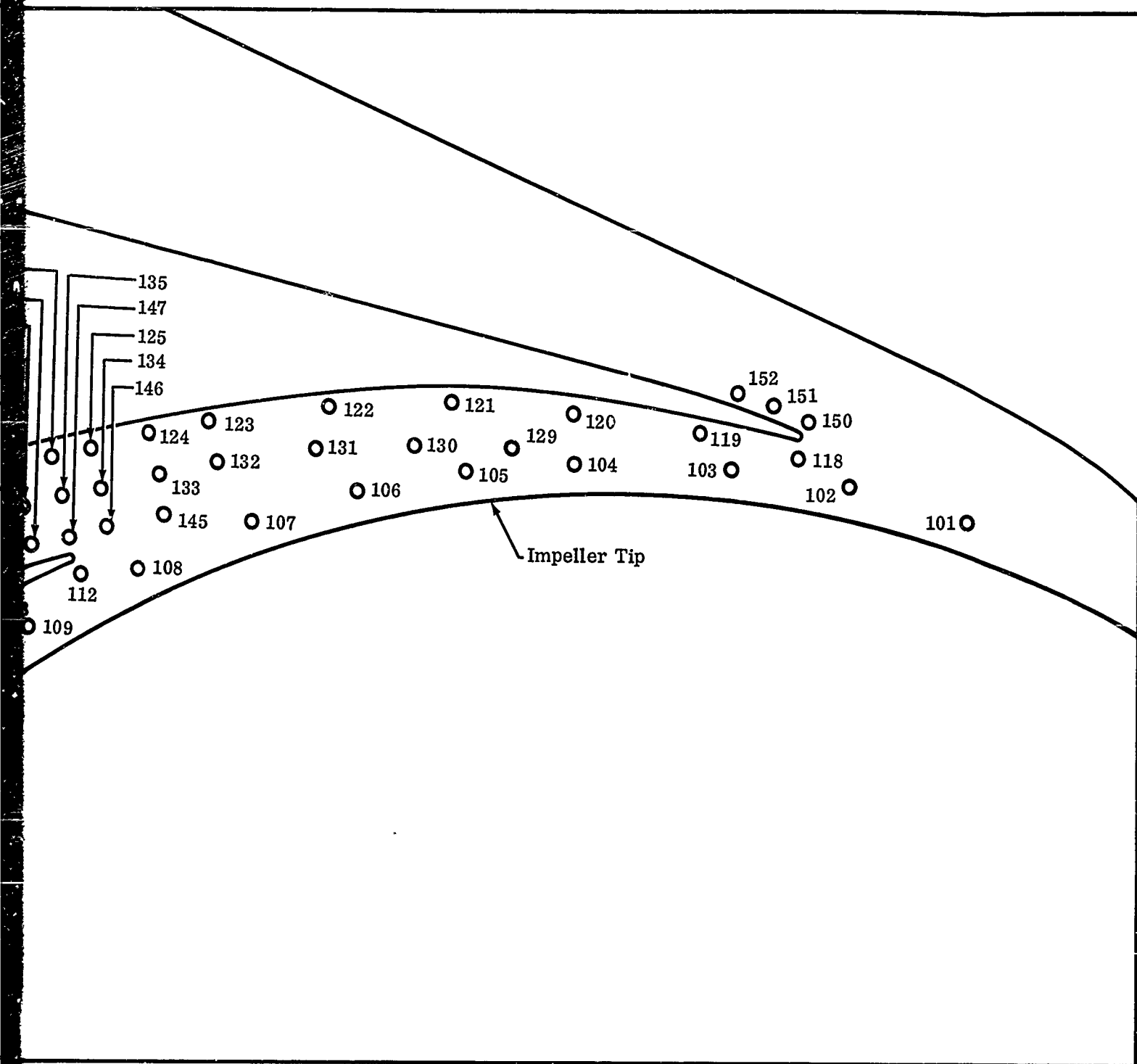


Figure 50. Diffuser Backplate Static-Pressure Tap Locations.





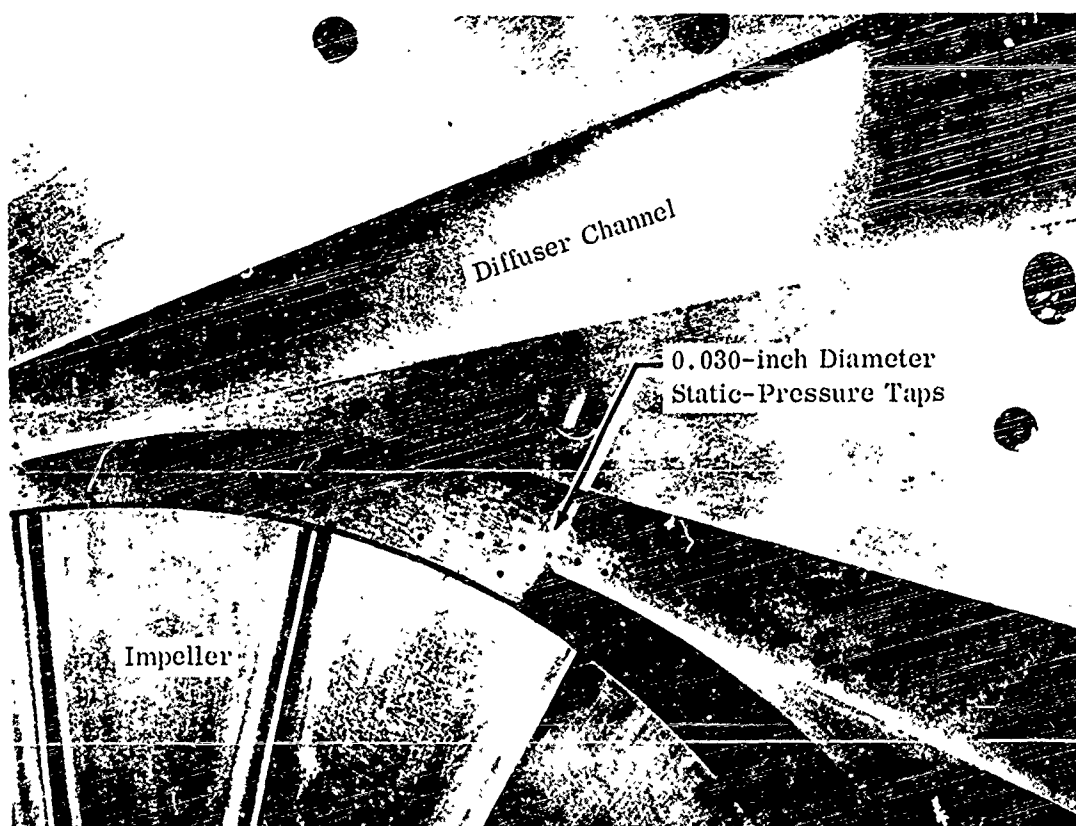


Figure 51. Static-Pressure Taps in Diffuser.

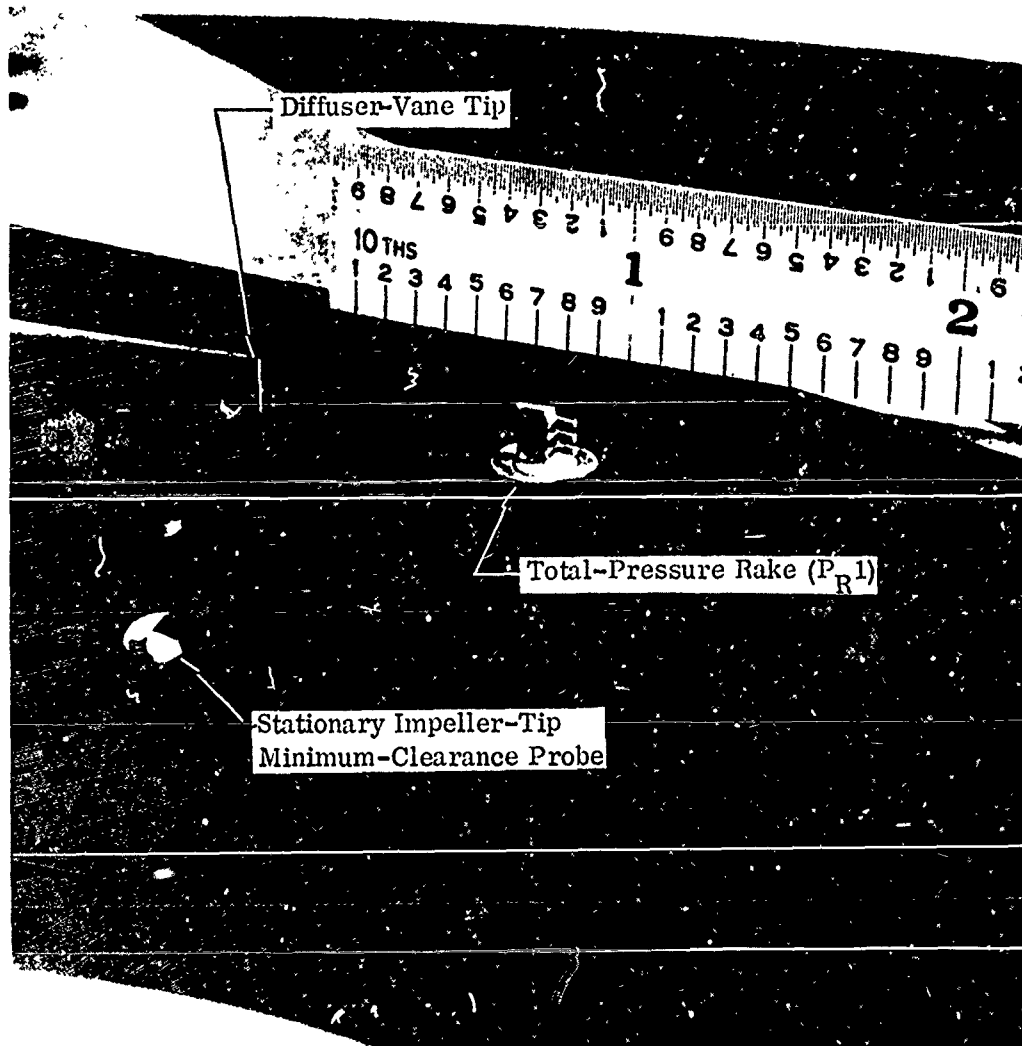


Figure 52. Total-Pressure Rake Installation.

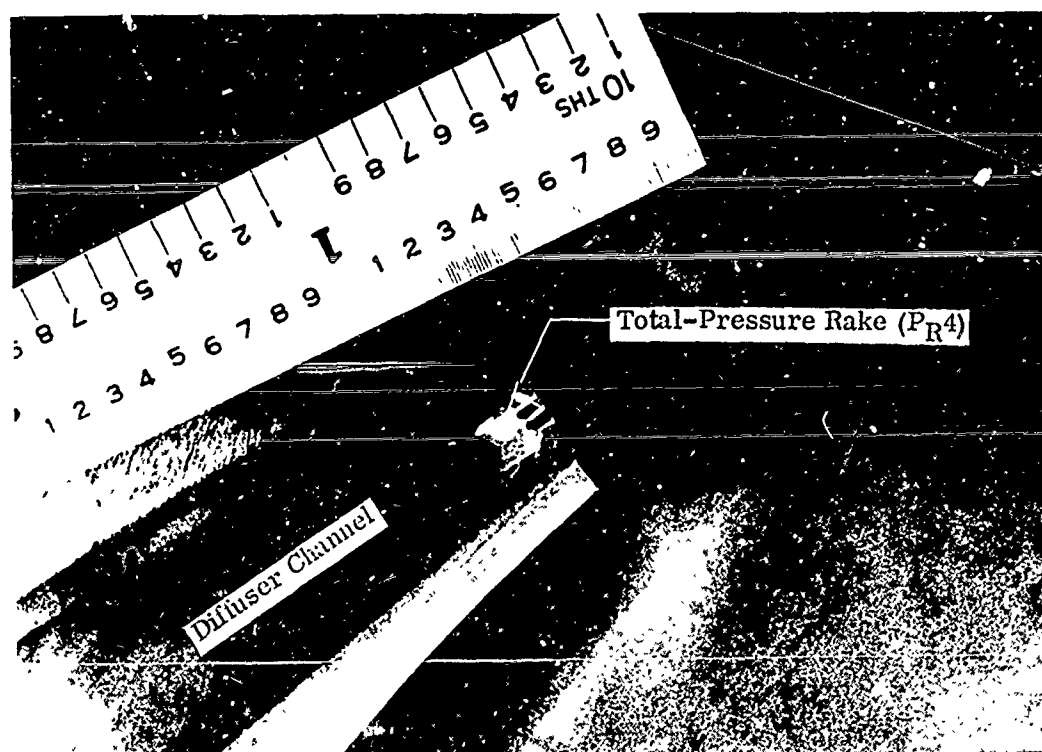


Figure 53. Total-Pressure Rake in Diffuser Throat.

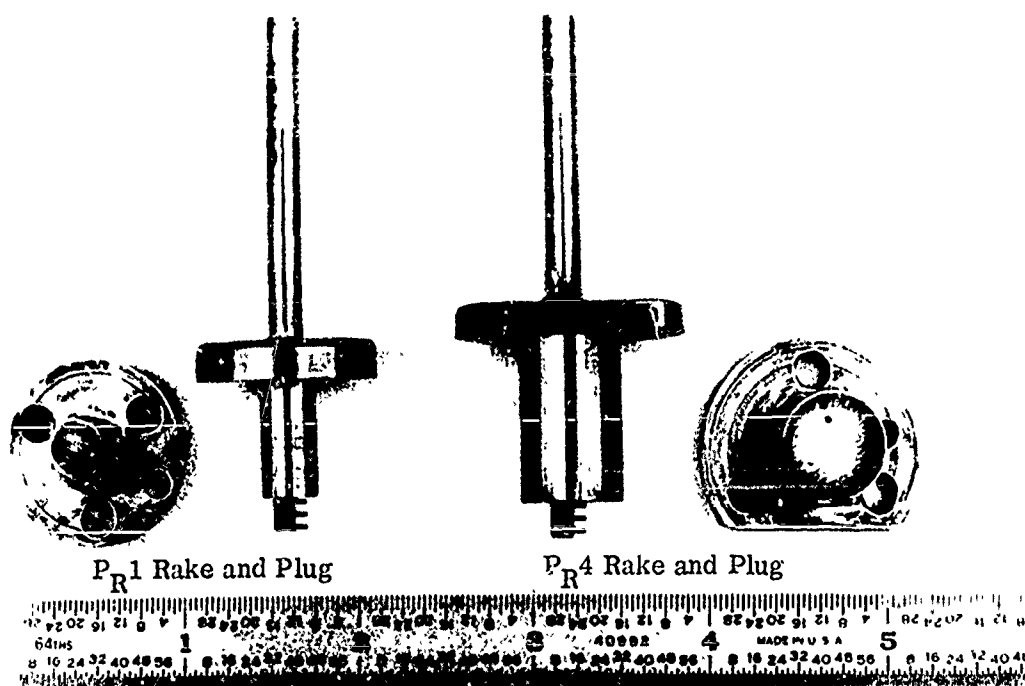


Figure 54. Total-Pressure Rakes and Plugs.

5.3 PERFORMANCE DATA ACQUISITION

Compressor performance data (temperature and pressure) were recorded by the digital-data system described in Section 4.1. In addition to the automatic digital recordings, impeller shroud, inlet duct, and collector static pressures were recorded manually on data sheets shown in Section 5.0 of Reference 1. The same manual-readout instruments described for the previous tests were used. Critical dimensions (such as impeller-tip clearance, blade height, diffuser-throat width, and throat height) affecting performance characteristics were measured for each configuration tested. Table IV lists the tests, speeds, diffuser-vane thicknesses and throat-height dimensions, impeller-tip clearances, and instrumentation probes used.

TABLE IV
DIFFUSER-VANE CONFIGURATIONS

Test No.	Corrected Rotor Speed (rpm)	Vane No.	Vane Thickness (in.)	Throat Width (in.)			Single-Throat Area (in. ²)	Impeller-Tip Clearance (in.)		Instrumentation Probes Installed		Dymec Data Recorded
				Min	Max	Avg ¹		Static	50,000 rpm	Total-Pressure Rakes (See Figure 40, Section 4.0 for -5, -8, and -9 rakes.)	Yaw Probes	
3351	50,000	V1	0.230	0.437	0.450	0.444	1.021	0.068	0.063			
3352	50,000	V1-1	0.200	0.437	0.450	0.444	0.888	0.038	0.028			
3352A	50,000	V1-1	0.200	0.437	0.450	0.444	0.888	0.038	0.027			X
3352B	50,000	V1-2	0.190	0.437	0.450	0.444	0.844	0.028	0.016			X
3352C	50,000	V1-3	0.183	0.437	0.450	0.444	0.813	0.027	0.016			X
3353	46,000	V1-3	0.183	0.437	0.450	0.444	0.813	0.027	0.016	-8 and -9 Vaneless Space (P_{R1} and P_{R2}) P_{T1} , T_{T1}		X
3353	46,000	V1-3	0.183	0.437	0.450	0.444	0.813	0.027	0.016			X
3353	50,000	V1-3	0.183	0.437	0.450	0.444	0.813	0.027	0.016			X
3353A	50,000	V1-3	0.183	0.437	0.450	0.444	0.813	0.027	0.016			X
3353B	50,000	V1-3	0.183	0.437	0.450	0.444	0.813	0.027	0.016			
3353C	50,000	V1-3	0.183	0.437	0.450	0.444	0.813	0.027	0.016	-9 in Vaneless Space (P_{R2})		X
3353D	50,000	V1-3	0.183	0.437	0.450	0.444	0.813	0.027	0.016	-9 in Center of Throat (P_{R4})		X
3353E	50,000	V1-3	0.183	0.437	0.450	0.444	0.813	0.027	0.016	-9 in Top of Throat (P_{R3})		X
3353F	50,000	V1-3	0.183	0.437	0.450	0.444	0.813	0.027	0.016	-9 in Bottom of Throat (P_{R5})		X
3354	50,000	V1-4	0.183	0.472	0.477	0.475	0.869	0.027	0.016	-9 in Center of Throat (P_{R4})		X
3354A	50,000	V1-4	0.183	0.472	0.477	0.475	0.869	0.027	0.016	-9 in Center of Throat (P_{R4})		X
3354B	50,000	V1-4	0.183	0.472	0.477	0.475	0.869	0.027	0.016	-9 in Top of Throat (P_{R3})		X
3355	50,000	V1-5	0.183	0.495	0.498	0.497	0.909	0.027	0.016			X
3356	50,000	V1-6	0.183	0.515	0.519	0.517	0.946	0.027	0.016			X
3356A	50,000	V1-6	0.183	0.515	0.519	0.517	0.946	0.027	0.016	-9 in Vaneless Space (P_{R2})		X
3357	50,000	V1-7	0.183	0.515	0.519	0.517	0.946	0.027	0.016			X
3358	50,000	V1-8	0.183	0.515	0.519	0.517	0.946	0.027	0.016			X
3358A	50,000	V1-8	0.183	0.515	0.519	0.517	0.946	0.027	0.016			X
3359	50,000	V1-9	0.183	0.515	0.519	0.517	0.946	0.027	0.016			X
3360	50,000	V1-10	0.183	0.515	0.519	0.517	0.946	0.027	0.016			X
3361	50,000	V1-10	0.183	0.515	0.519	0.517	0.946	0.027	0.016			X
3362	50,000	V1-10	0.183	0.515	0.519	0.517	0.946	0.027	0.016			X
3363	50,000	V1-11	0.183	0.515	0.519	0.517	0.946	0.027	0.016			X

TABLE IV
(Continued)

Test No.	Corrected Rotor Speed (rpm)	Vane No.	Vane Thickness (in.)	Throat Width (in.)			Single-Throat Area (in. ²)	Impeller-Tip Clearance (in.)		Instrumentation Probes Installed		Dymec Data Recorded
				Min	Max	Avg		Static	50,000 rpm	Total-Pressure Rakes (See Figure 40, Section 4.0 for -5, -8, and -9 rakes.)	Yaw Probes	
3364	50,000	V1-11	0.183	0.515	0.519	0.517	0.946	0.027	0.016			X
3365	50,000	V1-12	0.183	0.515	0.519	0.517	0.946	0.027	0.016			X
3366	50,000	V2	0.203	0.423	0.427	0.426	0.865	0.027	0.015			X
3366A	50,000	V2	0.203	0.423	0.427	0.426	0.865	0.027	0.015	-9 in Vaneless Space ($P_R^{(2)}$)		X
3366B	50,000	V2	0.203	0.423	0.427	0.426	0.865	0.027	0.015	-9 in Top of Throat ($P_R^{(3)}$)		X
3366C	50,000	V2	0.203	0.423	0.427	0.426	0.865	0.027	0.015	-9 in Center of Throat ($P_R^{(4)}$)		X
3366D	50,000	V2	0.203	0.423	0.427	0.426	0.865	0.027	0.015	-9 in Bottom of Throat ($P_R^{(5)}$)		X
3366E	50,000	V2	0.203	0.423	0.427	0.426	0.865	0.027	0.015	-8 in Vaneless Space ($P_R^{(1)}$)		X
3367	50,000	V2	0.203	0.4235	0.427	0.426	0.865	0.027	0.015			X
3368	35,000	V2-1	0.158	0.465	0.470	0.601	0.950	0.027	0.022			X
3368	40,000	V2-1	0.158	0.465	0.470	0.601	0.950	0.027	0.020			X
3368	45,000	V2-1	0.158	0.465	0.470	0.601	0.950	0.027	0.018			X
3368	50,000	V2-1	0.158	0.465	0.470	0.601	0.950	0.027	0.015			X
3368	51,850	V2-1	0.158	0.465	0.470	0.601	0.950	0.027	0.015			X
3369	50,000	V2-2	0.158	0.541	0.551	0.546	0.862	0.027	0.009			X
3369A	50,000	V2-2	0.158	0.541	0.551	0.546	0.862	0.027	0.009	-5 in Vaneless Space		X
3369B	50,000	V2-2	0.158	0.541	0.551	0.546	0.862	0.027	0.009	-5 in Center of Throat		X
3369C	51,850	V2-2	0.158	0.541	0.551	0.546	0.862	0.027	0.008			X
3370	35,000	V2-2	0.158	0.541	0.551	0.546	0.862	0.027	0.014			X
3370	40,000	V2-2	0.158	0.541	0.551	0.546	0.862	0.027	0.014			X
3370	45,000	V2-2	0.158	0.541	0.551	0.546	0.862	0.027	0.014			X
3370	51,850	V2-2	0.158	0.541	0.551	0.546	0.862	0.027	0.014			X
3370	53,000	V2-2	0.158	0.541	0.551	0.546	0.862	0.027	0.014			X
3370A	35,000	V2-2	0.158	0.541	0.551	0.546	0.862	0.027	0.014			X
3370A	40,000	V2-2	0.158	0.541	0.551	0.546	0.862	0.027	0.014			X
3370A	45,000	V2-2	0.158	0.541	0.551	0.546	0.862	0.027	0.014			X
3370A	50,000	V2-2	0.158	0.541	0.551	0.546	0.862	0.027	0.014			X

CONFIDENTIAL

6.0 (C) TEST RESULTS (U)

The results of the impeller and diffuser tests conducted during the second portion of the program are presented in this section. One impeller (with 2 modifications) was tested with various diffuser configurations. Of the 42 tests run, 9 were aimed at defining impeller performance, while the remaining runs were for gathering data to establish diffuser performance trends.

6.1 IMPELLER

The following discussion presents the test plan, measured data, and calculated results obtained from the impeller tests. All data were reviewed and curves were selected to provide a complete performance description of the impeller.

6.1.1 Test Plan

Table V presents the test plan for the RF-2 impeller; only the tests run to define impeller performance are tabulated. The other tests (run to evaluate diffuser performance) are presented in Section 6.2. The standard impeller test data were as follows:

- 1) Inlet temperature
- 2) Inlet total pressure
- 3) Inlet airflow
- 4) Static pressure along the inlet duct shroud
- 5) Static pressure along the inlet duct hub
- 6) Static pressure along the impeller shroud
- 7) Static pressure at the impeller exit
- 8) Collector temperature
- 9) Collector pressure

Special instrumentation was added for some tests to obtain additional data necessary in evaluating impeller performance. This information is also shown in Table V.

TABLE V IMPELLER TESTS				
Test No.	Speed (rpm)	Measurements	Vane No.	Remarks
3353	46, 000 and 50, 000	P_T^1 , T_{T^1} , P_R^1 , and P_R^2	V1-3	Leading Edge of Inducer Swept Impeller Blade Width Reduced to 0.135 in.
3353A	50, 000	P_T^1	V1-3	
3353C	50, 000	P_R^2	V1-3	
3356A	50, 000	P_R^2	V1-6	
3366A	50, 000	P_R^2	V-2	
3366E	50, 000	P_R^1	V-2	
3367	50, 000	Map Data Only	V-2	
3369A	50, 000	P_R^1	V2-2	
3370A	35, 000, 40, 000, 45, 000, 51, 850 and 53, 000	P_R^1	V2-2	
			V2-2	

6.1.2 Impeller Modifications

The first modification of the impeller was to sweep the leading edge of the inducer (shown in Figure 55). The modification was intended for investigation of the influence of inducer Mach number changes on impeller performance. The impeller was run with a previously tested diffuser (V2), without instrumentation probes at the impeller tip. A comparison plot of overall pressure ratio versus airflow for the swept and unswept leading-edge inducer (both with the V2 diffuser) is given in Figure 60 in the Test Results section. Because there was no measurable difference between the 2 impellers, and because overall impeller performance in the unswept configuration was already well defined, no further tests of this modification were necessary.

The impeller was modified a second time by reducing the blade width at the exit from 0.180 to 0.135 inch (shown in Figure 56). The reduction in blade width was expected to reduce exit mixing losses by increasing the jet-to-wake width ratio. This configuration was tested with instrumentation at the impeller tip, and the test results are presented with the other impeller data in the Test Results section.

6.1.3 Performance Measurements

To define the impeller performance, the following information was required:

- 1) Temperature rise
- 2) Pressure ratio
- 3) Vector diagrams
- 4) Slip factor
- 5) Blockage factor

Compressor Temperature Rise

The compressor temperature rise was used to determine adiabatic efficiency, and both are given in Section 6.1.4. The collector temperature measurement was used for this purpose.

The total-temperature profile at the tip of the impeller was measured for Test 3353 at 46,000 and 50,000 rpm. This profile was needed in continuity calculations for mass-averaging total-pressure data. These data, given in the Test Results section, show a large difference between the measured temperature at the tip of the impeller and the collector temperature. This same discrepancy was observed during the testing reported in Sections 6.0 and 7.0, and in Appendix VII of Reference 1.

CONFIDENTIAL

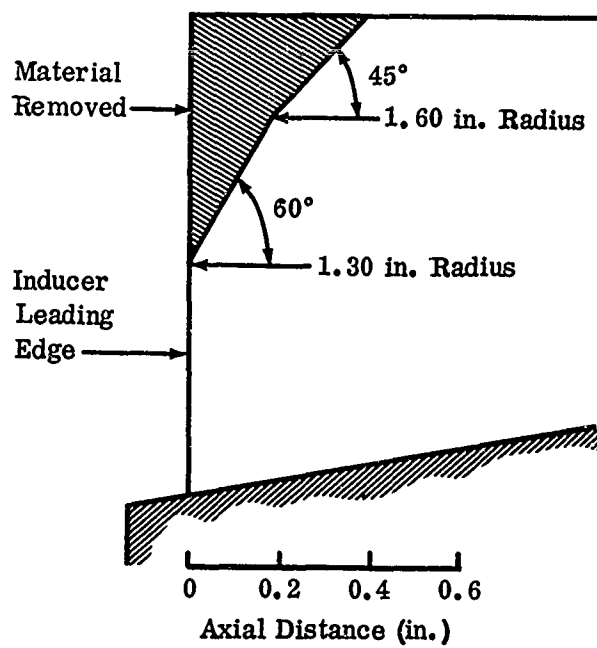


Figure 55. Inducer Leading-Edge Modification.

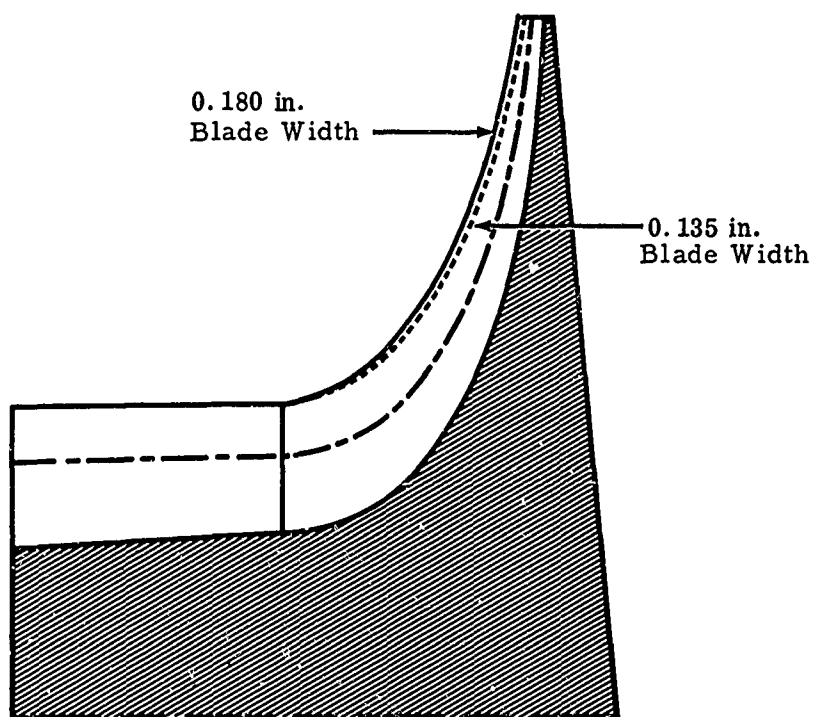


Figure 56. Reduced Blade Width Modification.

CONFIDENTIAL

Because the collector temperature was believed to be the true temperature rise of the impeller, the temperature profile at the tip was adjusted by decreasing each point on the profile by a constant ΔT until the mass-averaged total temperature of the resulting profile matched the collector temperature. The temperature-rise factor for the impeller was also calculated and is presented in Section 6.1.4. This factor was defined previously in Section 6.1 of Reference 1.

Pressure Ratio

Total-pressure profiles at the impeller tip were obtained with 3-probe rakes for all impeller tests except Test 3367 (inducer sweep test). In addition, yaw-probe flow-angle data were measured for Test 3353. Because these probes adversely affect overall performance, flow-angle profiles were not obtained for all tests; the profiles from Test 3353 were adjusted and used for the other impeller tests. This adjustment was made by setting the minimum angle at the same point in the passage as the maximum pressure, as confirmed by Test 3353. The remaining points were positioned so that the profile was similar to the measured profile. From these data, the airflow versus pressure ratio and the efficiency curves were obtained for the impeller.

Inlet Vector Diagram

The data required for inlet vector diagram are: 1) inlet static pressure, 2) inlet total temperature, and 3) inlet total pressure. From these data, the inlet vector diagrams and the plots of incidence variation along the blade were prepared.

Exit Vector Diagram

The exit vector diagrams were calculated from the mass-averaged values of total pressure, total temperature, flow angle, and the measured static pressure, using the method outlined in Section 6.1.1 of Reference 1.

Slip Factor

The slip factors and the variation of average slip factor with airflow were calculated as previously described in Section 6.1.1 of Reference 1.

Shroud Static Pressure

The static-pressure rise along the shroud of the impeller from inducer inlet to impeller exit is given in the Test Results section.

6.1.4 Test Results

The data obtained from the impeller tests are presented in this section. The arrangement of the data is as follows: 1) performance map, 2) measured data, and 3) calculated results. The evaluation of the results is given in Section 7.0.

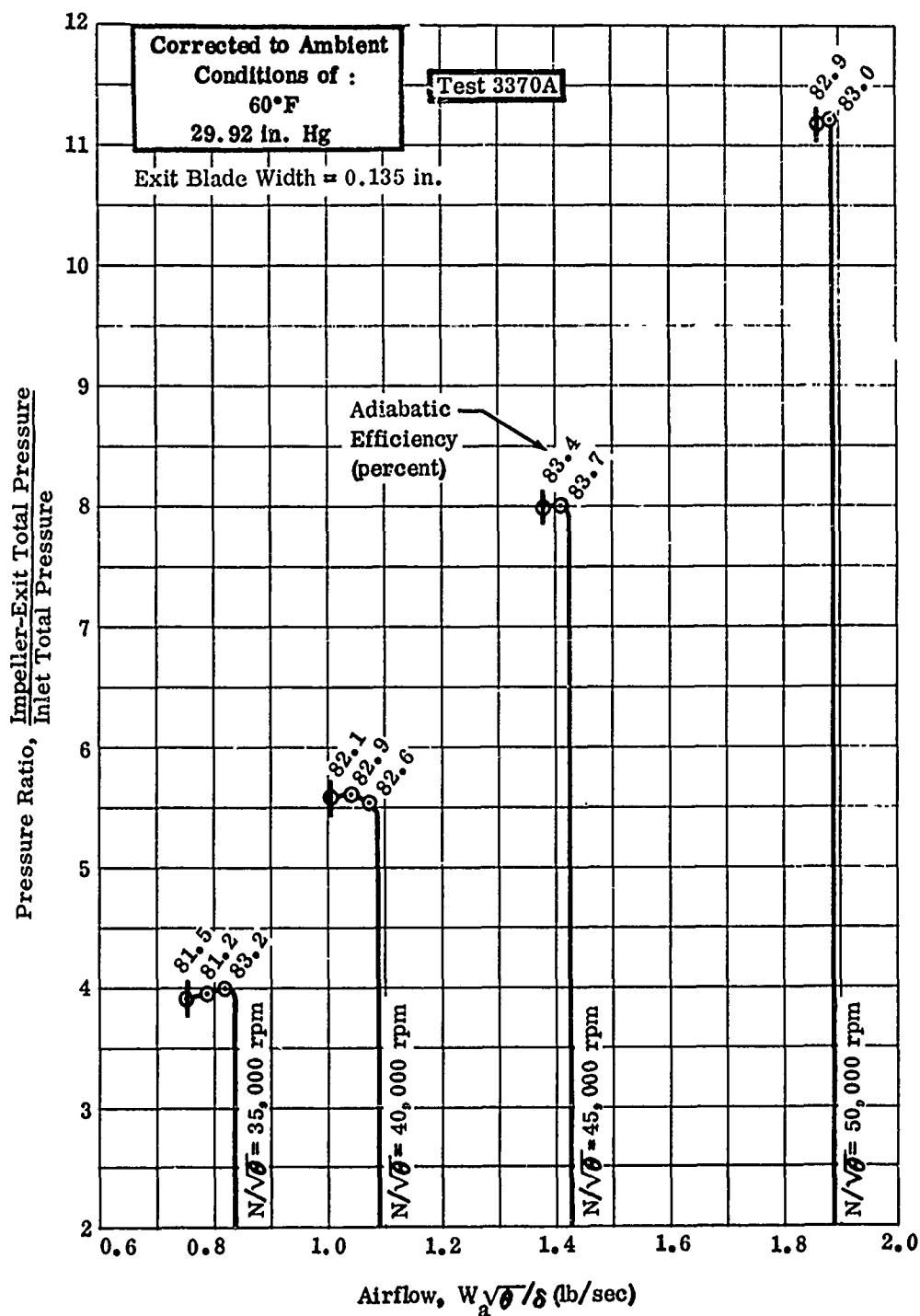


Figure 57. Performance of RF-2 Impeller with Reduced Blade Width.

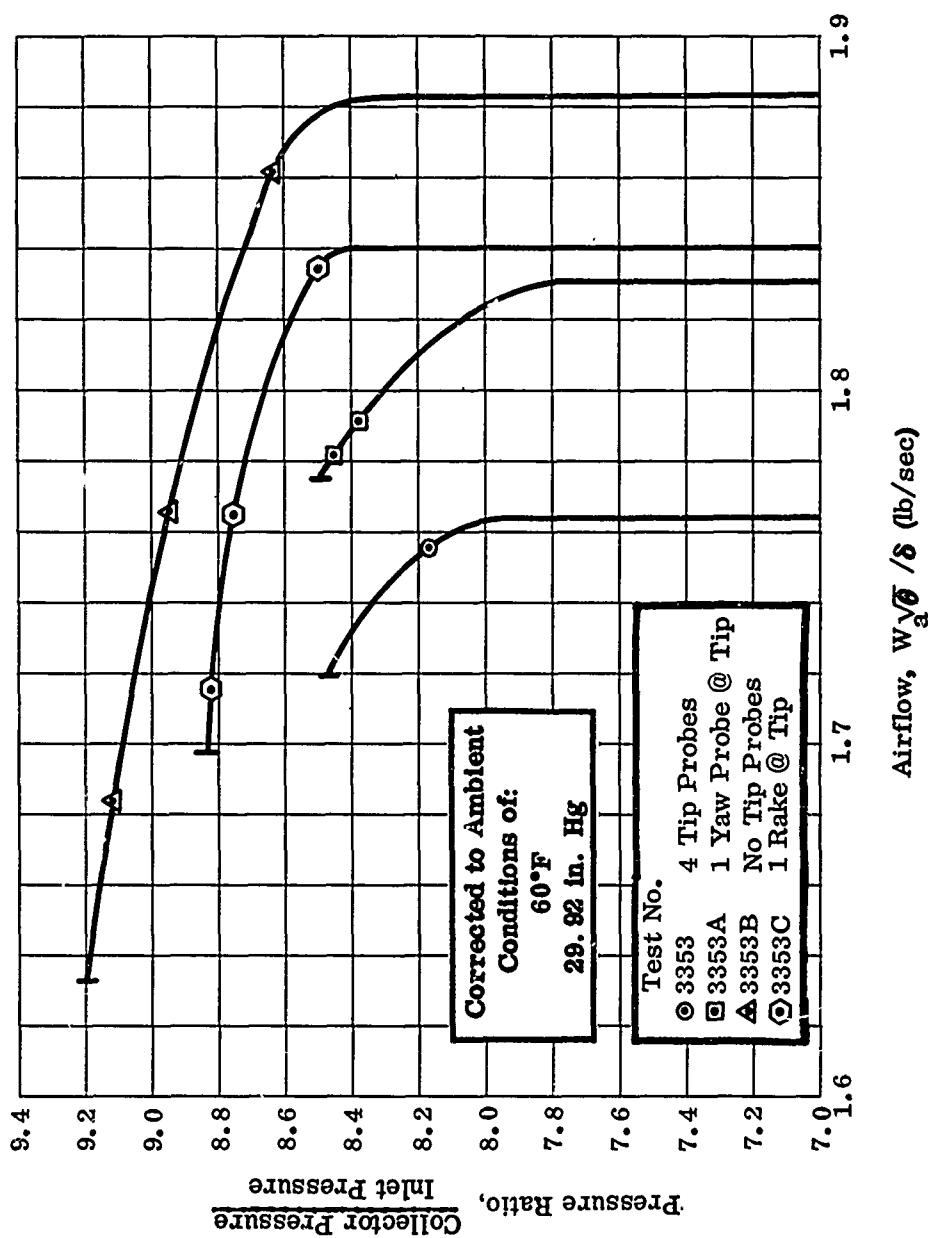


Figure 58. Pressure Ratio Versus Airflow.

CONFIDENTIAL

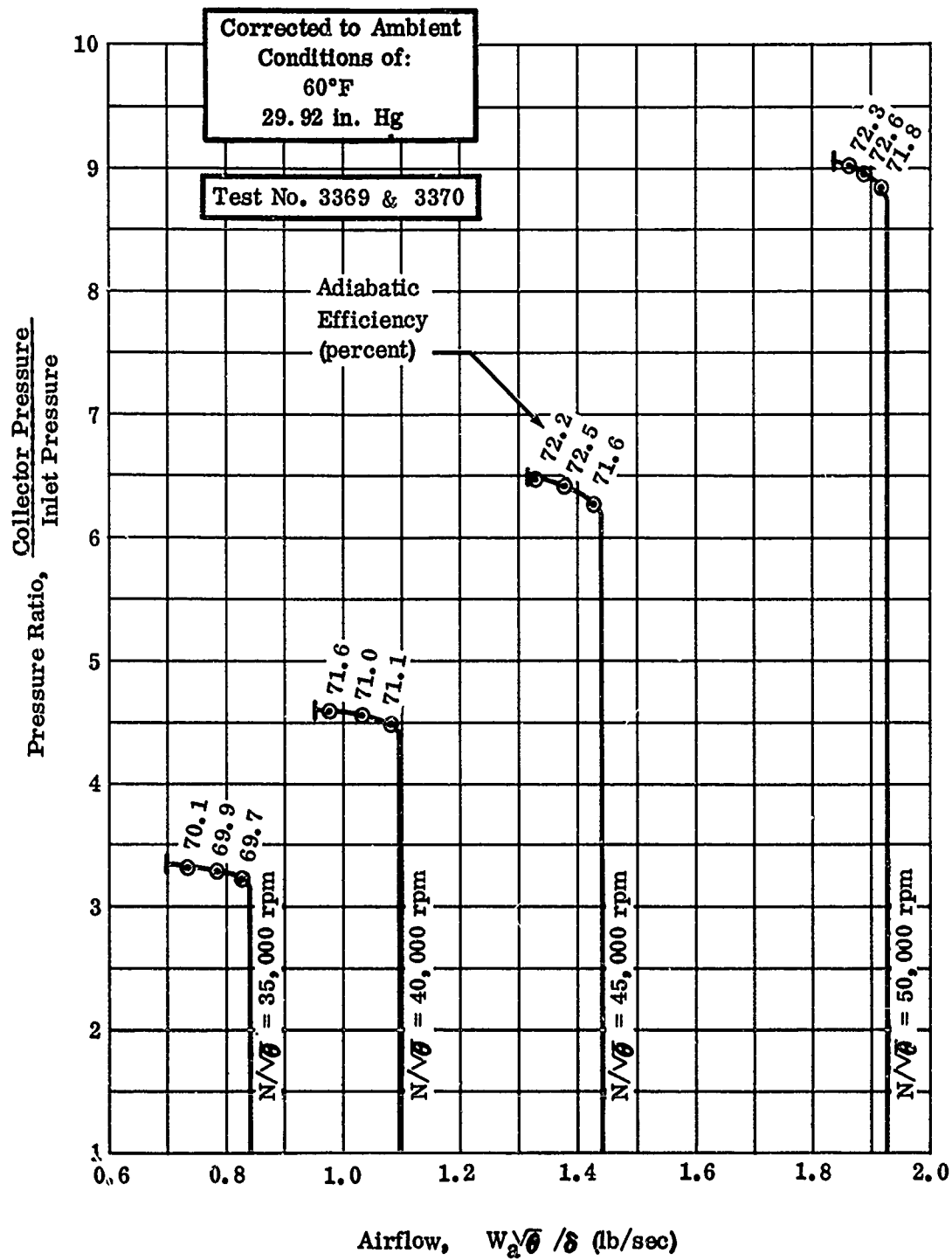


Figure 59. Pressure Ratio Versus Airflow.

CONFIDENTIAL

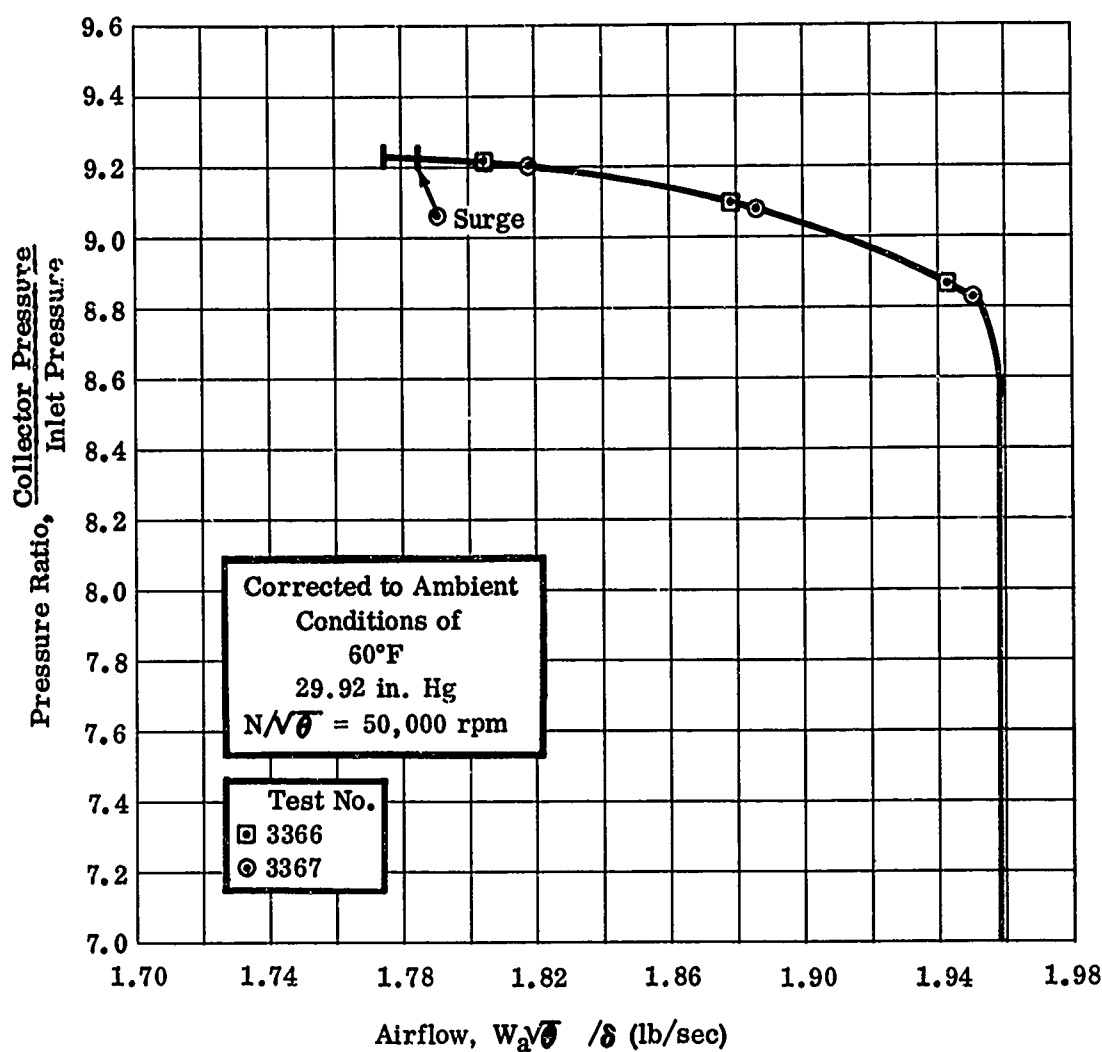


Figure 60. Pressure Ratio Versus Airflow.

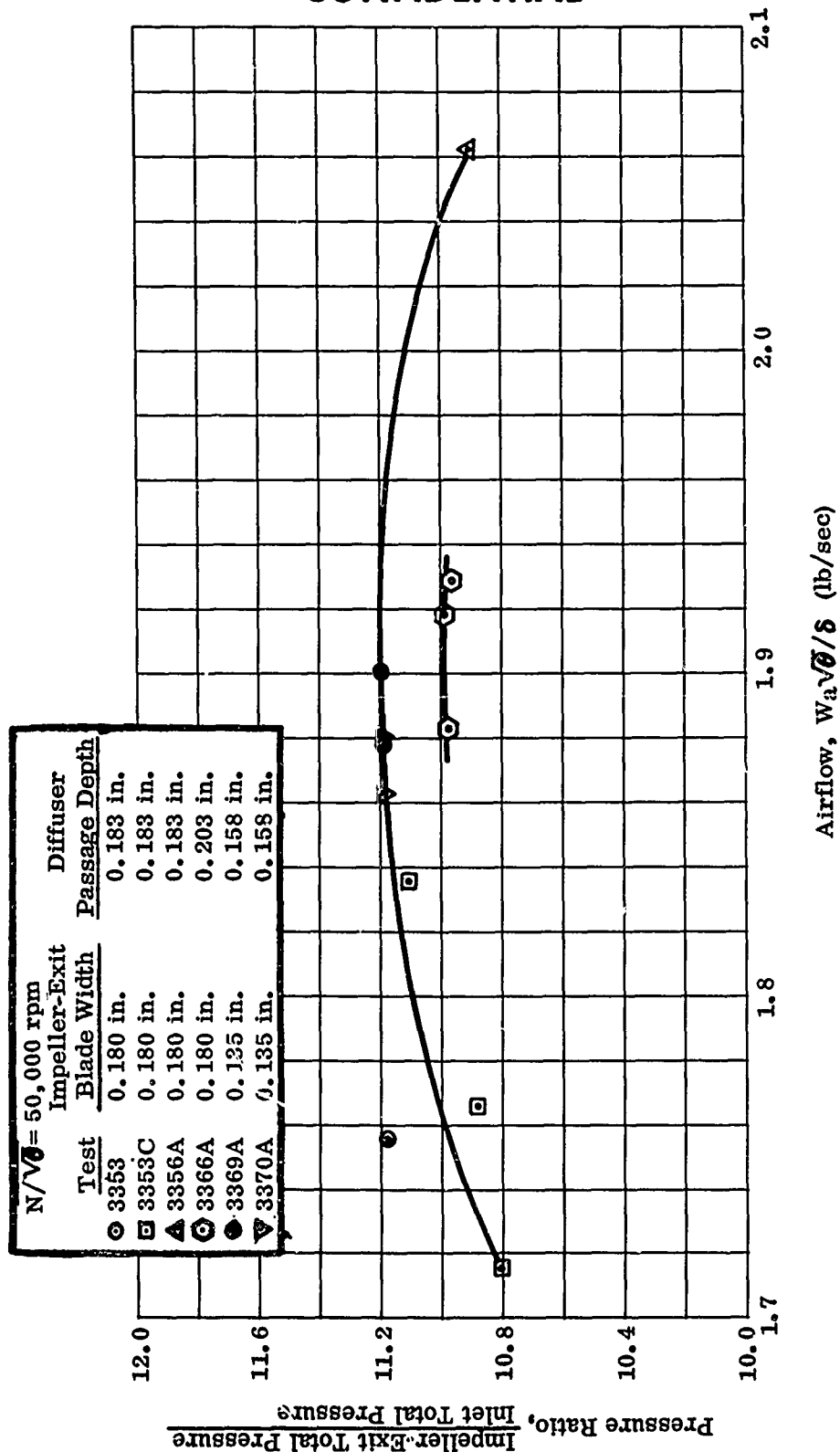


Figure 61. Pressure Ratio of RF-2 Impeller at Design Speed.

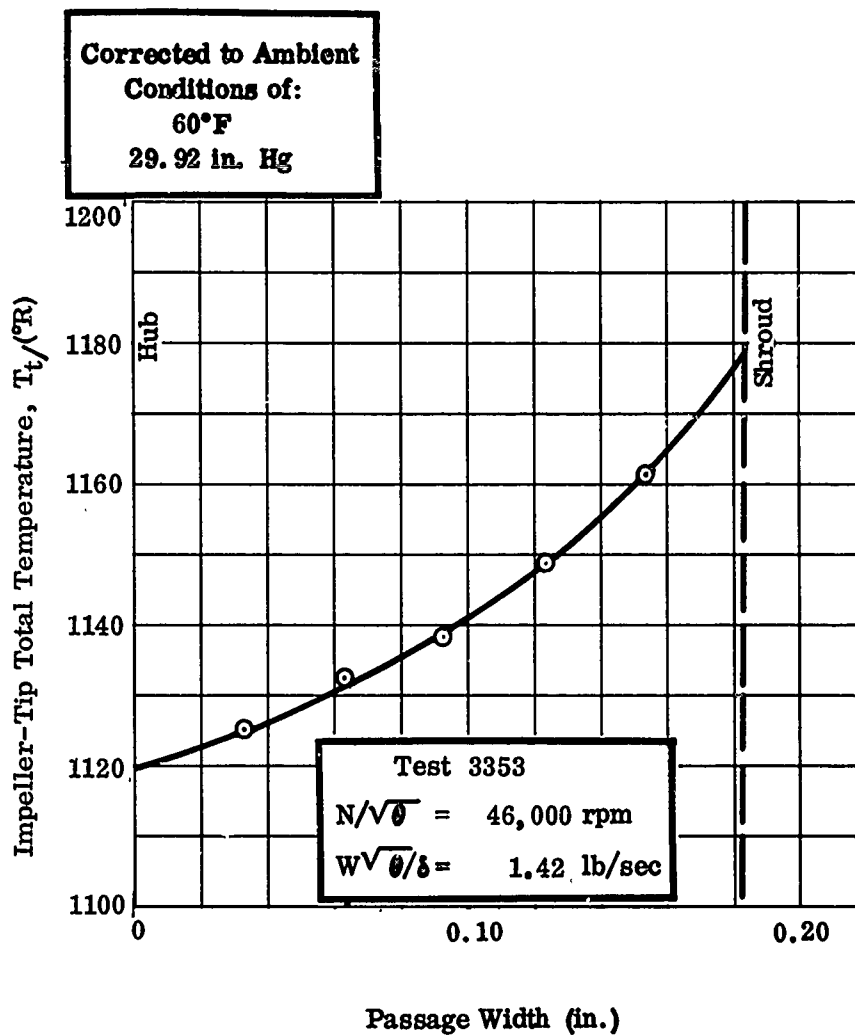


Figure 62. Impeller-Tip Total-Temperature Survey, RF-2.

CONFIDENTIAL

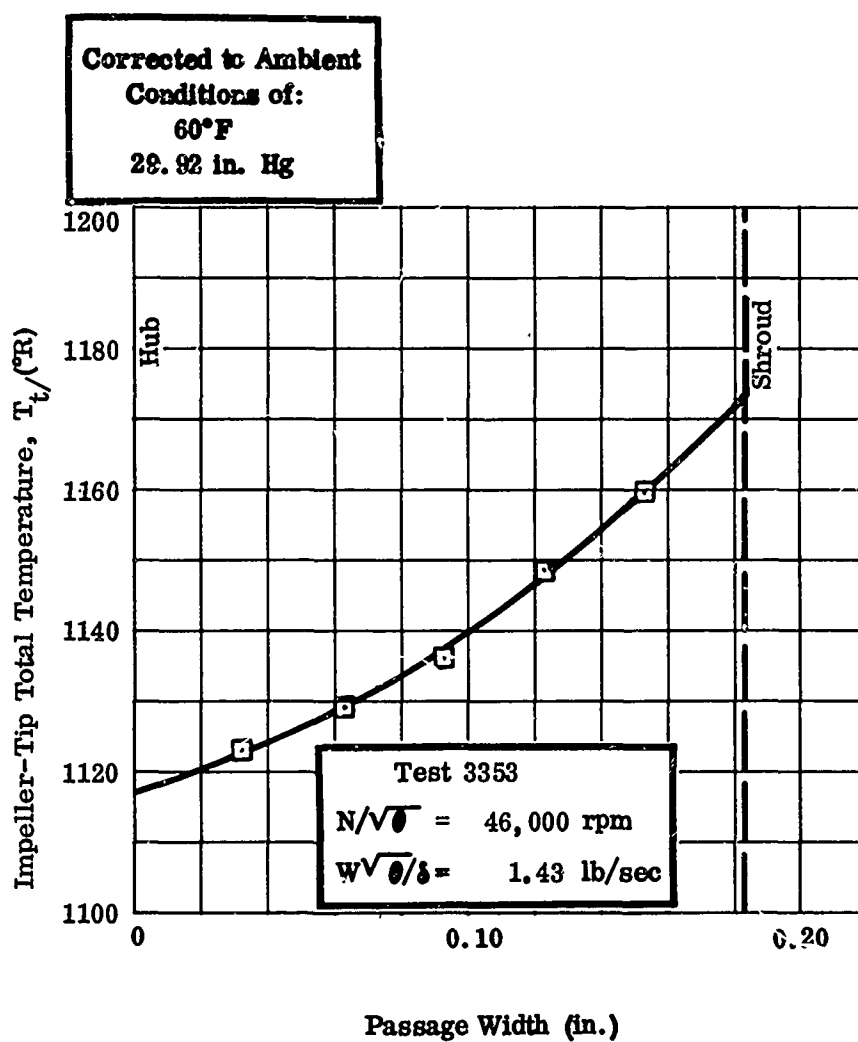


Figure 63. Impeller-Tip Total-Temperature Survey, RF-2.

CONFIDENTIAL

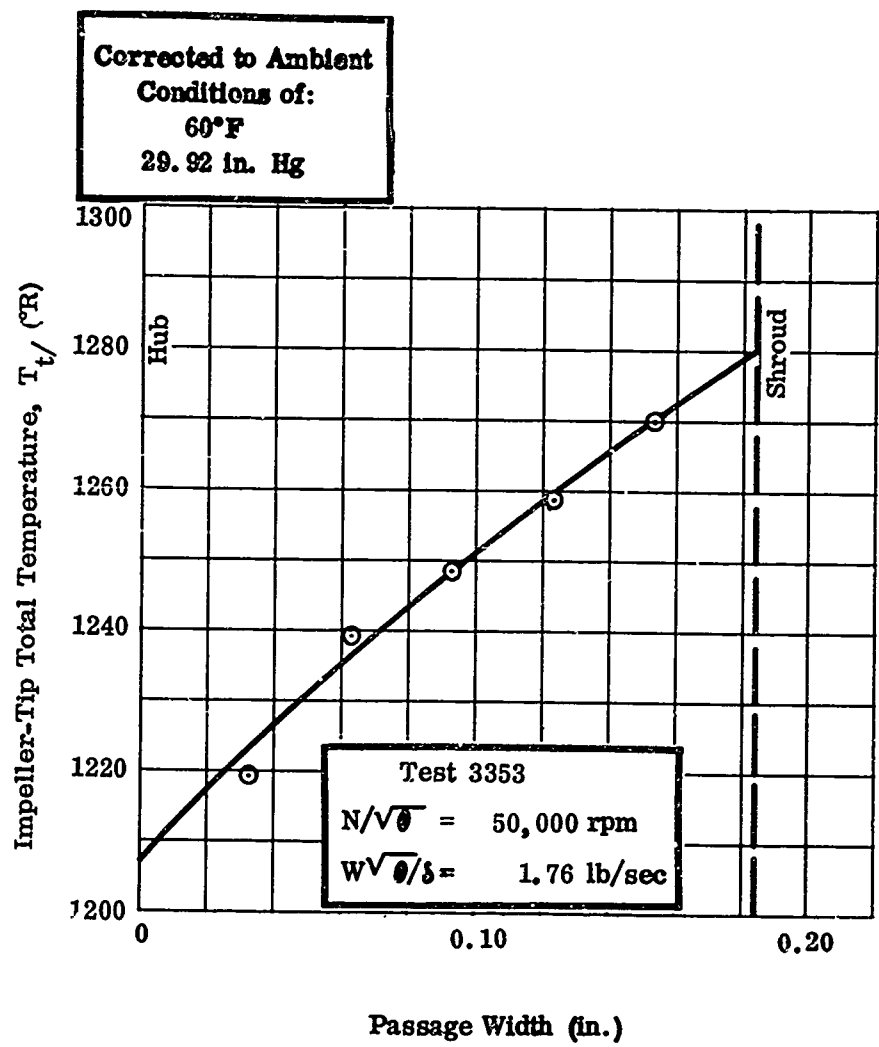


Figure 64. Impeller-Tip Total-Temperature Survey, RF-2.

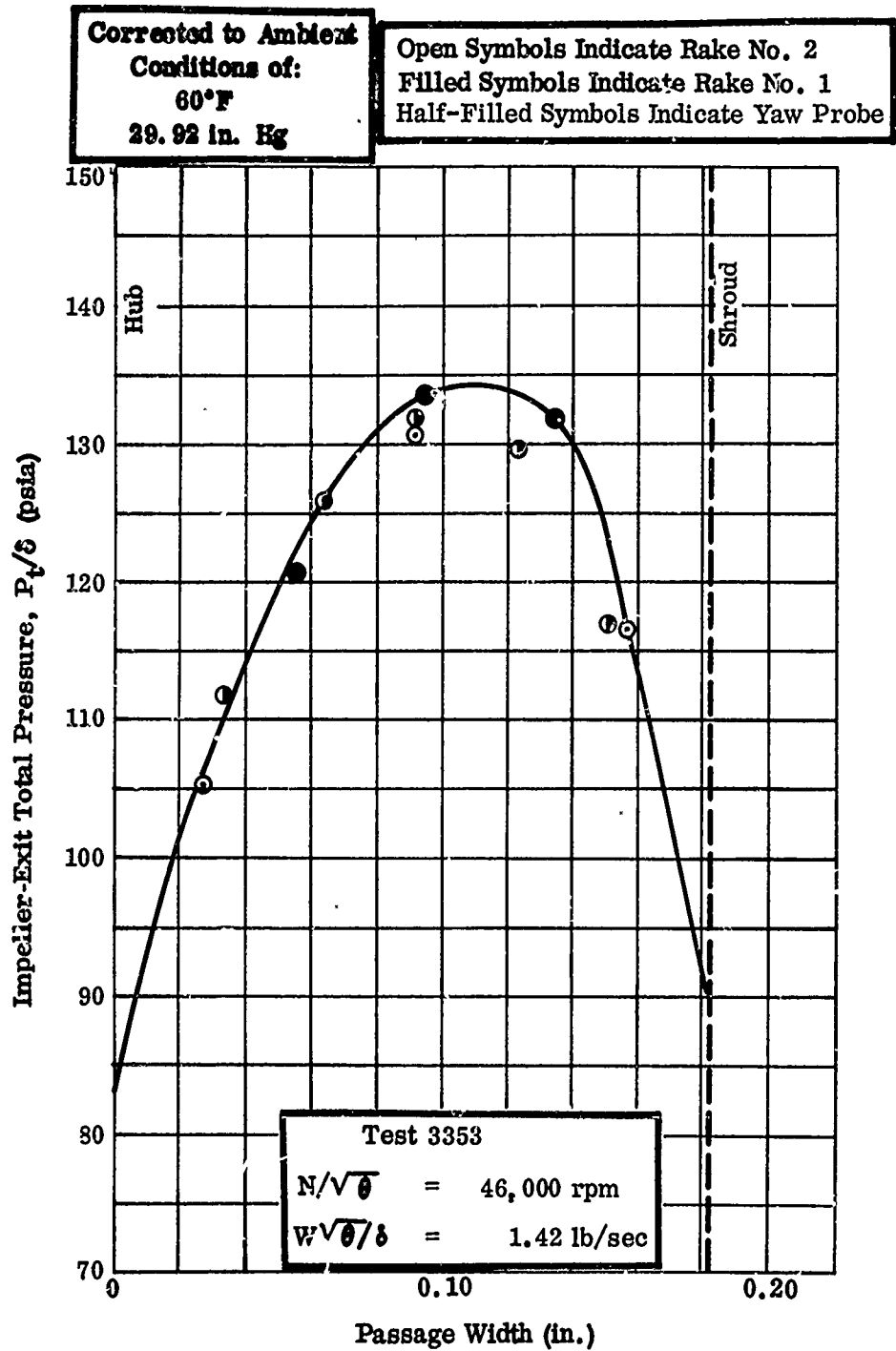


Figure 65. Impeller-Tip Total-Pressure Survey, RF-2.

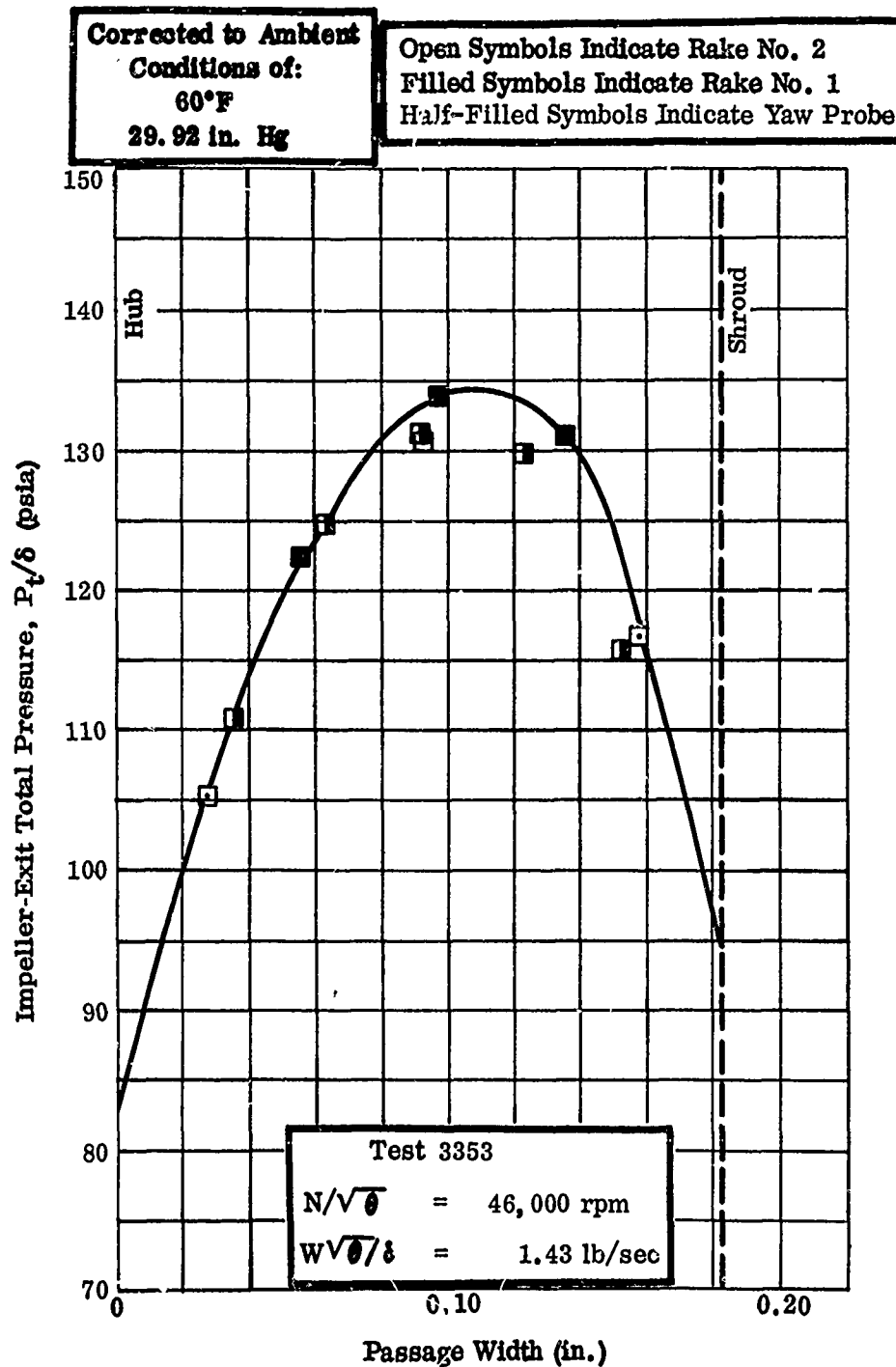


Figure 66. Impeller-Tip Total-Pressure Survey, RF-2.

CONFIDENTIAL

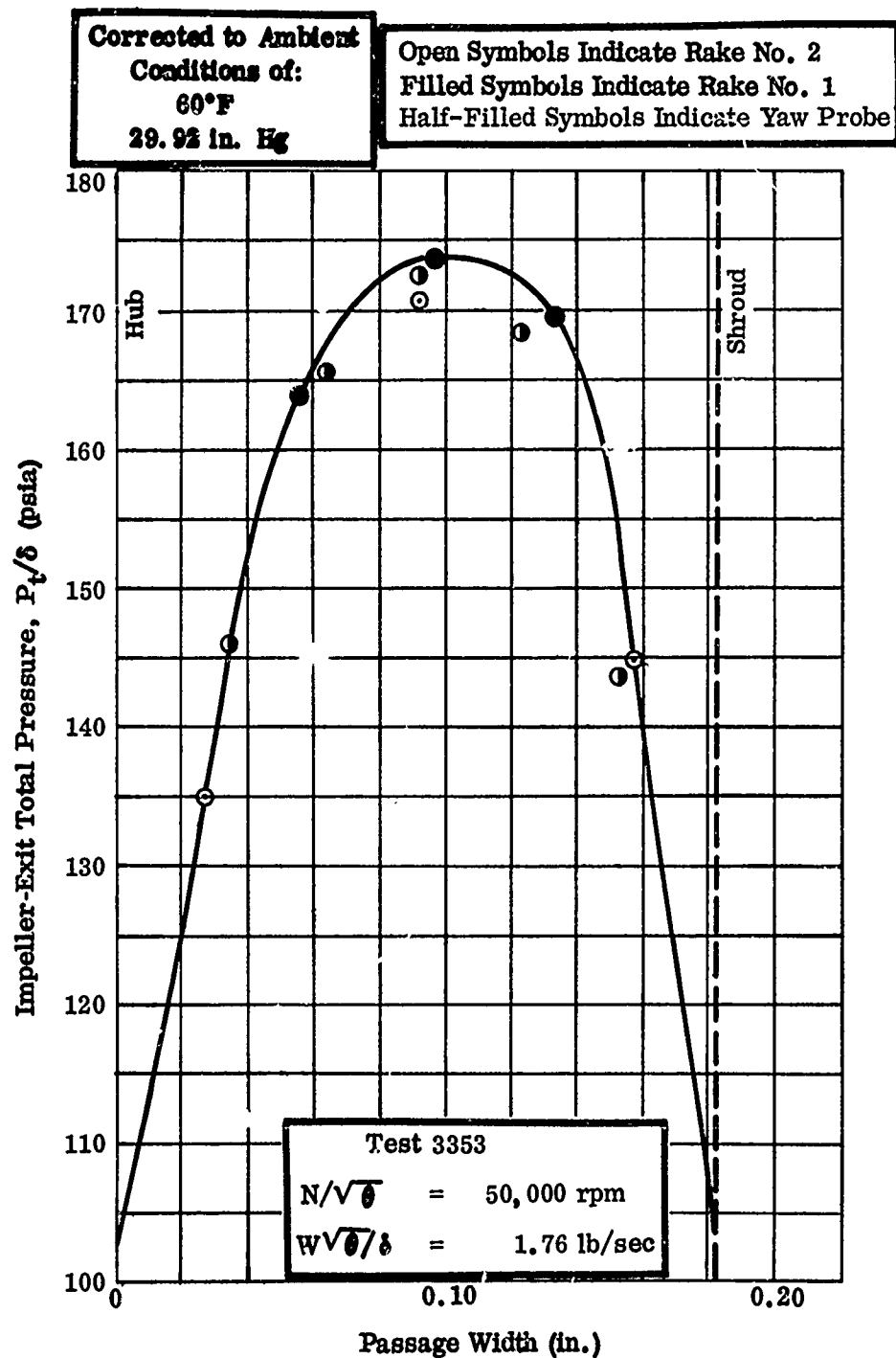


Figure 67. Impeller-Tip Total-Pressure Survey, RF-2.

CONFIDENTIAL

CONFIDENTIAL

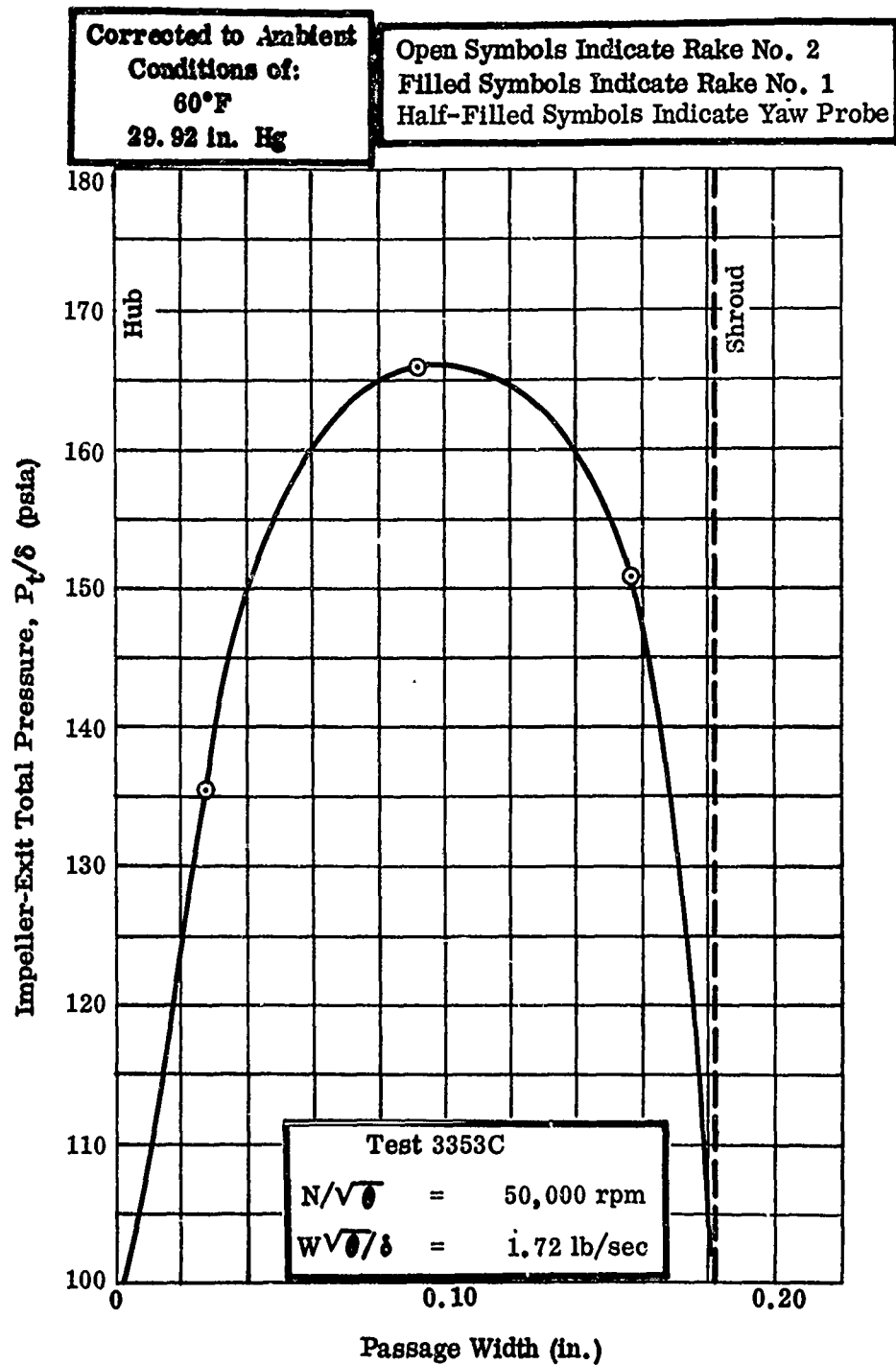


Figure 68. Impeller-Tip Total-Pressure Survey, RF-2.

CONFIDENTIAL

CONFIDENTIAL

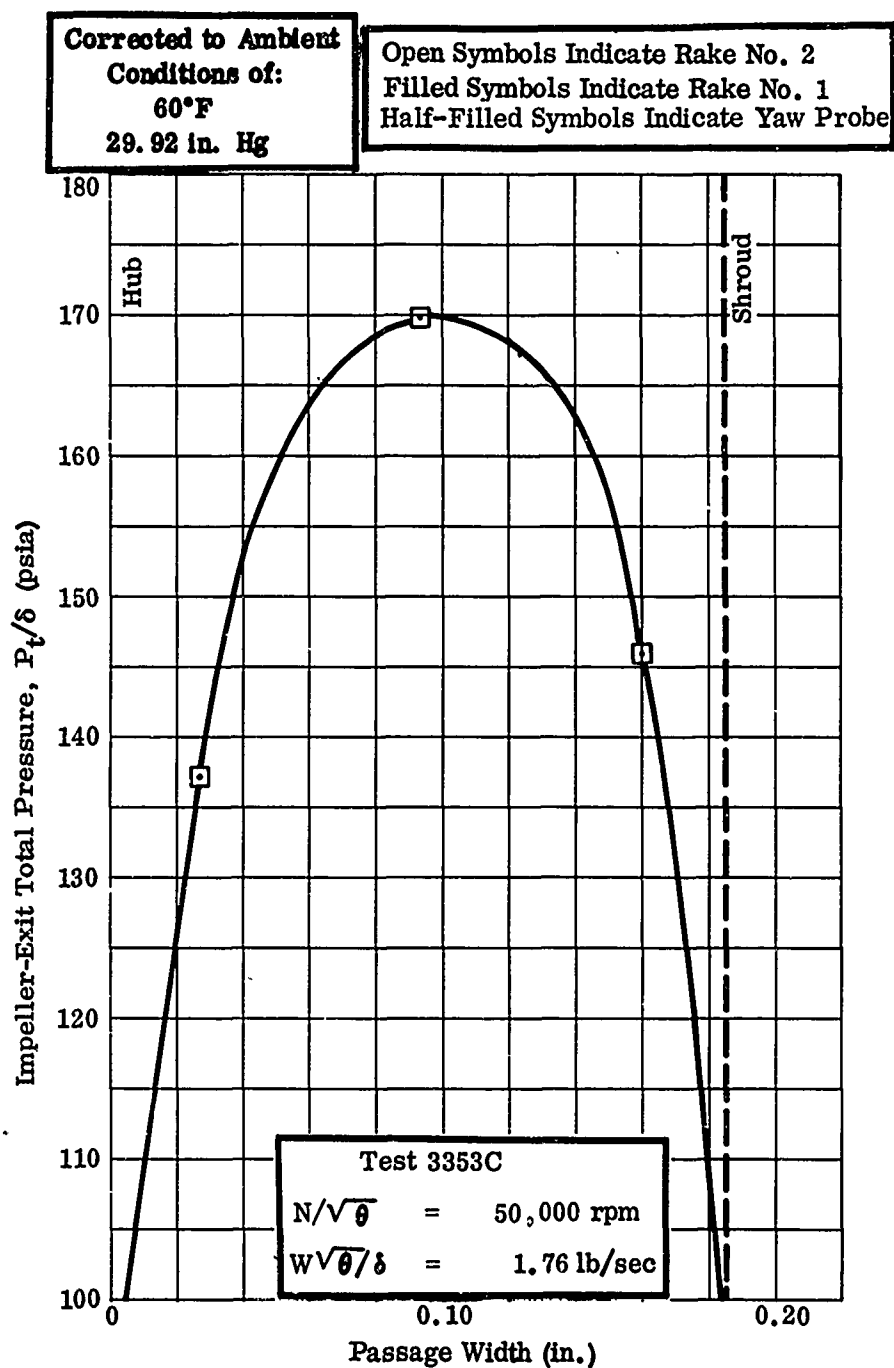


Figure 69. Impeller-Tip Total-Pressure Survey, RF-2.

CONFIDENTIAL

CONFIDENTIAL

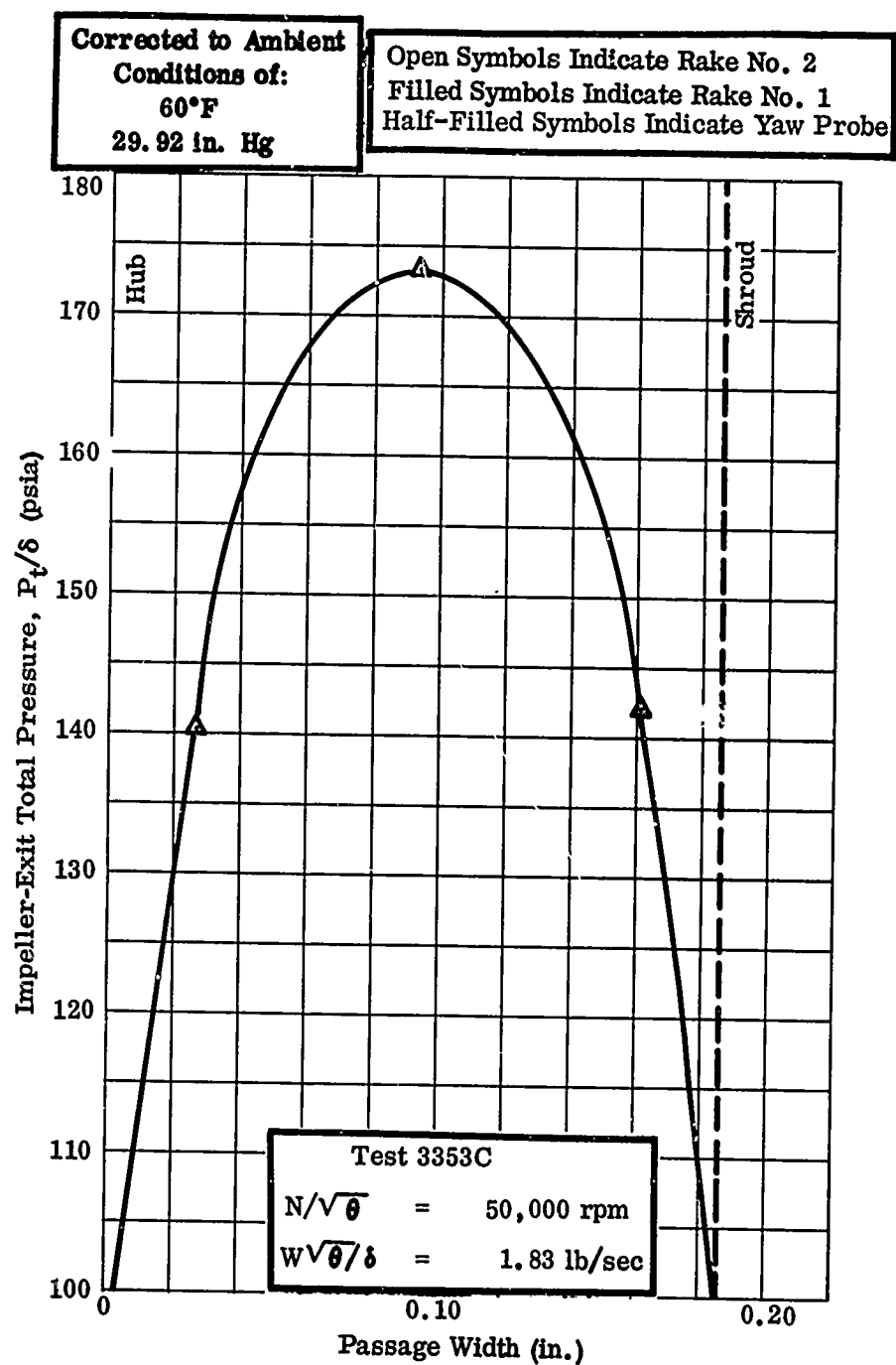


Figure 70. Impeller-Tip Total-Pressure Survey, RF-2.

CONFIDENTIAL

CONFIDENTIAL

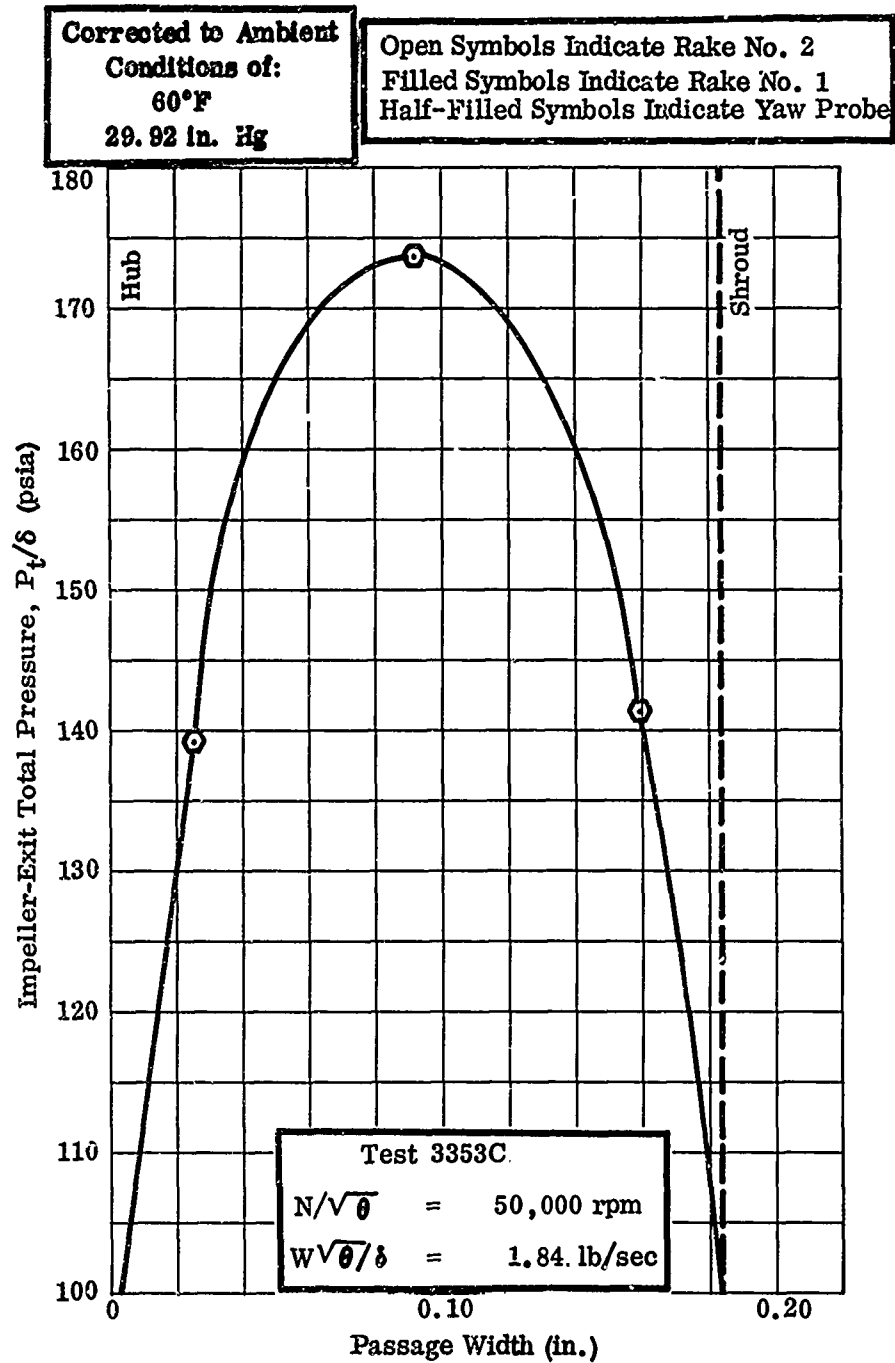


Figure 71. Impeller-Tip Total-Pressure Survey, RF-2.

CONFIDENTIAL

CONFIDENTIAL

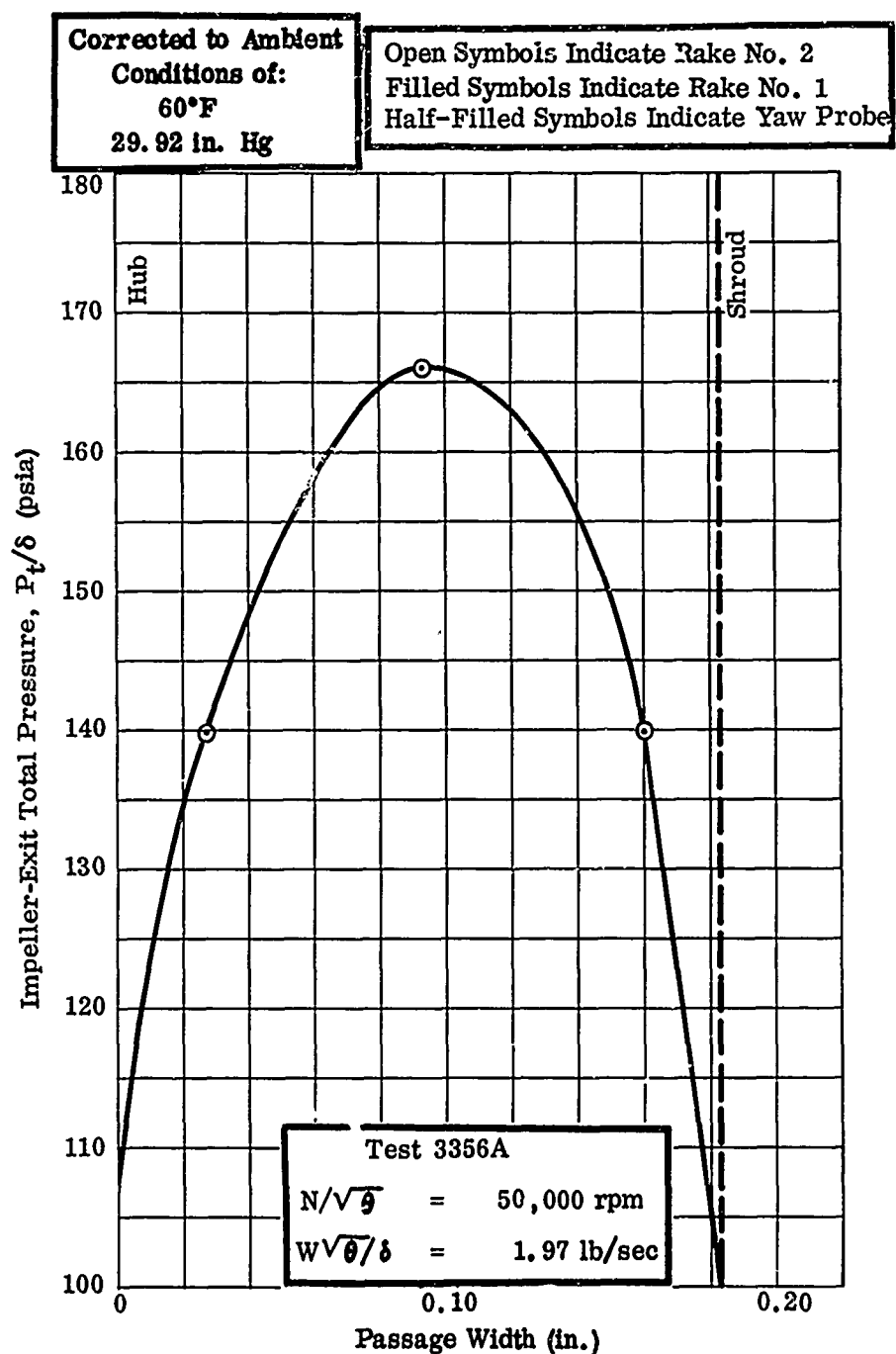


Figure 72. Impeller-Tip Total-Pressure Survey, RF-2.

CONFIDENTIAL

CONFIDENTIAL

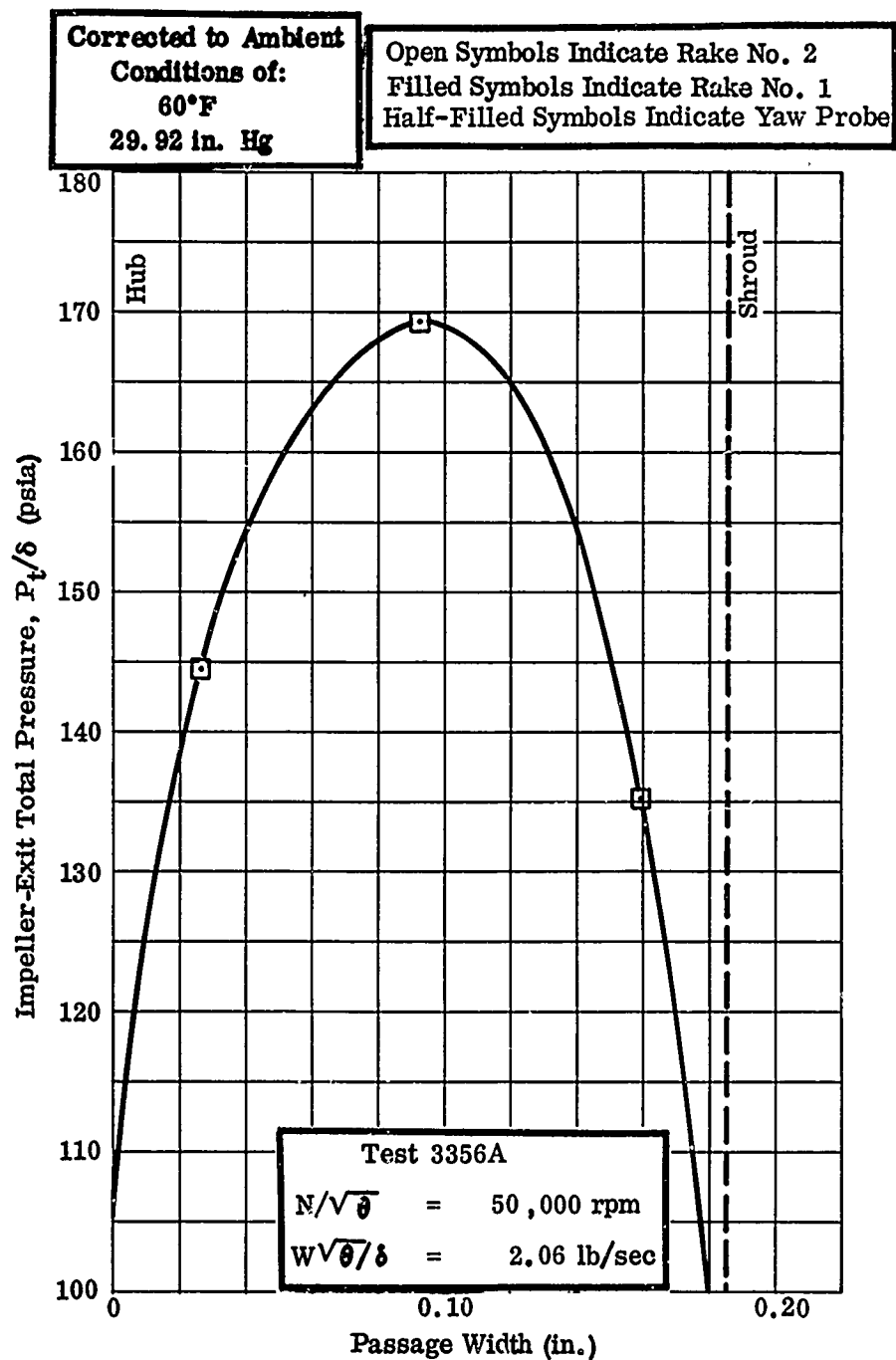


Figure 73. Impeller-Tip Total-Pressure Survey, RF-2.

CONFIDENTIAL

CONFIDENTIAL

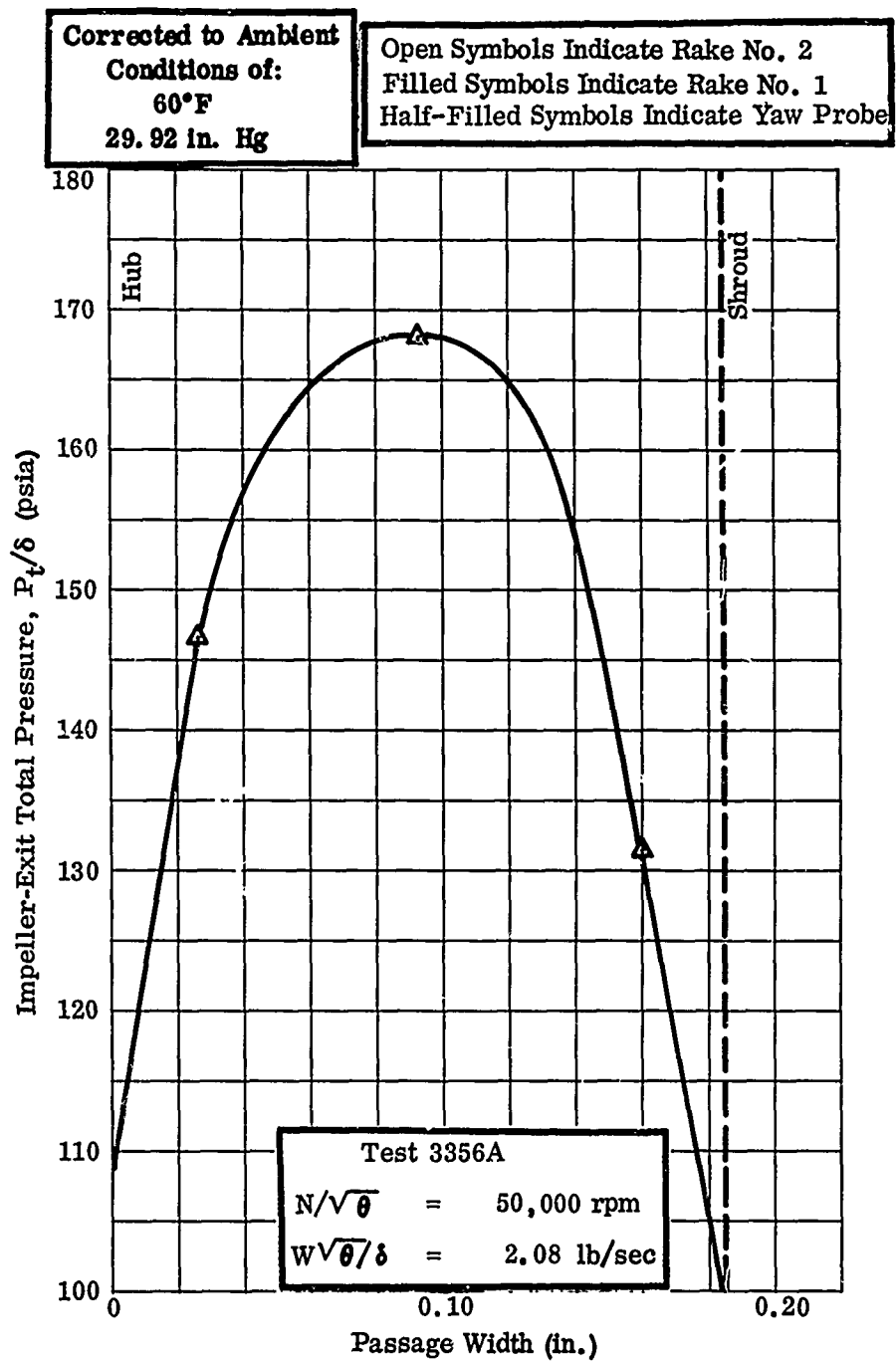


Figure 74. Impeller-Tip Total-Pressure Survey, RF-2.

CONFIDENTIAL

CONFIDENTIAL

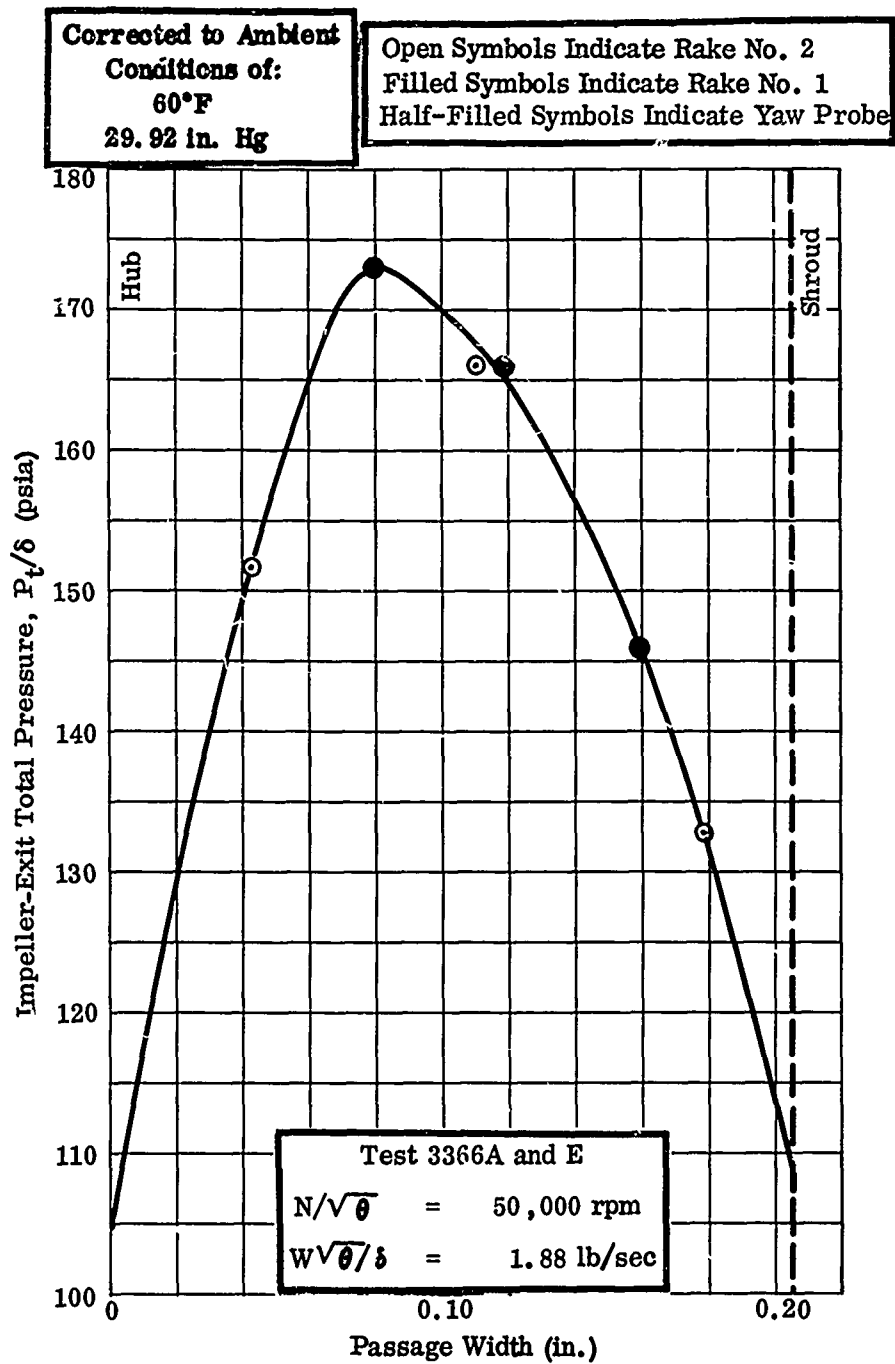


Figure 75. Impeller-Tip Total-Pressure Survey, RF-2.

100

CONFIDENTIAL

CONFIDENTIAL

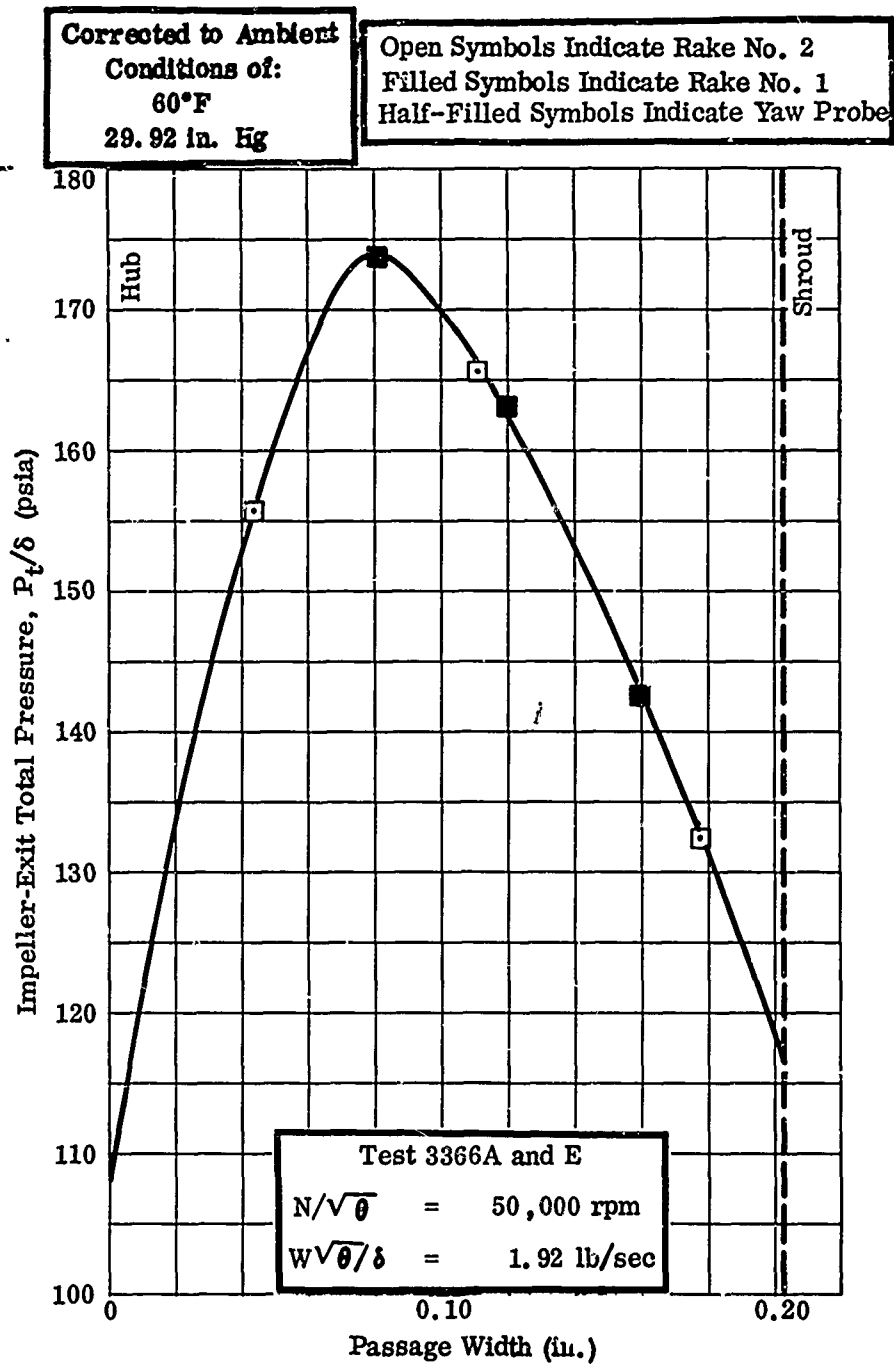


Figure 76. Impeller-Tip Total-Pressure Survey, RF-2.

CONFIDENTIAL

Corrected to Ambient
Conditions of:
60°F
29.92 in. Hg

Open Symbols Indicate Rake No. 2
Filled Symbols Indicate Rake No. 1
Half-Filled Symbols Indicate Yaw Probe

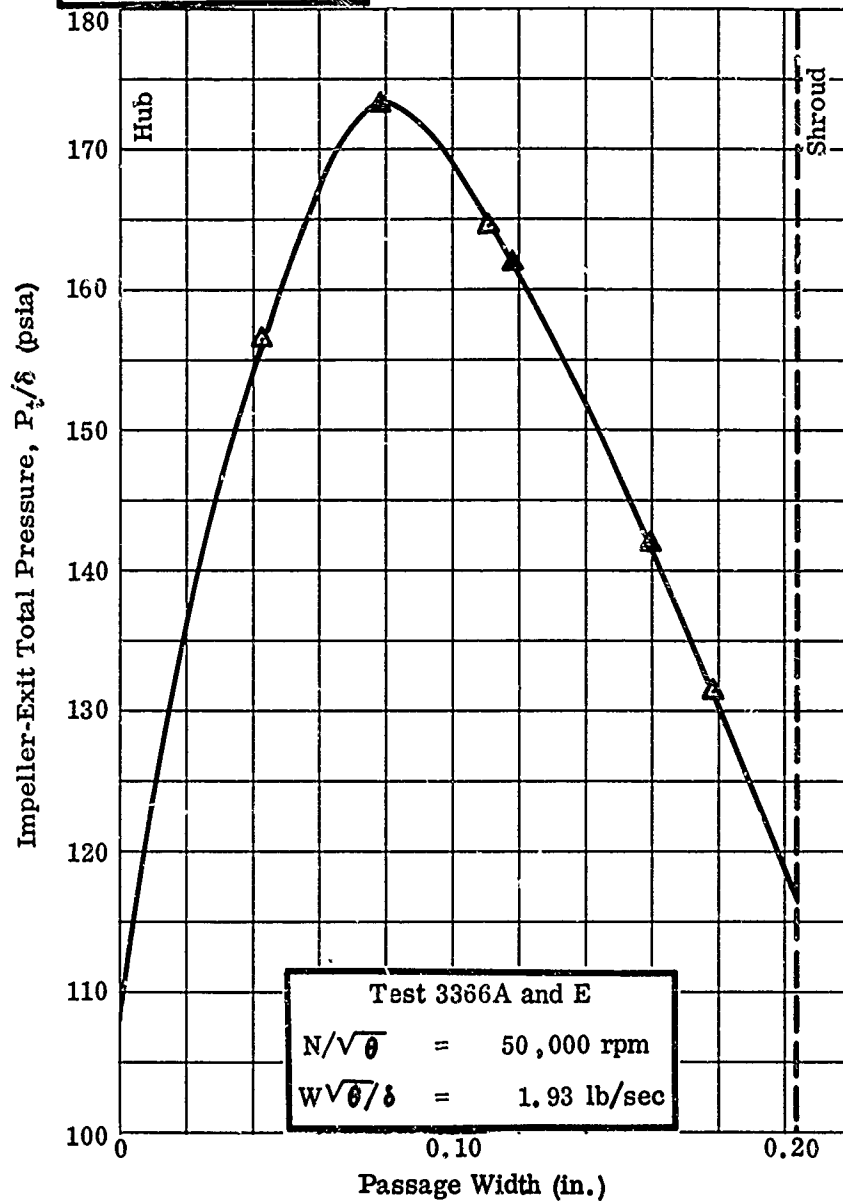


Figure 77. Impeller-Tip Total-Pressure Survey, RF-2.

CONFIDENTIAL

Corrected to Ambient
Conditions of:
60°F
29.92 in. Hg

Open Symbols Indicate Rake No. 2
Filled Symbols Indicate Rake No. 1
Half-Filled Symbols Indicate Yaw Probe

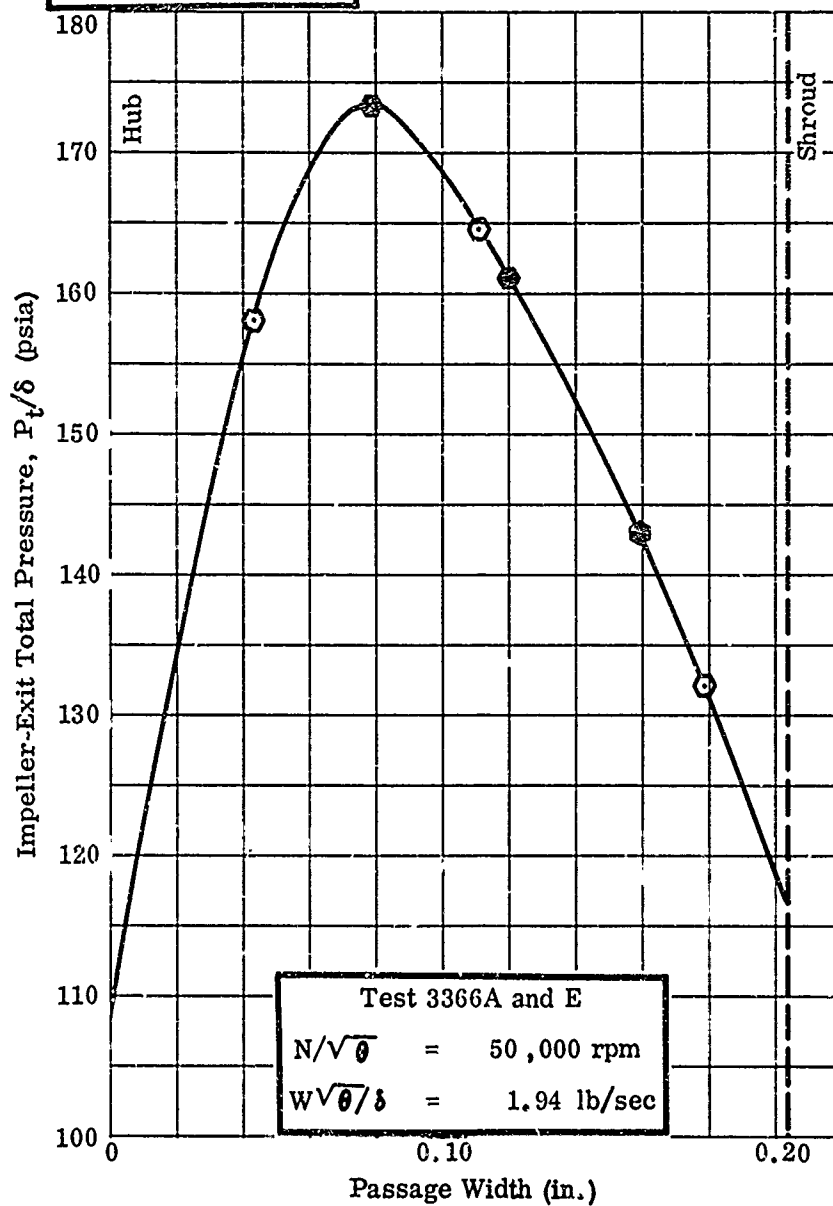


Figure 78. Impeller-Tip Total-Pressure Survey, RF-2.

CONFIDENTIAL

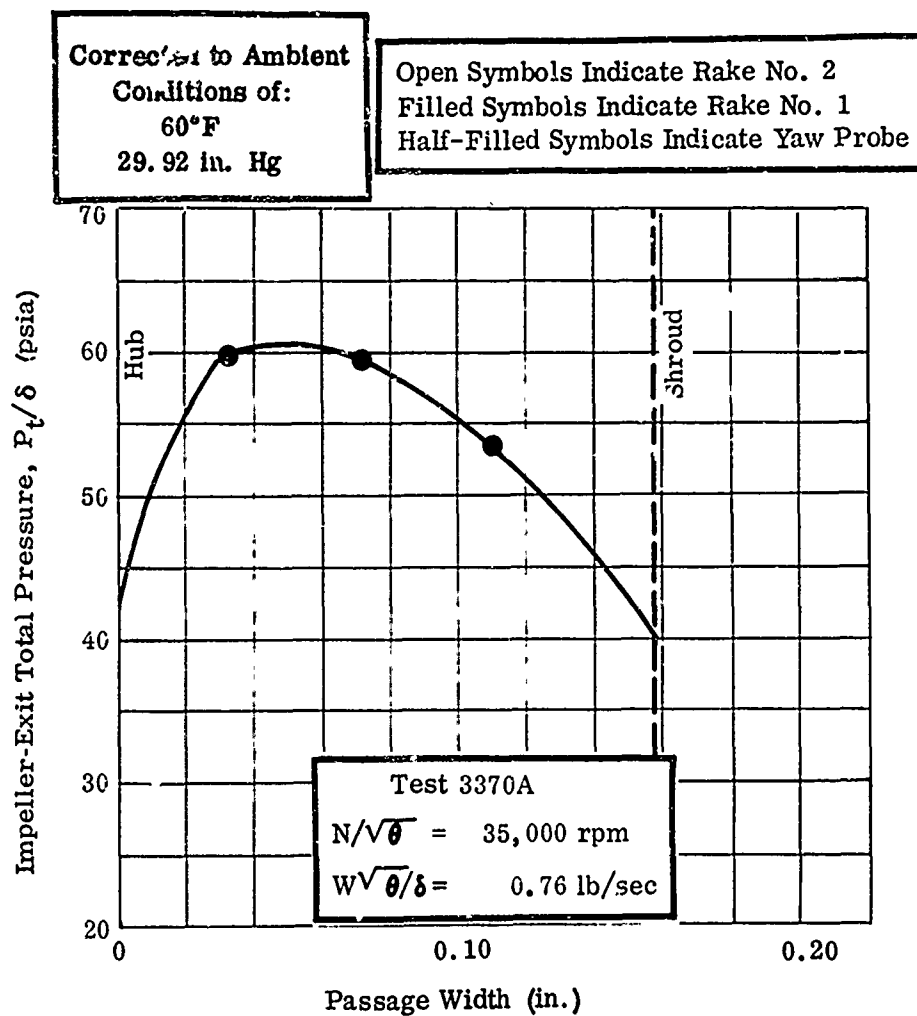


Figure 79. Impeller-Tip Total-Pressure Survey, RF-2.

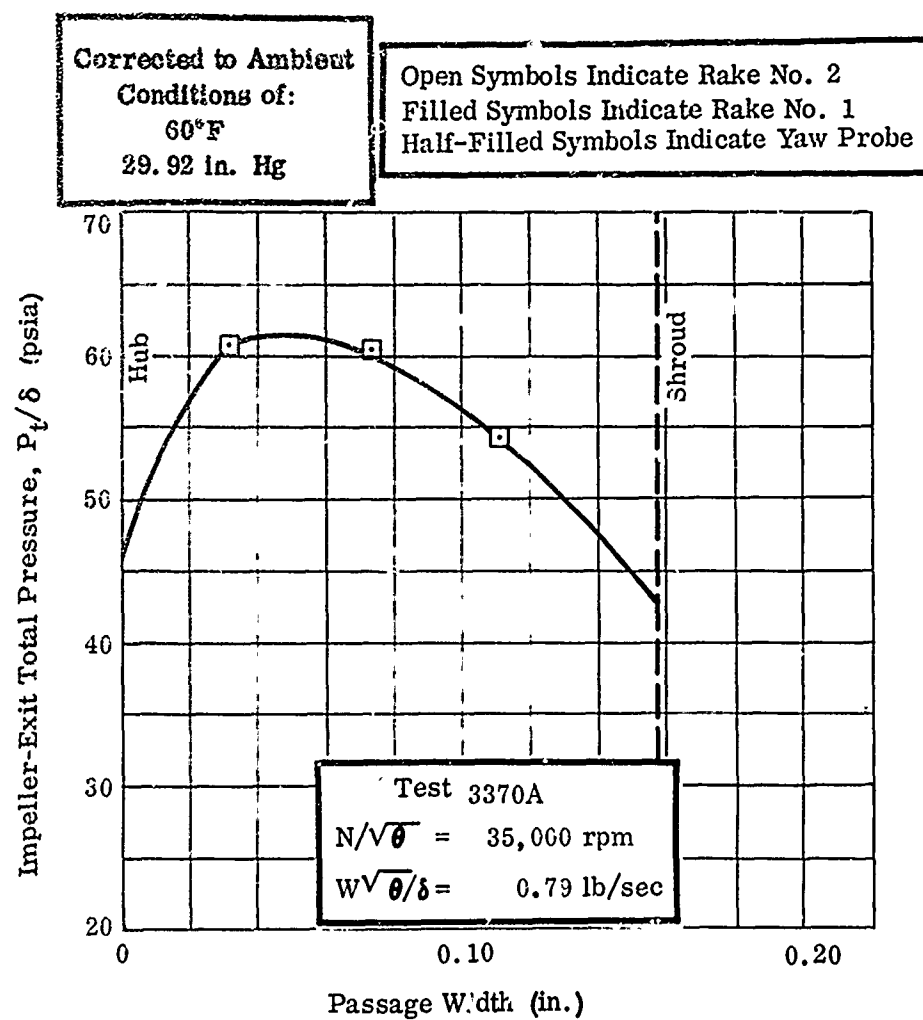


Figure 80. Impeller-Tip Total-Pressure Survey, RF-2.

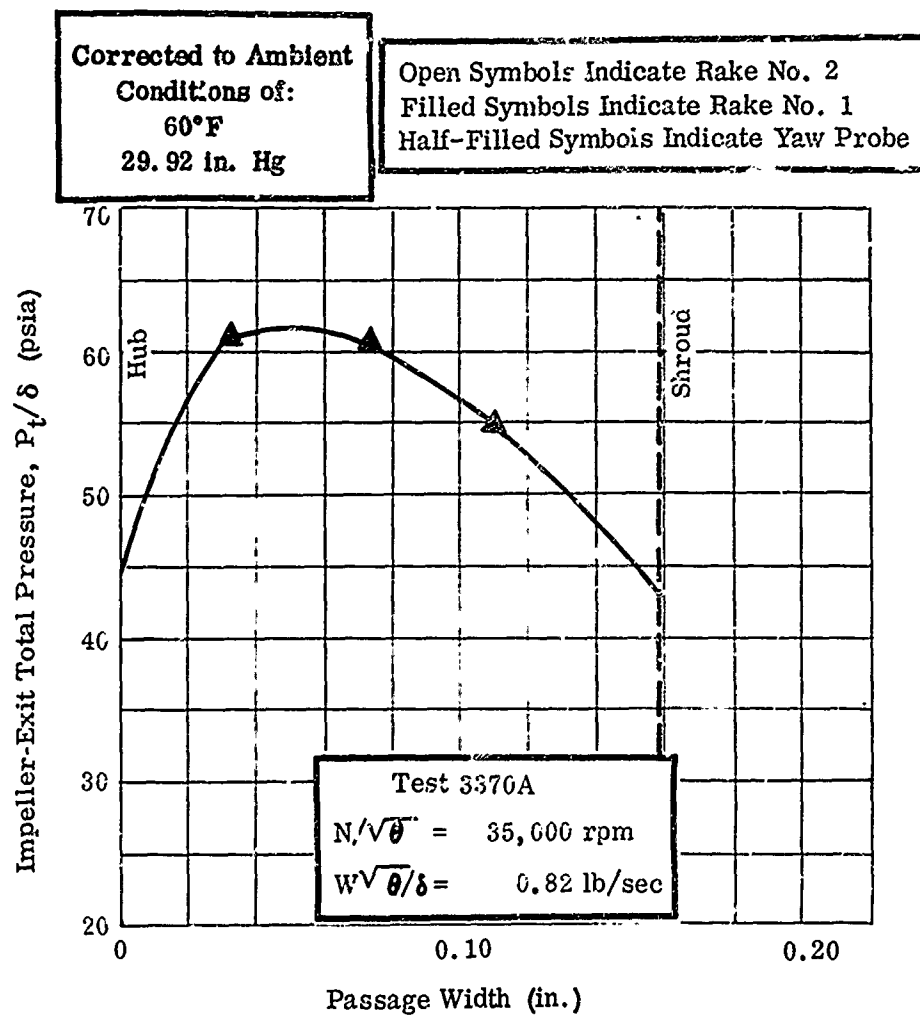


Figure 81. Impeller-Tip Total-Pressure Survey, RF-2.

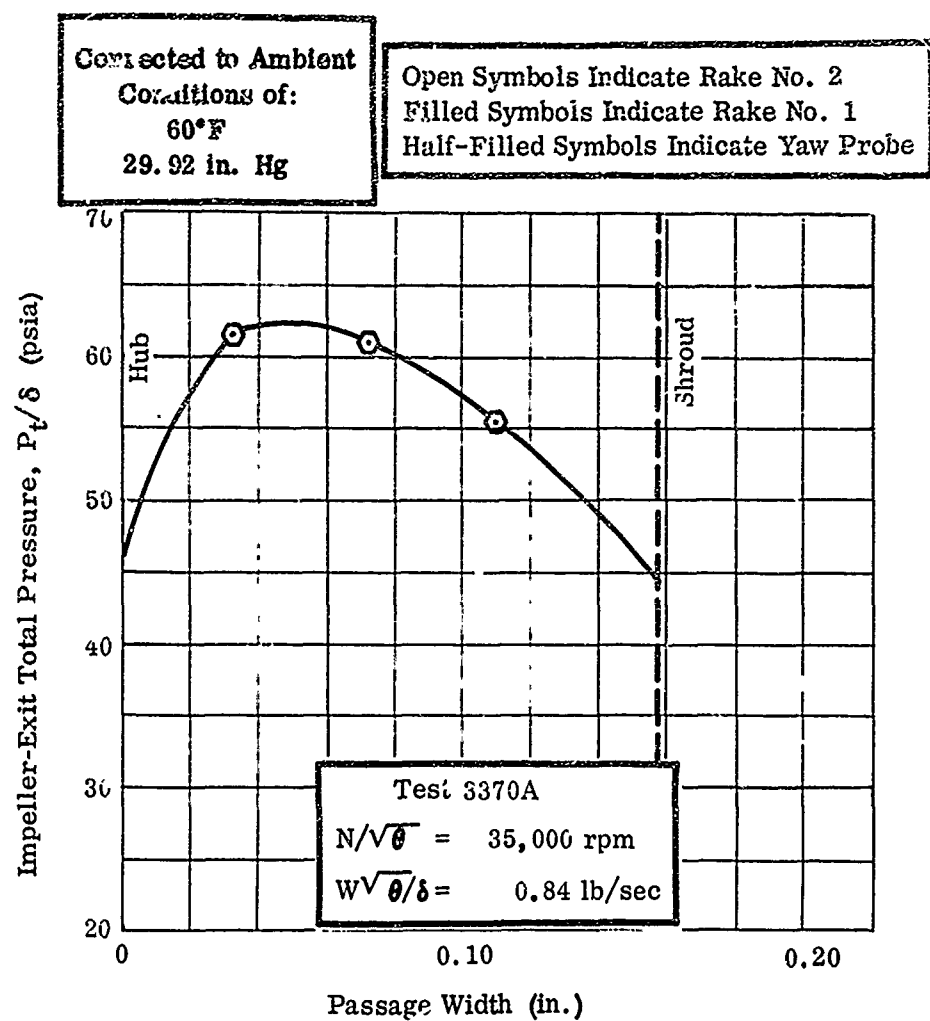


Figure 82. Impeller-Tip Total-Pressure Survey, RF-2.

CONFIDENTIAL

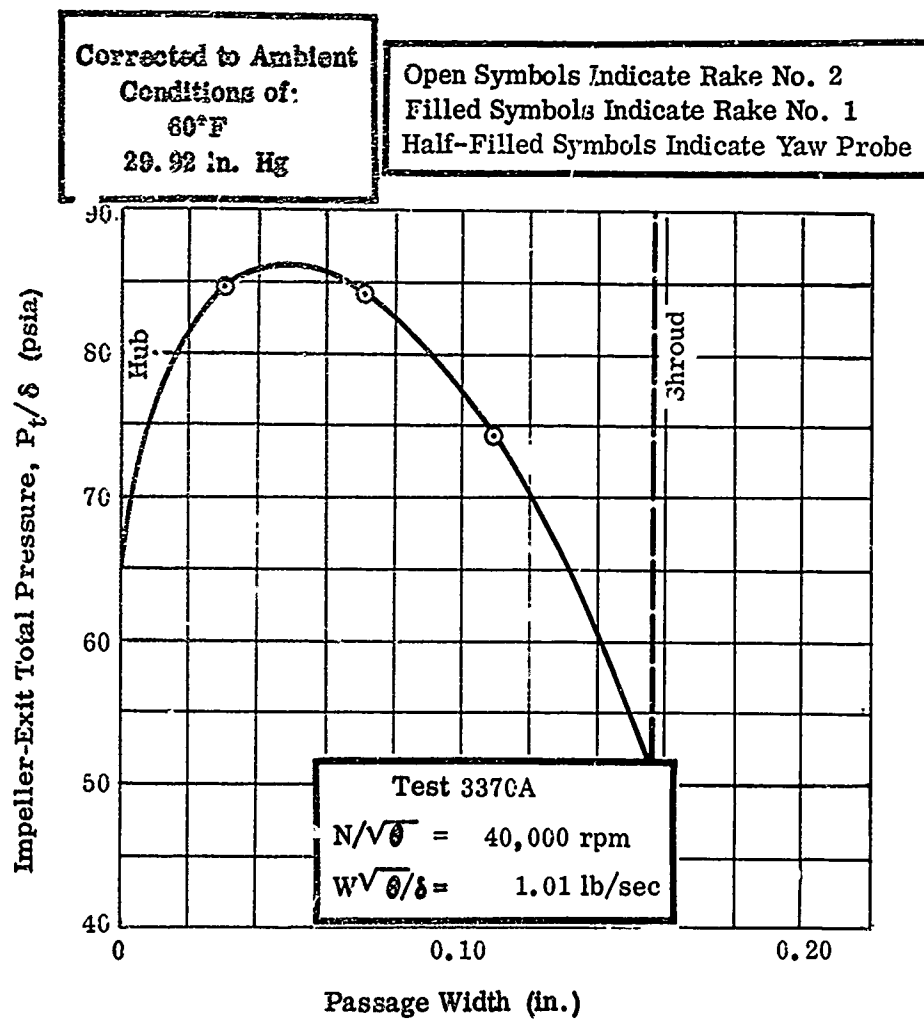


Figure 83. Impeller-Tip Total-Pressure Survey, RF-2.

CONFIDENTIAL

CONFIDENTIAL

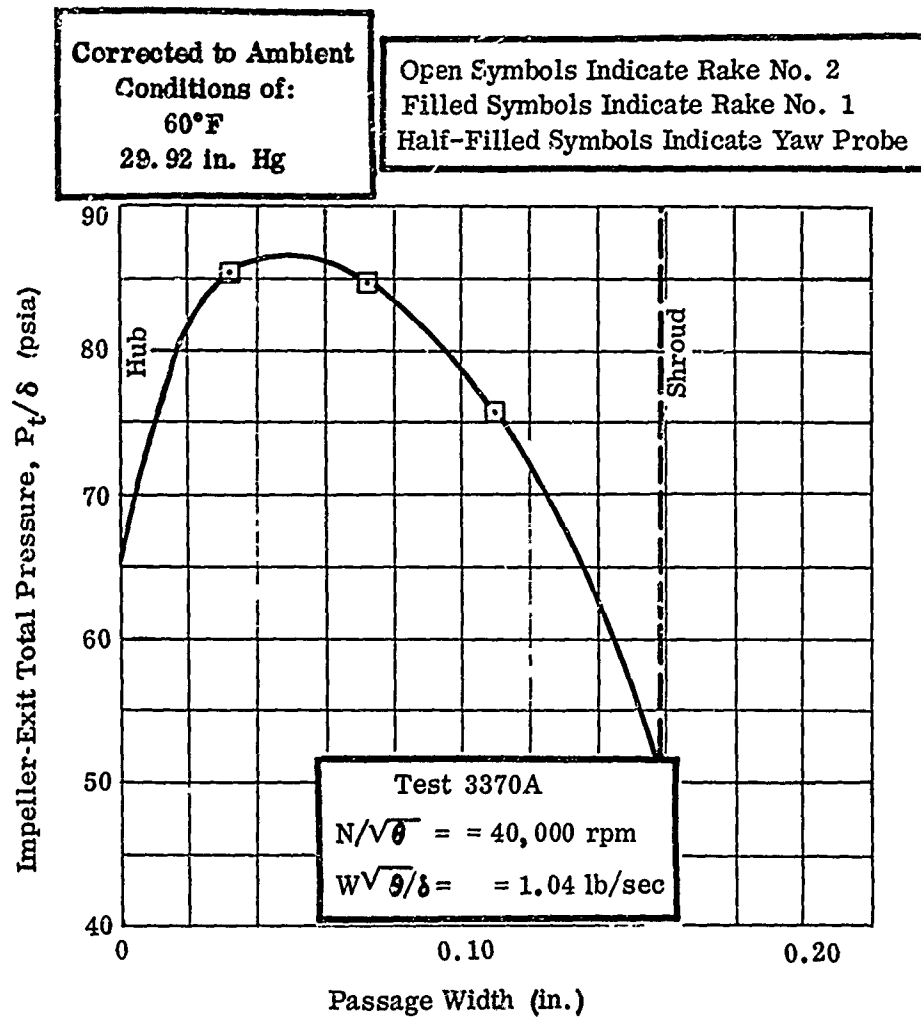


Figure 84. Impeller-Tip Total-Pressure Survey, RF-2.

CONFIDENTIAL

CONFIDENTIAL

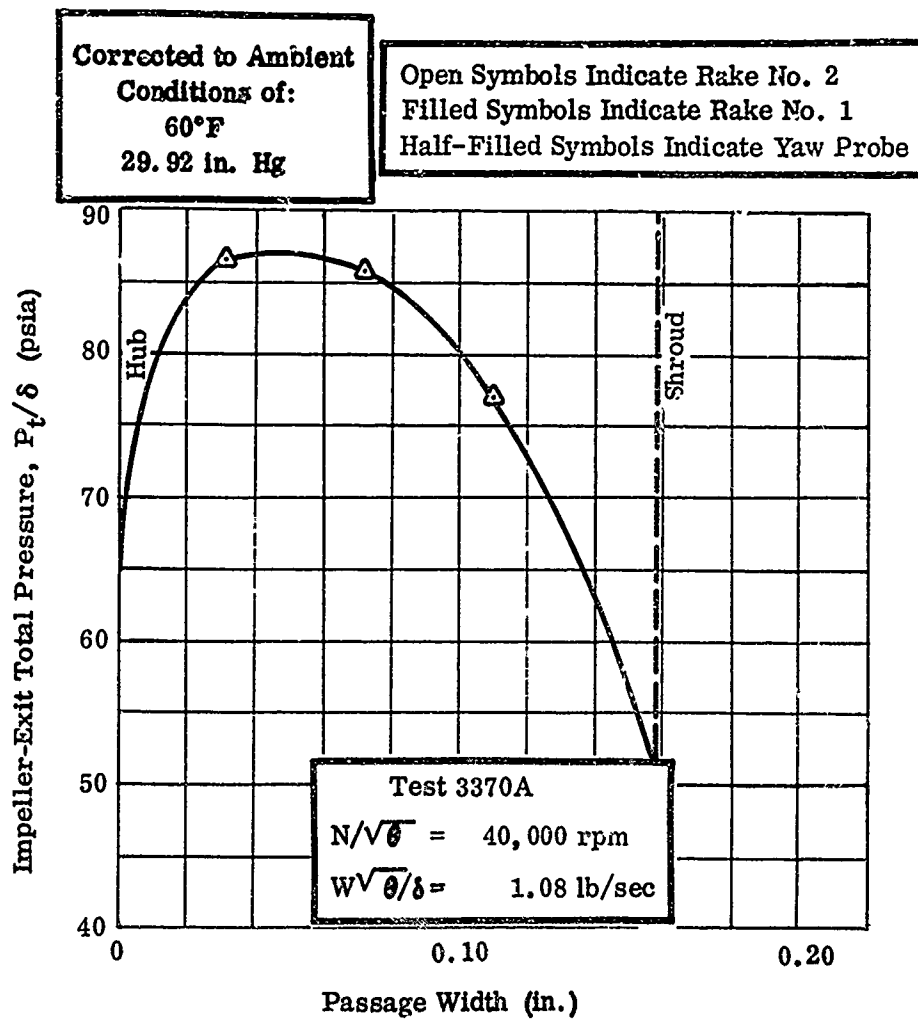


Figure 85. Impeller-Tip Total-Pressure Survey, RF-2.

CONFIDENTIAL

CONFIDENTIAL

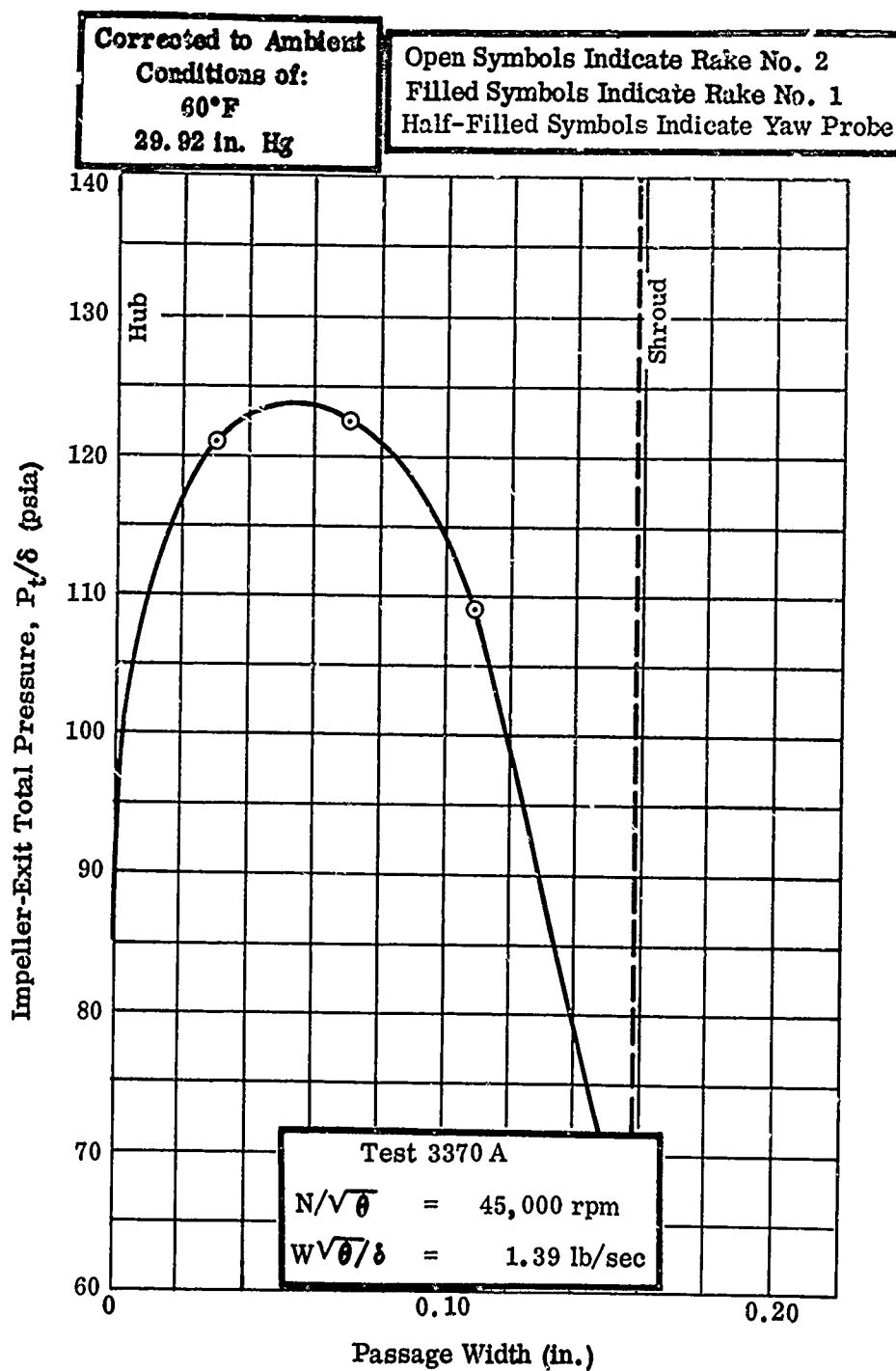


Figure 86. Impeller-Tip Total-Pressure Survey, RF-2.

CONFIDENTIAL

CONFIDENTIAL

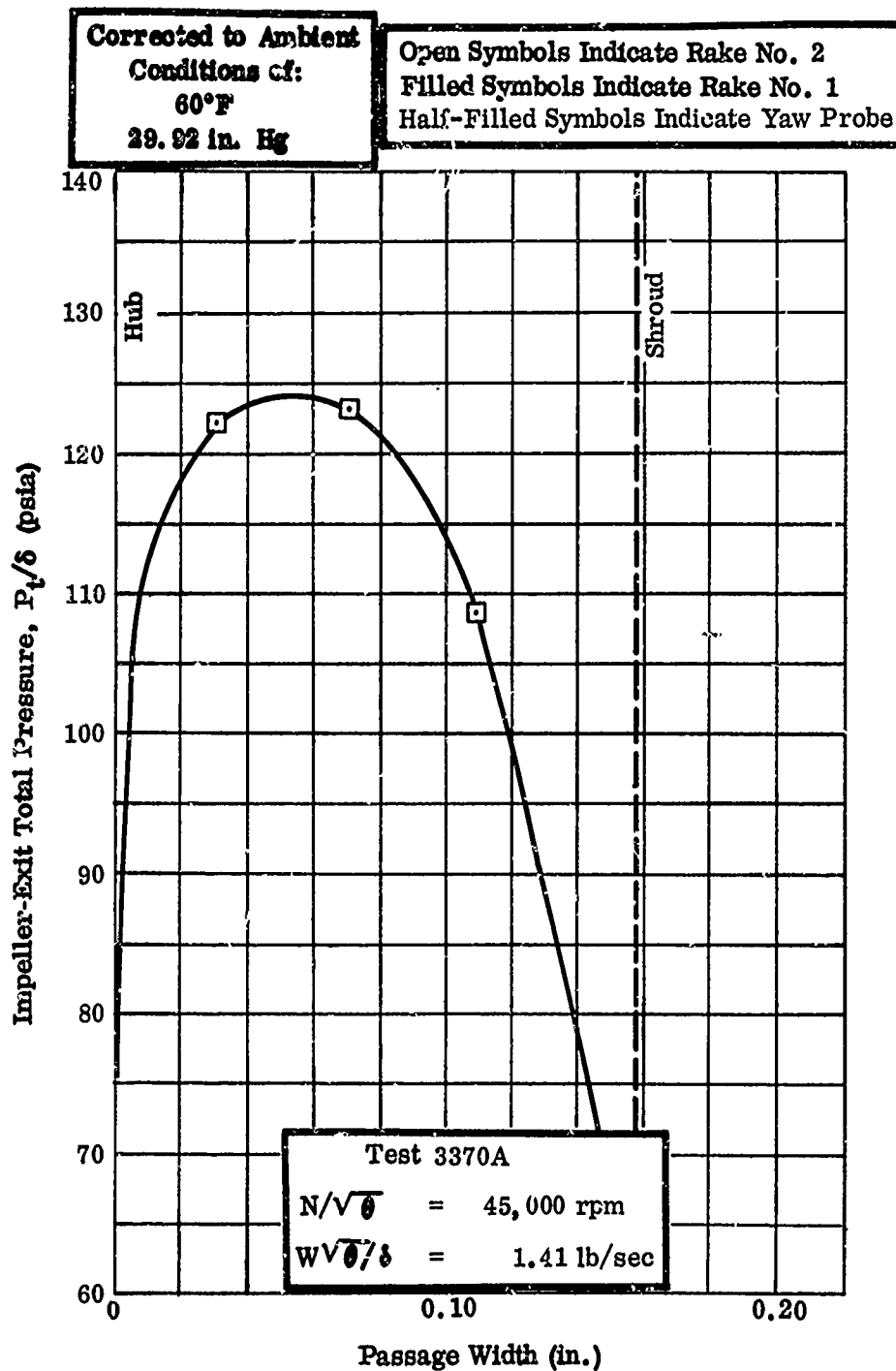


Figure 87. Impeller-Tip Total-Pressure Survey, RF-2.

CONFIDENTIAL

CONFIDENTIAL

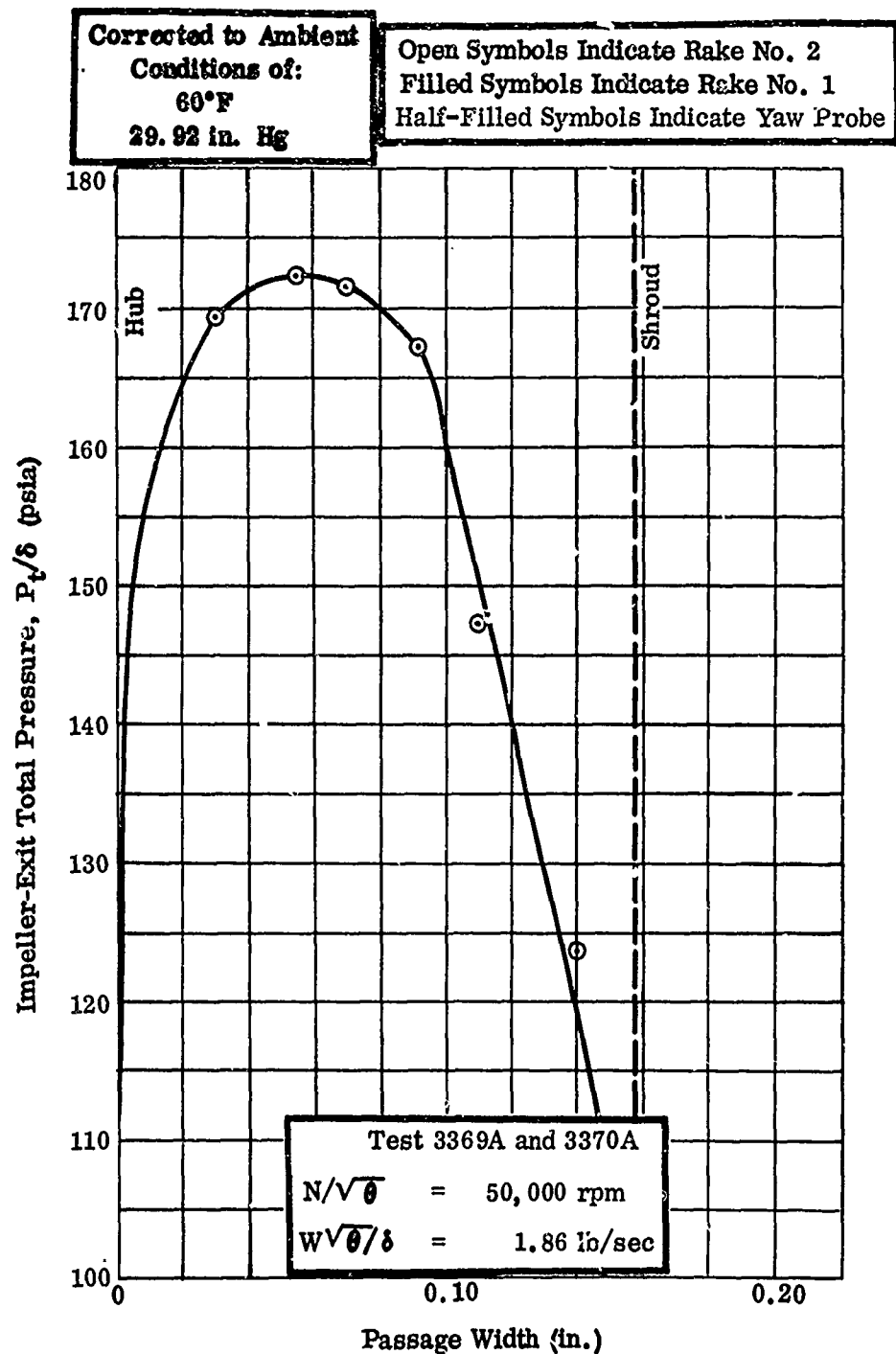


Figure 88. Impeller-Tip Total-Pressure Survey, RF-2.

CONFIDENTIAL

CONFIDENTIAL

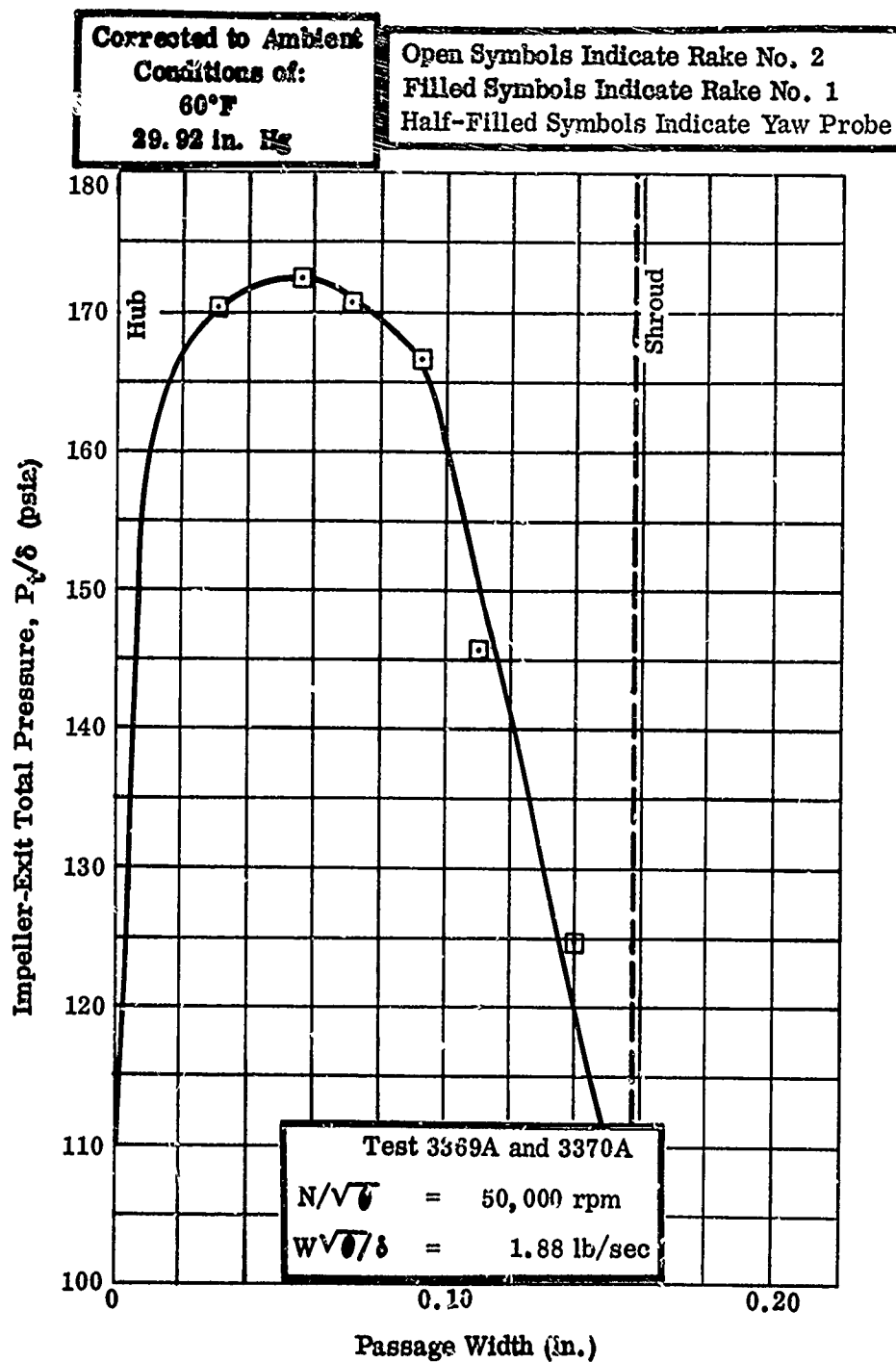


Figure 89. Impeller-Tip Total-Pressure Survey, RF-2.

CONFIDENTIAL

CONFIDENTIAL

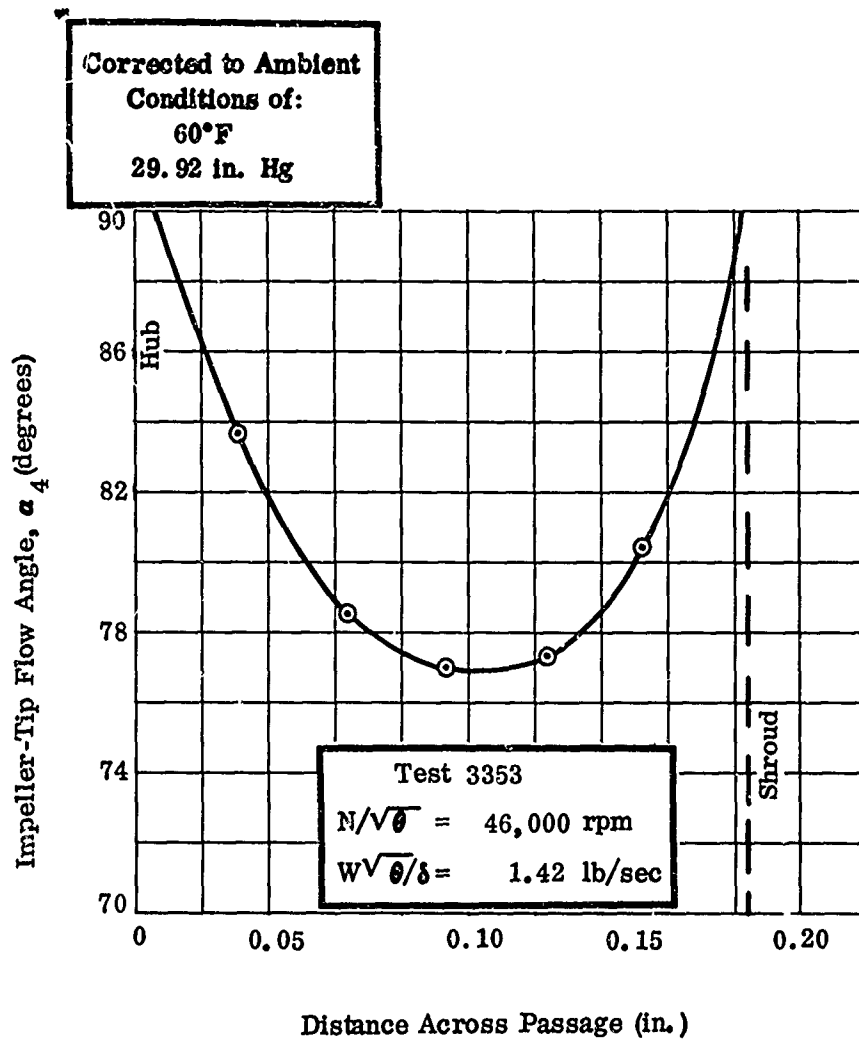


Figure 90. Impeller-Tip Flow-Angle Survey, RF-2.

CONFIDENTIAL

CONFIDENTIAL

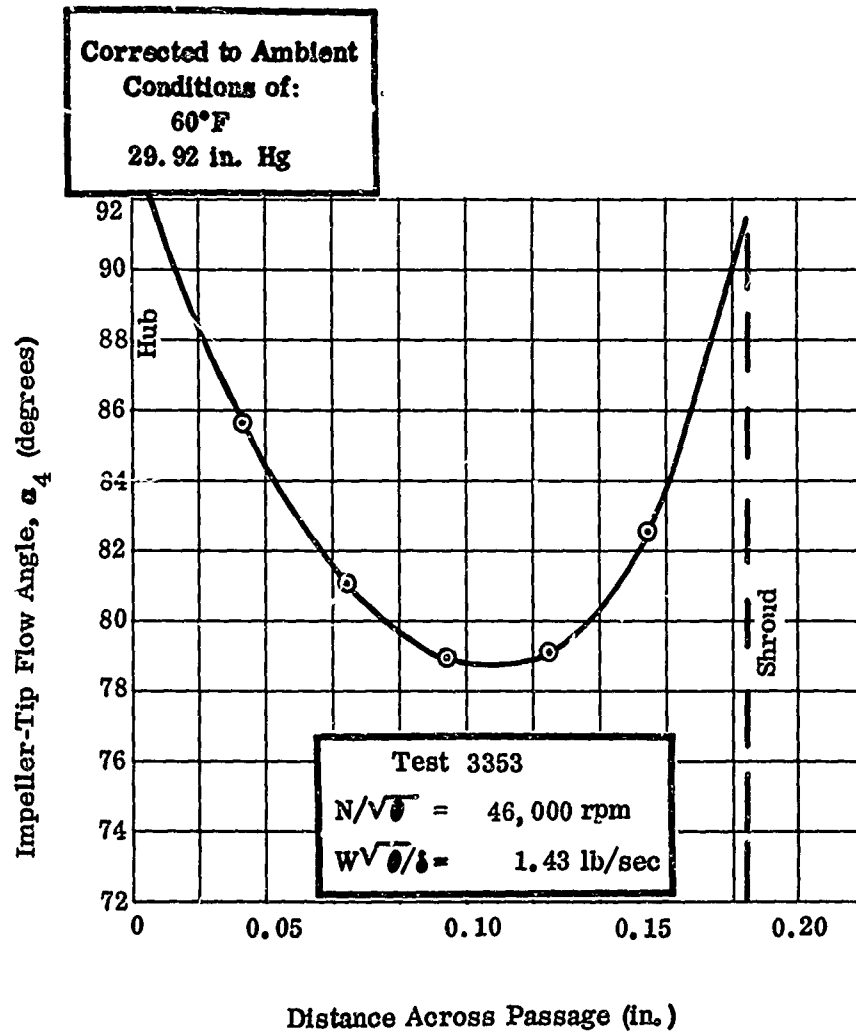


Figure 91. Impeller-Tip Flow-Angle Survey, RF-2.

CONFIDENTIAL

CONFIDENTIAL

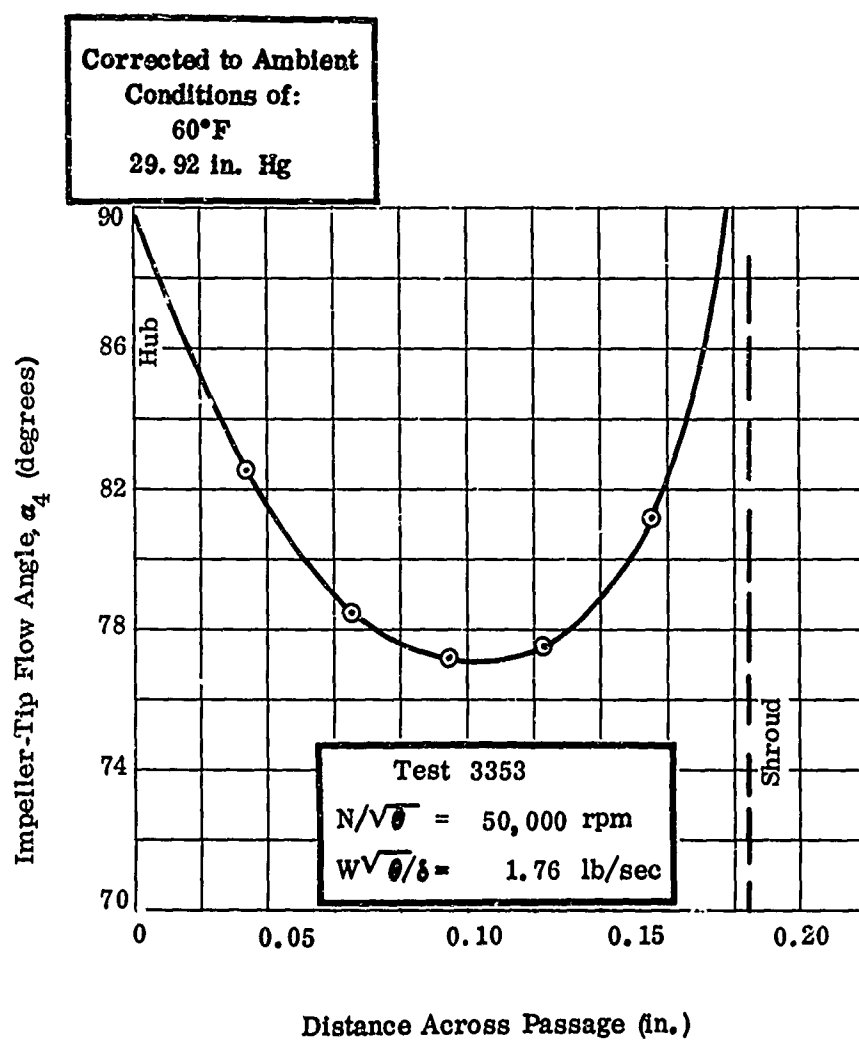


Figure 92. Impeller-Tip Flow-Angle Survey, RF-2.

CONFIDENTIAL

CONFIDENTIAL

Corrected to Ambient
Conditions of:
60°F
29.92 in. Hg

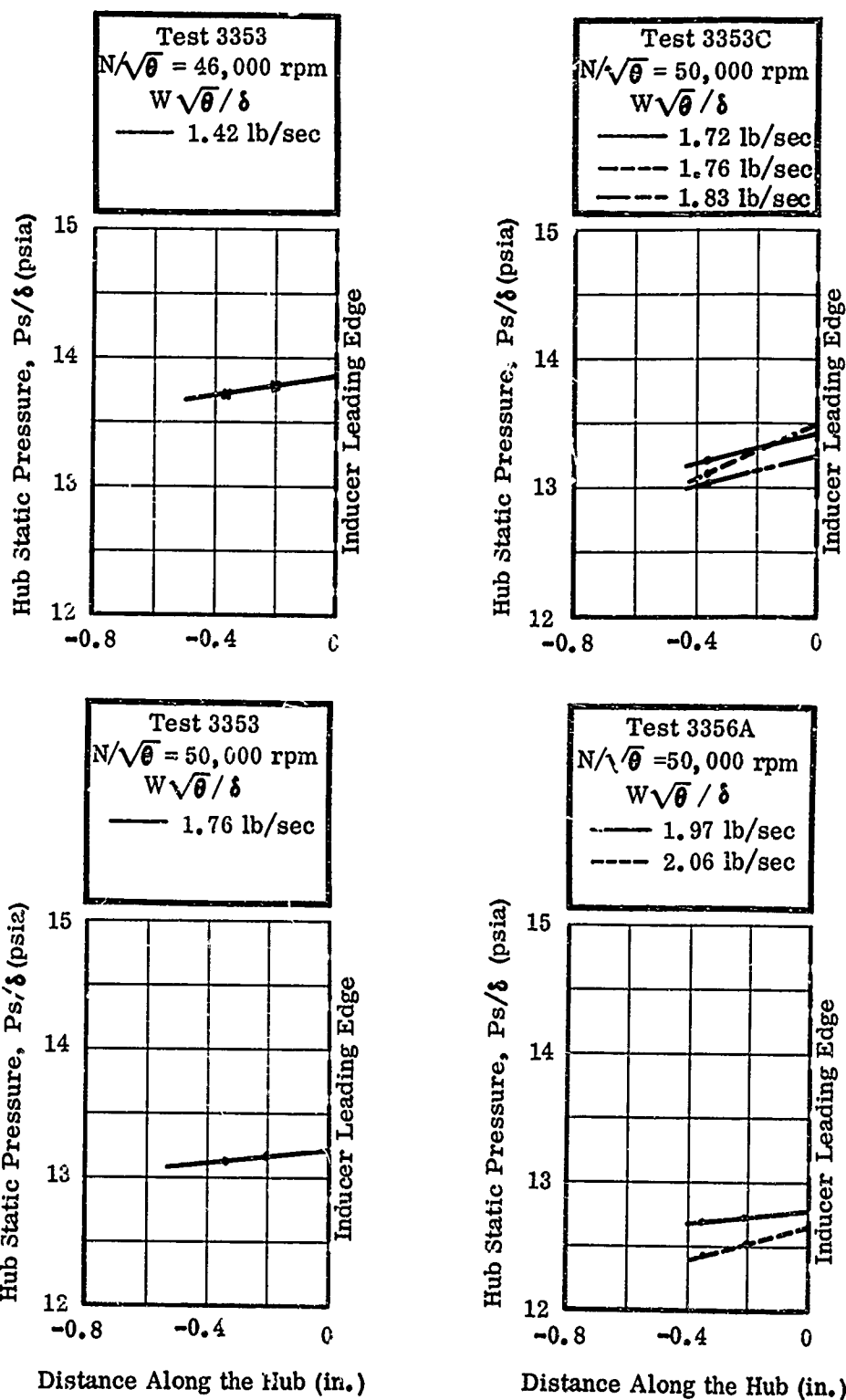
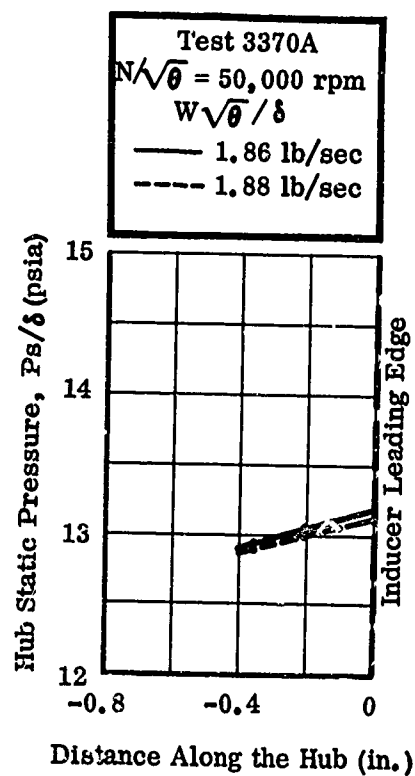
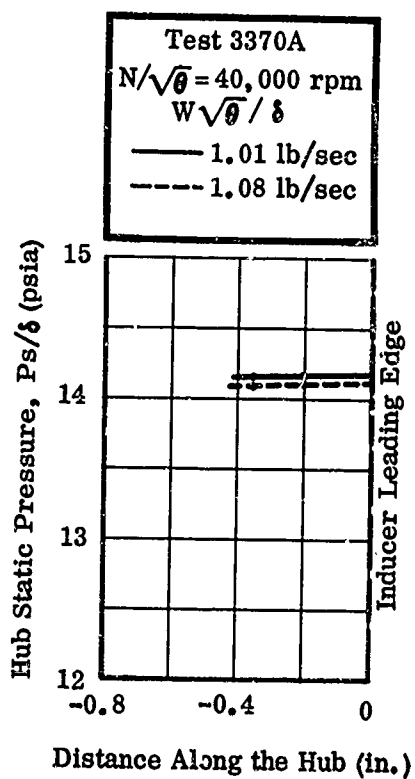
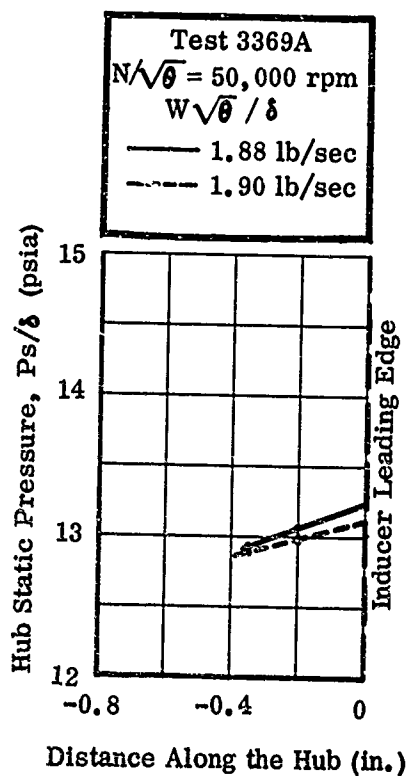
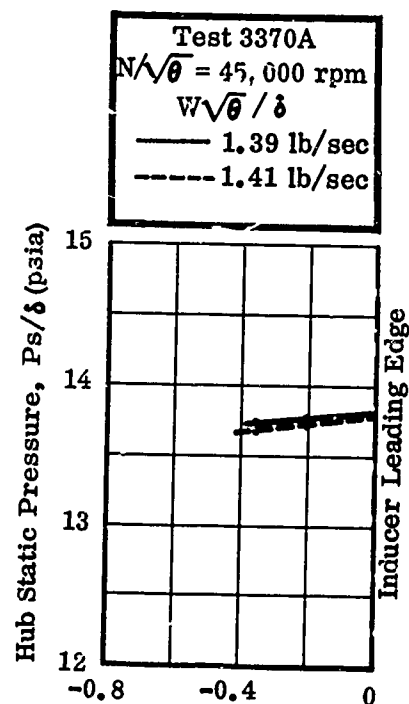
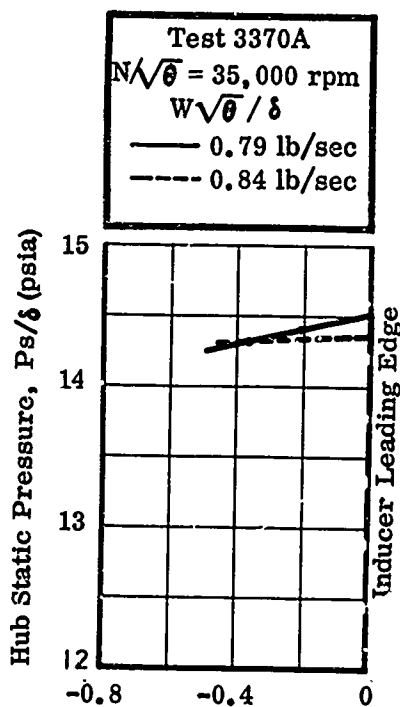
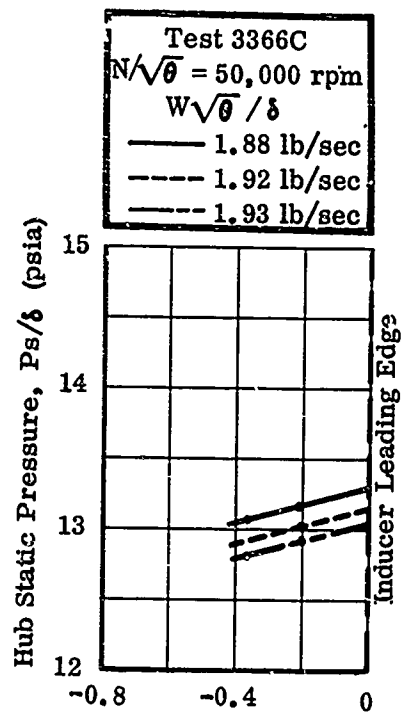


Figure 93. Inlet Duct Hub Static Pressures, RF-2.

CONFIDENTIAL



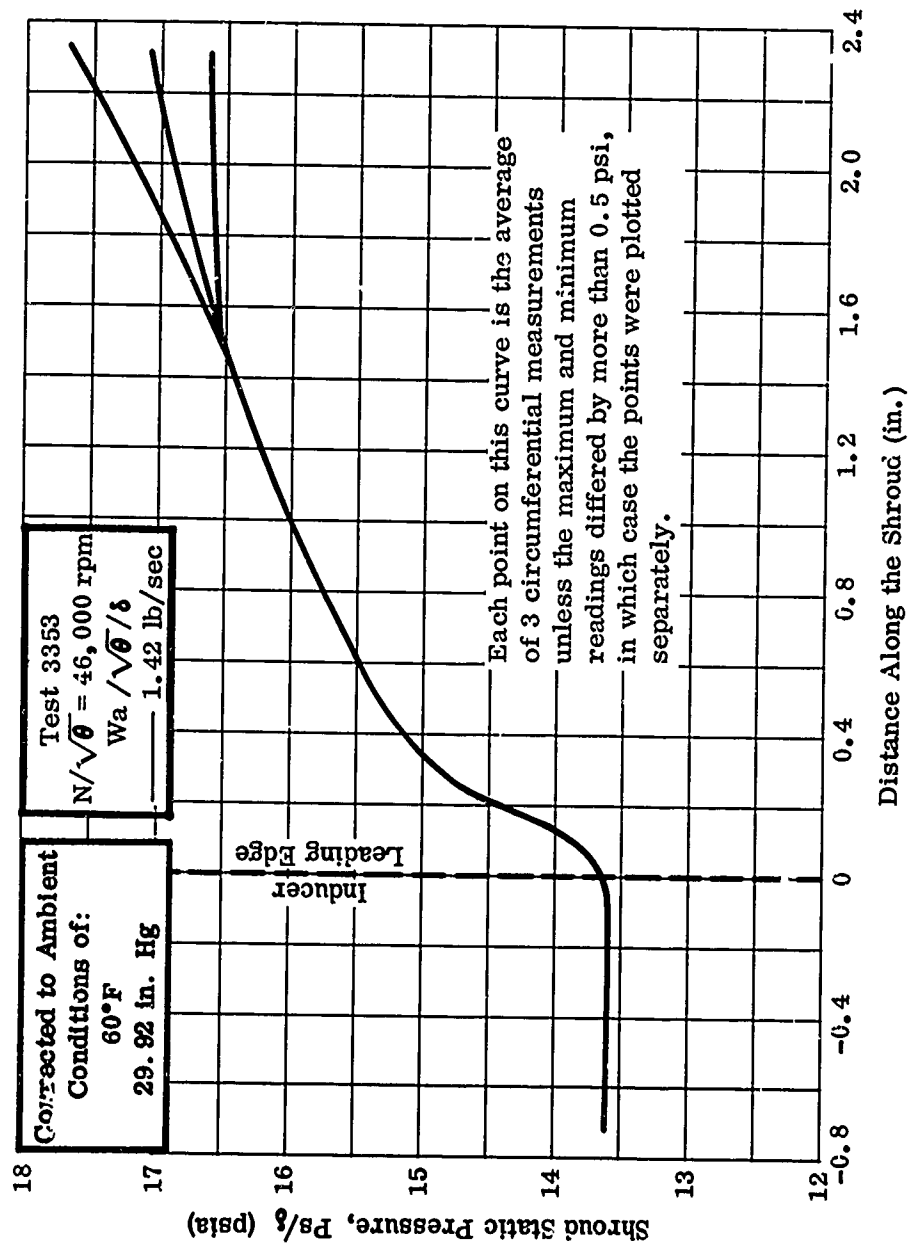


Figure 94. Inlet Duct and Inducer Shroud Static Pressures, RF-2.

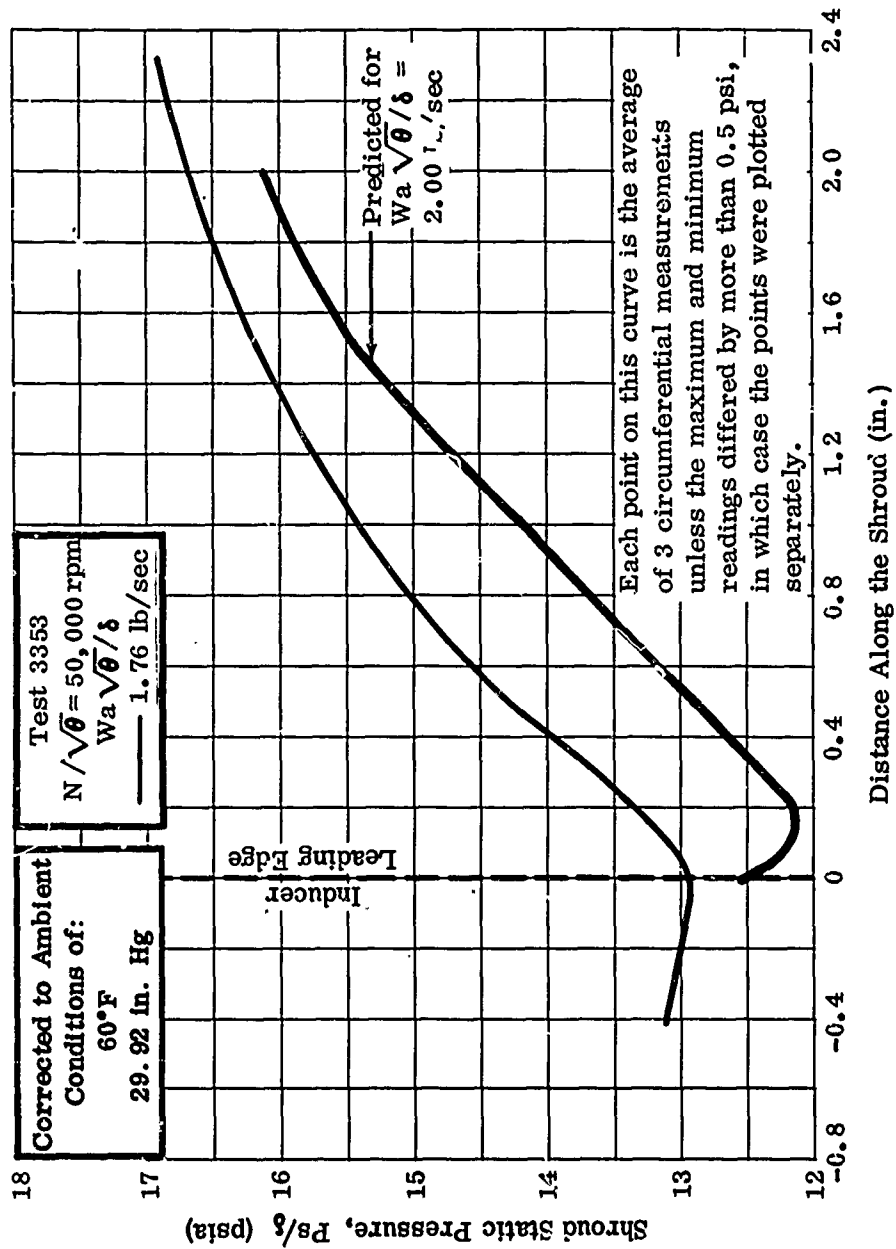


Figure 95. Inlet Duct and Inducer Shroud Static Pressures, RF-2.

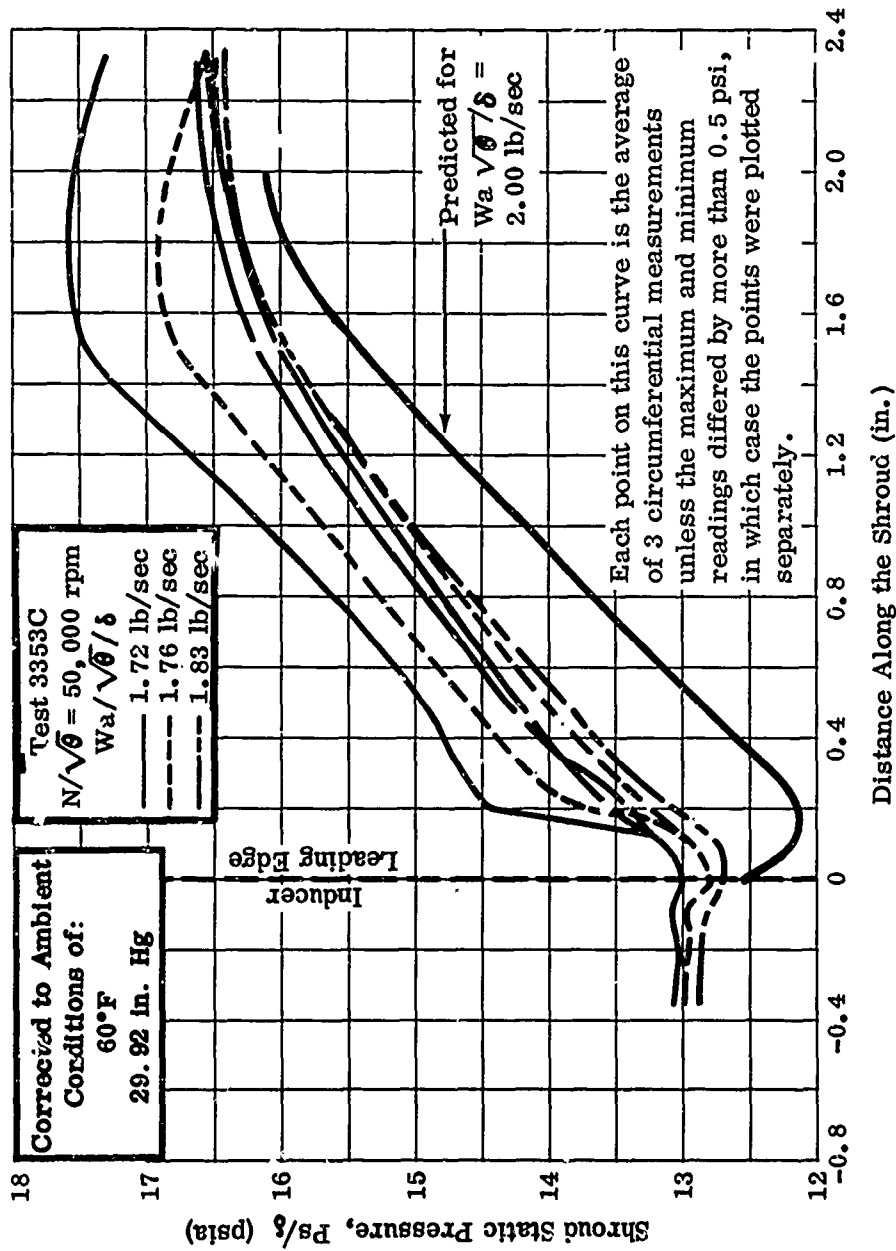


Figure 96. Inlet Duct and Inducer Shroud Static Pressures, RF-2.

CONFIDENTIAL

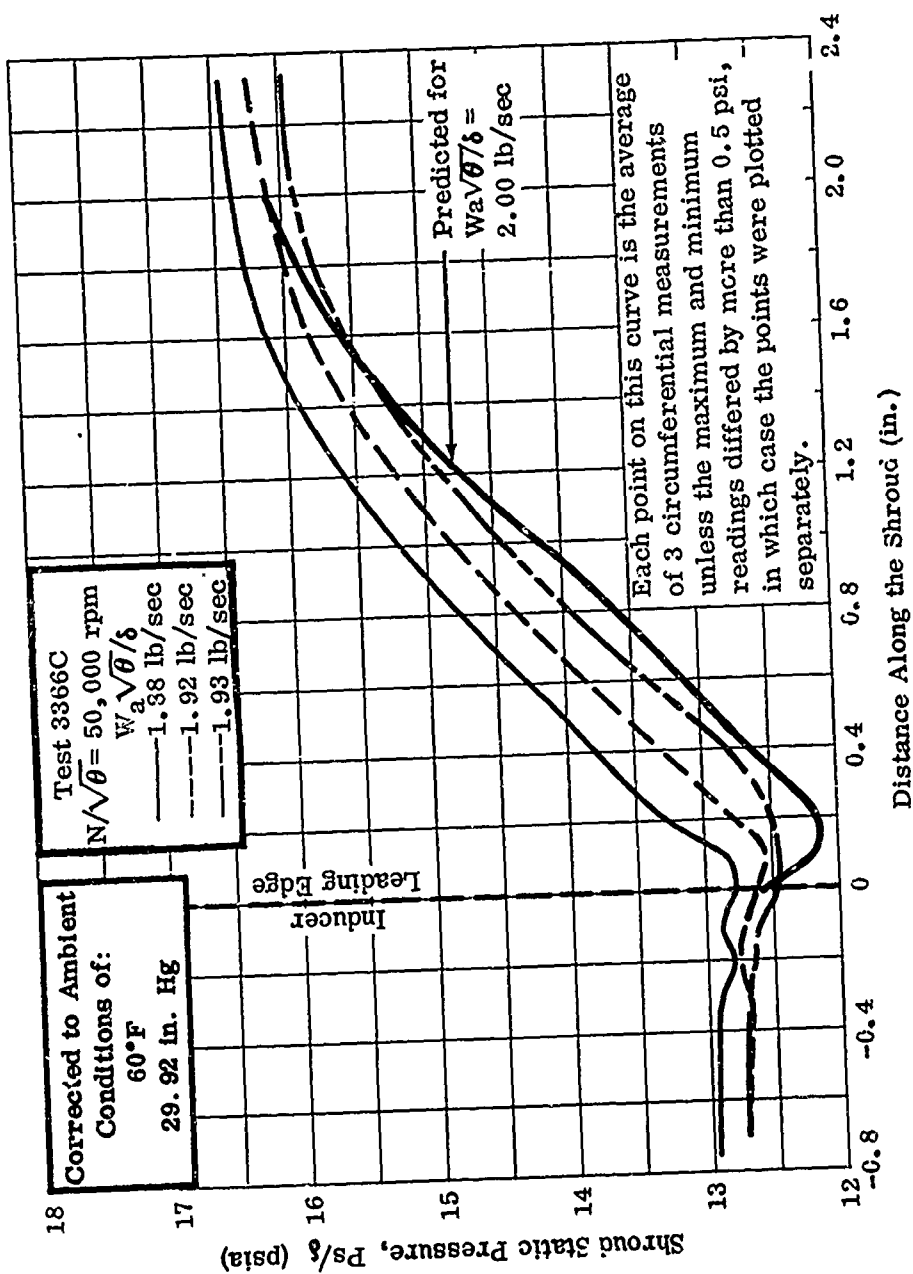


Figure 97. Inlet Duct and Inducer Shroud Static Pressures, RF-2.

CONFIDENTIAL

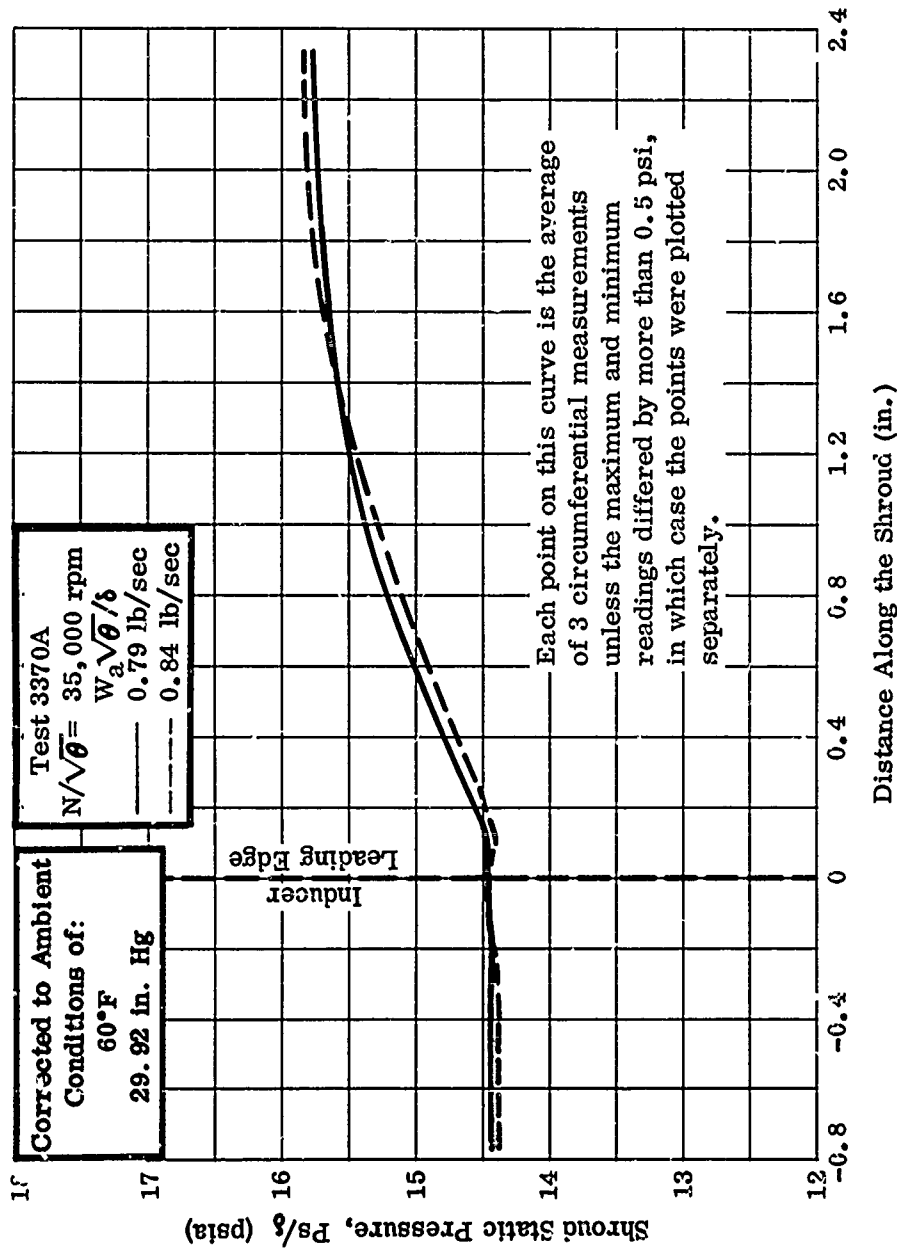


Figure 98. Inlet Duct and Inducer Shroud Static Pressures, RF-2.

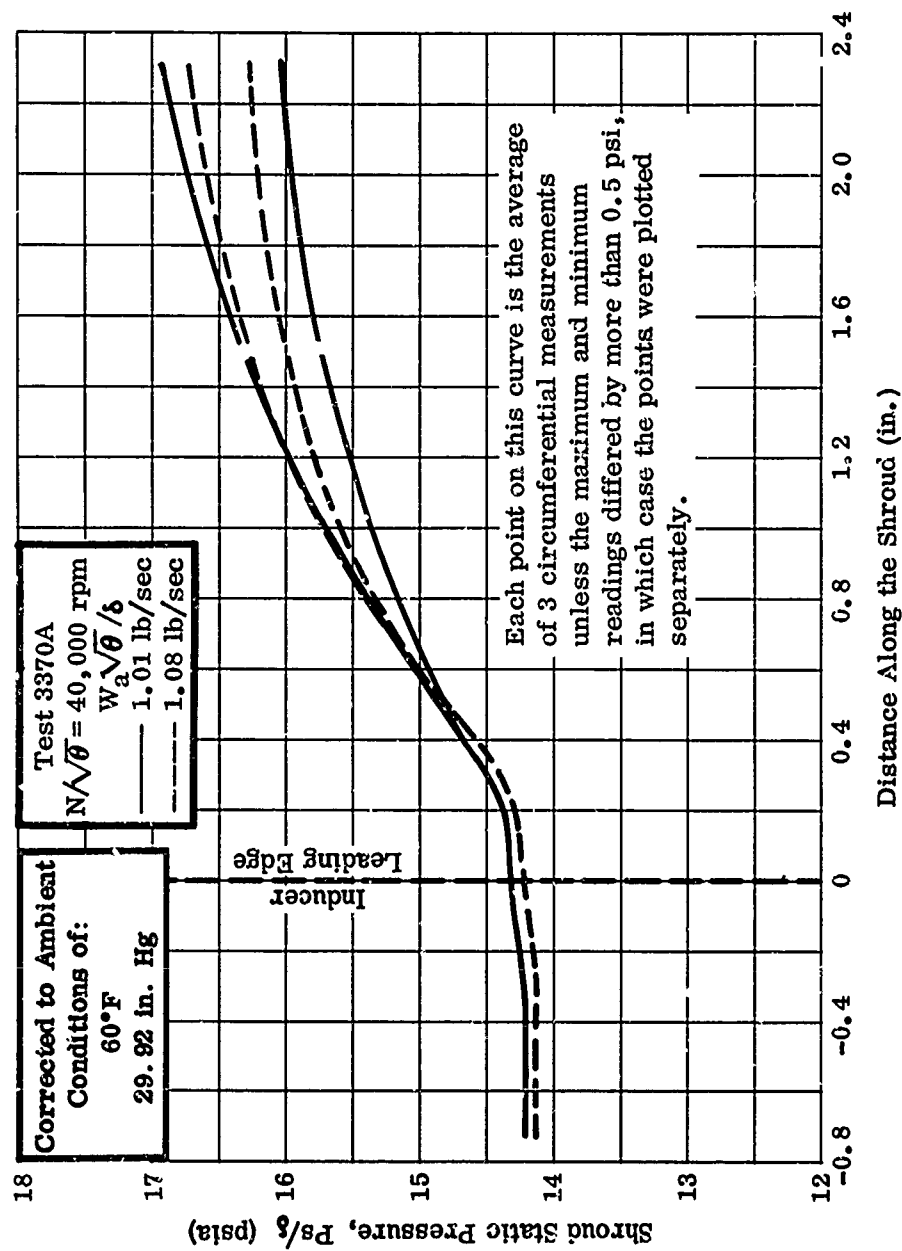


Figure 99. Inlet Duct and Inducer Shroud Static Pressures, RF-2.

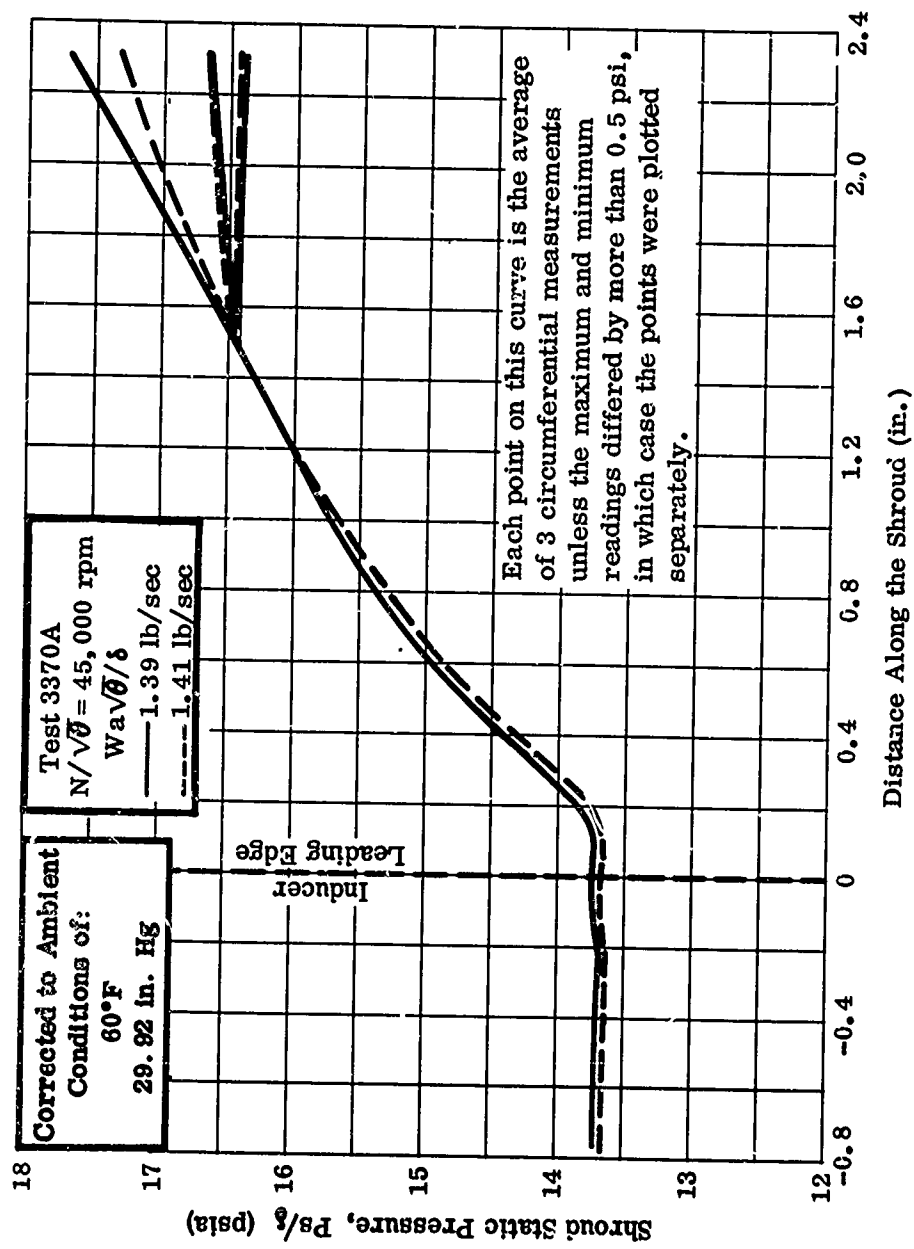


Figure 100. Inlet Duct and Inducer Shroud Static Pressures, RF-2.

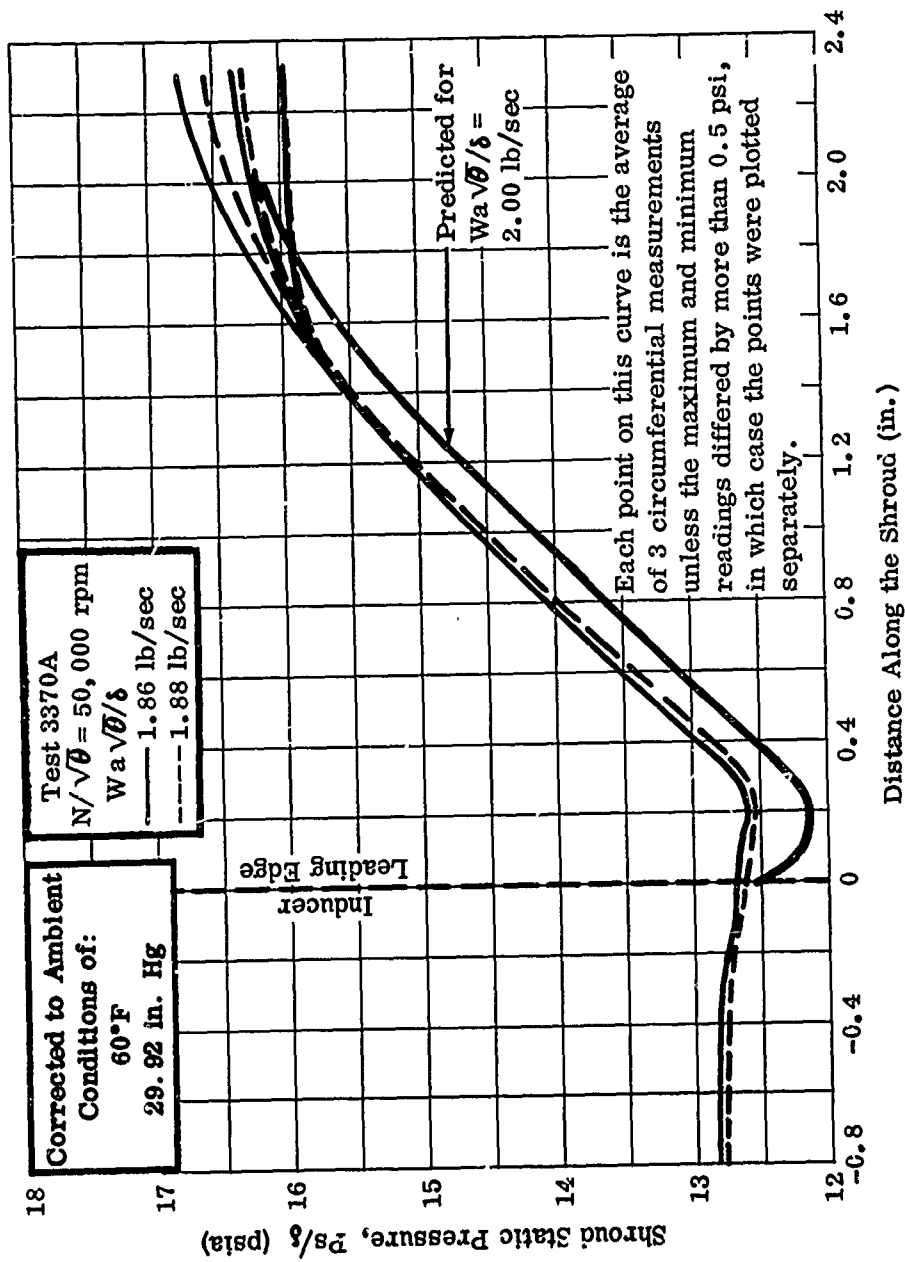


Figure 101. Inlet Duct and Inducer Shroud Static Pressures, RF-2.

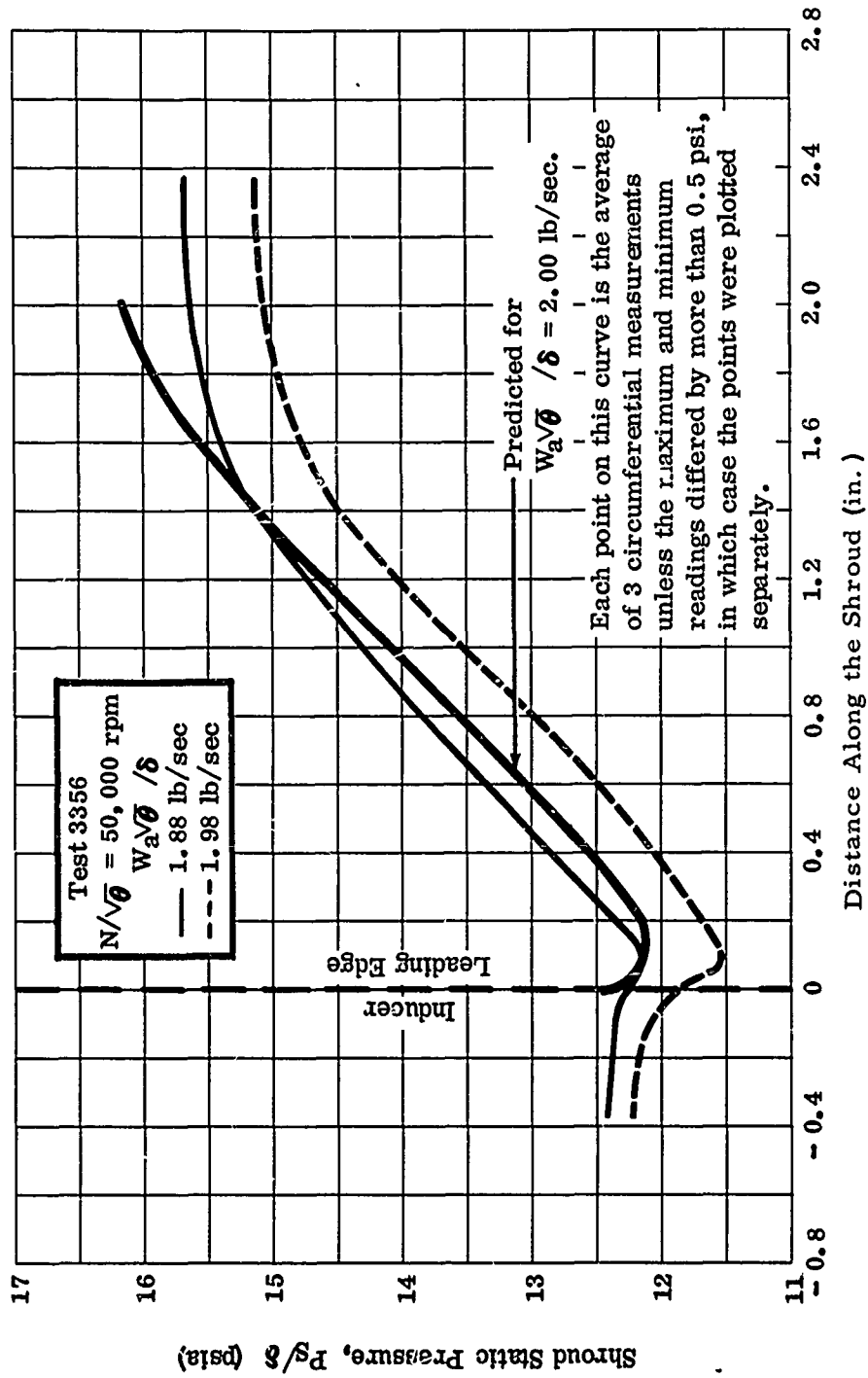


Figure 102. Inlet Duct and Inducer Shroud Static Pressures, RF-2.

CONFIDENTIAL

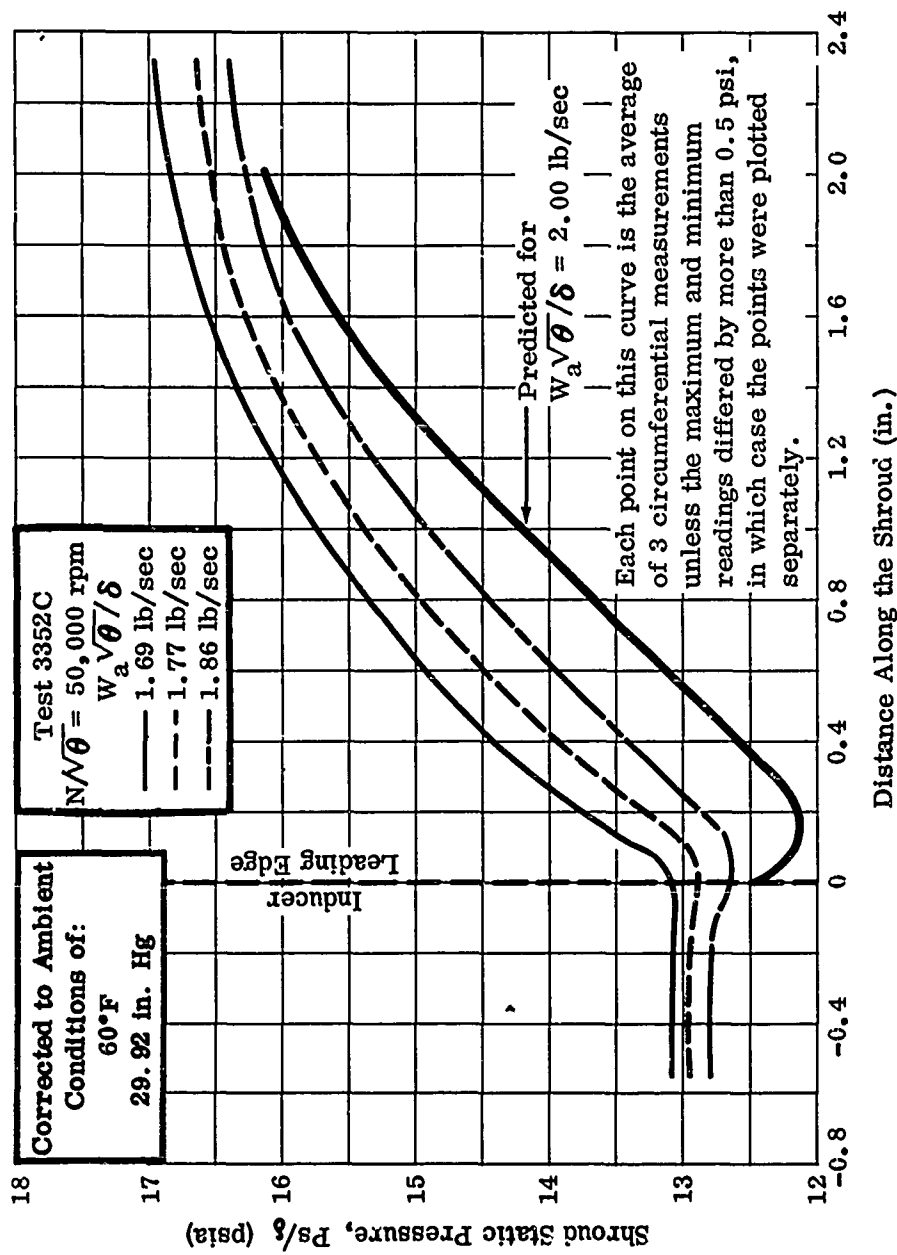


Figure 103. Inlet Duct and Inducer Shroud Static Pressure, RF-2.

CONFIDENTIAL

CONFIDENTIAL

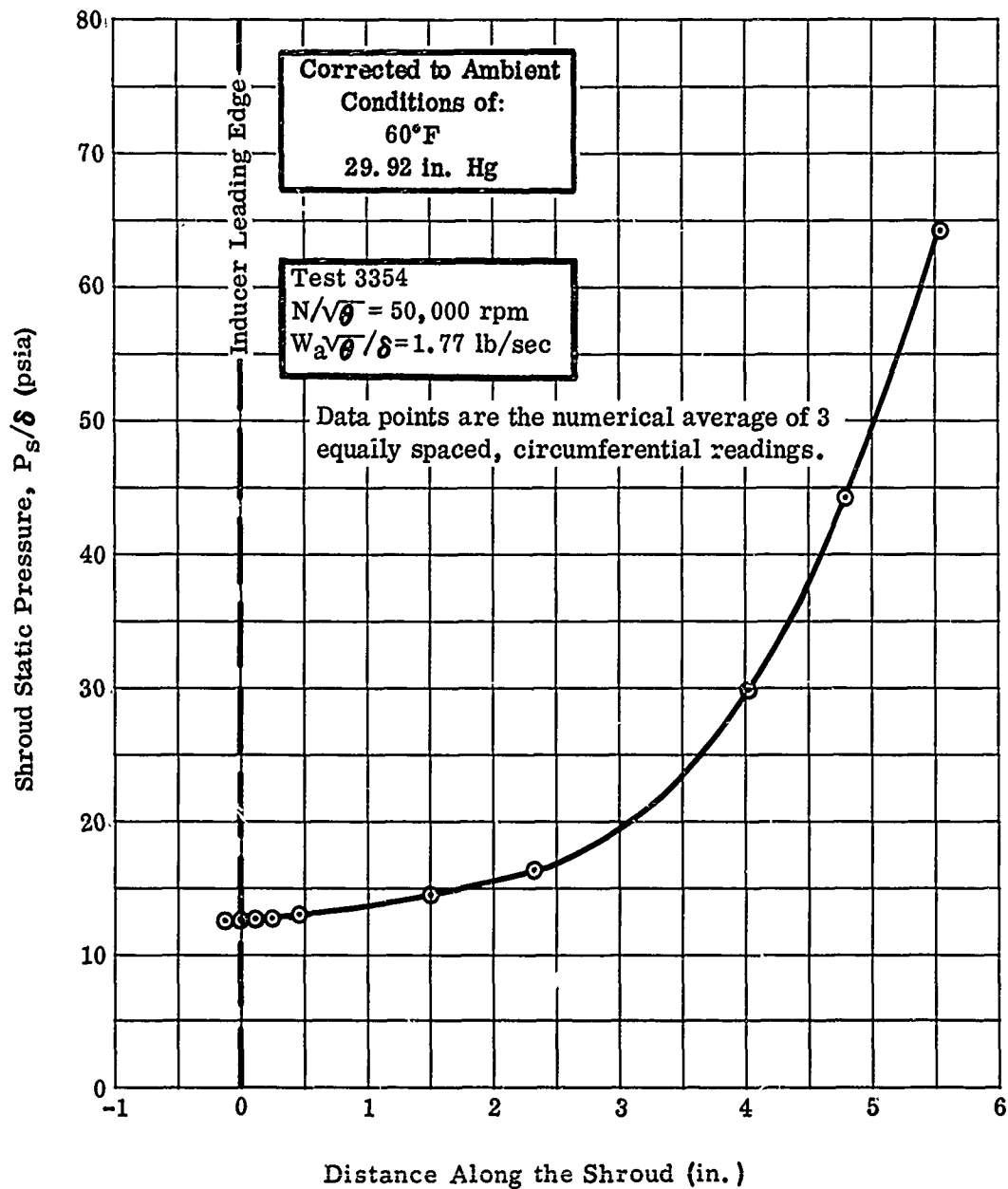


Figure 104. Static Pressure Along the Shroud, RF-2.

CONFIDENTIAL

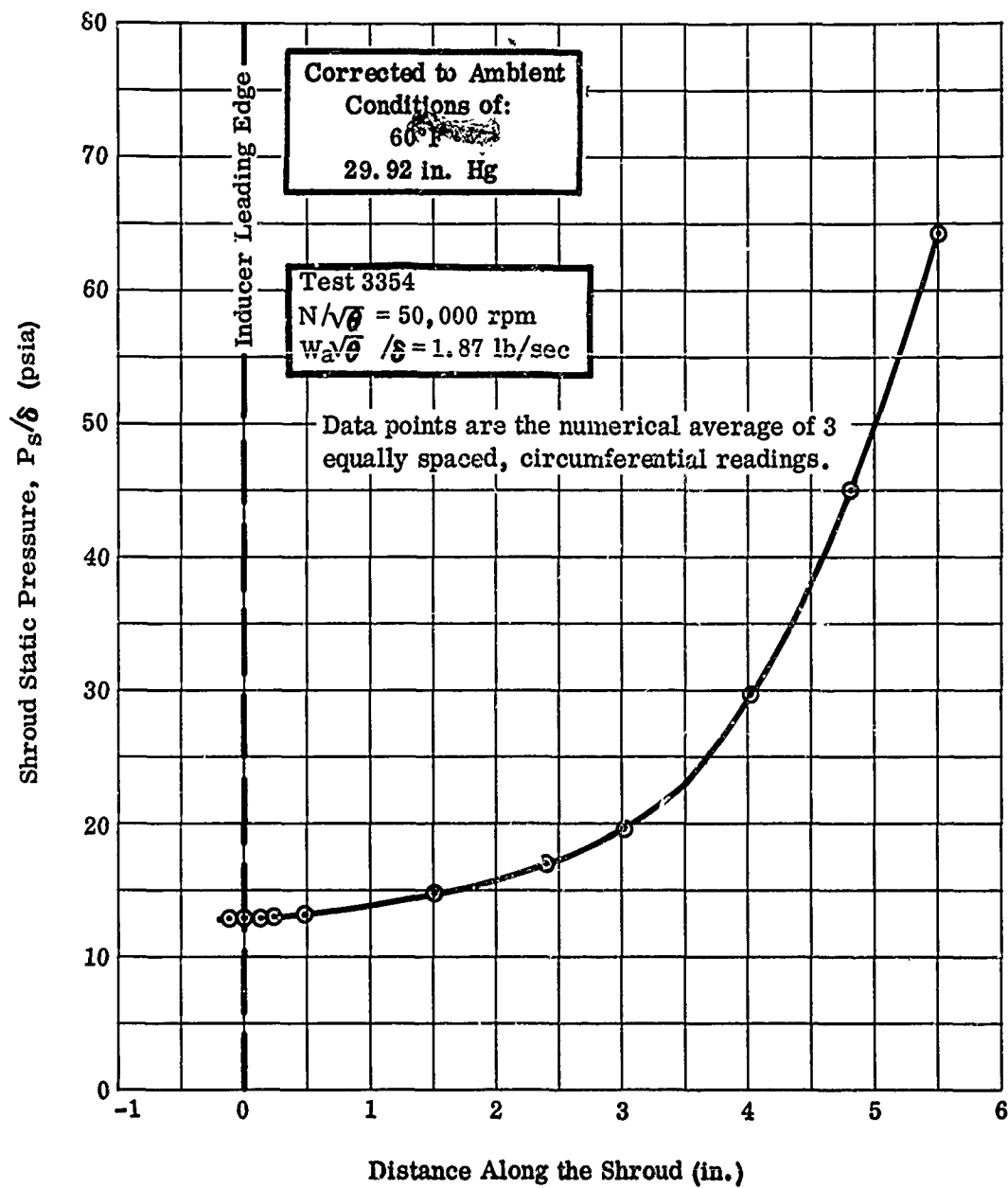


Figure 105. Static Pressure Along the Shroud, RF-2.

CONFIDENTIAL

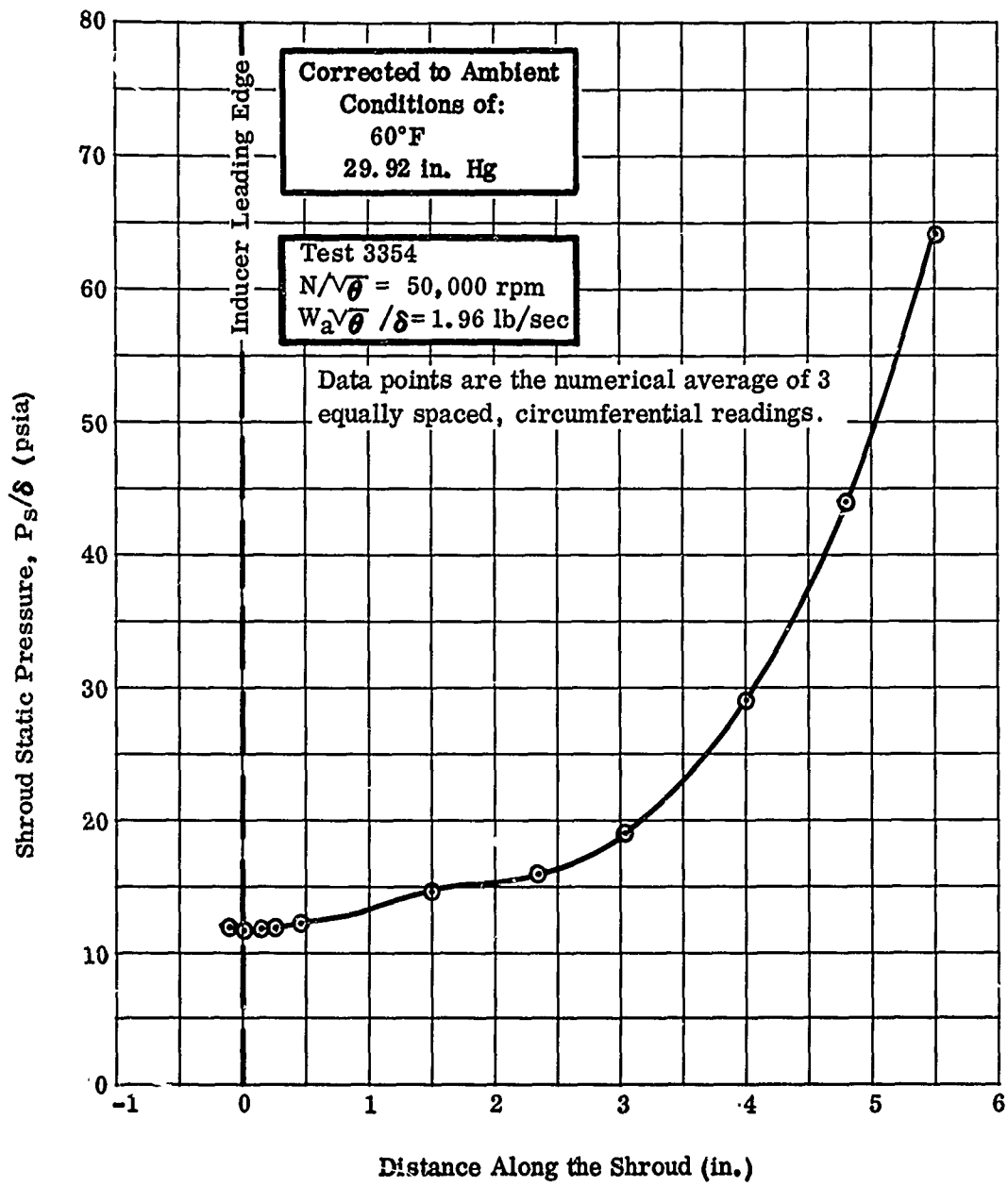


Figure 106. Static Pressure Along the Shroud, RF-2.

CONFIDENTIAL

CONFIDENTIAL

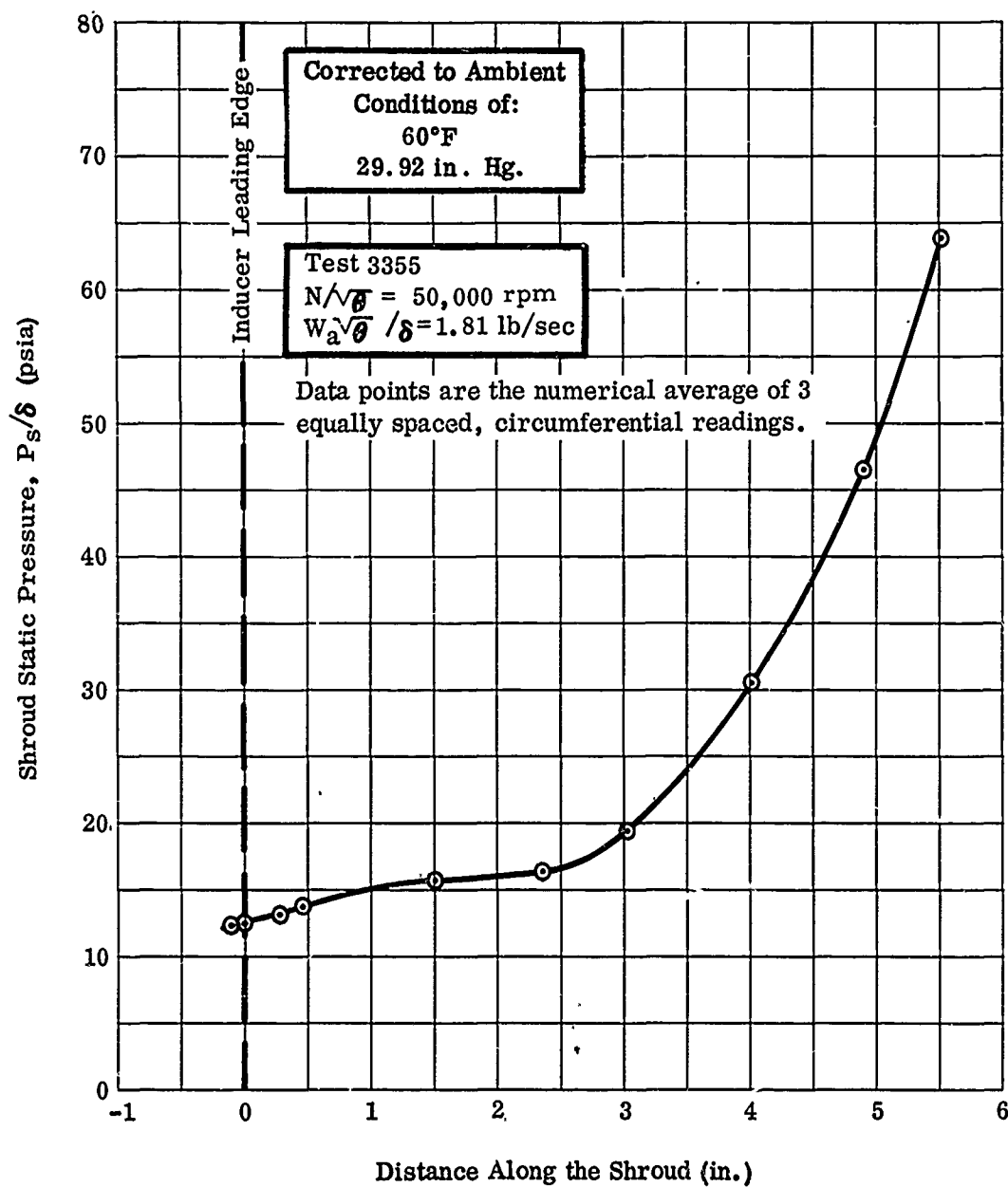


Figure 107. Static Pressure Along the Shroud, RF-2.

CONFIDENTIAL

CONFIDENTIAL

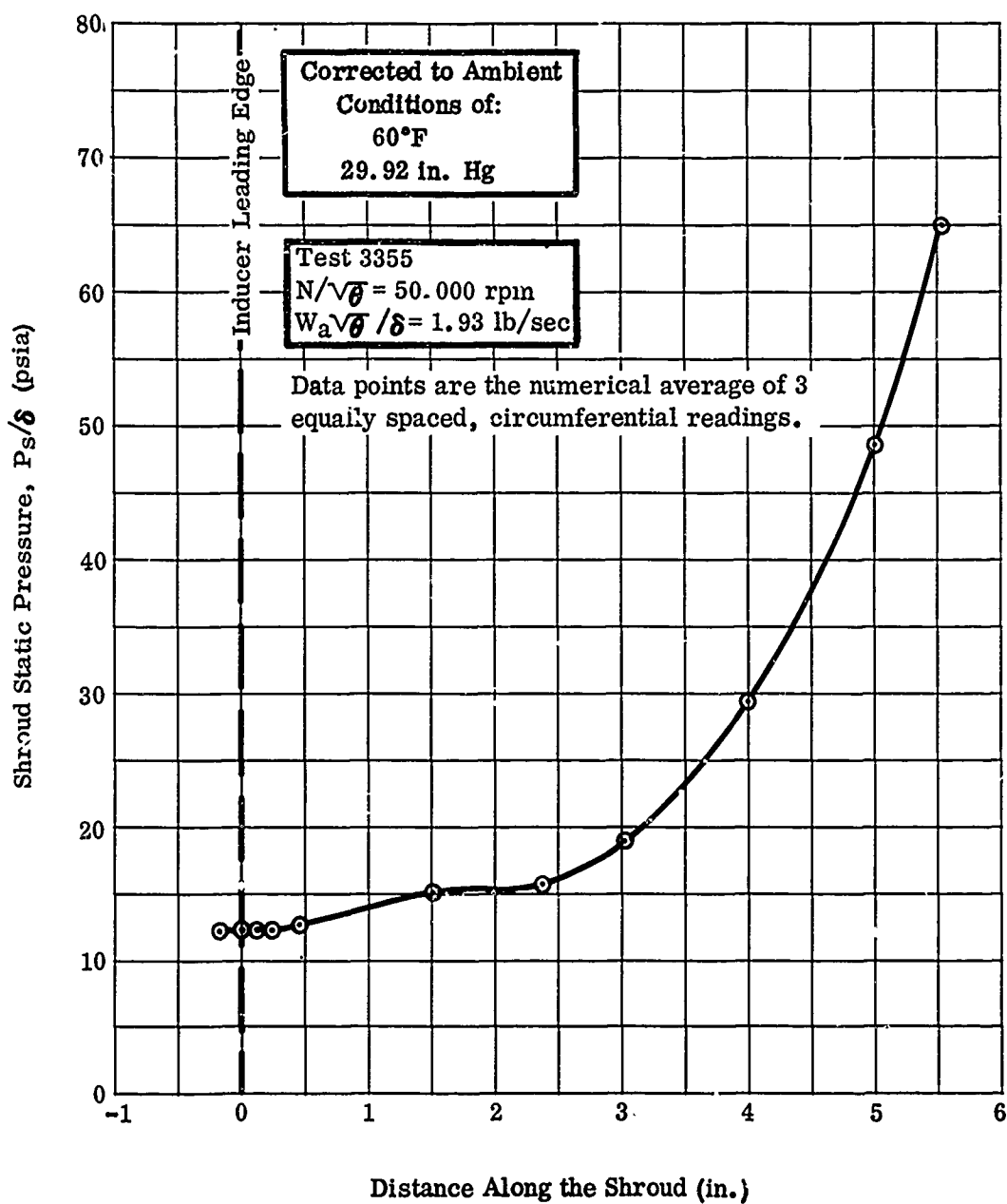


Figure 108. Static Pressure Along the Shroud, RF-2.

CONFIDENTIAL

CONFIDENTIAL

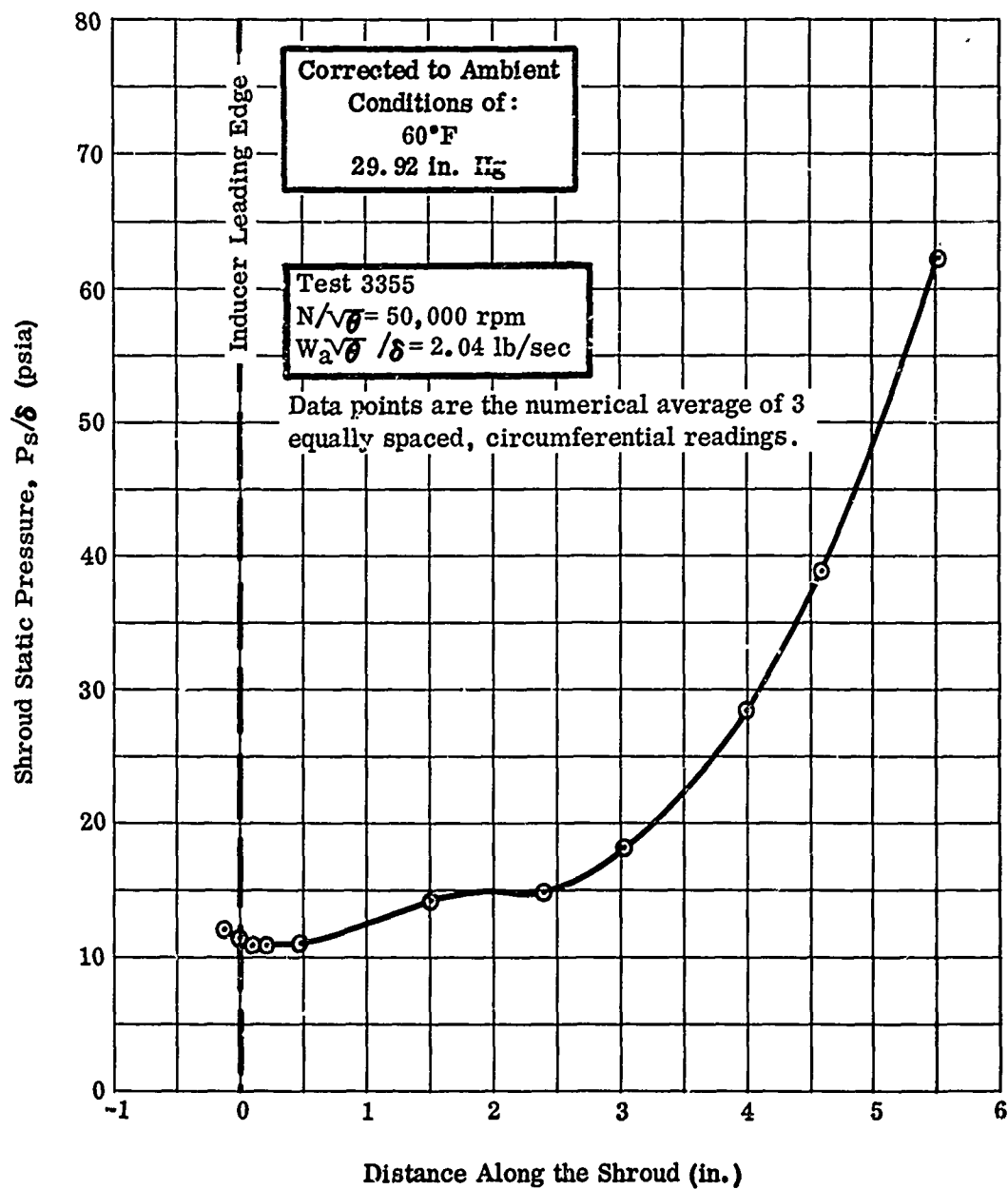


Figure 109. Static Pressure Along the Shroud, RF-2.

CONFIDENTIAL

CONFIDENTIAL

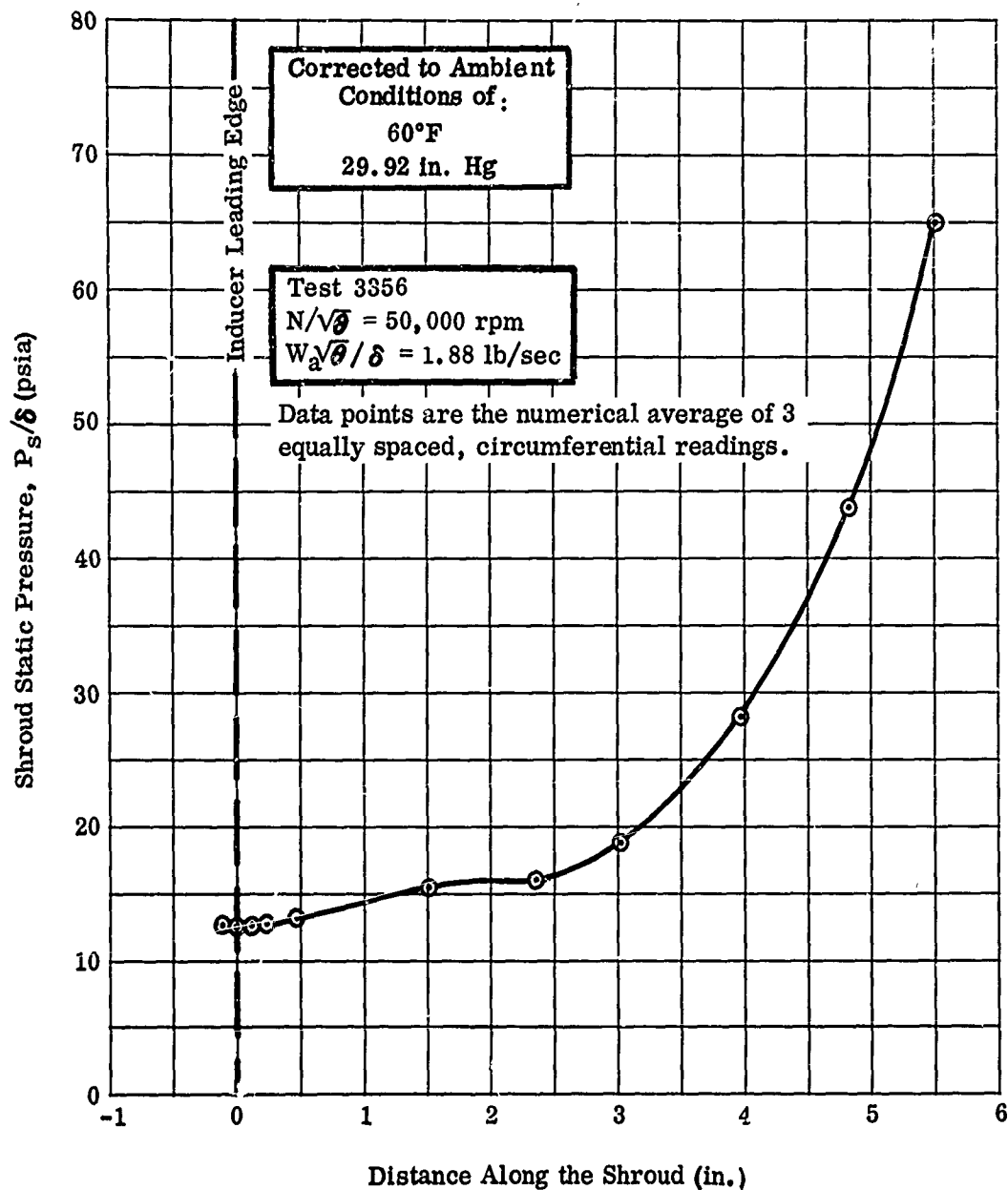


Figure 110. Static Pressure Along the Shroud, RF-2.

CONFIDENTIAL

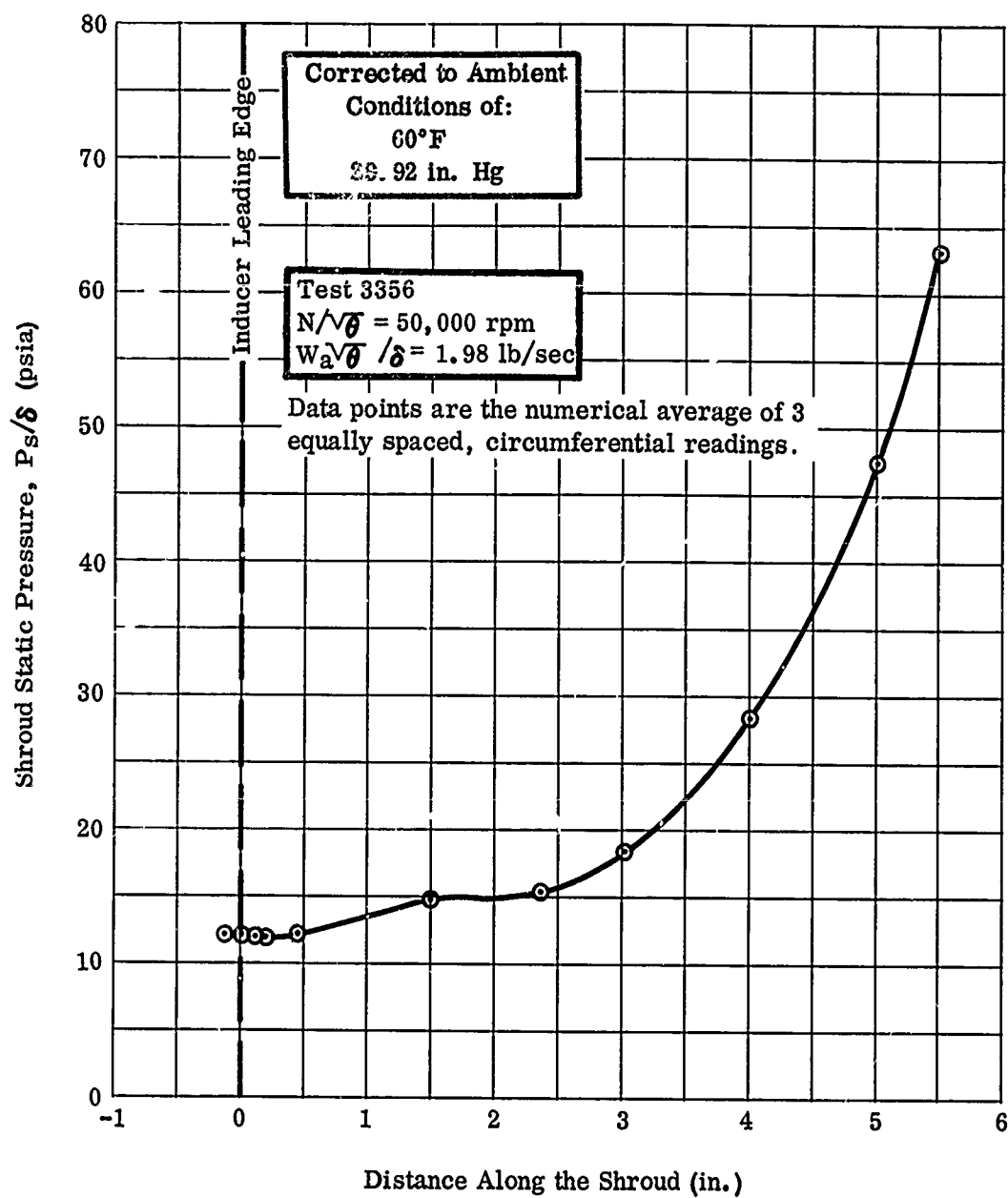


Figure 111. Static Pressure Along the Shroud, RF-2.

CONFIDENTIAL

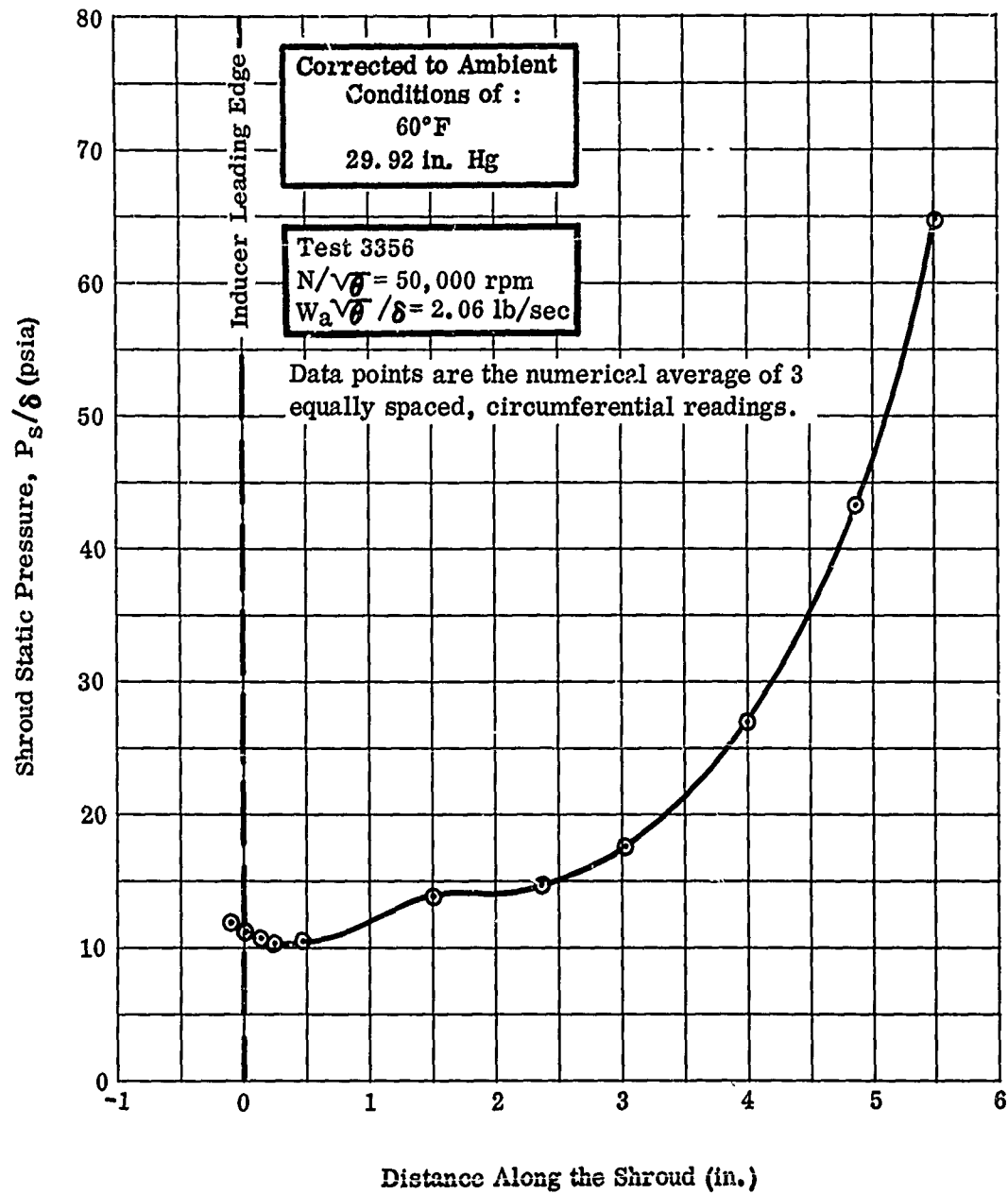


Figure 112. Static Pressure Along the Shroud, RF-2.

CONFIDENTIAL

CONFIDENTIAL

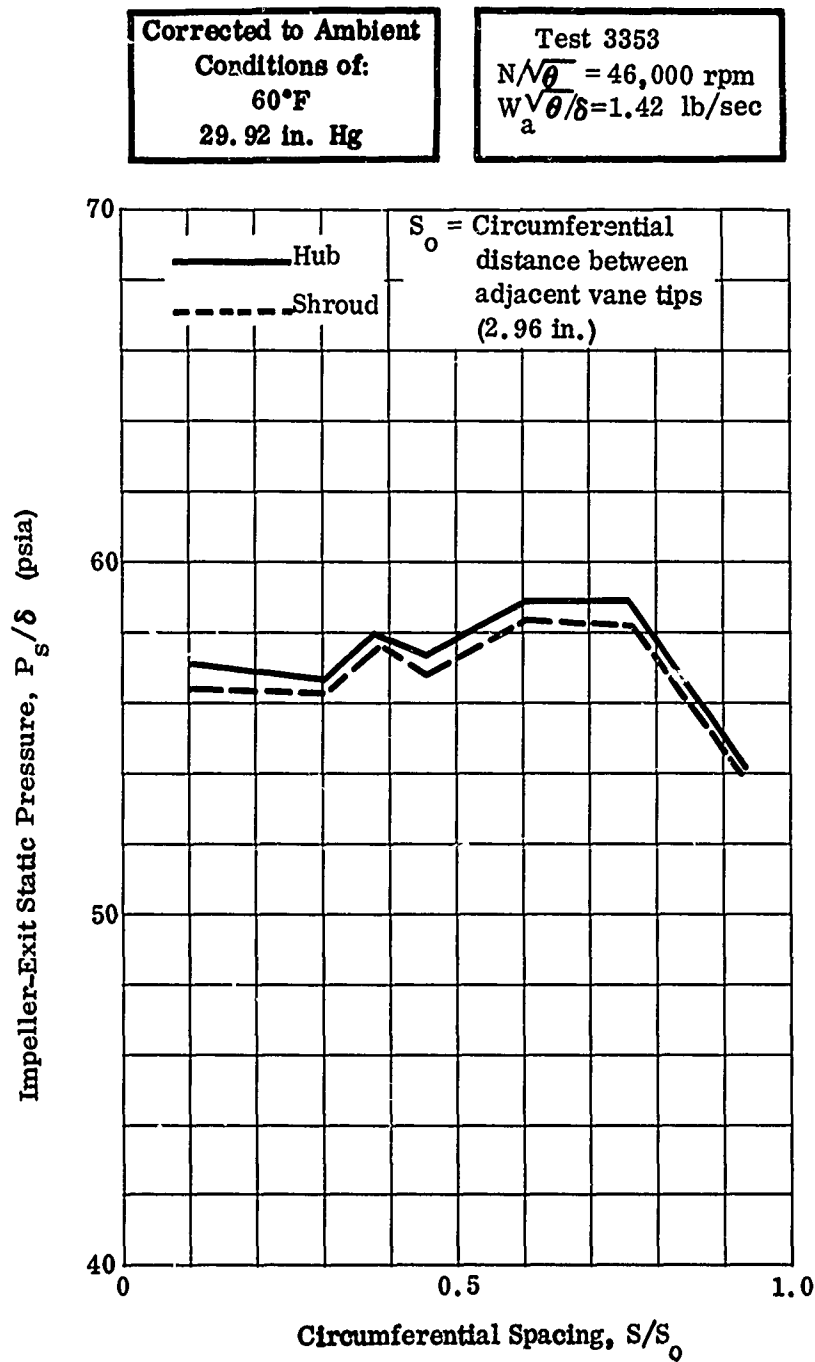


Figure 113. Circumferential Variation of Impeller-Exit Static Pressure.

CONFIDENTIAL

CONFIDENTIAL

Corrected to Ambient
Conditions of:
60°F
29.92 in. Hg

Test 3353
 $N/\sqrt{\theta} = 46,000 \text{ rpm}$
 $W_a \sqrt{\theta/\delta} = 1.43 \text{ lb/sec}$

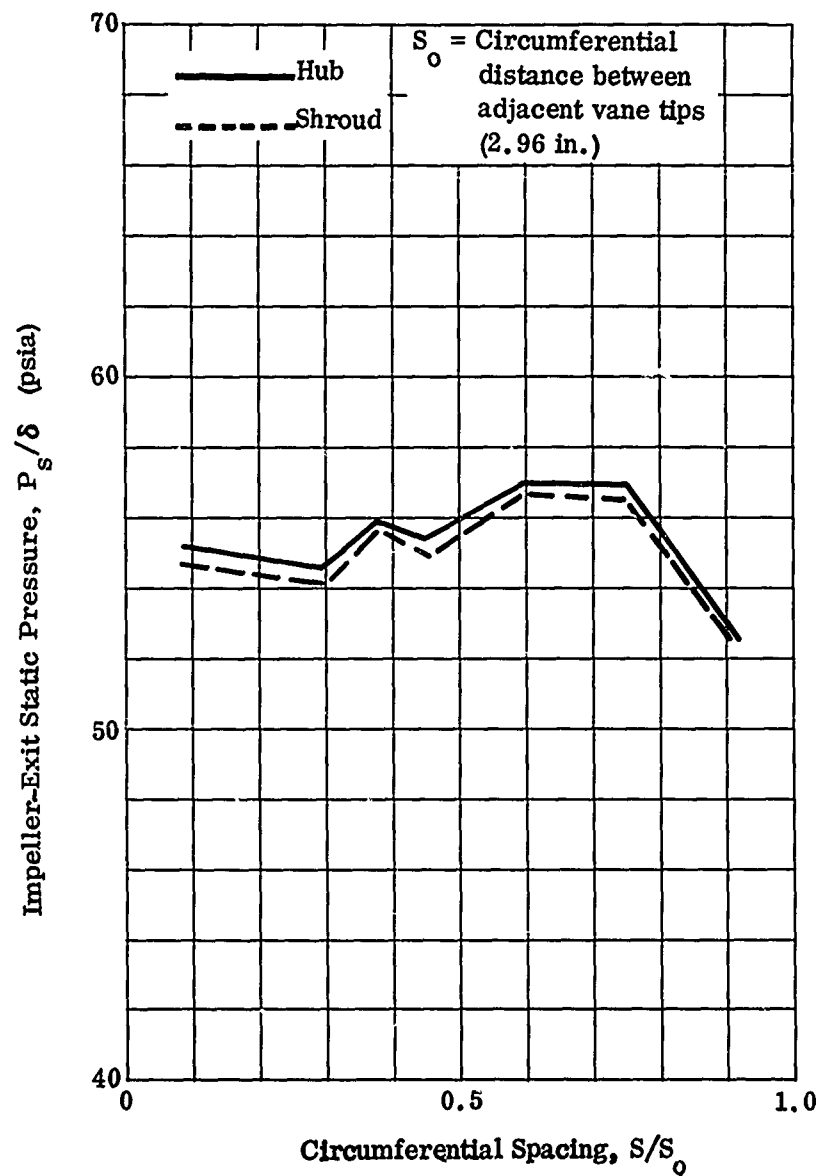


Figure 114. Circumferential Variation of Impeller-Exit Static Pressure.

CONFIDENTIAL

CONFIDENTIAL

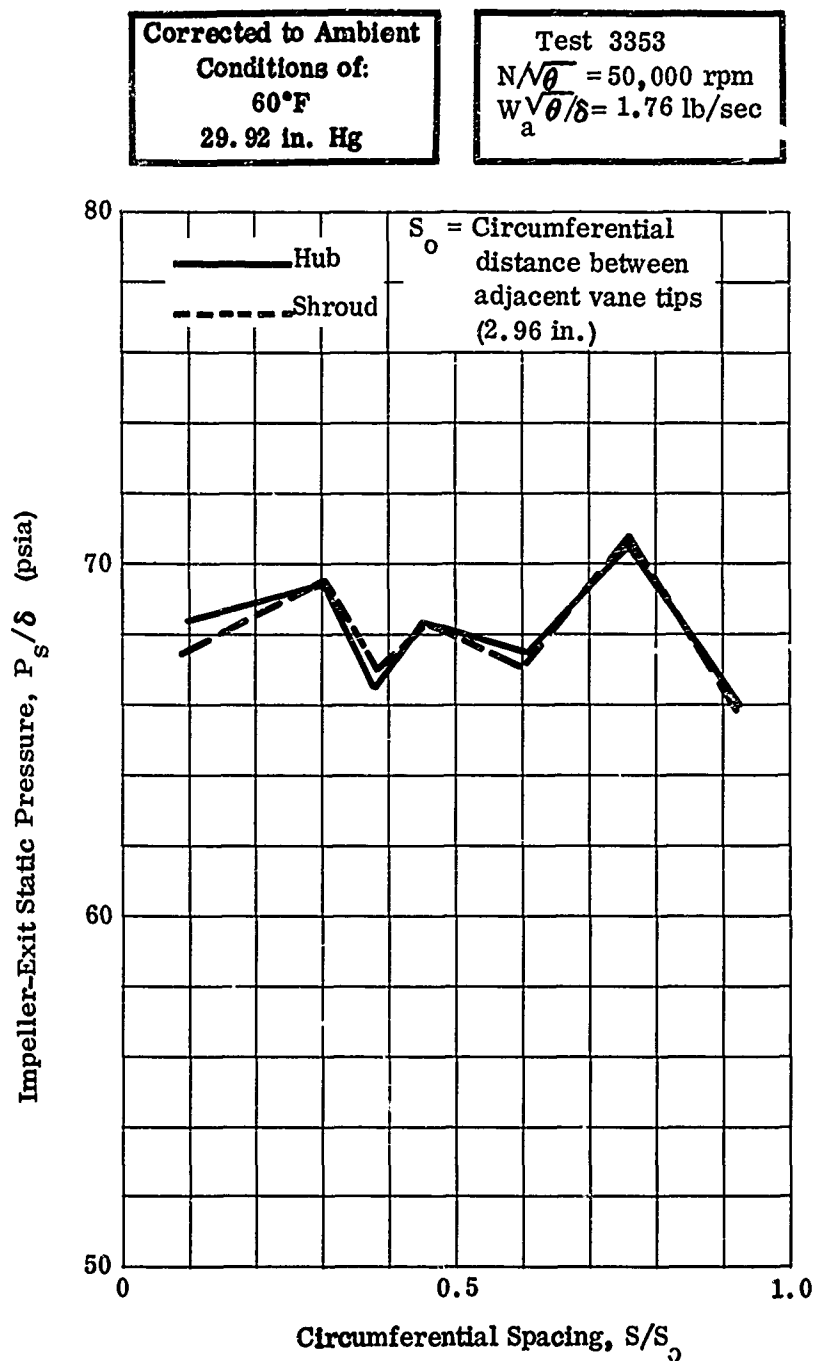


Figure 115. Circumferential Variation of Impeller-Exit Static Pressure.

CONFIDENTIAL

CONFIDENTIAL

Corrected to Ambient
Conditions of:
60°F
29.92 in. Hg

Test 3353C
 $N/\sqrt{\theta} = 50,000$ rpm
 $W_a \sqrt{\theta/\delta} = 1.72$ lb/sec

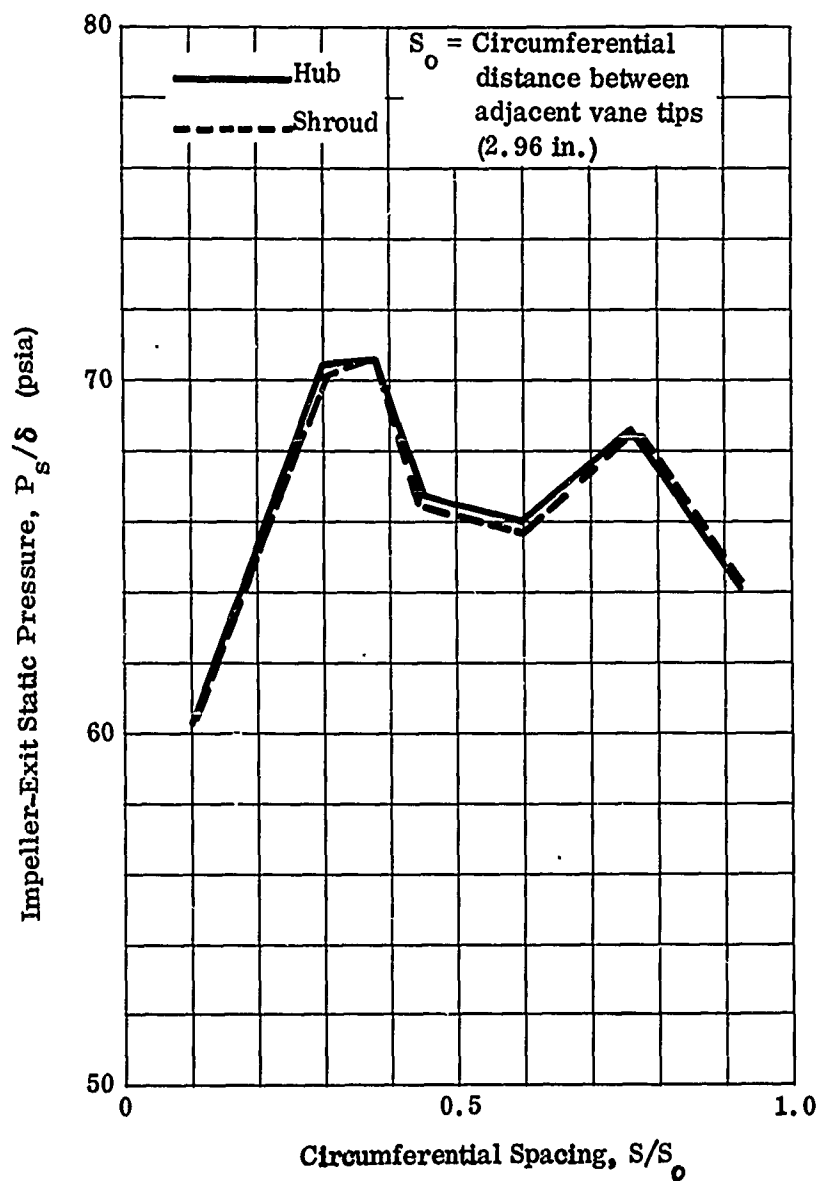


Figure 116. Circumferential Variation of Impeller-Exit Static Pressure.

CONFIDENTIAL

CONFIDENTIAL

Corrected to Ambient
Conditions of:
60°F
29.92 in. Hg

Test 3353C
 $N/\sqrt{\theta} = 50,000$ rpm
 $W_a \sqrt{\theta}/\delta = 1.76$ lb/sec

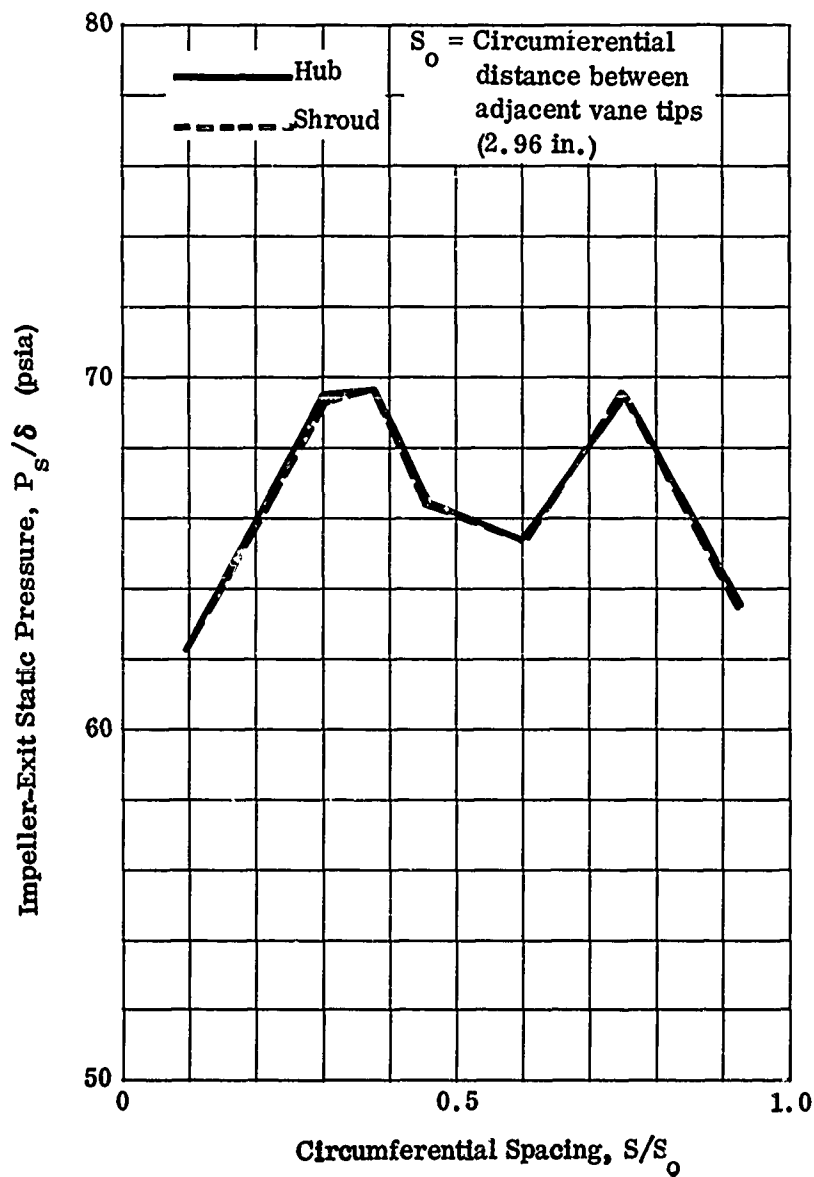


Figure 117. Circumferential Variation of Impeller-Exit Static Pressure.

CONFIDENTIAL

CONFIDENTIAL

Corrected to Ambient
Conditions of:
60°F
29.92 in. Hg

Test 3353C
 $N/\sqrt{\theta} = 50,000$ rpm
 $W_a \sqrt{\theta/\delta} = 1.83$ lb/sec

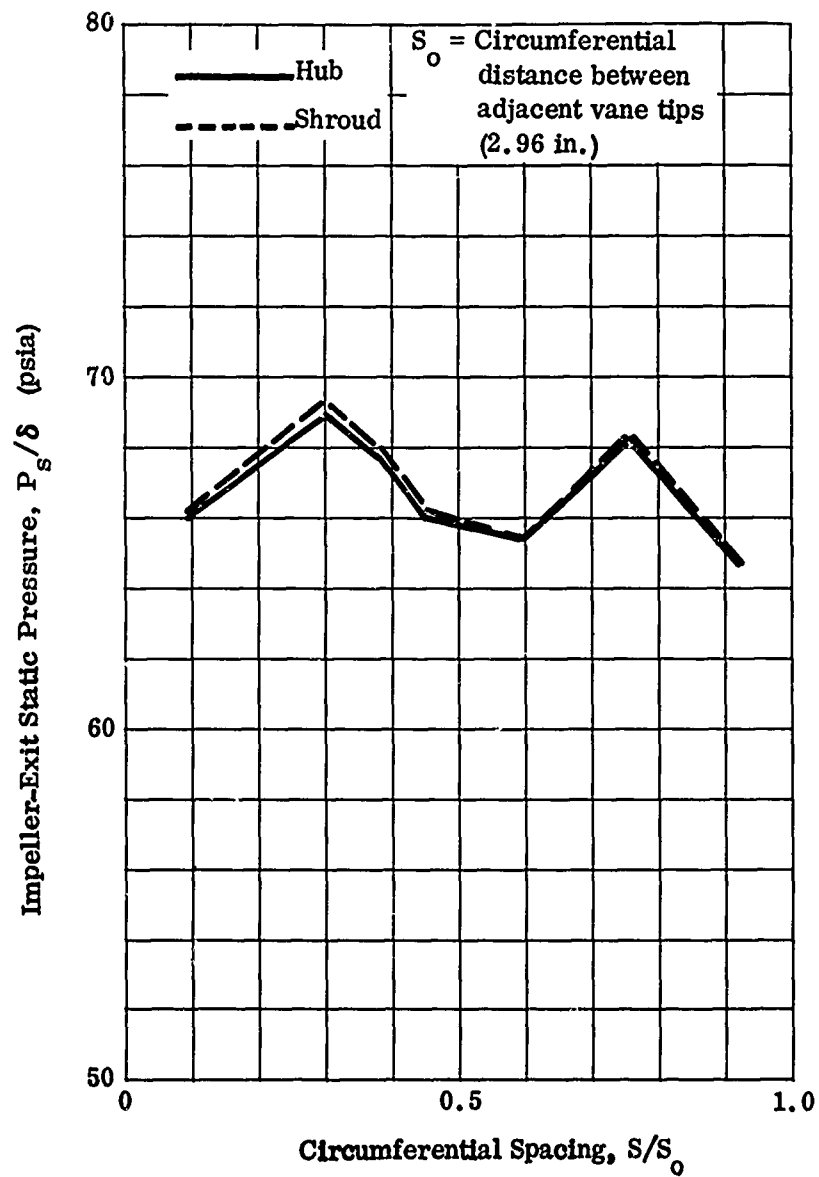


Figure 118. Circumferential Variation of Impeller-Exit Static Pressure.

CONFIDENTIAL

CONFIDENTIAL

Corrected to Ambient
Conditions of:
60°F
29.92 in. Hg

Test 3356A
 $N/\sqrt{\theta} = 50,000$ rpm
 $W\sqrt{\theta}/\delta = 1.97$ lb/sec



Figure 119. Circumferential Variation of Impeller-Exit Static Pressure.

CONFIDENTIAL

CONFIDENTIAL

Corrected to Ambient
Conditions of:
60°F
29.92 in. Hg

Test 3356A
 $N/\sqrt{\theta} = 50,000$ rpm
 $W_a/\sqrt{\theta/\delta} = 2.06$ lb/sec



Figure 120. Circumferential Variation of Impeller-Exit Static Pressure.

CONFIDENTIAL

CONFIDENTIAL

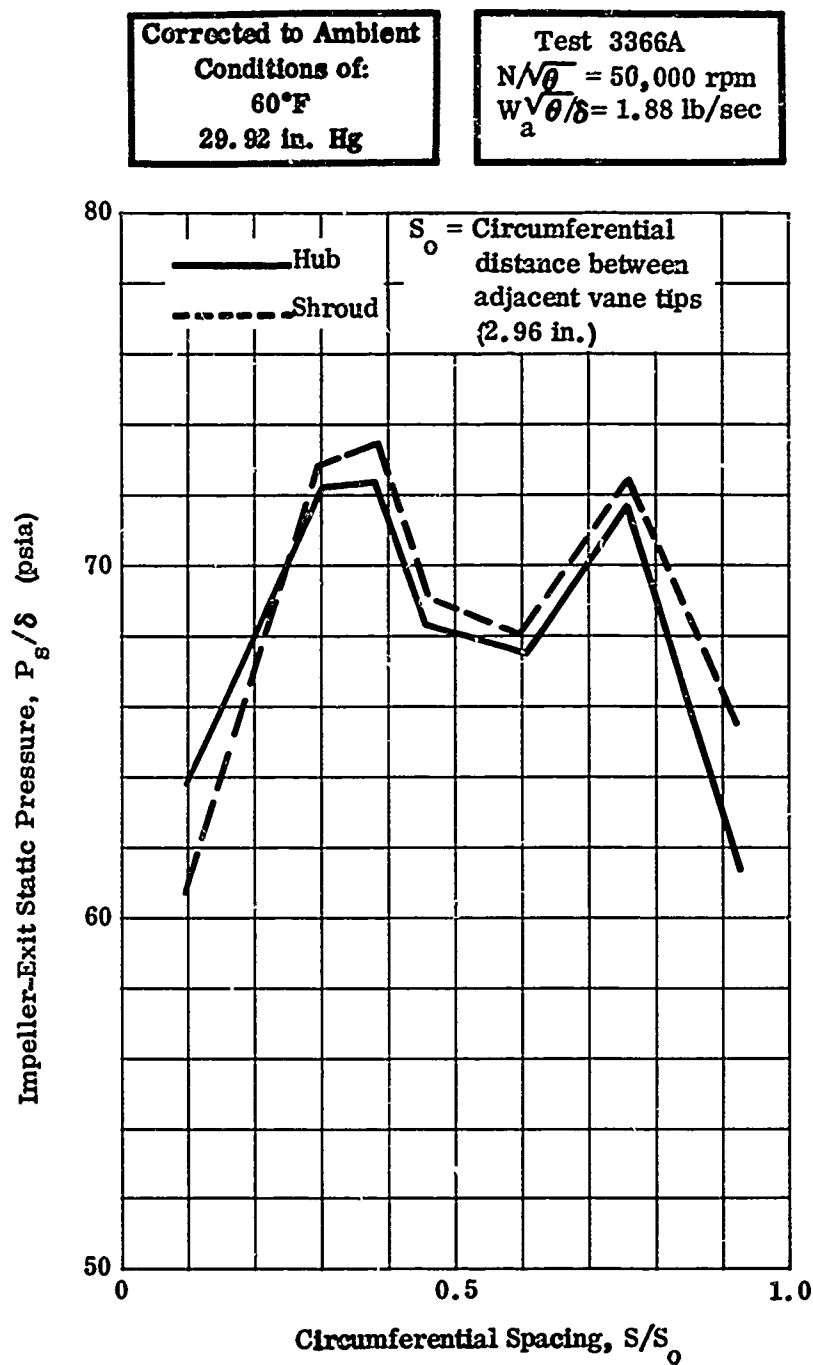


Figure 121. Circumferential Variation of Impeller-Exit Static Pressure.

CONFIDENTIAL

Corrected to Ambient
Conditions of:
60°F
29.92 in. Hg

Test 3366A
 $N/\sqrt{\theta} = 50,000$ rpm
 $W_a \sqrt{\theta/\delta} = 1.92$ lb/sec

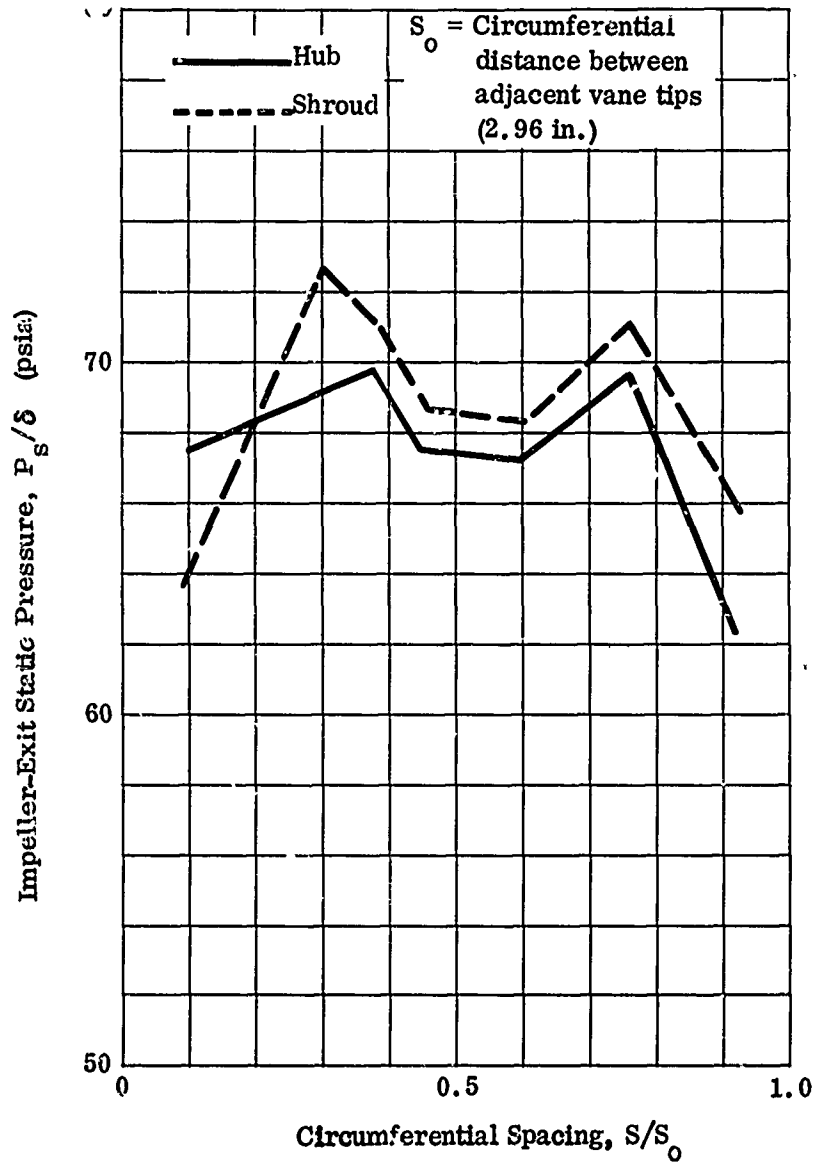


Figure 122. Circumferential Variation of Impeller-Exit Static Pressure.

CONFIDENTIAL

Corrected to Ambient
Conditions of:
60°F
29.92 in. Hg

Test 3366A
 $N/\sqrt{\theta} = 50,000$ rpm
 $W_a \sqrt{\theta/\delta} = 1.93$ lb/sec

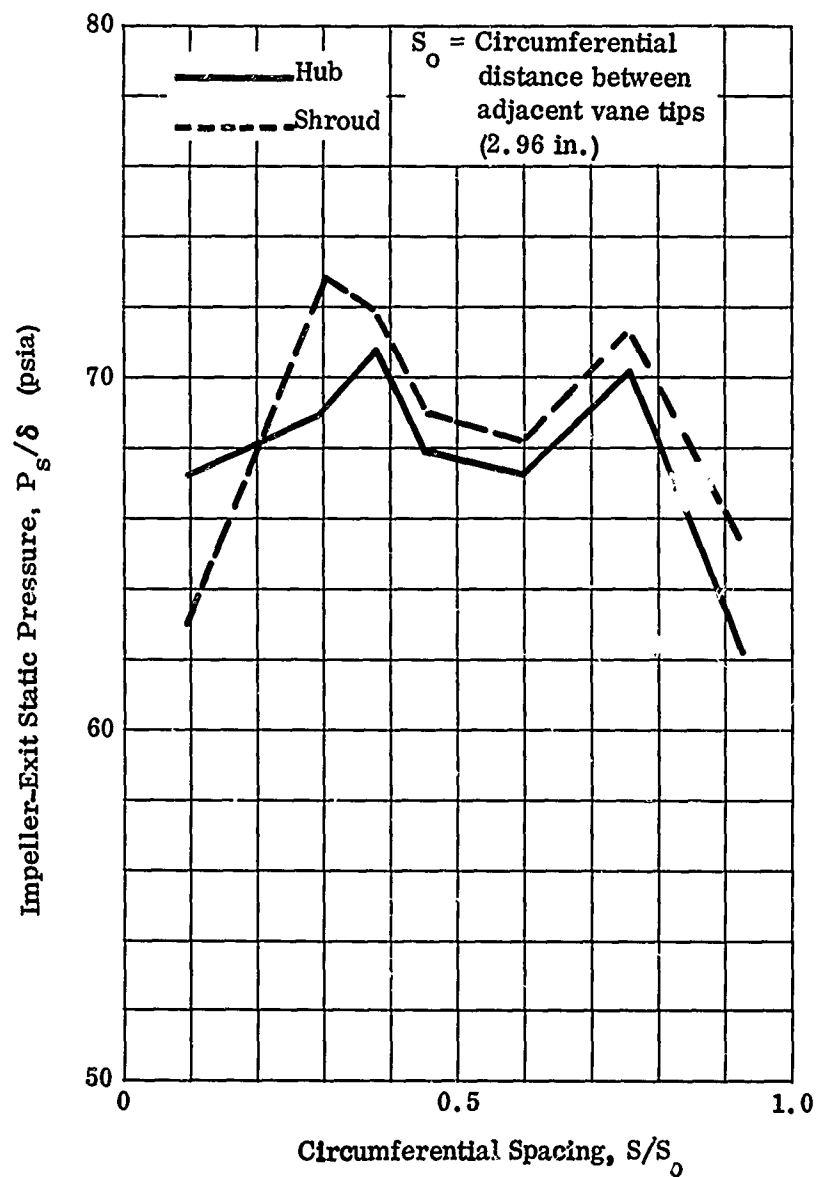


Figure 123. Circumferential Variation of Impeller-Exit Static Pressure.

CONFIDENTIAL

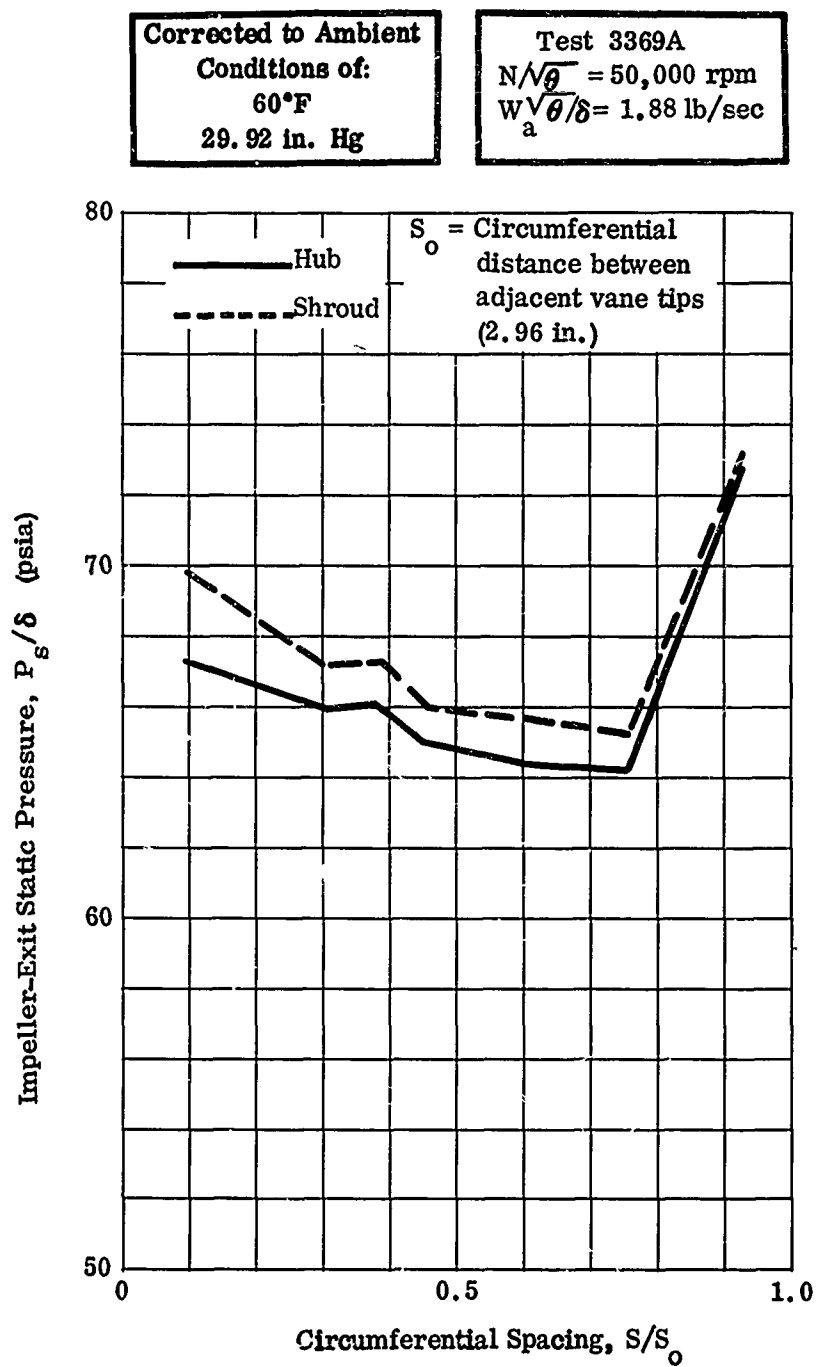


Figure 124. Circumferential Variation of Impeller-Exit Static Pressure.

CONFIDENTIAL

Corrected to Ambient
Conditions of:
60°F
29.92 in. Hg

Test 3369A
 $N/\sqrt{\theta} = 50,000$ rpm
 $W_a \sqrt{\theta/\delta} = 1.90$ lb/sec

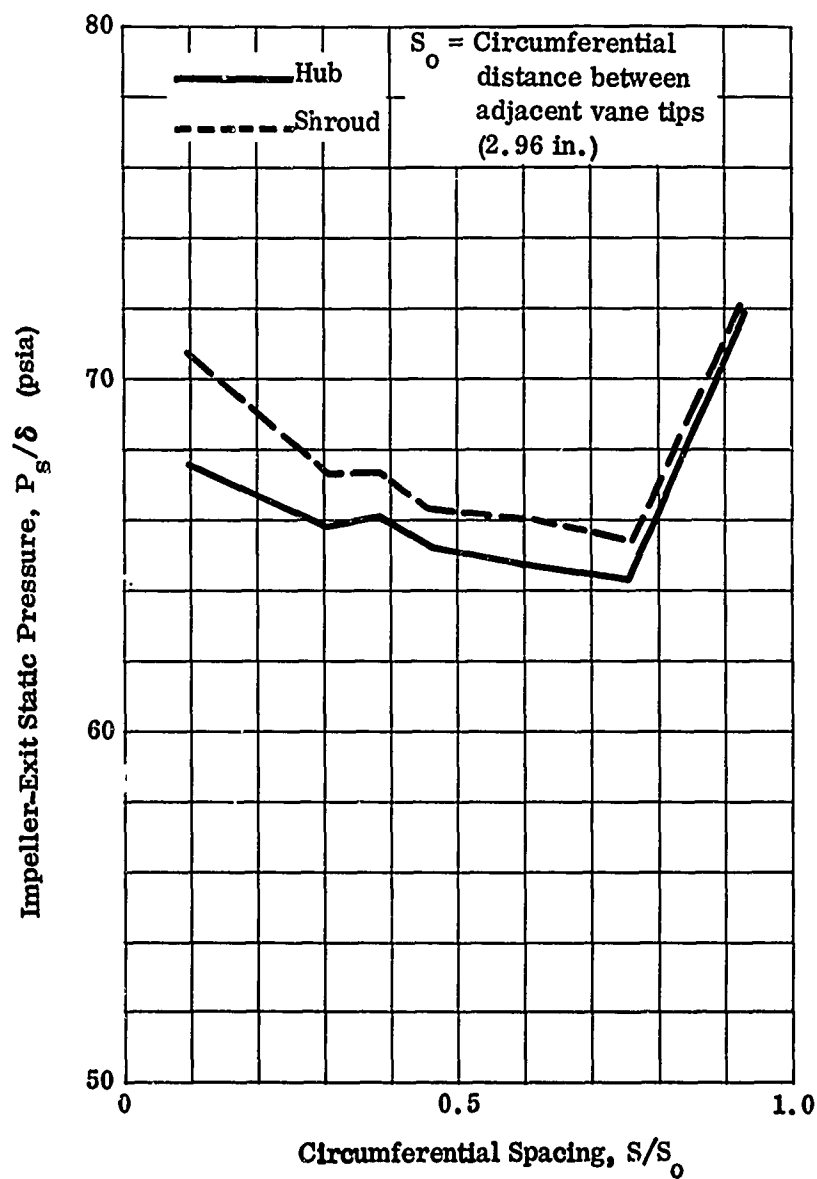


Figure 125. Circumferential Variation of Impeller-Exit Static Pressure.

CONFIDENTIAL

CONFIDENTIAL

Corrected to Ambient
Conditions of:
60°F
29.92 in. Hg

Test 3370A
 $N/\sqrt{\theta} = 35,000$ rpm
 $W\sqrt{\theta}/\delta = 0.76$ lb/sec

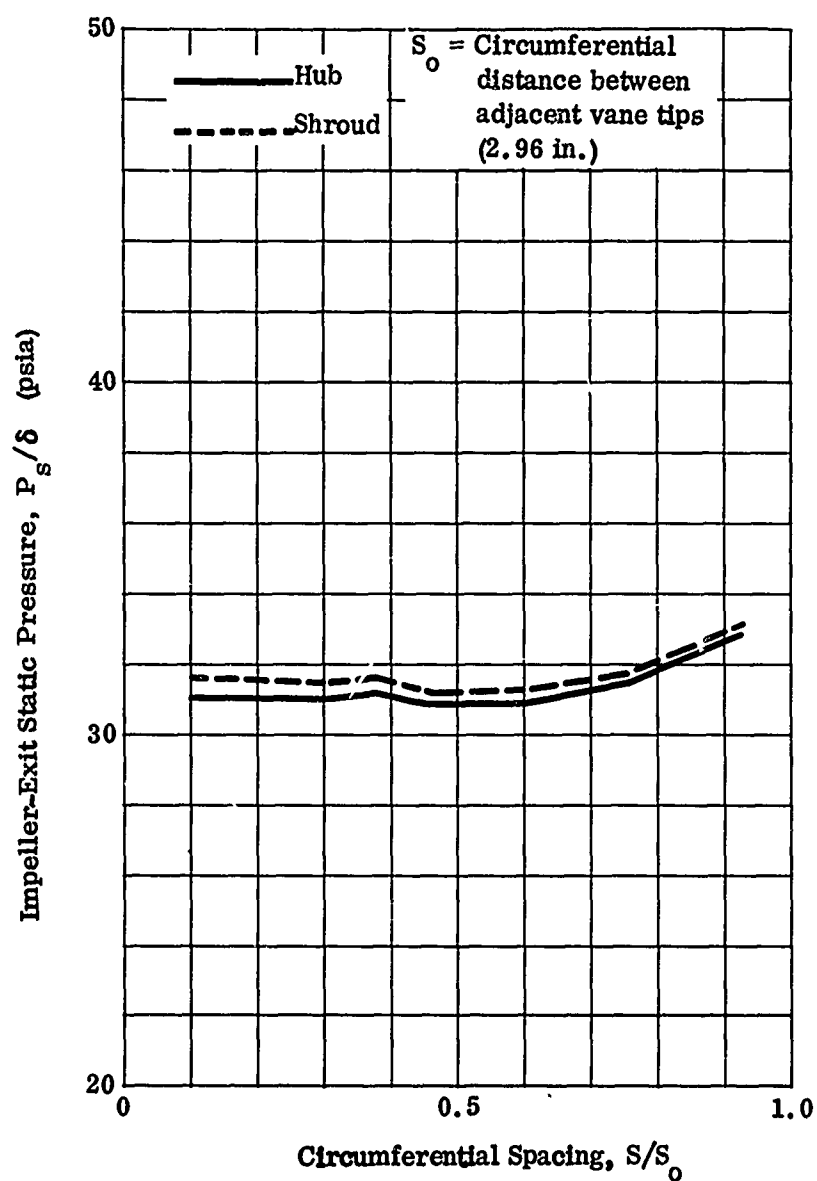


Figure 126. Circumferential Variation of Impeller-Exit Static Pressure.

CONFIDENTIAL

CONFIDENTIAL

Corrected to Ambient
Conditions of:
60°F
29.92 in. Hg

Test 3370A
 $N/\sqrt{\theta} = 35,000$ rpm
 $W_a \sqrt{\theta}/\delta = 0.79$ lb/sec

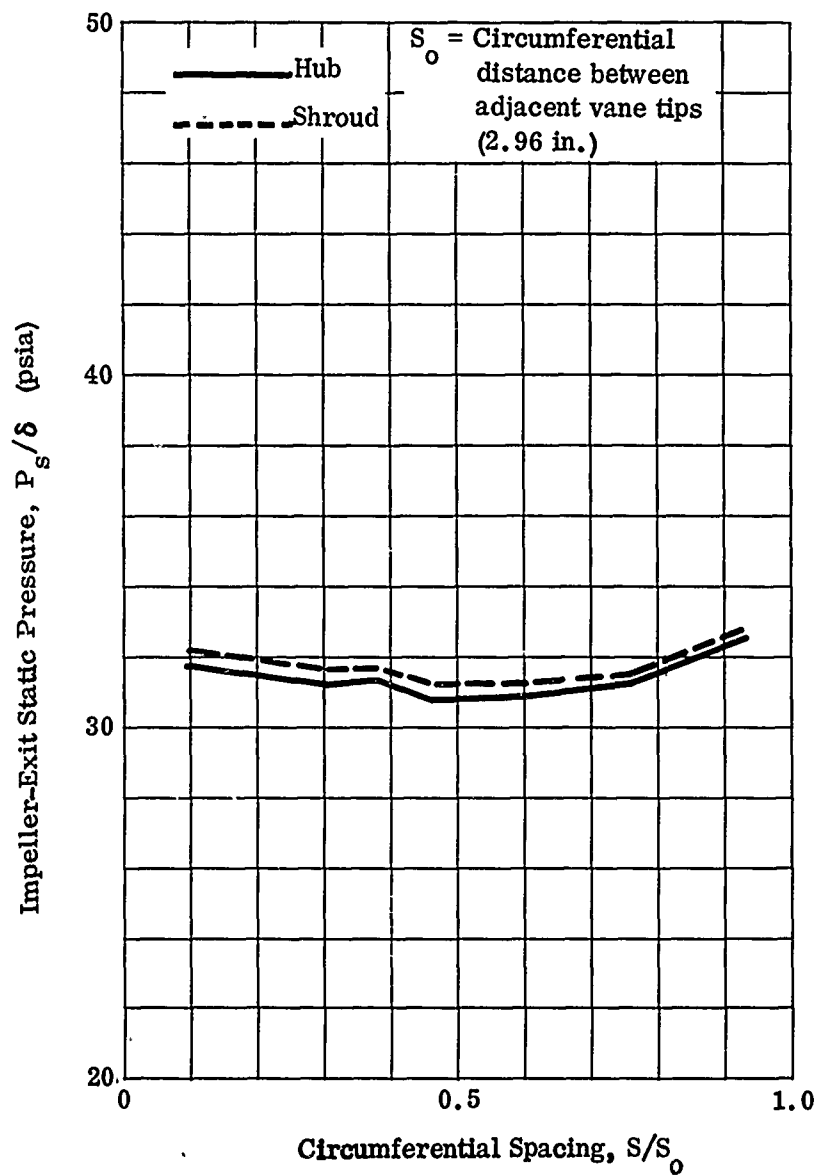


Figure 127. Circumferential Variation of Impeller-Exit Static Pressure.

CONFIDENTIAL

CONFIDENTIAL

Corrected to Ambient
Conditions of:
60°F
29.92 in. Hg

Test 3370A
 $N/\sqrt{\theta} = 35,000$ rpm
 $W_a \sqrt{\theta}/\delta = 0.82$ lb/sec

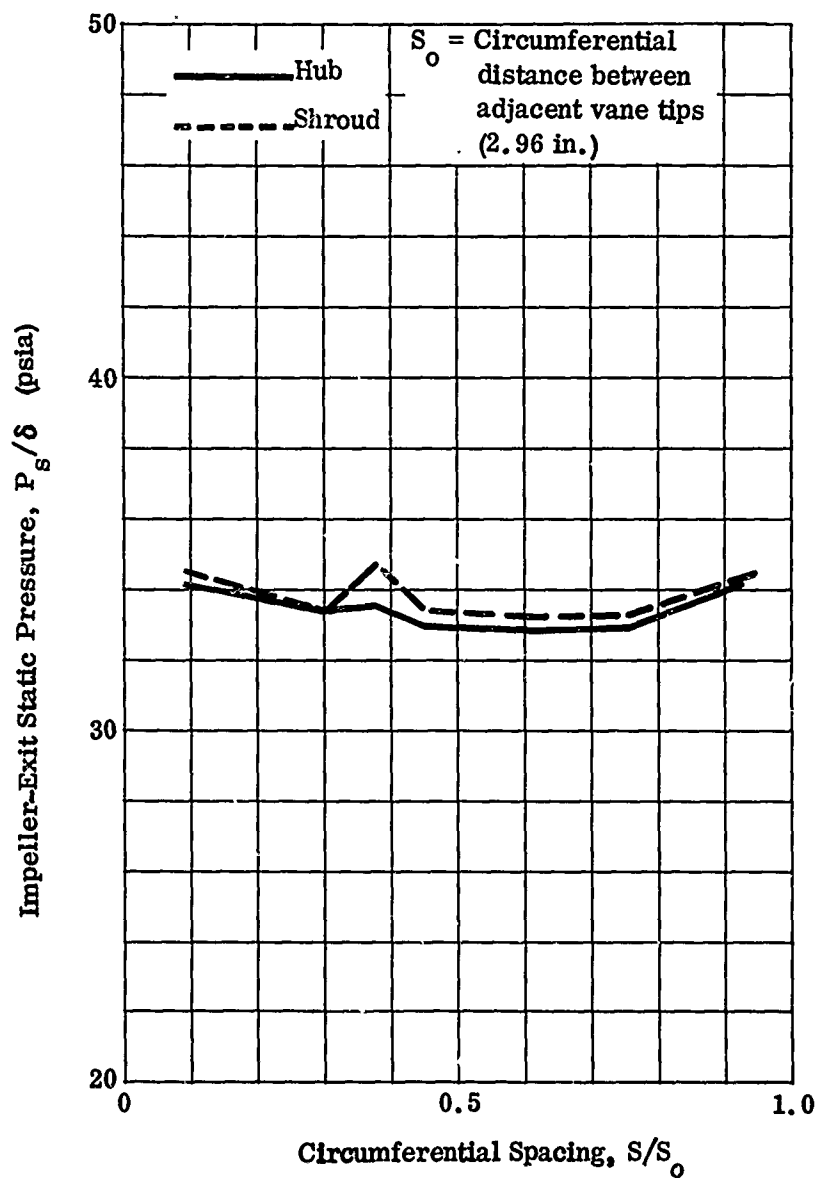


Figure 128. Circumferential Variation of Impeller-Exit Static Pressure.

CONFIDENTIAL

CONFIDENTIAL

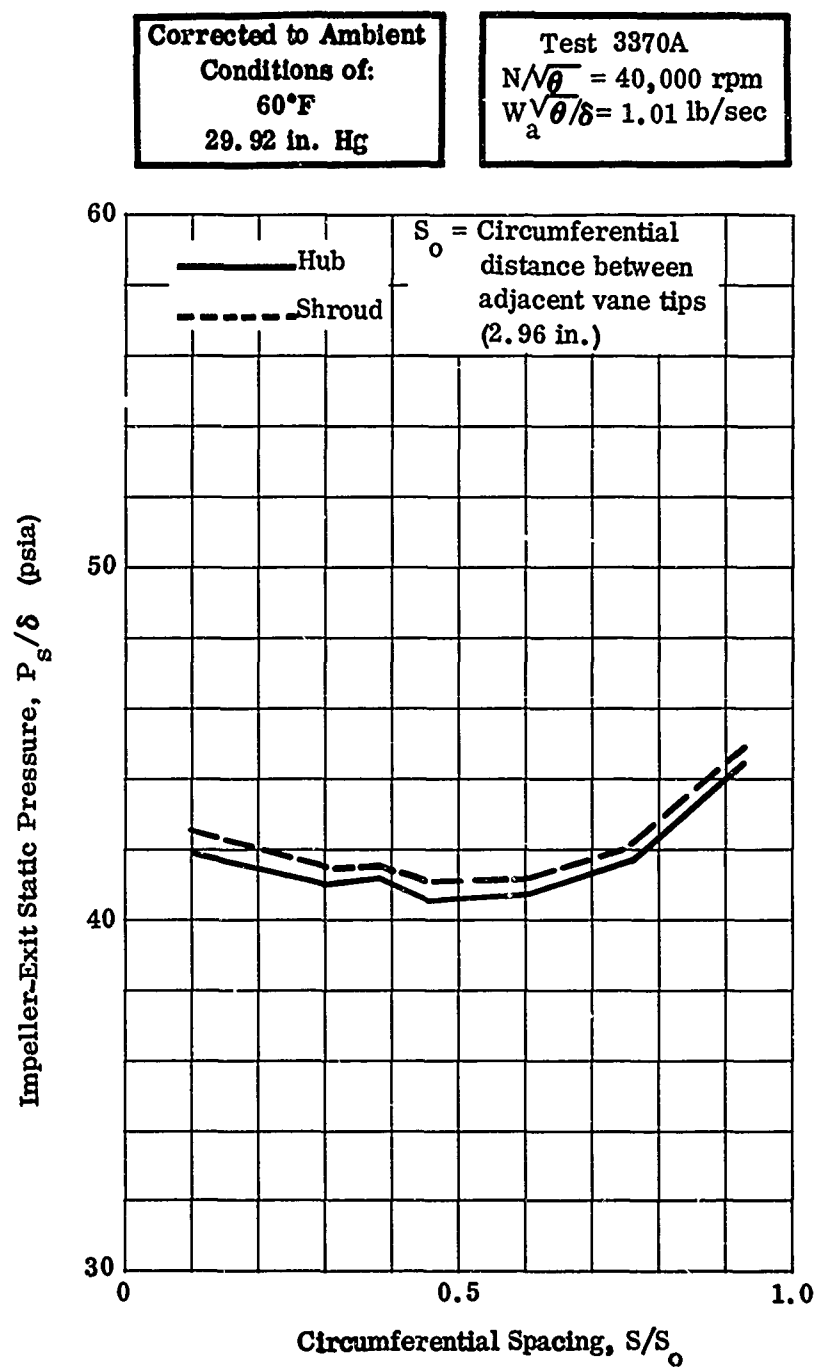


Figure 129. Circumferential Variation of Impeller-Exit Static Pressure.

CONFIDENTIAL

CONFIDENTIAL

Corrected to Ambient
Conditions of:
60°F
29.92 in. Hg

Test 3370A
 $N/\sqrt{\theta} = 40,000$ rpm
 $W_a \sqrt{\theta}/\delta = 1.04$ lb/sec

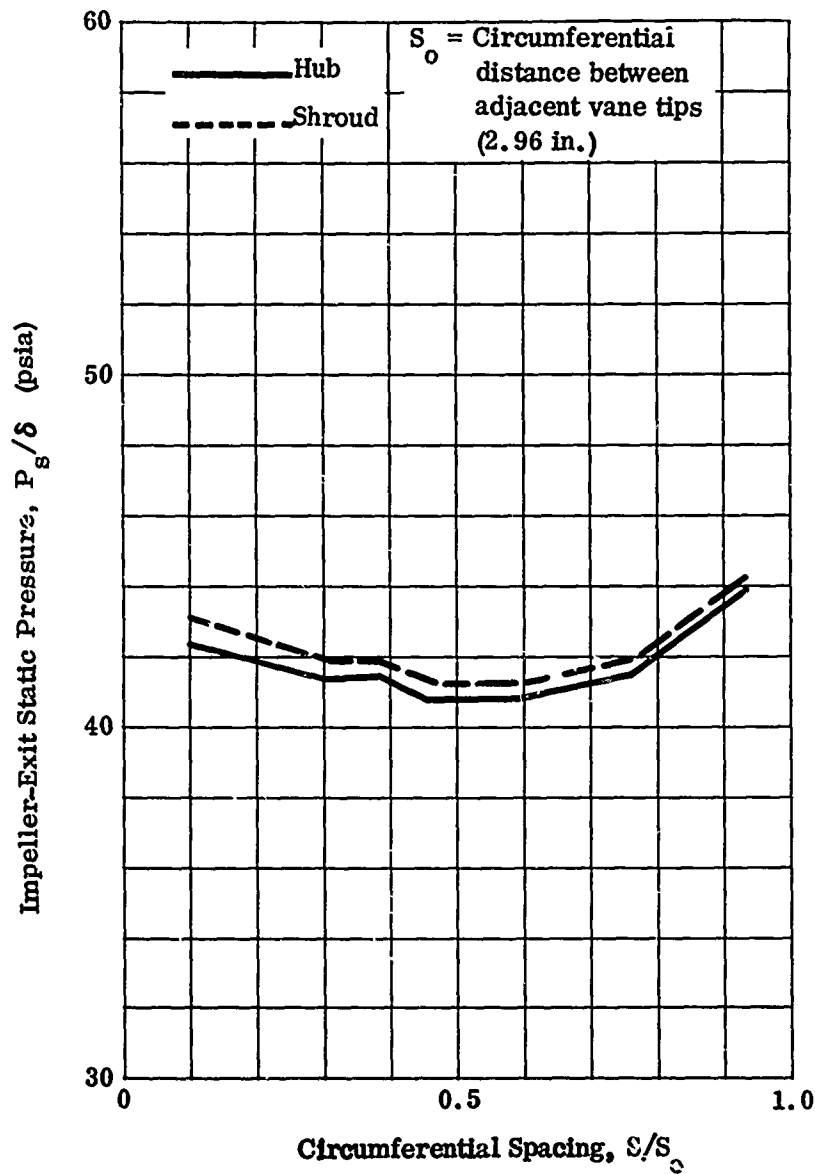


Figure 130. Circumferential Variation of Impeller-Exit Static Pressure.

CONFIDENTIAL

CONFIDENTIAL

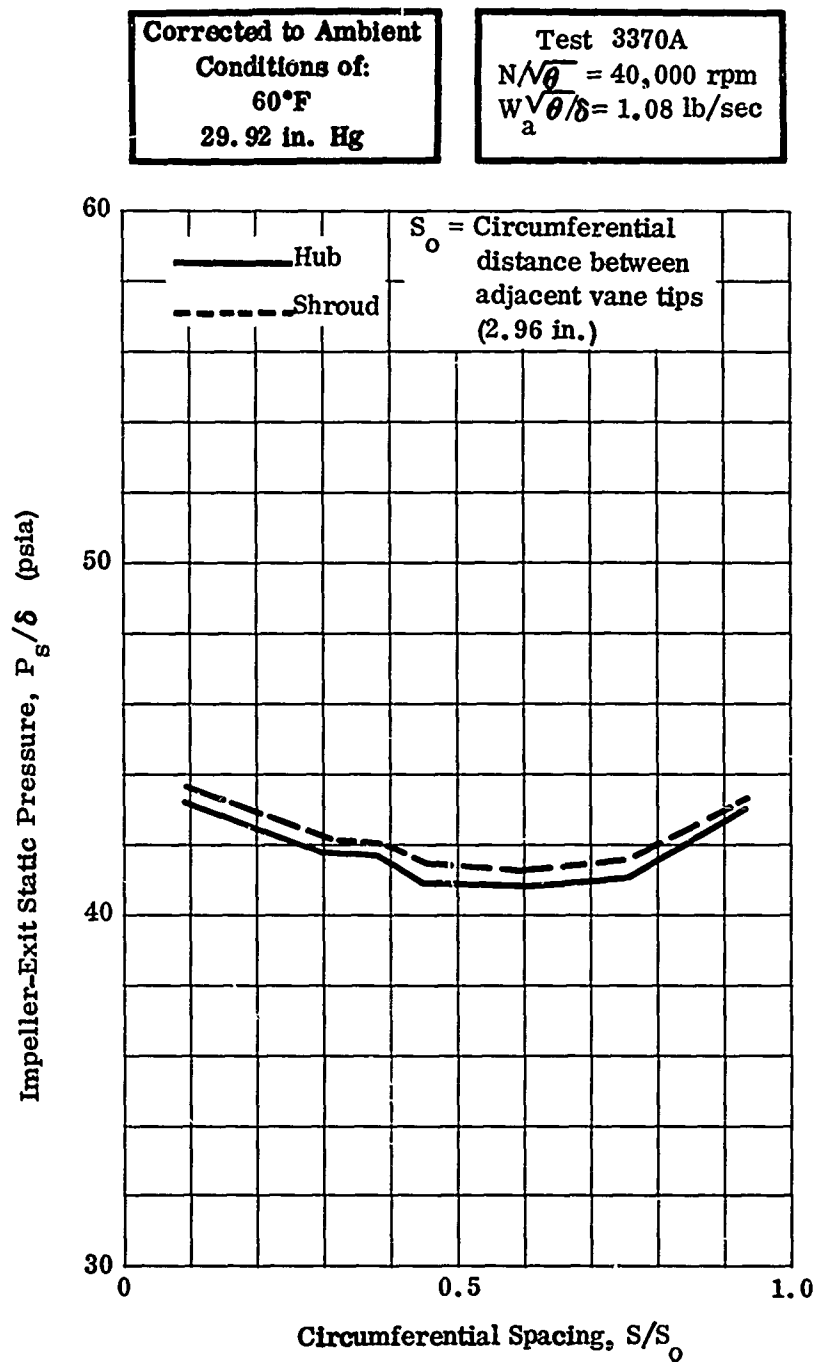


Figure 131. Circumferential Variation of Impeller-Exit Static Pressure.

CONFIDENTIAL

CONFIDENTIAL

Corrected to Ambient
Conditions of:
60°F
29.92 in. Hg

Test 3370A
 $N/\sqrt{\theta} = 45,000$ rpm
 $W_a \sqrt{\theta}/\delta = 1.39$ lb/sec

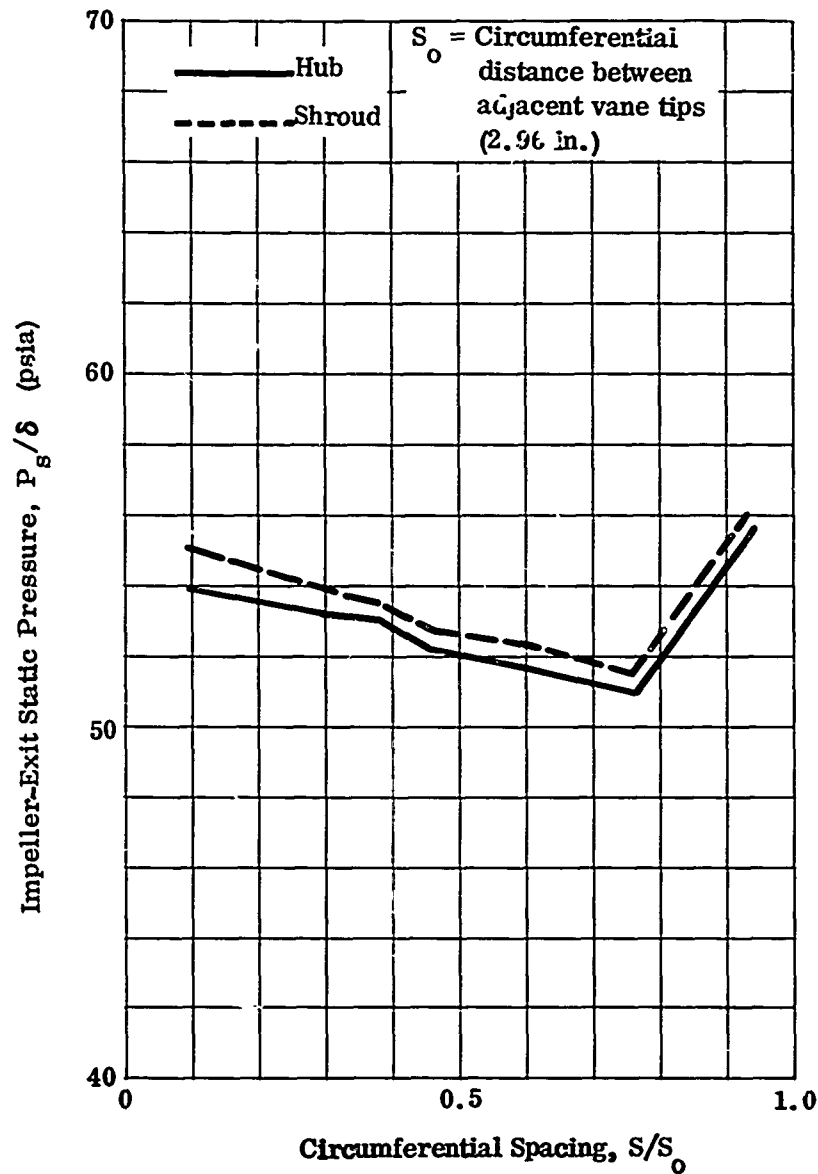


Figure 132. Circumferential Variation of Impeller-Exit Static Pressure.

CONFIDENTIAL

CONFIDENTIAL

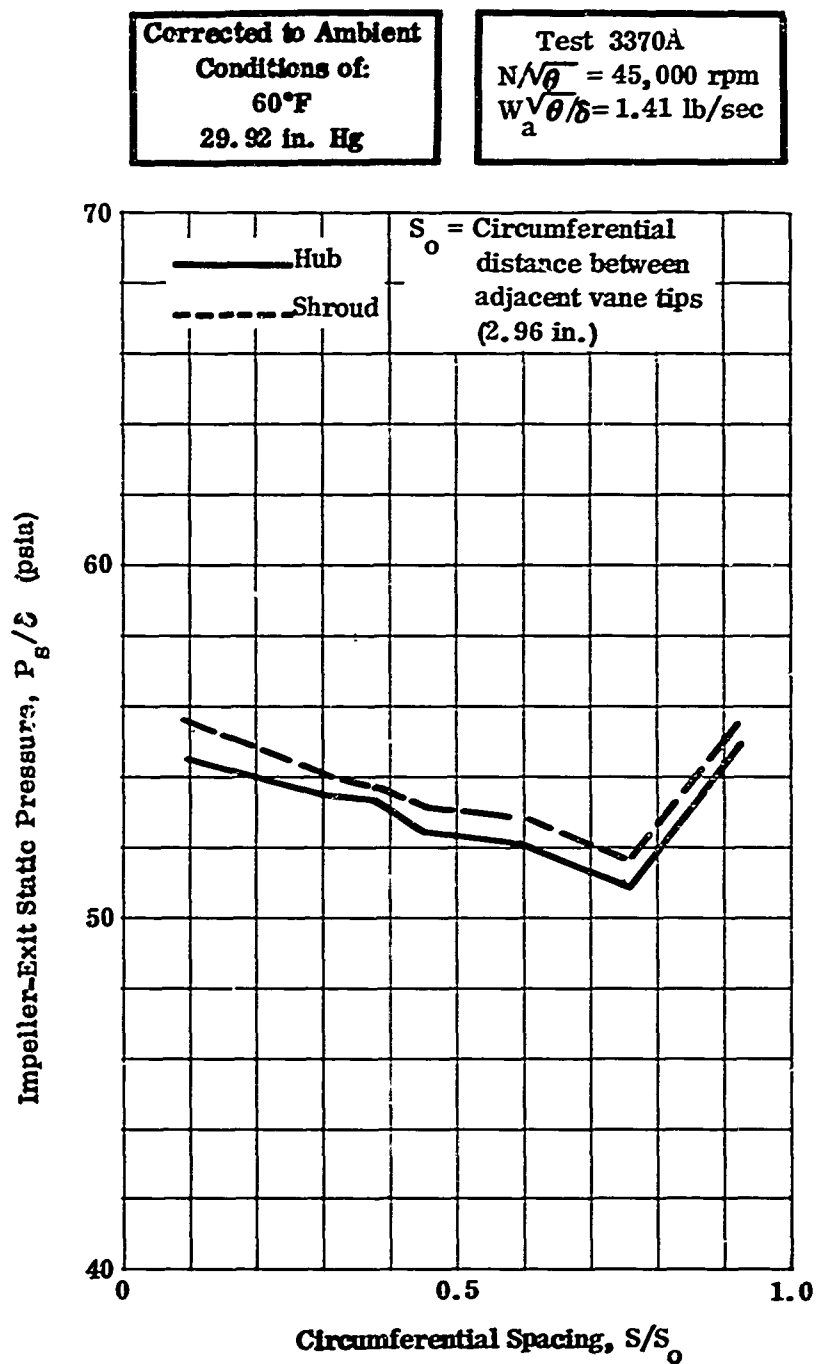


Figure 133. Circumferential Variation of Impeller-Exit Static Pressure.

CONFIDENTIAL

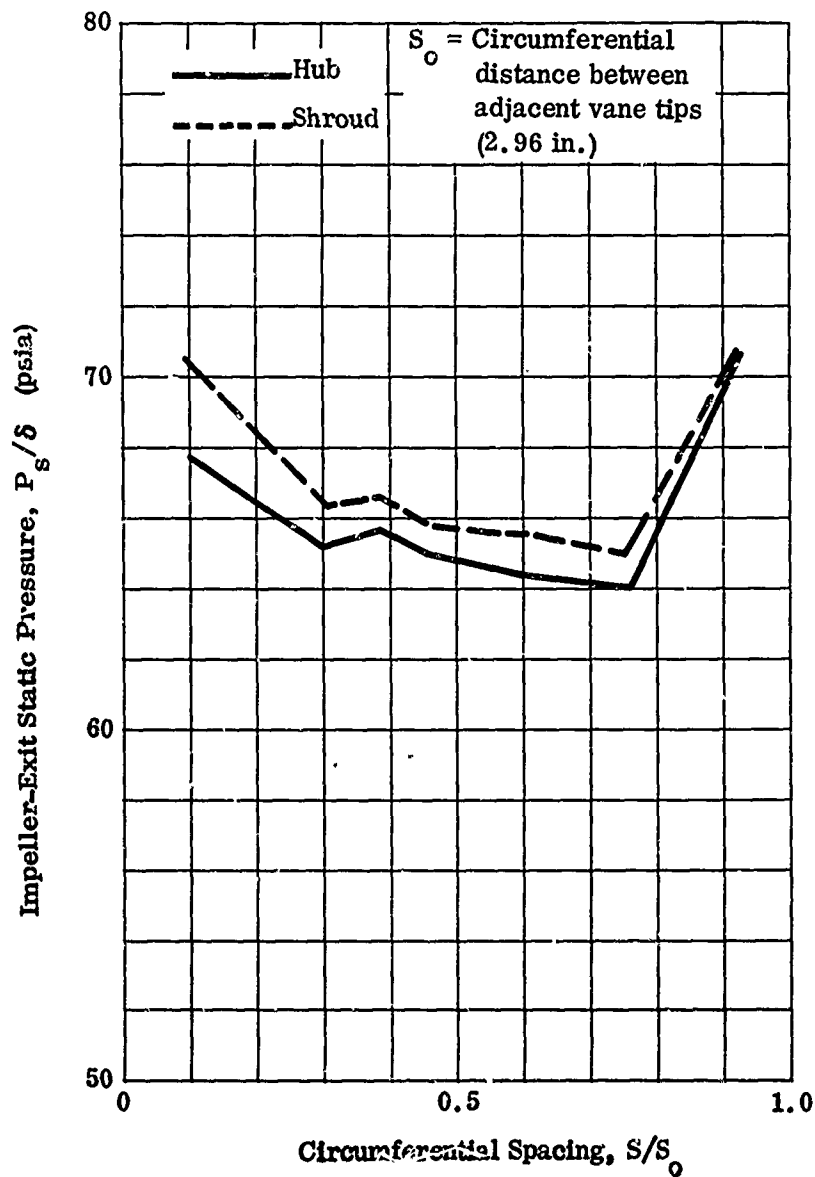
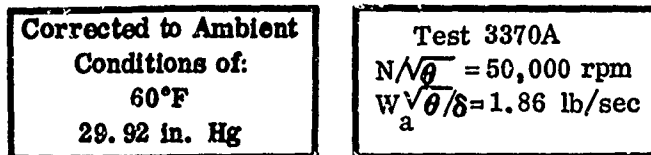


Figure 134. Circumferential Variation of Impeller-Exit Static Pressure.

CONFIDENTIAL

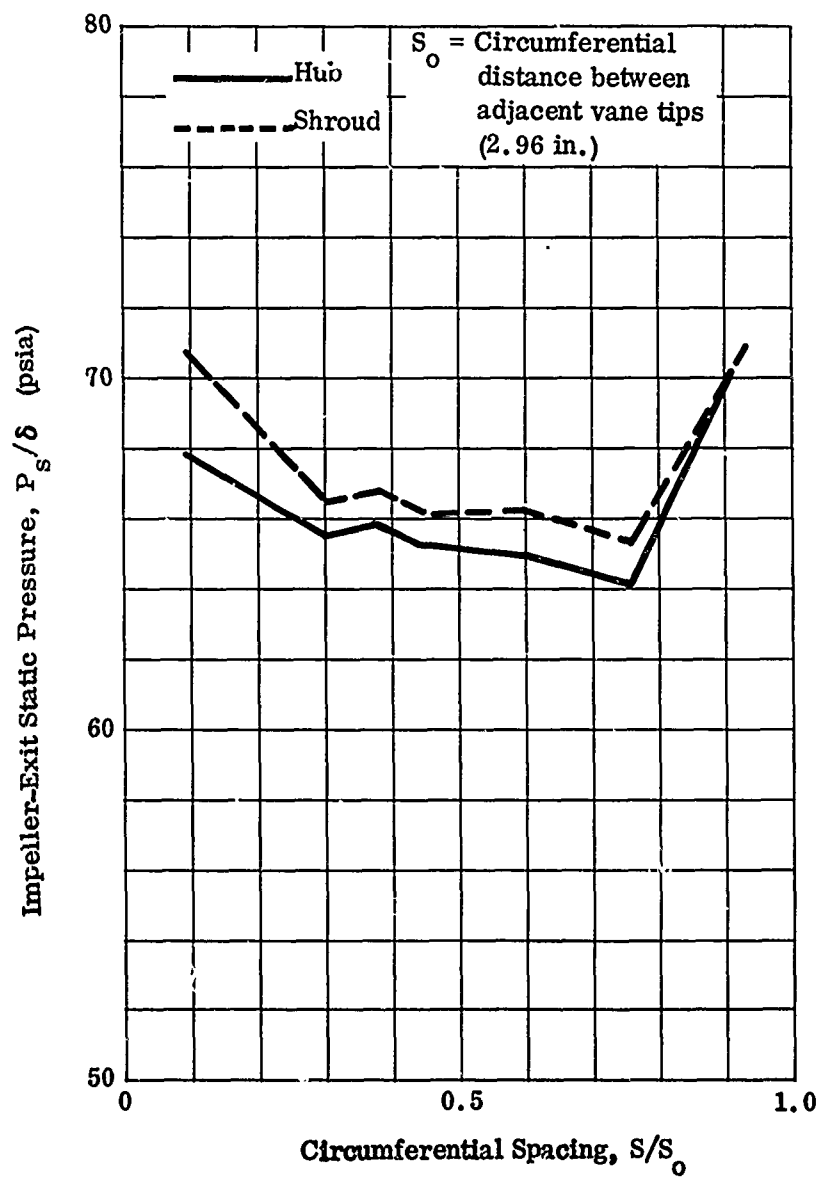
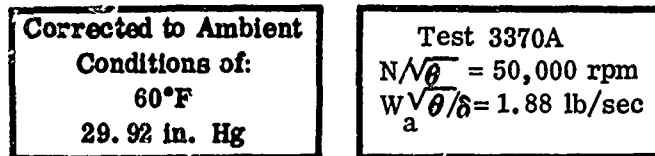


Figure 135. Circumferential Variation of Impeller-Exit Static Pressure.

CONFIDENTIAL

CONFIDENTIAL

Corrected to Ambient
Conditions of:
60°F
29.92 in. Hg

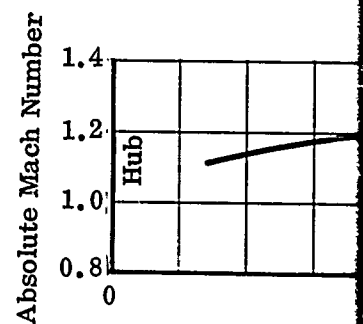
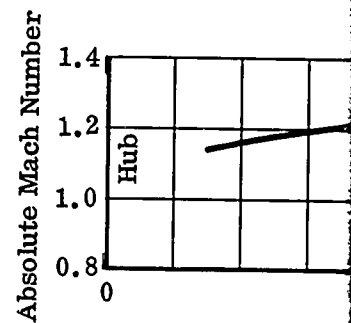
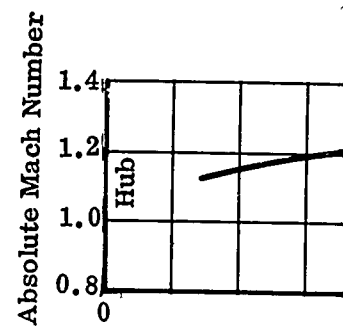
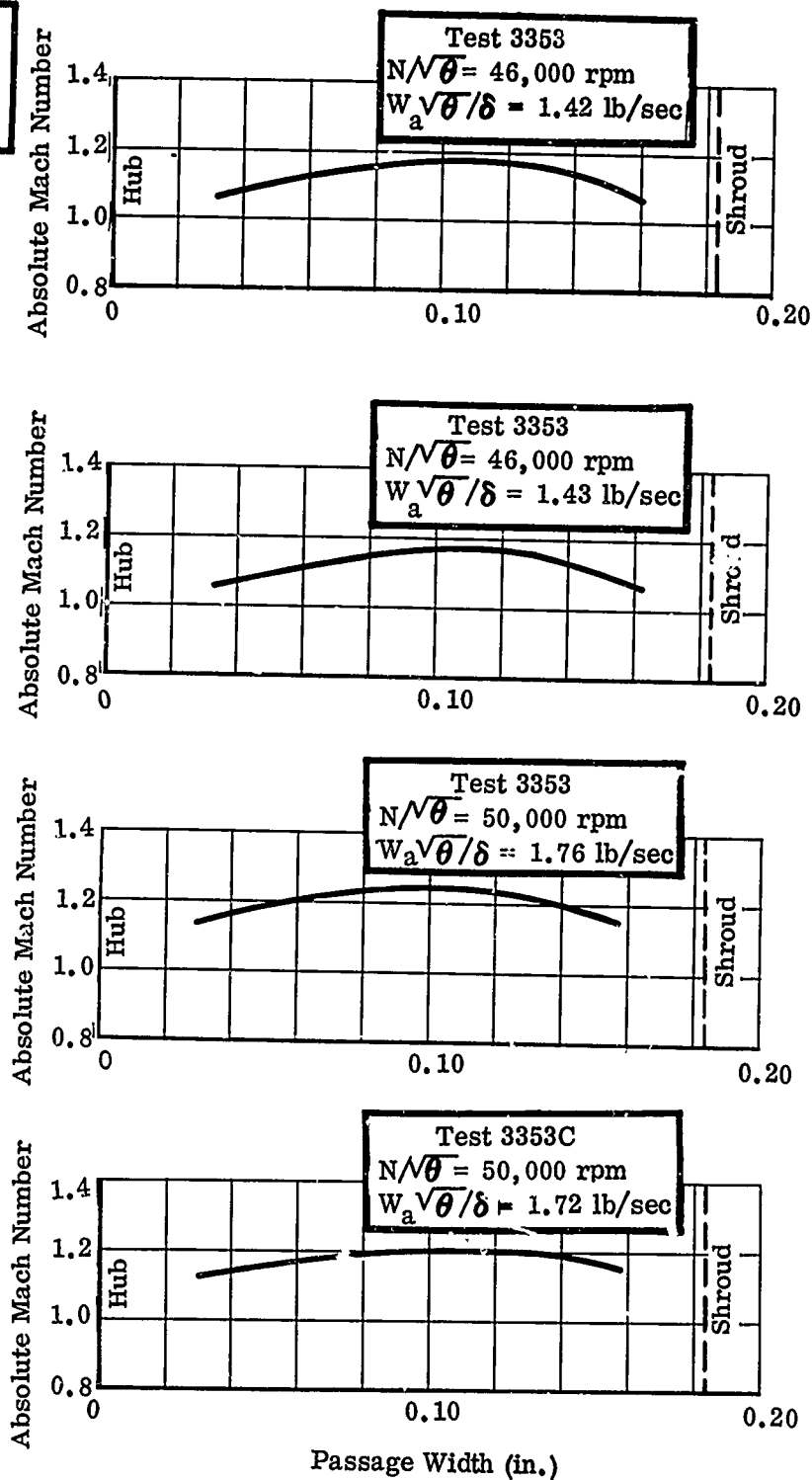
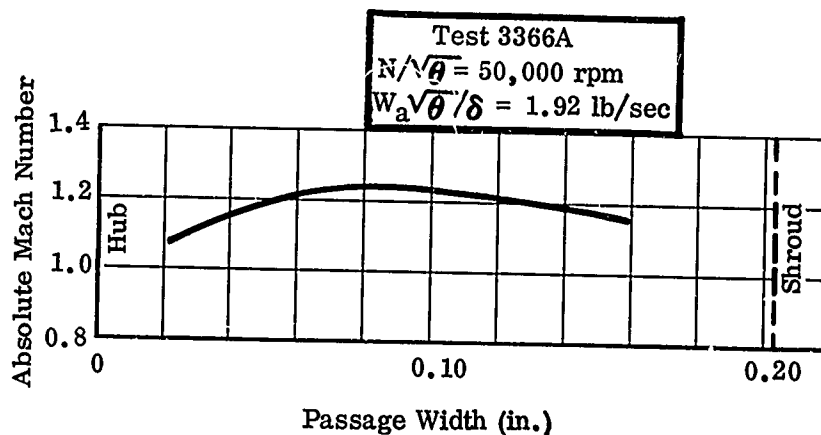
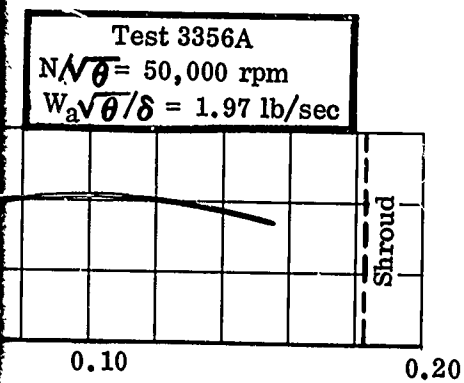
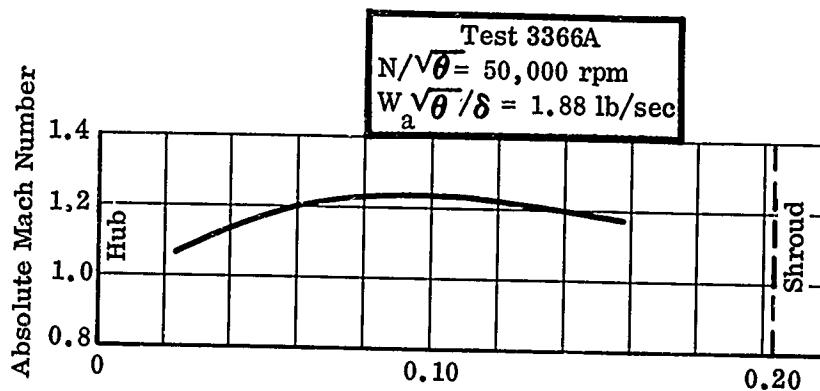
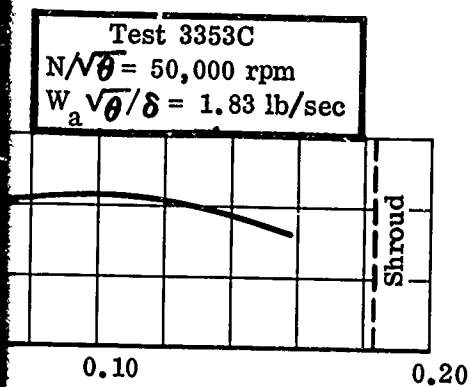
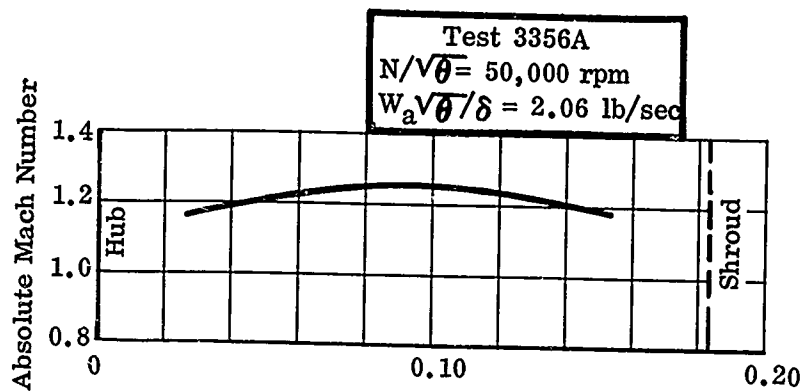
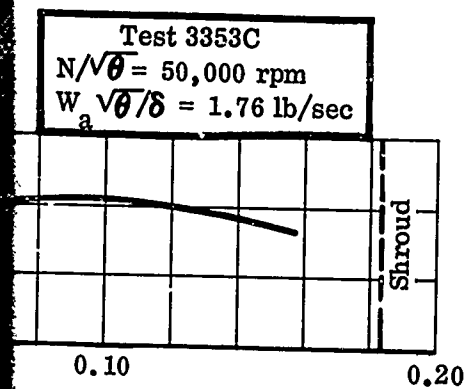


Figure 136. Impeller-Exit Mach Number Survey, RF-2.

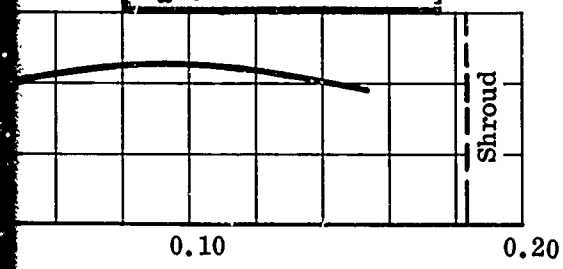
CONFIDENTIAL



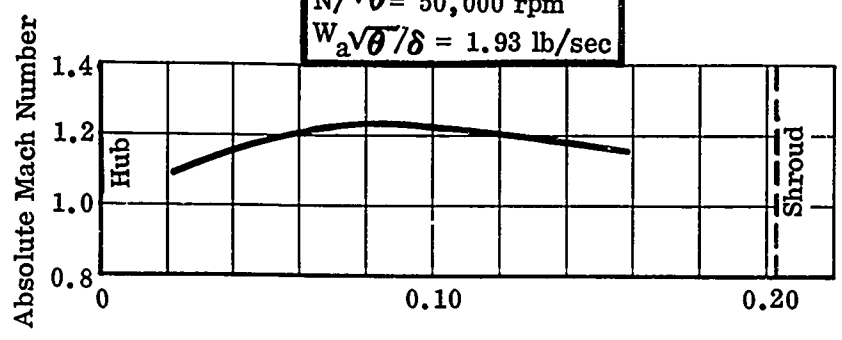
Passage Width (in.)

Passage Width (in.)

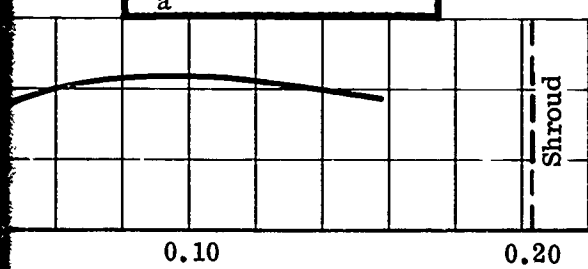
Test 3356A
 $N/\sqrt{\theta} = 50,000$ rpm
 $W_a\sqrt{\theta}/\delta = 2.06$ lb/sec



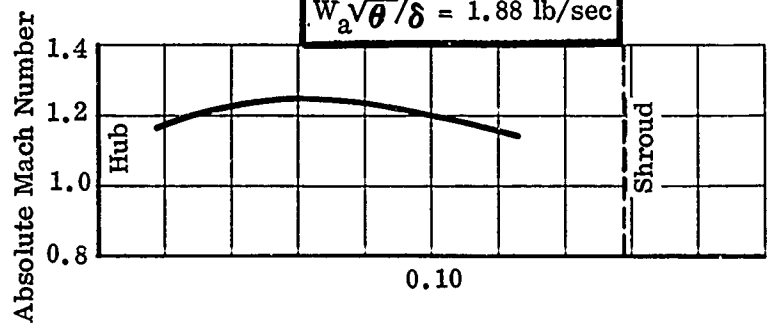
Test 3366A
 $N/\sqrt{\theta} = 50,000$ rpm
 $W_a\sqrt{\theta}/\delta = 1.93$ lb/sec



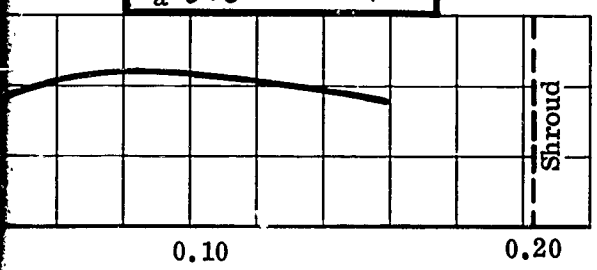
Test 3366A
 $N/\sqrt{\theta} = 50,000$ rpm
 $W_a\sqrt{\theta}/\delta = 1.88$ lb/sec



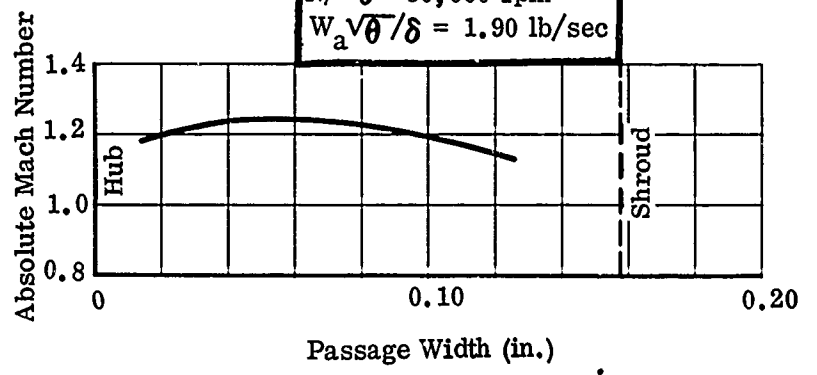
Test 3369A
 $N/\sqrt{\theta} = 50,000$ rpm
 $W_a\sqrt{\theta}/\delta = 1.88$ lb/sec



Test 3366A
 $N/\sqrt{\theta} = 50,000$ rpm
 $W_a\sqrt{\theta}/\delta = 1.92$ lb/sec



Test 3369A
 $N/\sqrt{\theta} = 50,000$ rpm
 $W_a\sqrt{\theta}/\delta = 1.90$ lb/sec



Passage Width (in.)

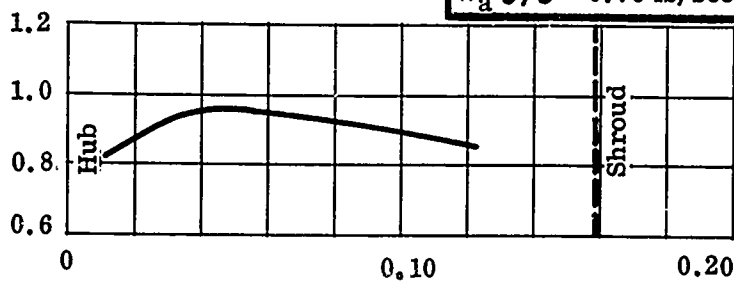
Passage Width (in.)

CONFIDENTIAL

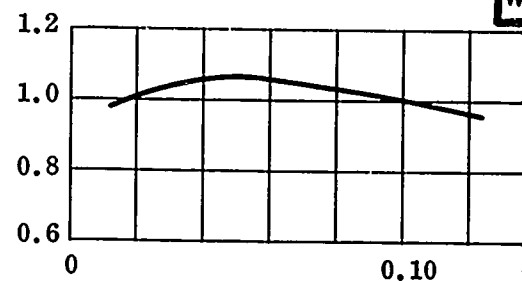
Test 3370A

$N/\sqrt{\theta} = 35,000$ rpm
 $W_a \sqrt{\theta/\delta} = 0.76$ lb/sec

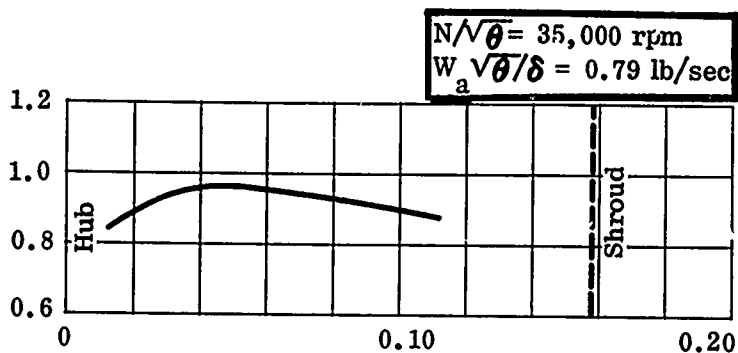
Absolute Mach Number



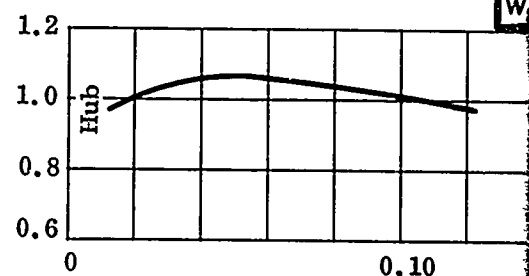
Absolute Mach Number



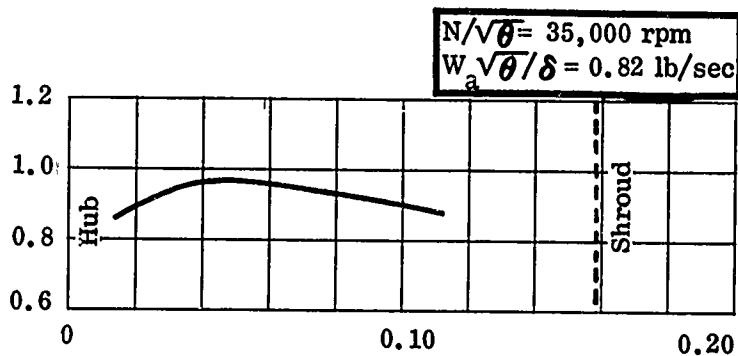
Absolute Mach Number



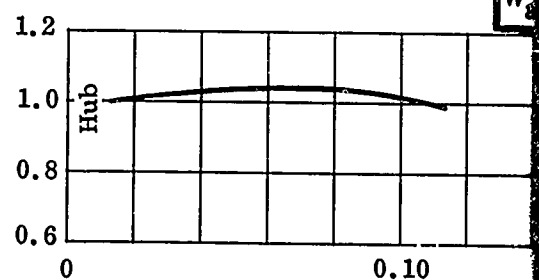
Absolute Mach Number



Absolute Mach Number



Absolute Mach Number



Passage Width (in.)

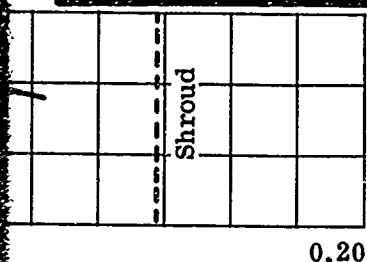
Passage Width (in.)

Figure 137. Impeller-Exit Mach Number Survey, RF-2.

CONFIDENTIAL

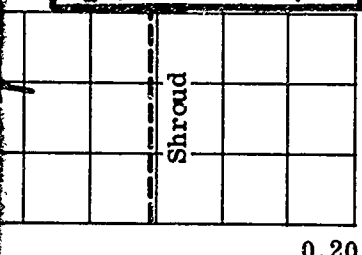
$$N/\sqrt{\theta} = 40,000 \text{ rpm}$$

$$W_a \sqrt{\theta}/\delta = 1.01 \text{ lb/sec}$$



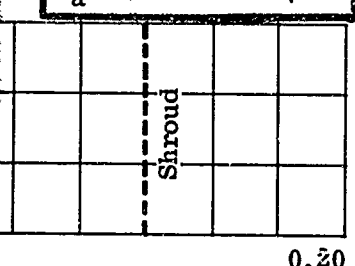
$$N/\sqrt{\theta} = 40,000 \text{ rpm}$$

$$W_a \sqrt{\theta}/\delta = 1.04 \text{ lb/sec}$$

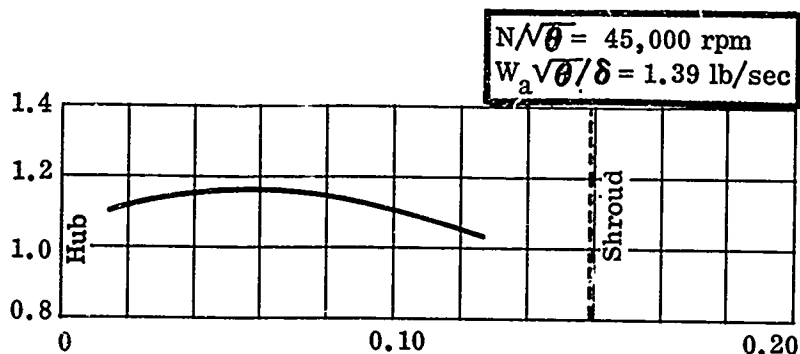


$$N/\sqrt{\theta} = 40,000 \text{ rpm}$$

$$W_a \sqrt{\theta}/\delta = 1.08 \text{ lb/sec}$$

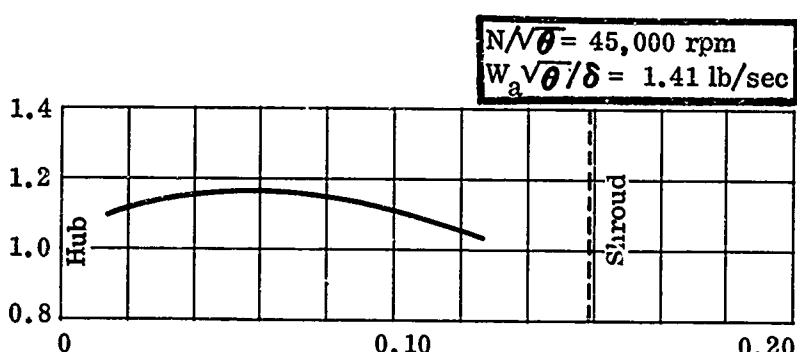


Absolute Mach Number



Absolute Mach Number

Absolute Mach Number

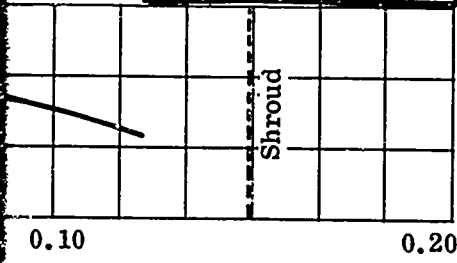


Absolute Mach Number

Passage Width (in.)

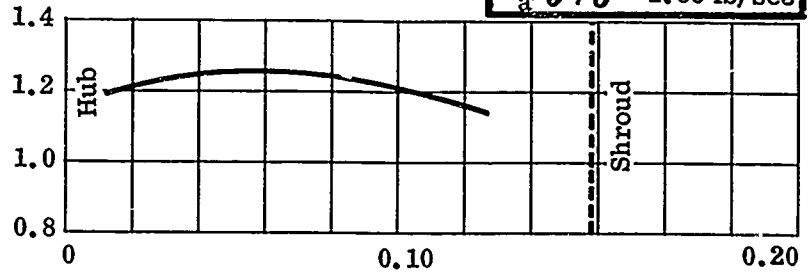
Width (in.)

$N/\sqrt{\theta} = 45,000 \text{ rpm}$
 $W_a \sqrt{\theta}/\delta = 1.39 \text{ lb/sec}$

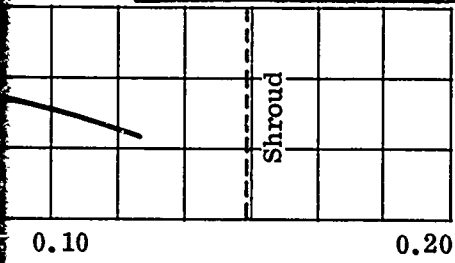


Absolute Mach Number

$N/\sqrt{\theta} = 50,000 \text{ rpm}$
 $W_a \sqrt{\theta}/\delta = 1.86 \text{ lb/sec}$

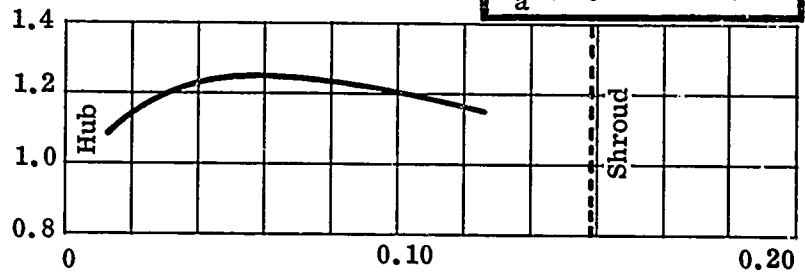


$N/\sqrt{\theta} = 45,000 \text{ rpm}$
 $W_a \sqrt{\theta}/\delta = 1.41 \text{ lb/sec}$



Absolute Mach Number

$N/\sqrt{\theta} = 50,000 \text{ rpm}$
 $W_a \sqrt{\theta}/\delta = 1.88 \text{ lb/sec}$



Passage Width (in.)

Passage Width (in.)

Corrected to Ambient
Conditions of:
60°F
29.92 in. Hg
All Velocities in fps

Test 3353

$N/\sqrt{\theta} = 46,000$ rpm

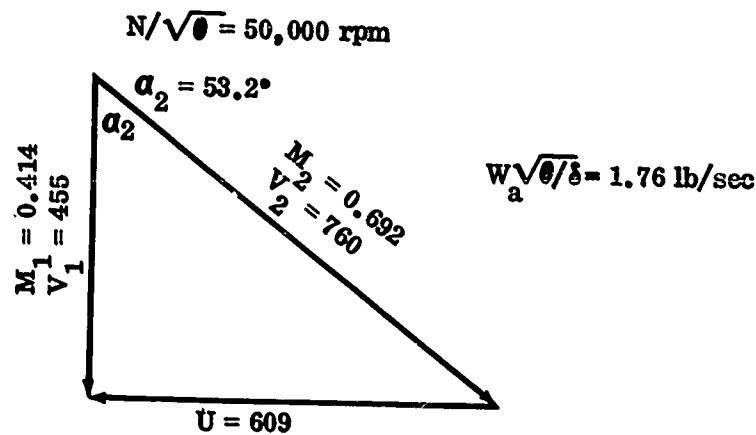
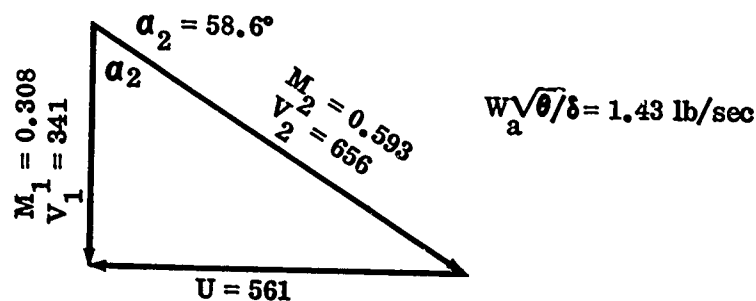
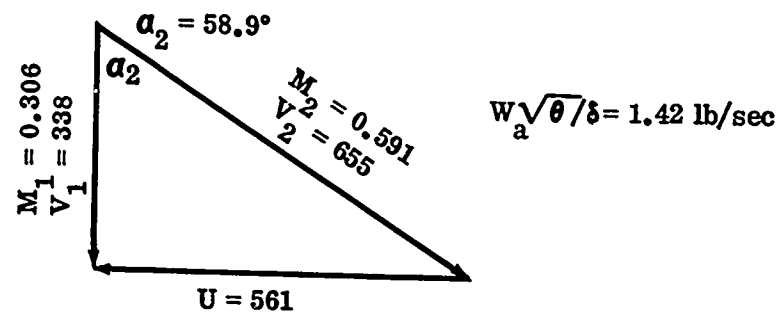


Figure 138. Inlet Vector Diagrams, RF-2.

CONFIDENTIAL

Corrected to Ambient
Conditions of:
60°F
29.92 in. Hg
All Velocities in fps

Test 3353C

$N/\sqrt{\theta} = 50,000$ rpm

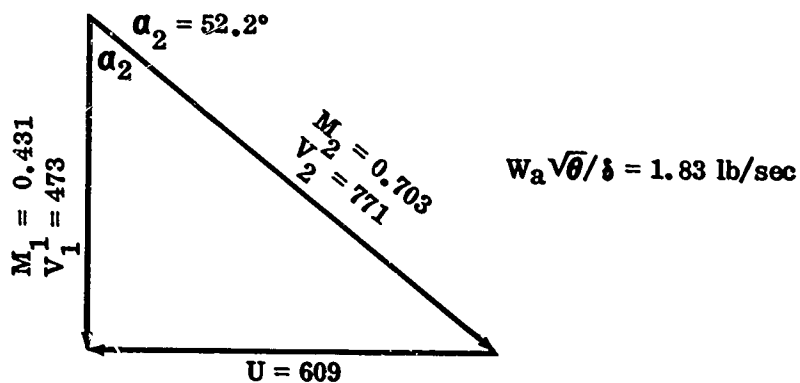
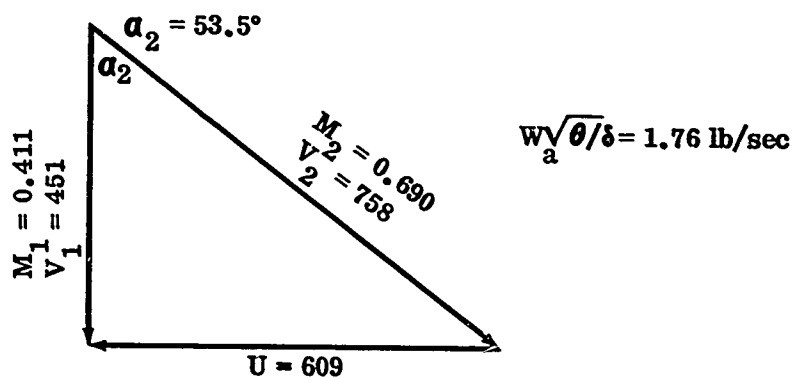
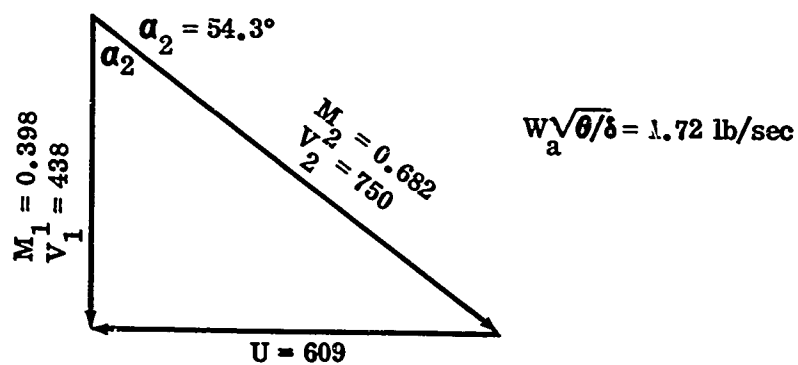


Figure 139. Inlet Vector Diagrams, RF-2.

CONFIDENTIAL

CONFIDENTIAL

Corrected to Ambient

Conditions of:

60°F

29.92 in. Hg

All Velocities in fps

Test 3366A

$N/\sqrt{\theta} = 50,000 \text{ rpm}$

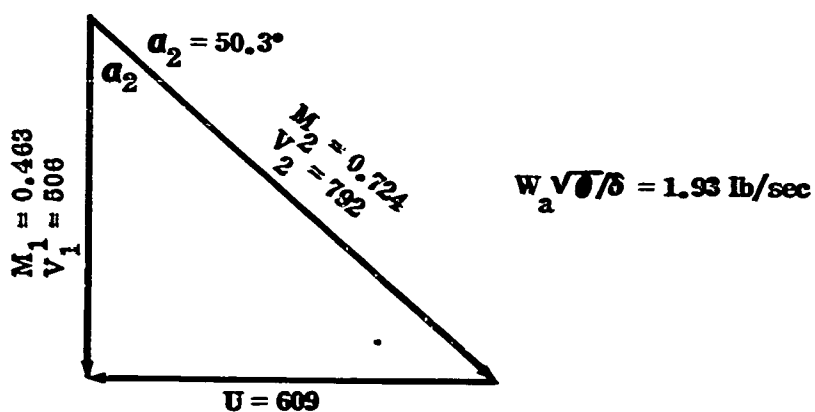
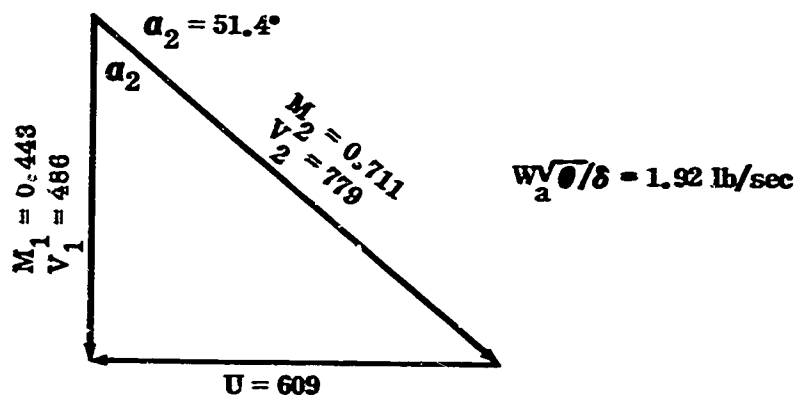
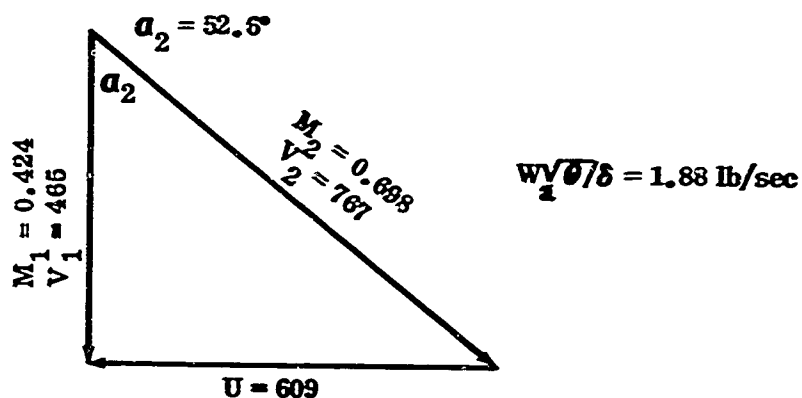


Figure 141. Inlet Vector Diagrams, RF-2.

CONFIDENTIAL

CONFIDENTIAL

Corrected to Ambient
Conditions of:
60°F
29.92 in. Hg
All Velocities in fps

Test 3369A

$N/\sqrt{\theta} = 50,000 \text{ rpm}$

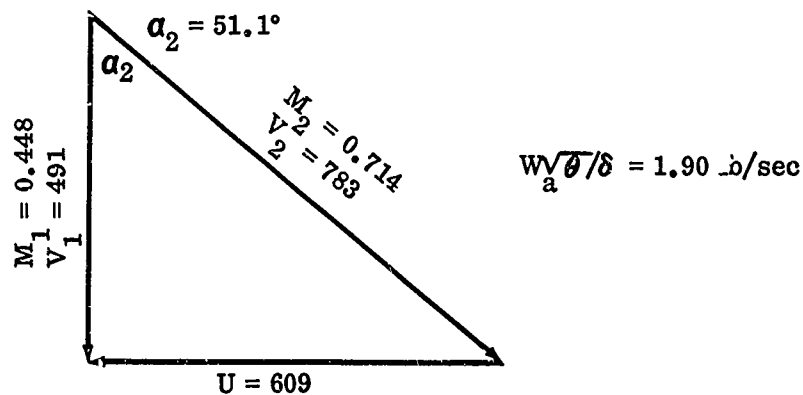
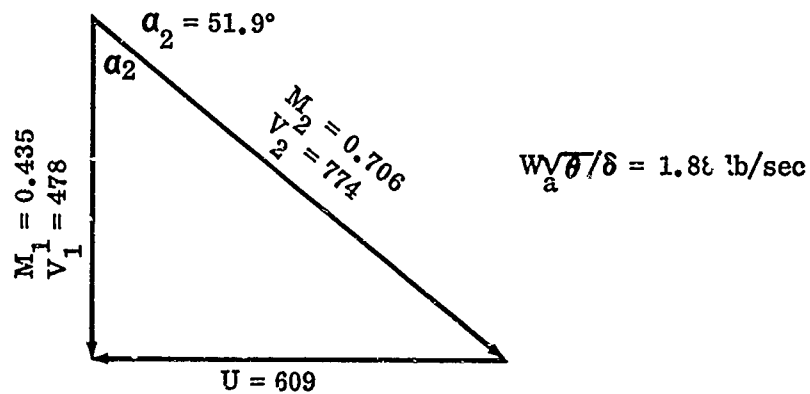


Figure 142. Inlet Vector Diagrams, RF-2.

CONFIDENTIAL

CONFIDENTIAL

Corrected to Ambient
Conditions of:
60°F
29.92 in. Hg
All Velocities in fps

Test 3370A

$N/\sqrt{\theta} = 35,000 \text{ rpm}$

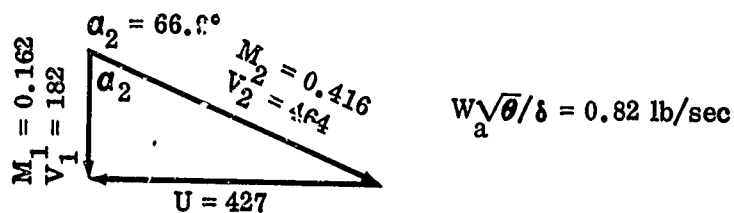
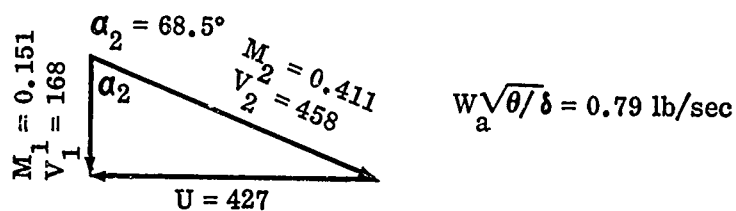
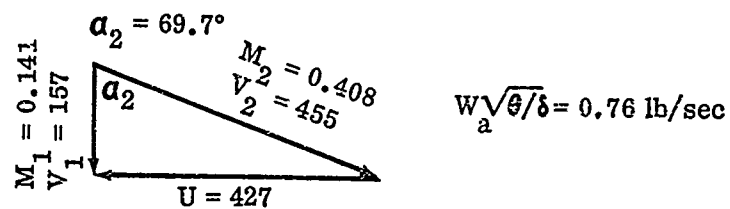


Figure 143. Inlet Vector Diagrams, RF-2.

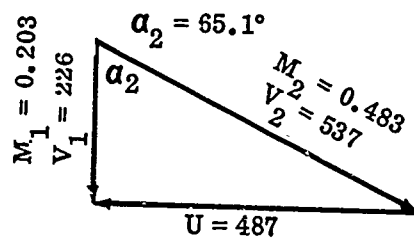
CONFIDENTIAL

CONFIDENTIAL

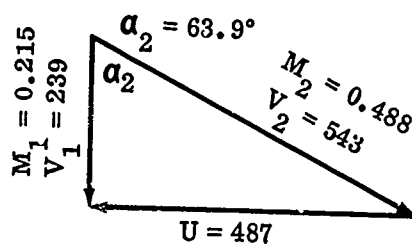
Corrected to Ambient
Conditions of:
60°F
29.92 in. Hg.
All Velocities in fps

Test 3370A

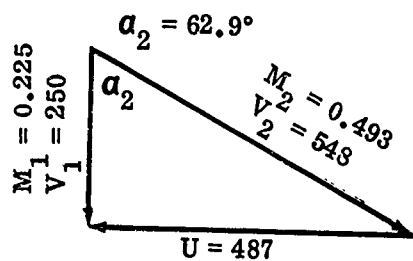
$N/\sqrt{\theta} = 40,000 \text{ rpm}$



$W_a \sqrt{\theta} / \delta = 1.01 \text{ lb/sec}$



$W_a \sqrt{\theta} / \delta = 104. \text{ lb/sec}$



$W_a \sqrt{\theta} / \delta = 1.08 \text{ lb/sec}$

Figure 144. Inlet Vector Diagrams, RF-2.

CONFIDENTIAL

CONFIDENTIAL

Corrected to Ambient
Conditions of :
60°F
29.92 in. Hg
All Velocities in fps

Test 3370A

$N/\sqrt{\theta} = 45,000$ rpm

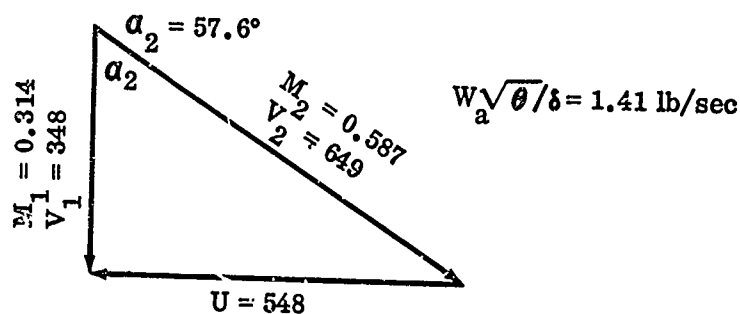
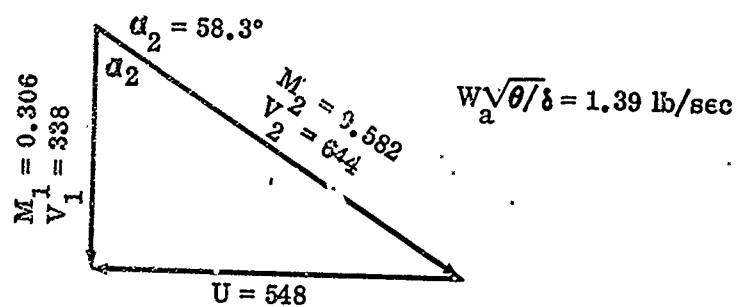


Figure 145. Inlet Vector Diagrams, RF-2.

CONFIDENTIAL

CONFIDENTIAL

Corrected to Ambient
Conditions of:
60°F
29.92 in. Hg
All Velocities in fps

Test 3370A

$N/\sqrt{G} = 50,000$ rpm

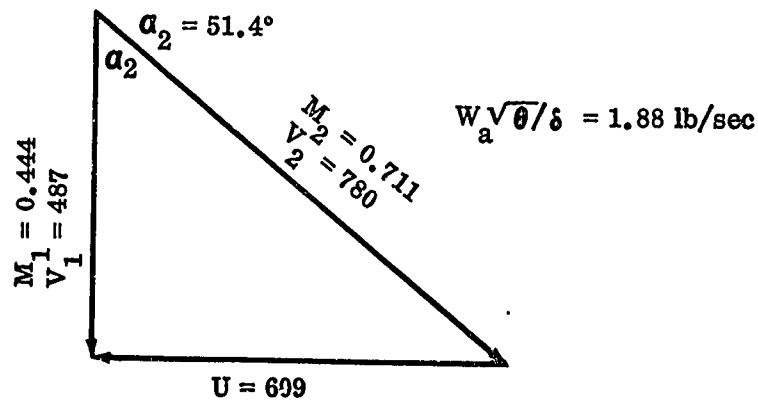
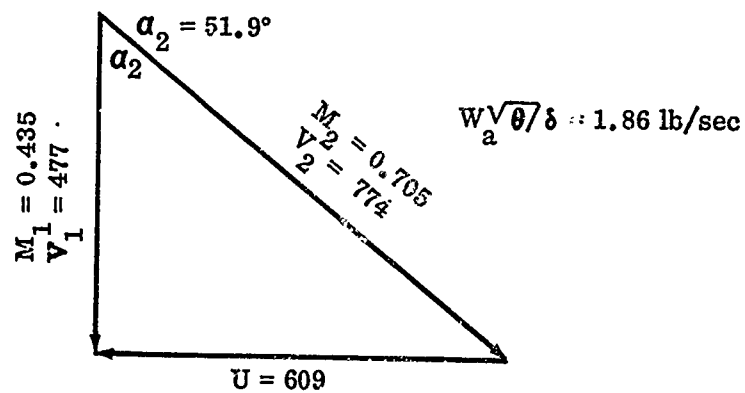


Figure 146. Inlet Vector Diagrams, RF-2.

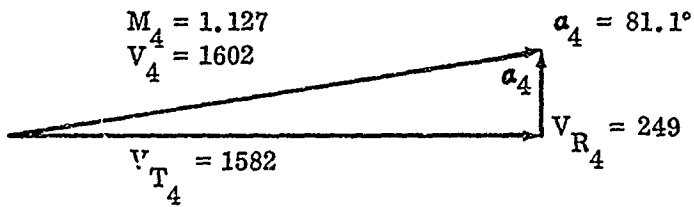
CONFIDENTIAL

CONFIDENTIAL

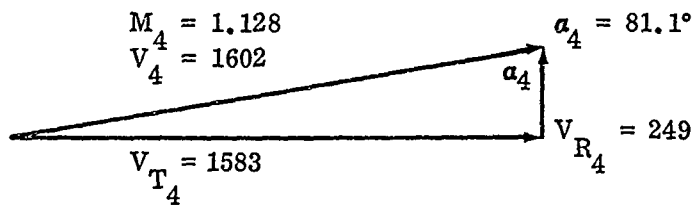
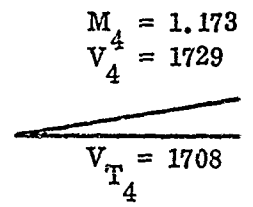
Corrected to Ambient
Conditions of:
60°F
29.92 in. Hg
All Velocities in fps

Test 3353

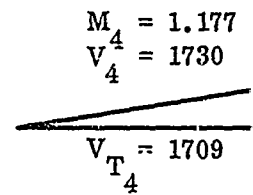
$N/\sqrt{\theta} = 46,000$ rpm



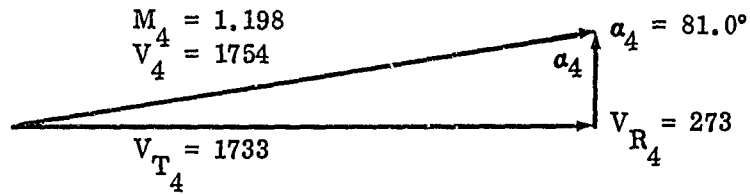
$$W_a \sqrt{\theta} / \delta = 1.42 \text{ lb/sec}$$



$$W_a \sqrt{\theta} / \delta = 1.43 \text{ lb/sec}$$



$N/\sqrt{\theta} 50,000$ rpm



$$W_a \sqrt{\theta} / \delta = 1.76 \text{ lb/sec}$$

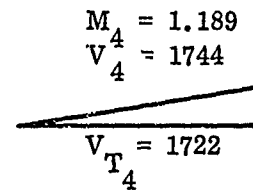


Figure 147. Exit Vector Diagrams at 1.028 Radius Ratio, RF-2.

CONFIDENTIAL

1

Test 3353C

$N/\sqrt{\theta} = 50,000$ rpm

$= 1.173$
 $= 1729$

$= 1708$

$\alpha_4 = 81.1^\circ$

α_4

$V_{R_4} = 268$

$W_a \sqrt{\theta}/\delta = 1.72$ lb/sec

$M_4 = 1.175$
 $V_4 = 1725$

$V_{T_4} = 1704$

$= 1.177$
 $= 1730$

$= 1709$

$\alpha_4 = 81.0^\circ$

α_4

$V_{R_4} = 269$

$W_a \sqrt{\theta}/\delta = 1.76$ lb/sec

$M_4 = 1.217$
 $V_4 = 1770$

$V_{T_4} = 1746$

$= 1.189$
 $= 1744$

$= 1722$

$\alpha_4 = 81.0^\circ$

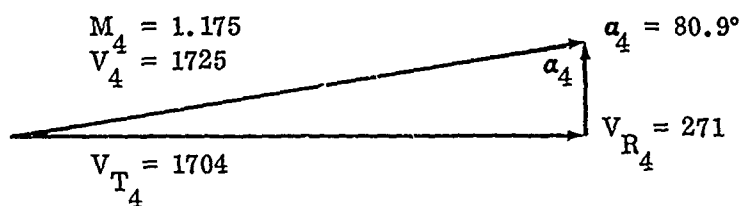
α_4

$V_{R_4} = 272$

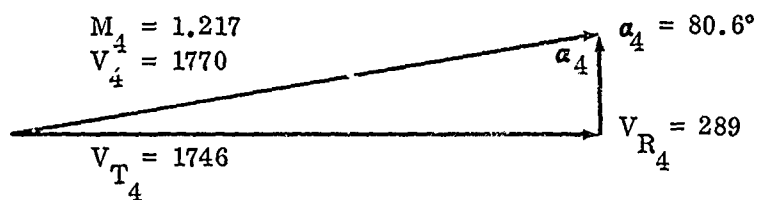
$W_a \sqrt{\theta}/\delta = 1.83$ lb/sec

Test 3356A

$N/\sqrt{\theta} = 50,000 \text{ rpm}$



$$W_a \sqrt{\theta} / \delta = 1.97 \text{ lb/sec}$$



$$W_a \sqrt{\theta} / \delta = 2.06 \text{ lb/sec}$$

CONFIDENTIAL

Corrected to Ambient
Conditions of:
60°F
29.92 in. Hg
All Velocities in fps

Test 3366A

$N/\sqrt{\theta} = 50,000$ rpm

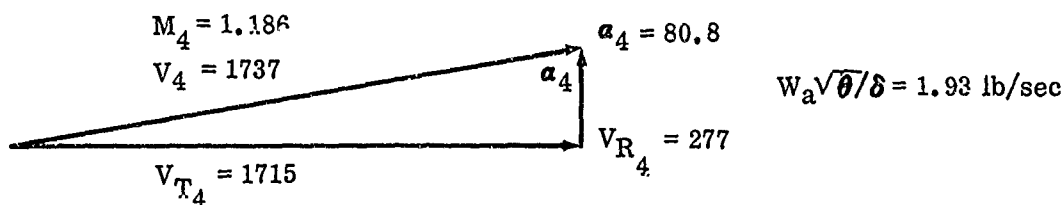
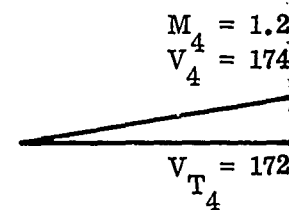
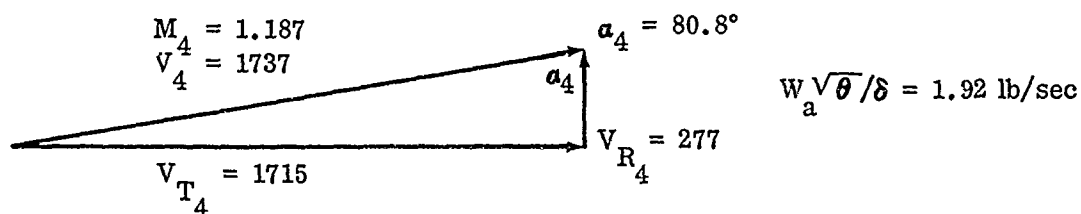
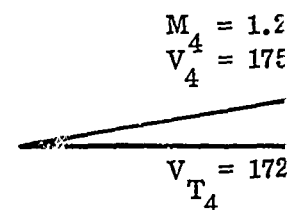
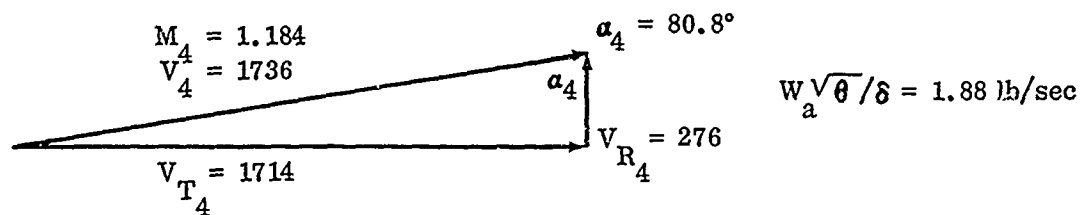
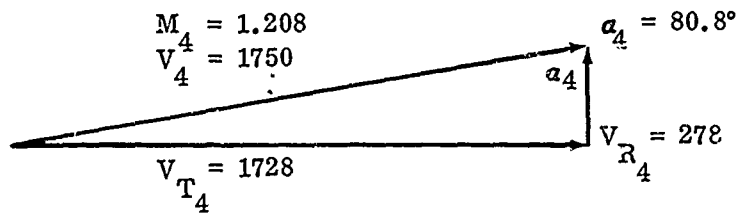


Figure 148. Exit Vector Diagrams at 1.028 Radius Ratio, RF-2.

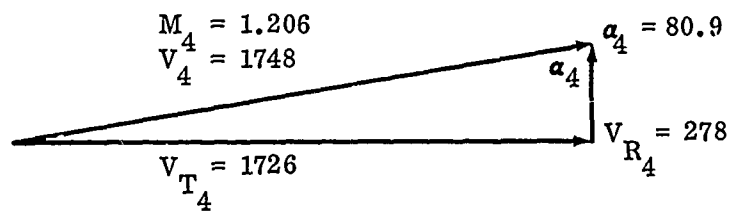
CONFIDENTIAL

Test 3369A

$N/\sqrt{\theta} = 50,000 \text{ rpm}$



$W_a \sqrt{\theta}/\delta = 1.88 \text{ lb/sec}$



$W_a \sqrt{\theta}/\delta = 1.90 \text{ lb/sec}$

CONFIDENTIAL

Corrected to Ambient
Conditions of:

60°F

29.92 in. Hg

All Velocities in fps

Test 3370A

$N/\sqrt{\theta} = 35,000 \text{ rpm}$

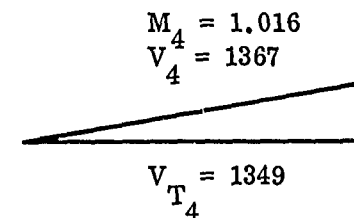
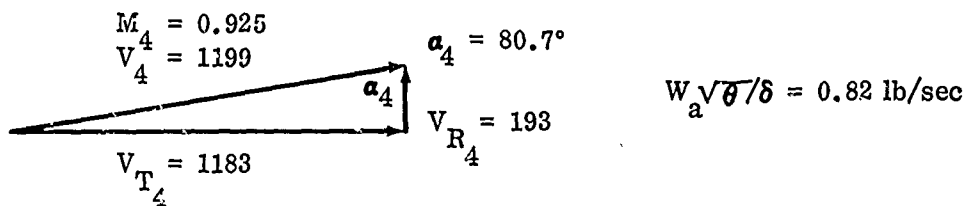
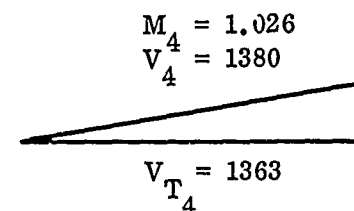
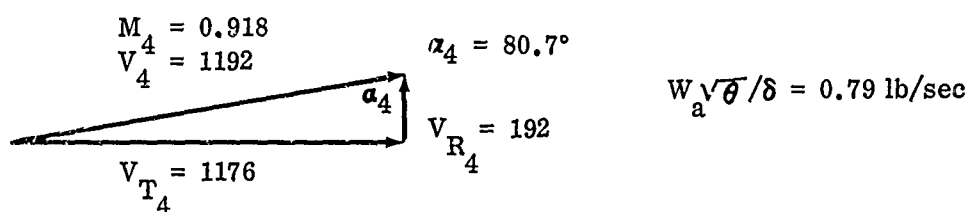
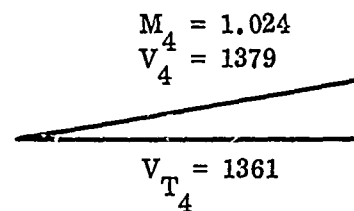
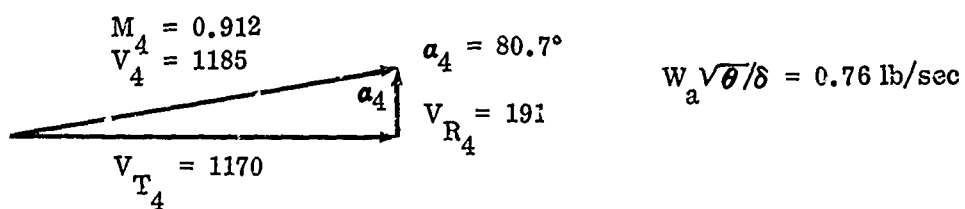


Figure 149. Exit Vector Diagrams at 1.028 Radius Ratio, RF-2.

CONFIDENTIAL

$$N/\sqrt{\theta} = 40,000 \text{ rpm}$$

$$\alpha_4 = 80.7^\circ$$

 α_4

$$V_{R_4} = 222$$

$$W_a \sqrt{\theta} / \delta = 1.01 \text{ lb/sec}$$

$$\alpha_4 = 80.7^\circ$$

 α_4

$$V_{R_4} = 222$$

$$W_a \sqrt{\theta} / \delta = 1.04 \text{ lb/sec}$$

$$\alpha_4 = 80.8^\circ$$

 α_4

$$V_{R_4} = 222$$

$$W_a \sqrt{\theta} / \delta = 1.08 \text{ lb/sec}$$

$$N/\sqrt{\theta} = 45,000 \text{ rpm}$$

$$M_4 = 1.123$$

$$V_4 = 1566$$

$$\alpha_4 = 80.8^\circ$$

 α_4

$$V_{R_4} = 250$$

$$V_{T_4} = 1546$$

$$W_a \sqrt{\theta} / \delta$$

$$M_4 = 1.122$$

$$V_4 = 1564$$

$$\alpha_4 = 80.8^\circ$$

 α_4

$$V_{R_4} = 250$$

$$V_{T_4} = 1543$$

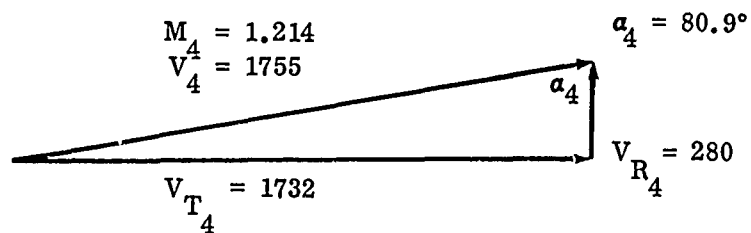
$$W_a \sqrt{\theta} / \delta$$

$$N/\sqrt{\theta} = 50,000 \text{ rpm}$$

0.8°

$$W_a \sqrt{\theta} / \delta = 1.39 \text{ lb/sec}$$

50

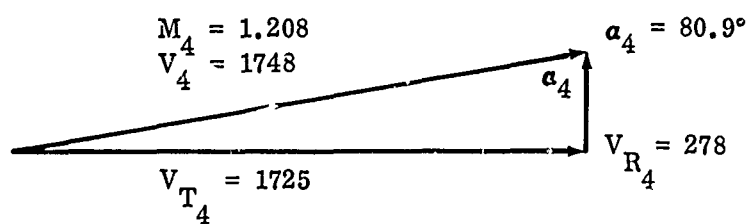


$$W_a \sqrt{\theta} / \delta = 1.86 \text{ lb/sec}$$

0.8°

$$W_a \sqrt{\theta} / \delta = 1.41 \text{ lb/sec}$$

250



$$W_a \sqrt{\theta} / \delta = 1.88 \text{ lb/sec}$$

CONFIDENTIAL

Corrected to Ambient
Conditions of:
60°F
29.92 in. Hg

All incidence values are with respect
to the vane pressure surface

Test 3353
 $N/\sqrt{\theta} = 46,000$ rpm
 $W \sqrt{\theta}/\delta$
— 1.43 lb/sec
--- 1.42 lb/sec

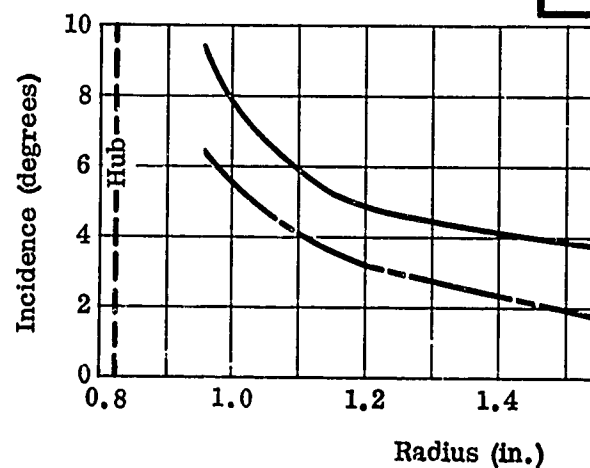
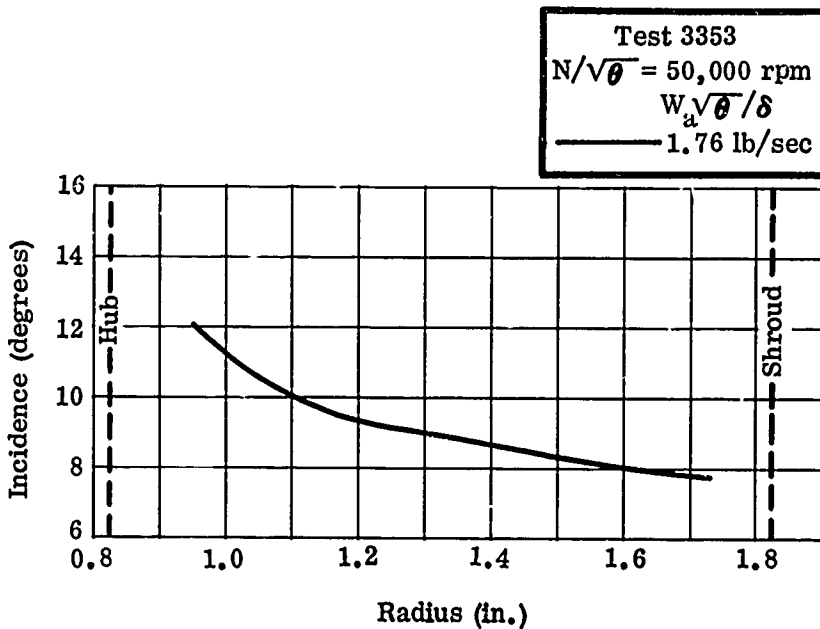
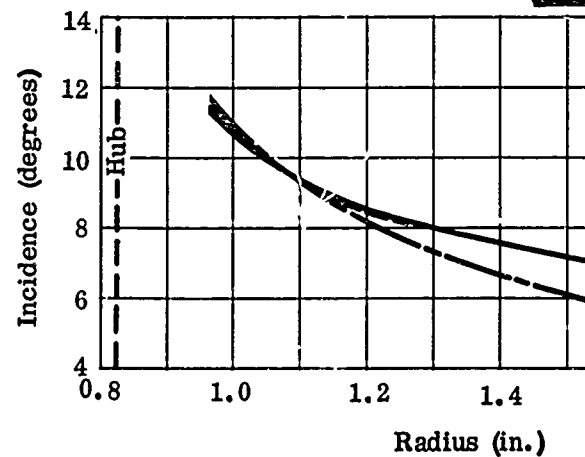
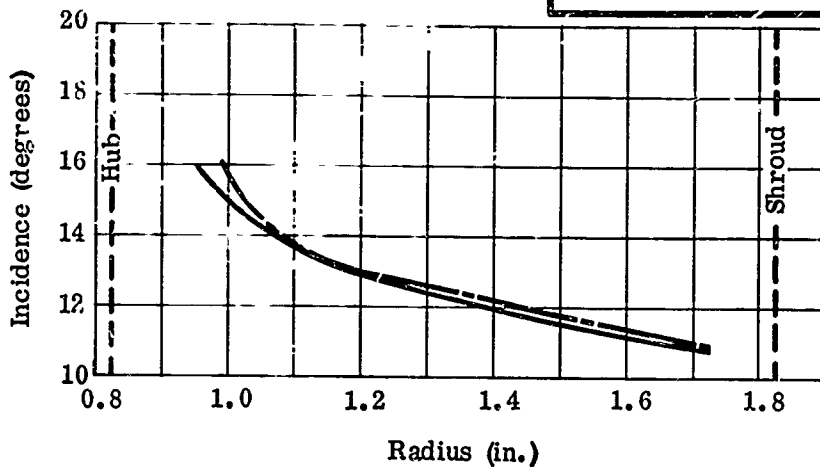
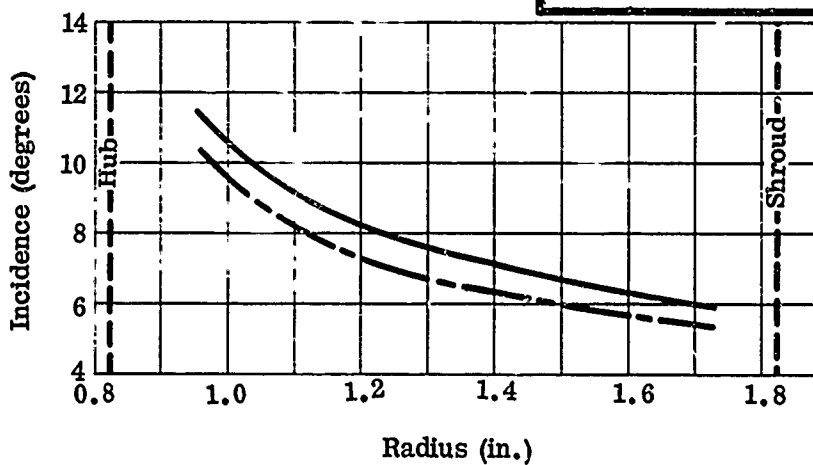
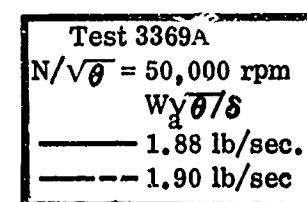
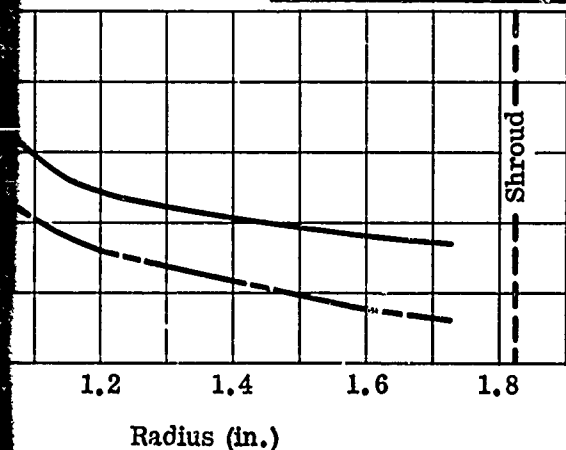
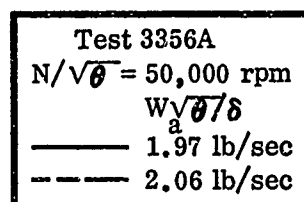
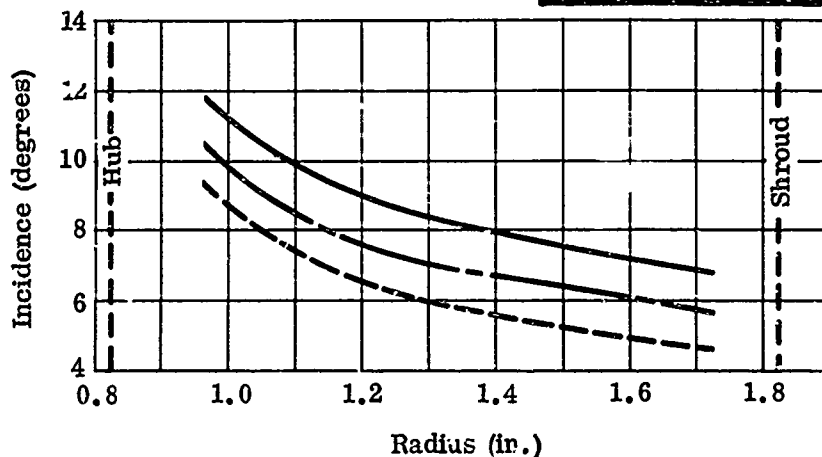
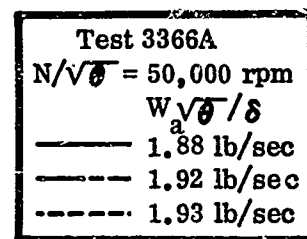
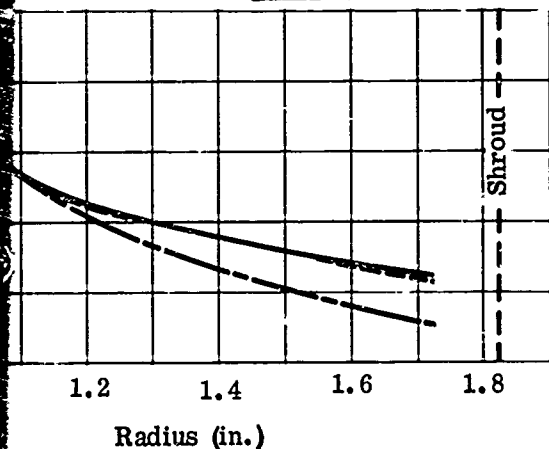
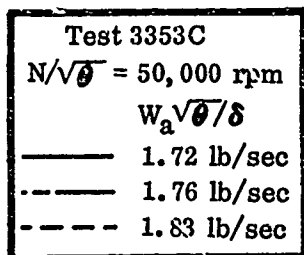


Figure 150. Inducer Incidence, RF-2.

CONFIDENTIAL



CONFIDENTIAL

All incidence values are with respect to the vane pressure surface

Corrected to Ambient
Conditions of:
56°F
25.92 in. Hg

Test 3370A
 $N/\sqrt{\theta} = 35,000$ rpm
 $W_a\sqrt{\theta}/\delta$
— 0.76 lb/sec
- - - 0.79 lb/sec
- - - 0.82 lb/sec

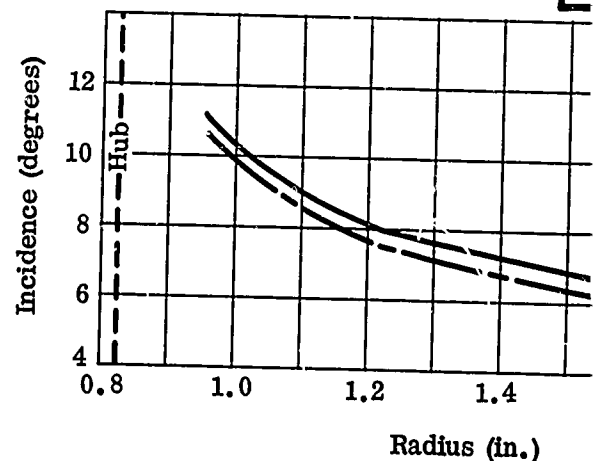
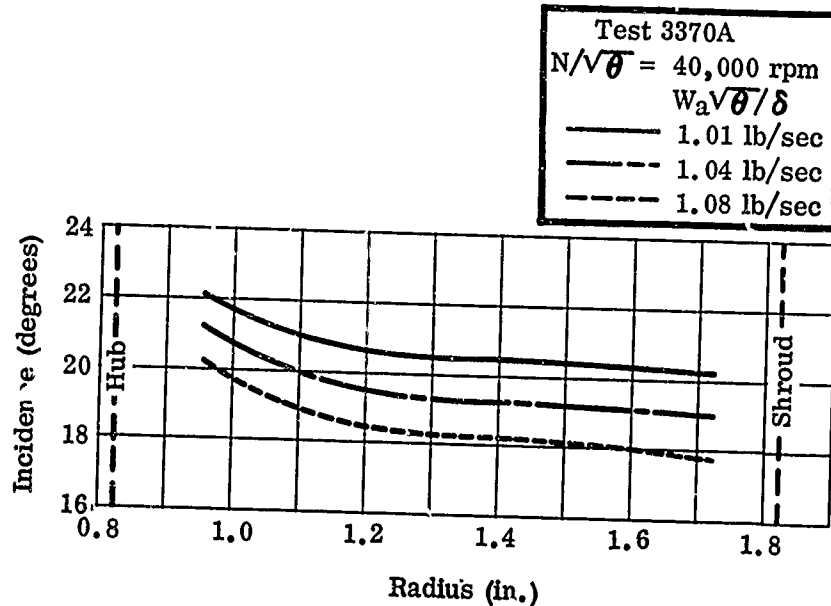
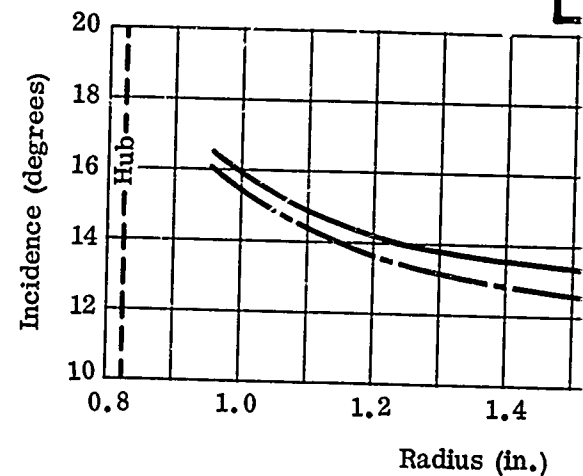
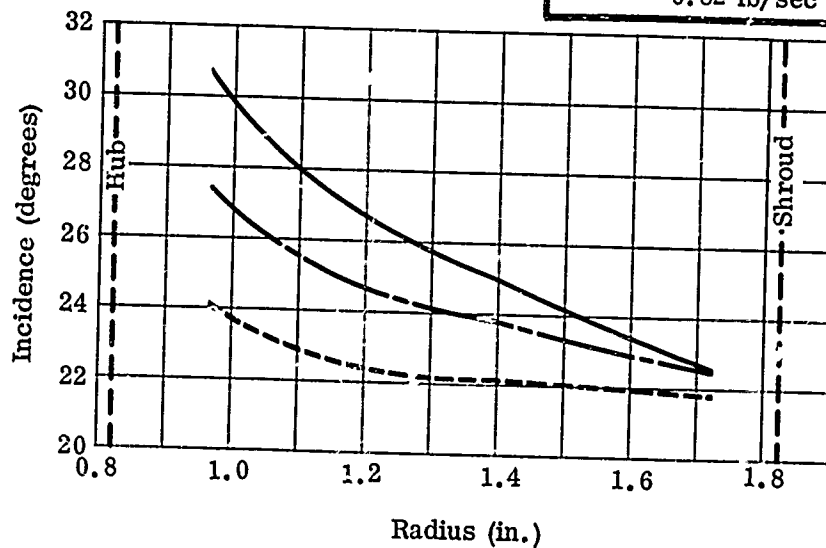


Figure 151. Inducer Incidence, RF-2.

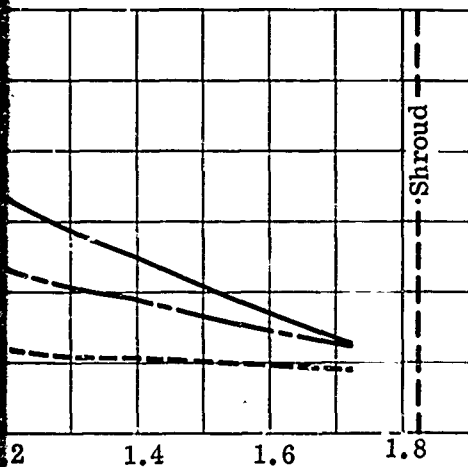
CONFIDENTIAL

CONFIDENTIAL

All incidence values are with respect to the vane pressure surface

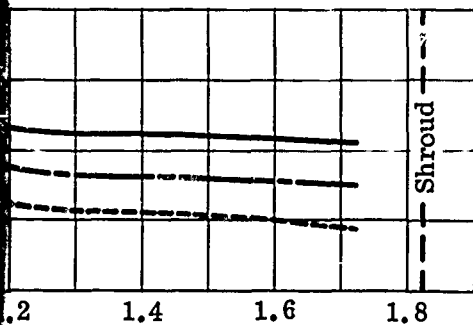
Table 1:

Test 3370A
 $N/\sqrt{\theta} = 35,000$ rpm
 $W_a\sqrt{\theta}/\delta$
 — 0.76 lb/sec
 - - 0.79 lb/sec
 - - - 0.82 lb/sec



Radius (in.)

Test 3370A
 $N/\sqrt{\theta} = 40,000$ rpm
 $W_a\sqrt{\theta}/\delta$
 — 1.01 lb/sec
 - - 1.04 lb/sec
 - - - 1.08 lb/sec

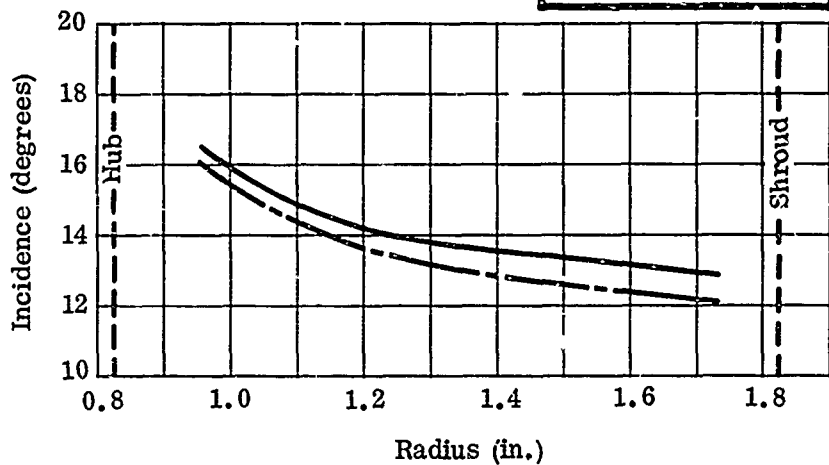


Radius (in.)

151. Inducer Incidence, RF-2.

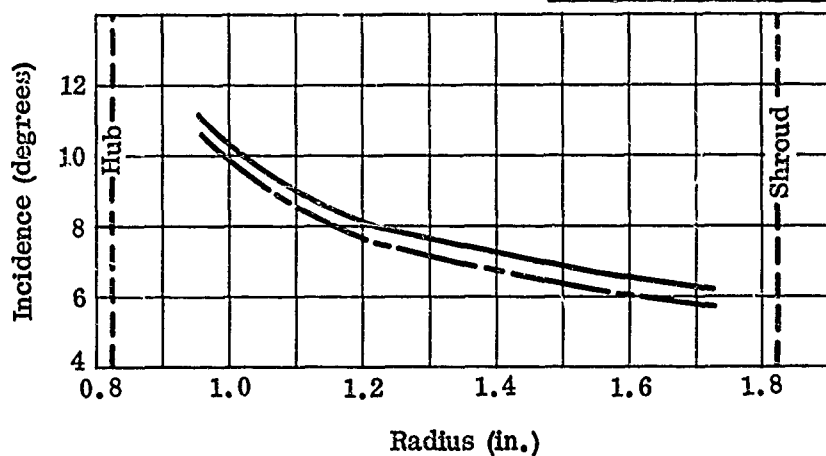
185

Test 3370A
 $N/\sqrt{\theta} = 45,000$ rpm
 $W_a\sqrt{\theta}/\delta$
 — 1.39 lb/sec
 - - 1.41 lb/sec



Radius (in.)

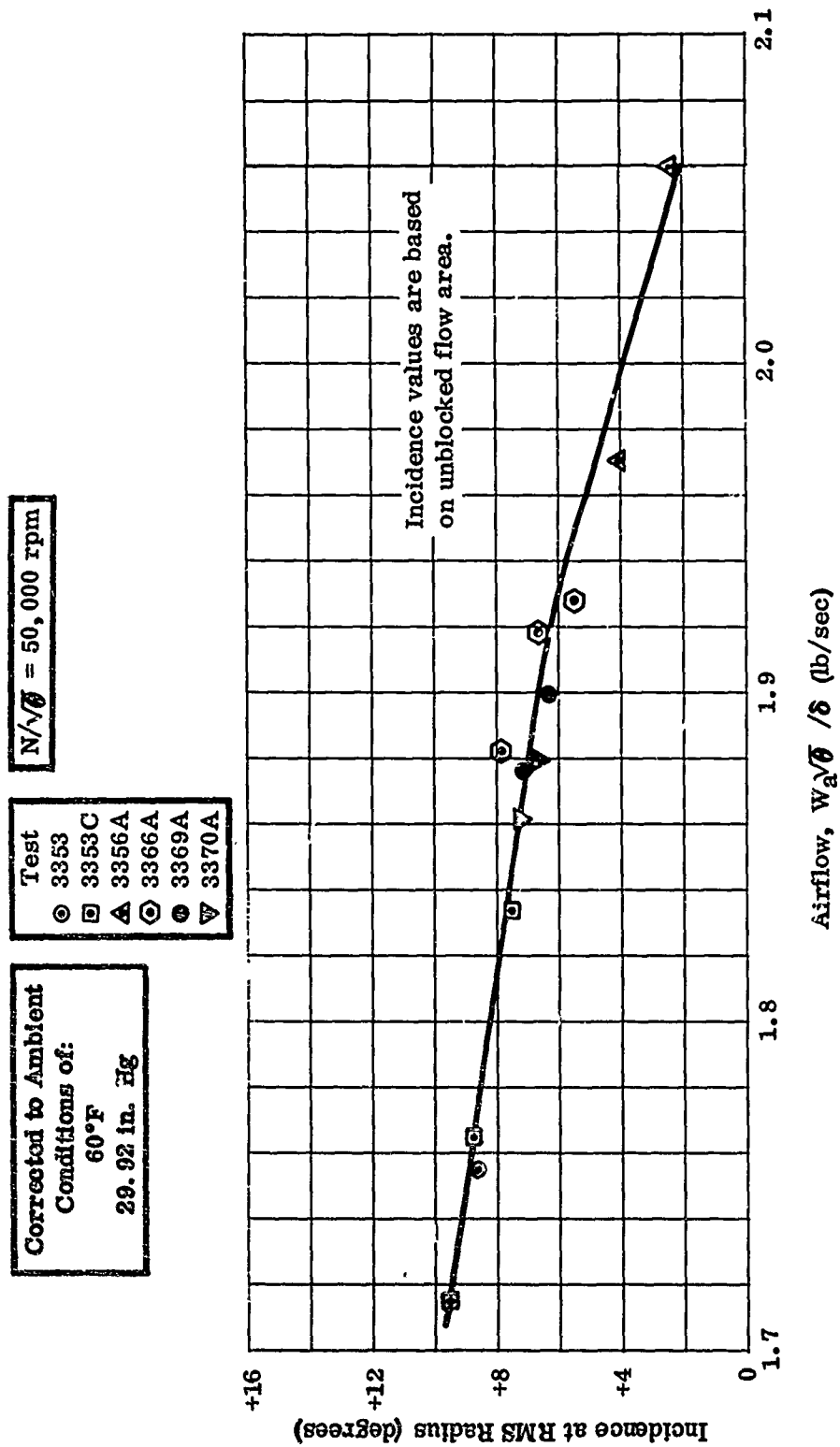
Test 3370A
 $N/\sqrt{\theta} = 50,000$ rpm
 $W_a\sqrt{\theta}/\delta$
 — 1.86 lb/sec
 - - 1.88 lb/sec



Radius (in.)

CONFIDENTIAL

CONFIDENTIAL



CONFIDENTIAL

Figure 152. Variation of Inducer Incidence with Airflow, RF-2.

CONFIDENTIAL

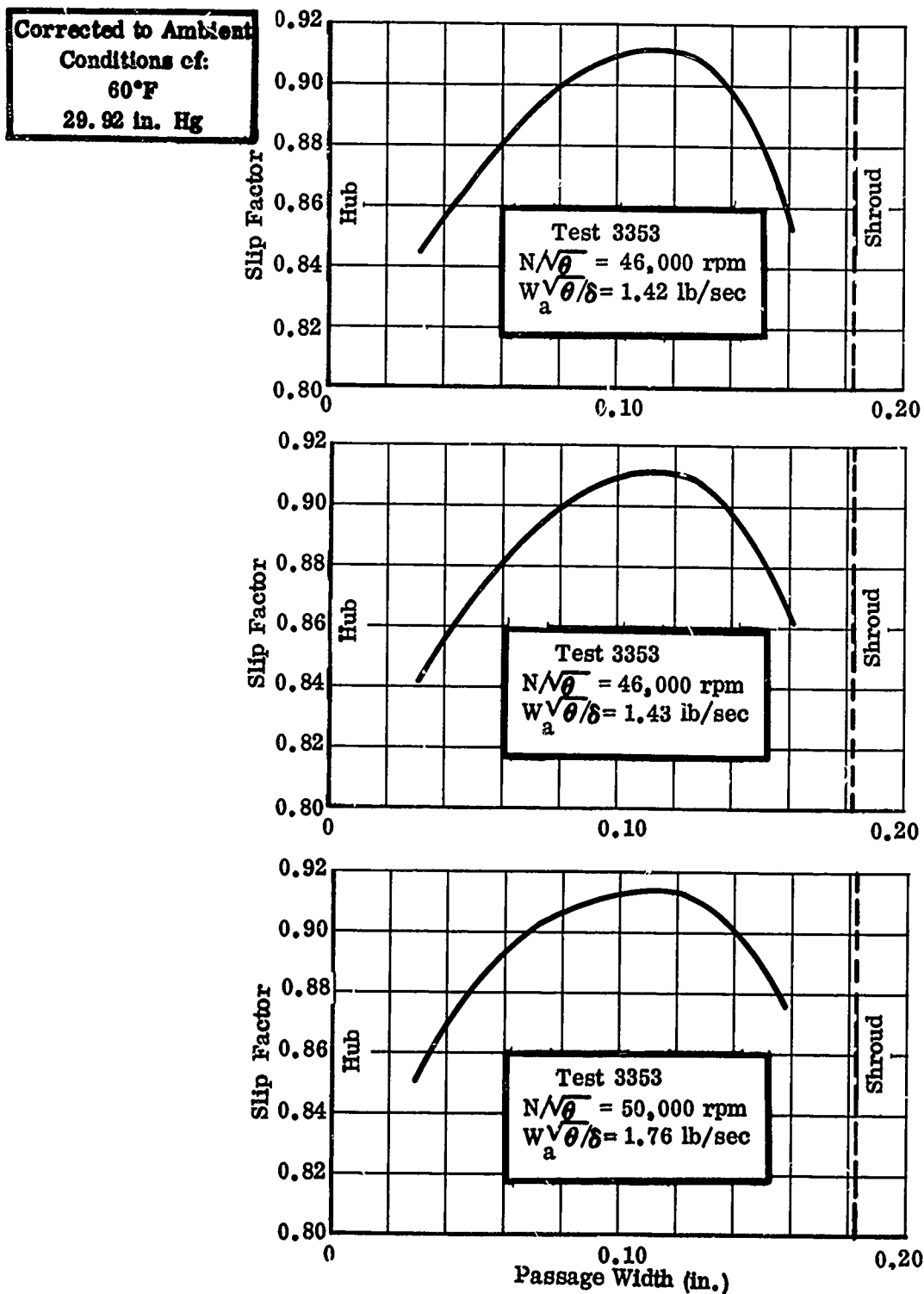


Figure 153. Variation of Slip Factor Across Impeller Tip, RF-2.

CONFIDENTIAL

CONFIDENTIAL

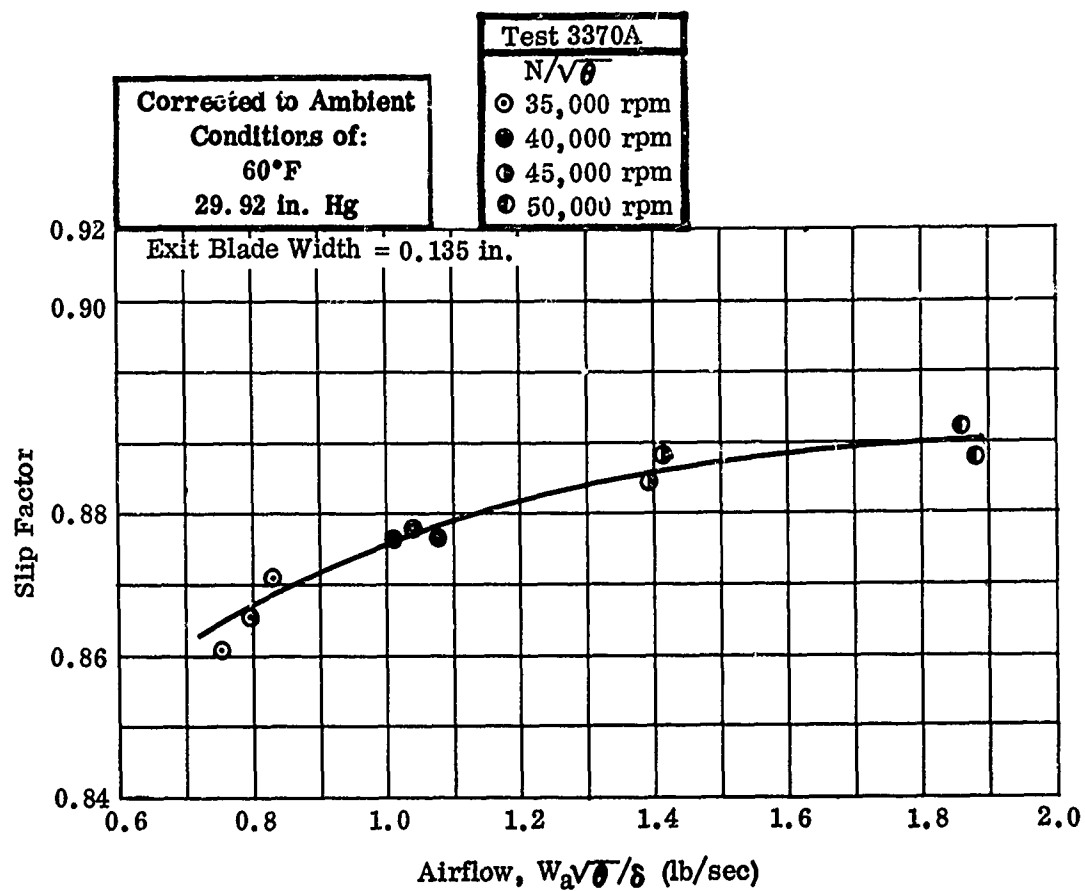
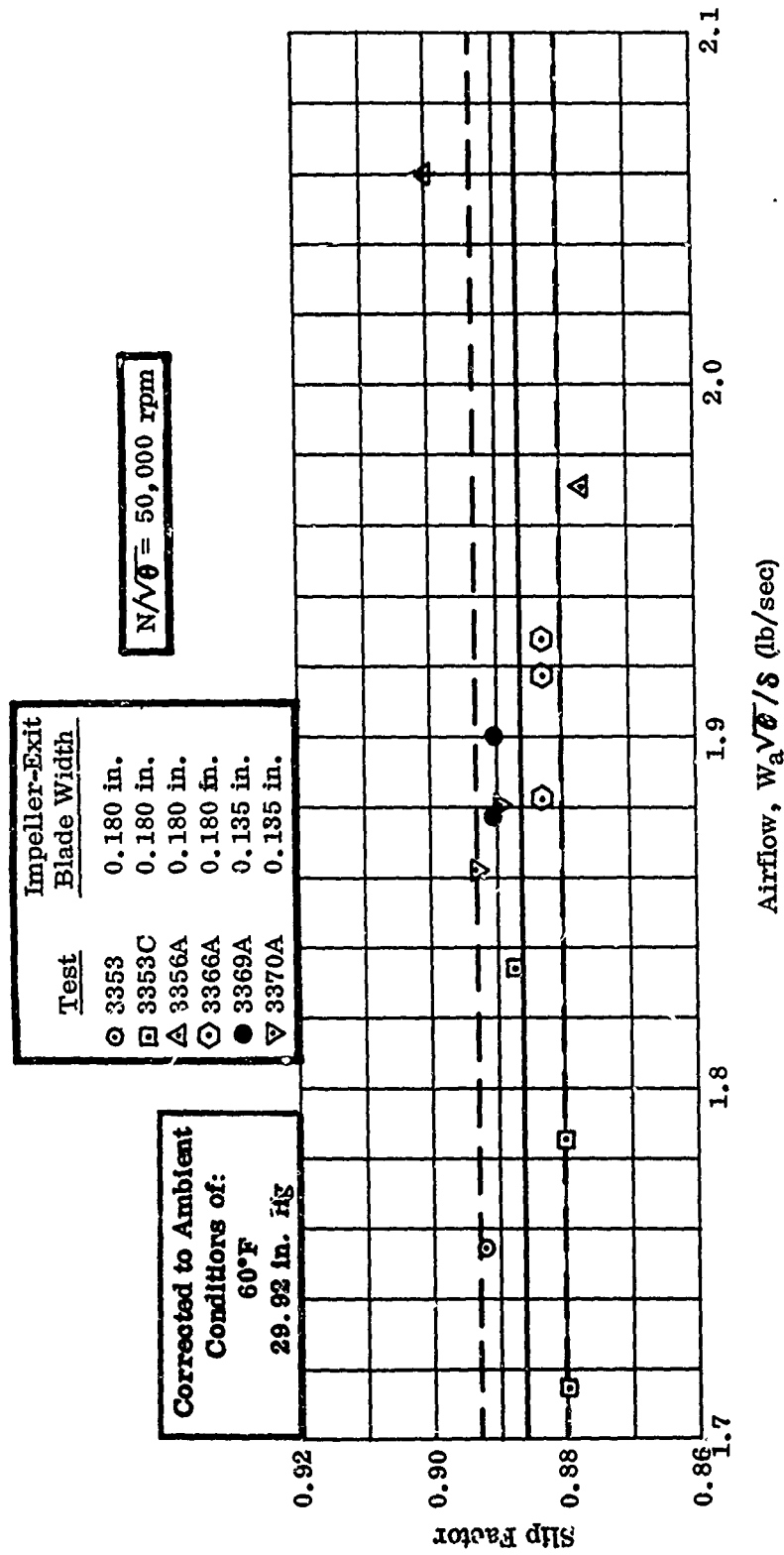


Figure 154. Variation of Average Slip Factor with Rotational Speed for RF-2 Impeller with Reduced Blade Width.

CONFIDENTIAL

CONFIDENTIAL



190

CONFIDENTIAL

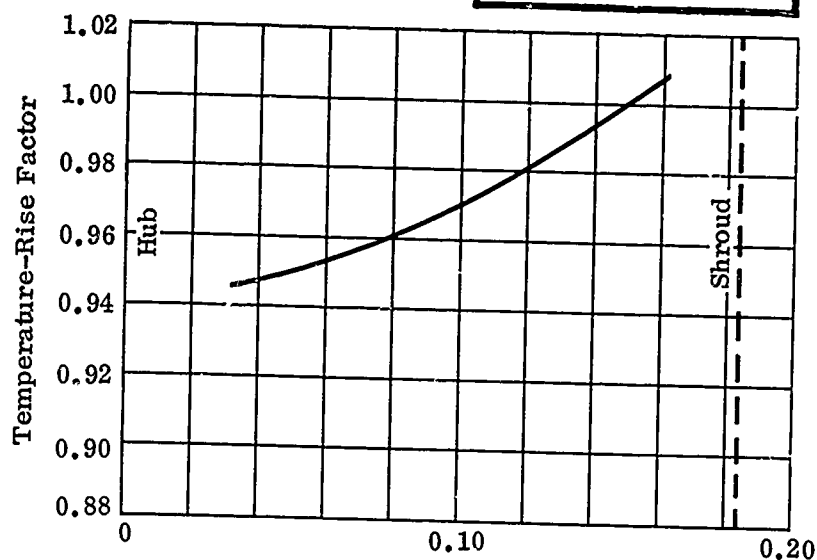
Figure 155. Average Slip Factor at Design Speed, RF-2.

CONFIDENTIAL

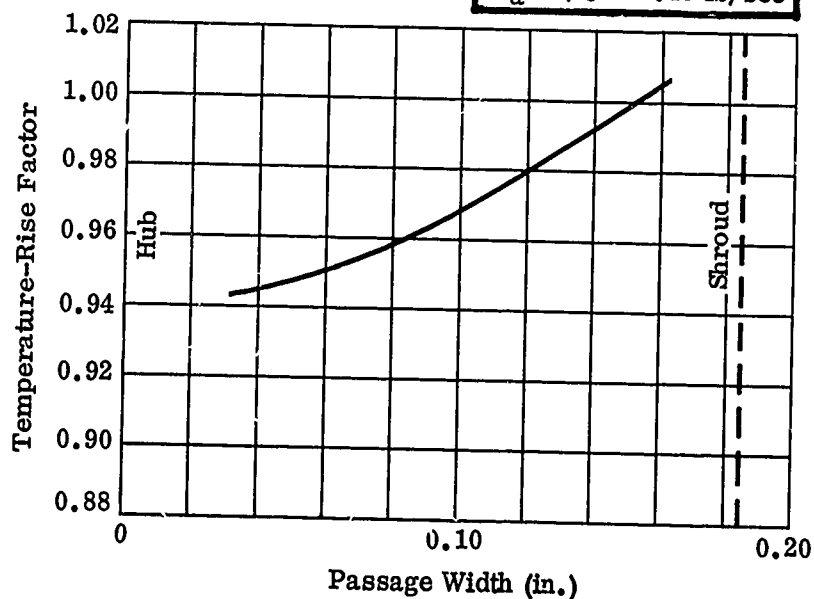
Corrected to Ambient
Conditions of:
60°F
29.92 in. Hg

Test 3353

$N/\sqrt{\theta} = 46,000$ rpm
 $W_a\sqrt{\theta}/\delta = 1.42$ lb/sec



$N/\sqrt{\theta} = 46,000$ rpm
 $W_a\sqrt{\theta}/\delta = 1.43$ lb/sec



$N/\sqrt{\theta}$
 $W_a\sqrt{\theta}/\delta$

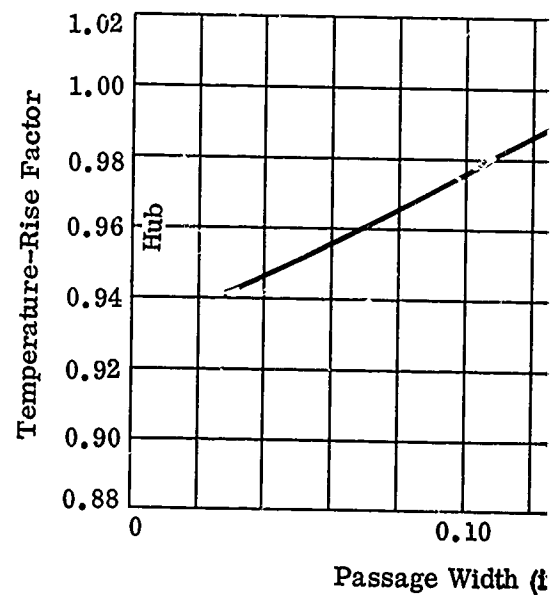
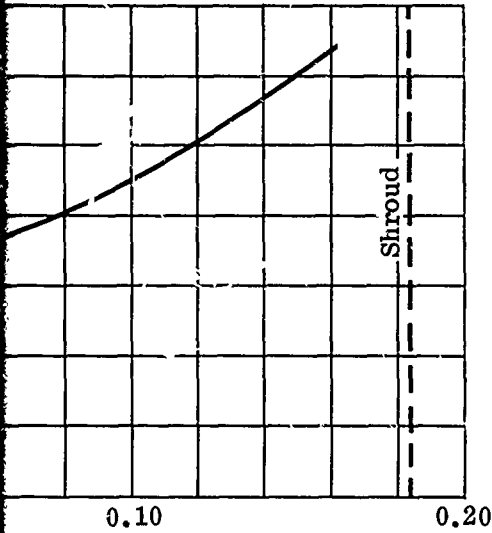


Figure 156. Variation of Temperature-Rise Factor Across Impeller Tip, RF-2.

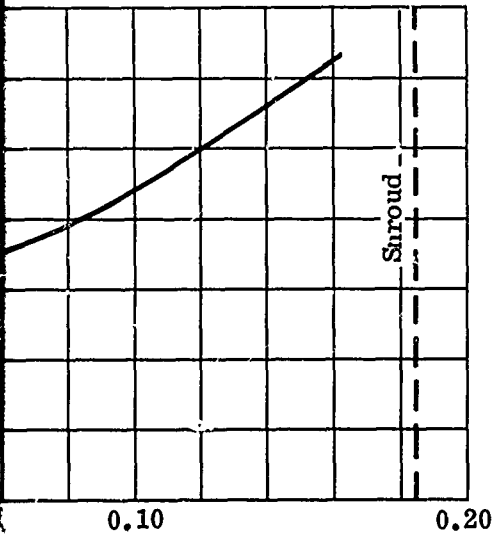
CONFIDENTIAL

Test 3353

$N/\sqrt{\theta} = 46,000 \text{ rpm}$
 $W_a\sqrt{\theta}/\delta = 1.42 \text{ lb/sec}$

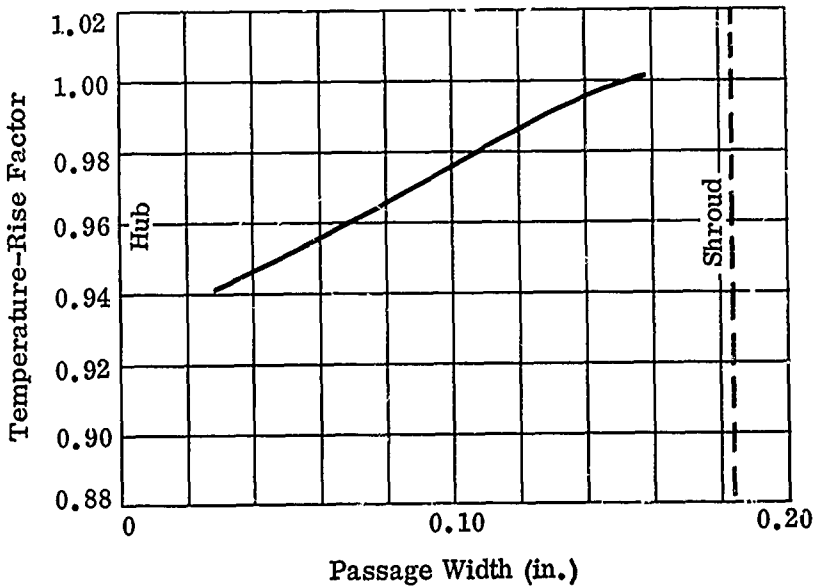


$N/\sqrt{\theta} = 46,000 \text{ rpm}$
 $W_a\sqrt{\theta}/\delta = 1.43 \text{ lb/sec}$



Test 3353

$N/\sqrt{\theta} = 50,000 \text{ rpm}$
 $W_a\sqrt{\theta}/\delta = 1.76 \text{ lb/sec}$



Passage Width (in.)
of Temperature-Rise Factor Across Impeller Tip, RF-2.

CONFIDENTIAL

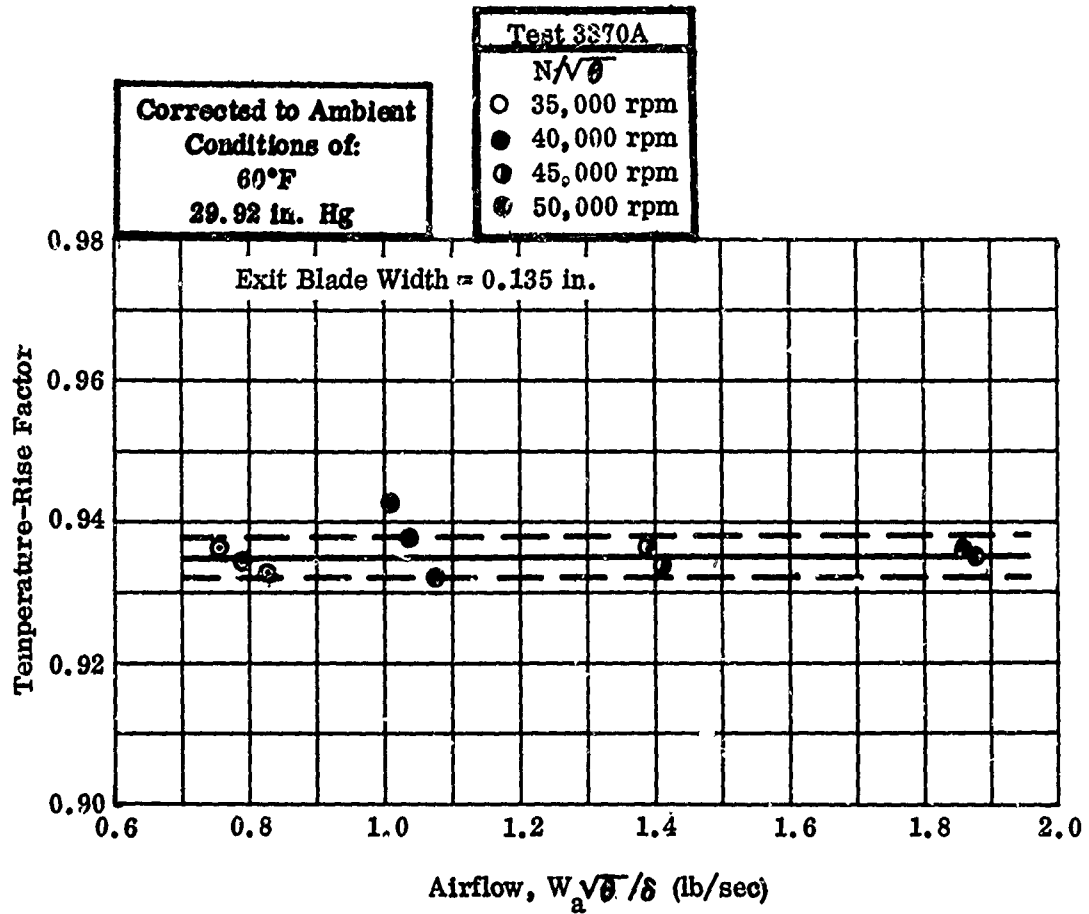
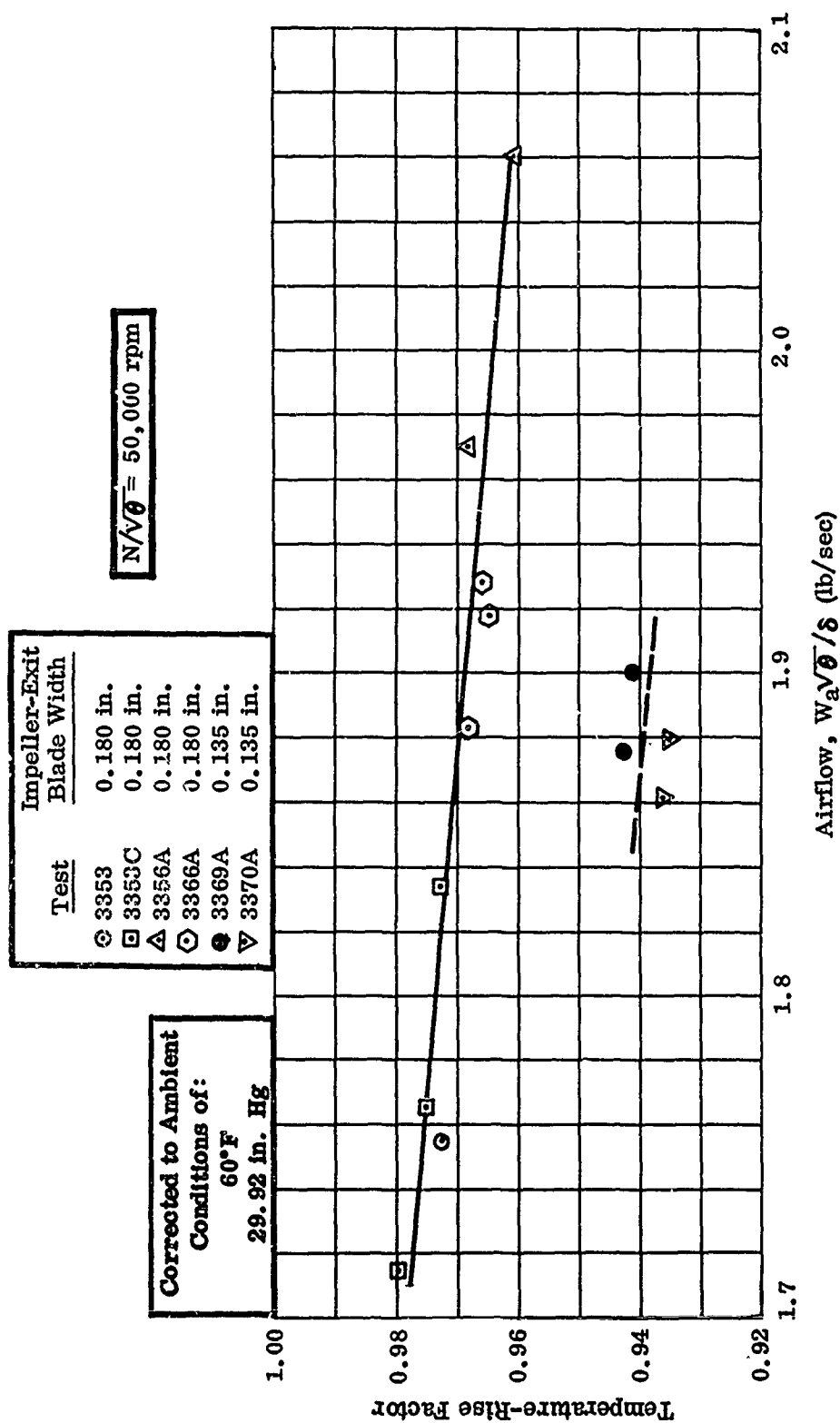


Figure 157. Variation of Average Temperature-Rise Factor with Rotational Speed for RF-2 Impeller with Reduced Blade Width.

CONFIDENTIAL

CONFIDENTIAL



CONFIDENTIAL

Figure 158. Average Temperature-Rise Factor at Design Speed, RF-2.

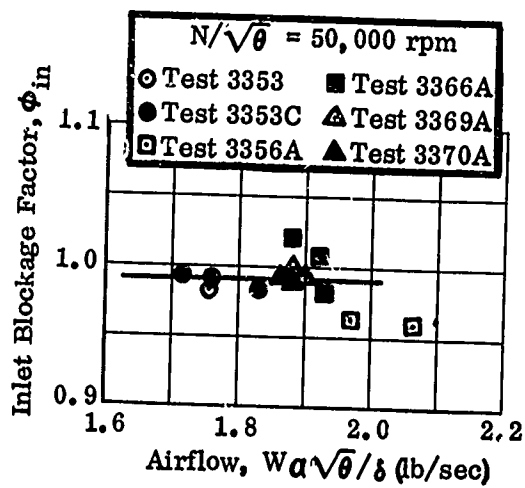
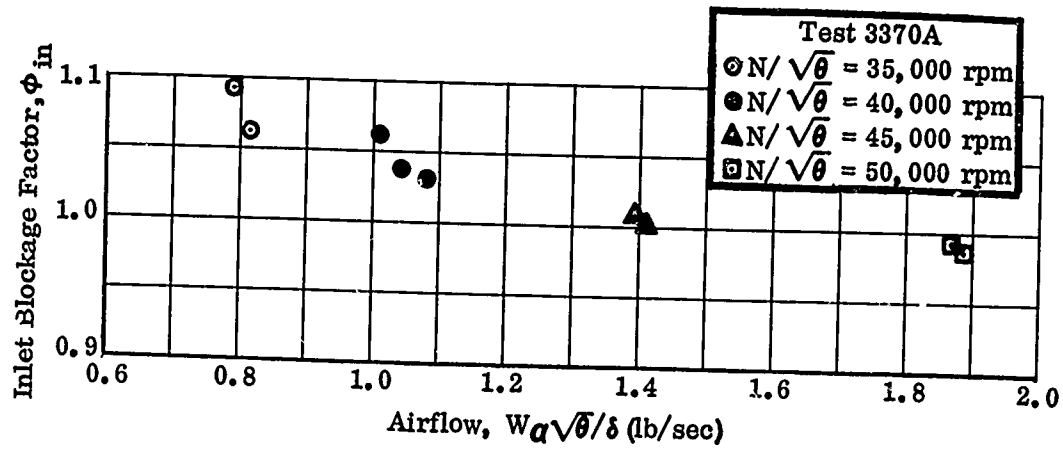


Figure 159. Inlet Blockage Factor Versus Airflow, RF-2.

CONFIDENTIAL

6.2 DIFFUSERS

This section of the report presents vane-island diffuser data collected during testing of the combined impeller-diffuser configuration. All data obtained were reviewed for graphical presentation of complete performance for each diffuser. Supplementary static-pressure data are presented in Appendix III.

6.2.1 Test Plan

The test plan for diffuser evaluation is presented in Table VI. The assessment of performance was based on the following measurements:

- 1) Static pressures in channels and vaneless and semivaneless spaces
- 2) Diffuser-throat total pressures
- 3) Collector total temperature
- 4) Collector pressure

The instrumentation used for each test in the series is shown in Table IV (Section 5.0).

6.2.2 Configurations Tested

During the test series, 16 vane configurations were investigated. These configurations are described in the following discussion.

V1

This configuration was used in the mechanical checkout of the test section and was as shown in Figure 14. The vane thickness for checkout purposes was 0.230 inch, instead of the design thickness of 0.180 inch shown in Table III.

V1-1

This vane was the same as V1 except that the thickness was reduced to 0.200 inch. Both V1 and V1-1 were run to establish impeller-tip clearances. Basic performance data were recorded in both tests.

TABLE VI
DIFFUSER TESTS

TABLE VI							
DIFFUSER TESTS							
Test No.	Diffuser No.	Measured		Diffuser Depth (in.)	Speed (rpm)	Measurements*	Remarks
		Total Throat Area (in. ²)					
3351	V1	1.021		0.230	50,000	Min Map Data	Mechanical Checkout Run and Reruns of Selected Points to Confirm Clearance Measurements
3352	V1-1	0.888		0.200	50,000	No Dymec Data	
3352A	V1-1	0.889		0.200	50,000		
3352B	V1-2	0.844		0.190	50,000		
3352C	V1-3	0.813		0.183	50,000		Aerodynamic Baseline Test Rerun of 3352C
3353B	V1-3	0.813		0.183	50,000	No Dymec Data	
3353D	V1-3	0.813		0.183	50,000	P _R ⁴	
3353E	V1-3	0.813		0.183	50,000	P _R ³	
3353F	V1-3	0.813		0.183	50,000	P _R ⁵	
3354	V1-4	0.869		0.183	50,000		
3354A	V1-4	0.869		0.183	50,000	P _R ⁴	
3354B	V1-4	0.869		0.183	50,000	P _R ³	

CONFIDENTIAL

TABLE VI (continued)

Test No.	Diffuser No.	Measured Total Throat Area (in. ²)	Diffuser Depth (in.)	Speed (rpm)	Measurements*	Remarks
3355	V1-5	0.909	0.183	50,000		
3356	V1-6	0.946	0.183	50,000		
3357	V1-7	0.946	0.183	50,000		
3358	V1-8	0.946	0.183	50,000		
3358A	V1-8	0.946	0.183	50,000		Wedge Separated Rerun of 3358 with Wedge Repaired
3359	V1-9	0.946	0.183	50,000		
3360	V1-10	0.946	0.183	50,000		
3361	V1-10	0.946	0.183	50,000		
3362	V1-10	0.946	0.183	50,000		
3363	V1-11	0.946	0.183	50,000		
3364	V1-11	0.946	0.183	50,000		
3365	V1-12	0.946	0.183	50,000		

CONFIDENTIAL

CONFIDENTIAL

TABLE VI (continued)

TABLE VI (continued)						
Test No.	Diffuser No.	Measured Total Throat Area (in. ²)	Diffuser Depth (in.)	Speed (rpm)	Measurements*	Remarks
3366	V2	0.865	0.203	50,000	<div>P_{R^3} P_{R^4} P_{R^5}</div>	0.020 Machined Off Frontplate to Accommodate 0.203 in. Vane Thickness
3366B	V2	0.865	0.203	50,000		
3366C	V2	0.865	0.203	50,000		
3366D	V2	0.865	0.203	50,000		
3368	V2-1	0.950	0.203	35,000, 40,000 45,000, 50,000 and 51,850		
3369	V2-2	0.862	0.158	50,000	P_{R^4}	Impeller Blade Width Reduced to 0.135 in.
3369B	V2-2	0.862	0.158	50,000		
3369C	V2-2	0.862	0.158	51,850		
3370	V2-2	0.862	0.158	35,000, 40,000 45,000, 51,850 and 53,000		
<div>*Inlet and collector pressures measured on all tests. Dymec data measured on all tests unless noted. P_{R^3} = Diffuser Throat Total Pressure Reake No. 3. P_{R^4} = Diffuser Throat Total Pressure Reake No. 4. P_{R^5} = Diffuser Throat Total Pressure Reake No. 5</div>						

See Figure 48, Section 5.

CONFIDENTIAL

CONFIDENTIAL

V1-2

The V1-2 configuration was the same as V1-1 except that its thickness was reduced further to 0.190 inch. Additional clearance and performance data were collected.

V1-3

For this modification, the thickness of V1-2 was reduced to 0.183 inch, essentially the design thickness. All other geometric parameters were the same as those shown in Figure 14.

V1-4

Because the airflow rate of V1-3 at design speed was lower than expected, it was believed that the throat blockage was higher than that accounted for in the design. For this reason, the throat height was increased by 6.9 percent. To maintain a parallel-walled throat, the vane contour ahead of the throat was also modified. The vane width was maintained at 0.183 inch.

V1-5

The V1-5 configuration was the third in the series aimed at determining the effect of increased throat area, and was obtained by reworking the V1-4 vanes. The throat height was increased by 4.6 percent; again the vane contour ahead of the throat was modified to maintain a parallel-walled throat.

V1-6

The throat area of the V1-5 configuration was enlarged an additional 4.1 percent, by increasing the throat height, to produce the V1-6 configuration. This modification, the fourth in this series, also required a change in the vane contour ahead of the throat. Figure 160 shows a comparison of the V1-3 and V1-6 configurations. The V1-4 and V1-5 vanes lie between the contours shown in Figure 160.

V1-7

The V1-7 configuration was obtained by modifying the V1-6. A 10-degree wedge was added to the diverging-channel wall at a 2:1 area ratio (see Figure 161). At this point, the 2:1 area-ratio channel was followed by a constant area section about 3 inches long. The test was aimed at determining the effect of changing overall area ratio.

CONFIDENTIAL

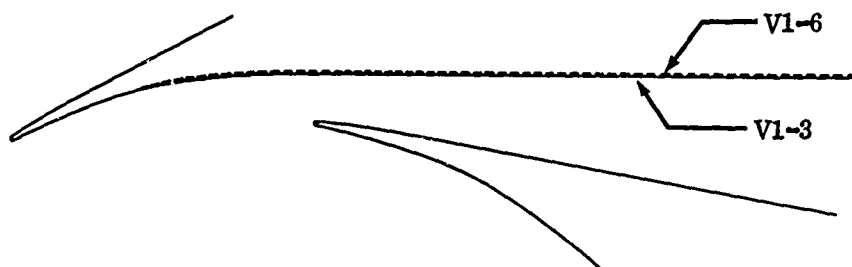


Figure 160. V1 Diffuser Vane Modifications.



Figure 161. V1 Diffuser Vane Modifications.

V1-8

A 5-degree wedge was added to the V1-6 configuration to obtain the V1-8 vanes. This wedge, added to the diverging wall of the channel, started at 0.500 inch from the leading edge of the vane (see Figure 162) and produced an asymmetrical channel with a divergence angle of 5 degrees. This test was run to determine the effect of changing divergence angle.

V1-9

The V1-9 configuration was the same as V1-8 except for a channel-divergence angle of 8 degrees (shown in Figure 162).

V1-10

For this configuration the V1-9 vanes were modified to produce a symmetrical channel divergence angle of 10 degrees (shown in Figure 162).

CONFIDENTIAL

CONFIDENTIAL

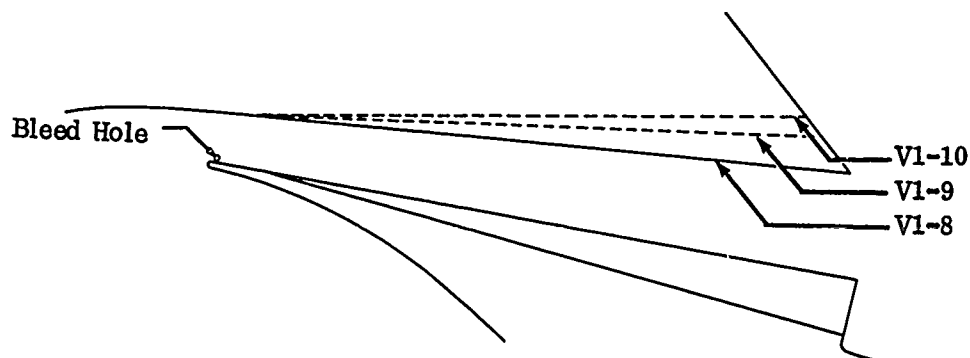


Figure 162. V1 Diffuser Vane Modifications.

V1-11

The V1-11 vane was a modification to V1-10 with a 10-degree asymmetrical channel-divergence angle (shown in Figure 163). A 5-degree wedge was added to the existing wedge, and the opposite wall was opened by 5 degrees.

V1-12

This configuration was identical to V1-11, except that a slot was machined on each side of the vane. This slot started at the middle of the throat and extended to a point approximately 1/2 inch from the tip on the suction surface (shown in Figure 163). This slot was provided to bleed the boundary layer internally from the throat to the suction surface.

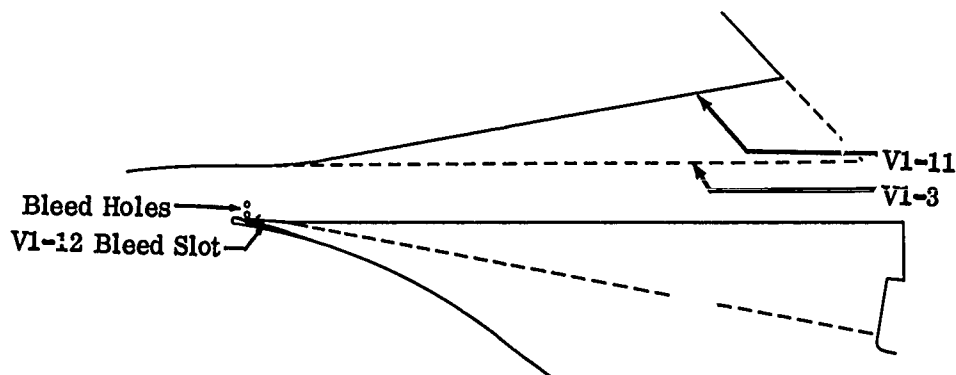


Figure 163. V1 Diffuser Vane Modifications.

CONFIDENTIAL

CONFIDENTIAL

All of the preceding modifications were accomplished with one set of vanes, the basic V1 configuration.

V2

The V2 vane-island diffuser (shown in Figure 164) required a new set of vanes. This configuration had a symmetrical channel-divergence angle of 10 degrees. The throat area was approximately the same as V1-4, but the vane width was 0.203 inch. Therefore, the required throat height for this configuration was smaller than V1-4.

V2-1

For this modification the throat area of V2 was enlarged by 9.8 percent by increasing the throat height, which required a modification to the vane contour ahead of the throat (shown in Figure 164).

V2-2

The V2-2 configuration had a throat area approximately equal to the throat area of the V2 diffuser. However, the vane thickness was reduced to 0.158, which required a larger throat height to maintain the desired throat area. The vane contour ahead of the throat was modified as shown in Figure 164.

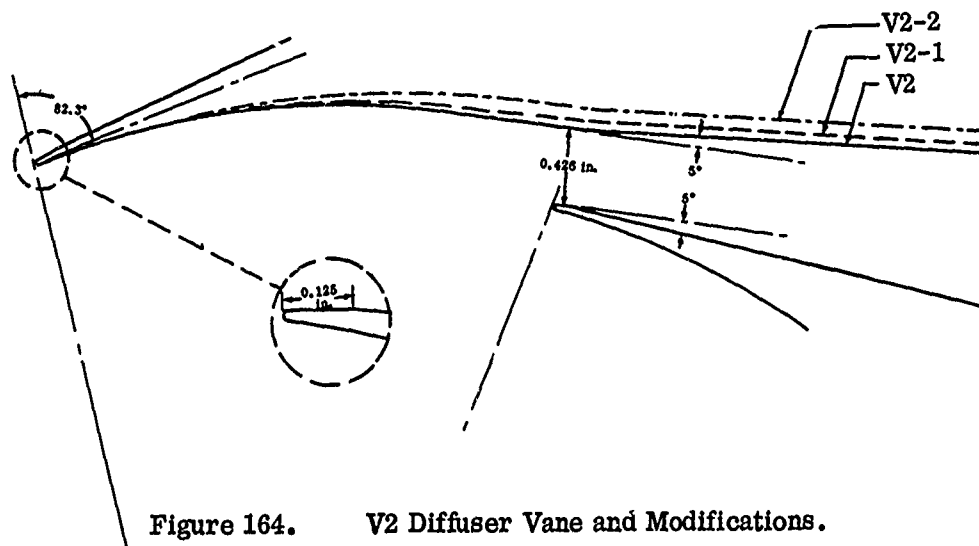


Figure 164. V2 Diffuser Vane and Modifications.

External Bleed Tests

During the V1 test series, an attempt was made to reduce throat blockage by bleeding the boundary layer. Two bleed tests were run with the V1-10 vanes (Tests 3361 and 3362) — the first with 0.032-inch-diameter holes drilled through the sideplates, and the second with the holes enlarged to 0.046 inch. The location of the hole is shown in Figure 163. In addition, a bleed test was conducted with the V1-11 vanes, using the same 0.046-inch-diameter holes as in V1-10 (Test 3363). A second test of V1-11, with 0.032-inch-diameter holes added, was run to increase the amount of bleed (Test 3364). Hole locations for V1-11 are shown in Figure 163.

6.2.3 Performance Measurements

Map Data

The curves of pressure ratio and efficiency versus airflow for representative tests in the series are given in the Test Results section. The pressure ratio shown is based on the numerically averaged collector pressure measurements, and the adiabatic efficiency is based on the numerical average of the collector temperatures.

Static-Pressure Measurements

The diffuser front and backplates were instrumented with 108 static-pressure taps. The locations of these taps and the test data (corrected for ambient conditions) are shown in Appendix III. In addition, significant test data are shown in the Test Results section.

Temperature Rise

The temperature rise of the compressor versus airflow for each test in the series is given in the Test Results section. The mean temperature rise and a $\pm 1/2$ -percent band for various groupings of tests are also shown on these curves for reference.

Diffuser-Throat Total Pressures

During this test series, measurements of the total pressure at the throat of the diffuser were taken with 3-probe total-pressure rakes for some diffuser configurations (see Table VI). Plots of diffuser throat total pressure versus diffuser width for these tests are shown in the Test Results section.

CONFIDENTIAL

6.2.4 Test Results

Representative data for all diffuser tests in this series are presented. Supplementary static-pressure data for these tests are contained in Appendix III.

CONFIDENTIAL

CONFIDENTIAL

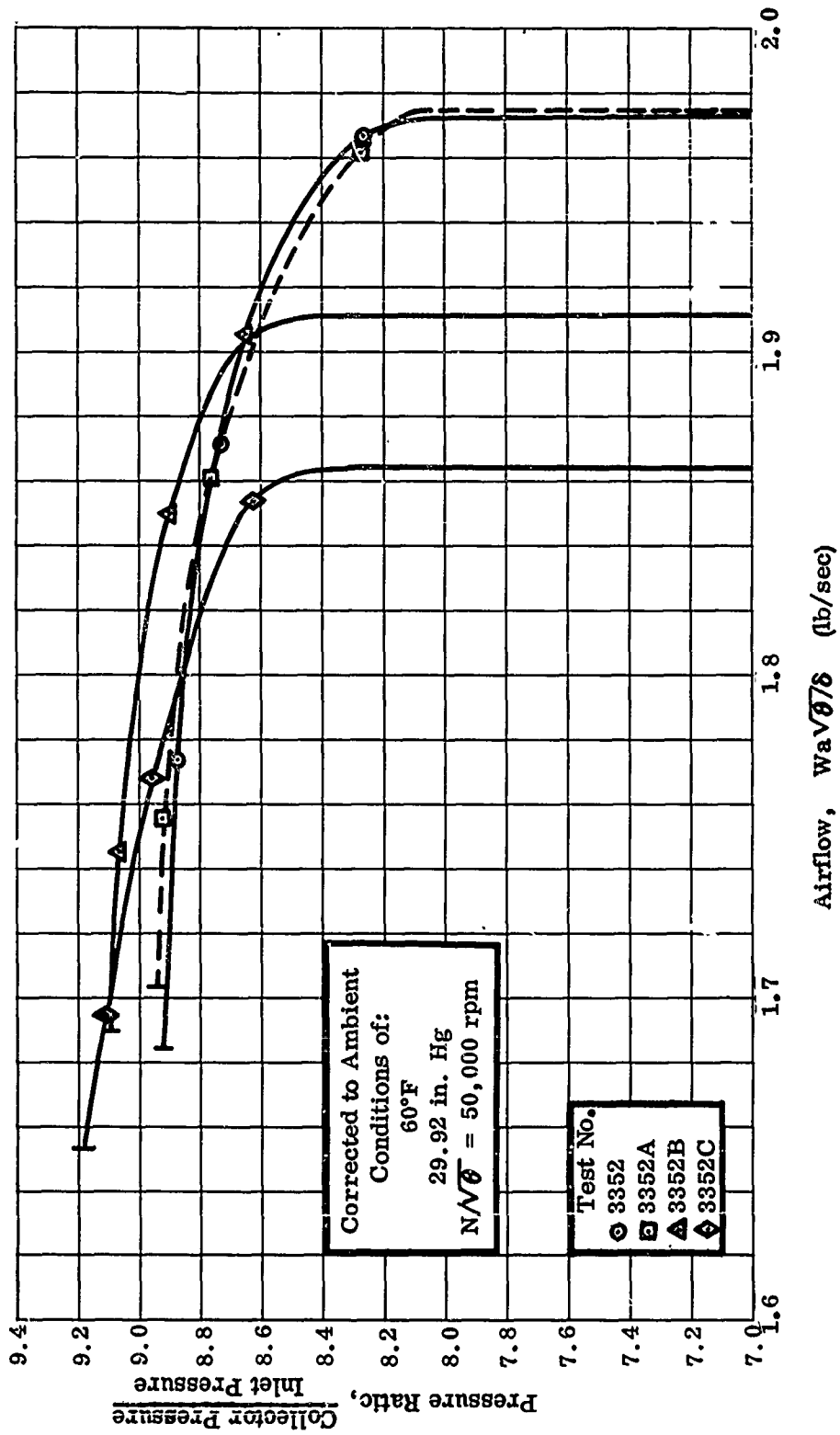


Figure 165. Pressure Ratio Versus Airflow.

CONFIDENTIAL

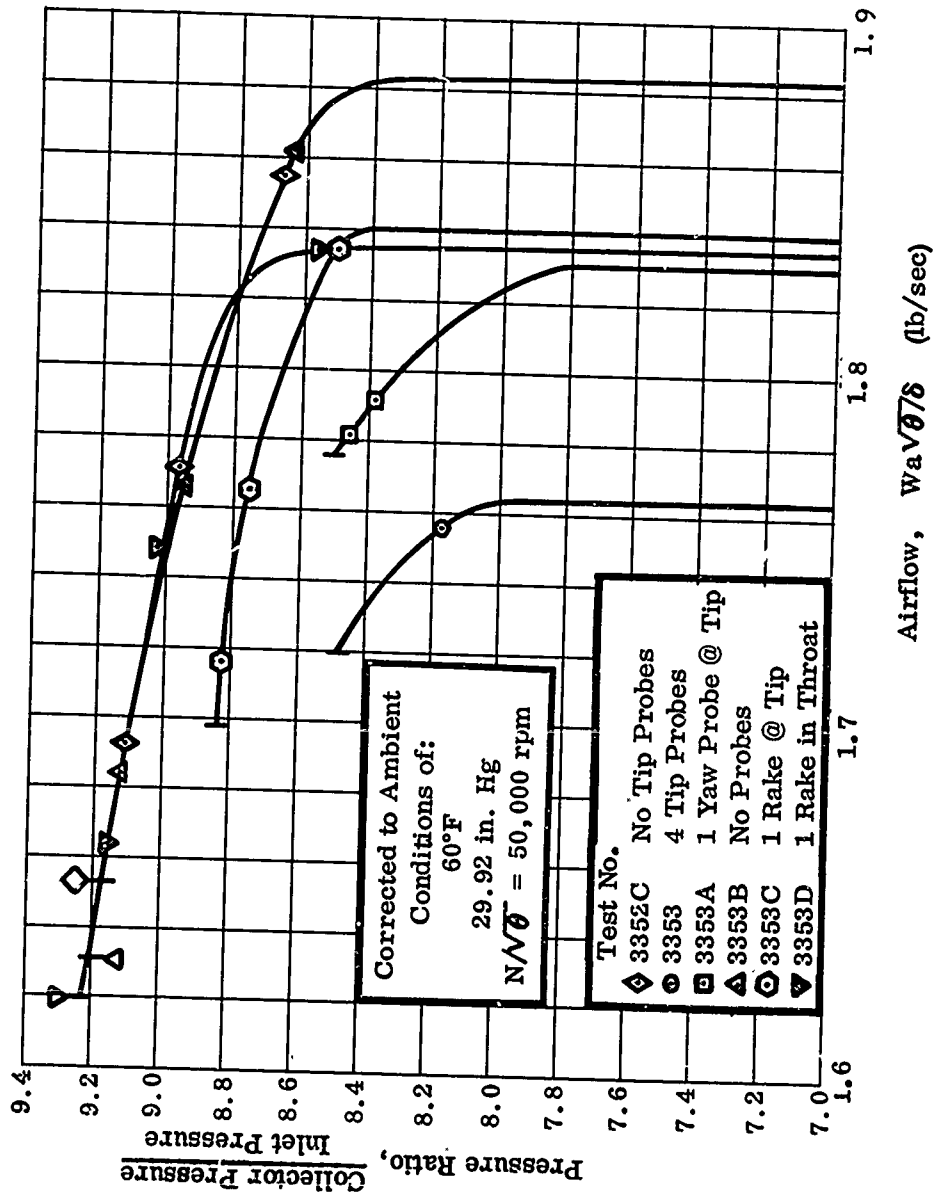


Figure 166. Pressure Ratio Versus Airflow.

CONFIDENTIAL

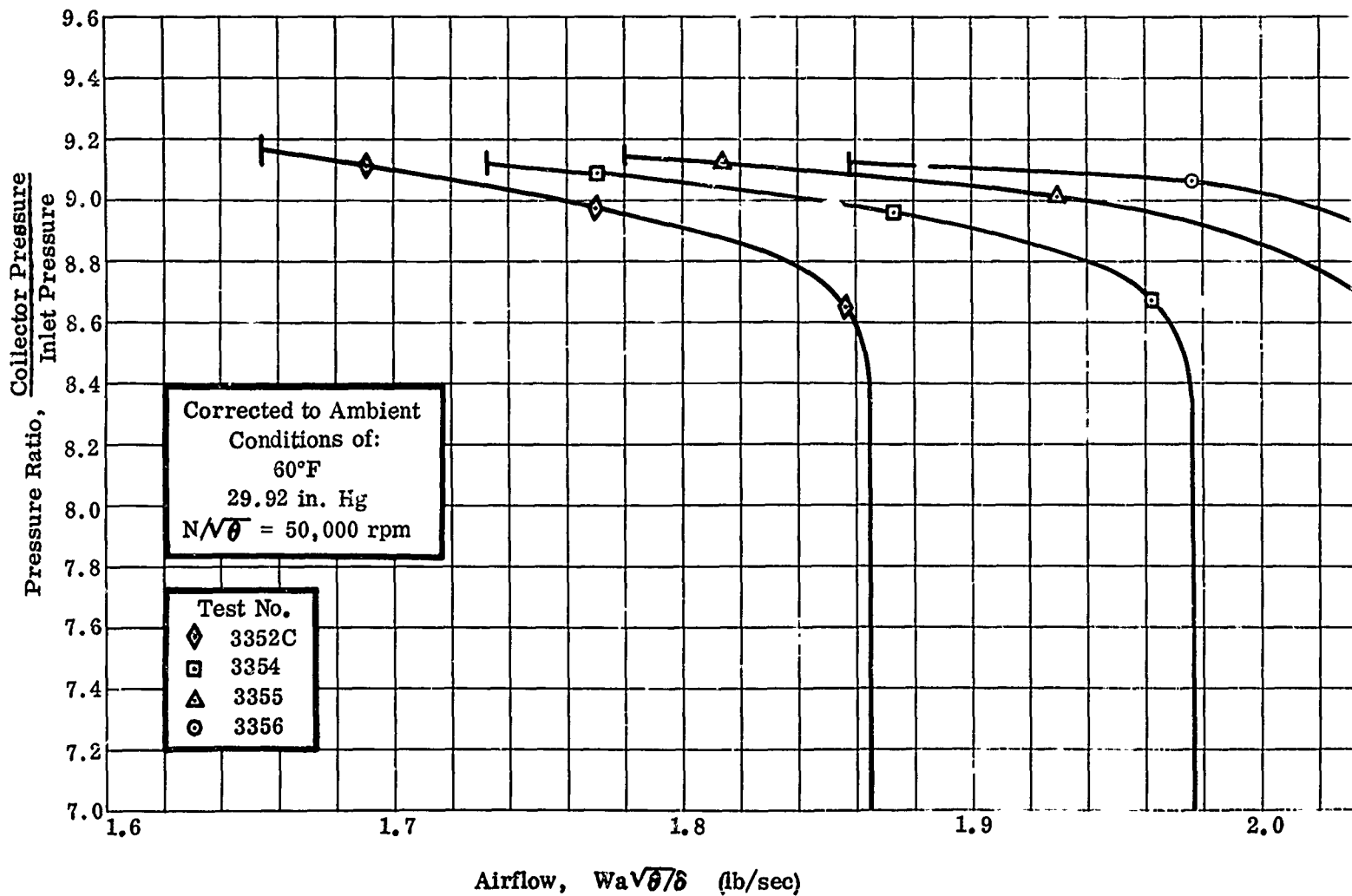
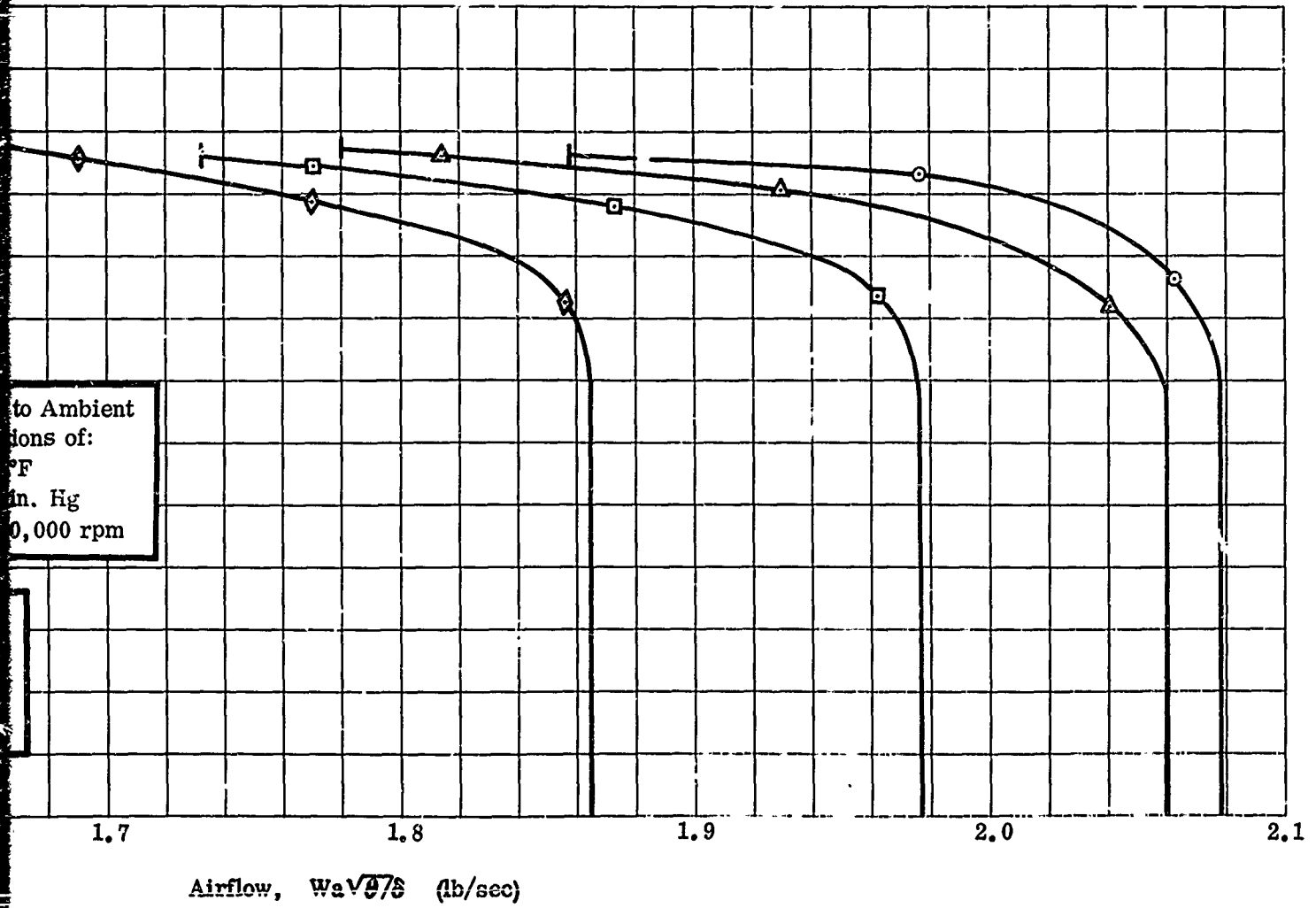


Figure 167. Pressure Ratio Versus Airflow.

CONFIDENTIAL

7
1

CONFIDENTIAL



Pressure Ratio Versus Airflow.

209

CONFIDENTIAL

2

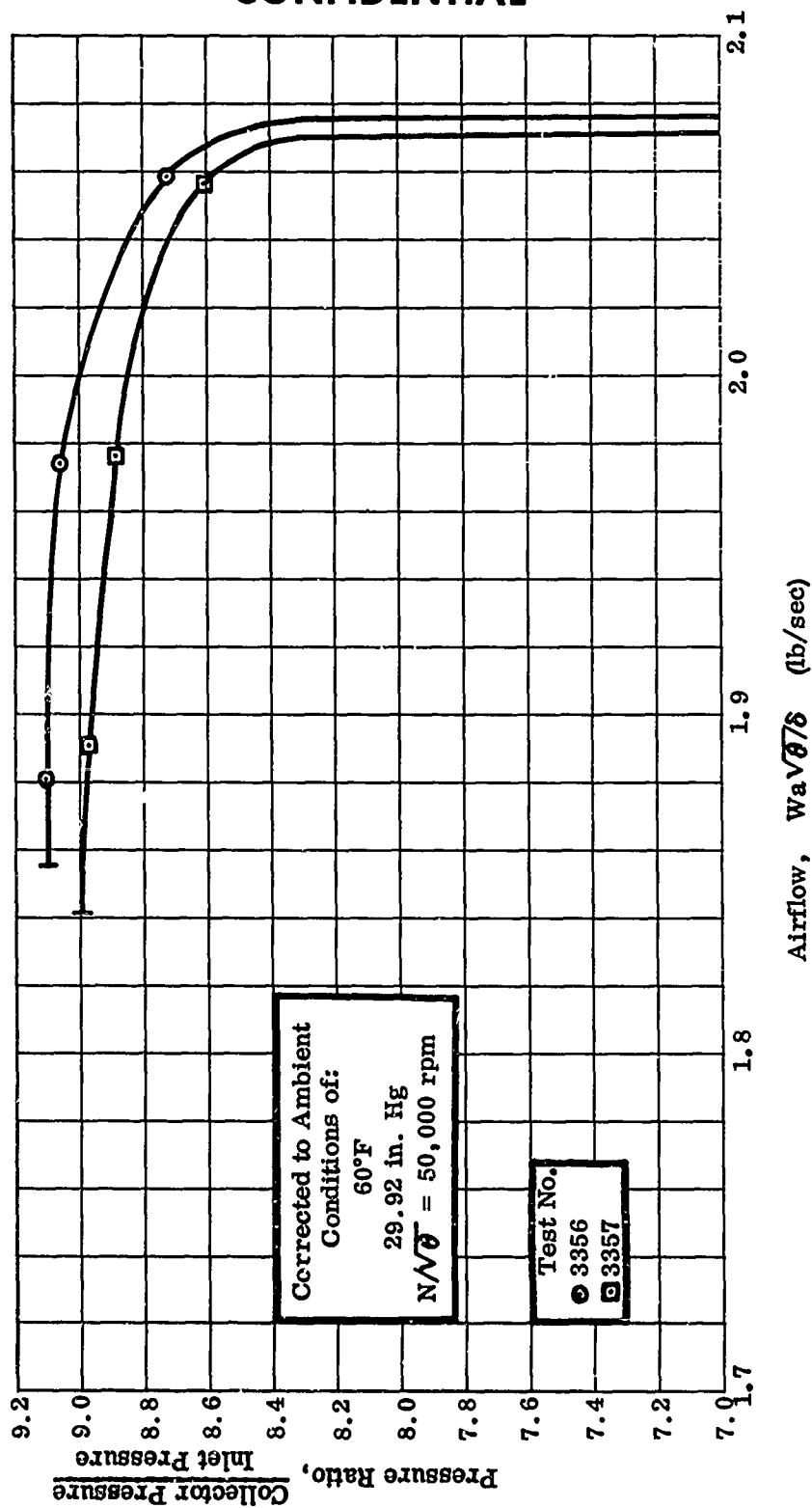


Figure 168. Pressure Ratio Versus Airflow.

CONFIDENTIAL

212

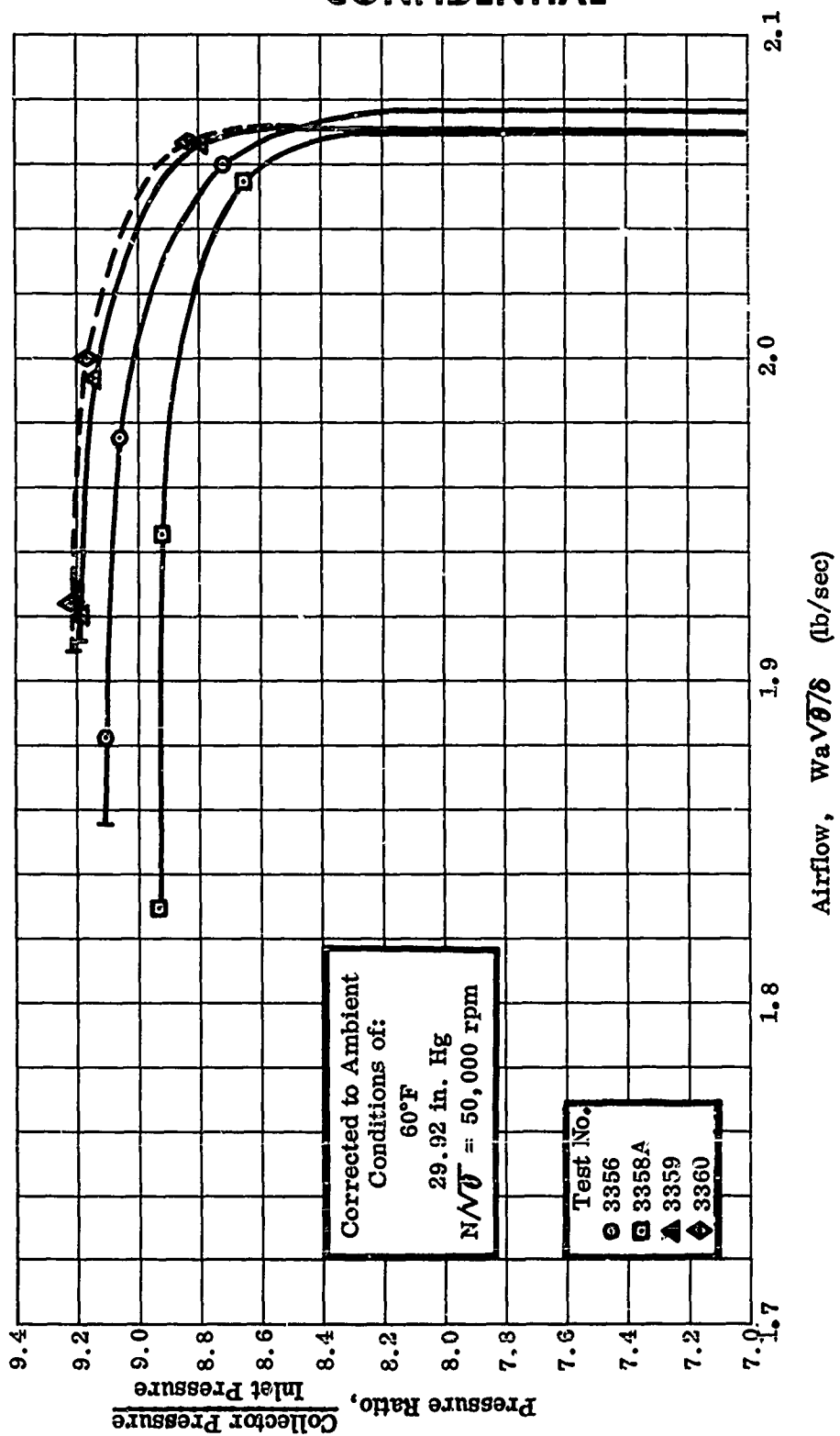


Figure 169. Pressure Ratio Versus Airflow.

CONFIDENTIAL

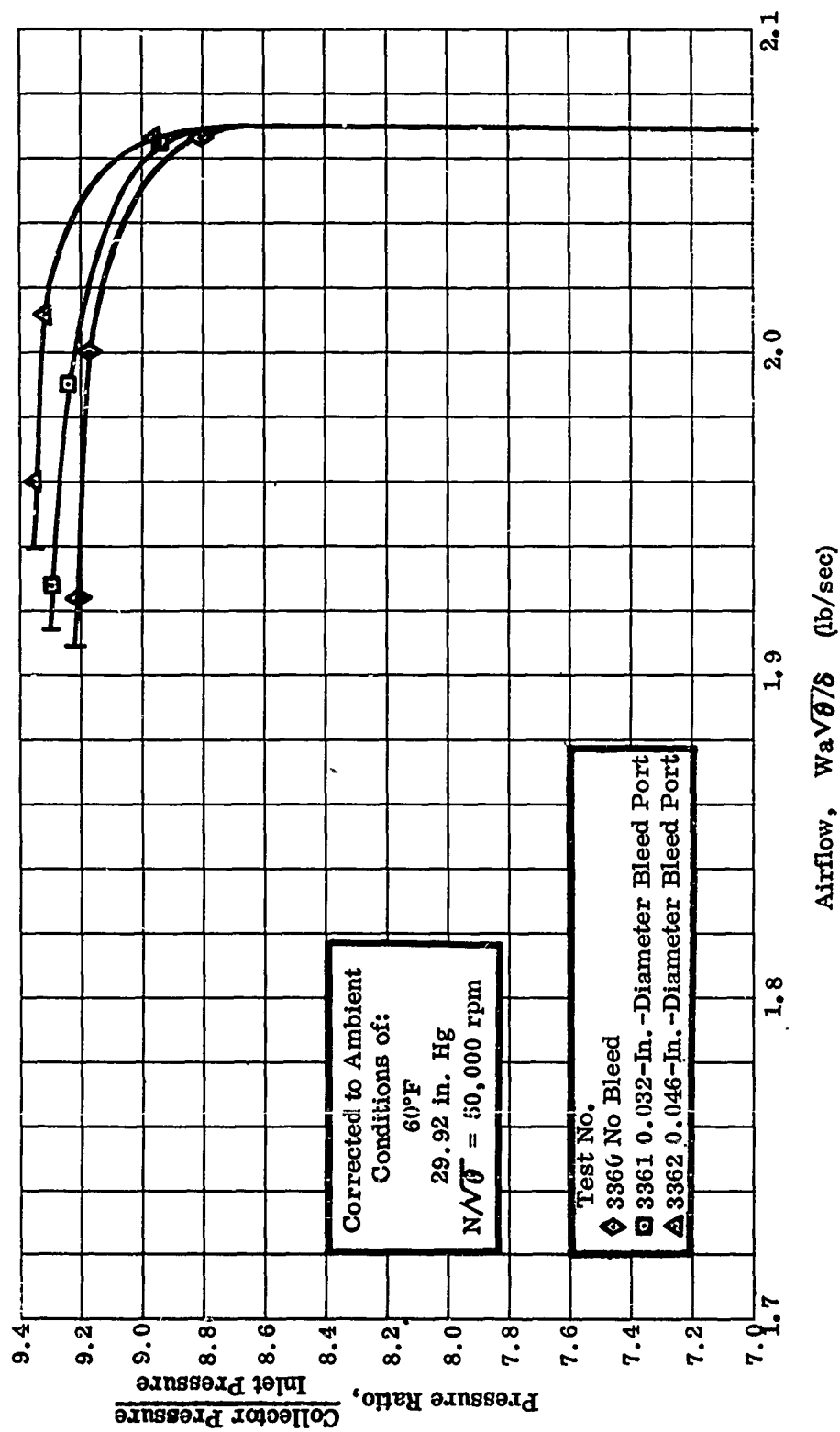


Figure 170. Pressure Ratio Versus Airflow.

CONFIDENTIAL

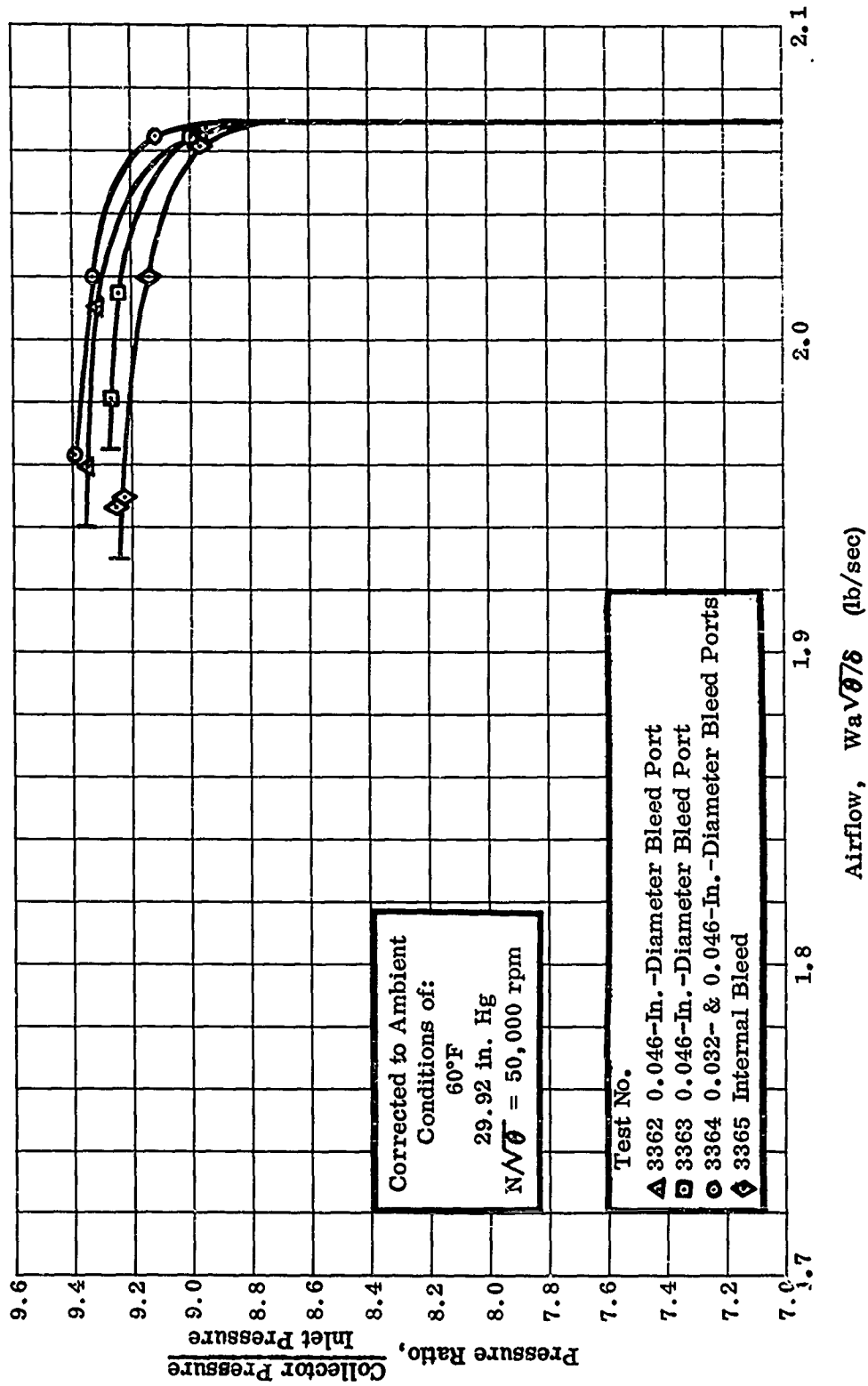


Figure 171. Pressure Ratio Versus Airflow.

CONFIDENTIAL

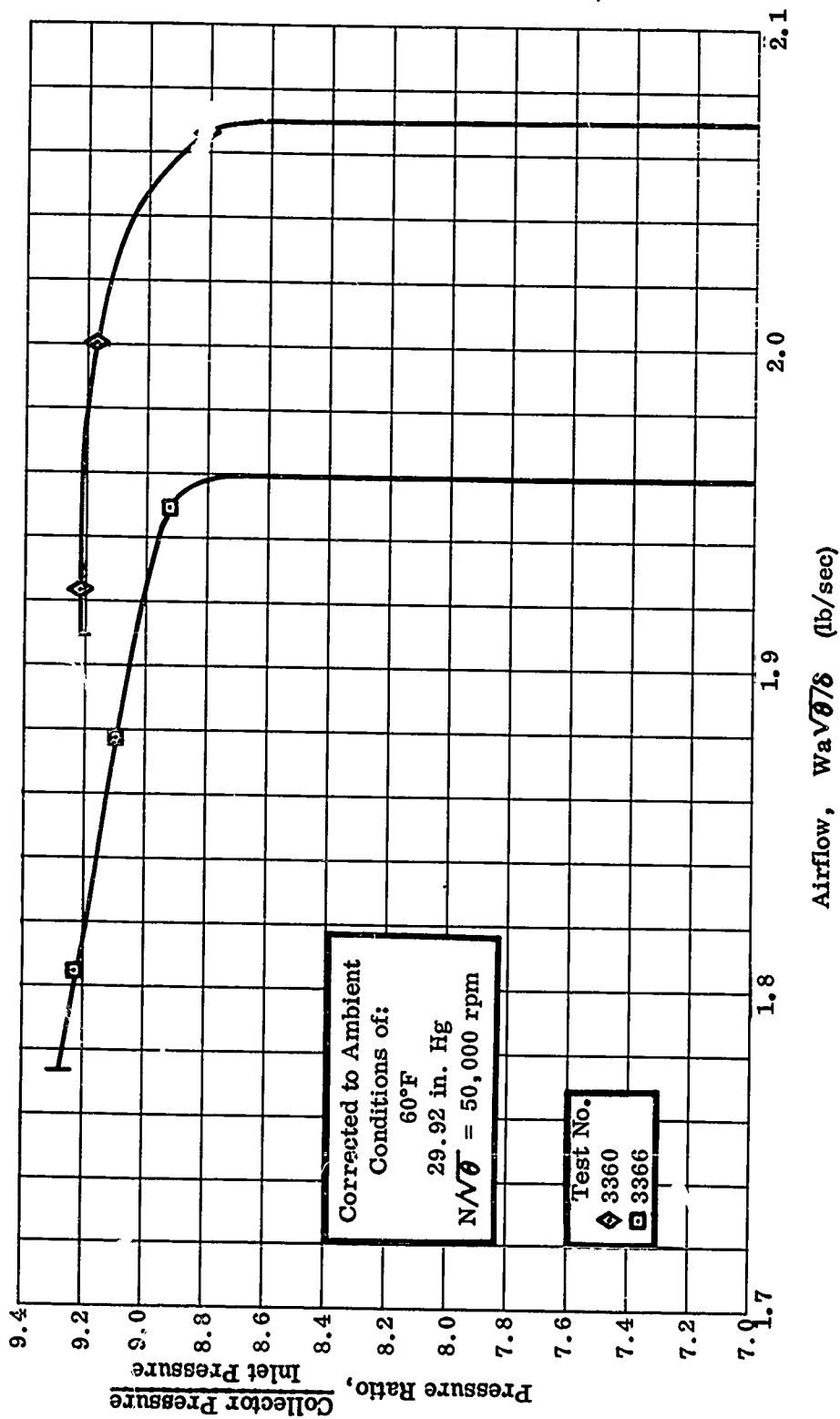


Figure 172. Pressure Ratio Versus Airflow.

CONFIDENTIAL

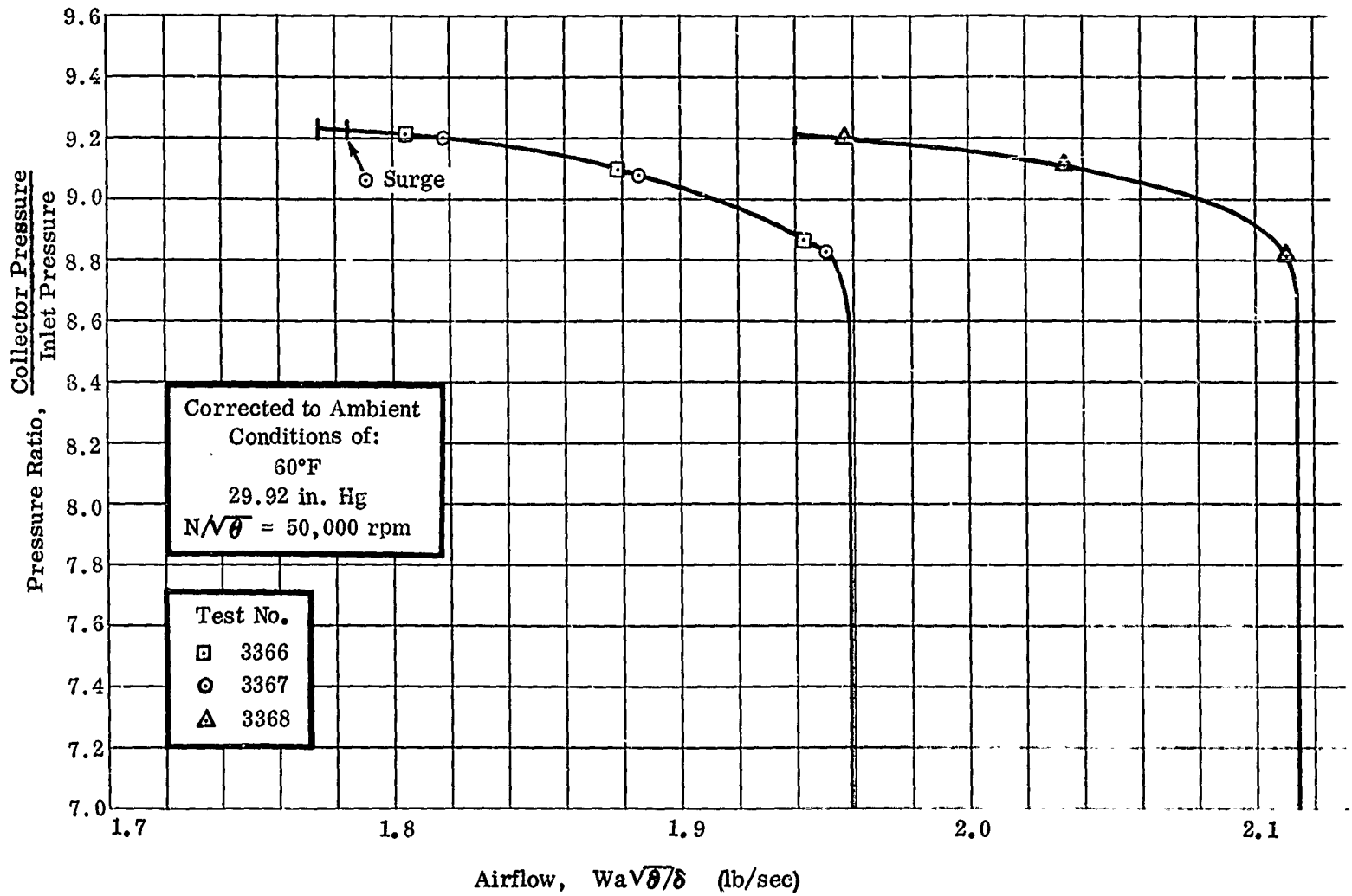
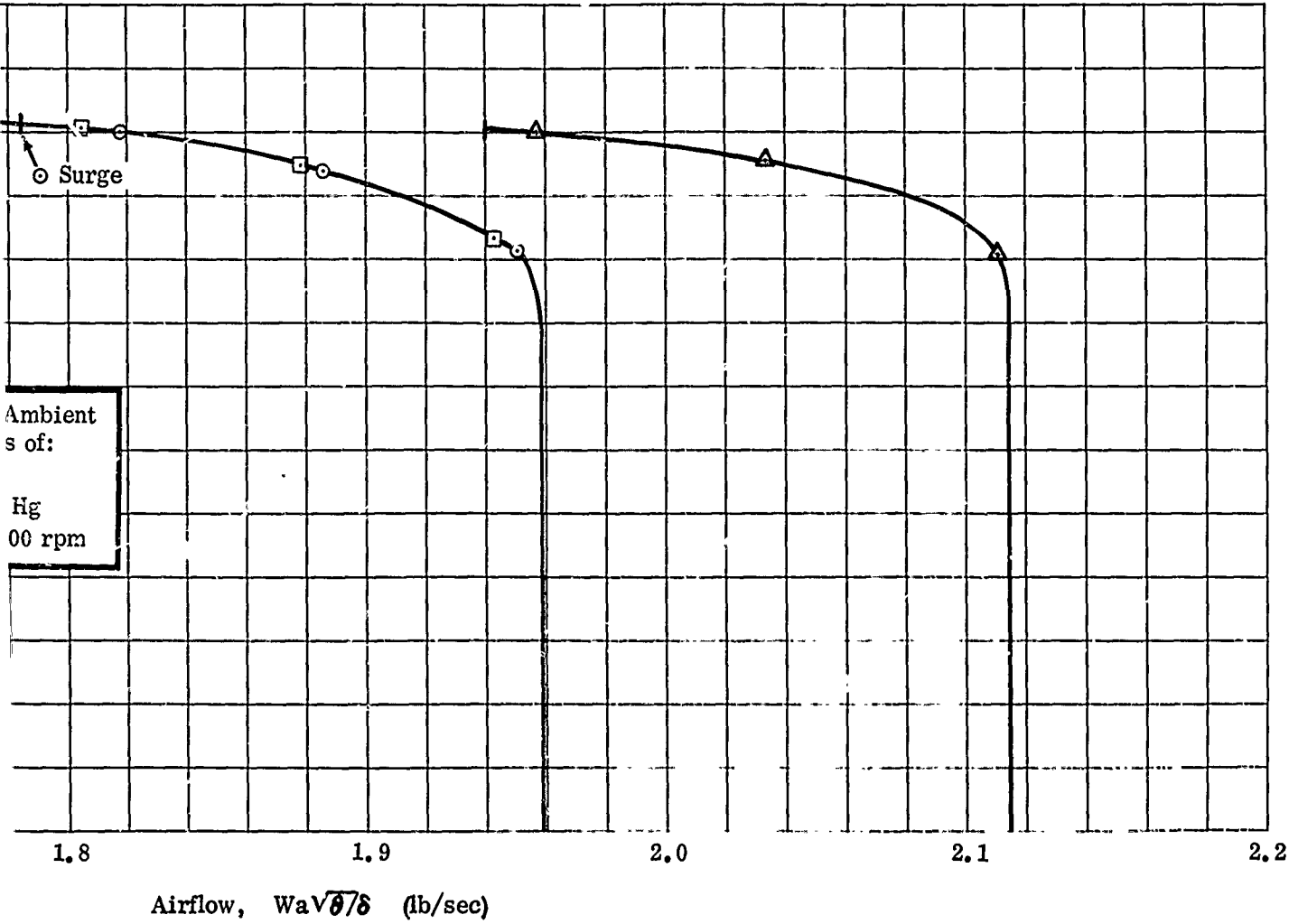


Figure 173. Pressure Ratio Versus Airflow.

CONFIDENTIAL

1



Pressure Ratio Versus Airflow.

217

2

CONFIDENTIAL

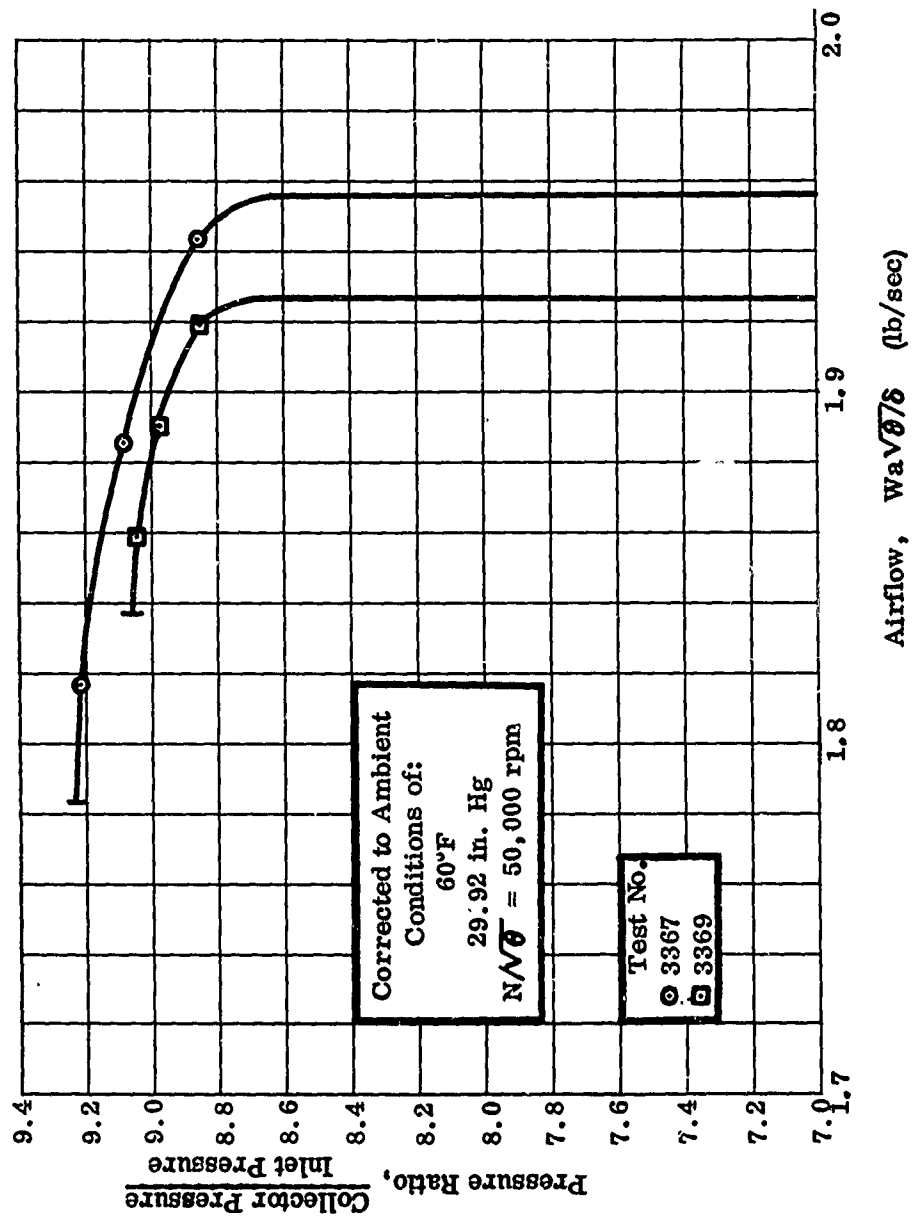


Figure 174. Pressure Ratio Versus Airflow.

CONFIDENTIAL

CONFIDENTIAL

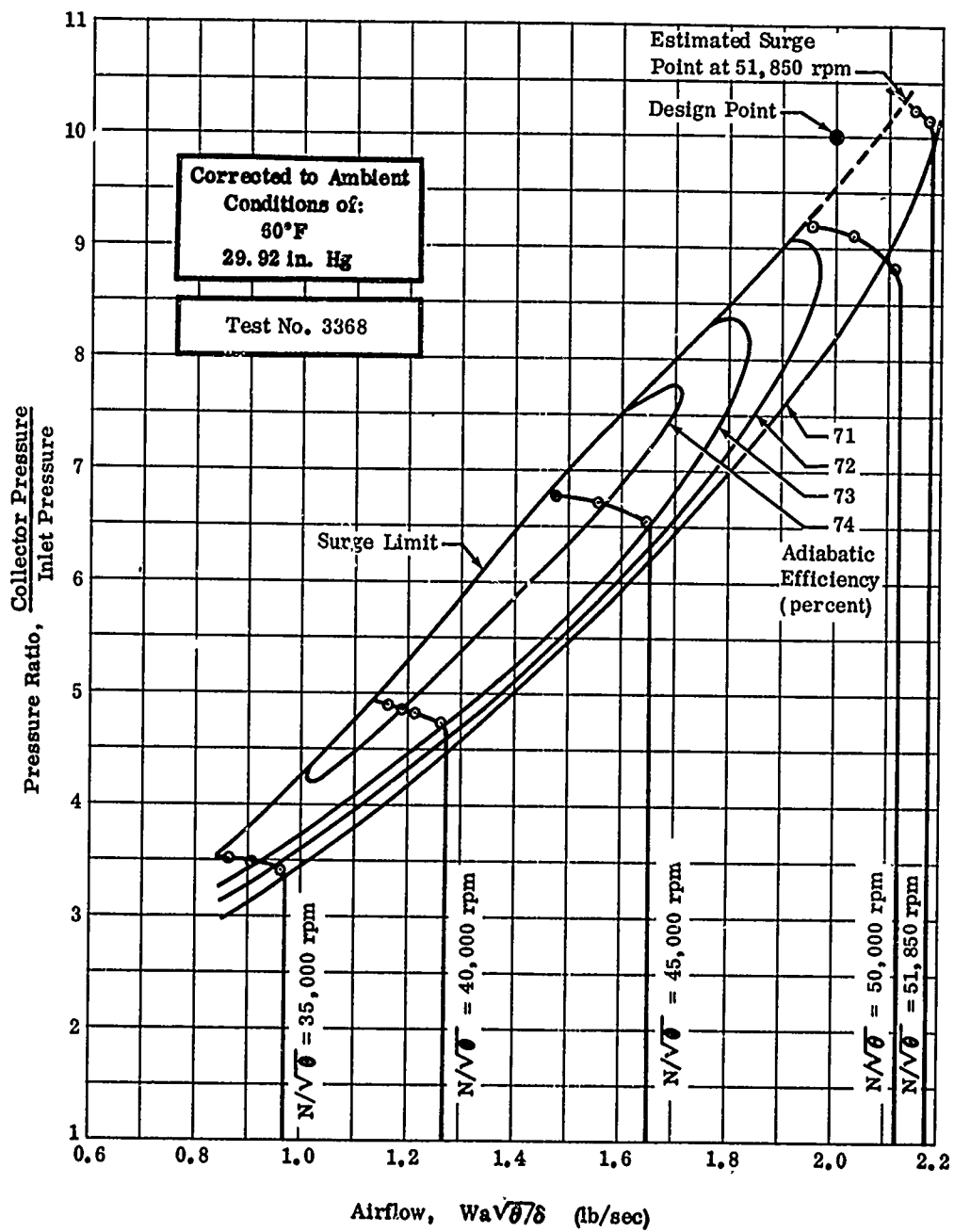


Figure 175. Pressure Ratio Versus Airflow.

CONFIDENTIAL

CONFIDENTIAL

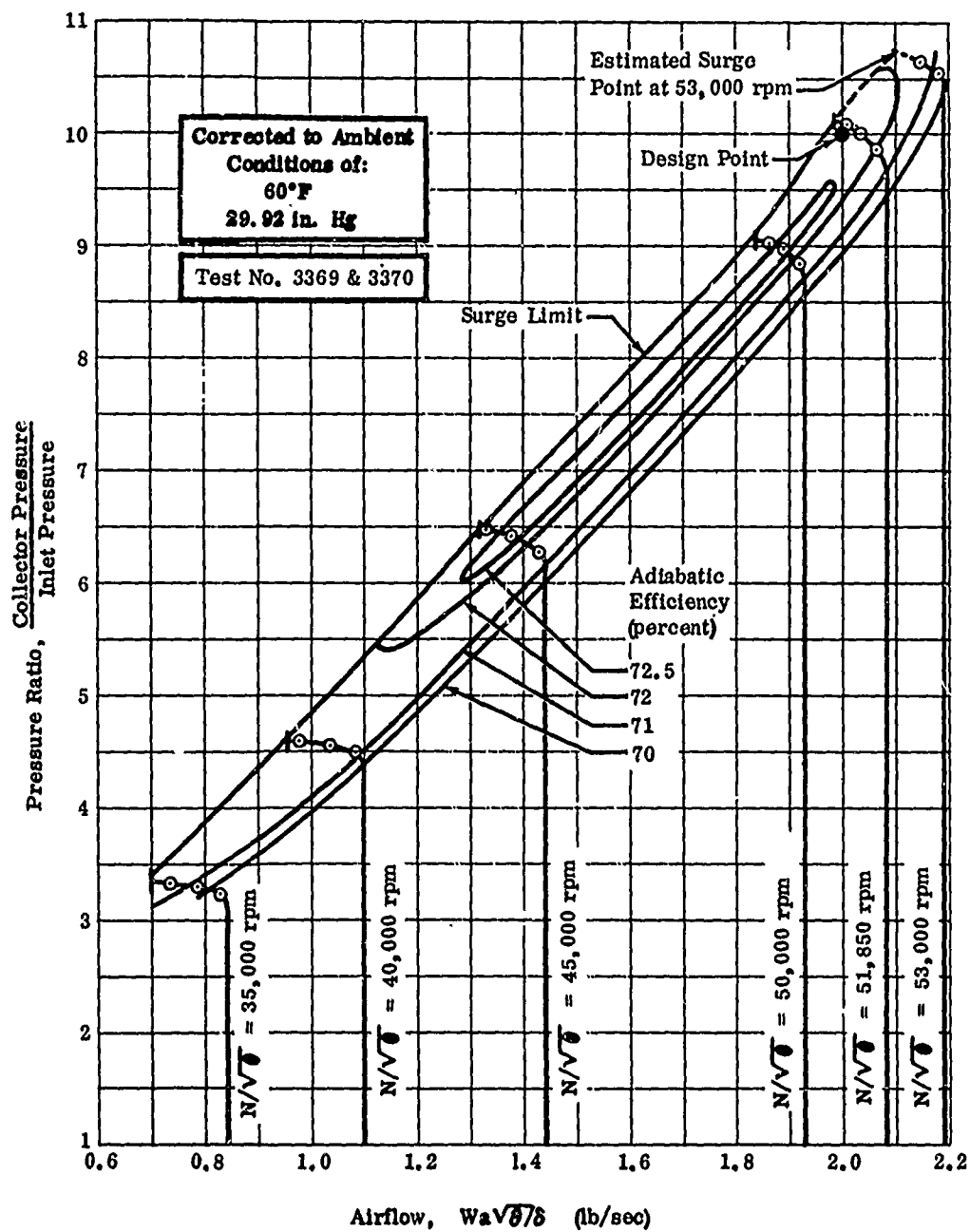


Figure 176. Pressure Ratio Versus Airflow.

CONFIDENTIAL

CONFIDENTIAL

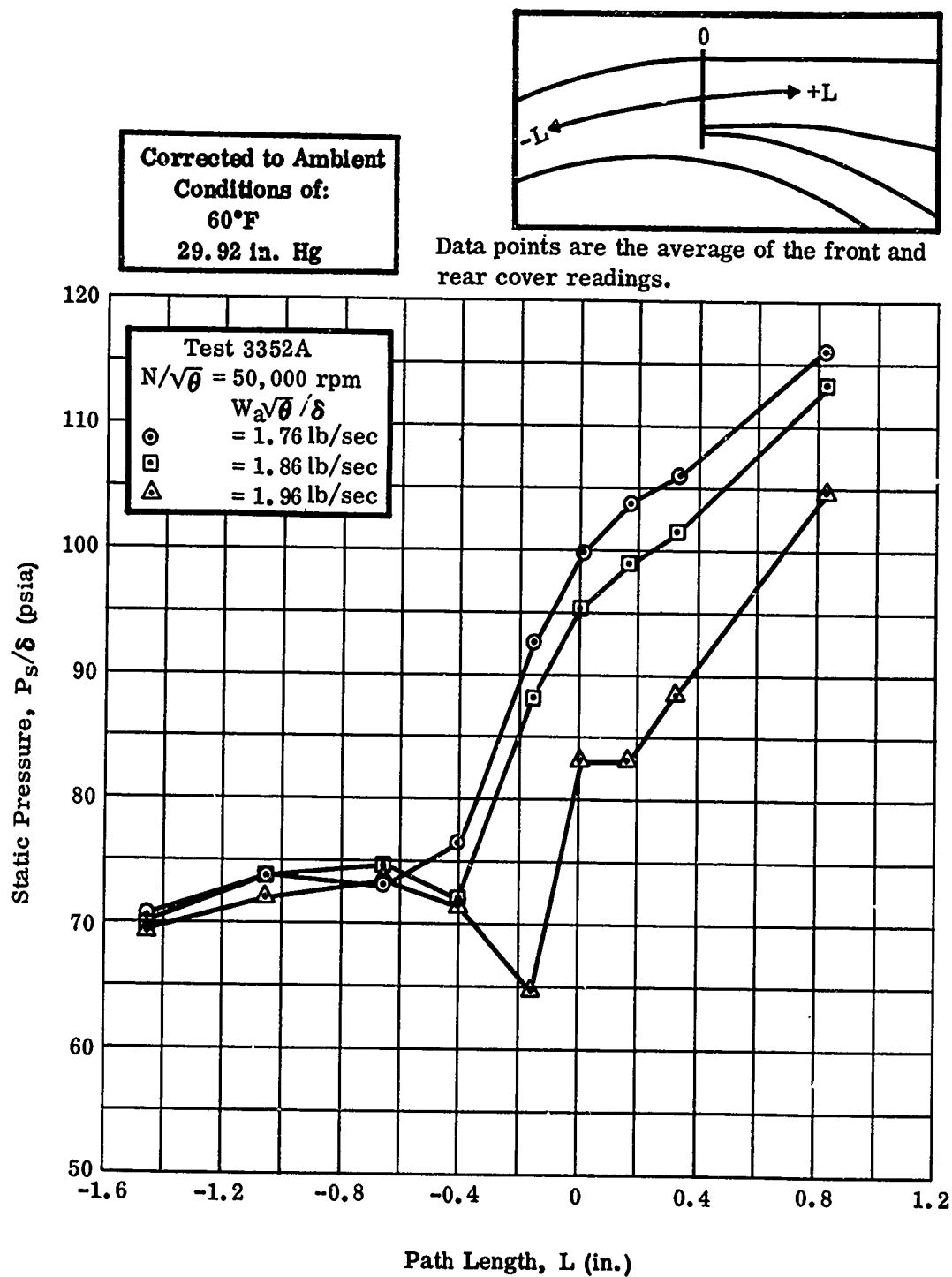


Figure 177. Static-Pressure Variation in Diffuser.

CONFIDENTIAL

CONFIDENTIAL

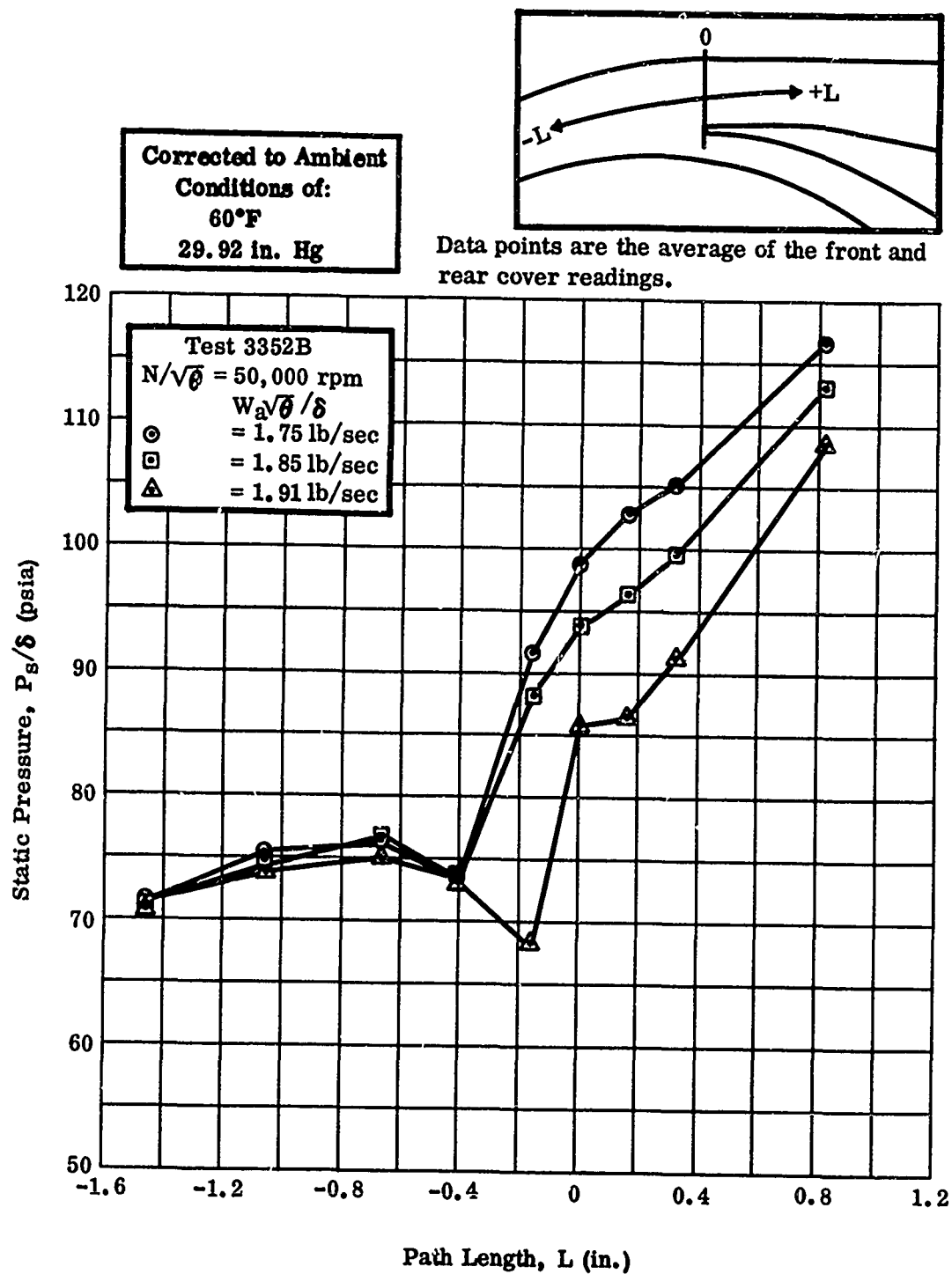


Figure 178. Static-Pressure Variation in Diffuser.

CONFIDENTIAL

CONFIDENTIAL

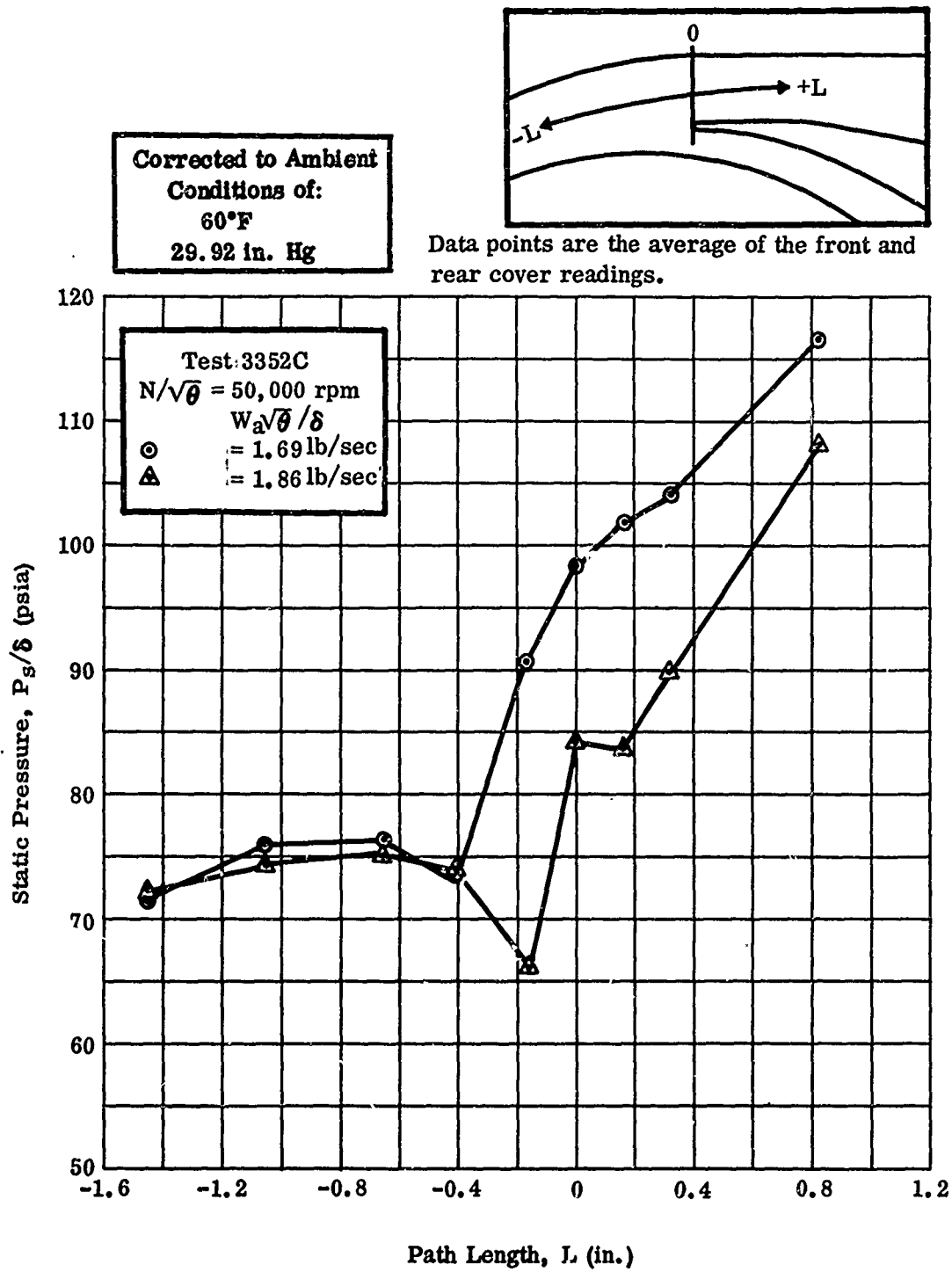


Figure 179. Static-Pressure Variation in Diffuser.

CONFIDENTIAL

CONFIDENTIAL

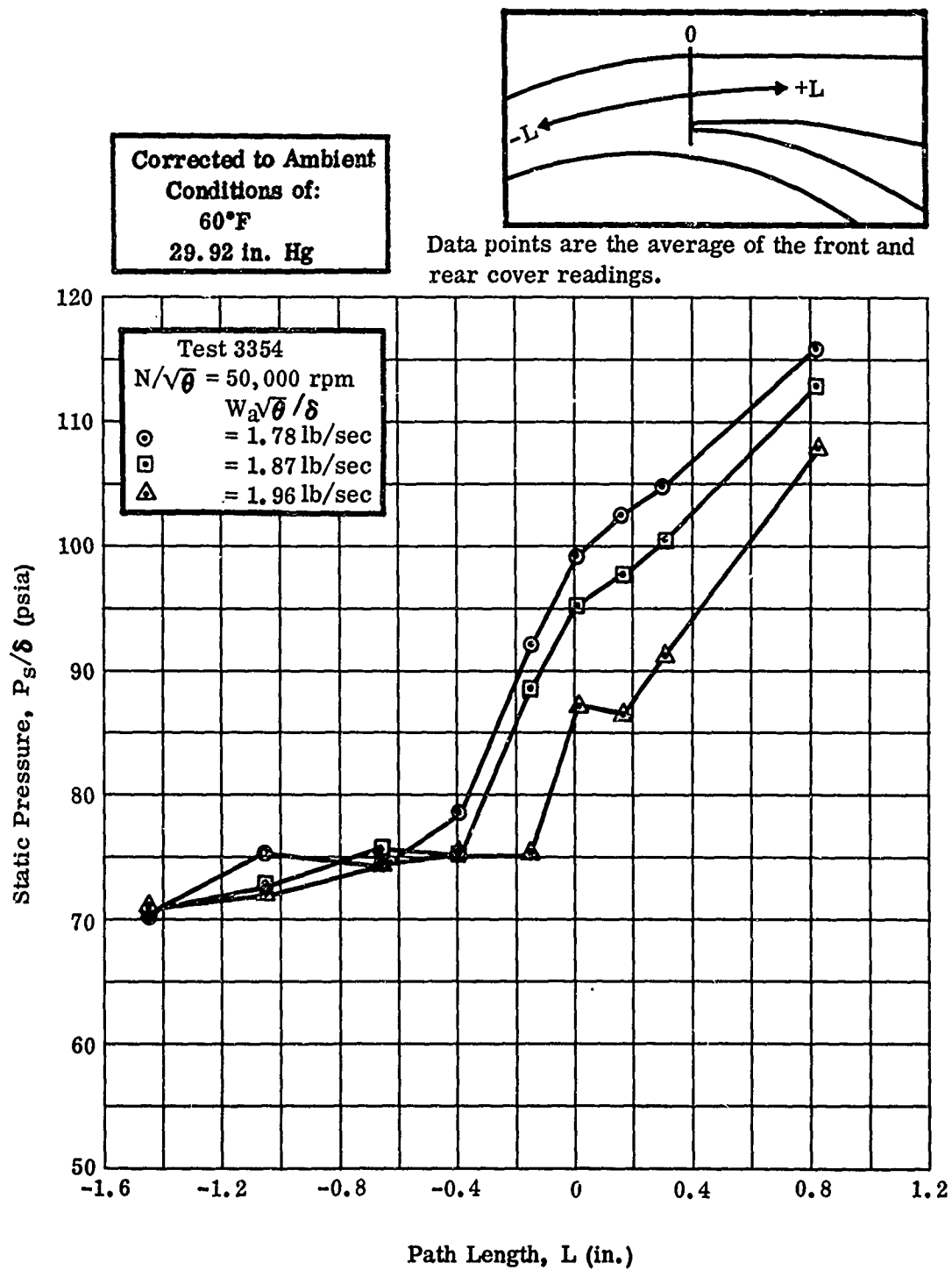
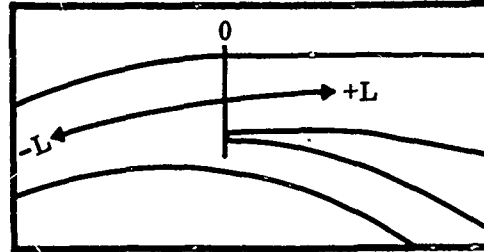


Figure 180. Static-Pressure Variation in Diffuser.

CONFIDENTIAL

CONFIDENTIAL

Corrected to Ambient
Conditions of:
60°F
29.92 in. Hg



Data points are the average of the front and rear cover readings.

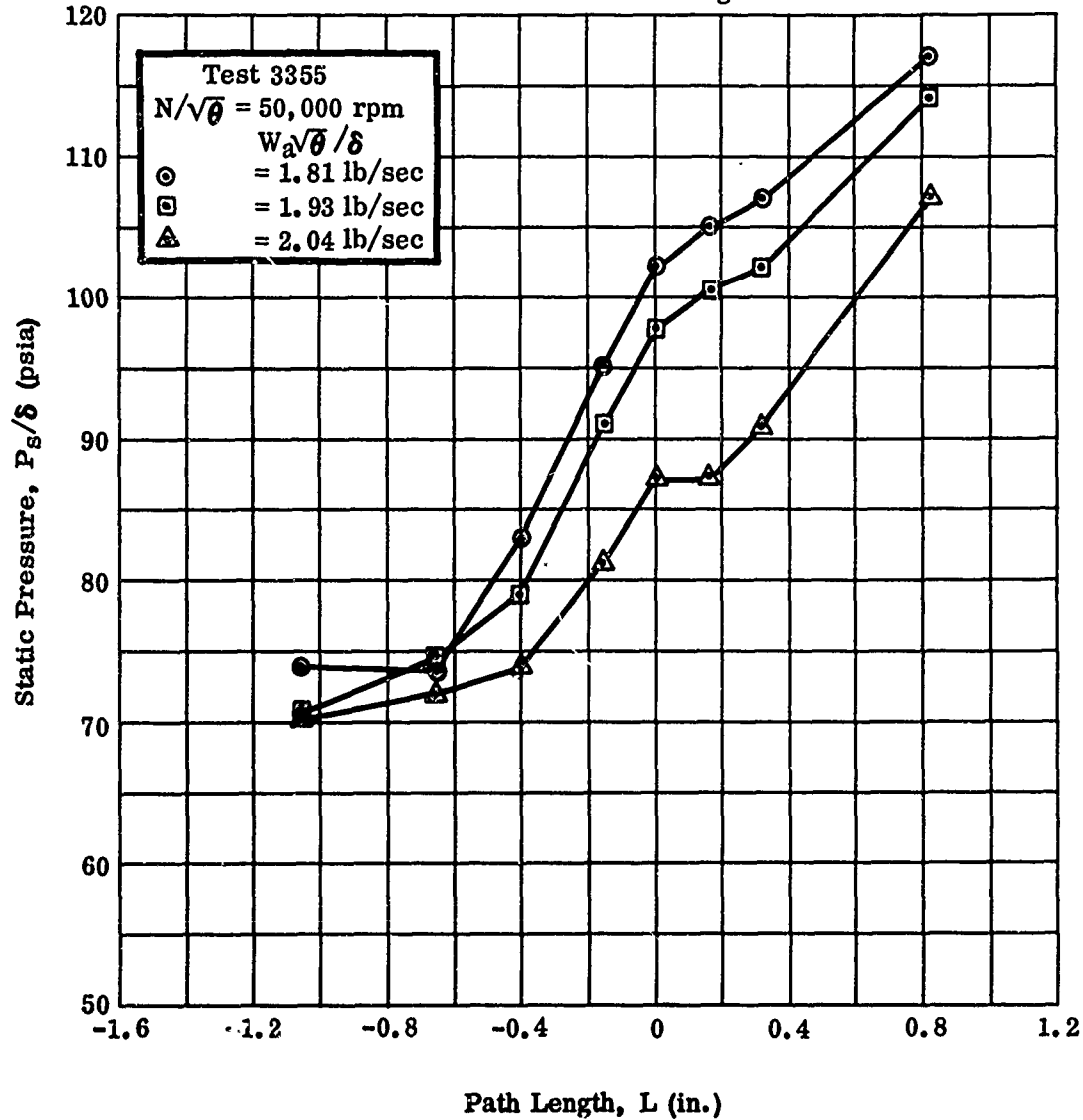
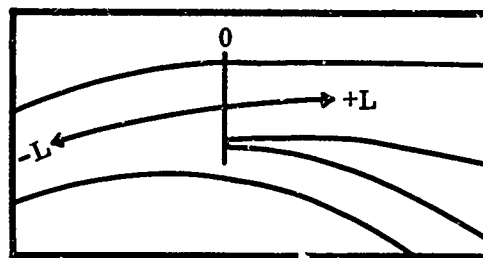


Figure 181. Static-Pressure Variation in Diffuser.

CONFIDENTIAL

CONFIDENTIAL

Corrected to Ambient
Conditions of:
60°F
29.92 in. Hg



Data points are the average of the front and rear cover readings.

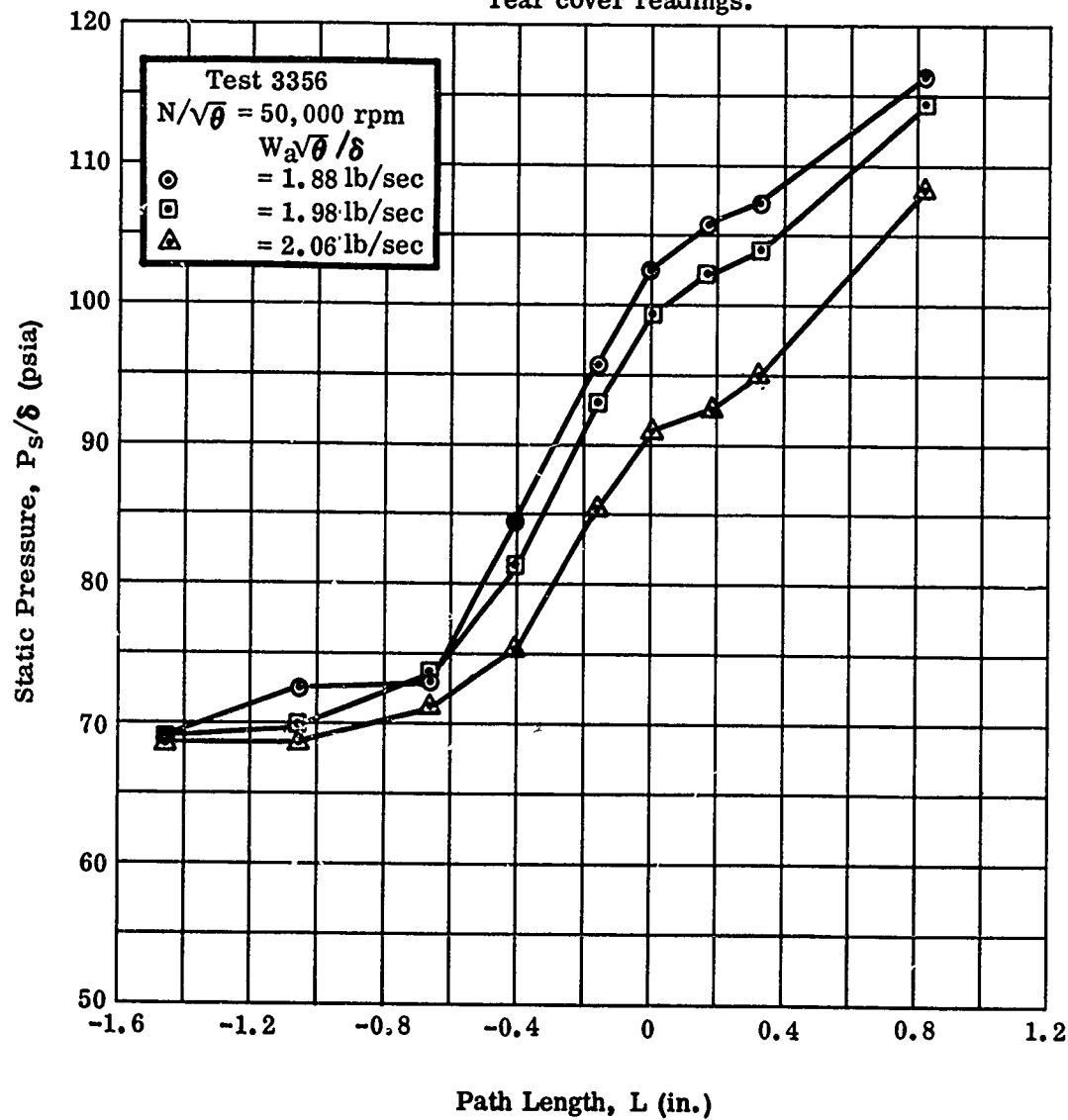


Figure 182. Static-Pressure Variation in Diffuser.

CONFIDENTIAL

CONFIDENTIAL

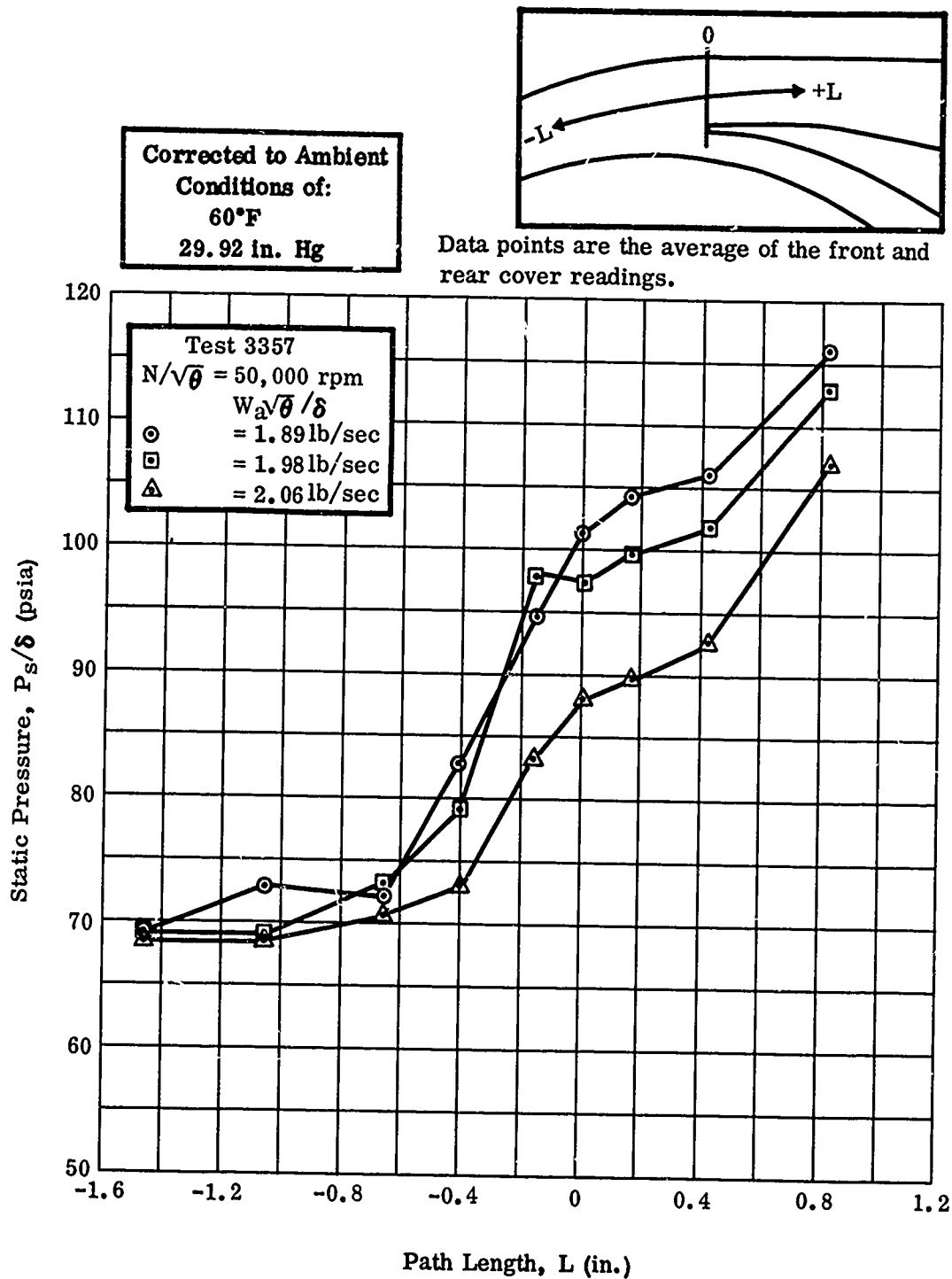
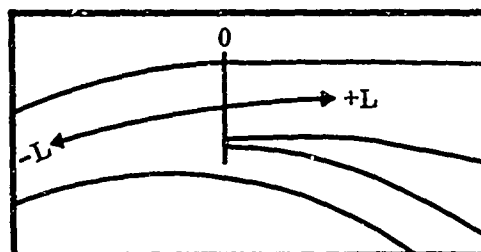


Figure 183. Static-Pressure Variation in Diffuser.

CONFIDENTIAL

CONFIDENTIAL

Corrected to Ambient
Conditions of:
60°F
29.92 in. Hg



Data points are the average of the front and rear cover readings.

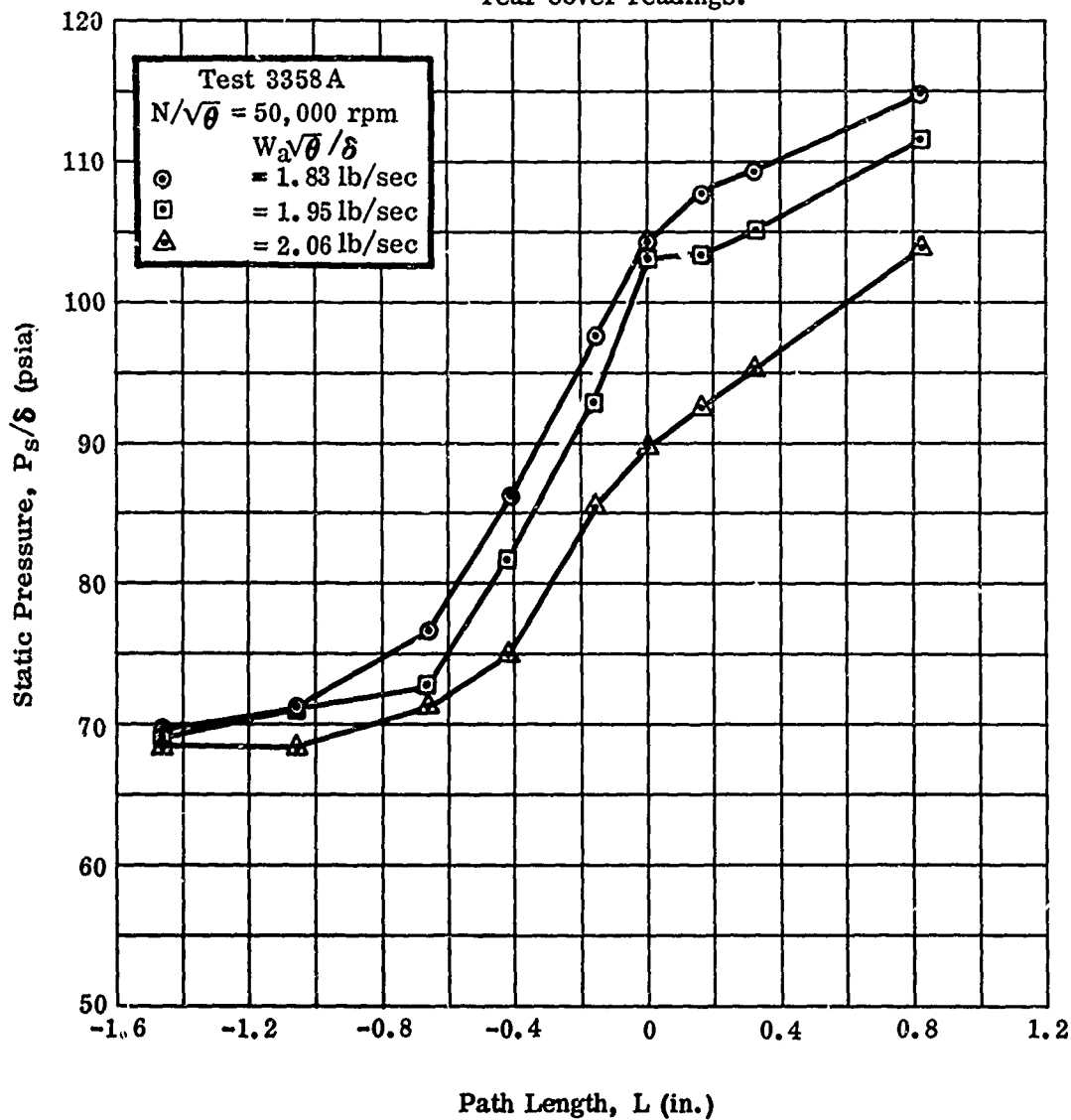


Figure 184. Static-Pressure Variation in Diffuser.

CONFIDENTIAL

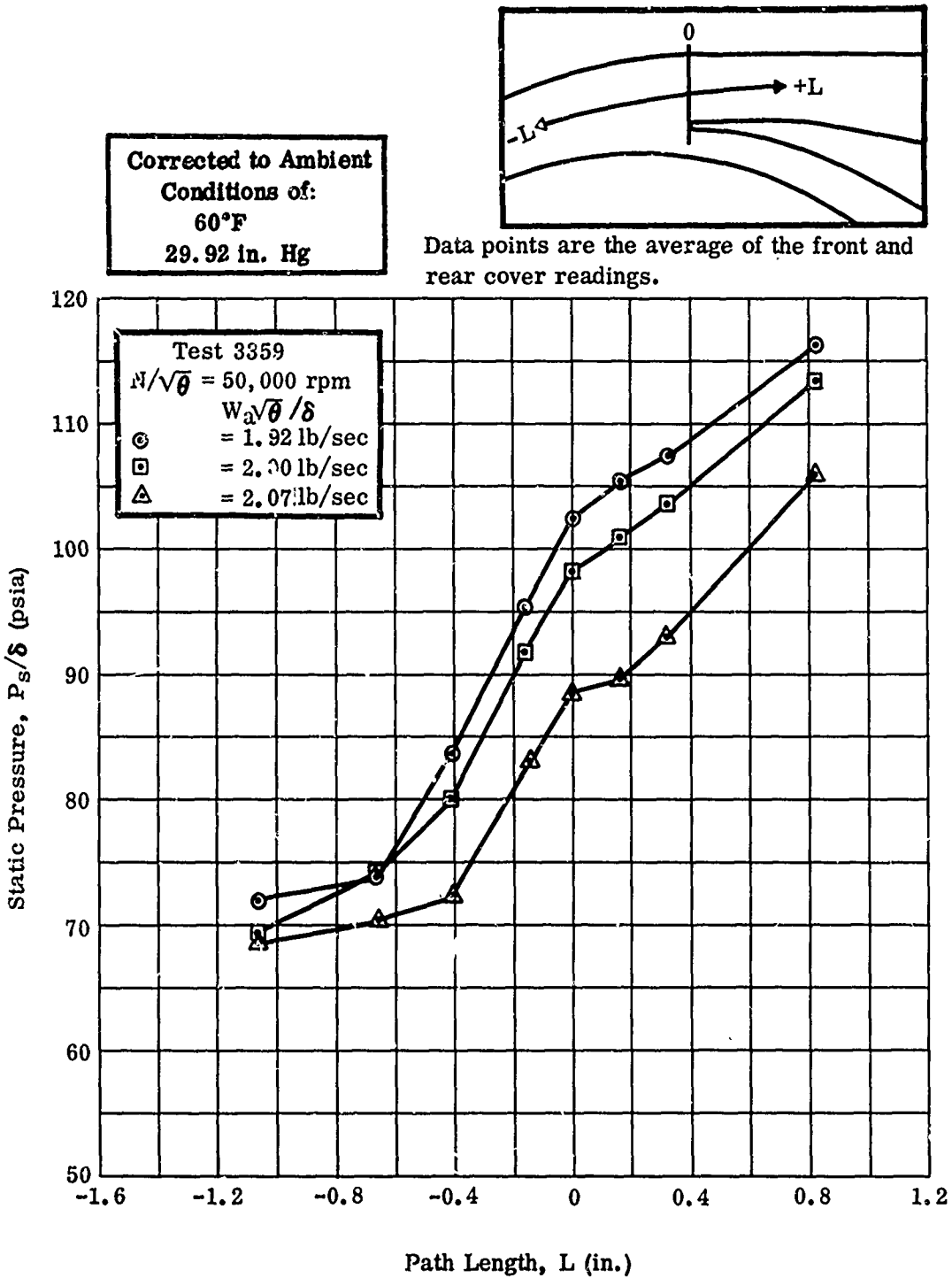


Figure 185. Static-Pressure Variation in Diffuser.

CONFIDENTIAL

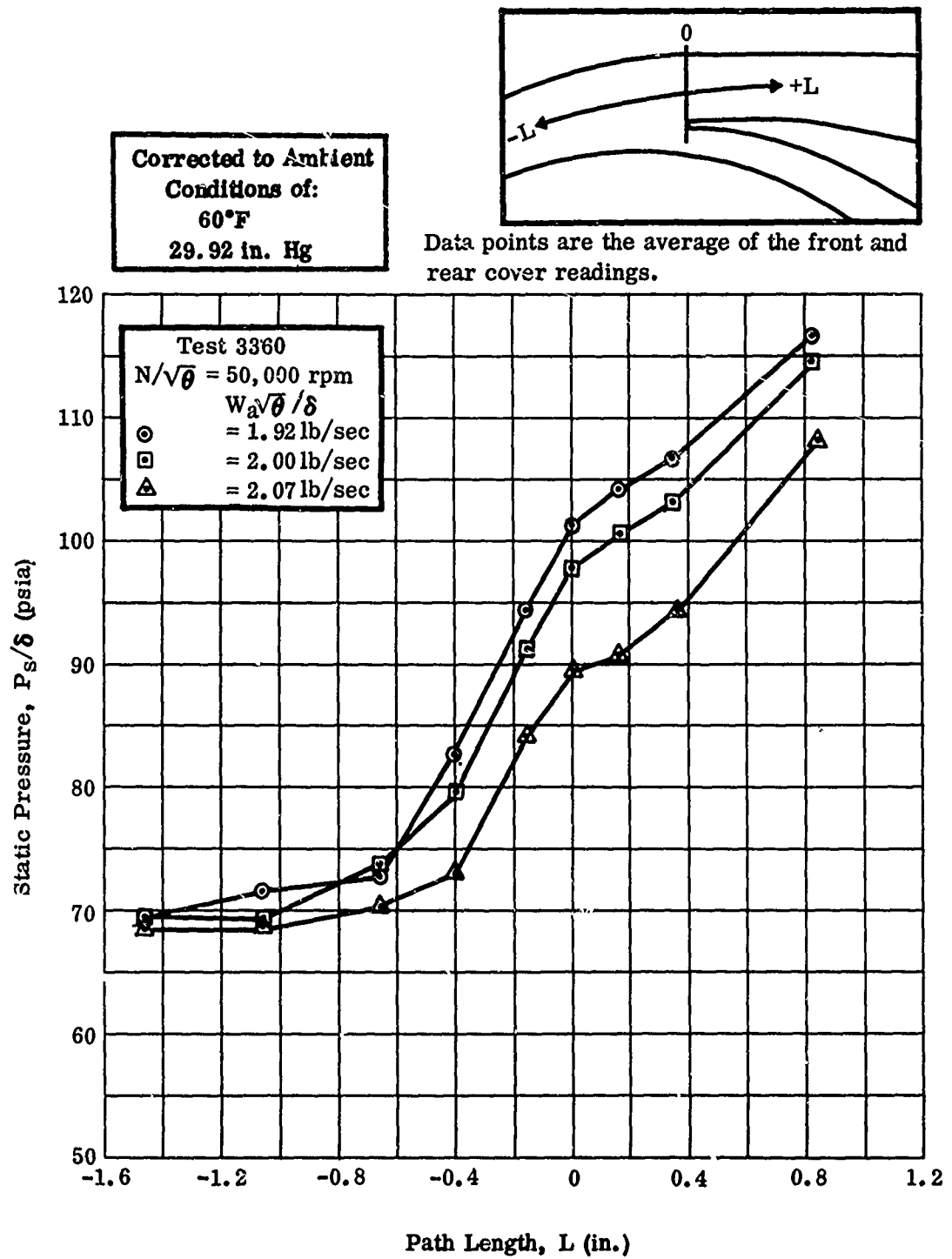


Figure 186. Static-Pressure Variation in Diffuser.

CONFIDENTIAL

CONFIDENTIAL

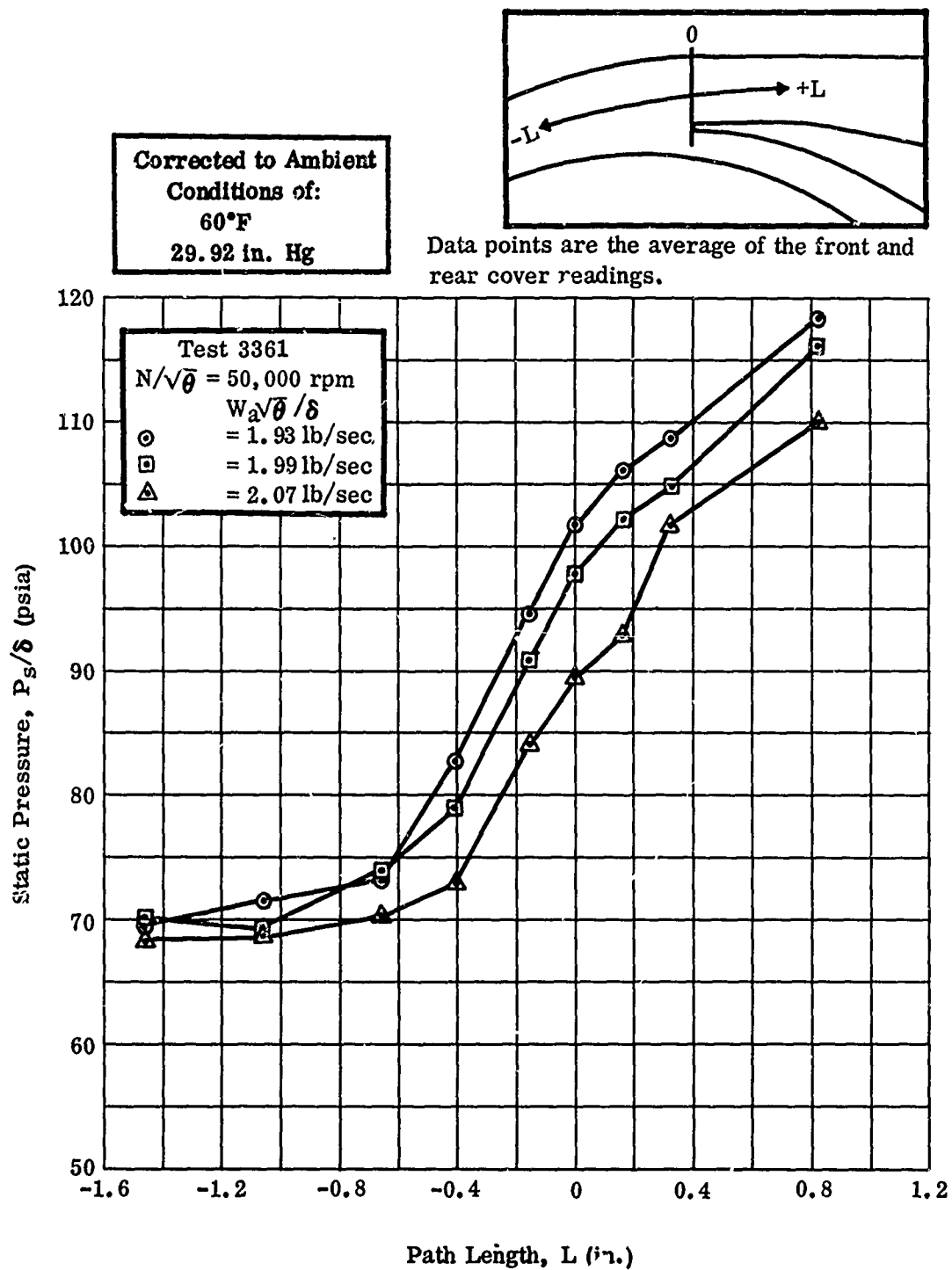
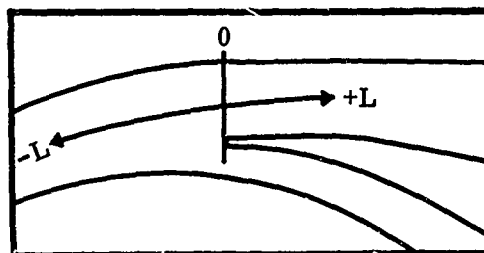


Figure 187. Static-Pressure Variation in Diffuser.

CONFIDENTIAL

CONFIDENTIAL

Corrected to Ambient
Conditions of:
60°F
29.92 in. Hg



Data points are the average of the front and rear cover readings.

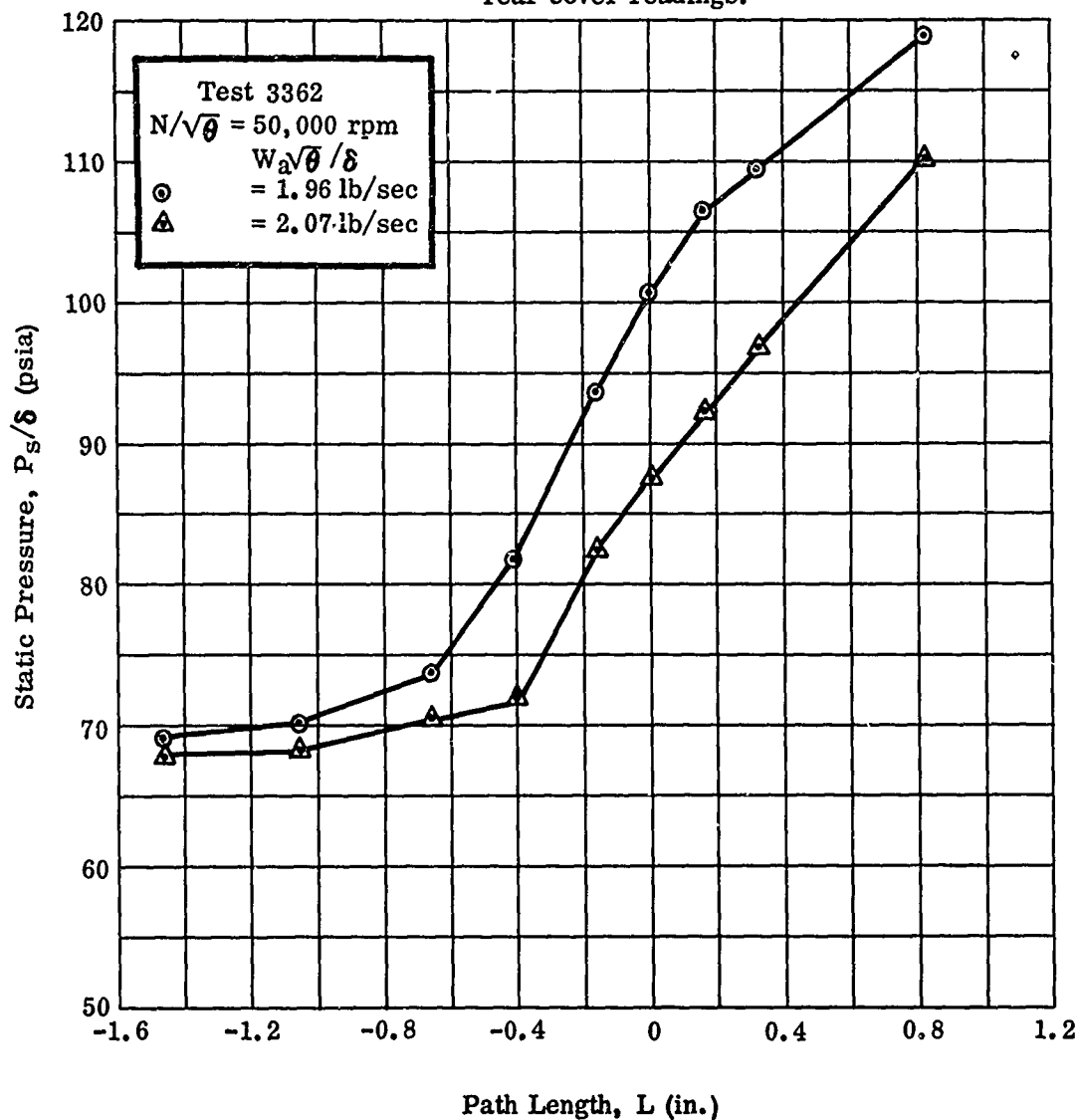


Figure 188. Static-Pressure Variation in Diffuser.

CONFIDENTIAL

CONFIDENTIAL

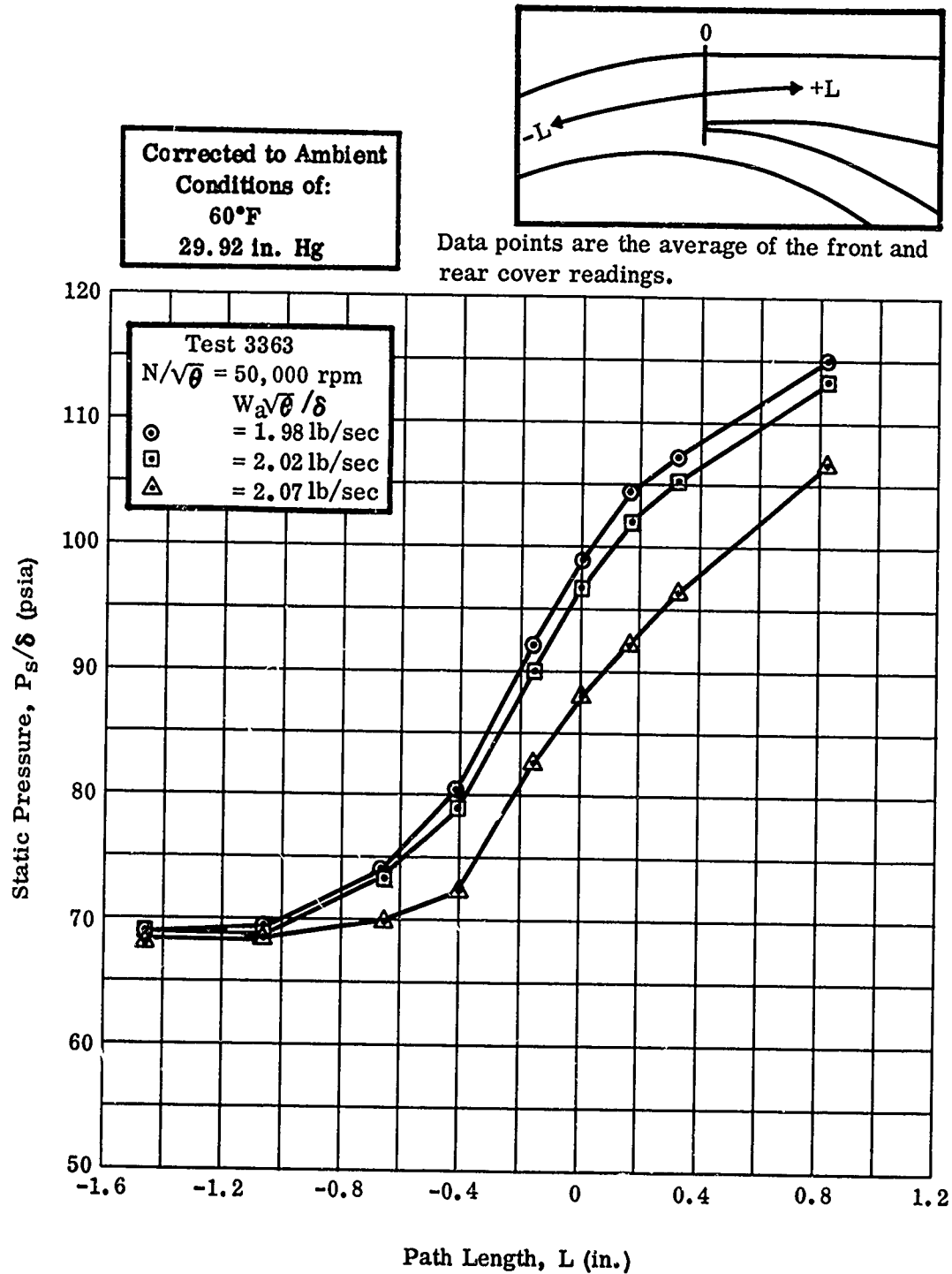
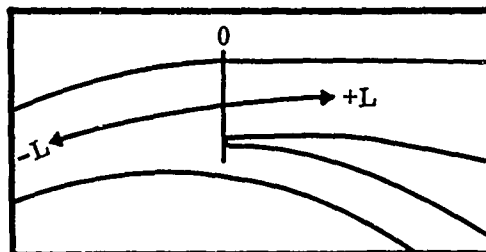


Figure 189. Static-Pressure Variation in Diffuser.

CONFIDENTIAL

CONFIDENTIAL



Corrected to Ambient
Conditions of:
60°F
29.92 in. Hg

Data points are the average of the front and rear cover readings.

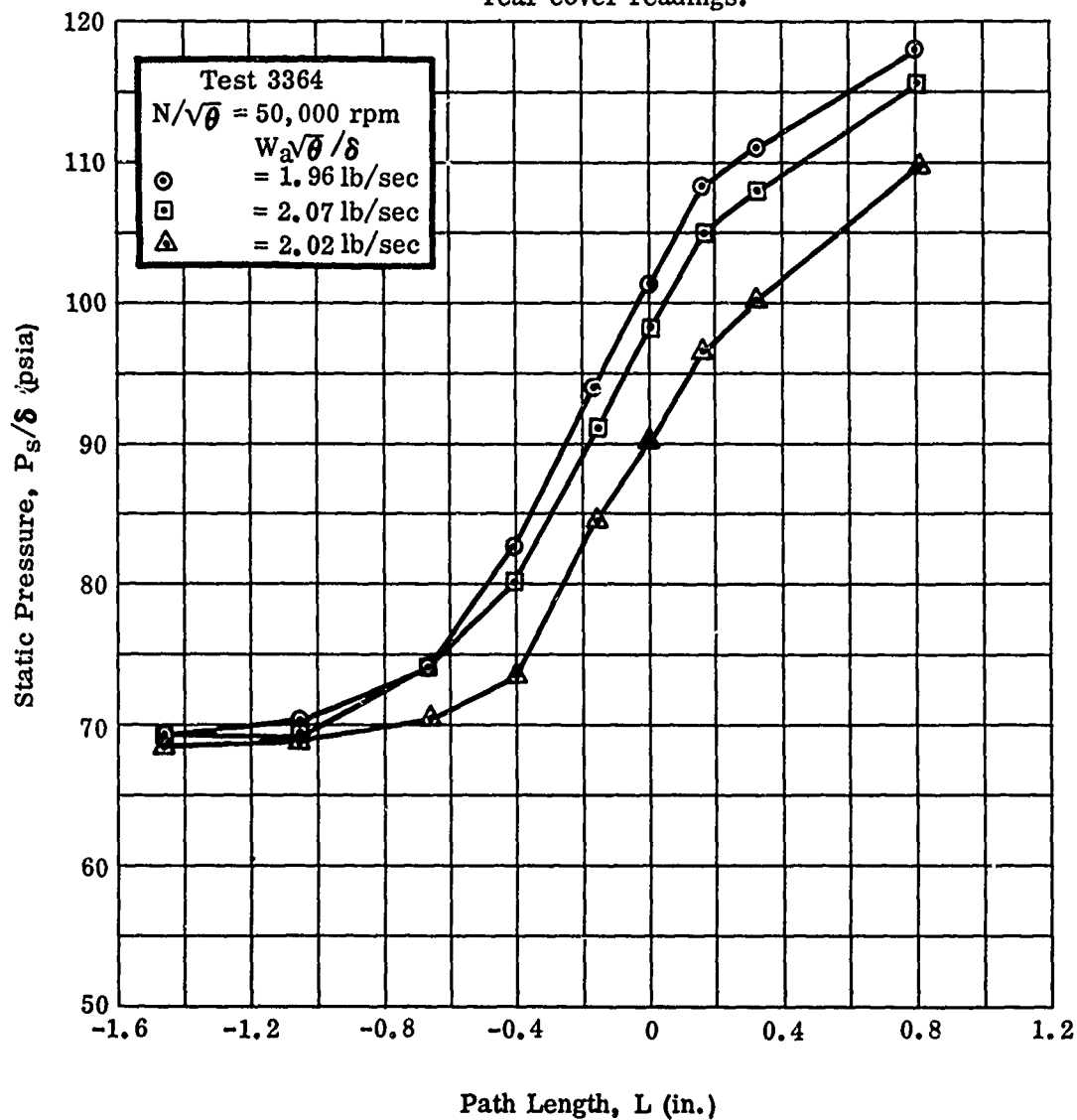
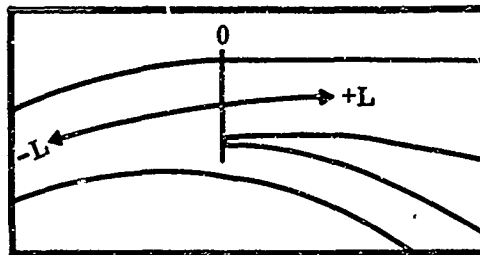


Figure 190. Static-Pressure Variation in Diffuser.

CONFIDENTIAL

CONFIDENTIAL

Corrected to Ambient
Conditions of:
60°F
29.92 in. Hg



Data points are the average of the front and rear cover readings.

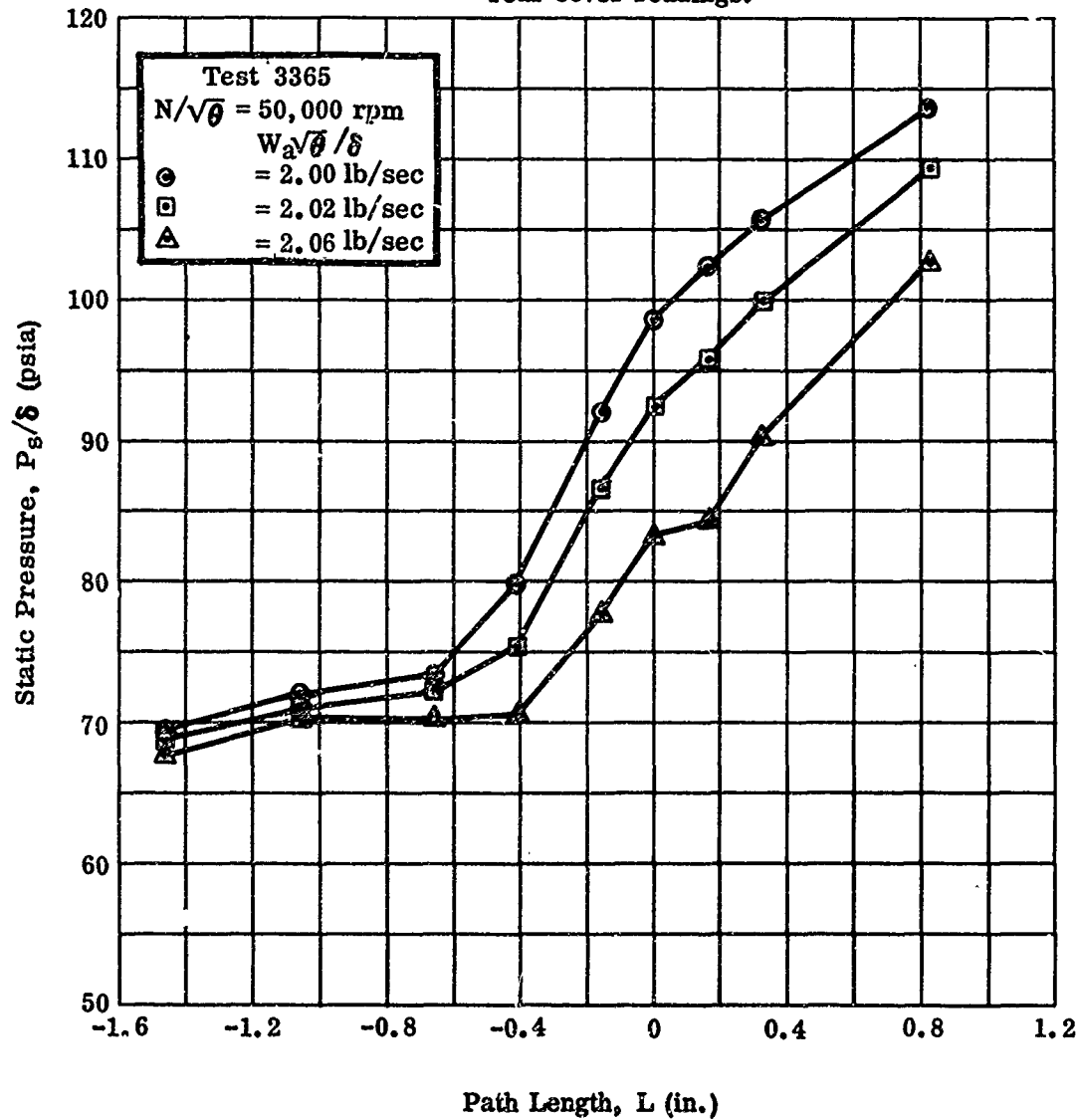


Figure 191. Static-Pressure Variation in Diffuser.

CONFIDENTIAL

CONFIDENTIAL

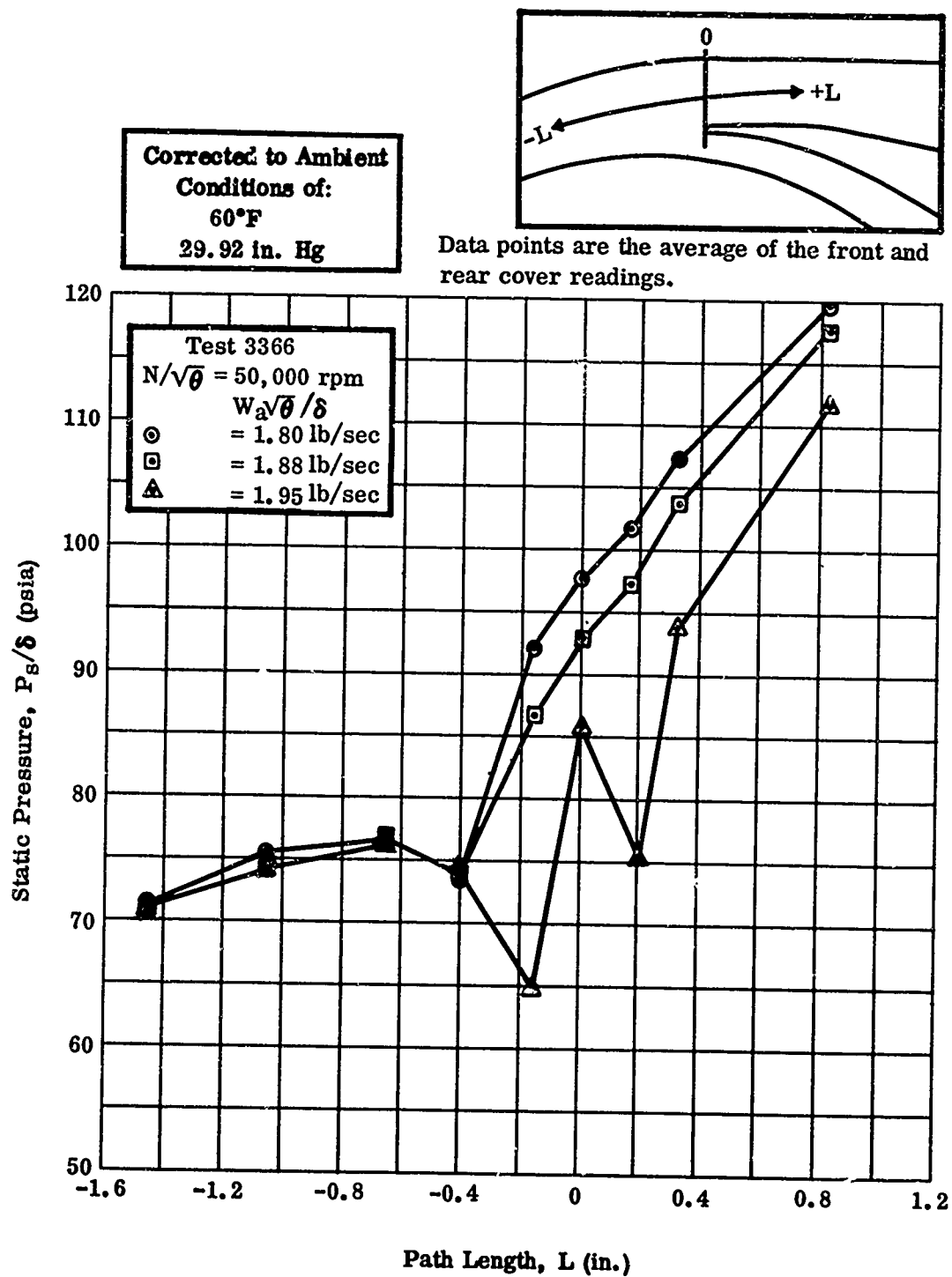


Figure 192. Static-Pressure Variation in Diffuser.

CONFIDENTIAL

CONFIDENTIAL

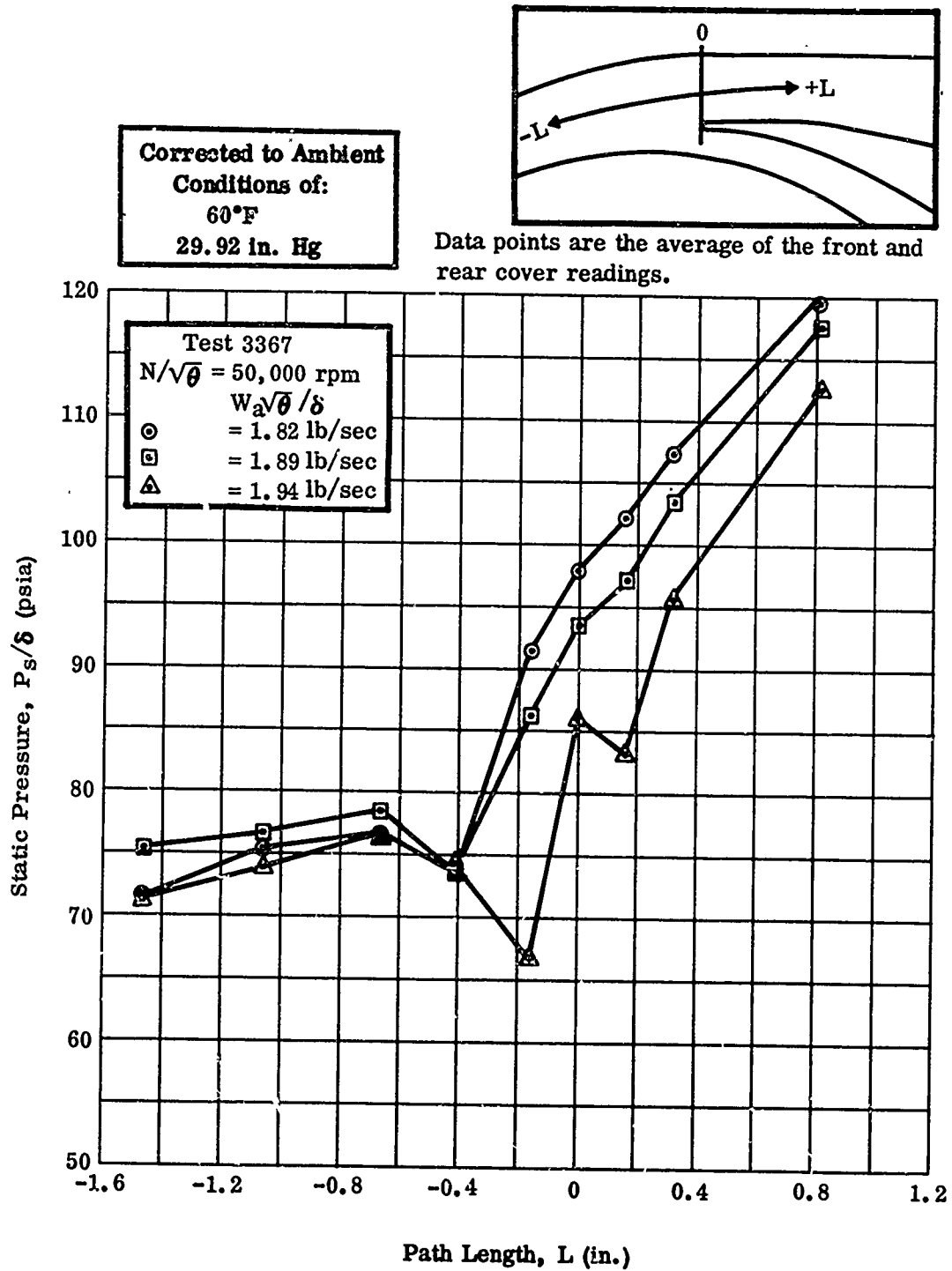
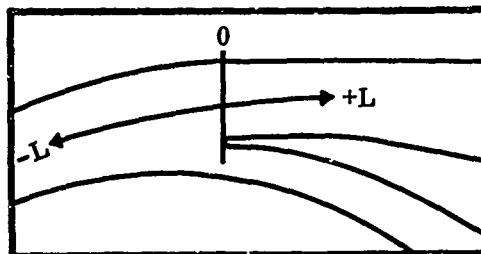


Figure 193. Static-Pressure Variation in Diffuser.

CONFIDENTIAL

CONFIDENTIAL

Corrected to Ambient
Conditions of:
60°F
29.92 in. Hg



Data points are the average of the front and rear cover readings.

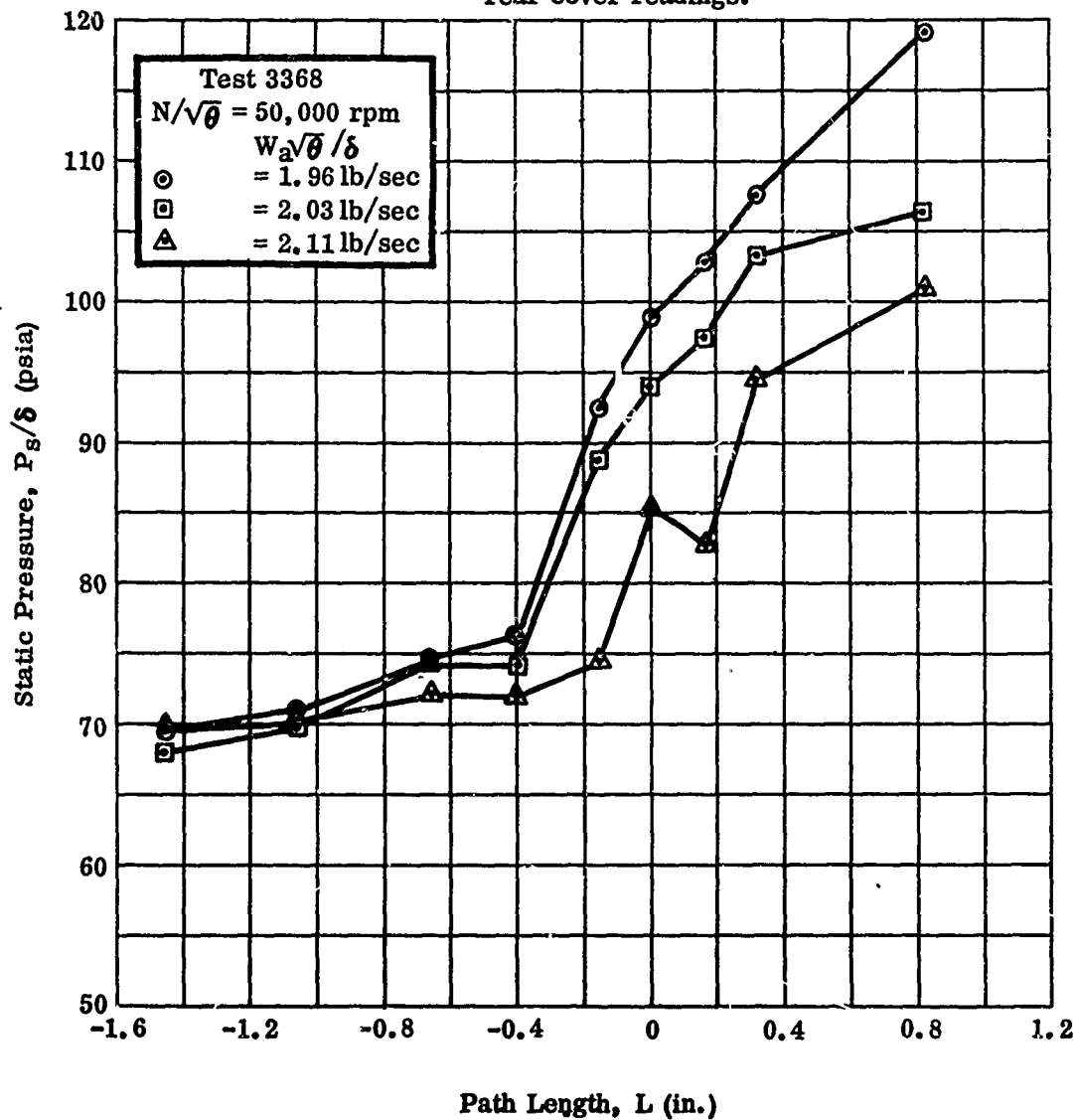
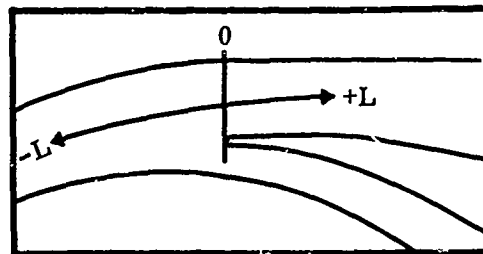


Figure 194. Static-Pressure Variation in Diffuser.

CONFIDENTIAL

CONFIDENTIAL

Corrected to Ambient
Conditions of:
60°F
29.92 in. Hg



Data points are the average of the front and rear cover readings.

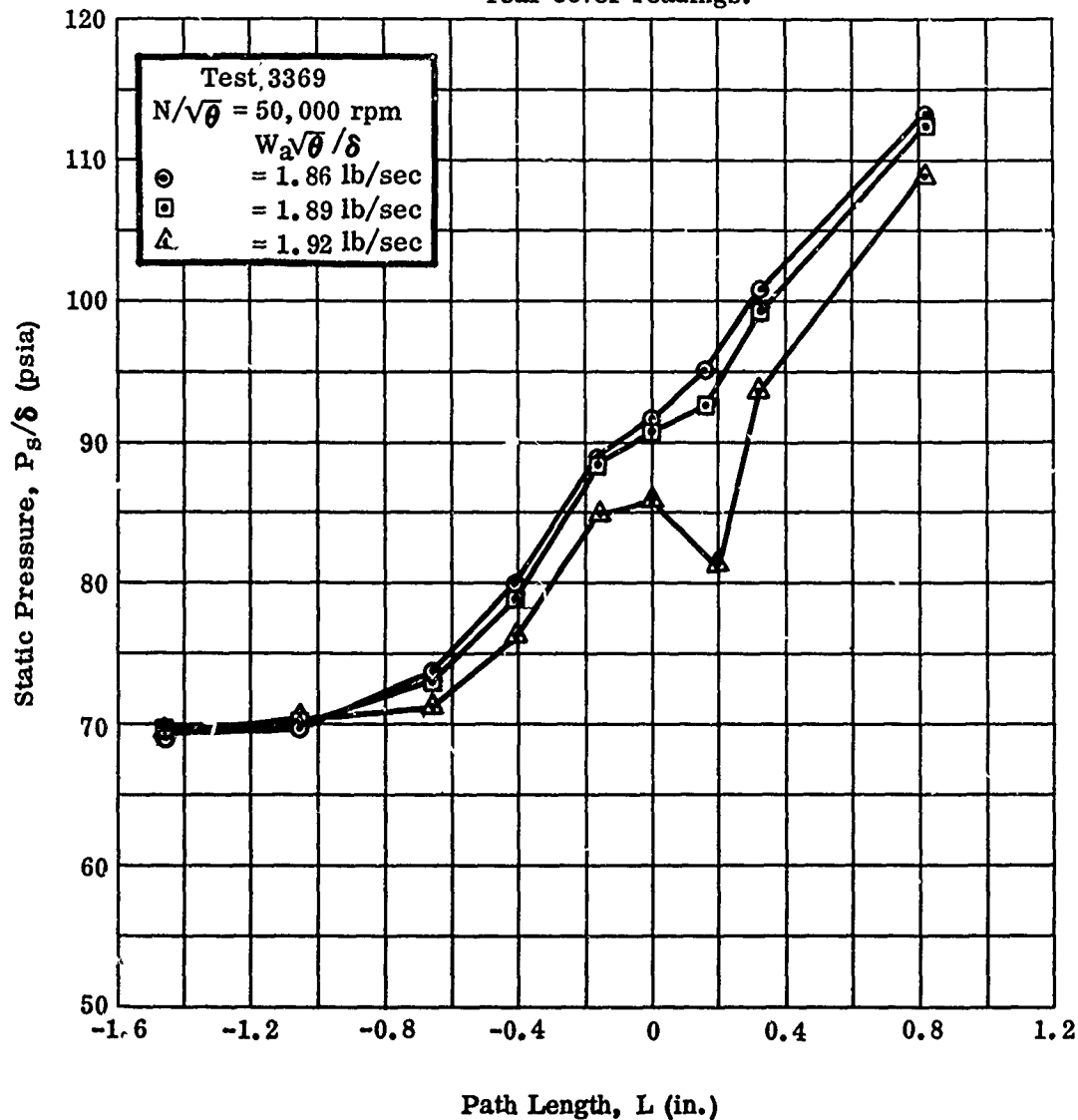


Figure 195. Static-Pressure Variation in Diffuser.

CONFIDENTIAL

CONFIDENTIAL

Corrected to Ambient
Conditions of:
60°F
29.92 in. Hg
 $N/\sqrt{\theta} = 50,000$ rpm

Temperature Rise, $\Delta T/\theta = \frac{\text{Collector Temperature} - \text{Inlet Temperature}}{\theta}$

— — — — — $\pm 1\%$ of Mean Temperature Rise

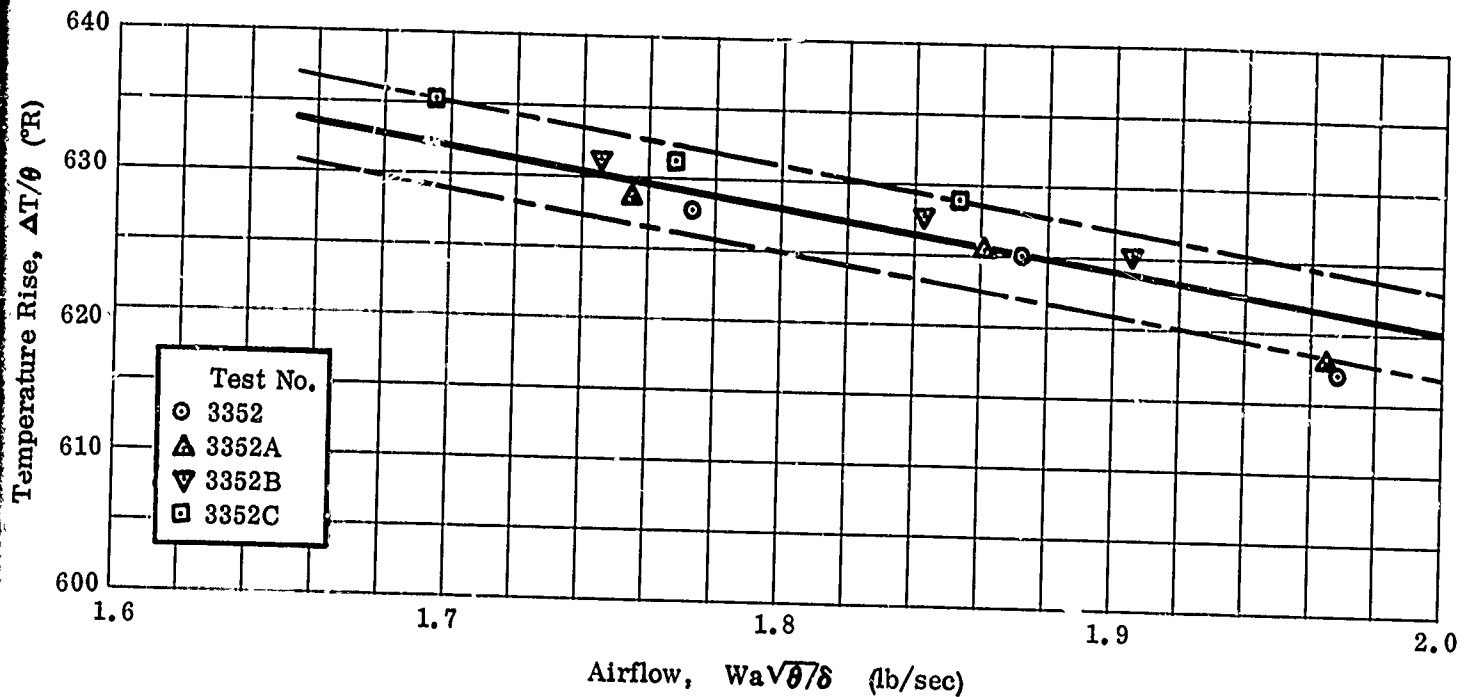
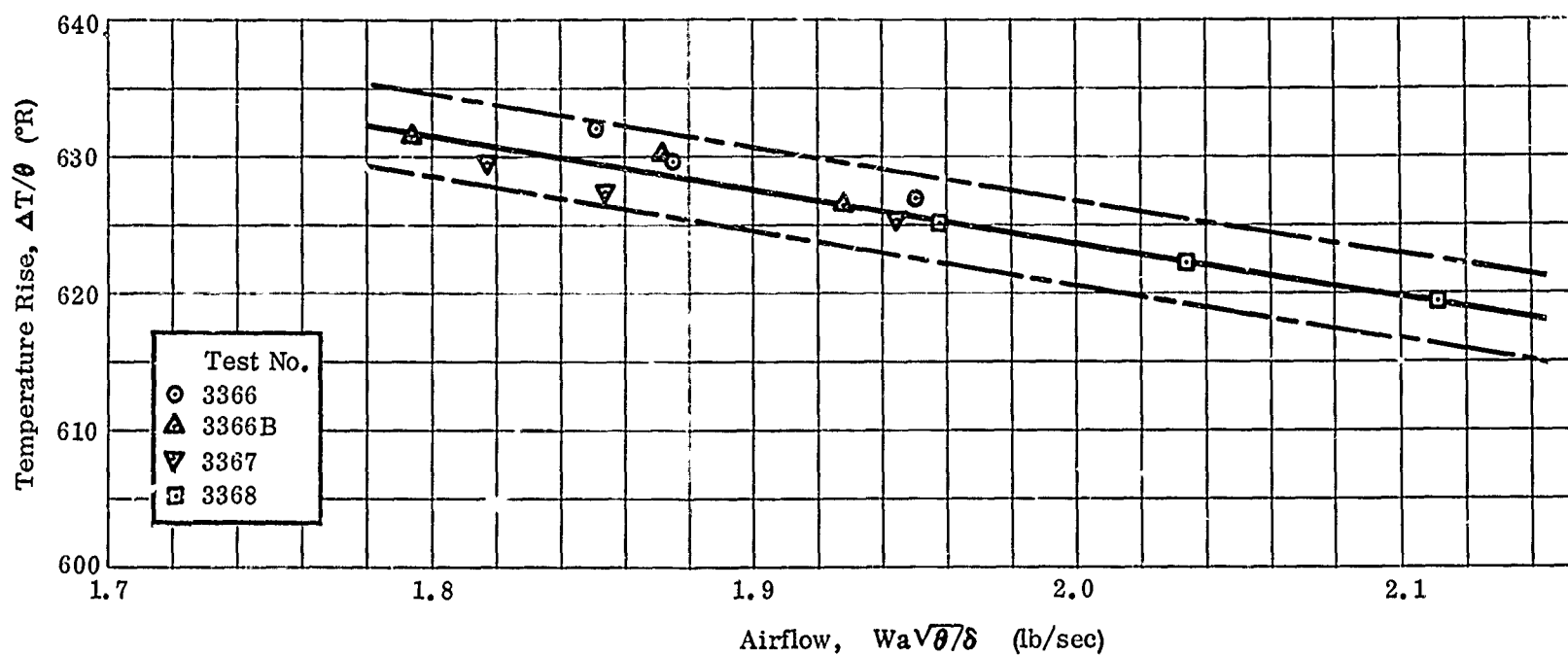
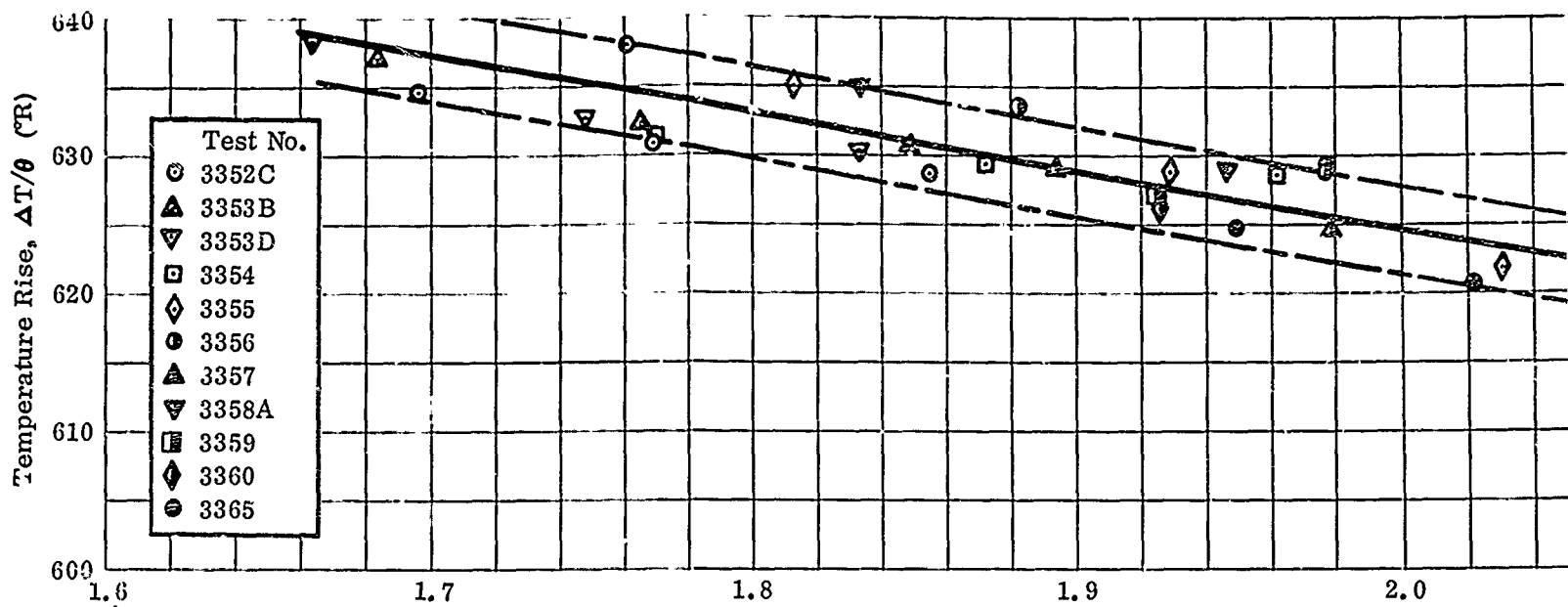
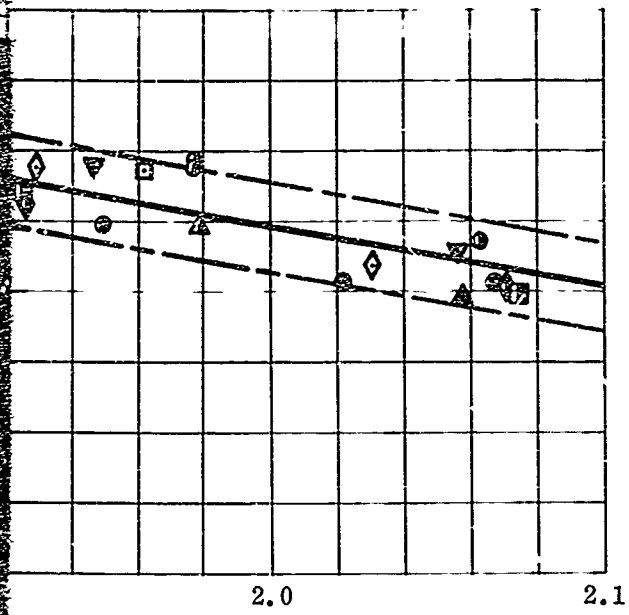


Figure 196. Temperature Rise Versus Airflow.

CONFIDENTIAL

1





CONFIDENTIAL

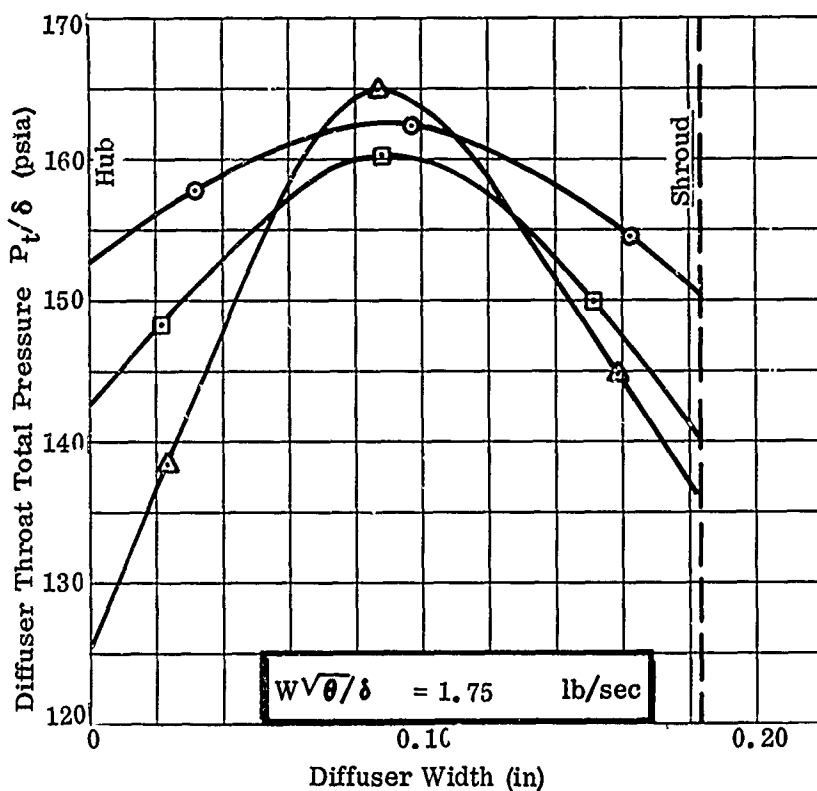
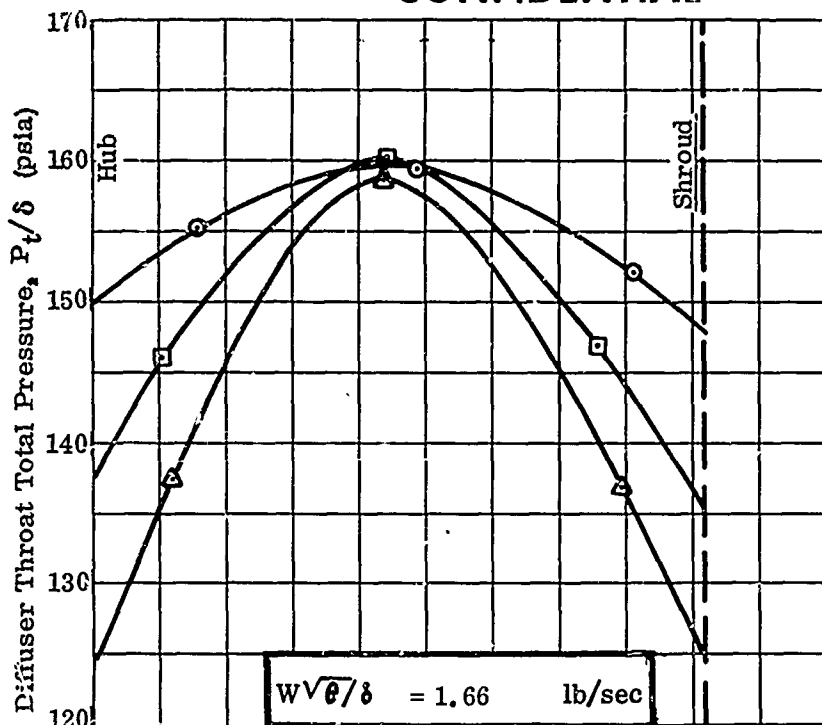


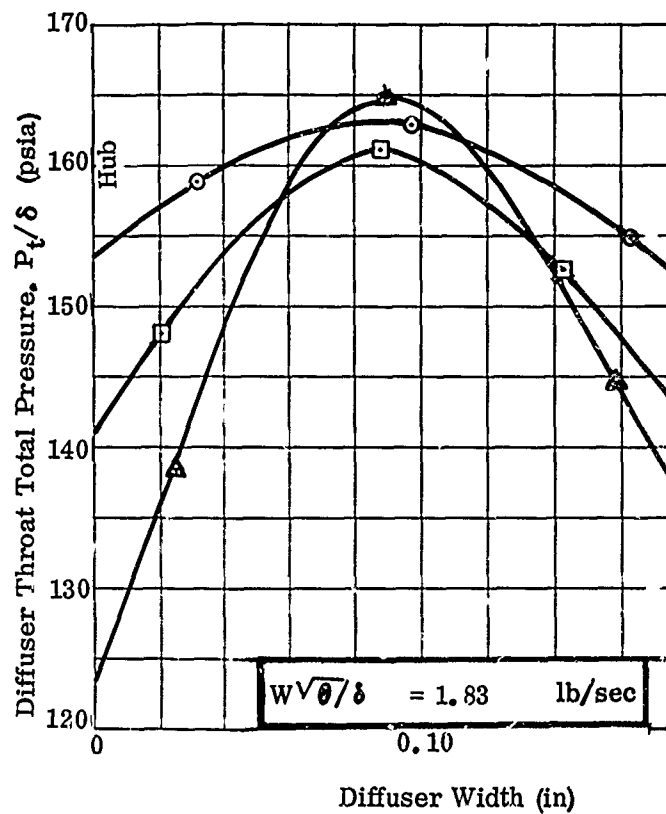
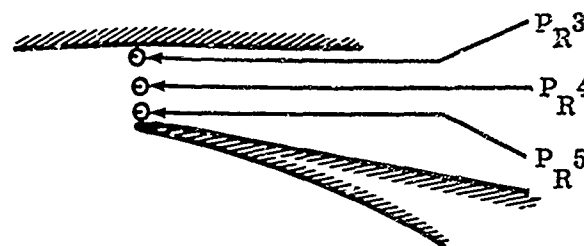
Figure 197. Diffuser-Throat Total Pressure Versus Width.

243

CONFIDENTIAL

Corrected to Ambient
Conditions of:
60°F
29.92 in. Hg
 $N/\sqrt{\theta} = 50,000 \text{ rpm}$

○
□
△



↑

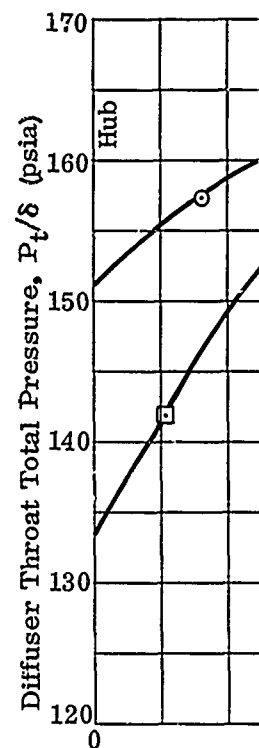
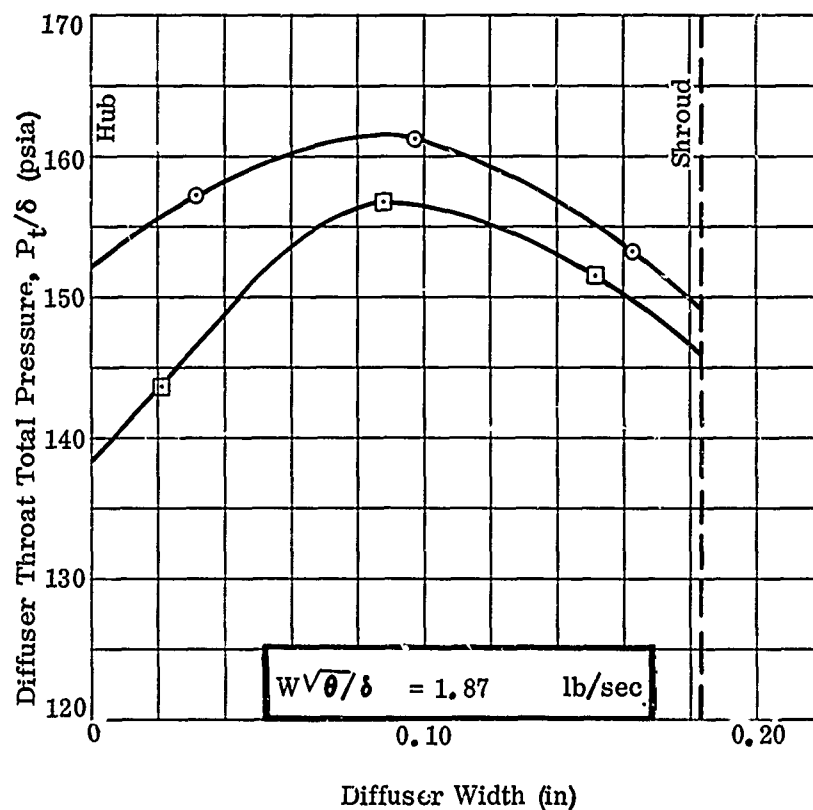
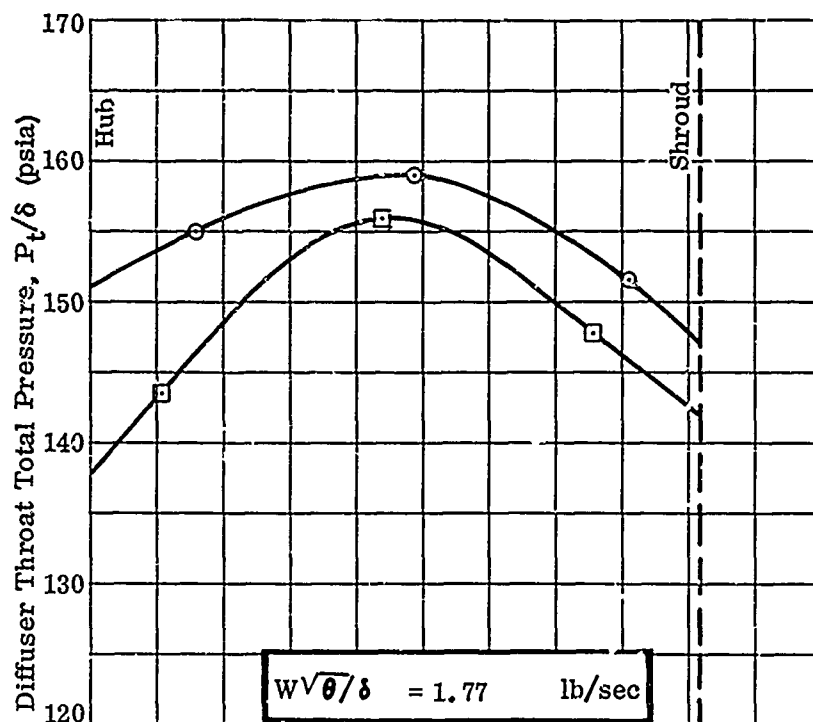
Test No.

R³ 3353E

R⁴ 3353D

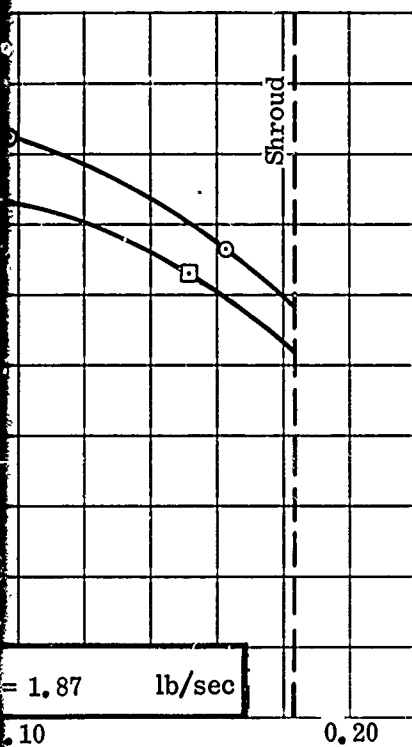
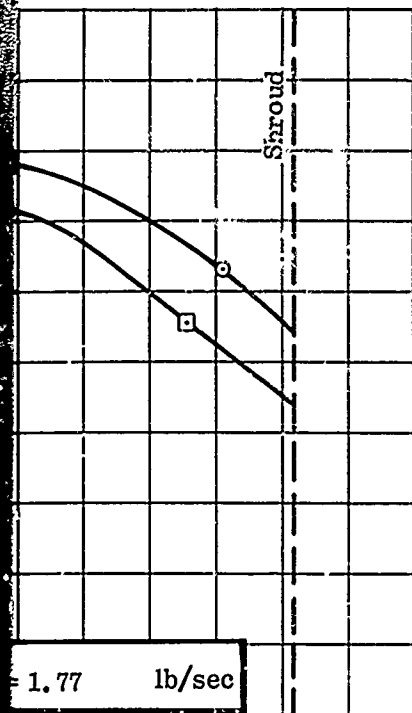
R⁵ 3353F

Corrected
Condit:
60°
29.92
 $N/\sqrt{\theta} = 50$

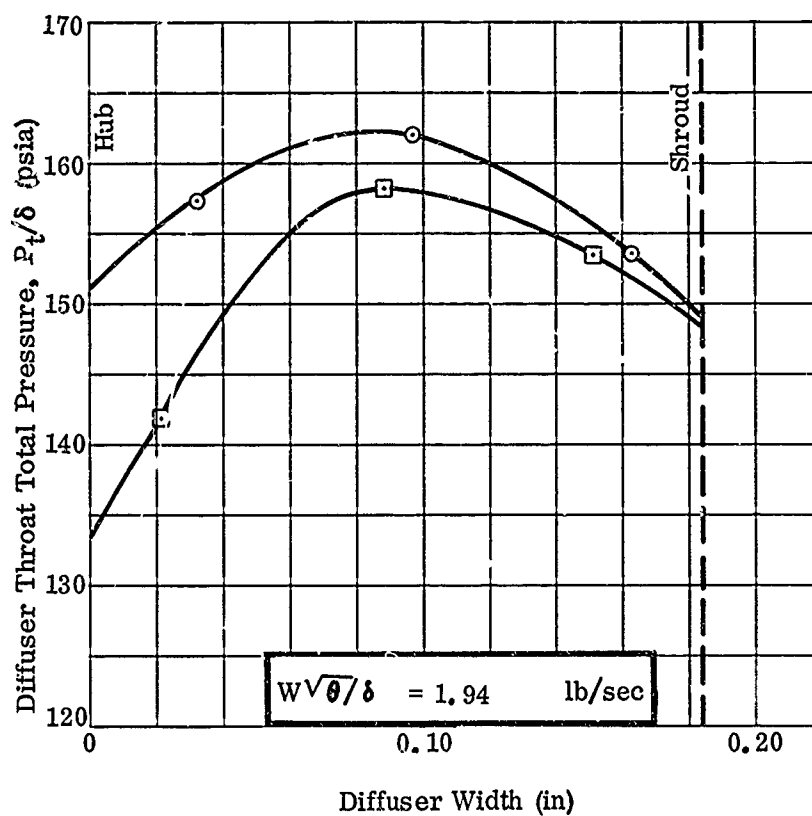
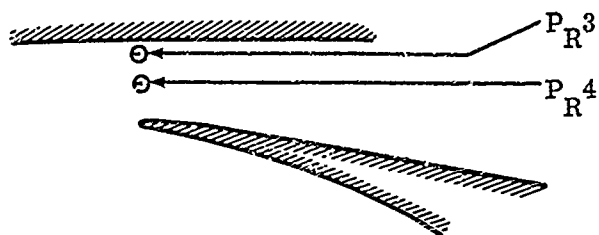


Corrected to Ambient
Conditions of:
60°F
29.92 in. Hg
 $N/\sqrt{\theta} = 50,000$ rpm

Test No.
○ P_R 3 3354B
□ P_R 4 3354A



er Width (in)



CONFIDENTIAL

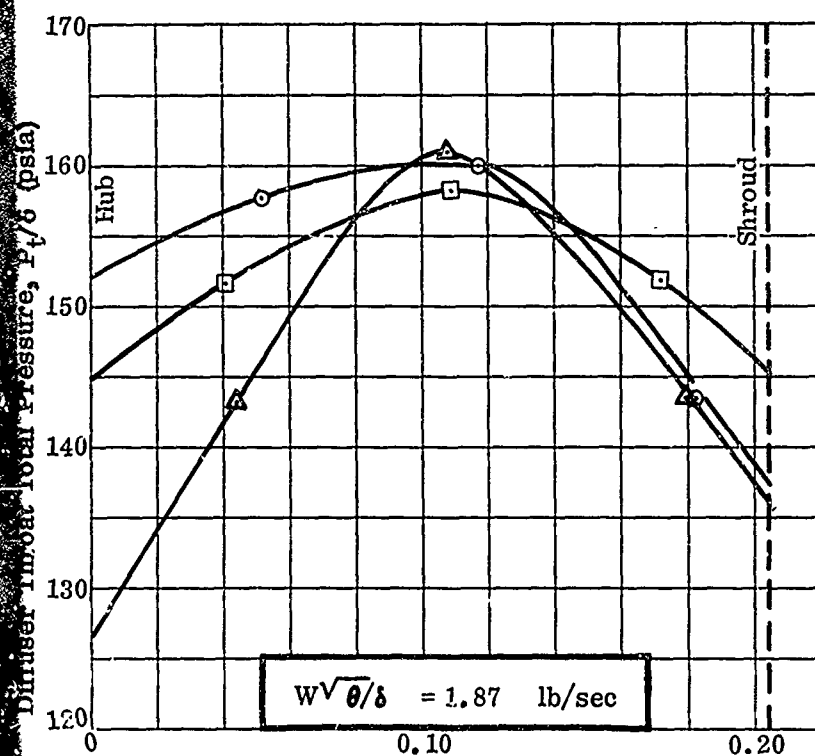
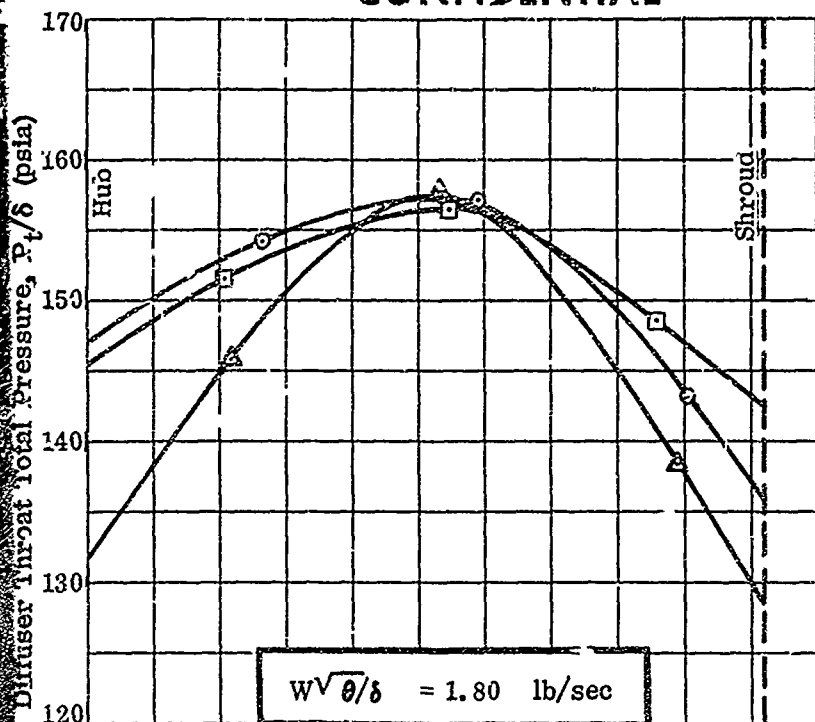


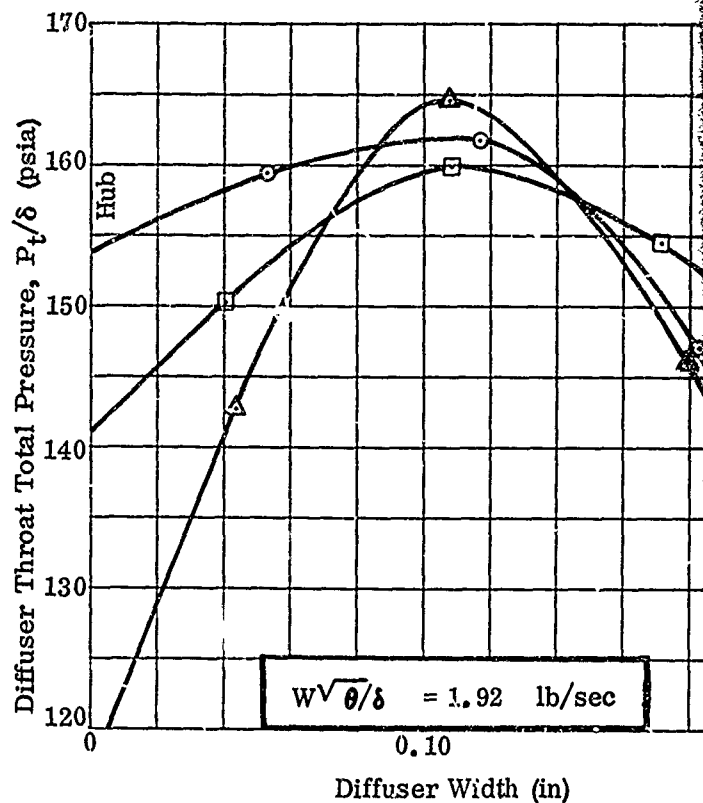
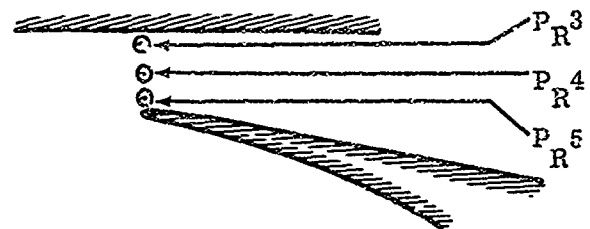
Figure 198. Diffuser-Throat Total Pressure Versus Width.

245

CONFIDENTIAL

Corrected to Ambient
Conditions of:
60°F
29.92 in. Hg
 $N/\sqrt{\theta} = 50,000 \text{ rpm}$

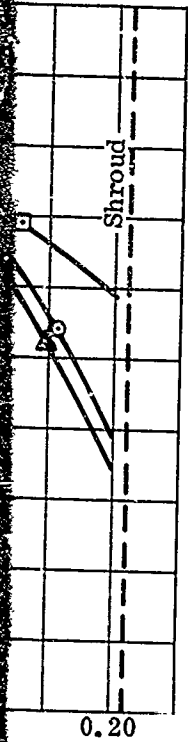
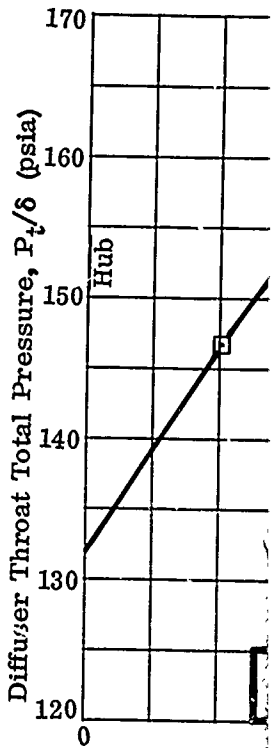
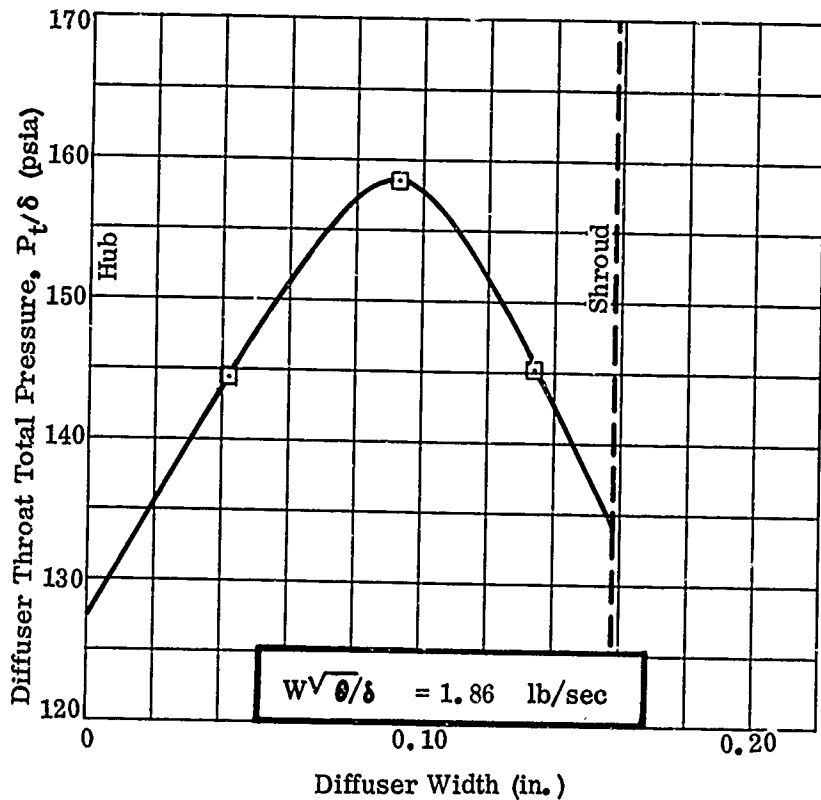
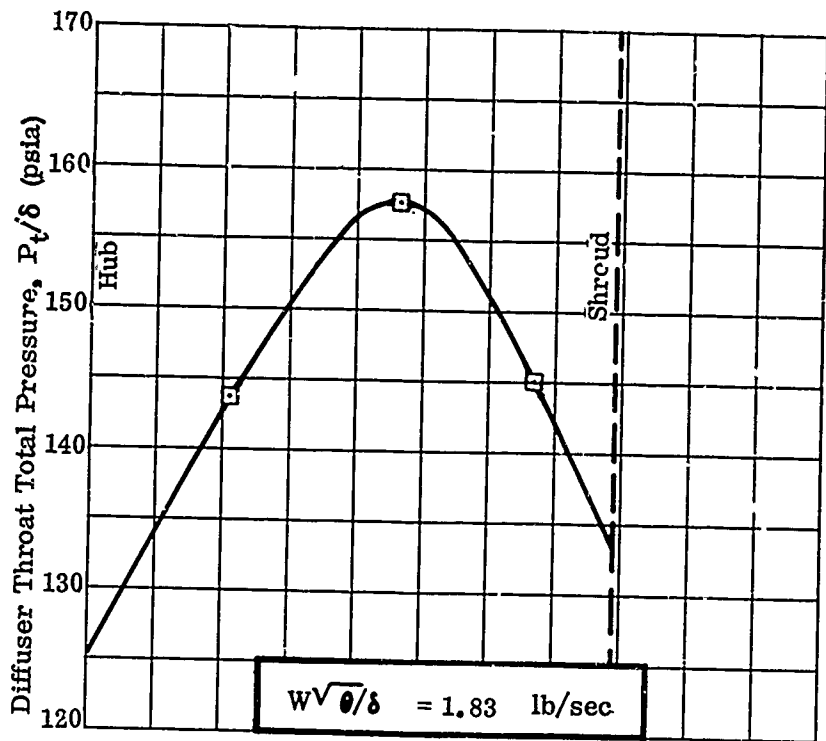
T_a
 $\circ P_R$
 $\square P_R$
 $\triangle P_R$
 ΔP_R



↑

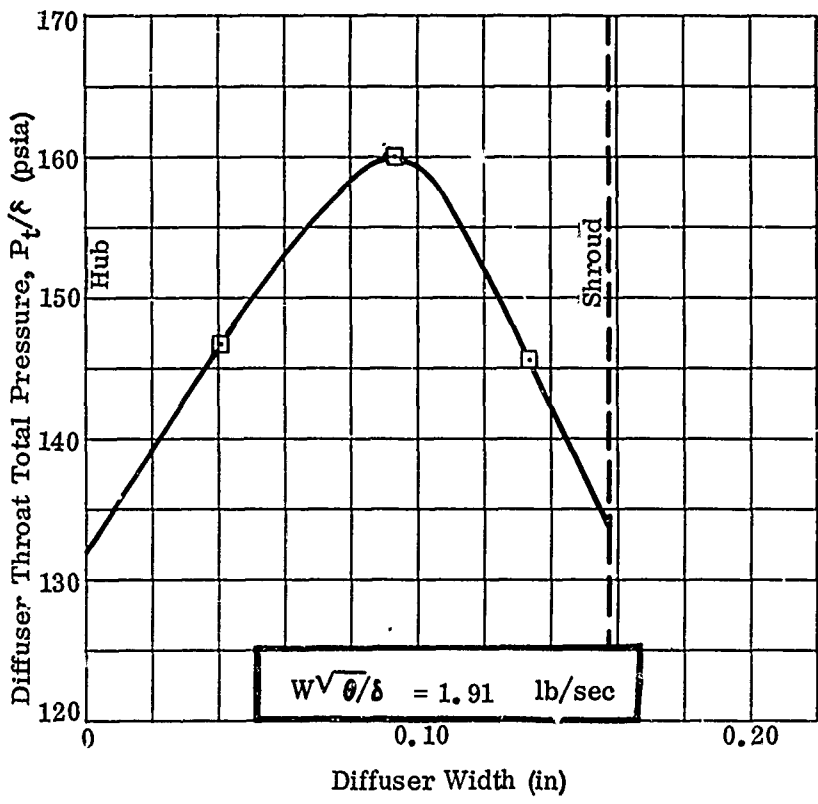
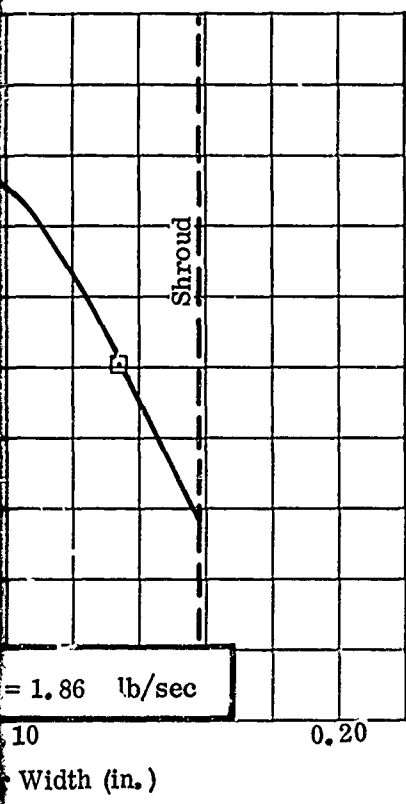
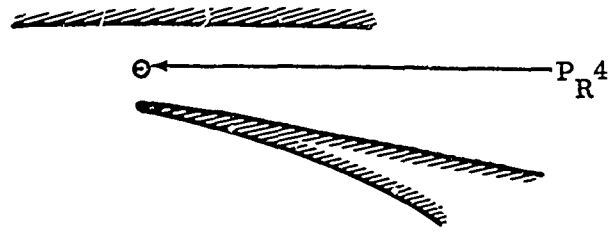
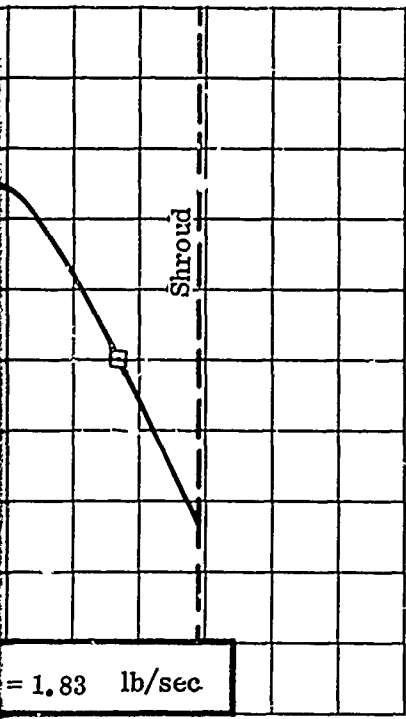
Test No.
 P_R 3 3366B
 P_R 4 3366C
 P_R 5 3366D

Corrected
 Condition
 60°
 29.92 in Hg
 $N/\sqrt{\theta} = 50$



Corrected to Ambient
Conditions of:
60°F
29.92 in. Hg
 $N/\sqrt{\theta} = 50,000$ rpm

Test No.
 P_R^4 3369



CONFIDENTIAL

7.0 (C) EVALUATION OF TEST RESULTS (U)

The design methods and flow model theories discussed in Reference 1 required further test and analysis to help confirm these methods. The new impeller and diffuser discussed in this section were designed with this in mind, and the information presented in Reference 1 was used for the design of this new compressor. The new compressor was tested, and the performance of each component was measured using techniques similar to those used on the previous components. In addition, several impeller and diffuser modifications were tested. These studies further contributed to the flow models and increased compressor performance above that of the initial tests.

7.1 IMPELLER TESTS

The impeller investigation was conducted with the new impeller design RF-2, described in Section 2.1. Two modifications of the RF-2 were also tested. The test results of the design configuration will be discussed, followed by an explanation of the 2 modifications and test results.

The performance of the RF-2 was monitored in the same manner as that of the RF-1 and the workhorse impellers; i.e., probes to measure total pressure, total temperature and flow angle were installed at a radius ratio of about 1.03. Static pressure was also measured at the inlet and along the shroud.

7.1.1 Tests of the Design Configuration

Based on the earlier tests of the workhorse impeller, the design value of the slip factor for the RF-2 impeller was selected at 0.93. Introducing this value of slip factor into the loss analysis described in Section 7 of Reference 1, the predicted pressure ratio for the RF-2 impeller was 12.1:1. With an allowance of 3 percent for disk friction and recirculation (temperature-rise factor = 0.96), the predicted impeller adiabatic efficiency was 84.6 percent.

The measured performance of the design configuration of the RF-2 impeller at the design airflow of 2.00 pounds per second was as follows:

Pressure Ratio	11.1:1
Adiabatic Efficiency	79.6%

The inducer incidence at the RMS radius for the design airflow was about +4 degrees. This incidence was calculated with respect to the pressure surface of the blading, since the benching operation performed on the inducer leading edge made the determination of the blade angle on the suction surface quite difficult.

During the test evaluation of the impeller and diffuser design geometries, 4 separate diffuser throat area settings were used. This change in throat area made it possible to determine the performance of the impeller over a wide range of airflows. As shown in Figure 139a, the impeller pressure ratio was nearly constant at 11.2:1 over an incidence range from +5 degrees to +8 degrees (an airflow range from 1.81 pounds per second to 1.96 pounds per second). The pressure ratio decreased as the incidence was increased beyond +8 degrees or decreased below +5 degrees.

The impeller efficiency was constant at 79.6 percent over a wide range of incidence angles, +2 degrees to +8 degrees (an airflow range from 1.81 pounds per second to 2.06 pounds per second) as shown in Figure 139b. The efficiency began to decrease when the inducer incidence was increased beyond +6 degrees. This performance decrease with increasing incidence most likely resulted from an upstream shift of the separation point in the inducer.

As shown in Figure 155, the test value of the slip factor was approximately 0.89. Insertion of this value in the previously mentioned loss analysis resulted in a predicted impeller pressure ratio of 11.0:1, which is within 1 percent of the measured pressure ratio at the design point.

Effect of Probes on Impeller

The insertion of several probes into the flow passage at the impeller-tip survey station had an adverse effect on the flow range of the compressor, as shown from performance curves for Tests 3353, 3353A, and 3353B (Figure 166). Tests 2370 and 3370A, which were run later in the program, also showed similar results (Figures 57 and 176). In Test 3353, 2 total-pressure rakes, 1 traversing yaw probe, and 1 traversing temperature probe were installed at the survey station. The resulting influence on the compressor pressure ratio and airflow range was considerable.

For Tests 3353B and 3370, all probes at the tip were removed. The influence of 1 traversing yaw probe can be identified by comparing Tests 3353B and 3353A, while the influence of a single total-pressure rake can be seen by comparing Tests 3353B and 3353C and Tests 3370 and 3370A. Part of the adverse effects of the probes on the compressor performance can be attributed to their influence on the diffuser performance. Some effect, however, is felt upstream as far as the inducer; this effect is demonstrated by the static-pressure rise along the shroud in the inducer section from Tests 3353, 3353C and 3352C (Figures 95, 96 and 103). In these figures, each point on the curve represents the numerical average of 3 equally spaced, circumferential static-pressure measurements unless the maximum and minimum measurement differed by more than 0.5 psi, in which case the points were plotted separately. The inducer pressure fields are quite

CONFIDENTIAL

Corrected to Ambient
Conditions of:
60°F
29.92 in. Hg

$N/\sqrt{\theta} = 50,000 \text{ rpm}$

Pressure ratios are based
on the mass-averaged
impeller-exit total pressure.

Test	Impeller Blade Width	Diffuser Passage Width
⊙ 3353	0.180 in.	0.183 in.
□ 3353C	0.180 in.	0.183 in.
△ 3356A	0.180 in.	0.183 in.
⊙ 3366A	0.180 in.	0.203 in.
● 3369A	0.135 in.	0.158 in.
▽ 3370A	0.135 in.	0.158 in.

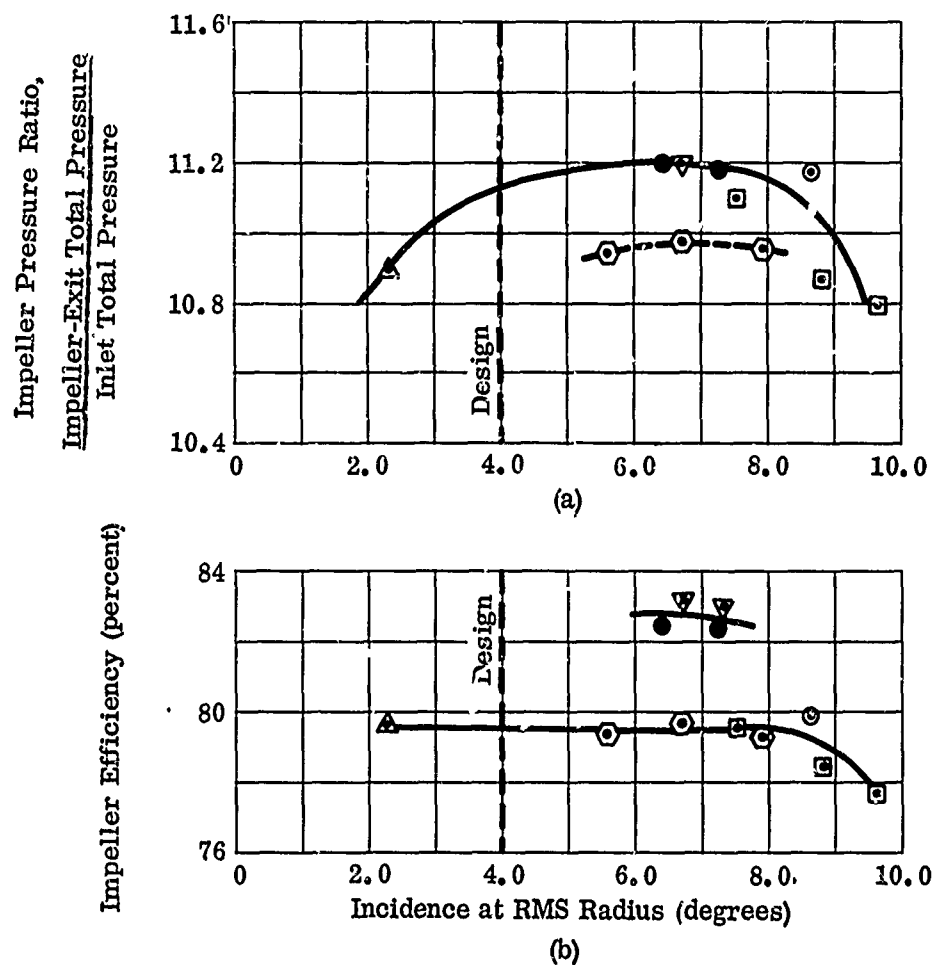


Figure 199. Variation of Performance with Incidence, RF-2.

CONFIDENTIAL

different for the 3 cases compared; 4 tip probes (Test 3353), single tip probe (Test 3353C), no tip probes (Test 3352C).

Because of this marked influence of the probes on the flow within the impeller, and because of the airflow range limitation, it was decided that further tests would be conducted with only the single miniature total-pressure rake to monitor impeller performance. Therefore, flow-angle surveys and total-temperature surveys were only obtained at 3 test points for Test 3353: 2 at 46,000 rpm and 1 at 50,000 rpm.

Mass-Averaged Impeller Data Analysis

Since the impeller-exit flow-angle and temperature measurements were limited to only 3 data points, it was necessary to generate angle and temperature profiles for the other test points, so that a quasi-mass-averaged pressure ratio could be obtained. The influence of changes in airflow at a given rotational speed on the quantitative level and shape of the angle profiles was observed during the RF-1 data analysis.

Changes in rotational speed also affected the profiles. These trends were used in conjunction with the RF-2 data to generate profiles for all test points. The RF-2 measured temperature profiles (Figures 62, 63 and 64) show that the temperature is highest in the shroud region for both 46,000 rpm and 50,000 rpm, and that the temperature gradient from the hub to the shroud increased as the rotational speed was increased. The temperature profiles at speeds other than 46,000 and 50,000 rpm were generated by assuming that the hub-to-shroud gradient varied linearly with rotational speed. The level of the profile was adjusted by using the collector temperature as a guide.

There was little change in either the level or the shape of the measured angle profiles with rotational speed or airflow, as shown in Figures 90, 91 and 92. The relative independence of the measured exit flow angles from rotational speed and airflow was also evidenced during the testing program of the RF-1 impeller (see Figure 263 in Reference 1). Therefore, for mass-averaging purposes, the measured profiles from Test 3353 were used for all other tests with the same diffuser passage depth (0.183 inch). For other passage depths, the same profile level with adaptations was used: (1) to match the minimum flow angle with the maximum total pressure across the passage and (2) to adjust the angles near the walls for the increased or decreased passage depth.

Discussion of Impeller Performance Trends

It is felt that the performance trends of the impeller, which were discussed earlier in this section, require further explanation to clarify apparent

CONFIDENTIAL

CONFIDENTIAL

discrepancies in the data. The mass-averaged pressure ratios for the various tests are shown in Figure 61 as a function of airflow.

The impeller performance at low airflow is represented by 4 data points: 1 for Test 3353 and 3 for Test 3353C. The test rig geometry was identical for these 2 tests, but the tip instrumentation differed, as explained previously. The representative curve of impeller performance shown in Figure 61 is drawn with a positive slope, following the trend of the data from Test 3353C, since there was less probe influence. The curve in this low-airflow region represents the impeller performance with a probe installed at the tip. The diffuser-throat total pressures obtained for tests without impeller-tip instrumentation indicate that the impeller performance is constant in this region (Figure 200).

The peak pressures for the tests of the narrow-blade-width configuration (Tests 3369A and 3370A) were nearly the same as those observed for the highest airflow data point for Test 3353C. Therefore, the representative curve was drawn through those points and continued to the highest airflow data point at 2.06 pounds per second (Figure 61). This leads one to ask why the mass-averaged pressure ratio for Test 3366A lies about 2 percent below the curve, although the peak values are in line with the other data, as shown in Figure 61. This can be explained by referring to Figures 67 and 75 where the measured total-pressure profiles are presented for Test 3353 and Test 3366A respectively. As the diffuser passage depth was increased from 0.183 inch (Test 3353) to 0.203 inch (Test 3366A), the total-pressure profile became more peaked, as shown in Figure 201. Through the mass-averaging procedure, this led to a lower pressure ratio by 2 percent.

The original front-cover geometry (0.183-inch passage width) is compared with the modified front cover (0.203-inch passage width) in Figure 202. The small change in shroud geometry may have affected the flow in the shroud region through an alteration in the recirculation pattern or a local separation.

Shroud Static-Pressure Rise and Inducer Analysis

As in previous tests, the static-pressure rise along the shroud was used to monitor changes in impeller performance. As shown by the data plotted in Figure 102, the static pressure in the inducer section is about 0.5 psi below the predicted level at the design airflow. This difference in pressure is mainly attributable to the fact that the static pressure of the entering flow in the shroud region is lower than the predicted level by 0.5 psi. For the design analysis, it was assumed that the flow was uniform just upstream of the inducer inlet. This assumption resulted in a constant static pressure from hub to shroud at the inlet station. Due to the effects of the tapered inducer blades, the inlet flow migrates toward the shroud and a negative radial static-pressure gradient results. For the test point shown in Figure 102 at 1.98 pounds per second, the measured static-

CONFIDENTIAL

CONFIDENTIAL

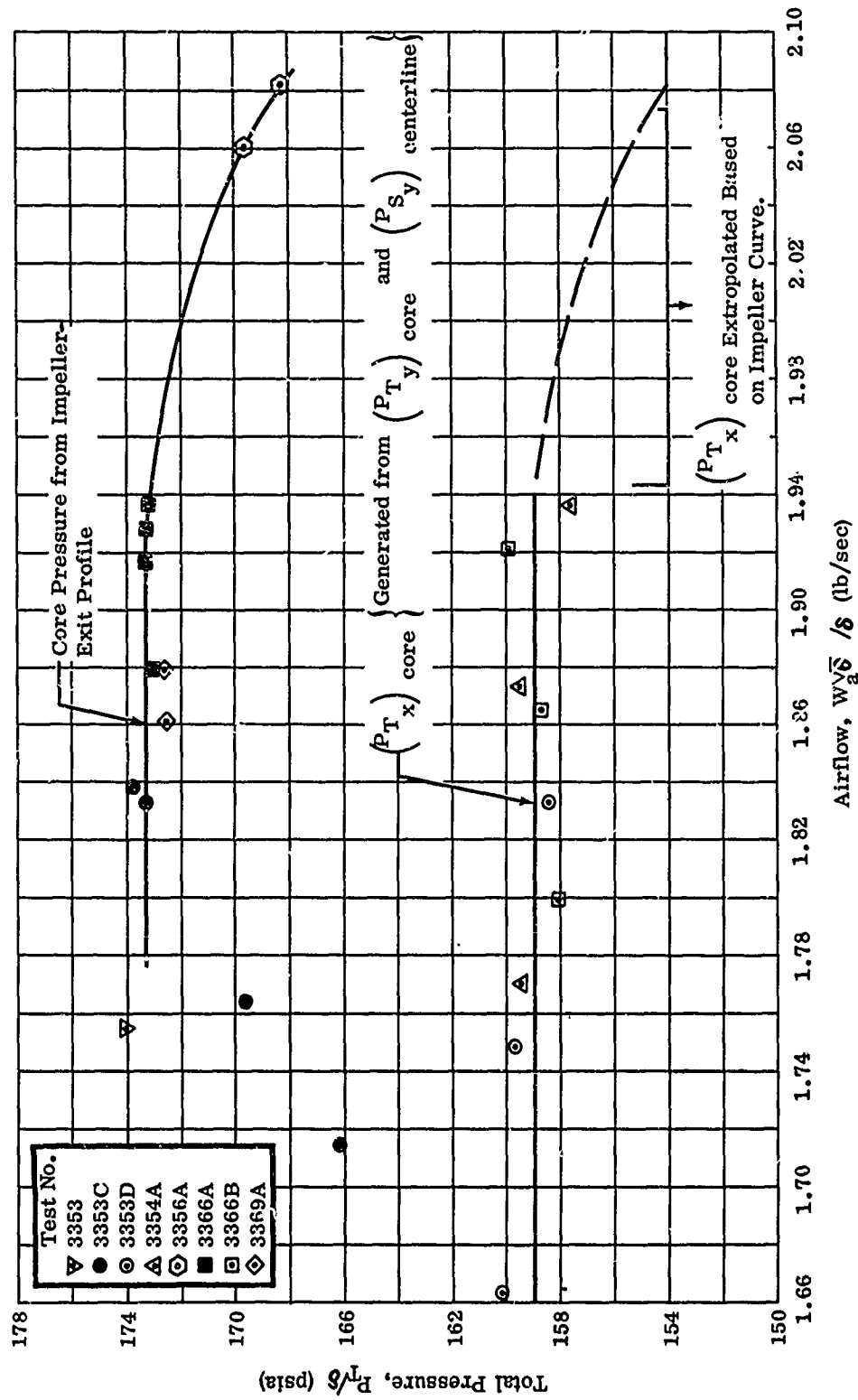


Figure 200. Impeller Core and Throat Total Pressure Versus Airflow, RF-2.

CONFIDENTIAL

CONFIDENTIAL

$$N/\sqrt{\theta} = 50,000 \text{ rpm}$$

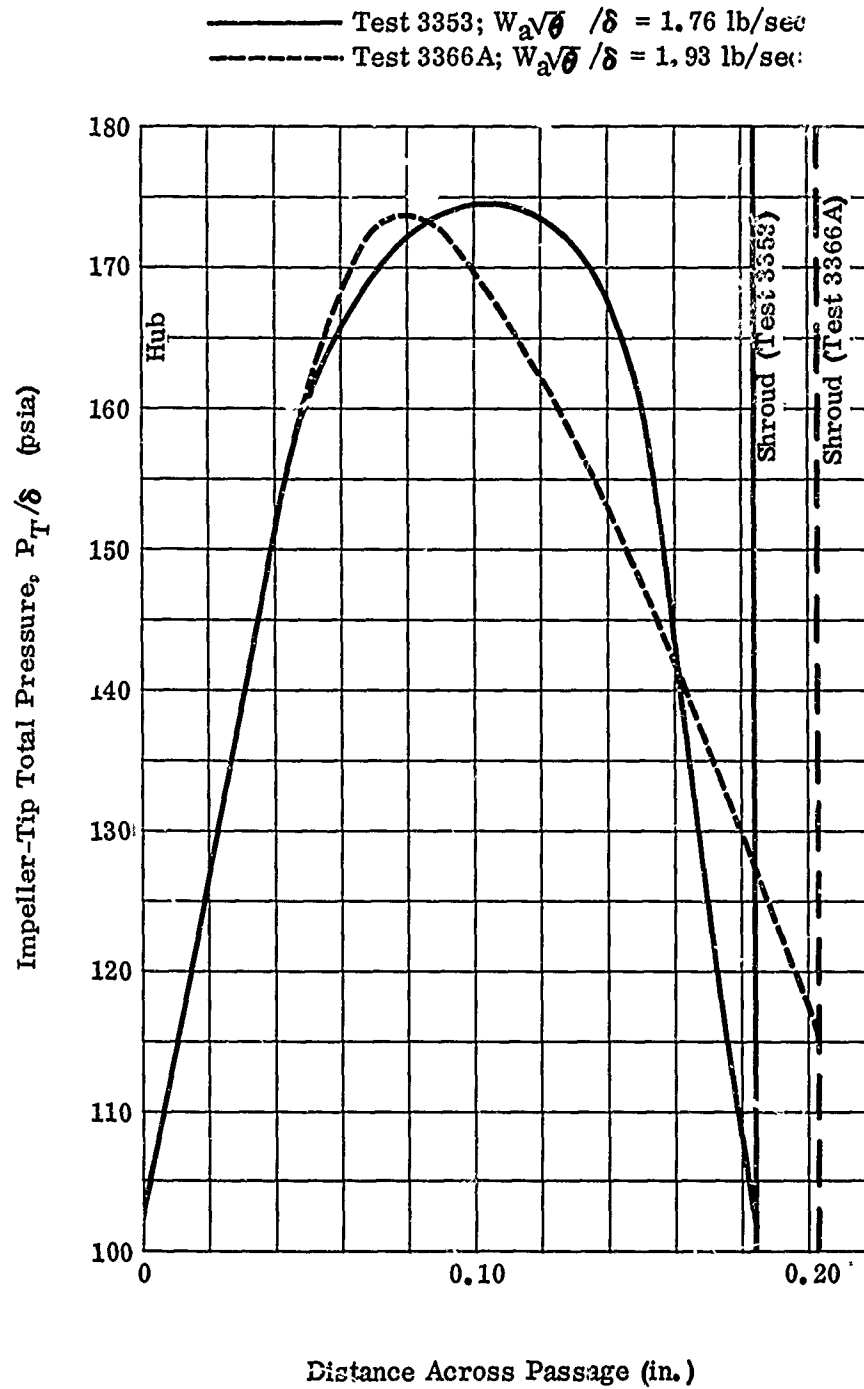


Figure 201. Comparison of Impeller-Exit Total Pressure, RF-2.

CONFIDENTIAL

CONFIDENTIAL

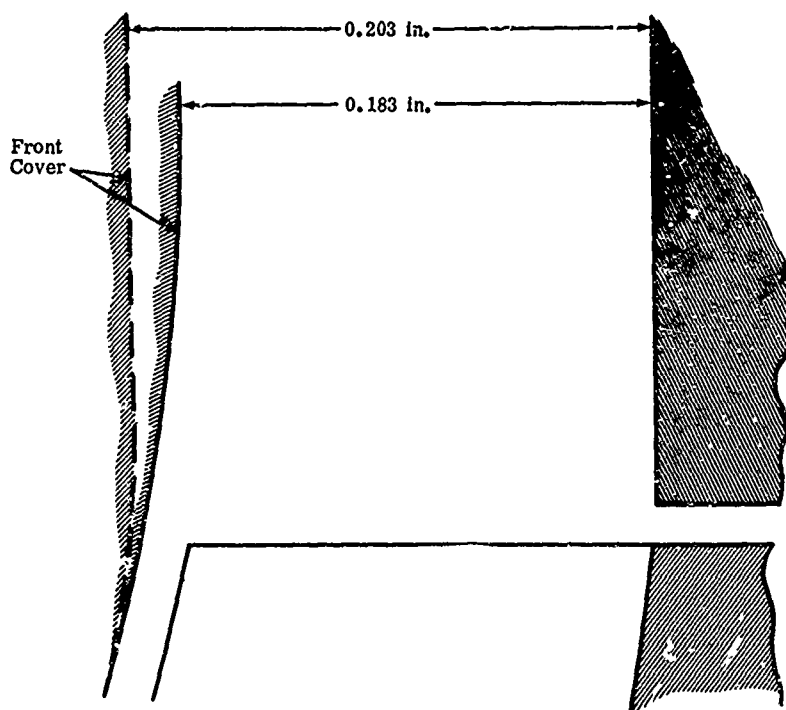


Figure 202. Front-Cover Modification.

pressure gradient dp_s/dR was -0.81 psi per inch, which results in a static-pressure difference of 0.33 psi between the flow at the RMS radius and the shroud radius. This difference demonstrates that the average static pressure (RMS radius) was within 0.17 psi of the predicted level, although the flow at the shroud was lower by 0.50 psi. The fact that the level of the static pressure along the shroud is below the predicted values does not mean that the inducer was not operating per the design analysis. When the actual inlet conditions are studied, it is seen that the conditions at the tip of the inducer are not as predicted. In fact, the plots in Figure 102 show that the static-pressure rise is about the same as that predicted for the first 1.4 inches. The static pressure downstream of the 1.4 -inch station levels off, indicating that the flow must have separated from the blading in this region. When the design values of the relative total pressure and temperature at the 1.4 -inch station are used with the measured shroud static pressure at that point (14.5 psia), the flow velocity is computed to be 675 fps. If this is interpreted as the average (midway between the blades) flow velocity in the tip region, the velocity on the suction surface at this station can be obtained by using the blade-to-blade solution from the design analysis. This solution gives a suction-surface velocity of 803 fps and a relative Mach number of 0.72 . For the impeller-design loss analysis, the predicted relative Mach number at the separation point ($M = 0.73$), and therefore the relative Mach number of the jet flow at the exit, shows good agreement with the previous solution. In addition, by using the

CONFIDENTIAL

CONFIDENTIAL

minimum shroud static pressure (11.55 psia) with the corresponding design values of relative total pressure and temperature, the maximum average flow velocity can be calculated. The resulting velocity was 985 fps. From this analysis the separation velocity ratio of the average flow ($V_{\text{maximum}}/V_{\text{separation}}$) was determined to be 1.46. The velocity ratio used in the design loss analysis was 1.40. The close agreement between the assumed and calculated Mach number at separation and the separation velocity ratio lends support to the loss analysis presented in Section 7 of Reference 1.

To prevent the premature impeller choke experienced by the RF-1 and the workhorse impellers, the RF-2 impeller was designed with lower inlet relative Mach numbers and lower blade blockage in the inducer inlet region. As a result, the choking airflow of RF-2 was 3.8 percent higher than the design, as shown by the performance curve for Test 3356 in Figure 167.

Temperature-Rise Factor and Slip Factor

As mentioned previously in this section, the test value for the slip factor of the RF-2 impeller was about 0.89. This value is predicted by the modified form of Eckert's equation. (As discussed in Section 7.1 of Reference 1, the slip factor predicted for the workhorse impeller using Eckert's equation did not agree with the test data.) The average temperature-rise factor for the RF-2 impeller at the design airflow of 2.00 pounds per second was 0.96. The temperature-rise factor increased linearly as airflow decreased (the value at an airflow of 1.72 pounds per second being about 0.01 higher than the value at the design airflow).

The difference between the compressor work, represented by the temperature-rise factor, and the useful (Euler) work, represented by the slip factor, is a measure of the temperature rise resulting from disk friction and recirculation. For the RF-2 impeller, this difference was 0.07, indicating that the maximum possible impeller adiabatic efficiency was 93 percent.

The lowest slip factor is shown to be in the region of the walls (Figure 153). The temperature-rise factor, on the other hand, increases almost linearly from the hub to the shroud, with the values at the shroud near unity. Variation of the difference between these 2 parameters across the passage is shown in Figure 203. Due to the trends discussed above, this difference, TRF-SF, is largest near the walls (the largest difference at the shroud). This is as expected, due to the influence of the clearance space on recirculation.

7.1.2 First Modification — Inducer Leading-Edge Sweep

For tests of the compressor with only the diffuser-throat total-pressure instrumentation installed in the airstream downstream of the impeller tip, it was

CONFIDENTIAL

CONFIDENTIAL

Test 3353

Corrected to Ambient
Conditions of:
60°F
29.92 in. Hg

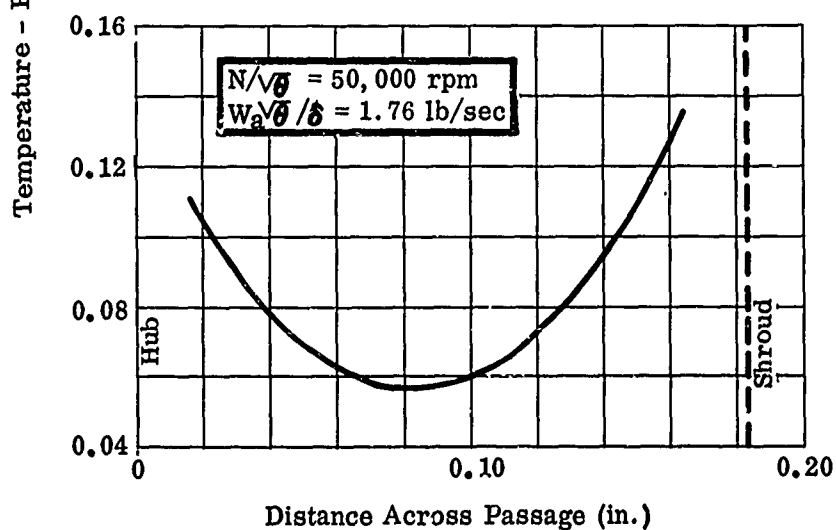
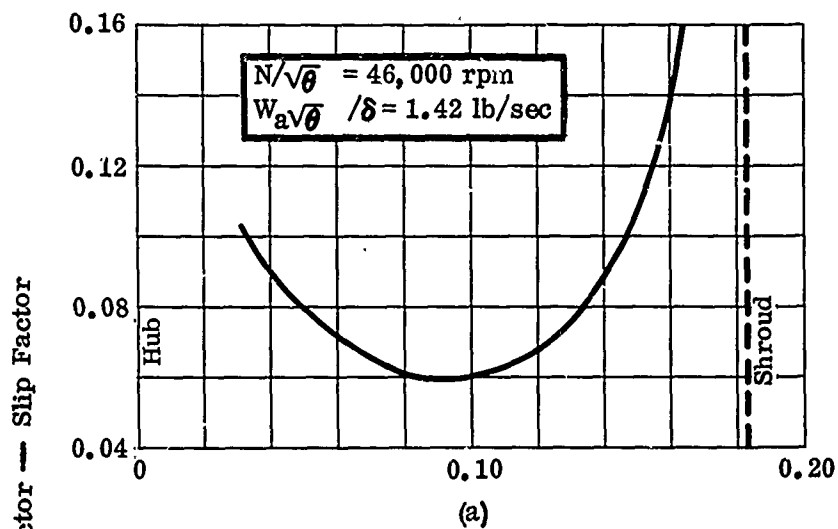


Figure 203. Difference Between Temperature-Rise Factor and Slip Factor, RF-2.

CONFIDENTIAL

CONFIDENTIAL

observed that little change in the impeller pressure ratio occurred over an airflow range of about 15 percent. Over this flow range, the inducer incidence varied by nearly 7 degrees. Interpreting the total pressure of the core flow in the diffuser throat as an indicator of impeller performance, the variation of the impeller pressure ratio over the test airflow range is shown in Figure 200. This constant performance suggested that a considerable portion of the inducer blading was operating at an incidence-Mach number combination outside the separation-effects boundary (Figure 377 of Reference 1). Since the incidence variation produced no significant change in impeller performance, this also suggested that the inducer was operating to the right of the separation-effects boundary, as shown in Figure 204 (line A-A'). If the inducer were forced to operate along line A-A', early separation would take place along the suction surface. The separation point has a marked influence on the impeller-exit mixing loss, as discussed in Section 7.1 of Reference 1. The impeller flow model argues that relative diffusion takes place in the impeller passage up to the point of separation after which the flow continues as a constant Mach number jet. The jet fills the passage as dictated by continuity

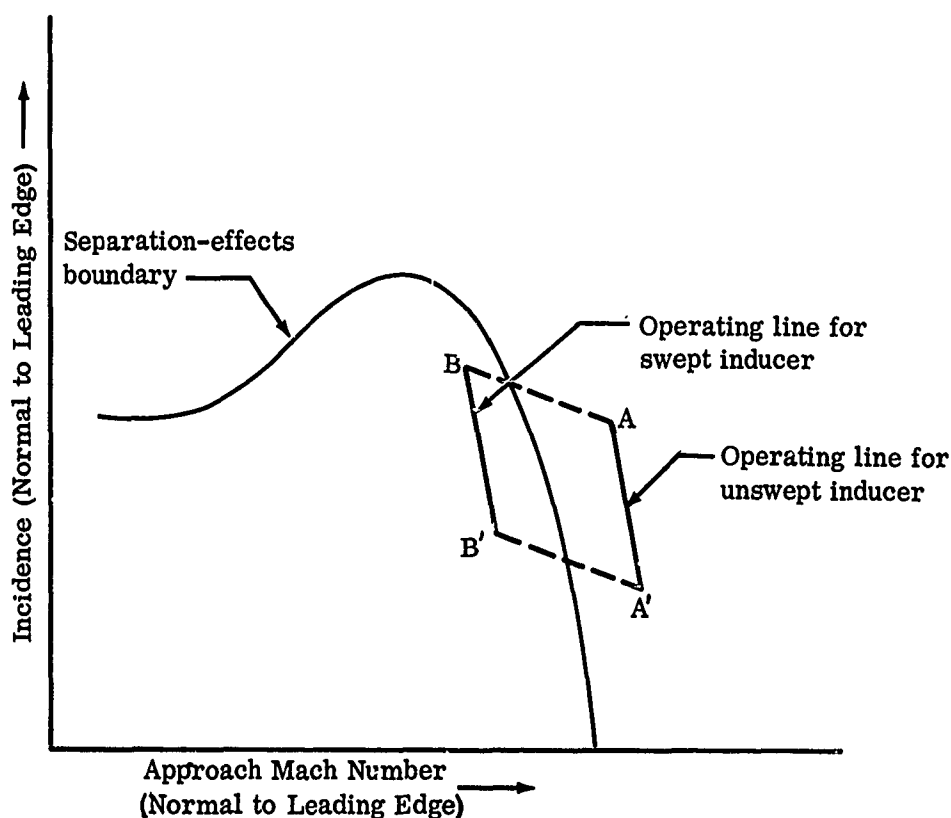


Figure 204. Assumed Relationship Between the Inducer Operating Line and the Separation-Effects Boundary.

CONFIDENTIAL

CONFIDENTIAL

with the remaining area occupied by a wake. The exit mixing loss was shown to be a function of the ratio of wake width to blade pitch. If the inducer operated in a region along the line A-A' (Figure 204), the impeller loss would be greater than expected.

It was planned, therefore, to sweep the inducer leading edge; this would reduce the approach Mach number normal to the inducer leading edge and bring the inducer operating line within the region of no separation effects for this blading (Figure 204, line B-B'). The final leading-edge configuration was as shown in Figure 55.

It was realized that the sweep would result in increased incidence on the blading. One increment in incidence is due to the sweep itself, as seen from the relationship of incidence and sweep.

The expression is:

$$\frac{\Delta i}{i_{\infty}} = \sec \psi - 1$$

where:

Δi = increment in incidence (degrees)

i_{∞} = incidence on unswept blading (degrees)

ψ = sweep angle (degrees)

The second increment in incidence is due to the blade camber. By cutting back the blade, the metal angle at the leading edge is reduced (becoming more axial). The radial variation of incidence for the design airflow is shown in Figure 205. In spite of the increased incidence, it was expected that the impeller performance would improve due to the decrease in the inlet relative Mach number normal to the blade leading edge if the incidence-Mach number condition was causing early separation in the inducer. The test results showed no change in impeller performance. The overall compressor performance with the swept-leading-edge inducer installed was nearly identical to that with the original inducer installed, as shown in Figure 60 (Test 3367 compared with Test 3366). This suggests that there was no change in impeller performance. Two possibilities exist for explaining the lack of improvement. First, the changes in the inlet Mach number and incidence normal to the leading edge resulting from the sweep may not have brought the operating line of the inducer inside the region of no separation effects (Figure 206). A second possibility is that the high Mach number flow and the ensuing shocks in the leading-edge region of the blades did not affect the diffusion and, therefore, the separation

CONFIDENTIAL

CONFIDENTIAL

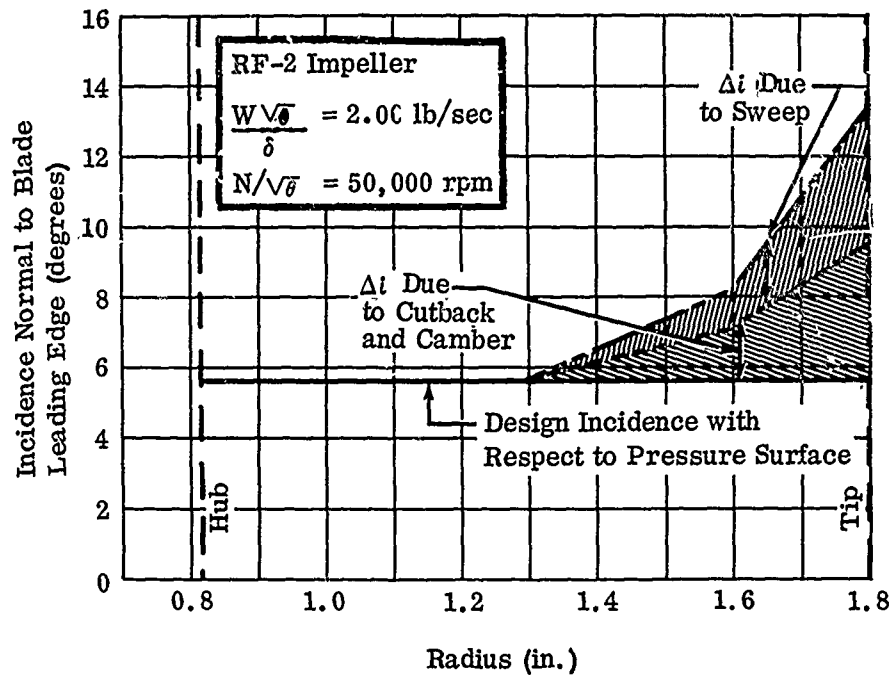


Figure 205. Incidence Changes Due to Sweep and Cutback, RF-2.

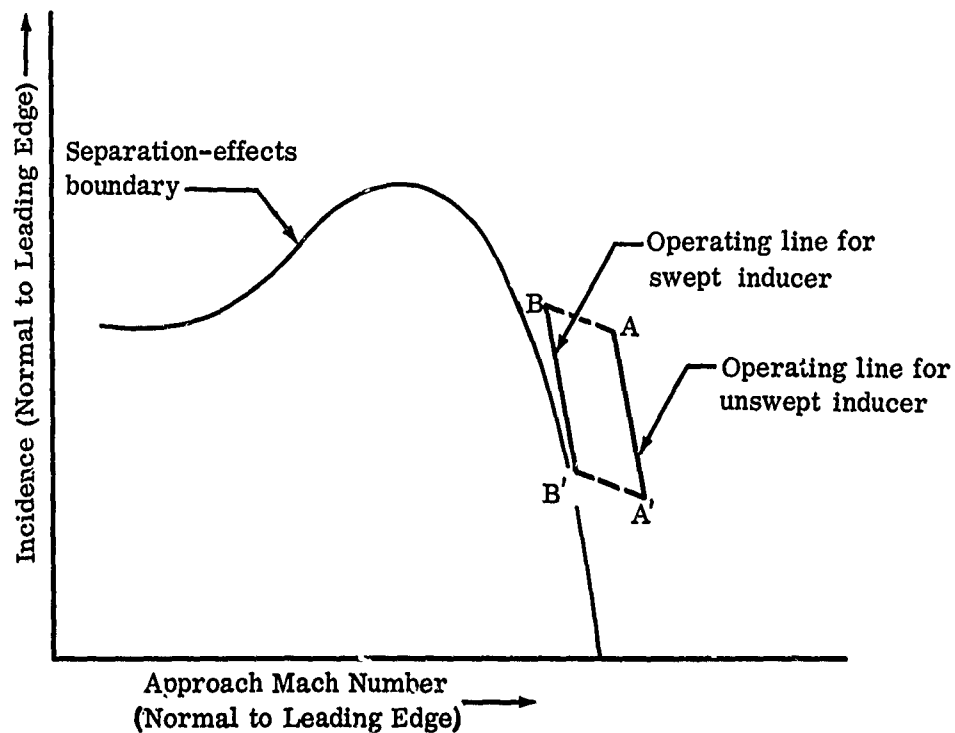


Figure 206. Assumed Relationship Between the Inducer Operating Line and the Separation-Effects Boundary.

CONFIDENTIAL

CONFIDENTIAL

point within the inducer (Figure 207). This test indicates that a swept inducer is not effective for high subsonic designs with radial-element blading.

7.1.3 Second Modification — Impeller-Exit Blade Width Reduction

The design loss analysis of the RF-2 impeller had indicated that approximately 75 percent of the peripheral area at the tip was occupied by low-energy wake fluid ($\epsilon = 0.75$). The predicted loss in total pressure through the exit mixing process was about 17 percent. The influence of ϵ in determining the exit mixing loss is illustrated in Figures 369 through 371 of Reference 1.

By adopting the constant Mach number-jet flow model described in Section 7.1 of Reference 1, it follows that by reducing the geometric area at the tip of the impeller, the jet would occupy a larger percentage of the area. This area change would result in a smaller value of ϵ and a smaller loss through the mixing process. To decrease the geometric area at the impeller tip, the blade width of the impeller was reduced from 0.180 to 0.135 inch (Figure 56).

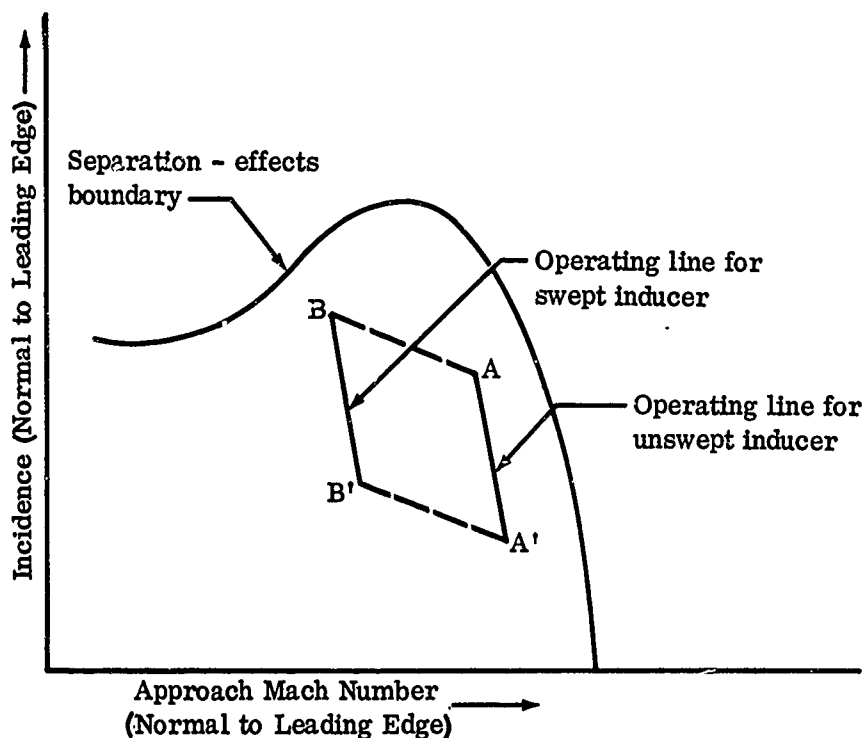


Figure 207. Assumed Relationship Between the Inducer Operating Line and the Separation-Effects Boundary.

CONFIDENTIAL

Careful consideration had to be given to the resulting diffuser design, so that the impeller performance improvement was not nullified by a degradation in diffuser performance. Two-dimensional diffuser tests conducted as part of this program and reported in Appendix XI of Reference 1 showed that it was possible to obtain acceptable static-pressure recovery with a 0.25-throat-aspect-ratio diffuser. The aspect ratio of the modified diffuser was 0.29. Therefore, a considerable reduction in diffuser performance was not expected.

The flow model showed a decrease of ϵ from 0.75 to 0.65 with this modification. The parameter λ , which is the tangent of the bulk-mean absolute flow angle at the tip, also decreased. The net effect was a 4- to 5-percent improvement in the impeller pressure ratio, provided the useful work of the impeller remained constant. By changing ϵ , the energy imparted to the air by the impeller will also change, as discussed below.

Every known method for predicting the useful work (slip factor) of centrifugal impellers incorporates the number of blades as one of the inputs (see References 3 and 4). Several of the methods are:

Busemann

$$SF = \frac{1 - \sqrt{\cos \beta_{B2}}}{Z^{0.70}} \quad (3)$$

Stanitz

$$\begin{aligned} SF &= 1 - 0.315 \left[\frac{2\pi}{Z} \sin \left(\frac{\phi}{2} \right) \right] \\ &= 1 - \frac{1.98}{Z} \quad (\text{radial impeller, } \phi = 180^\circ) \end{aligned} \quad (4)$$

Eckert (Modified)

$$SF = \frac{1}{1 + \frac{\tau \cos \beta_{B2}}{2Z \left[1 - \left(\frac{d_{RMS}}{D_{tip}} \right) \right]}} \quad (5)$$

where:

SF = impeller slip factor

Z = number of impeller blades

CONFIDENTIAL

CONFIDENTIAL

β_{B2} = angle between blade mean line and the meridional plane at the exit (for straight, radial blades $\beta_{B2} = 0^\circ$)

d_{RMS} = root mean square diameter at impeller inlet

D_{tip} = impeller-tip diameter

Introducing the geometry of the RF-2 impeller into the above relationships gives:

Busemann

$$SF = 1 - \frac{1}{Z^{0.70}} \quad (6)$$

Stanitz

$$SF = 1 - \frac{1.98}{Z} \quad (7)$$

Eckert (Modified)

$$SF = \frac{1}{1 + \frac{\pi}{1.39 Z}} \quad (8)$$

For the jet-flow model adopted for the analysis of the RF-2 impeller, the pitch of the jet flow is $(1 - \epsilon) \frac{2\pi R}{Z}$ rather than $\frac{2\pi R}{Z}$, as shown in Figure 208.

Therefore, an equivalent number of blades Z_{eq} can be introduced. This parameter represents the number of blades required to produce the jet pitch if all channels flowed full. The equivalent number of blades and the actual number of blades are related by the expression

$$Z_{eq} = \frac{Z}{1 - \epsilon} \quad (9)$$

Substituting

$$Z_{eq} = \frac{18}{1 - \epsilon} \quad (\text{RF-2 impeller})$$

for Z in the previous slip factor equations, the relationships between slip factor and ϵ become:

Busemann

$$SF = 1 - 0.132 (1 - \epsilon)^{0.70} \quad (10)$$

CONFIDENTIAL

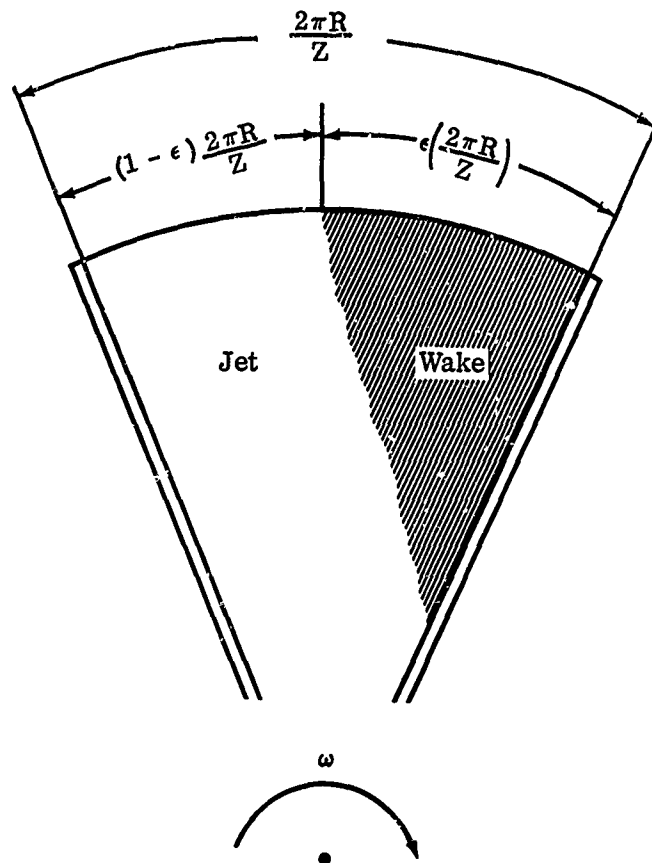


Figure 208. Jet-Wake Flow Model.

Stanitz

$$SF = 1 - 0.110 (1 - \epsilon) \quad (11)$$

Eckert (Modified)

$$SF = \frac{24.9}{(28.0 - \pi \epsilon)} \quad (12)$$

Therefore, for a given impeller, the slip factor is only a function of ϵ ; and $d(SF)/d\epsilon$ was determined as a function of ϵ for the RF-2 impeller, as shown in Figure 209. The average value of $d(SF)/d\epsilon$ from the 3 methods listed above in the region of interest ($0.65 \leq \epsilon \leq 0.75$) is 0.12. This indicates that the predicted decrease in ϵ from 0.75 to 0.65 would result in a decrease in the slip factor of 0.012.

CONFIDENTIAL

CONFIDENTIAL

The test data showed that, at the design speed, the peak value of the exit total-pressure profile as well as the mass-averaged total pressure were nearly the same as those measured for the wider blade width (Figures 61 and 200). The temperature-rise factor, however, decreased nearly 0.03. On the basis of the slip factor argument, this decrease indicated that the recirculation effects were also reduced.

To estimate the increase in impeller performance, the predicted change in ϵ and the corresponding change in slip factor were incorporated into an analysis with the measured impeller pressure ratio and the predicted internal losses. The results indicate that the exit mixing losses were reduced by about 3 percent; the pressure ratio remained constant, although the useful work input was reduced by 1.3 percent. This loss reduction agreed favorably with the 4- to 5-percent improvement predicted by the loss analysis. This agreement further substantiates the impeller flow model and the exit mixing loss analysis.

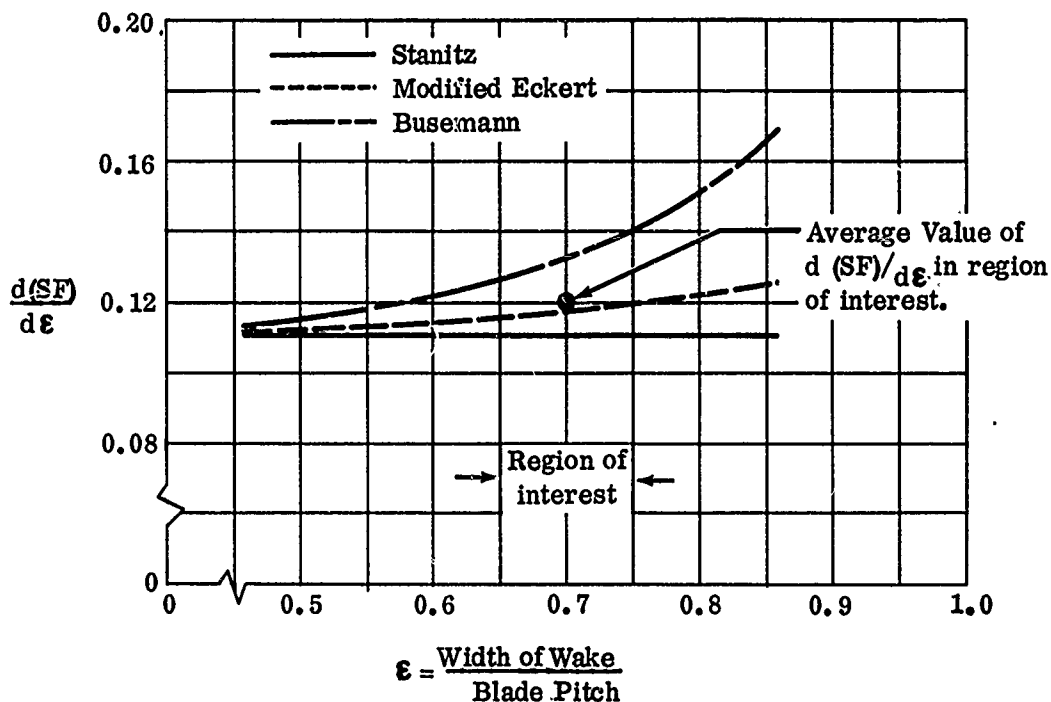


Figure 209. Variation of Slip Factor with the Ratio of Wake Width to Blade Pitch, RF-2.

CONFIDENTIAL

At the design speed, the performance of the narrow-blade-width impeller was:

Impeller Pressure Ratio = 11.2:1

Impeller Adiabatic Efficiency= 83%

The impeller efficiency was nearly constant at all speeds. At the low speeds the diffuser limited the airflow, causing the inducer to operate at high incidence.

7.1.4 Discussion of Pressure Measurements

The 3 impellers tested with diffuser vanes installed (workhorse, RF-1 and RF-2) were analyzed in the same manner to determine their performance; i. e., the readings of the total-pressure rakes at a radius ratio of about 1.03 were interpreted as the total pressures after the exit mixing process had been completed. The measured total-pressure profiles were averaged to determine the pressure ratio of each impeller. In comparing the performance of the RF-2 and the workhorse impellers, several contradictory pieces of data were found to exist. The mass-averaged pressure ratio of the workhorse impeller was 11.6:1 (corrected for IGV loss), while that of the RF-2 was 11.2:1. A comparison of the core total pressures at the diffuser throat, however, indicated that the RF-2 impeller delivered about 6 psi more pressure than the workhorse impeller (Figure 210). The average static pressure at the 1.03 radius ratio was 3 psi higher for the RF-2 impeller than for the workhorse impeller (68 psia versus 65 psia). The design absolute Mach numbers at the exit for both impellers were about 1.27. Using the ratio of the static to total pressures corresponding to a Mach number of 1.27, the 3-psi static-pressure difference gives an 8-psi difference in total pressure. This agrees quite favorably with the 6-psi total-pressure difference indicated by readings at the throat.

If both the 1.03-radius-ratio and the diffuser-throat total pressures are accepted as being correct, then the total-pressure recovery in the region between the 1.03 radius ratio and the diffuser-throat entrance must be about 7 percent higher for the case of the RF-2 impeller. Since the vaneless space diffuser geometry is essentially the same for both compressors, a large difference in loss would not be expected. Of these 2 pieces of data, the readings taken at the 1.03 radius ratio are more suspect because of the unsteady operating environment produced by the jet-wake flow emanating from the impeller. The flow at the diffuser throat is more steady; therefore, probe error is reduced. For these tests, the time-averaged total pressure is measured; however, the true mass-averaged value is in error. For example, the expression for the time-averaged absolute total pressure at the impeller rim (prior to any mixing) is as follows:

$$\left(P_{T_a} \right)_{t-a} = (1 - \epsilon) \left(P_{T_a} \right)_{jet} + \epsilon \left(P_{T_a} \right)_{wake} \quad (13)$$

CONFIDENTIAL

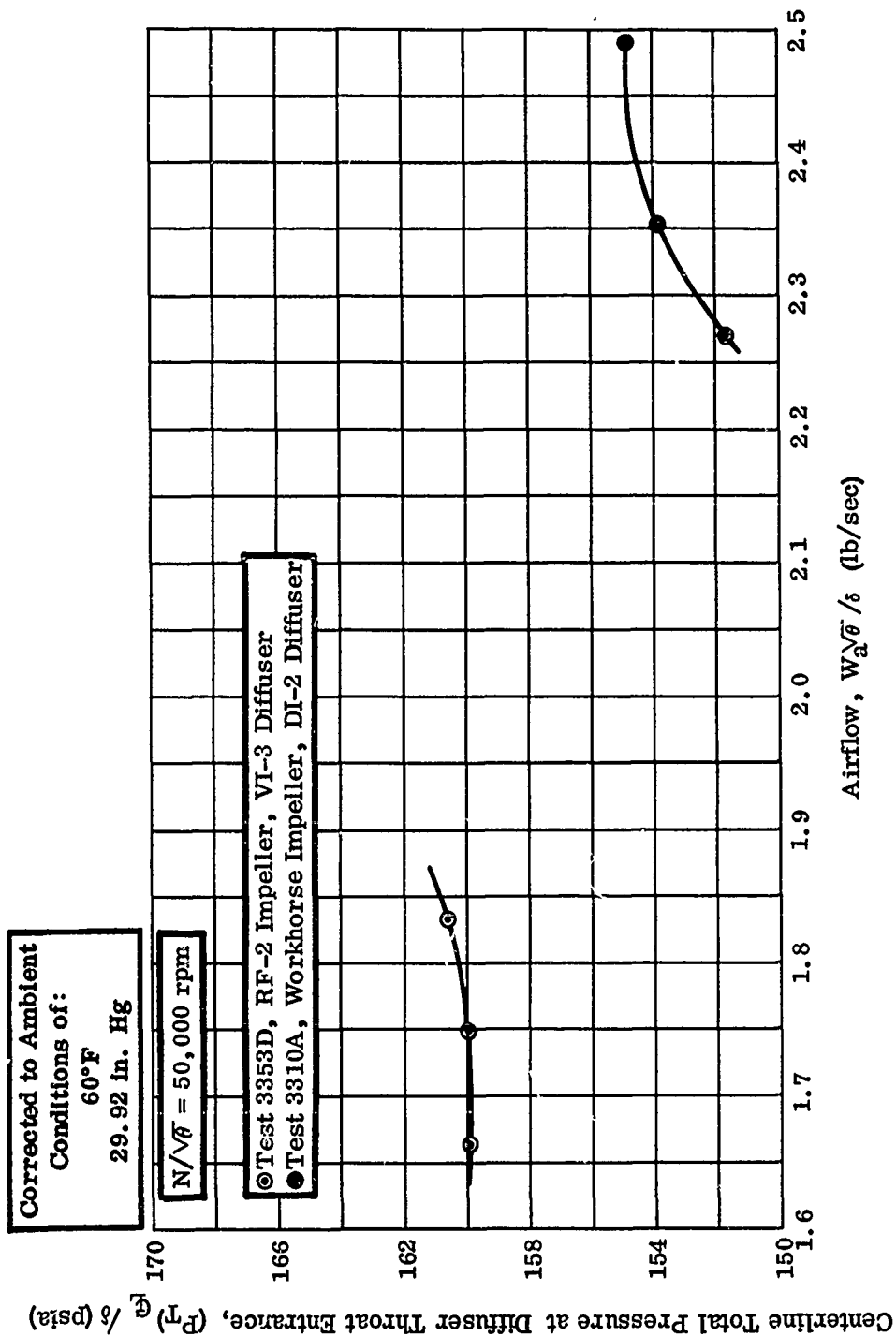


Figure 210. Centerline Total Pressures at the Diffuser-Throat Entrance for Tests 3310A and 3353D.

CONFIDENTIAL

The expression for $(P_{T_a})_{t-a}$ assumes:

- 1) Zero through flow in the wake
- 2) Constant through-flow velocity in the jet

where:

P_{T_a} = absolute total pressure

ϵ = ratio of wake width to blade pitch

and the subscript, $t-a$, refers to the time-averaged value.

Representative values for the different quantities involved in the above expression are $(P_{T_a})_{jet} = 205$ psia; $(P_{T_a})_{wake} = 175$ psia; $\epsilon = 0.75$.

For this case $(P_{T_a})_{t-a} = 182$ psia. The mass-averaged value of the total pressure, consistent with the previously stated assumptions, is 205 psia. For the representative case the total-pressure reading is about 11 percent low. At the 1.03 radius ratio, some mixing has taken place and the error is not as large as indicated by the example cited above. The 11-percent difference serves as an upper limit on the probe error introduced by the pulsating flow. This simple flow model, however, does not explain why a higher total pressure was indicated for the workhorse impeller than for the RF-2 impeller. According to the impeller flow model, the probes would see about the same type of pulsating flow in both cases. If the probes indicated low pressures for the RF-2, they would also indicate low for the workhorse. It is felt, nonetheless, that the wake-jet flow pattern in proximity to the impeller tip introduces errors in the sense described above into the total-pressure measurements obtained at the 1.03 radius ratio. The data suggest that for high-pressure-ratio impellers, where large separated regions are common, the diffuser-throat core total pressure is a better indicator of the impeller performance. The analysis of Dean and Senoo (Reference 5) shows that for impellers similar to the workhorse and the RF-2, the mixing process might extend to a radius ratio of 1.08 (see Figure 399 in Reference 1). The loss analysis using the test slip factor of 0.89, which was discussed in Section 7.1.1, predicted an impeller pressure ratio of 11.0:1. This agrees within 2 percent with the core total pressure at the throat entrance (159 psia).

7.2 DIFFUSER

In the centrifugal compressor, about half of the static-pressure rise occurs in the diffuser. It is therefore necessary to ensure that the diffuser operates as efficiently as possible. To do this, the flow mechanisms through the diffuser must be understood and ways must be found to correct deficiencies.

CONFIDENTIAL

CONFIDENTIAL

Initially, in the simple analytical flow model of the diffuser, it is considered that flow through the vaneless and semivaneless spaces follows a modified log-spiral curve to the diffuser throat. Generally, the vane thicknesses are also taken into consideration, requiring a further modification to the log-spiral streamline shape in the semivaneless space. The flow decelerates to subsonic velocities at the throat entrance and further diffuses in the subsonic diffuser channel.

During the course of this program, it was found that the flow was quite different from the flow in the above simple case. The flow does not diffuse by some simple process, but in general, diffuses very little in the vaneless and semivaneless spaces. When the flow leaves the impeller tip at a supersonic Mach number ($M = 1.0$ to 1.3), the velocity remains nearly constant to some point near the vane leading edge, where the supersonic flow is terminated by a throat entry shock. The entry shock decreases in strength from surge to maximum airflow. Near maximum airflow the shock is weakest and curves into the diffuser throat rather than being quite normal as is the case near surge. The characteristic shape of the entry shock also changes for different diffuser models. In some cases the shock appears to be of high strength like a single normal shock, and in other cases, there are a series of weak shocks similar to the duck-shock system shown by Neumann and Lustwerk (Reference 6).

Oil traces from earlier schlieren tests show evidence of secondary flow bleeding the boundary layer from the suction surface. Therefore, the likelihood of uniform boundary layer on the walls of the diffuser throat is small. In fact, total-pressure surveys of the diffuser throat show a boundary-layer buildup on the pressure surface and the diffuser side walls, suggesting that the suction surface is nearly free of boundary layer. Subsonic flow follows the entry shock; however, tests have shown that a lambda shock also occurs on the pressure surface of the vane leading edge, indicating that the flow reaccelerates in this region. The strength of the lambda shock changes from surge to maximum airflow, but in contrast to the entry shock, it is strongest at maximum airflow, as would be expected from the change in incidence with increased airflow. There is a possibility that the lambda shock separates the pressure-surface boundary layer where maximum shock strength occurs.

In addition to the observed flow phenomena associated with these shocks, the jet-wake mixing process from the impeller tip further complicates definition of the flow. The radius ratio required to mix out the wakes can be estimated using a study by Johnston and Dean (Reference 7).

With these different flow processes occurring in the diffuser, it is apparent that a simple 1-dimensional flow model will not suffice to define the flow accurately. The flow model put forth in Reference 1 shows the change in entry-shock strength with airflow. The diffuser-channel static-pressure recovery is related to the diffuser-throat blockage and Mach number upstream of the entry shock. The

CONFIDENTIAL

CONFIDENTIAL

strengths of the lambda and the entry shocks previously were treated as a single shock. Further analysis of data from the new diffuser model, V1, indicated that these shocks should be treated separately, as shown in the discussions which follow.

7.2.1 Diffuser Tests

The first tests of the new compressor were run with the V1 diffuser vanes. Test results of the design configuration showed that overall compressor performance was below expectations. Because test data also indicated that the previously observed performance deficiencies with the RF-1, MF-1, and workhorse impellers had been corrected, further investigations were concentrated on the diffuser. It was believed that performance improvement could be obtained with reductions in throat blockage, as shown earlier in Section 7.2 of Reference 1, or by modifying channel-divergence angles. Analyses of test data were conducted to determine the effects of upstream-shock Mach number and boundary-layer blockage at the diffuser throat on diffuser-channel static-pressure recovery. The matching of the impeller and diffuser was also studied to determine how the diffuser static-pressure recovery could be improved.

Because the impeller and diffuser are tested together, it was possible to obtain diffuser data for every impeller test run. Section 5.0 shows details of the diffuser static-pressure instrumentation. As shown in the following discussion of compressor performance and as shown in Section 7.1, impeller performance was nearly constant across the airflow range. Therefore, it was possible to relate changes in compressor performance to the particular diffuser under investigation.

Decreased Clearance Tests

In initial tests of the compressor, checkout runs were necessary to reduce impeller-tip clearance to the design value of 0.015 to 0.020 inch. The diffuser throat area was larger than design for the first wide-clearance tests. Vane width was reduced in 3 steps to reduce the clearance and bring the diffuser throat area to the design value. Figure 165 shows the compressor speed line resulting from each vane-width reduction. The speed line from Test 3352C (Figure 165) shows compressor performance for the design configuration. The overall compressor performance was less than expected, although consistent with the DI-2 diffuser shown in Reference 1 (Test 3310).

Probe Tests

Instrumentation was installed at the impeller tip and the diffuser throat to determine performance of both the impeller and diffuser; however, this instrumentation was not used simultaneously at the impeller tip and the diffuser throat.

CONFIDENTIAL

CONFIDENTIAL

Figure 166 shows the effect of instrumentation on the overall compressor performance. For Test 3353, complete impeller-tip instrumentation was installed, and the overall pressure ratio was reduced more than 1/2 atmosphere. When all probes except the yaw probe were removed, total pressure still was low despite an airflow increase, as shown in Figure 166. The yaw probe was replaced with a smaller total-pressure rake for Test 3353C, and both total pressure and airflow increased. The speed line from Test 3353D shows that a single total-pressure rake installed in the diffuser throat did not affect the compressor pressure ratio. For this test, maximum airflow was reduced as expected because of the reduced effective flow area in 1 channel.

Increased Throat-Area Tests

Referring again to Figure 166, the design configuration did not pass the design airflow of 2.0 pounds per second; therefore, the diffuser throat area was increased in 3 steps to reach design conditions and extend the airflow range until the impeller reached maximum airflow. The resulting compressor speed lines are compared with those from Test 3352C in Figure 167. The maximum airflow was increased by 12 percent from Test 3352C to Test 3356. The compressor showed essentially no change in pressure ratio as the airflow was increased, which suggests that the impeller and diffuser performance were constant across the entire airflow change. The maximum range achieved was 16 percent in Test 3355. For this test series, maximum airflow increased in proportion to the throat area increase except in Test 3356, when the inducer section of the impeller was choked at the full-flow line. The impeller performance was expected to increase as the airflow was increased because of the reduced inducer-flow-incidence angle. This performance change did not occur (Section 7.1). However, the impeller shroud static-pressure rise showed that the impeller was performing close to design and that the compressor performance deficiency largely was caused by the diffuser, as shown by the measured static-pressure recovery.

Divergence Angle Tests

The V1 diffuser tested thus far was designed with a 10 degree asymmetrical divergence angle, as shown in Figure 14. It was planned that changes in divergence angle and symmetry would be evaluated to determine the geometry for best performance. The diffuser channel was modified into 3 configurations. Sketches of each diffuser modification are shown in Figure 162, and results of these tests are shown in Figure 169. The 10-degree asymmetrical channel was changed to a 5-degree asymmetrical channel, and a 2-percent pressure-ratio reduction resulted. This change in performance was found to be in agreement with the single-channel diffuser data presented in Appendix XII of Reference 1. The second channel modification was to increase the divergence angle to 8 degrees by cutting a 3-degree wedge out of the vane suction surface. This test (3359) resulted

CONFIDENTIAL

CONFIDENTIAL

in a small pressure-ratio increase over the 10-degree asymmetrical test (3356) which was used as a base point. The vane suction surface was again modified to increase the suction surface divergence to 5 degrees, and a 10-degree symmetrical divergence angle and another small increase in pressure ratio resulted. These channel modifications resulted in a 2-percent overall pressure-ratio improvement; however, the channel static-pressure recovery was still below the expected value. A complete analysis of the diffuser data was conducted to determine ways of further improving performance.

7.2.2 Discussion of Data and Results

The diffuser test data from the workhorse tests showed a strong dependence of diffuser-channel static-pressure recovery on throat blockage and Mach number upstream of the entry shock. V1 was analyzed in the same manner as DI-1, DI-2 and DI-3 to determine diffuser performance and to establish whether a correlation of data existed. The static-pressure ratio across the entry shock was determined by using the test data shown in Appendix III. The average static pressure at the throat exit was used for P_y , and the lowest static pressure ahead of the shock was used for P_x (see Figures 177 through 195). The analysis method included consideration of the strength of both the entry and downstream lambda shocks. It should be noted that the entry-shock system of V1 appeared to be spread out further along the streamlines than the entry-shock system of DI-1 or DI-2, where the shock appeared to be more concentrated. However, for purposes of analyses, the static-pressure rise was treated as a single shock, which appears to be valid (as suggested in Reference 6, and in Reference 8, page 141). Mach numbers upstream (M_x) and downstream (M_y) of the shock were found from the static-pressure ratio. The throat total pressure (P_{T_y}) and blockage (B) were determined, where:

$$1 - B = \frac{\text{one-dimensional flow area}}{\text{geometric throat area}} \quad (14)$$

The channel static-pressure recovery was found from:

$$C_P = \frac{P_{\text{collector}} - P_{S_y}}{P_{T_y} - P_{S_y}} \quad (15)$$

The channel static-pressure recovery with respect to blockage is presented in Figure 211. Good agreement was found between the single-channel diffuser data (Appendix XII of Reference 1) and the V1 diffuser data. The Mach number upstream of the entry shock is shown with respect to throat blockage in Figure 212. These results showed trends similar to the results of the analysis for Mach number and blockage presented in Section 7.2 of Reference 1.

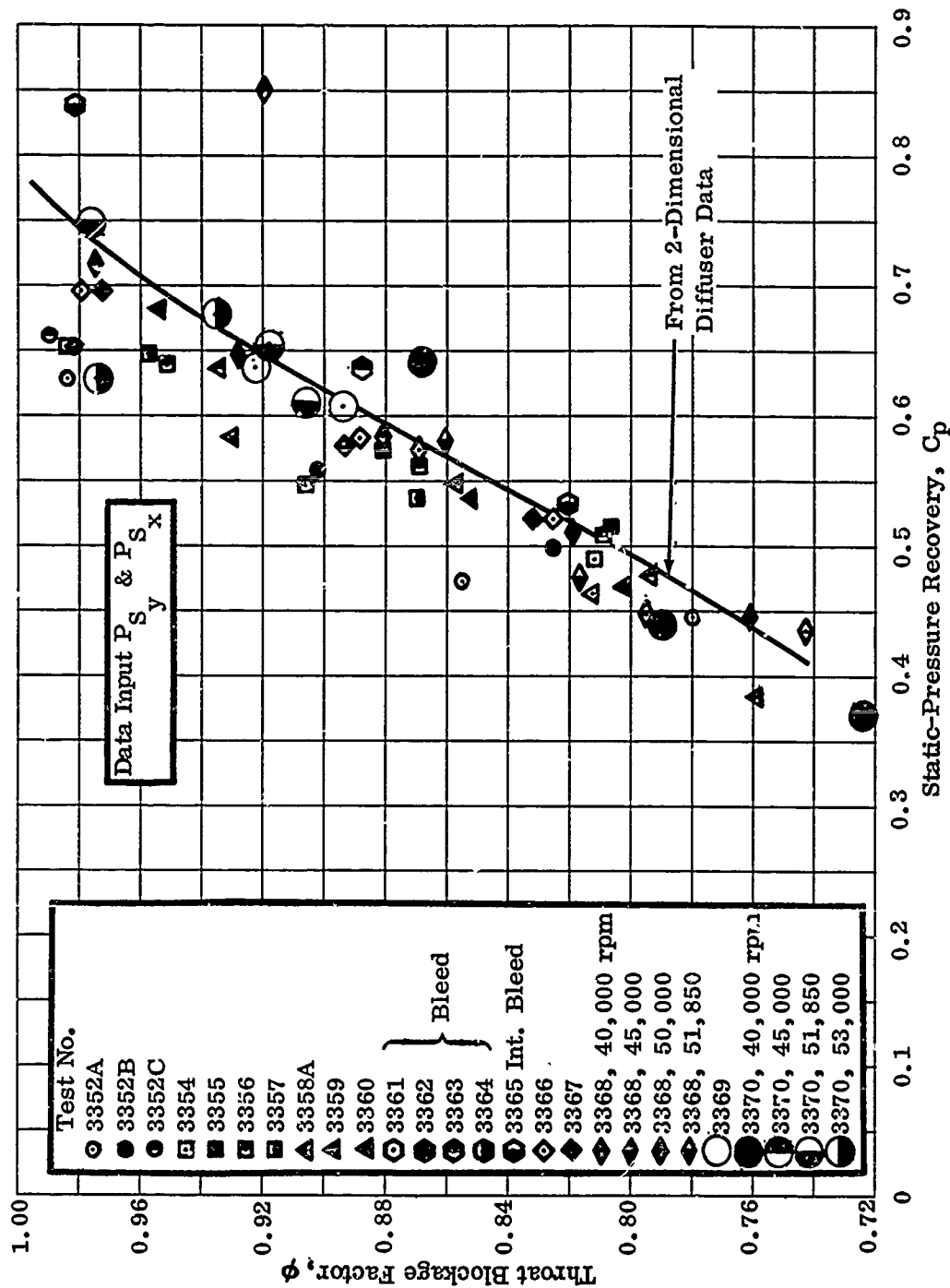


Figure 211. Comparison of Pressure Recovery for Compressor Channel with 2-Dimensional Diffuser Data.

CONFIDENTIAL

The good agreement was significant because preliminary analysis of this test data did not show high blockage factors (1-B) and high static-pressure recovery (0.70 to 1.0), as shown in Figure 211. Each test showed that the blockage factor increased with airflow; however, the indicated throat total pressure from continuity considerations apparently was reduced at a more rapid rate, resulting in performance below the target. The strong dependence of static-pressure recovery on blockage was apparent. The indicated total pressure suggested that the impeller performance was reduced with an airflow increase or that an increased pressure loss occurred in the vaneless and semivaneless spaces with increased airflow.

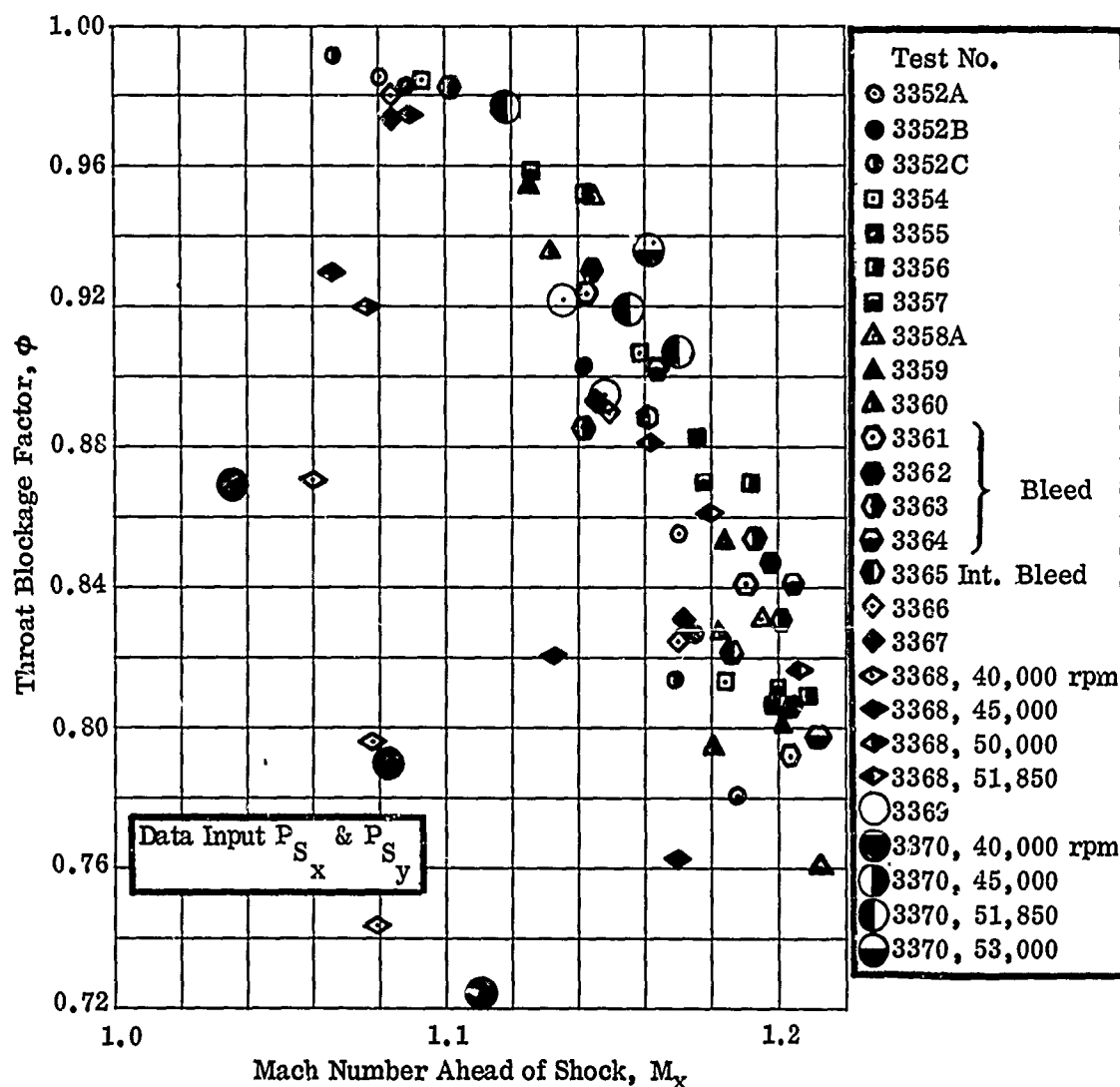


Figure 212. Throat Blockage Factor Versus Mach Number Ahead of Shock.

CONFIDENTIAL

CONFIDENTIAL

Total pressure data at the impeller tip and at the diffuser throat were analyzed to determine changes with airflow, and total pressure at both locations was found to be uniform within ± 1 percent. Figure 213 shows the core total pressure measured at the diffuser throat. These data show that the total pressure measured at the diffuser throat is nearly constant with airflow; therefore, the performance should increase (with improved static-pressure recovery) or the calculated static-pressure recovery is in error and is actually much lower. The calculated throat total pressure resulting from the preceding analysis (Figure 214) was compared with measured throat total-pressure data (Figure 213). The data scatter was found to be very large (± 8 percent from a mean curve fit), suggesting that the impeller total pressure also drops rapidly with airflow.

There is no fundamental reason why the impeller total pressure should vary strongly over this small airflow range, provided that the impeller passages are not choked. Further, impeller performance might be expected to be independent of the diffuser configuration; however, the opposite is reflected in Figure 215. As the throat area was increased for some tests, the speed line moved toward increased airflow, as was expected. But in each case, the indicated impeller performance (determined by diffuser-throat total pressure) dropped off rapidly as maximum airflow (diffuser choke) was approached. Because total pressure deduced from the analysis (Figure 215) is also much higher at surge than the measured values shown in Figure 213, it is concluded that the analysis results shown in Figures 214 and 215 are erroneous. It should be noted that the middle points (line 5 measured on each speed line) do agree quite well with the measured total-pressure data shown in Figure 216. This observation leads to the question of the validity of the remaining data at lines 3 and 7 (near surge and maximum airflow, respectively). The relative positions of lines 3, 5 and 7 on a speed line are shown in Figure 249.

At maximum airflow, it has been shown from the previous schlieren photographs and static-pressure distributions presented in Reference 1 that flow in the throat is highly 3-dimensional. In some cases, the shock curves back into the throat and the lambda shock increases in strength, so that choosing the proper P_x values becomes difficult. Therefore, the line 7 analysis is subject to question. At surge airflow, the case is less definitive, but the entry shock does move out ahead of the entrance, as shown by the static-pressure distributions (see Section 6.2). This shift may extend the shock into the impeller mixing region, where again selection of P_x may be difficult and total pressure may vary considerably over the length of the extended shock.

Since the result of the above analysis had proven to be invalid, the diffuser was reanalyzed using the measured static pressure and the total pressure at the diffuser throat corrected for the shock loss. Initially, only the tests with measured total pressure at the diffuser throat were reanalyzed to determine throat blockage, static-pressure recovery, and Mach number ahead of the entry shock.

CONFIDENTIAL

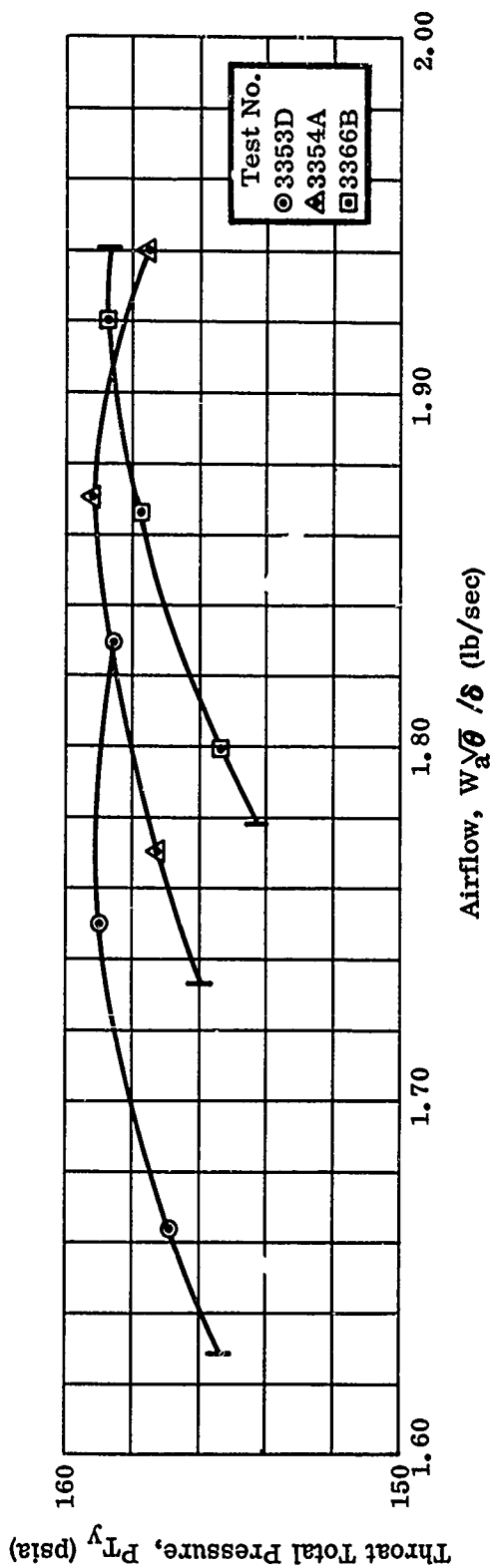


Figure 213. Diffuser-Throat Total Pressure Versus Airflow.

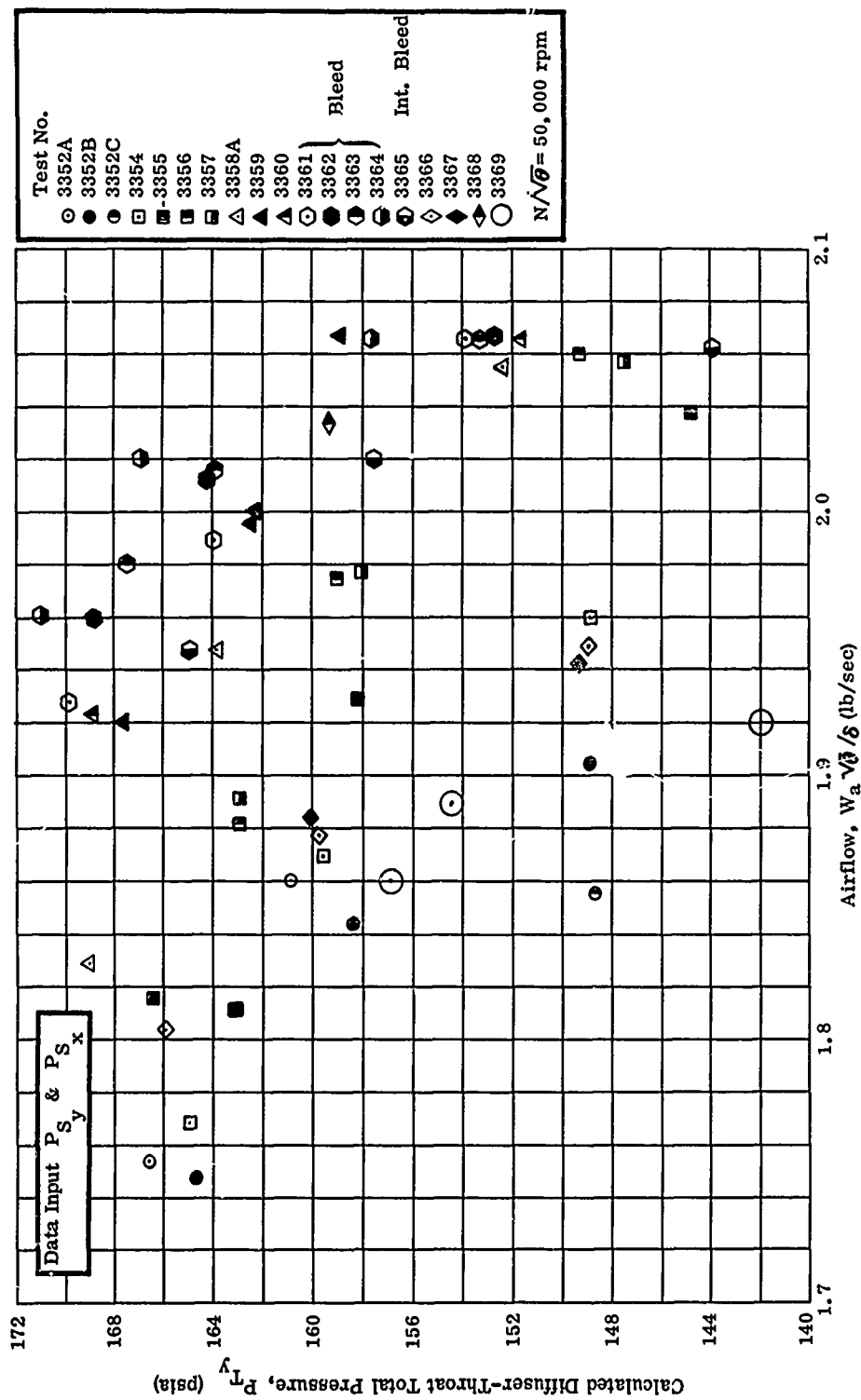


Figure 214. Calculated Diffuser-Throat Total Pressure.

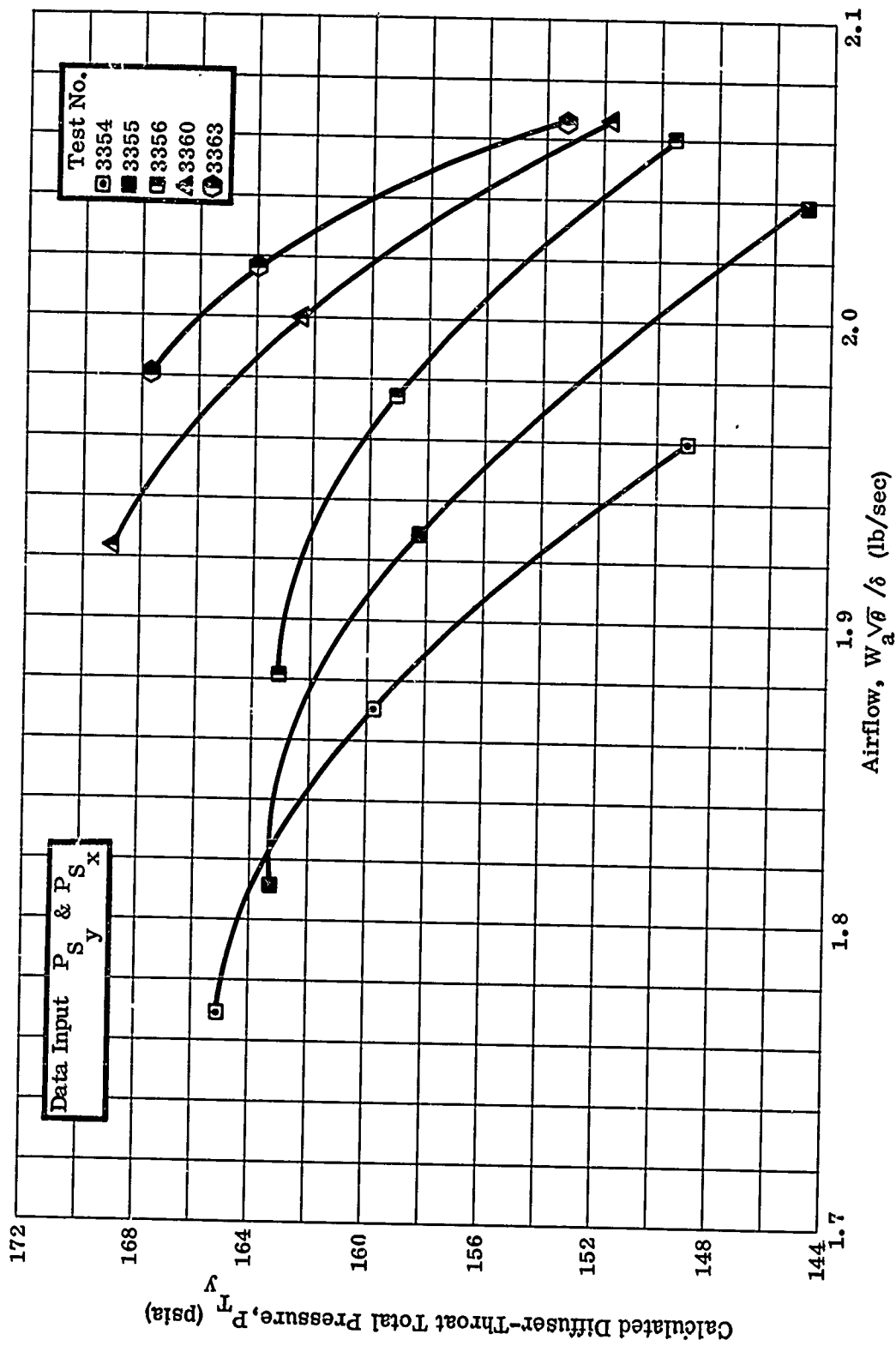


Figure 215. Calculated Diffuser-Throat Total Pressure Versus Airflow.

CONFIDENTIAL

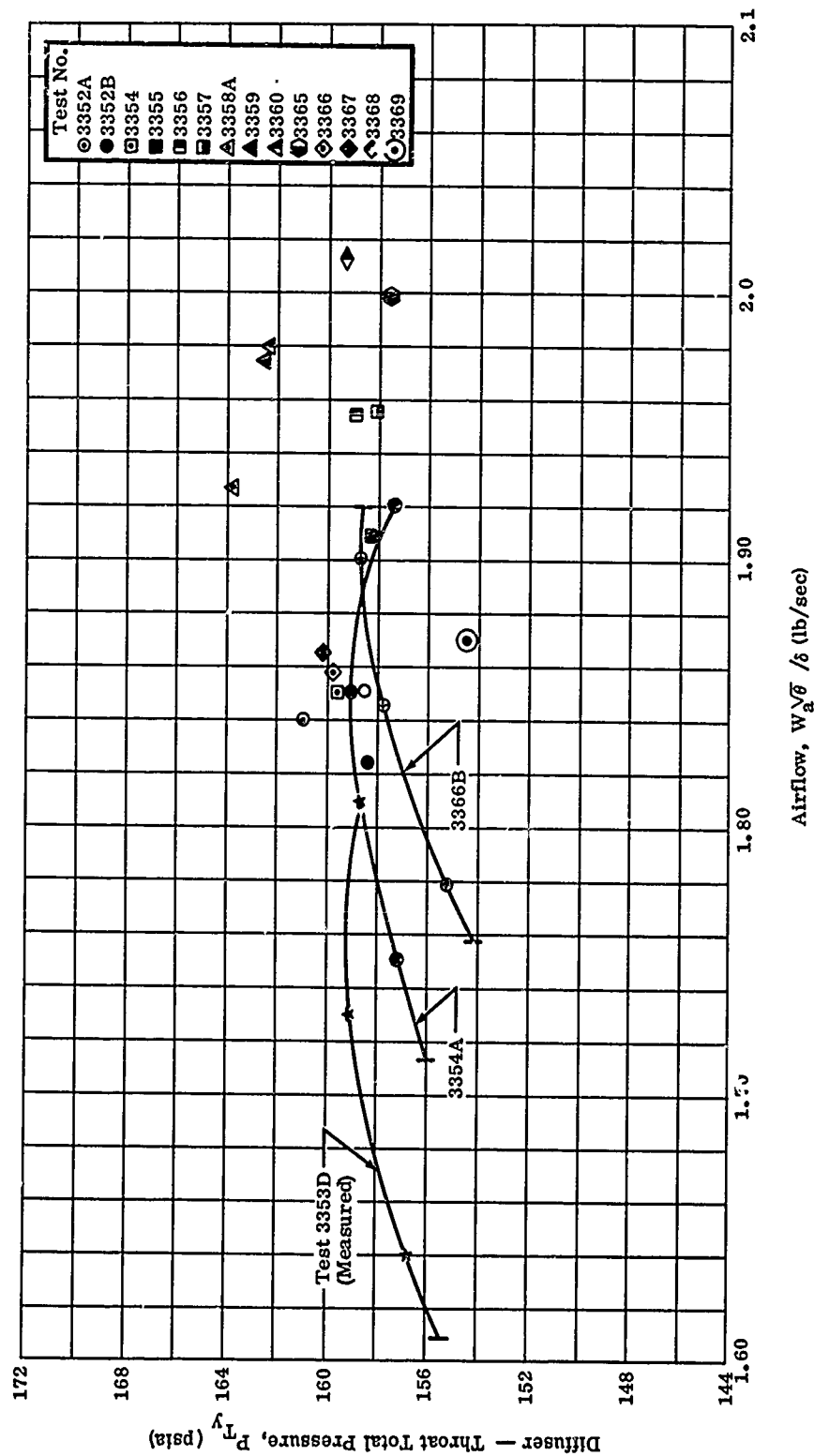


Figure 216. Comparison of Measured and Calculated Throat Total Pressure.

CONFIDENTIAL

CONFIDENTIAL

The resulting static-pressure recovery from this second analysis clustered around the single-channel diffuser data but did not show the previously observed large spread between maximum and minimum values. Because this analysis appeared to show better closure of the data, the remaining tests were analyzed in a similar manner. Variation of the average core total pressure P_{T_x} (corrected for the shock loss) with respect to airflow was determined, as shown in Figure 200 (page 252). This total-pressure curve was determined from 3 tests and was believed acceptable provided that the impeller pressure output was linear with airflow for various tests. To show the constant impeller output, the static pressure along the impeller shroud is presented in Figures 104 through 112. These figures show that the impeller static-pressure rise was nearly the same for each test, and suggests that a single curve through the data is valid. In each case, the static pressure was found to agree at a constant airflow (see Figure 217); therefore, it was concluded that at a given airflow, the impeller did perform the same for different diffuser tests, and that the measured throat total pressure could be used for all tests with the same impeller.

The throat total-pressure data with the mean curve used in the analysis and the impeller-tip-core total pressure are shown in Figure 200. The throat pressure data were extrapolated to higher airflows using the impeller-tip pressures as a guide.

The static-pressure recovery and throat blockage, therefore, could be calculated for all tests. The results of this analysis are shown in Figure 218. Again static-pressure recovery clusters around the 2-dimensional single-channel data ($C_p = 0.52$); however, the spread is small compared to the first analysis shown in Figure 211. The analysis with total pressure shows that the performance of the impeller and diffuser changed very little for all tests, as reflected by the overall compressor-performance speed lines shown in Section 6.2.

A comparison of the static-pressure recovery with respect to blockage for the 2 analyses shows that the results of the first analysis at line 5 agree quite well with all of the calculated results from the second analysis (using measured throat total pressure). However, the comparison again suggests that the line 3 and line 7 data of the first analysis may be in question.

The change in throat blockage with respect to the Mach number ahead of the entry shock has less influence on the throat blockage than was shown in the first analysis, Figure 219.

Therefore, it was necessary to investigate other causes of large throat blockage. Distortion of the velocity profile at the diffuser throat (not considering the boundary-layer displacement thickness near the walls) accounts for a large part of the blockage, as will be shown below. The throat was divided into 9 areas with a total-pressure measurement at the center of each area. The measured total

CONFIDENTIAL

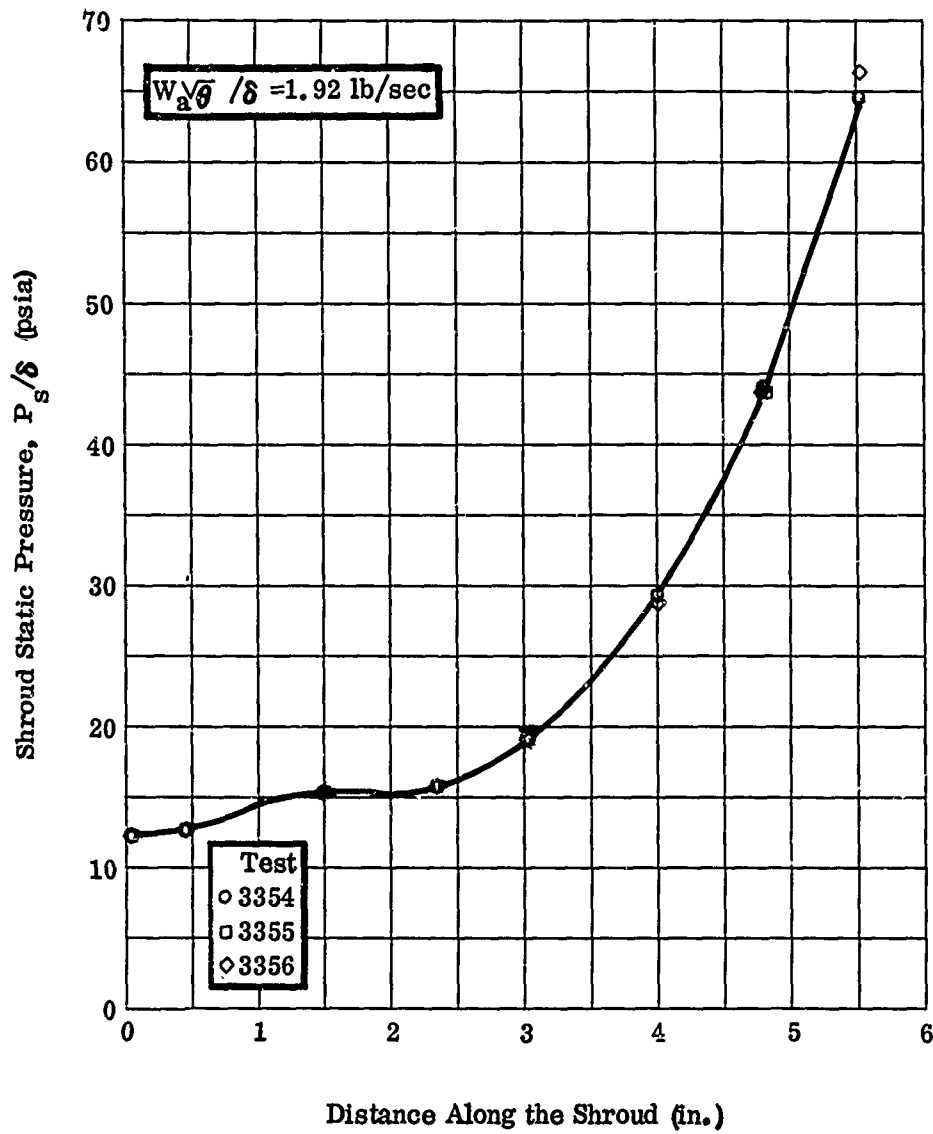


Figure 217. Comparison of Static Pressure Along Shroud for 3 Tests, RF-2.

CONFIDENTIAL

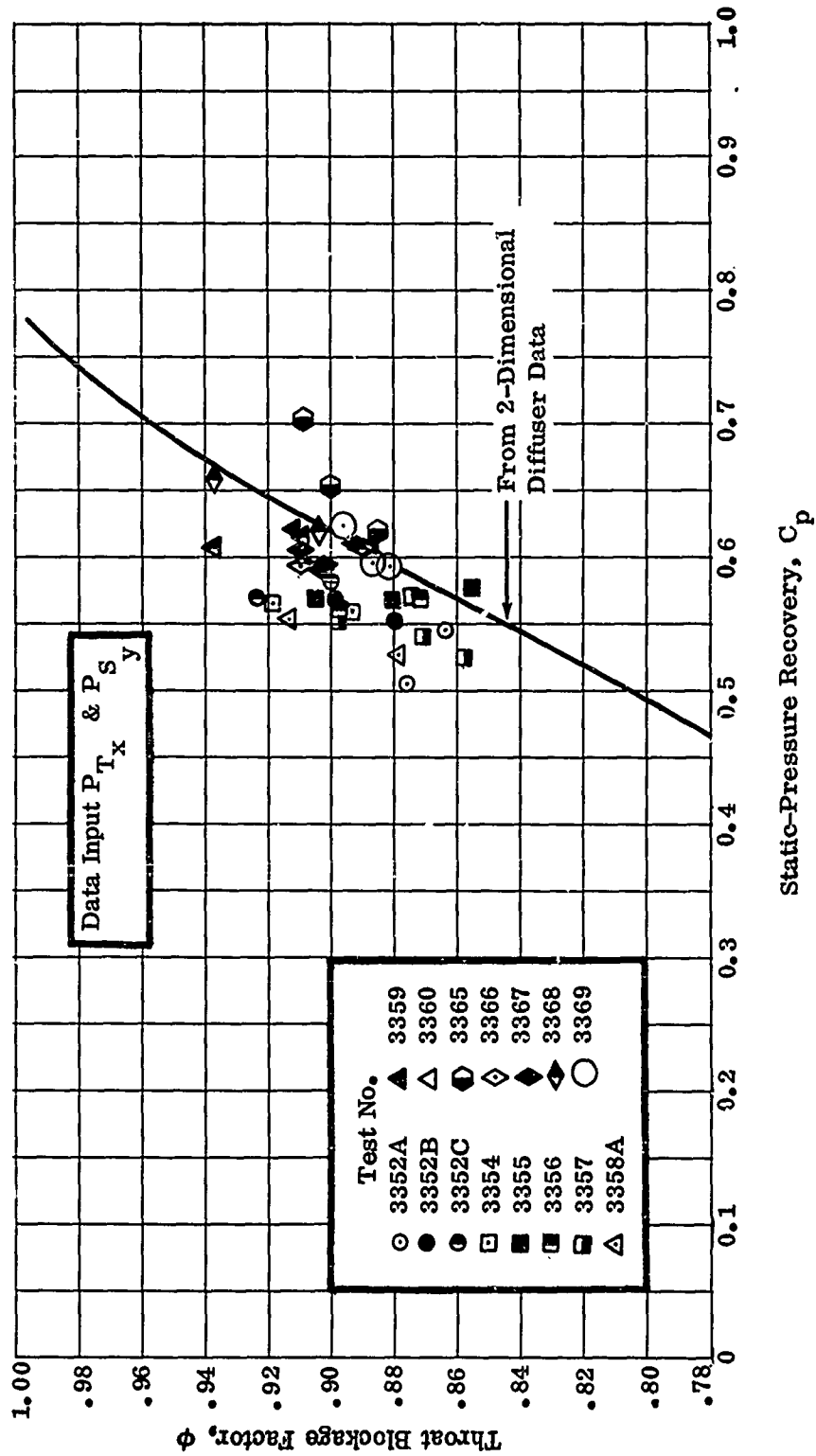


Figure 218. Comparison of Pressure Recovery for Compressor Channel with 2-Dimensional Diffuser Data.

CONFIDENTIAL

CONFIDENTIAL

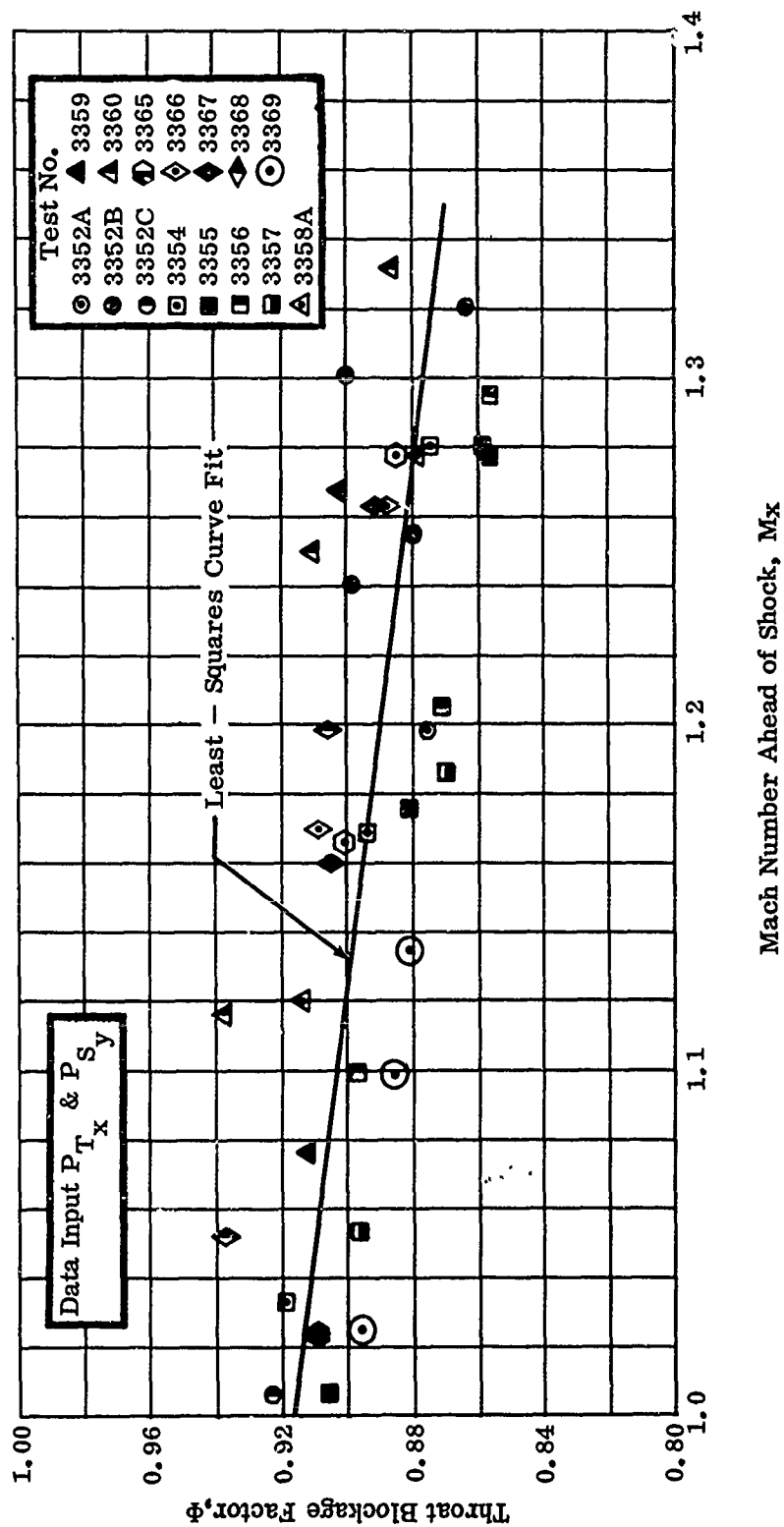


Figure 219. Throat Blockage Factor Versus Mach Number Ahead of Shock.

CONFIDENTIAL

CONFIDENTIAL

pressures and static pressures were used along with the total-temperature measurements to calculate the airflow in each area. The incremental airflows were then summed to obtain the total calculated airflow. The ratio of the airflow calculated by the above method to the airflow corresponding to the peak total pressure shows the blockage due to velocity-profile distortion. The resulting blockage was 5.5 percent. From overall continuity calculations, total blockage for this data point was 14 percent. Therefore, the wall boundary layer must account for the remaining 8.5 percent. Using flat-plate boundary-layer analysis, δ^* was calculated to be near 0.006. If a symmetrical boundary layer is assumed, the resulting blocking of 9 percent is very close to the above difference. Therefore, the blockage from the velocity profile, combined with the boundary-layer thickness, gives reasonable correlation with the blockage from the throat total-pressure analysis.

Throat Blockage

From the data analysis, it was apparent that the throat blockage must be reduced to increase the diffuser performance. Several methods under consideration to reduce the blockage were to bleed the boundary layer at the throat and to change the throat geometry. Further analysis suggested that these methods could be effective.

Boundary-Layer Bleed — Because diffuser performance was shown to be dependent on the throat blockage, boundary-layer bleed was considered as a possible way to reduce blockage. Therefore, tests were conducted to determine if a small bleed (1 to 2 percent) could substantially improve the static-pressure coefficient. Analysis had shown that the collector pressure could be increased up to 11 psi if the static-pressure recovery were increased from 0.52 to 0.70. Single-channel diffuser data had shown that this target was a high but attainable value.

The total-pressure data measured at the diffuser throat suggested the nature of the boundary layer. The core flow appeared to be T-shaped, spreading across the upper portion of the passage as shown in Figure 220.

This boundary-layer shape was also suggested from schlieren photographs with oil streaks on the side walls, which indicated that secondary flow was bleeding the boundary layer on the suction surface and directing it toward the pressure surface (Section 7.2 of Reference 1).

From these observations, it was expected that 1 set of bleed holes machined in each channel throat near the pressure surface would result in a reduction in throat blockage. For the initial bleed test, an 0.032-inch-diameter hole was drilled in both the front and the rear plates (Figure 221).

CONFIDENTIAL

CONFIDENTIAL

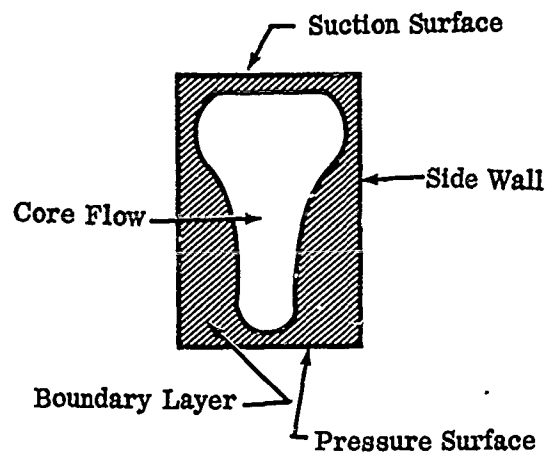


Figure 220. Cross Section of Diffuser-Throat
Core Flow and Boundary Layer.

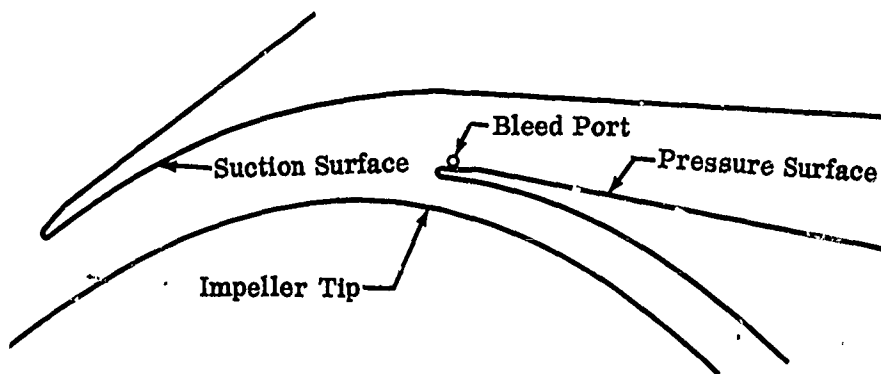


Figure 221. Sketch of Diffuser with 0.032-Inch Bleed Port.

CONFIDENTIAL

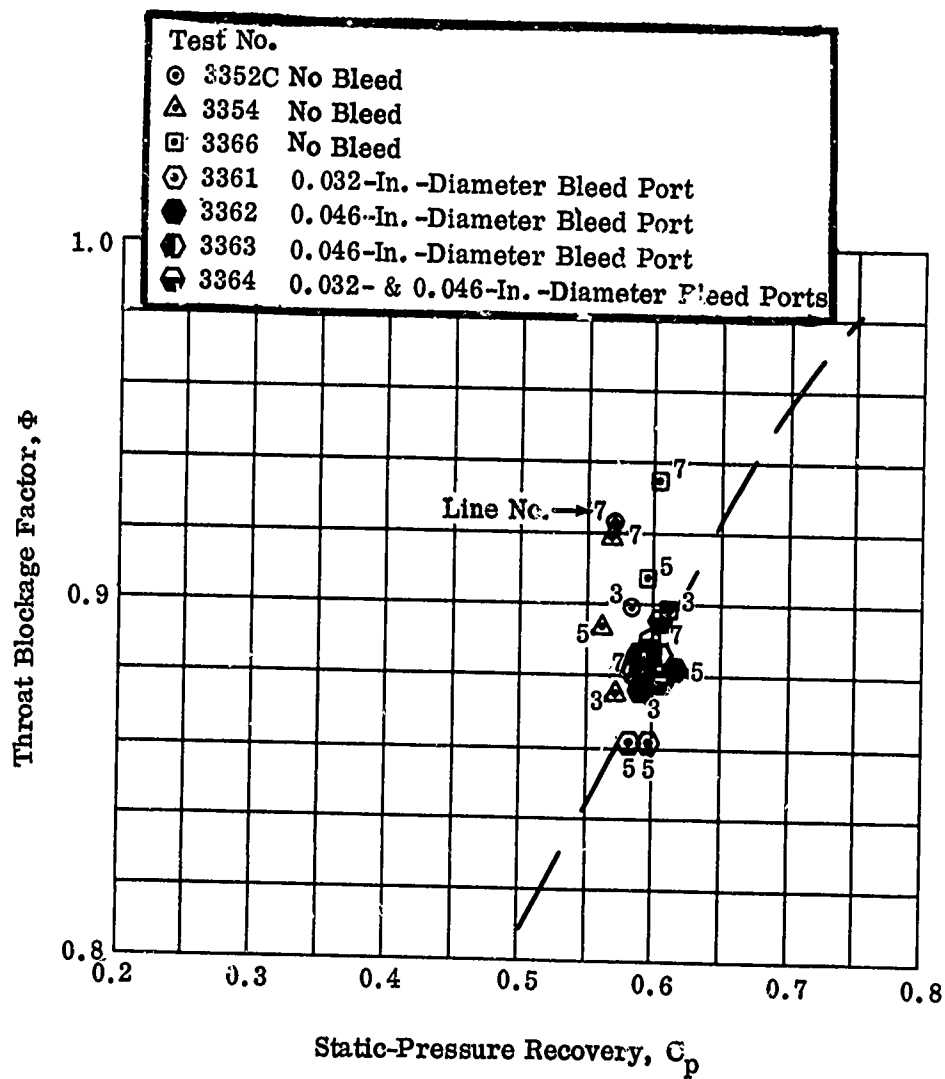


Figure 222. Comparison of Static-Pressure Recovery for Bleed and Non-Bleed Diffuser Tests.

CONFIDENTIAL

If a flow coefficient of 0.6 is assumed, 0.75 percent of the airflow was bled during this test. A comparison of the compressor speed line with and without bleed is shown in Figure 170. A small increase (+1 percent) in pressure ratio was obtained with this bleed modification.

The bleed ports were increased to 0.046 inch diameter in a second test to increase the total bleed to 1.5 percent of the airflow. The compressor pressure ratio was increased by 2 percent over the case without bleed; this was equivalent to a 0.045 increase in static-pressure recovery. The change in throat blockage and the static-pressure recovery of the bleed and non-bleed tests are shown in Figure 222.

Both bleed tests had resulted in an increase of the overall compressor total pressure. A second bleed port was installed in the side walls (as shown in Figure 223) to increase the bleed and further reduce the throat blockage (Test 3364). The results of the test showed that the compressor pressure ratio was again increased (+0.1 atmosphere). A change in the channel geometry (Test 3363) prior to the third bleed test (Test 3364) resulted in a slight improvement in overall compressor pressure ratio, as shown in Figure 171; however, the pressure ratio increase resulting from the additional bleed ports is probably more correctly represented by the dashed curve shown in Figure 224. This test showed the highest pressure ratio obtained thus far with the new impeller and diffuser.

Further external bleed tests were not conducted; however, the results showed that overall compressor performance improvement could be obtained from reduced throat blockage. The total pressure ratio was increased nearly 3 percent because of the estimated 2.7-percent airflow bleed.

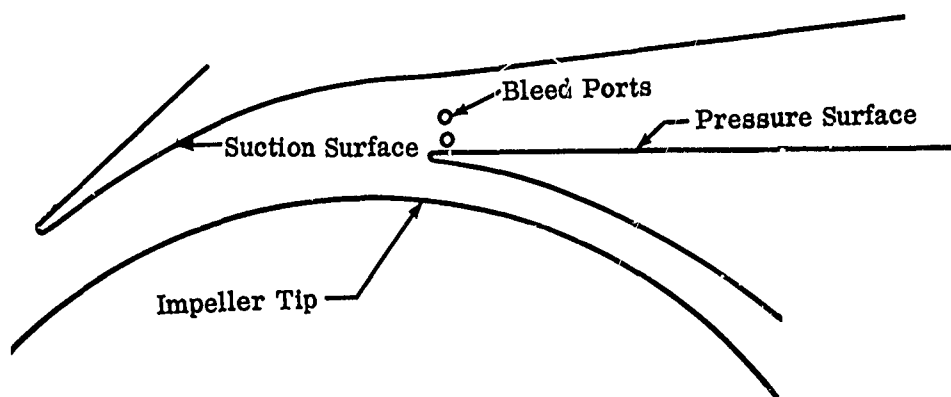


Figure 223. Sketch of Diffuser Showing Location of Second Bleed Port.

CONFIDENTIAL

CONFIDENTIAL

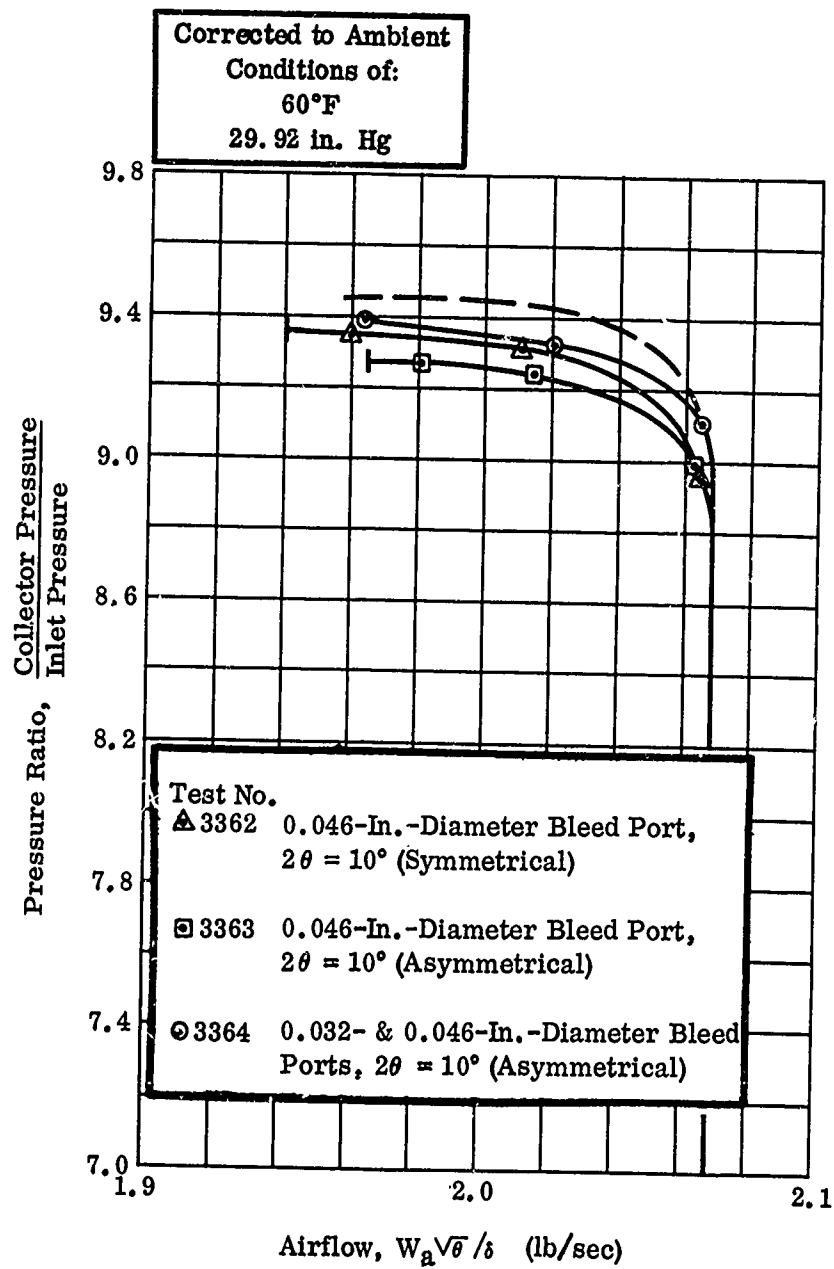


Figure 224. Pressure Ratio Versus Airflow.

CONFIDENTIAL

CONFIDENTIAL

A second effect of the airflow bleed was that the overall compressor temperature rise decreased with bleed. Figure 225 shows the comparison of temperature rise for bleed and non-bleed tests with respect to airflow

It is reasoned that the bleed affects the pressure distribution outside the impeller tip (Appendix III) and reduces the amount of reverse flow, which changes the temperature-rise factor while the slip factor remains a constant. The temperature rise was reduced nearly 1.0 percent for the bleed tests.

The increased pressure ratio and reduced temperature rise resulted in an increase in compressor performance that more than offset the percent of bleed airflow. For example, in a high-performance engine, where turbine cooling is required, it is suggested that this bleed air be used in the cooling process. In a conventional engine cycle, this cooling bleed air to the turbine accounts for a loss in the cycle. Bleed air could be drawn from the diffuser throat and be useful by improving the compressor performance while cooling the turbine. The bleed tests have also provided additional insight into the behavior of diffuser flow.

Examination of the static-pressure recovery with respect to blockage correlation resulting from the throat total-pressure analysis of non-bleed tests shows that

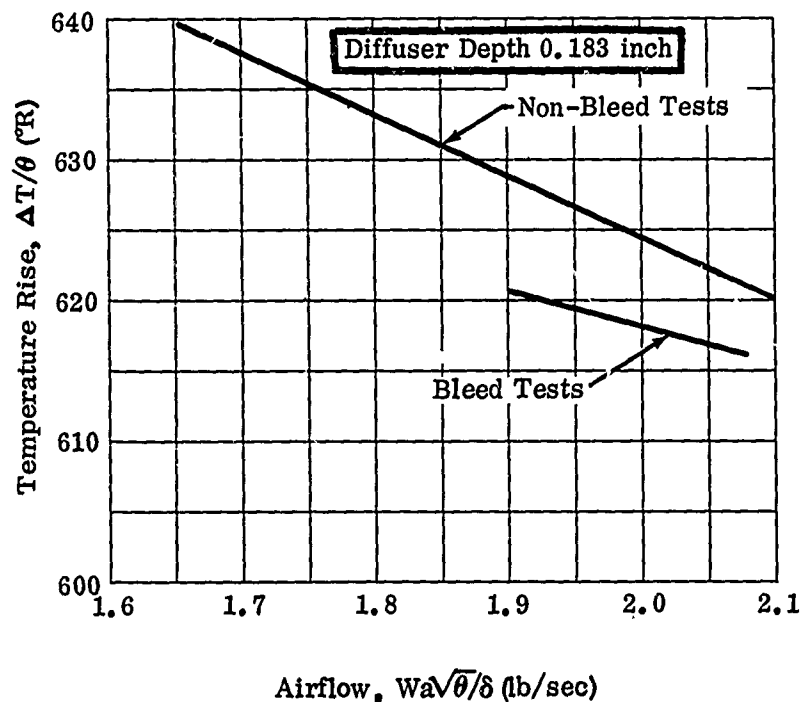


Figure 225. Comparison of Temperature Rise for Bleed and Non-Bleed Tests.

CONFIDENTIAL

the static-pressure recovery is essentially constant for many cases. Several tests are shown in Figure 222. In each case, the static-pressure recovery for line 3 falls on the 2-dimensional channel-diffuser curve and lies above the curve at lines 5 and 7. This trend suggests that the static-pressure recovery did not increase with reduced blockage; this is opposite to the trend shown in data from the 2-dimensional diffuser tests (Appendix XII of Reference 1). It was further noted that all points from the boundary-layer bleed tests fell closely on the 2-dimensional diffuser curve; i. e., for the bleed tests there was no drift toward worse performance on going from line 3 toward line 7, as shown in Figure 222. This difference in static-pressure recovery for the bleed and non-bleed tests suggests that the effect of bleed was to pull line 5 and line 7 points onto the curve on top of the line 3 point. The effect of bleed was significant at line 7 (near maximum airflow) but was not significant at line 3 (near surge); this is the reverse of what would be expected, since the blockage is maximum near surge and the bleed should have been most effective at the maximum blockage point. This difference suggests that the bleed ports may be affecting the lambda shock at the vane leading edge. Figure 226 shows the lambda shock relative to the bleed ports.

Examination of the pressure data shows a large increase in lambda shock strength from surge toward maximum airflow. For example, in Test 3352C at line 3, the recompression $\Delta P = 3$ psi, and at line 7, the $\Delta P = 10$ psi. These pressures near line 7 suggest that the lambda shock may be strong enough to separate the boundary layer on the pressure surface at the beginning of the diverging section. The bleed ports may have thinned the boundary layer after the lambda shock and eliminated the throat separation, which previously was detrimental to static-pressure recovery of the diffuser.

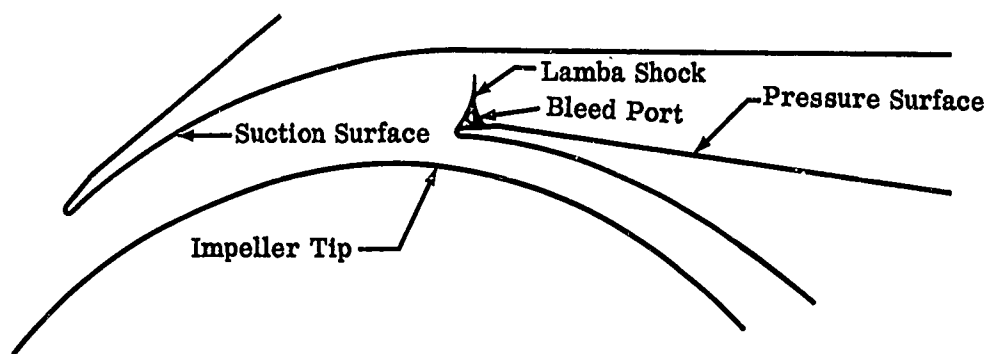


Figure 226. Sketch of Lambda Shock Relative to Bleed Ports.

CONFIDENTIAL

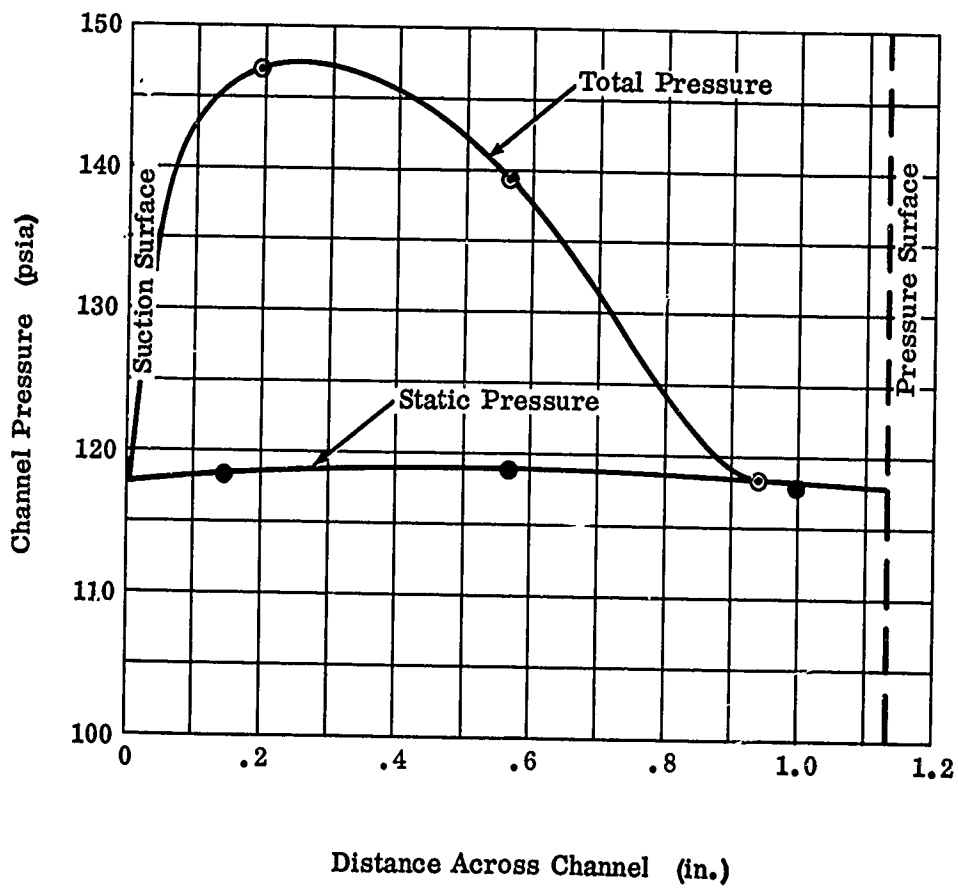
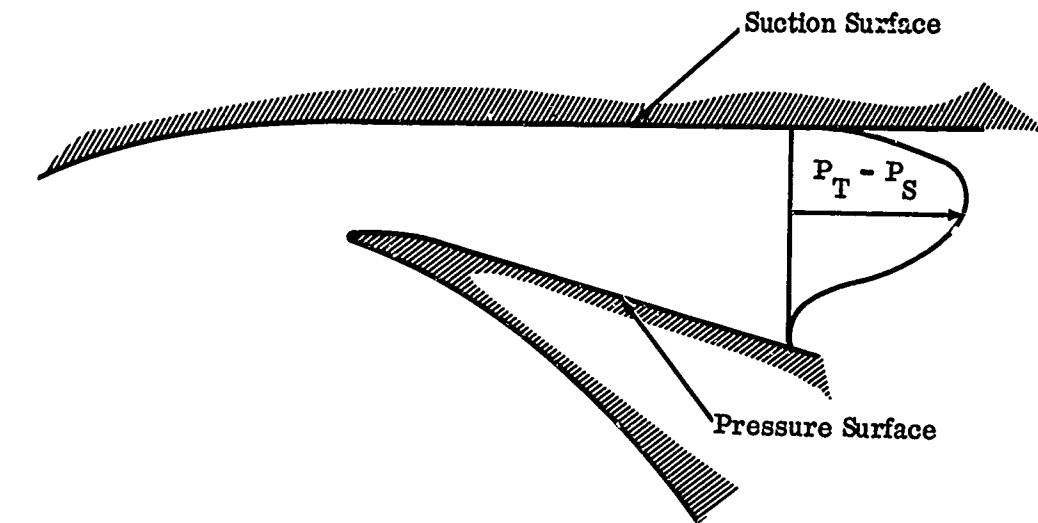


Figure 227. DI-1 Channel Pressures at 2:1 Area Ratio.

CONFIDENTIAL

Total-pressure measurements in the diffuser channel of DI-1 at an area ratio of 2.0 also suggest that the flow is separated near the pressure surface. Note the drop in the total-pressure profile near the pressure surface (see Figure 227). It is unlikely that the bleed ports affected the boundary layer over a large area. However, there was a marked compressor improvement, showing the validity of the bleed tests.

Throat Geometry — As discussed under boundary-layer bleed, the measured total pressure at the throat and the schlieren-oil-trace photographs show that the boundary layer in the diffuser throat is concentrated on the side walls (Figure 401 of Reference 1). The total-pressure profiles in the diffuser throat are shown in Figure 228. These observations suggest that the throat blockage can be reduced by increasing the aspect ratio (depth/height) for a constant throat area.

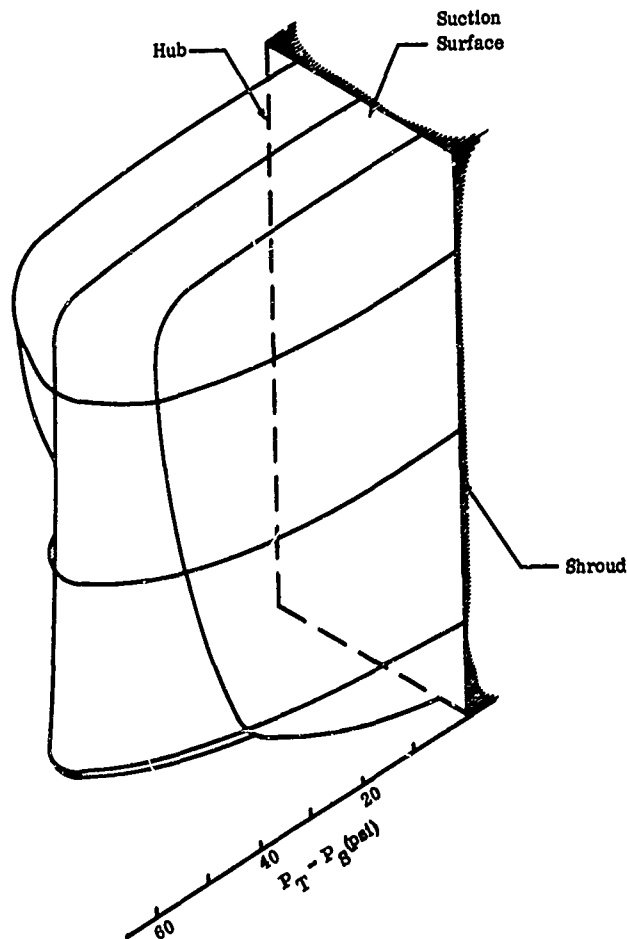


Figure 228. Diffuser-Throat Total-Pressure Profile.

CONFIDENTIAL

The profile is quite steep across the depth of the diffuser and is flat from the suction to the pressure surface along midchannel. With the sharp drop in pressure on the side walls, it is reasonable to assume that the boundary layer is concentrated on these walls, in contrast to the suction surface, which shows a relatively flat total-pressure profile. To evaluate this concept, the diffuser was modified to increase the throat depth and to reduce the throat height. The throat depth was increased from 0.183 to 0.203 inch, which was the maximum change that could be made to match the impeller-tip width. Test results of this modified diffuser are shown in Figures 172 and 173. The pressure ratio was increased 0.1 atmosphere. Figure 172 shows a comparison of the test results for the reference and modified diffusers based on the maximum airflow.

A third test (3369) was run later in the program at a reduced throat depth of 0.158 inch. A comparison of throat blockage for the 3 diffuser aspect ratios (Figure 229) shows that the throat blockage decreased with increased throat depth. The diffuser-throat area was nearly constant in each test. Considering the dependence of static-pressure recovery on throat blockage, Figure 229 suggests that this relationship is not universal but could be correlated with diffuser-throat geometry.

From Reneau (Reference 9), static-pressure-recovery maps were correlated for different values of the parameter $2\delta^*/W$, where W is the throat height in the plane of divergence. Reneau's experiments were 2-dimensional with no boundary layer on the side walls; therefore, it is clear that the $2\delta^*/W$ parameter is valid. In the

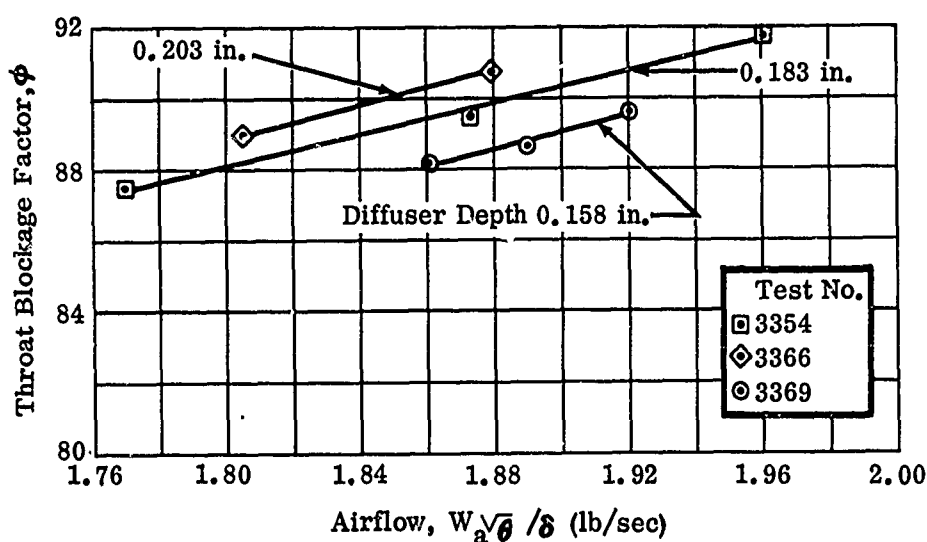


Figure 229. Comparison of Blockage Factor Versus Airflow for Various Diffuser Depths.

CONFIDENTIAL

2-dimensional diffuser for the compressor, however, the boundary layer is on the opposite walls from Reneau's experiment. Therefore, the recovery should be correlated against a parameter $2\delta^*/b$ where b is the diffuser depth (see Figure 416 of Reference 1). However, blockage may be as effective a parameter as $2\delta^*/b$ when correlated with diffuser-throat aspect ratio. It can be shown that blockage varies with aspect ratio (at constant δ^* on all walls) as:

$$B = 2 \frac{\delta^*}{\sqrt{A_t}} \frac{1 + AR}{\sqrt{AR}} \quad (16)$$

where:

- B = blockage
- δ^* = displacement thickness
- A_t = throat area
- AR = aspect ratio = b/W

The blockage varies with respect to aspect ratio, as shown in Figure 230.

This trend suggests that an increased aspect ratio in the region of conventional compressor design (up to 1.0) will reduce throat blockage and improve diffuser recovery for the symmetrical boundary-layer case as well as the case with the boundary layer concentrated on only 2 walls.

A second diffuser performance gain from increasing aspect ratio is also suggested from the 2-dimensional diffuser data presented in Appendix XII of Reference 1. Aspect ratio is plotted against static-pressure recovery for all cases at the same divergence angle ($2\delta = 10$ degrees) and L/W ($L/W = 10$) (Figure 231). Complete curves cannot be shown because data are available at only 2 aspect ratios (0.25 and 5.7).

The low-aspect-ratio data show better recovery than the high-aspect-ratio cases at the same throat blockage. In addition, the recovery must be zero at an aspect ratio of zero. These observations suggest that, for a constant throat blockage and low aspect ratio (probably below 1.0), an increase in aspect ratio will result in a substantial increase in static-pressure recovery and that further increase in aspect ratio will finally result in a decrease in static-pressure recovery.

From the compressor tests run to evaluate throat geometry (Tests 3366 and 3369), it has been shown that best static-pressure recovery occurs at an aspect ratio greater than 0.25. A suggested shape of the complete curve is shown in Figure 232.

CONFIDENTIAL

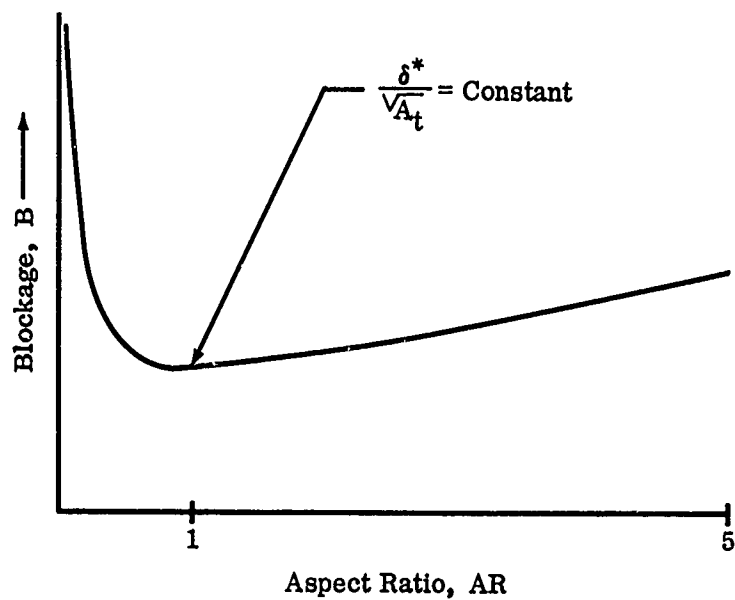


Figure 230. Blockage Versus Aspect Ratio.

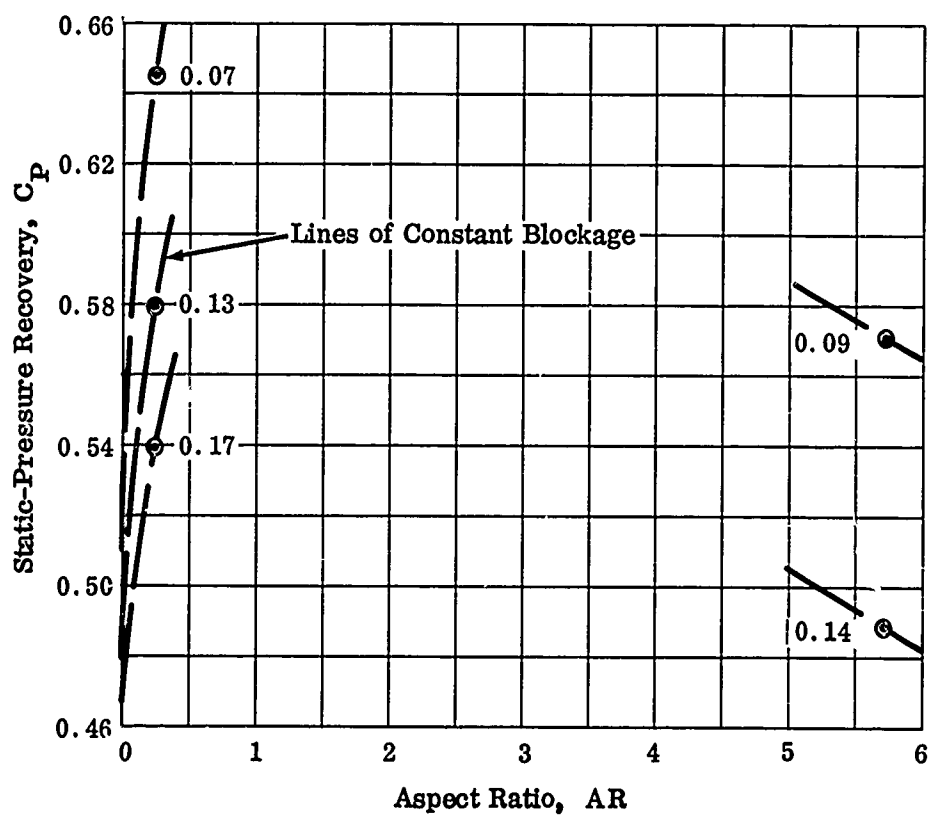


Figure 231. Static-Pressure Recovery Versus Aspect Ratio.

CONFIDENTIAL

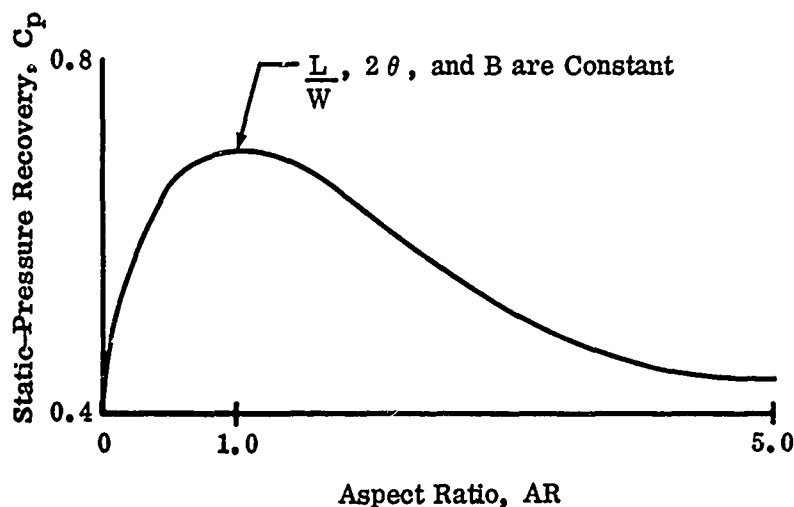


Figure 232. Suggested Trend of Static-Pressure Recovery Versus Aspect Ratio.

This concept is extremely important to the diffuser designer, because the aspect ratio must be selected with great care for best performance. It may also be true that the aspect ratio for best performance will shift with changing blockage and channel geometry.

7.3 OVERALL COMPRESSOR

The impeller and diffusers discussed in the previous sections were tested to obtain overall compressor maps. Figure 175 shows the compressor map with the impeller at the design tip width. Figure 176 shows the compressor map for the narrow-width impeller. The target-pressure ratio of 10:1 was obtained at an efficiency of 72 percent. Somewhat higher efficiency was demonstrated at design speed (50,000 rpm). Airflow range up to 16 percent was demonstrated at pressure ratios between 9.0 and 10.0:1.

The impeller design techniques presented in Reference 1 appear to apply within the scope of tests conducted for this program. The parameter κ seems to provide guidance in designing the nose region of the inducer blading to prevent separation of the flow at the leading edge. The low κ designs, workhorse and RF-2 impellers, had better performance than the RF-1 impeller with higher κ . Transonic inlet Mach numbers are associated with small-diameter, high-pressure-ratio impeller designs. In this Mach number regime, care must be taken to insure that excessive overvelocities do not occur on the suction surface of the blading near the leading edge. If the overvelocity is too large, the flow will

separate at a high Mach number, and large exit mixing losses ensue. One of the overvelocity-prediction methods presented in Section 7.1 of Reference 1 is used to evaluate different blade shapes (nose shape, blade camber, blade thickness) at the design incidence and Mach number. Due to the effects of the adjacent blades and the clearance space, the prediction methods do not provide a true quantitative value for the overvelocity. It is felt, however, that the methods do provide a basis for comparing the relative merits of various designs. Diffusion factor, an axial-rotor loading parameter, should be used in the design of axial inducers. Although little could be done to evaluate the effects of the blade-to-blade Coriolis forces on inducer performance, it is believed that the axial inducer concept presented in Reference 1 should be followed.

For the RF-2 impeller, the test data suggest that the flow separates from the inducer blading at the predicted Mach number. Agreement was also obtained between the calculated and measured impeller pressure ratio. These correlations indicate the validity of the flow model and loss analysis presented in Section 7.1 of Reference 1.

Some additions can be made to the diffuser flow model presented in Reference 1. In particular, the throat shape parameter (aspect ratio) was shown to have an important influence on the diffuser design. Since static-pressure recovery peaks with respect to aspect ratio, the proper selection of aspect ratio can be very influential to the compressor performance. Runstadler's 2-dimensional data also suggest that the peak performance with aspect ratio may shift with changes in divergence angle or L/W . Therefore, attempts to increase aspect ratio (such as an increased number of vanes) must be done with great care. Further basic data would be helpful to the designer to map a complete diffuser operating range.

The static-pressure recovery was again shown to vary with throat blockage; however, the change in blockage for the diffusers tested is not as great as originally predicted from the analysis. The difference in predicted results from the 2 diffuser analyses presented in this report shows the necessity of accurately determining the pressures at the diffuser throat when blockage and static-pressure recovery are to be determined.

CONFIDENTIAL

8.0 (C) CONCLUSIONS (U)

The results of this program have provided essential information for defining means by which to achieve pressure ratios in the range of 10:1 at adiabatic efficiencies of about 80 percent. Although the targeted efficiency was not demonstrated in tests of the overall compressor, several significant milestones were established, producing new understanding of transonic flows in impellers and diffusers. In this regard, the following major conclusion was reached:

There are no known fundamental reasons preventing the development of a high-pressure-ratio centrifugal stage. Pressure ratios of about 10.6:1 were demonstrated at efficiency levels that remained nearly the same as those at lower pressure ratios. In reviewing earlier compressor programs of this type, where large gains in pressure ratio were achieved (notably the modified T60 compressor described in Reference 1), 4 years of concentrated development was required to raise efficiency to the 80 percent goal at a pressure ratio of approximately 6:1. However, prior research, which produced an efficiency of only 73 percent, was necessary as the starting point from which to identify future program details. It is believed that the Army research program described in this report now has advanced to the point where continued effort will produce similarly rewarding results. In addition, the broader understanding of impellers and diffusers which resulted from this program is considered a stronger base for further development than was available in the earlier program.

In reviewing program results, several detailed conclusions can be drawn from the data presented in Sections 6.0 and 7.0 of this report and Reference 1. Each item listed below was considered a questionable or unknown quantity when the program was planned. All are believed to be essential to successful development of high-pressure-ratio single-stage centrifugal compressors.

- 1) An airflow range of up to 15 percent of full flow is possible at pressure ratios between 9 and 10:1. In addition, impeller pressure ratio is nearly constant with changing airflow across a speed line, despite an inducer incidence variation of about 6 degrees from full flow to surge.
- 2) Exit mixing of the jet and wake at the impeller tip contributes the largest share of the overall impeller loss. Flow separation from the suction surface of the impeller will produce jet flow along the pressure surface—the earlier this separation, the larger the wake will be at the exit. It was shown that the resulting loss in total pressure was a function of the exit wake width-to-blade pitch ratio, which is dependent on the amount of relative diffusion which takes place in the impeller up to the point of separation. The separation can be related to inducer-entrance blade shape, Mach number, and flow conditions by a nose-shape parameter, κ , derived from airfoil theories. The value of the airfoil analogy was demonstrated by the design and test of RF-2 discussed in this report.

CONFIDENTIAL

CONFIDENTIAL

- 3) At high-pressure-ratio conditions, an entry shock is located upstream of the diffuser-vane leading edge. Primarily, the increase in static pressure in the diffuser results from a combination of static-pressure rise across the entry shock and through the channel. Little static-pressure rise takes place in the vaneless and semivaneless spaces before the entry shock. The strength of the shock is set by the continuity requirements in the subsonic throat downstream of the entry shock and by the back-pressure in the channel. As the compressor airflow is reduced from maximum airflow toward surge at constant rpm, the shock strength is increased because the diffuser-throat subsonic Mach number is reduced.
- 4) The channel static-pressure recovery is a function of diffuser-throat blockage and aspect ratio. Channel static-pressure recovery increases with reduced diffuser-throat blockage. With increasing aspect ratio and constant throat blockage, static-pressure recovery reaches a maximum and then decreases. Best recovery at constant blockage appears to be a function of diffuser geometry; i.e., L/W and 2θ . For a given number of channels, an increase in design airflow will result in a more favorable aspect ratio than was required for the 2.0 pounds per second selected for this program and will also provide a lower blockage.

The performance of the impeller and diffuser are interrelated. The diffuser width and hence the throat-aspect ratio are dependent upon the impeller-tip width which must be kept small to minimize the impeller-exit mixing loss. If the inducer is designed to extend the separation point toward the exit of the passage, where the relative Mach number is lower, the impeller-tip width can be designed wider while maintaining a constant wake-jet-width ratio and a constant exit mixing loss. The result will be a more favorable throat geometry and a diffuser performance gain.

- 5) There is no subsonic critical Mach number in 2-dimensional channel diffusers, contrary to the literature reviewed. Static-pressure recovery is nearly constant with increasing throat Mach number up to 1.0. Reduction in back pressure causes flow acceleration in the diverging channel, terminating with a shock. However, static-pressure recovery deteriorates rapidly as Mach numbers upstream of the channel shock reach the range of 1.1 to 1.2.
- 6) Boundary-layer bleed at the diffuser throat will increase the static-pressure recovery of the channel, and reduced throat blockage will result. In a high-performance-engine design, it may be possible to use the bleed air for cooling in a high-temperature turbine.

CONFIDENTIAL

9.0 (C) RECOMMENDATIONS (U)

Data from the numerous tests run in this program have shown that the goals, as originally established, can be met with continued research. Further, there are no identifiable fundamental and technical reasons to prevent attainment of the target. Although the efficiency goal of 80 percent was not achieved, the research demonstrated the application of fluid dynamic principles to the design of impellers and diffusers for high-pressure-ratio compressors. On separate runs, overall pressure ratios in excess of 10:1 and airflow ranges of about 15 percent were shown. Both are considered important background from which to devise a plan for continuation of this work. In addition, the detailed studies shown in this report will provide the basis for new investigations. An enlargement of these studies is strongly recommended, with the ultimate goal of incorporating the resulting centrifugal compressor into a small-gas-turbine engine.

9.1 (C) INDUCER INVESTIGATION (U)

The first step in an inducer program must be to continue the investigation of nose shapes and the related effects of inlet Mach number and incidence. The goal of this program should be to increase the amount of possible relative diffusion in the impeller and, therefore, to favorably influence the overall impeller and diffuser performance. A portion of the study should be aimed at establishing best possible diffusion within the geometrical blockage and fluid dynamic limitations, and should be applied to the high subsonic and supersonic Mach number regimes. Available knowledge of transonic wings should be applied as a first analytical step. Analysis should include calculations of boundary-layer growth, the transonic flow field, the influence of shocks, and the final boundary-layer state at the beginning of the subsonic diffusion. The nose-shape parameter κ should be more thoroughly investigated, and inducer tests to evaluate analytical predictions should be conducted. Combined with this investigation, studies should be made to determine a useful method for predicting the point of separation in the impeller. A program of this scope should result in a better understanding of the limitations and potentials of the centrifugal compressor as applied to both high- and low-pressure-ratio designs.

9.2 (C) IMPELLER-EXIT MIXING (U)

The impeller-exit mixing loss analysis used in this program results from a comprehensive theory of the loss makeup. However, more experimental confirmation is necessary to test the theory critically. An investigation of this loss analysis, with an impeller designed to vary the discharge pattern, is recommended. Total-pressure probes installed to measure the relative pressure combined with hot wire instruments in the vaneless space should provide a good view of the impeller-exit conditions. Discharge patterns in the impeller may be varied by using screens installed at the impeller tip and by changing the impeller-tip width. If the impeller wheel speeds are excessive for experimental work, the

impeller could be designed for a closed-loop Freon system which would provide high Mach number conditions at low wheel speeds.

9.3 (C) DIFFUSER (U)

It is recommended that investigations be continued to determine ways to reduce the diffuser-throat blockage. As shown from the experiments of this program, the static-pressure recovery of the diffuser channel varies directly with the diffuser-throat blockage. Further effort should be directed toward the understanding of the effects of diffuser-throat geometry and channel geometry on the diffuser-throat blockage. The throat geometry and blockage are also related to the impeller-exit vaneless space geometry; therefore, this investigation might be combined with the impeller-exit mixing studies.

Further effort should be directed toward single-channel diffuser tests to obtain more basic data in the Mach number region of interest. These data should be correlated with a diffuser aspect ratio and blockage or a parameter such as $2\delta^*/b$ in a manner similar to Reneau's incompressible diffuser studies but with the boundary layer in the plane of divergence rather than on the diverging walls.

9.4 (C) CASCADE DIFFUSER (U)

This program was primarily directed toward investigation of channel-type diffusers. It is recommended that a study be conducted to evaluate cascade diffusers at similar Mach number levels. This type of diffuser has shown promise at subsonic entrance Mach numbers; however, no work was found in the literature for cascade diffusers at supersonic entrance Mach numbers. Limited cascade tests were conducted at entrance Mach number levels up to 1.3 during this program; however, a thorough evaluation of the cascade was not conducted.

(U) REFERENCES

- 1 Element Design and Development of Small Centrifugal Compressor, USAAVLABS Technical Report 67-30, US Army Aviation Materiel Laboratories, Fort Eustis, Virginia, August 1967.
- 2 Pearcey, H.H., "Shock-Induced Separation and Its Prevention by Design and Boundary Layer Control", Boundary Layer and Flow Control, Edited by Lachman, G.V., Volume 2, Pergamon Press, New York, New York, 1961.
- 3 Stahler, Alfred F., The Slip Factor, ASME 64 GTP-1, 1963.
- 4 Wiesner, Frank J., A Review of Slip Factors for Centrifugal Impellers, ASME 66 WA/FE-18, 1967.
- 5 Dean, R.C., and Senoo, Y., "Rotating Wakes in Vaneless Diffusers", Journal of Basic Engineering, Volume 82, Series D, September 1960.
- 6 Neumann, E.P., and Lustwerk, F., "Supersonic Diffusers for Wind Tunnels", Journal of Applied Mechanics, June 1949.
- 7 Johnston, J.P., and Dean, R.C., "Losses in Vaneless Diffusers of Centrifugal Compressors and Pumps", Journal of Basic Engineering, Volume 87, Series D, 1965.
- 8 Shapiro, Ascher H., The Dynamics and Thermodynamics of Compressible Fluid Flow, Volumes I and II, The Rolland Press Company, New York, New York, 1953.
- 9 Reneau, L.R., Johnston, J.P., and Kline, S.J., Performance and Design of Straight, Two-Dimensional Diffusers, Thermosciences Division Report No. PD-8, Stanford, California, September 1964.
- 10 Roark, R.J., Formulas for Stress and Strain, McGraw-Hill Book Company, New York, New York, 1954.

(U) APPENDIX I
IMPELLER STRESS AND VIBRATION ANALYSIS

Analysis of the RF-2 inducer-impeller showed that the design is satisfactory for operation within the proposed test range (page 315). If operation outside this range for prolonged periods will be necessary, a bench test to check the accuracy of the blade frequencies shown in Figure 238 is recommended. In this case, special attention should be given to vibratory conditions around 41,000 and 52,500 rpm.

In addition to the usual stress and vibration analyses outlined in Appendix II of Reference 1, a Boeing-developed triaxial stress and deflection program was used. The program employs a finite element idealization of the impeller blade and disk, in conjunction with the direct-stiffness method, to determine the 3-dimensional elastic deflections and stresses. The results provide design information which is essential to the optimization of bore-pilot length and position. Running clearances for the blade may also be estimated from the deflections obtained.

The results in Figure 243 show Mises-Hencky stresses which have been derived from the triaxial-stress distribution according to the following formula:

$$S_{M-H} = 0.707 \sqrt{(\sigma_x - \sigma_r)^2 + (\sigma_r - \sigma_\theta)^2 + (\sigma_\theta - \sigma_x)^2 + 3\tau_{xr}^2} \quad (17)$$

where:

- σ_x = axial normal stress (psi)
- σ_r = radial normal stress (psi)
- σ_θ = tangential normal stress (psi)
- τ_{xr} = shear stress in the x-r plane (psi)

The stresses were calculated at the centroid of a finite element in the cylindrical-coordinate system as shown in Figure 233.

The stresses described above and the deflections shown in Figure 244 were based on the assumption that the material has remained elastic. It was necessary to modify this assumption after the part was proof-spun, based on results of previous tests with similar impellers. Proof-spinning induces a considerable compressive prestress in the bore of an impeller, and subsequent running of the impeller at design speed does not produce the same stress distribution. The effect is to reduce the bore stresses shown in Figure 243 by an amount

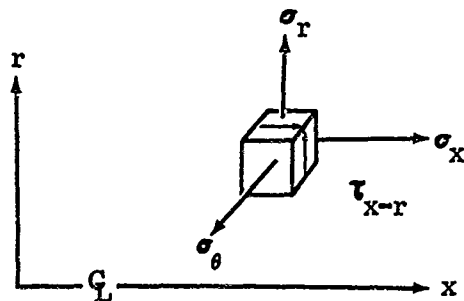


Figure 233. Coordinate System for Triaxial-Stress and Deflection Analysis.

proportional to the compressive prestress. Because the prestress, in effect, increases the elastic range of the impeller, the predicted operating deflections were expected to be quite accurate.

The calculated minimum safety factors for steady-state operation at 50,000 rpm and an impeller inlet temperature of 60°F are as follows:

- 1) Blade safety factor is 1.21 to minimum 0.2-percent yield stress (including $\pm 12,000$ -psi vibratory stress).
- 2) Disk safety factors are 1.75 to minimum 0.2-percent yield stress and 1.97 to minimum ultimate stress.

The calculated minimum safety factors for momentary operation at 55,000 rpm (10-percent overspeed) and an impeller inlet temperature of 60°F are as follows:

- 1) Blade safety factor is 1.28 to minimum 0.2-percent yield stress (not including the above $\pm 12,000$ -psi vibratory stress).
- 2) Disk safety factors are 1.45 to minimum 0.2-percent yield stress and 1.63 to minimum ultimate stress.

The weight of the inducer-impeller is 7.64 pounds, and the mass moment of inertia is 0.106 lb-in.-sec².

Figures 234 through 244 present the results of stress and vibration analyses for the P.F-2 inducer-impeller.

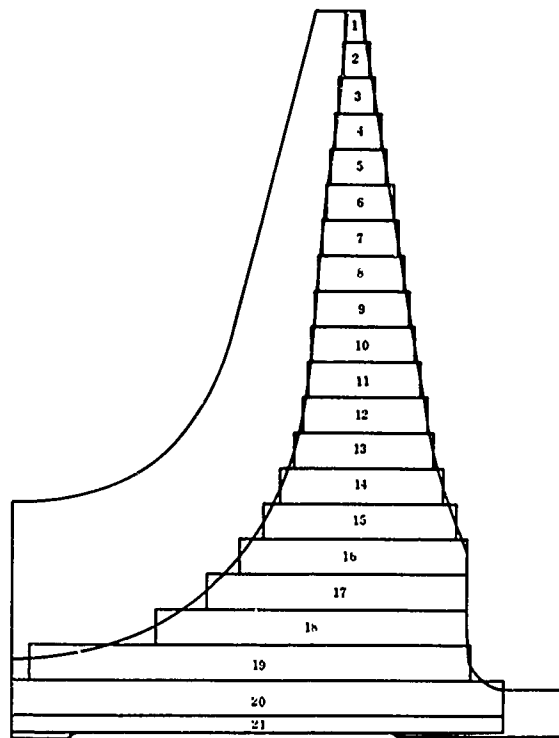


Figure 234. Disk and Blade Profile of RF-2 Impeller.

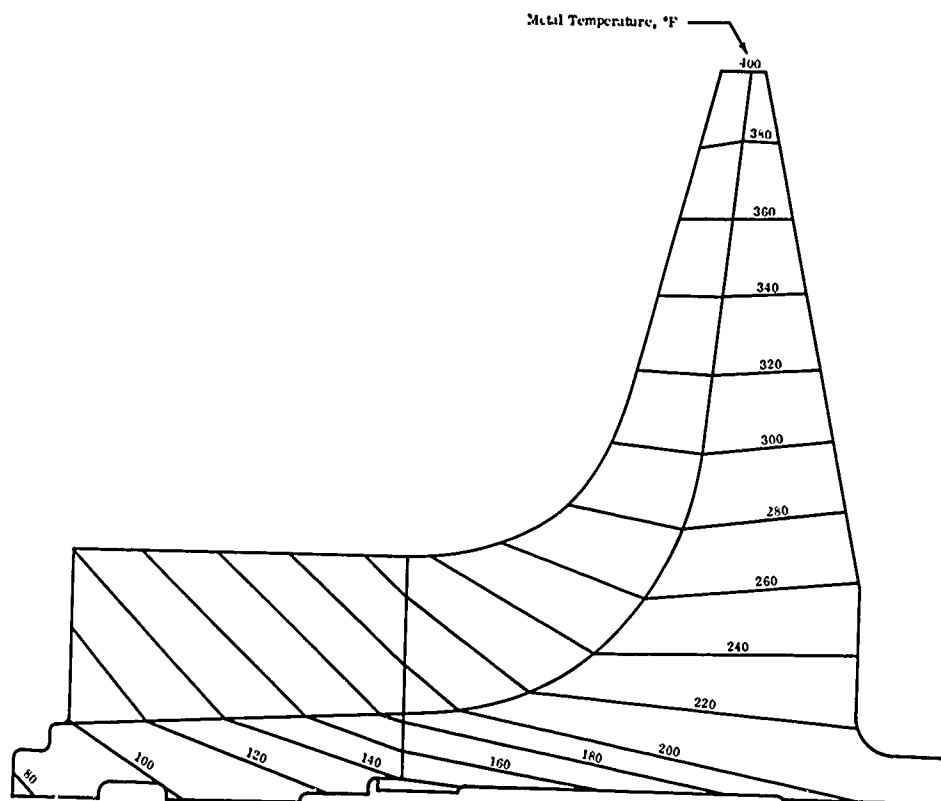


Figure 235. Temperature Distribution of RF-2 Inducer-Impeller.

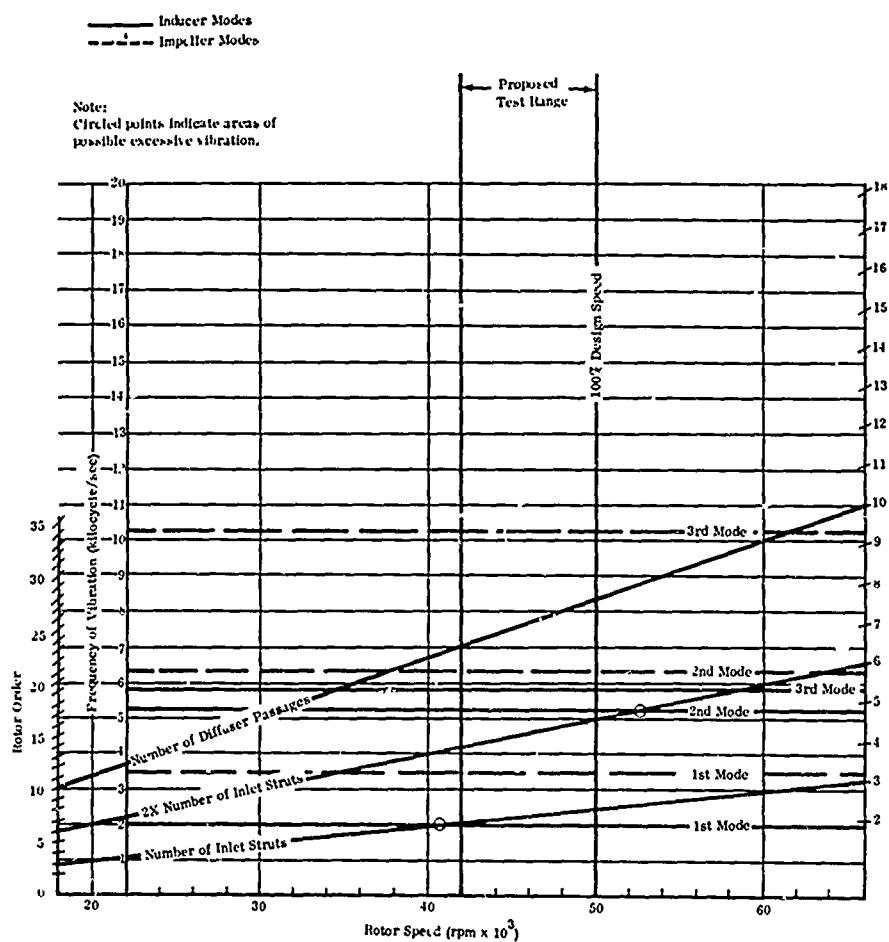


Figure 238. Campbell Diagram for RF-2.

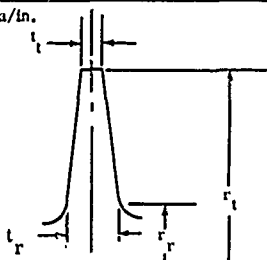
Radial Flow Blade Root Stress, Force/in., Weight/in., and Mass Moment of Inertia/in.									
Material: Titanium, 6Al-4V Speed, N = 50,000 rpm Density, $\gamma = 0.160 \text{ lb/in.}^3$									
									
Blade Station No.			1	7	12	14	18	20	22
Computer Input									
1	r_t	in.	1.800	1.800	1.800	1.839	2.711	4.316	4.570
2	r_r	in.	0.813	0.871	0.918	0.958	1.431	2.313	4.070
3	t_t	in.	0.0445	0.0346	0.020	0.030	0.030	0.030	0.0454
4	t_r	in.	0.0634	0.0576	0.055	0.055	0.055	0.055	0.055
Computer Output									
1	F'	lb/in.	773	631	485	577	1,240	3,110	1,230
2	S_{root}	lb/in. ²	12,200	11,000	8,820	10,500	22,600	56,600	22,400
3	$I' \times 10^4$	$\frac{\text{lb-in.}^2 \cdot \text{sec}}{\text{in.}}$	0.378	0.311	0.237	0.295	0.939	3.76	1.94
4	$W' \times 10^2$	lb/in.	0.852	0.685	0.529	0.599	0.870	1.36	0.102

Figure 239. Blade Stress Calculations for RF-2.

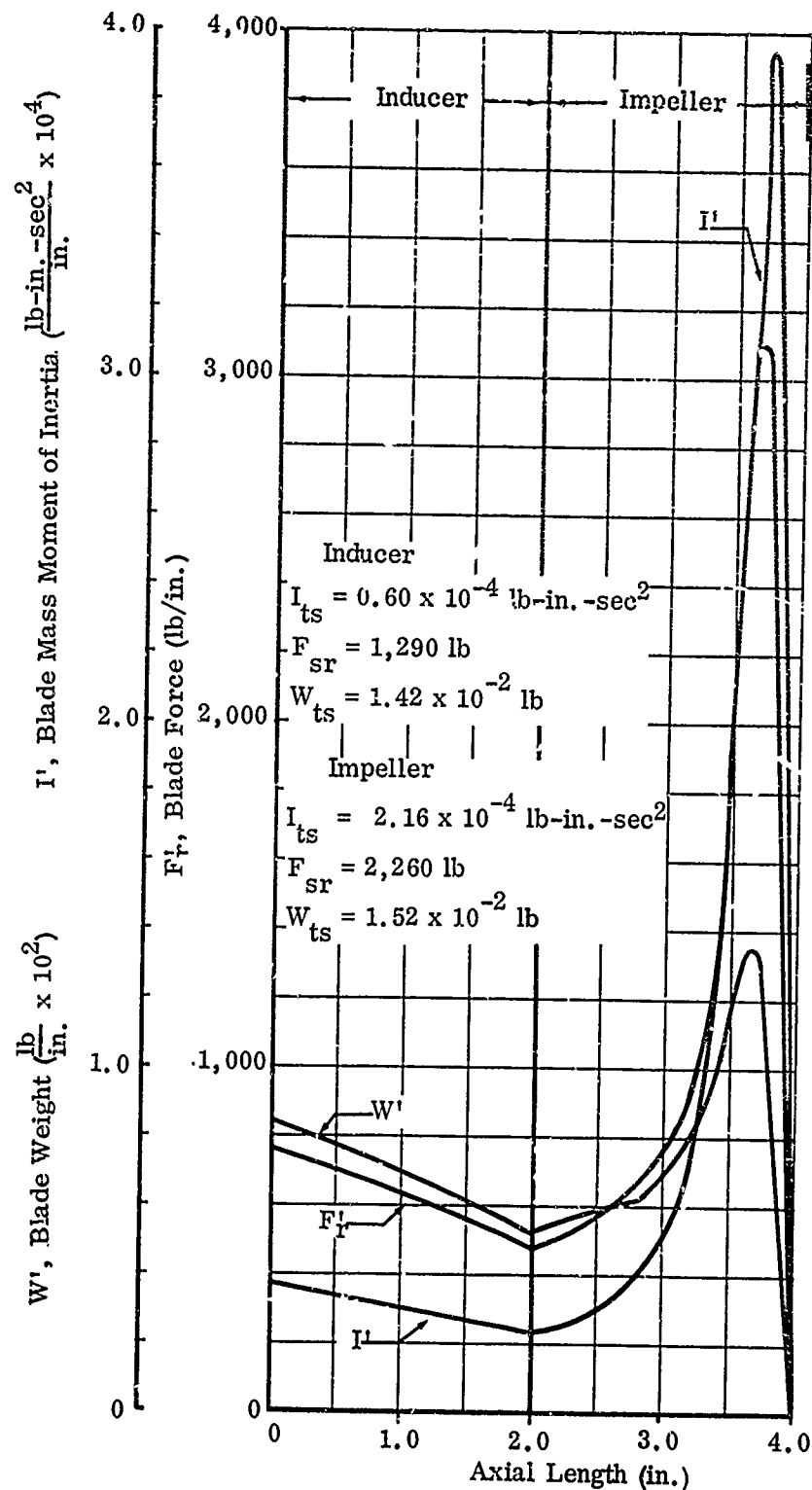


Figure 240. RF-2 Impeller-Blade Force, Weight, and Inertia.

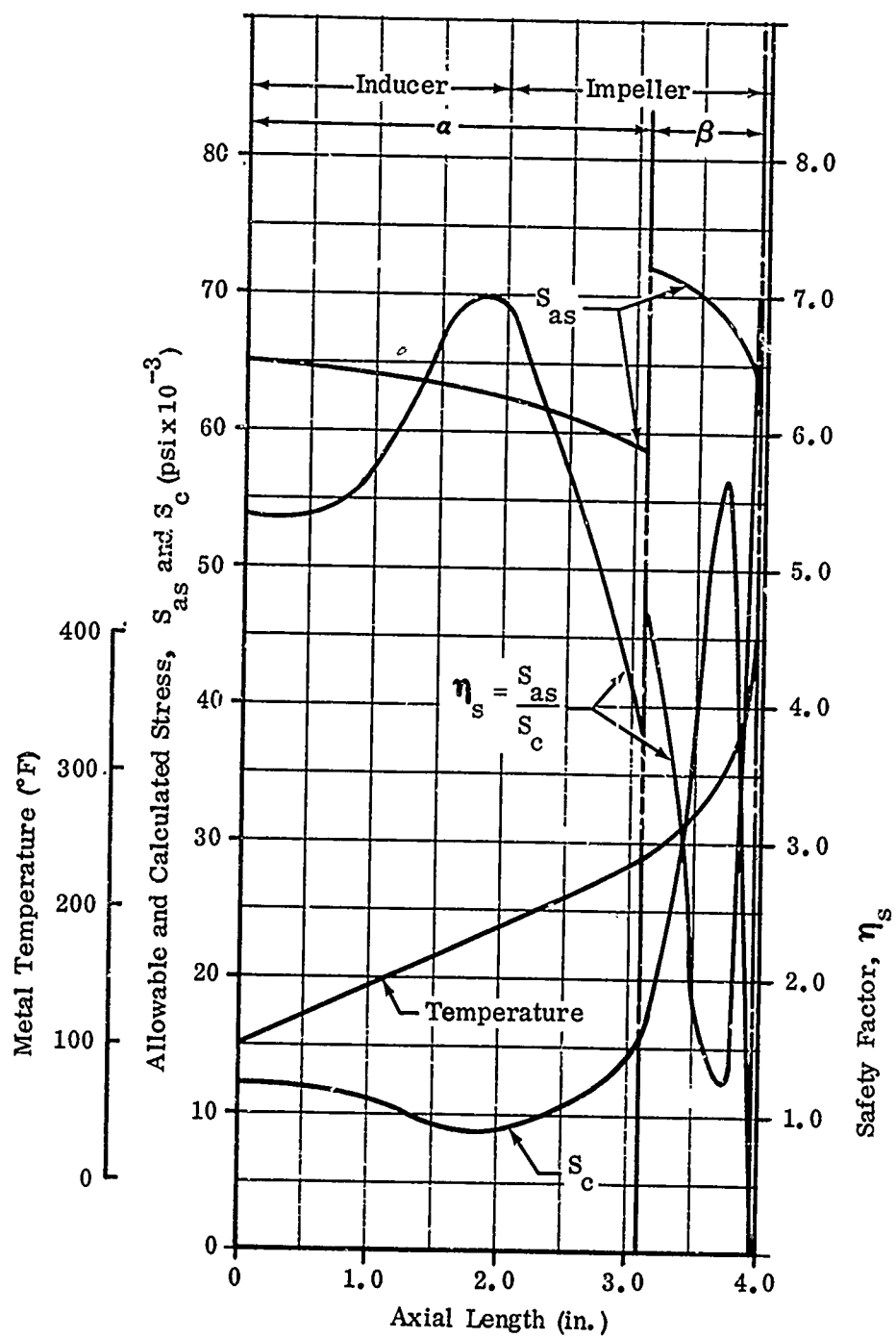


Figure 241. Blade-Root Stress, Temperature, and Safety Factor for RF-2.

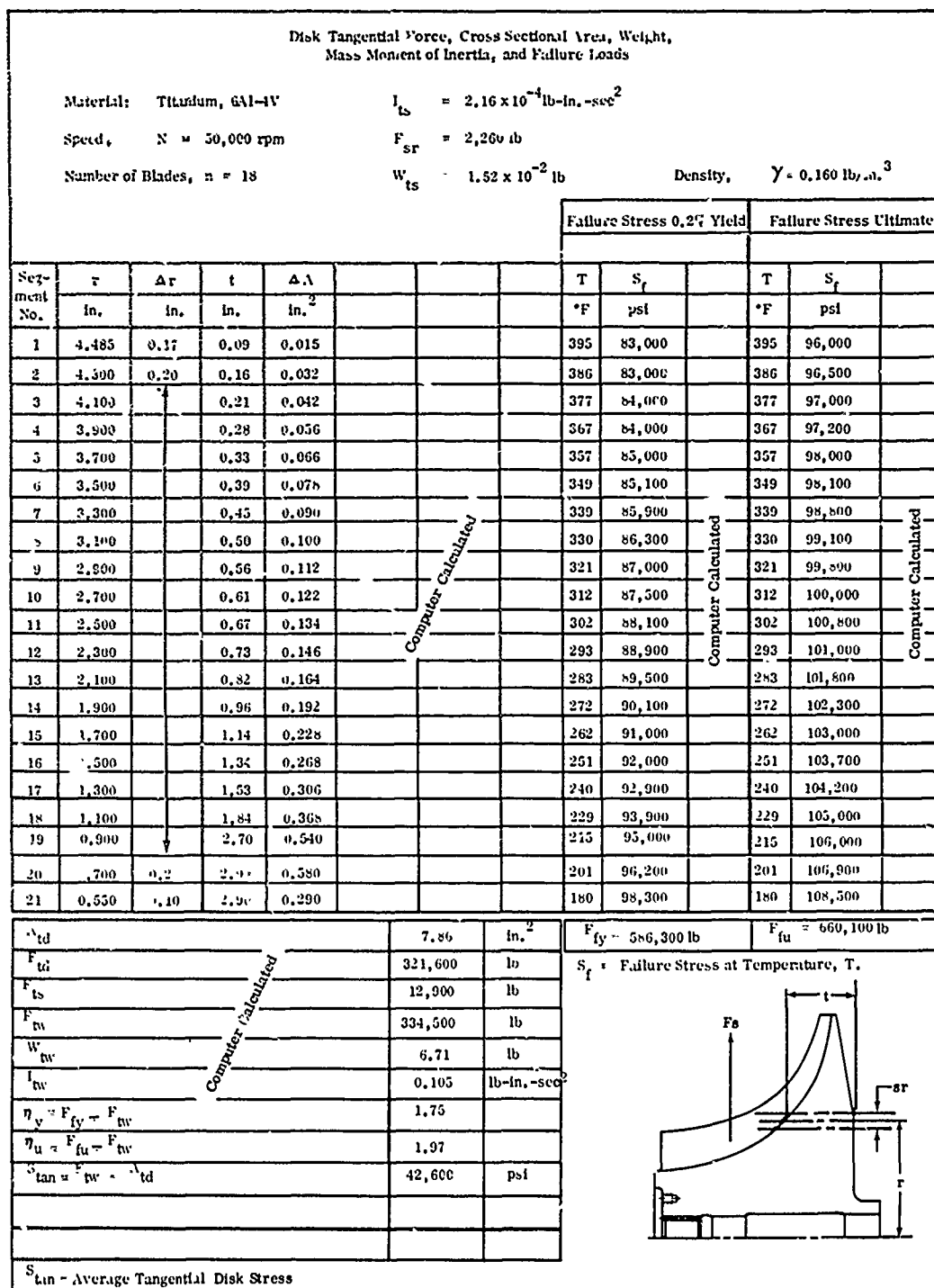


Figure 242. Disk Calculations for RF-2 Impeller.

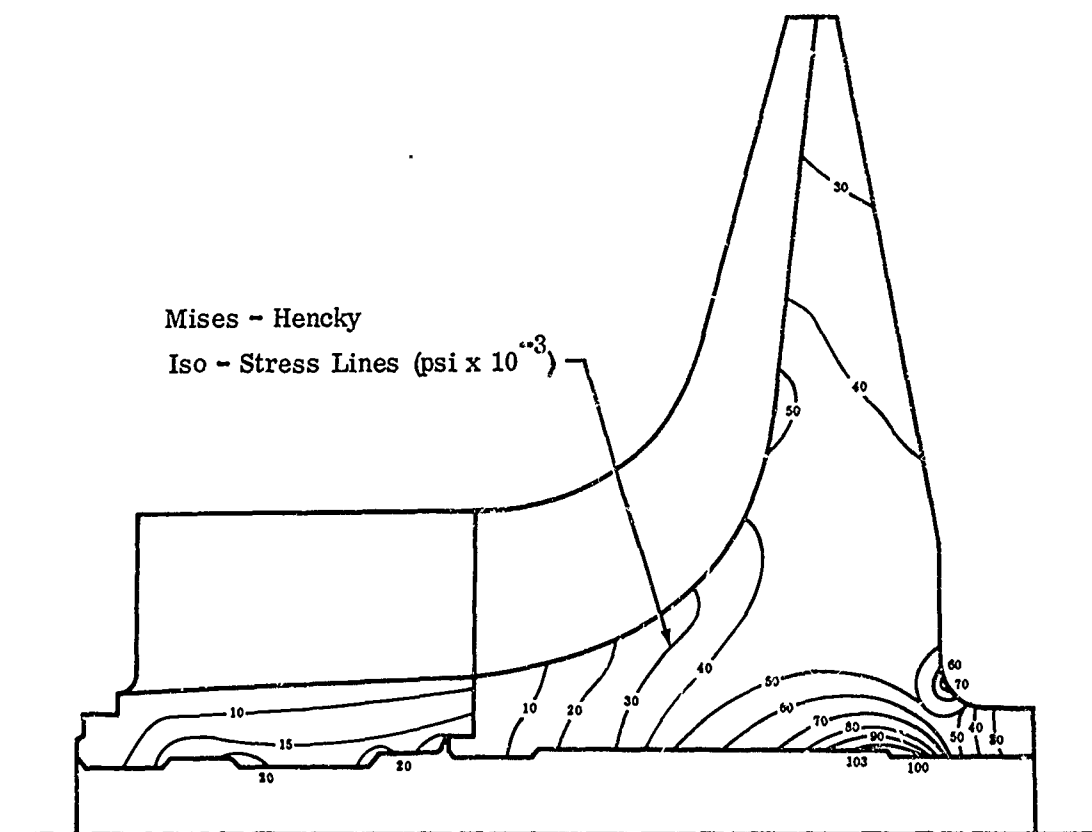


Figure 243. Predicted Impeller Disk Stress Distribution Before Proof-Spin.

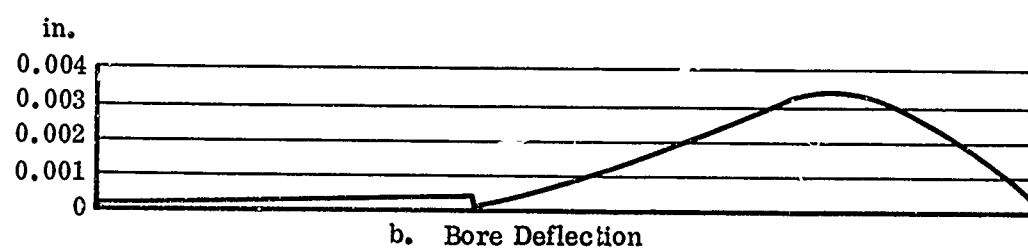
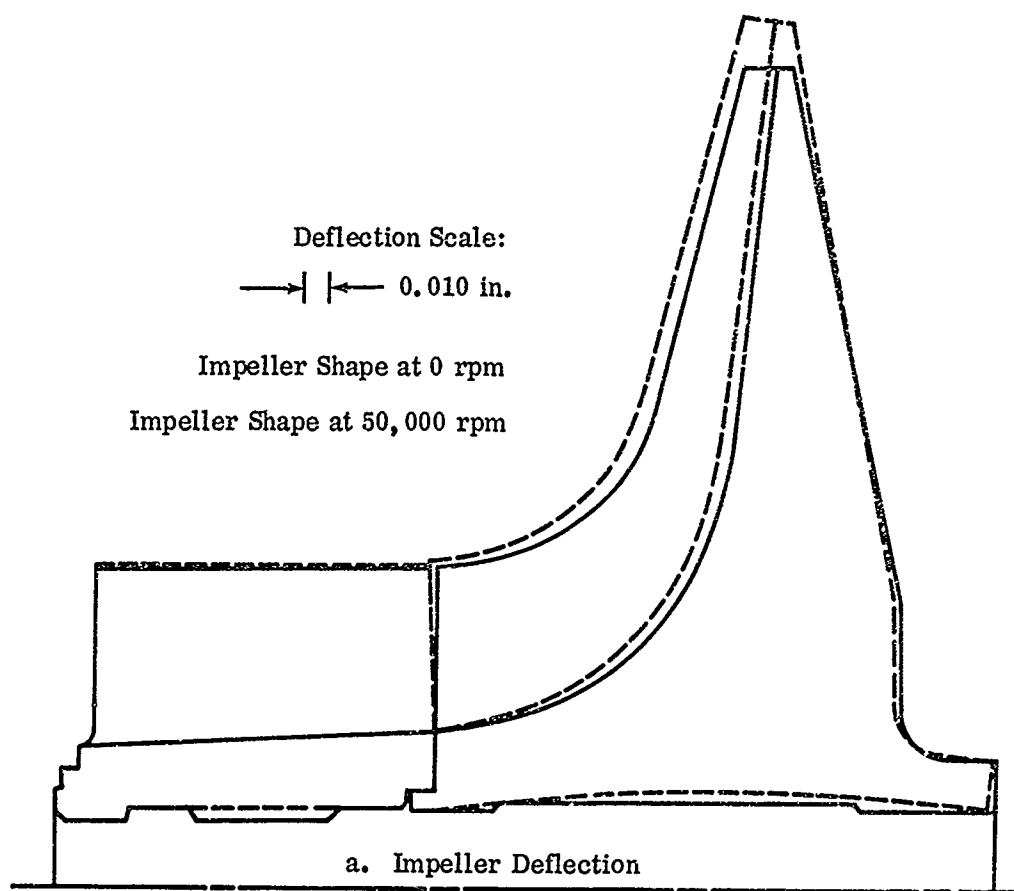


Figure 244. Predicted Impeller Deflection Before Proof-Spin.

(U) APPENDIX II
MECHANICAL DESIGN ANALYSIS

1.0 INTRODUCTION

A modification to the diffuser test rig was required to evaluate a 2-piece impeller-inducer rotor. The new impeller-inducer design required a new inlet, shroud, and diffuser for the diffuser test rig. This appendix presents the design analysis for this test-rig modification.

2.0 DIFFUSER TEST SECTION

The design of the 2-piece impeller test rig was an adaptation of the diffuser test rig. The rotor system was identical to the diffuser test rig (Reference 1) except for a longer and lighter weight impeller. The length of the RF-2 impeller is 4.8 inches compared to the 4.2-inch length of the workhorse impeller. The weight of the RF-2 impeller is 7.46 pounds, while the workhorse impeller weighed 13.0 pounds. The maximum speed requirement remained at 55,000 rpm. Design operating temperatures ranged from ambient at the inlet to 750°F at the diffuser exit. The unit was designed to operate at various back pressures and at a number of constant-speed increments from 33,000 through 55,000 rpm. Instrumentation was provided for measurement of static and total pressures and total temperatures. The schlieren window installation was redesigned for the RF-2 test rig. The windows were never installed, however, since the schlieren system was not utilized for the tests covered by this report.

The configuration was a cantilevered rotor system with the shaft passing through the impeller. All bearing supports were flexible to provide versatility in controlling the critical speeds to be encountered. Thrust loads from the high pressure at the impeller backface were counteracted by a balance disk on the opposite end of the shaft from the impeller.

2.1 BEARING SYSTEM

The rotor system was designed as a stiff-shaft assembly, supported by 2 hydrodynamic floating-sleeve bearings. A titanium impeller was precision fitted to the shaft. In a similar manner, a thrust-balance disk was attached to the aft or coupling end of the shaft. Thrust load was carried in both the forward and aft directions by hydrodynamic slipper bearings. A damped, resilient support for the forward radial bearing was incorporated during the previously reported operational development of the unit to accommodate radial loads caused by shaft vibration. The reverse-thrust slipper bearing was capable of carrying both radial and thrust loads in a 3-bearing rotor system. Except for the new impeller, the rotor system is identical to the diffuser rig rotor system shown in Figure 54 of Volume II of Reference 1.

Hydrodynamic full-floating journal bearings were used as the main support for the rotor system. The design and operating characteristics of the full-floating journal bearings are discussed in Appendix III of Reference 1.

2.2 ROTOR DYNAMICS ANALYSIS

As with analyses of the previous configurations, the critical speed of synchronous-whirl and the respective mode shapes were determined using a mathematical model consisting of 10 mass points and 8 coincident hinged joints with rotational springs.

The results of the rotor analysis, showing variation in the critical speeds as a function of bearing stiffness, T_n , are represented in Figure 245 with the corresponding mode shapes shown in Figure 246. The first and second critical speeds were noted to be essentially non-bending modes at K values up to 100,000 pounds per inch and to be at speeds below 20,000 rpm. Operational experience with the previous diffuser test rig indicated that these modes were not troublesome and that the shaft displacement resulting from them was easily accommodated by the clearance of the journal bearings. The third critical, however, was the first bending mode and was noted to occur at 53,000 to 60,000 rpm for the expected bearing-system stiffness. This calculated critical speed was about 100 rpm higher than the previous diffuser test rig rotor. The third critical speed, therefore, was considered to be unchanged by the new 2-piece configuration, and the modified rotor system was projected to have the same dynamic-operating characteristics as the previous diffuser test rig.

2.3 DIFFUSER AND COLLECTOR BOLT STRESS

The bolt stress for the diffuser clamping bolts was calculated for a maximum pressure of 145 psig on the total area of the diffuser plates. This assumption was for the case of collector pressure applied over the full area between the diffuser plates, including the diffuser islands.

Separating force:

$$\begin{aligned} P &= pA = 145 (r_2^2 - r_1^2) \pi \\ &= 145 [(12.5)^2 - (1.8)^2] 3.14 = 69,500 \text{ lb} \end{aligned} \quad (18)$$

Load per bolt:

$$P/\text{Bolt} = \frac{69,500}{30} = 2,300 \text{ lb}$$

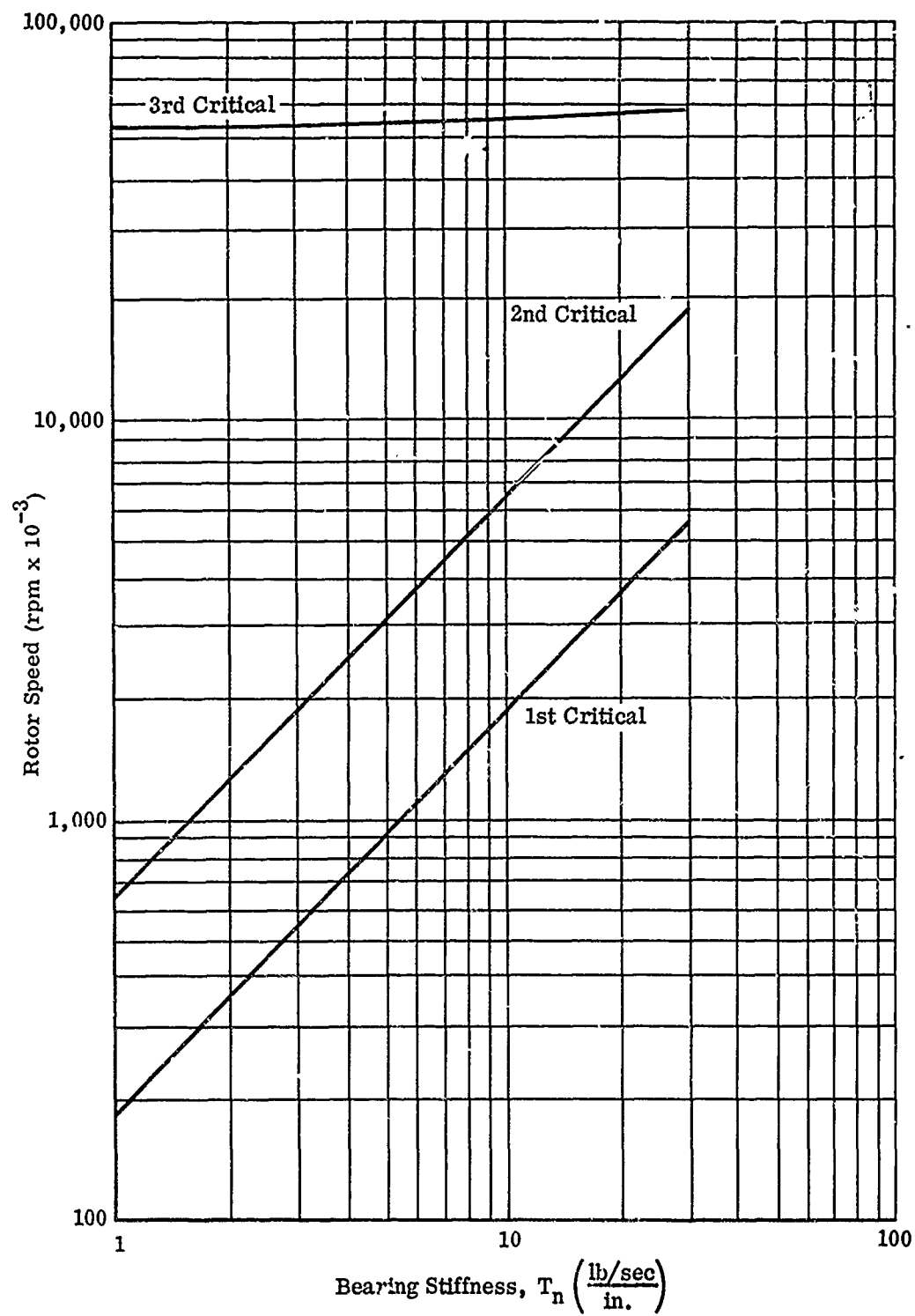
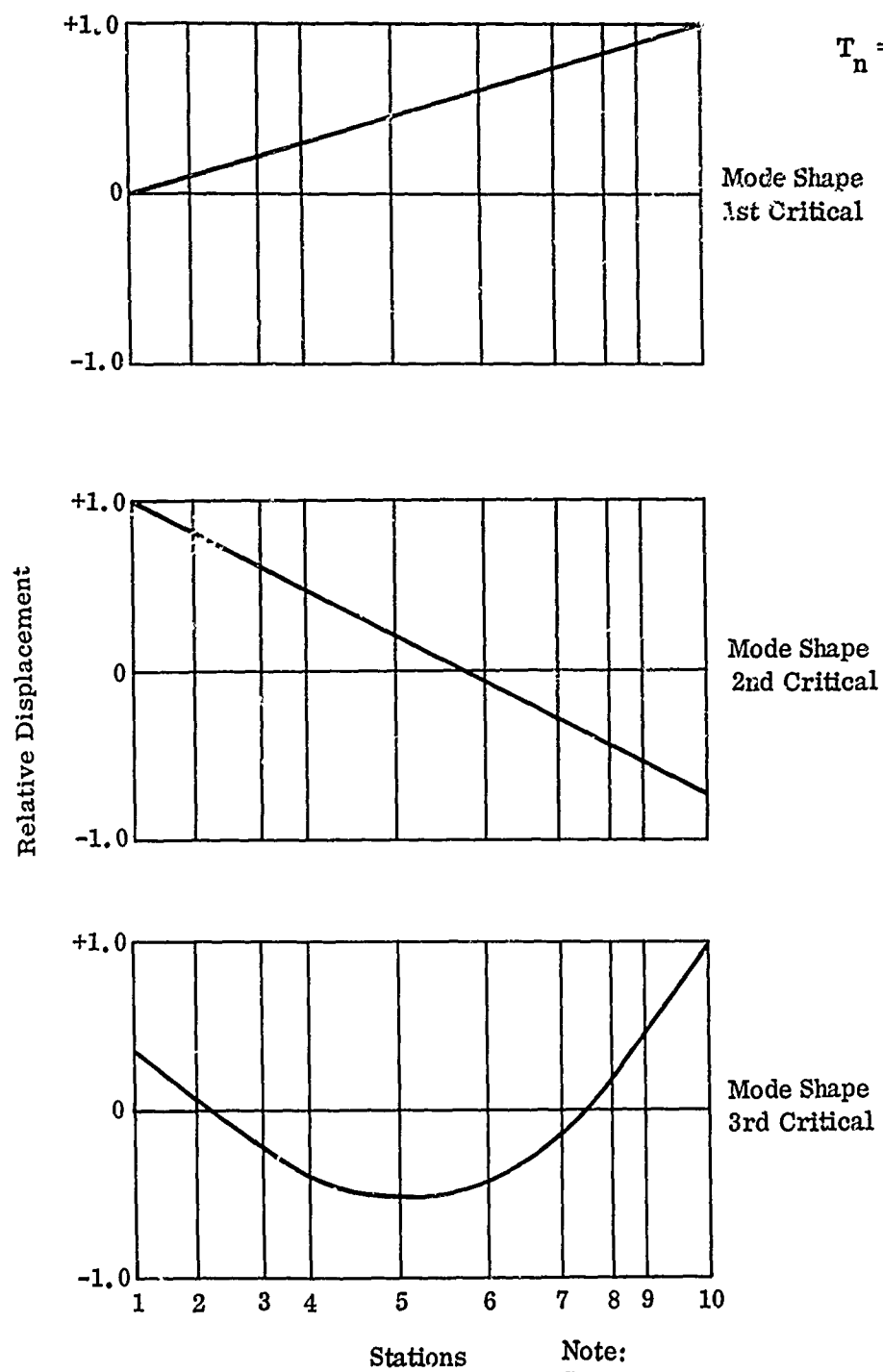


Figure 245. Bearing Stiffness Versus Rotor Speed.



Note:
See Reference 1 (Section 2.4 and
Appendix III) for station locations.

Figure 246. Shaft Mode Shapes.

Bolt stress for 1/4-inch bolts:

$$\sigma = \frac{P}{A} = \frac{2300}{\pi D^2} = \frac{2300}{0.0371} = 62,000 \text{ psi} \quad (19)$$

where σ is the average stress for 30 bolts.

For the case of 145 psig pressure applied to only the diffuser passages and shroud annulus areas:

$$\begin{aligned} \text{Total area} &= \pi \left[r_2^2 - r_1^2 \right] + (\text{number of passages}) (\text{area per passage}) \\ &= \pi \left[(5.1)^2 - (1.8)^2 \right] + 10 \left(\frac{2.0}{2} \right) (7.25) \\ &= 71.5 + 72.5 = 144 \text{ in.}^2 \end{aligned} \quad (20)$$

Separating force:

$$P = pA = 145 (144) = 20,800 \text{ lb} \quad (18)$$

Bolt stress:

$$\sigma = \frac{20,800}{30(0.0371)} = 19,000 \text{ psi}$$

where σ is the average stress for 30 bolts.

The collector skin stress and bolt stress were also calculated for 145 psig internal pressure. The dimensional configuration is shown in Figure 247.

From Reference 10 (page 224, case 20), the skin stress at Point A is:

$$\sigma_A = \frac{pb}{t} \left(\frac{2a-b}{2a-2b} \right) \quad (21)$$

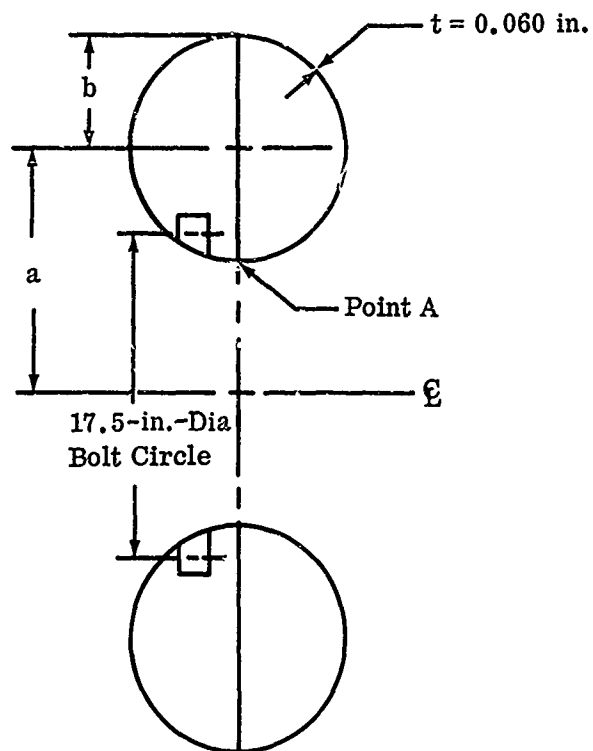


Figure 247. Collector Configuration for Stress Calculations.

where:

$$a = 10.8 \text{ in.}$$

$$b = 2.0 \text{ in.}$$

$$t = 0.060 \text{ in.}$$

$$p = 145 \text{ psi}$$

$$\sigma_A = \frac{145 (2.0)}{0.060} \left[\frac{21.6 - 2.0}{21.6 - 4.0} \right]$$

$$\sigma_A = \frac{145 (2.0)}{0.060} \left[\frac{19.6}{17.6} \right] = 5,460 \text{ psi}$$

The bolt stress for 10 bolts restraining the collector at a bolt circle of 17.5-inch diameter was calculated. The bolt force is:

$$\begin{aligned}
 F &= \sigma_A t \pi D \\
 &= (5,400) (0.060) (3.14) (17.5) = 17,800 \text{ lb}
 \end{aligned}
 \tag{22}$$

The bolt stress for ten 1/4-inch-diameter bolts is:

$$\sigma = \frac{17,800}{10 (0.0371)} = 48,000 \text{ psi}$$

2.4 DIFFUSER DEFLECTION

The axial deflection of the diffuser backplate was calculated for the same pressure load as above, distributed over the total plate area. From Reference 10 (page 200, case 19), the maximum axial deflection as shown in Figure 248 will be:

$$y_{\max} = -\frac{3W(m^2-1)}{16m^2Et^3} \left[a^4 + 3b^4 - 4a^2b^2 - 4a^2b^2 \ln \frac{a}{b} + \frac{16a^2b^4}{a^2-b^2} \left(\ln \frac{a}{b} \right)^2 \right] \tag{23}$$

where:

$$W = 145 \text{ psig}$$

$$m = \frac{1}{\nu} = \frac{1}{0.33} = 3.0$$

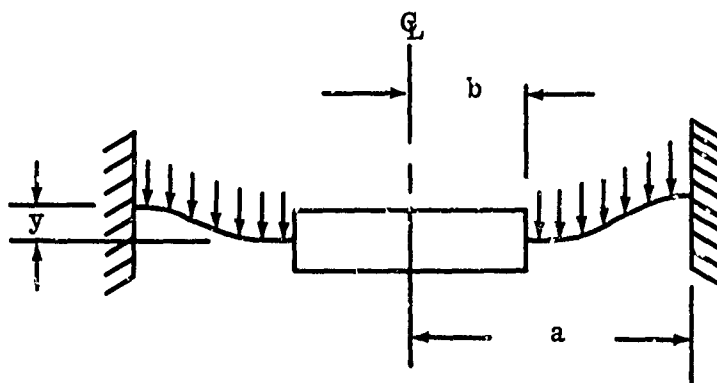


Figure 248. Diffuser Backplate Configuration for Deflection Calculation.

$$E = 29.0 \times 10^6 \text{ psi}$$

$$t = 0.70 \text{ in.}$$

$$a = 5.4 \text{ in.}; a^2 = 29.2 \text{ in.}^2; a^4 = 852 \text{ in.}^4$$

$$b = 3.5 \text{ in.}; b^2 = 12.25 \text{ in.}^2; b^4 = 150 \text{ in.}^4$$

$$\frac{a}{b} = 1.54; \ln \frac{a}{b} = 0.431$$

$$\begin{aligned} y_{\max} &= \frac{3(145)(8)}{(16)(9)(29.0 \times 10^6)(0.343)} \left[852 + 3(150) - 4(358)(0.431) + \right. \\ &\quad \left. \frac{16(4360)}{16.6} 0.185 \right] \\ &= \frac{3(145)(8)}{16(9)(29 \times 10^6)(0.343)} \left[352 + 450 - 1430 - 606 + 779 \right] \\ &= \frac{3(145)(8)}{16(9)(29.0 \times 10^6) 0.343} \left[245 \right] = 0.0006 \text{ in.} \end{aligned}$$

where $y_{\max} = 0.0006 \text{ in.}$ is the predicted axial deflection for the diffuser plate.

The deflection for each passage was calculated with the same distributed pressure of 145 psig. The diffuser bolt pattern was assumed to form a rectangular support with all edges rigidly supported as a cantilever. The force calculated on each diffuser passage is:

$$P = pA = 145 (1.0 \text{ wide})(3.75 \text{ long}) = 513 \text{ lb}$$

From Reference 10 (page 203, case 36),

$$y_{\max} = \frac{0.1422 W b^4}{E t^3 (1 + 2.21 a^3)} \quad (24)$$

where:

$$a = \frac{b}{a} = \frac{2.25}{3.75} = 0.60$$

$$b^4 = 0.13$$

$$t = 0.35 \text{ in.}; t^3 = 0.043 \text{ in.}^3$$

$$m = \frac{1}{\gamma} = \frac{1}{0.33} = 3.0$$

$$y_{\max} = \frac{0.1422 (145) (2.25)^4}{(29 \times 10^6) [1 + 2.21 (0.216)] t^3}$$

$$= \frac{0.1422 (145) (255)}{(29 \times 10^6) (1.478) (0.043)}$$

$$y_{\max} = 0.000285 \text{ in.}$$

where y_{\max} is the predicted maximum deflection at the center of the passage.

2.5 INLET-SHROUD ALUMINUM INSERT STRESS

The thermal expansion and resultant stress for the inlet-shroud aluminum insert was calculated for a temperature rise of 380°F. The coefficients of thermal expansion for 6061 aluminum and low carbon steel are 13.4×10^{-6} and 6.5×10^{-6} in./in.°F, respectively. The aluminum diametral growth will be:

$$\begin{aligned} \Delta D_{al} &= \alpha_{al} D \Delta T \\ &= (13.4 \times 10^{-6}) (5.40) (380) \\ &= 0.0275 \text{ in.} \end{aligned} \tag{25}$$

The steel diametral growth will be:

$$\begin{aligned} \Delta D_{st} &= \alpha_{st} D \Delta T \\ &= 6.5 \times 10^{-6} (5.40) (380) \\ &= 0.0134 \text{ in.} \end{aligned} \tag{26}$$

The interference at 380°F with a line-to-line contact at 60°F will be:

$$\begin{aligned} \text{interference} &= 0.0275 - 0.0134 \\ &= 0.0141 \text{ in.} \end{aligned}$$

The compressive stress of the aluminum for the above interference will be:

$$\sigma_{al} = \frac{XD}{2 h_{al}} \quad (27)$$

where equal deflection for the aluminum and steel gives.

$$\alpha_{al} \Delta T - \frac{XD}{2E_{al}h_{al}} = \alpha_{st} \Delta T + \frac{XD}{2E_{st}h_{st}} \quad (28)$$

$$\sigma_{al} = \frac{XD}{2 h_{al}} = \frac{(\alpha_{al} - \alpha_{st})(\Delta T) E_{al}}{1 + \frac{E_{al}h_{al}}{E_{st}h_{st}}} \quad (28a)$$

$$\begin{aligned} \sigma_{al} &= \frac{(13.4 - 6.5)(10^{-6})(380)(10 \times 10^6)}{1 + \frac{1(0.5)}{3(6)}} \\ &= \frac{6.9 \times 10^{-6}(380)(10 \times 10^6)}{1.0278} \\ &= 25,500 \text{ psi} \end{aligned}$$

The tensile stress of the steel will be:

$$\begin{aligned} \sigma_{st} &= \frac{XD}{2h_{st}} = \frac{(\alpha_{al} - \alpha_{st})(\Delta T)(E_{st})}{1 + \frac{E_{st}h_{st}}{E_{al}h_{al}}} \quad (29) \\ &= \frac{(6.9 \times 10^{-6})(380)(30 \times 10^6)}{1 + \frac{3(6)}{1(0.5)}} \\ &= \frac{6.9(380)(30)}{37} = 2,100 \text{ psi} \end{aligned}$$

The differential diametral growth between the mating steel shroud and the aluminum insert was 0.014 inch. This differential growth results in a compressive stress of 25,500 psi for aluminum and a tensile stress of 2,100 psi for steel.

The steel stress was low enough for infinite life. The aluminum stress corresponded to 0.2 percent yield endurance life of 100 hours; however, this life was sufficient for the planned test program.

The axial growth of the aluminum insert due to the thermal stress was calculated as:

$$\begin{aligned}\epsilon_{\text{axial}} &= \frac{\sigma_{\text{radial}}}{E} \\ &= \frac{25,500}{10 \times 10^6} = 0.00255 \text{ in./in.}\end{aligned}\tag{30}$$

For an axial length of 0.25 inch, the growth was calculated as:

$$\begin{aligned}\Delta X_{\text{axial}} &= 0.25 (0.00255) \\ &= 0.0006 \text{ in.}\end{aligned}$$

The axial differential growth for the aluminum insert was expected to be 0.0006 inch.

2.6 CONCLUSIONS

The design analyses for the modified 2-piece impeller indicated that the design was structurally sound for the planned operating conditions. The rotor dynamic analysis resulted in critical-operating speeds essentially identical to those of the diffuser test rig which used the workhorse impeller rotor system. The inducer-impeller stress and blade-vibration analyses are given in Appendix I of this report.

(U) APPENDIX III
DIFFUSER TEST DATA

This appendix contains the static-pressure measurements on the side walls of the diffuser in the vaneless space, the semivaneless space and the channels for the 10-vane-island diffuser configurations that were tested. The data is presented in tabular form with a sketch showing the location of each pressure tap with respect to the vane. The pressures given are in psia and are corrected to a standard day. The speed given is corrected ($N/\sqrt{\theta}$) in rpm, and airflows are corrected ($W_a\sqrt{\theta}/\delta$) in pounds per second. Each table of data also gives total throat area and depth. Since this appendix supplements the data of Section 6, the line number is given to facilitate cross reference for each test. The relative positions of lines 3, 5, and 7 on the speed lines of a compressor map are shown in Figure 249.

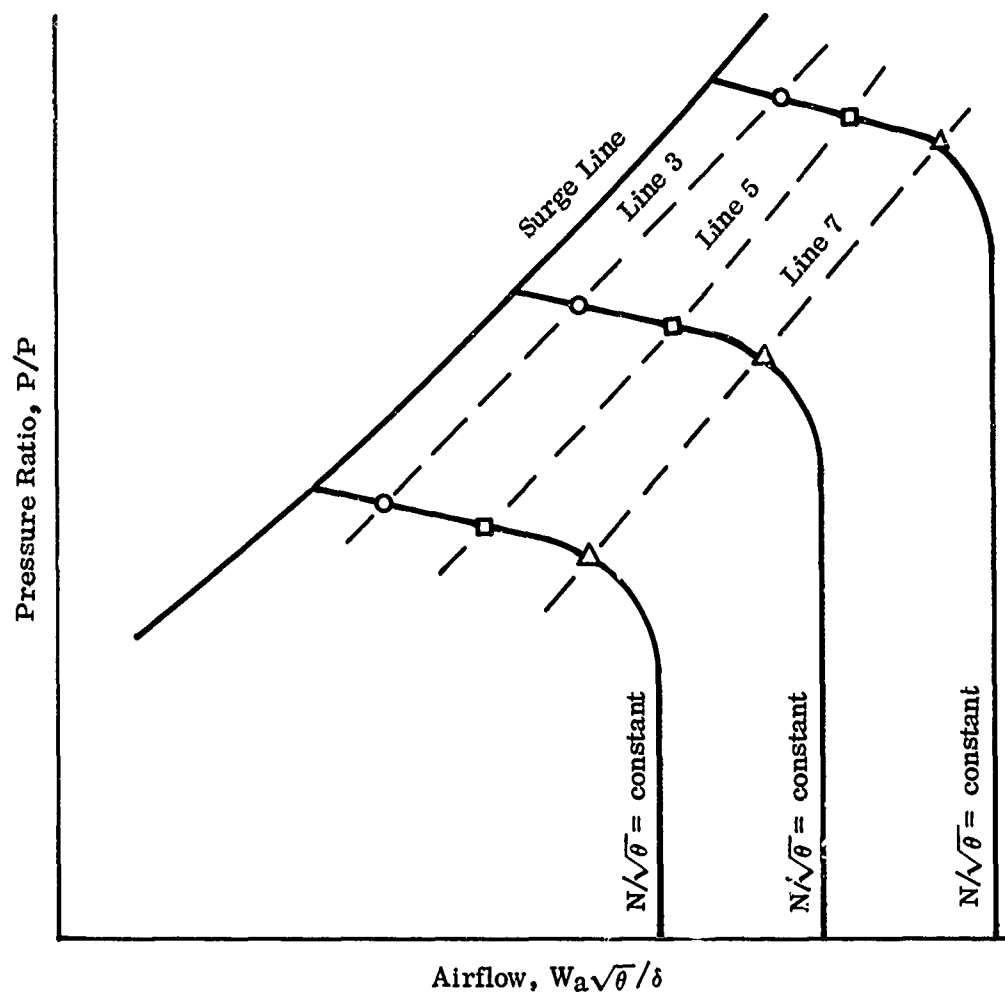


Figure 249. Relative Positions of Lines 3, 5 and 7 on the Speed Lines of a Compressor Map.

Corrected Diffuser Data
Static Pressure, P_s/δ (psia)

Test No. 3352A, Line 3
Configuration V1-1

Throat Size $\left\{ \begin{array}{l} \text{Total Area} = 0.889 \text{ in.}^2 \\ \text{Depth} = 0.200 \text{ in.} \end{array} \right.$

Speed, $N/\sqrt{\theta} = 50,000$ rpm

Airflow, $W_a \sqrt{\theta/\delta} = 1.76$ lb/sec

Tap No.	Static Pressure	Tap No.	Static Pressure	Tap No.	Static Pressure	Tap No.	Static Pressure
49	67.3	76	107.6	103	51.6	130	70.6
50	81.2	77	72.0	104	71.8	131	74.0
51	47.7	78	70.6	105	67.2	132	73.6
52	73.2	79	74.1	106	68.9	133	75.9
53	67.9	80	73.8	107	66.8	134	97.7
54	69.8	81	77.1	108	78.8	135	99.9
55	67.2	82	92.6	109	52.7	136	104.0
56	81.0	83	100.3	110	72.4	137	106.1
57	48.5	84	104.0	111	74.5	138	116.3
58	73.9	85	106.2	112	82.5	139	113.4
59	70.7	86	116.2	113	60.3	140	86.7
60	86.0	87	122.6	114	78.7	141	129.9
61	60.6	88	128.1	115	77.7	142	130.0
62	79.4	89	129.9	116	75.7	143	130.8
63	77.3	90	130.5	117	78.6	144	131.0
64	76.0	91	130.8	118	85.8	145	73.2
65	77.0	92	130.9	119	59.7	146	90.4
66	86.7	93	74.4	120	78.5	147	105.3
67	59.2	94	90.9	121	75.2	148	103.4
68	78.6	95	104.5	122	79.3	149	105.4
69	75.3	96	103.0	123	78.4	150	143.4
70	79.2	97	105.7	124	77.3	151	140.7
71	78.6	98	104.5	125	94.2	152	144.5
72	79.7	99	122.1	126	100.1	157	
73	94.1	100	125.9	127	104.7	158	
74	100.1	101	66.8	128	107.5	159	
75	104.6	102	79.6	129	71.5	160	

Corrected Diffuser Data
Static Pressure, P_s/δ (psia)

Test No. 3352A, Line 5
Configuration V1-1

Throat Size $\left\{ \begin{array}{l} \text{Total Area} = 0.889 \text{ in.}^2 \\ \text{Depth} = 0.200 \text{ in.} \end{array} \right.$

Speed, $N/\sqrt{\theta} = 50,000 \text{ rpm}$

Airflow, $W_a\sqrt{\theta}/\delta = 1.86 \text{ lb/sec}$

Tap No.	Static Pressure	Tap No.	Static Pressure	Tap No.	Static Pressure	Tap No.	Static Pressure
49	69.2	76	103.6	103	54.2	130	69.6
50	74.7	77	72.0	104	70.6	131	73.7
51	54.4	78	69.7	105	67.4	132	74.6
52	70.3	79	74.1	106	68.1	133	71.2
53	67.3	80	75.1	107	68.4	134	88.2
54	67.2	81	72.4	108	73.8	135	95.6
55	68.4	82	88.6	109	55.5	136	99.1
56	74.7	83	96.2	110	72.0	137	101.7
57	55.1	84	99.2	111		138	113.5
58	72.2	85	101.9	112	83.8	139	111.5
59	70.5	86	113.4	113	63.2	140	85.3
60	84.8	87	120.5	114	77.1	141	127.7
61	63.6	88	126.2	115	77.7	142	127.7
62	78.4	89	127.7	116	74.6	143	128.7
63	77.8	90	128.3	117	76.7	144	128.9
64	75.1	91	128.6	118	86.5	145	68.6
65	75.3	92	128.7	119	63.1	146	86.5
66	85.4	93	69.3	120	77.0	147	100.2
67	62.2	94	86.8	121	74.7	148	97.0
68	77.7	95	101.5	122	78.0	149	100.9
69	75.2	96	97.6	123	79.5	150	136.1
70	78.0	97	101.2	124	70.3	151	133.3
71	79.7	98	101.3	125	89.5	152	138.4
72	73.6	99	115.7	126	95.9	157	
73	89.4	100	120.9	127	100.4	158	
74	95.9	101	68.1	128	103.5	159	
75	100.1	102	74.9	129	71.9	160	

Corrected Diffuser Data

Static Pressure, P_s/δ (psia)

Test No. 3352A, Line 7
Configuration

Throat Size $\left\{ \begin{array}{l} \text{Total Area} = 0.889 \text{ in.}^2 \\ \text{Depth} = 0.200 \text{ in.} \end{array} \right.$

Speed, $N/\sqrt{\theta} = 50,000 \text{ rpm}$

Airflow, $W_a\sqrt{\theta/\delta} = 1.96 \text{ lb/sec}$

Tap No.	Static Pressure	Tap No.	Static Pressure	Tap No.	Static Pressure	Tap No.	Static Pressure
49	67.4	76	90.5	103	64.2	130	69.6
50	63.5	77	69.6	104	67.3	131	72.0
51	63.5	78	69.5	105	67.3	132	73.2
52	66.7	79	72.3	106	67.0	133	71.1
53	66.6	80	74.0	107	67.1	134	64.9
54	66.4	81	72.5	108	63.7	135	82.4
55	66.5	82	64.9	109	66.0	136	83.1
56	63.2	83	84.2	110	67.9	137	88.3
57	64.2	84	83.5	111	68.8	138	105.0
58	67.6	85	88.9	112	84.6	139	105.1
59	68.2	86	105.2	113	69.9	140	80.9
60	81.1	87	113.3	114	73.0	141	120.0
61	70.5	88	118.6	115	75.9	142	120.4
62	74.8	89	120.0	116	74.2	143	121.1
63	76.7	90	120.6	117	75.8	144	121.3
64	75.2	91	121.0	118	85.8	145	68.7
65	74.9	92	121.2	119	70.2	146	65.1
66	81.3	93	69.1	120	72.8	147	87.4
67	69.0	94	65.4	121	74.4	148	79.9
68	73.9	95	89.6	122	76.8	149	88.2
69	75.3	96	80.1	123	78.2	150	86.7
70	77.2	97	88.7	124	69.6	151	106.4
71	78.8	98	88.5	125	66.1	152	120.1
72	73.5	99	78.1	126	82.8	157	
73	66.1	100	105.2	127	85.5	158	
74	83.1	101	68.0	128	90.3	159	
75	85.4	102	64.3	129	69.8	160	

Corrected Diffuser Data

Static Pressure, P_s/δ (psia)

Test No. 3352B, Line 3
Configuration V1-2

Throat Size $\left\{ \begin{array}{l} \text{Total Area} = 0.845 \text{ in.}^2 \\ \text{Depth} = 0.190 \text{ in.} \end{array} \right.$

Speed, $N/\sqrt{\theta} = 50,000 \text{ rpm}$

Airflow, $W_a\sqrt{\theta}/\delta = 1.75 \text{ lb/sec}$

Tap No.	Static Pressure	Tap No.	Static Pressure	Tap No.	Static Pressure	Tap No.	Static Pressure
49	70.2	76	107.4	103	55.1	130	71.2
50	80.5	77	74.3	104	73.1	131	75.3
51	52.5	78	71.9	105	69.5	132	75.8
52	74.0	79	76.2	106	68.7	133	72.5
53	69.9	80	77.1	107	70.2	134	91.3
54	69.2	81	74.7	108	75.1	135	98.7
55	70.7	82	92.1	109	56.3	136	102.4
56	79.6	83	99.7	110	73.8	137	104.7
57	55.9	84	103.1	111	72.5	138	116.4
58	74.7	85	105.6	112	85.3	139	113.4
59	73.1	86	117.1	113	63.7	140	85.2
60	88.6	87	124.4	114	78.8	141	131.4
61	63.8	88	130.4	115	79.6	142	131.6
62	80.5	89	132.3	116	76.1	143	132.4
63	80.1	90	132.9	117	77.9	144	132.6
64	77.3	91	133.2	118	88.2	145	70.1
65	77.3	92	133.3	119	63.0	146	89.4
66	89.2	93	71.7	120	79.4	147	104.0
67	62.1	94	90.5	121	76.8	148	99.9
68	80.4	95	104.8	122	79.5	149	103.7
69	77.7	96	101.7	123	80.9	150	104.4
70	80.2	97	105.1	124	73.0	151	101.7
71	81.8	98	104.8	125	92.5	152	105.0
72	76.5	99	102.4	126	98.8	157	---
73	93.2	100	106.2	127	103.4	158	---
74	99.6	101	69.8	128	106.4	159	---
75	104.1	102	79.1	129	73.3	160	88.4

Corrected Diffuser Data
Static Pressure, P_s/δ (psia)

Test No. 3352B, Line 5
Configuration V1-2

Throat Size $\left\{ \begin{array}{l} \text{Total Area} = 0.845 \text{ in.}^2 \\ \text{Depth} = 0.190 \text{ in.} \end{array} \right.$

Speed, $N/\sqrt{\theta} = 50,000 \text{ rpm}$

Airflow, $W_a\sqrt{\theta/\delta} = 1.84 \text{ lb/sec}$

Tap No.	Static Pressure	Tap No.	Static Pressure	Tap No.	Static Pressure	Tap No.	Static Pressure
49	70.7	76	102.4	103	59.3	130	71.1
50	70.2	77	73.9	104	71.8	131	73.8
51	58.8	78	71.9	105	69.7	132	75.9
52	71.7	79	74.9	106	68.5	133	72.5
53	69.4	80	74.4	107	70.4	134	85.4
54	68.4	81	75.0	108	67.9	135	93.2
55	70.3	82	86.7	109	61.4	136	96.0
56	68.6	83	94.6	110	72.0	137	99.2
57	60.1	84	97.0	111	73.0	138	113.0
58	72.1	85	100.2	112	86.5	139	110.7
59	72.8	86	113.8	113	66.9	140	83.1
60	87.1	87	121.7	114	76.4	141	128.6
61	68.0	88	127.8	115	79.5	142	128.6
62	78.6	89	129.4	116	76.0	143	129.5
63	80.5	90	130.0	117	77.2	144	129.8
64	77.3	91	130.3	118	86.6	145	70.2
65	76.6	92	130.4	119	66.5	146	84.0
66	87.7	93	71.8	120	77.5	147	98.0
67	66.2	94	85.2	121	76.4	148	93.1
68	79.0	95	100.3	122	78.2	149	98.6
69	77.7	96	94.8	123	81.1	150	98.7
70	79.0	97	99.8	124	72.0	151	95.8
71	82.1	98	100.5	125	85.9	152	100.2
72	75.6	99	96.1	126	93.4	157	---
73	86.8	100	101.3	127	97.6	158	---
74	94.4	101	70.8	128	101.5	159	---
75	98.2	102	70.3	129	73.2	160	88.4

Corrected Diffuser Data
Static Pressure, P_s/δ (psia)

Test No. 3352B, Line 7
Configuration V1-2

Throat Size $\left\{ \begin{array}{l} \text{Total Area} = 0.845 \text{ in.}^2 \\ \text{Depth} = 0.190 \text{ in.} \end{array} \right.$

Speed, $N/\sqrt{\rho} = 50,000 \text{ rpm}$

Airflow, $W_a\sqrt{\theta/\delta} = 1.91 \text{ lb/sec}$

Tap No.	Static Pressure	Tap No.	Static Pressure	Tap No.	Static Pressure	Tap No.	Static Pressure
49	69.6	76	94.3	103	65.2	130	71.2
50	65.7	77	72.1	104	70.0	131	73.5
51	64.5	78	71.9	105	69.2	132	74.1
52	69.5	79	74.5	106	68.7	133	72.3
53	68.8	80	76.4	107	69.1	134	67.2
54	68.2	81	74.9	108	65.6	135	84.9
55	68.6	82	69.2	109	67.4	136	86.3
56	65.2	83	87.3	110	69.7	137	91.2
57	65.8	84	87.4	111	71.2	138	108.3
58	69.8	85	92.6	112	86.0	139	107.4
59	70.6	86	109.2	113	71.2	140	82.1
60	84.7	87	117.8	114	74.4	141	124.2
61	72.5	88	123.6	115	78.1	142	124.5
62	77.0	89	125.1	116	76.0	143	125.3
63	79.5	90	125.7	117	77.4	144	125.5
64	77.6	91	126.0	118	88.0	145	70.1
65	77.0	92	126.2	119	71.0	146	67.5
66	85.0	93	71.4	120	75.1	147	90.4
67	70.5	94	68.4	121	76.0	148	82.4
68	77.0	95	93.2	122	78.3	149	91.2
69	77.6	96	83.7	123	80.1	150	90.3
70	79.4	97	92.5	124	71.4	151	84.2
71	81.3	98	92.7	125	68.1	152	92.9
72	75.9	99	83.9	126	85.4	157	---
73	68.8	100	94.1	127	88.6	158	---
74	86.5	101	70.1	128	78.3	159	---
75	89.3	102	66.6	129	71.5	160	88.4

Corrected Diffuser Data

Static Pressure, P_s/δ (psia)

Test No. 3352C, Line 3
Configuration V1-3

Throat Size $\left\{ \begin{array}{l} \text{Total Area} = 0.813 \text{ in.}^2 \\ \text{Depth} = 0.183 \text{ in.} \end{array} \right.$

Speed, $N/\sqrt{\theta} = 50,000 \text{ rpm}$

Airflow, $W_a\sqrt{\theta/\delta} = 1.69 \text{ lb/sec}$

Tap No.	Static Pressure	Tap No.	Static Pressure	Tap No.	Static Pressure	Tap No.	Static Pressure
49	70.8	76	106.9	103	56.0	130	71.4
50	79.2	77	74.9	104	73.4	131	75.7
51	54.2	78	72.2	105	69.9	132	75.4
52	74.2	79	76.6	106	69.0	133	71.9
53	70.3	80	77.5	107	70.8	134	90.6
54	69.6	81	74.5	108	75.9	135	97.8
55	71.1	82	91.3	109	57.4	136	101.6
56	77.3	83	99.2	110	73.9	137	103.7
57	55.5	84	102.3	111	73.0	138	116.4
58	75.1	85	104.9	112	85.5	139	112.8
59	73.6	86	117.0	113	64.5	140	83.8
60	89.6	87	124.5	114	78.4	141	131.6
61	64.9	88	130.6	115	80.0	142	131.6
62	80.4	89	132.4	116	76.4	143	132.5
63	80.5	90	133.0	117	77.9	144	132.7
64	77.5	91	133.3	118	88.6	145	69.4
65	77.2	92	133.4	119	63.8	146	88.6
66	90.2	93	71.5	120	79.6	147	103.6
67	62.8	94	90.0	121	77.2	148	98.3
68	80.5	95	104.4	122	79.9	149	103.1
69	78.2	96	100.6	123	81.3	150	104.2
70	80.6	97	104.3	124	72.3	151	101.4
71	82.3	98	104.4	125	91.7	152	104.9
72	75.8	99	101.8	126	98.2	157	
73	92.5	100	105.9	127	102.8	158	
74	99.0	101	70.2	128	105.9	159	
75	103.5	102	78.1	129	73.8	160	

Corrected Diffuser Data

Static Pressure, P_s/δ (psia)

Test No. 3352C, Line 5
Configuration V1-3

Throat Size $\left\{ \begin{array}{l} \text{Total Area} = 0.813 \text{ in.}^2 \\ \text{Depth} = 0.183 \text{ in.} \end{array} \right.$

Speed, $N/\sqrt{\theta} = 50,000$ rpmAirflow, $W_a\sqrt{\theta}/\delta = 1.77$ lb/sec

Tap No.	Static Pressure	Tap No.	Static Pressure	Tap No.	Static Pressure	Tap No.	Static Pressure
49	71.1	76	93.5	103	67.2	130	72.4
50	67.1	77	73.0	104	71.3	131	74.8
51	67.0	78	73.3	105	70.3	132	74.8
52	70.9	79	76.0	106	70.0	133	73.2
53	70.0	80	77.6	107	70.3	134	66.6
54	69.7	81	76.2	108	66.9	135	84.2
55	70.0	82	67.5	109	70.0	136	84.2
56	66.7	83	86.8	110	71.0	137	89.9
57	68.9	84	85.3	111	71.8	138	106.9
58	71.1	85	91.9	112	86.3	139	107.6
59	71.5	86	109.7	113	73.0	140	80.7
60	86.6	87	118.6	114	74.8	141	125.0
61	74.4	88	124.4	115	78.8	142	125.2
62	78.0	89	125.9	116	77.4	143	126.0
63	80.1	90	126.5	117	78.7	144	126.2
64	79.0	91	126.8	118	88.1	145	70.9
65	78.2	92	127.0	119	72.4	146	66.6
66	86.9	93	72.9	120	76.6	147	90.3
67	72.0	94	67.4	121	77.3	148	80.1
68	78.3	95	93.1	122	79.5	149	90.4
69	78.7	96	82.0	123	81.4	150	90.6
70	80.8	97	92.0	124	72.9	151	83.0
71	82.6	98	92.6	125	68.2	152	92.8
72	77.2	99	82.8	126	84.6	157	
73	69.0	100	94.1	127	86.8	158	
74	85.8	101	71.3	128	92.3	159	
75	87.5	102	67.5	129	72.3	160	

Corrected Diffuser Data

Static Pressure, P_s/δ (psia)

Test No. 3352C, Line 7
Configuration V1-3

Throat Size $\left\{ \begin{array}{l} \text{Total Area} = 0.813 \text{ in.}^2 \\ \text{Depth} = 0.183 \text{ in.} \end{array} \right.$

Speed, $N/\sqrt{\theta} = 50,000 \text{ rpm}$

Airflow, $W_a\sqrt{\theta}/\delta = 1.85 \text{ lb/sec}$

Tap No.	Static Pressure	Tap No.	Static Pressure	Tap No.	Static Pressure	Tap No.	Static Pressure
49	70.4	76	92.5	103	67.1	130	71.6
50	66.3	77	72.3	104	70.6	131	74.0
51	66.2	78	72.6	105	69.6	132	74.0
52	70.1	79	75.2	106	69.3	133	72.5
53	69.3	80	76.8	107	69.5	134	65.8
54	69.0	81	75.4	108	66.1	135	83.2
55	69.2	82	66.8	109	69.1	136	83.3
56	65.9	83	85.8	110	70.2	137	88.9
57	68.1	84	84.5	111	71.0	138	107.8
58	70.3	85	90.9	112	85.4	139	106.5
59	70.8	86	108.6	113	72.2	140	79.9
60	85.7	87	117.3	114	74.0	141	123.9
61	73.6	88	123.0	115	78.0	142	123.9
62	77.2	89	124.5	116	76.6	143	123.8
63	79.3	90	125.1	117	77.8	144	125.0
64	78.1	91	125.4	118	87.2	145	70.1
65	77.4	92	125.6	119	71.6	146	65.8
66	86.0	93	72.2	120	75.8	147	89.4
67	71.3	94	66.6	121	76.5	148	79.2
68	77.5	95	92.1	122	78.6	149	89.5
69	77.9	96	81.2	123	80.5	150	89.6
70	80.0	97	91.0	124	72.2	151	82.2
71	81.8	98	91.6	125	67.5	152	91.8
72	76.4	99	81.9	126	83.6	157	
73	68.2	100	93.1	127	85.9	158	
74	84.9	101	70.6	128	91.3	159	
75	86.5	102	66.8	129	71.6	160	

Corrected Diffuser Data

Static Pressure, P_s/δ (psia)

Test No. 3353D, Line 3
Configuration V1-3

Throat Size $\left\{ \begin{array}{l} \text{Total Area} = 0.813 \text{ in.}^2 \\ \text{Depth} = 0.183 \text{ in.} \end{array} \right.$

Speed, $N/\sqrt{\theta} = 50,000 \text{ rpm}$

Airflow, $W_a\sqrt{\theta}/\delta = 1.66 \text{ lb/sec}$

Tap No.	Static Pressure	Tap No.	Static Pressure	Tap No.	Static Pressure	Tap No.	Static Pressure
49	70.0	76	107.5	103	55.4	130	72.5
50	80.7	77	75.0	104	73.3	131	76.8
51	52.9	78	72.5	105	70.0	132	75.2
52	74.5	79	77.0	106	70.1	133	73.9
53	70.8	80	76.2	107	69.6	134	92.3
54	70.8	81	74.3	108	77.7	135	98.5
55	69.9	82	92.1	109	56.5	136	103.5
56	79.8	83	99.8	110	74.3	137	105.0
57	54.0	84	103.4	111	72.9	138	117.5
58	75.6	85	105.7	112	84.3	139	124.7
59	73.5	86	117.4	113	64.3	140	130.5
60	89.7	87	124.5	114	79.2	141	132.2
61	63.8	88	130.4	115	80.8	142	133.0
62	80.9	89	128.5	116	77.1	143	133.2
63	80.4	90	132.5	117	79.6	144	133.4
64	77.5	91	133.1	118	88.9	145	71.0
65	79.1	92	133.3	119	63.9	146	89.8
66	90.1	93	71.5	120	80.4	147	105.0
67	61.9	94	90.7	121	78.4	148	101.7
68	80.5	95	104.5	122	81.3	149	104.6
69	78.6	96	101.8	123	80.9	150	105.6
70	81.5	97	105.2	124	73.6	151	103.0
71	81.1	98	104.7	125	92.5	152	106.4
72	75.8	99	102.7	126	99.6	157	---
73	93.5	100	106.5	127	104.6	158	---
74	99.7	101	69.5	128	107.2	159	---
75	104.5	102	79.1	129	74.6	160	90.3

Corrected Diffuser Data
Static Pressure, P_s/δ (psia)

Test No. 3353D, Line 5
Configuration V1-3

Throat Size $\left\{ \begin{array}{l} \text{Total Area} = 0.813 \text{ in.}^2 \\ \text{Depth} = 0.183 \text{ in.} \end{array} \right.$

Speed, $N/\sqrt{\theta} = 50,000 \text{ rpm}$

Airflow, $W_a\sqrt{\theta/\delta} = 1.75 \text{ lb/sec}$

Tap No.	Static Pressure	Tap No.	Static Pressure	Tap No.	Static Pressure	Tap No.	Static Pressure
49	72.5	76	103.7	103	59.6	130	72.9
50	69.7	77	76.8	104	71.3	131	75.8
51	59.0	78	73.1	105	70.9	132	77.1
52	71.5	79	76.2	106	69.3	133	74.8
53	71.1	80	73.2	107	71.2	134	86.9
54	69.5	81	75.3	108	67.9	135	94.4
55	71.5	82	87.0	109	61.4	136	98.0
56	68.1	83	95.5	110	72.4	137	100.6
57	60.5	84	98.0	111	74.0	138	115.0
58	72.9	85	101.2	112	86.7	139	122.9
59	74.3	86	114.9	113	67.7	140	129.1
60	89.2	87	122.9	114	77.3	141	130.6
61	68.3	88	129.0	115	81.8	142	131.4
62	79.2	89	127.0	116	77.6	143	131.5
63	81.7	90	131.3	117	78.4	144	131.8
64	78.0	91	131.5	118	89.4	145	71.9
65	78.0	92	131.6	119	67.0	146	85.2
66	89.7	93	72.2	120	77.9	147	100.3
67	65.9	94	85.9	121	78.9	148	95.8
68	79.2	95	101.2	122	80.2	149	100.2
69	79.2	96	95.8	123	82.8	150	101.0
70	80.4	97	100.8	124	73.5	151	97.7
71	83.0	98	131.6	125	87.3	152	102.2
72	76.3	99	97.3	126	95.2	157	---
73	87.4	100	102.4	127	99.6	158	---
74	95.3	101	72.1	128	103.4	159	---
75	99.4	102	70.4	129	76.3	160	90.2

Corrected Diffuser Data

Static Pressure, P_s/δ (psia)

Test No. 3353D, Line 7
Configuration V1-3

Throat Size $\left\{ \begin{array}{l} \text{Total Area} = 0.813 \text{ in.}^2 \\ \text{Depth} = 0.183 \text{ in.} \end{array} \right.$

Speed, $N/\sqrt{\theta} = 50,000 \text{ rpm}$

Airflow, $W_a\sqrt{\theta/\delta} = 1.83 \text{ lb/sec}$

Tap No.	Static Pressure	Tap No.	Static Pressure	Tap No.	Static Pressure	Tap No.	Static Pressure
49	71.3	76	79.6	103	66.2	130	73.1
50	66.5	77	75.1	104	69.6	131	74.9
51	66.5	78	73.3	105	71.5	132	75.9
52	69.3	79	75.3	106	69.5	133	74.9
53	71.4	80	77.3	107	69.8	134	66.0
54	69.4	81	75.6	108	66.1	135	81.4
55	69.6	82	66.4	109	69.2	136	78.8
56	66.0	83	83.6	110	70.7	137	36.6
57	68.4	84	78.8	111	71.1	138	107.2
58	70.7	85	87.9	112	84.4	139	116.1
59	70.9	86	107.1	113	73.0	140	121.9
60	85.5	87	116.2	114	75.1	141	123.4
61	73.5	88	122.0	115	78.9	142	124.1
62	77.7	89	120.0	116	78.2	143	124.4
63	79.4	90	124.0	117	78.9	144	124.6
64	78.9	91	124.3	118	86.9	145	72.0
65	78.5	92	124.5	119	71.5	146	65.4
66	85.9	93	72.3	120	75.3	147	88.7
67	70.4	94	65.6	121	79.6	148	76.8
68	76.3	95	90.5	122	79.8	149	87.4
69	80.2	96	77.4	123	81.8	150	89.3
70	80.4	97	88.4	124	73.6	151	77.2
71	82.2	98	90.3	125	67.9	152	89.6
72	76.5	99	76.5	126	81.0	157	---
73	68.1	100	90.1	127	82.3	158	---
74	81.8	101	61.3	128	89.1	159	---
75	82.2	102	86.8	129	75.0	160	90.6

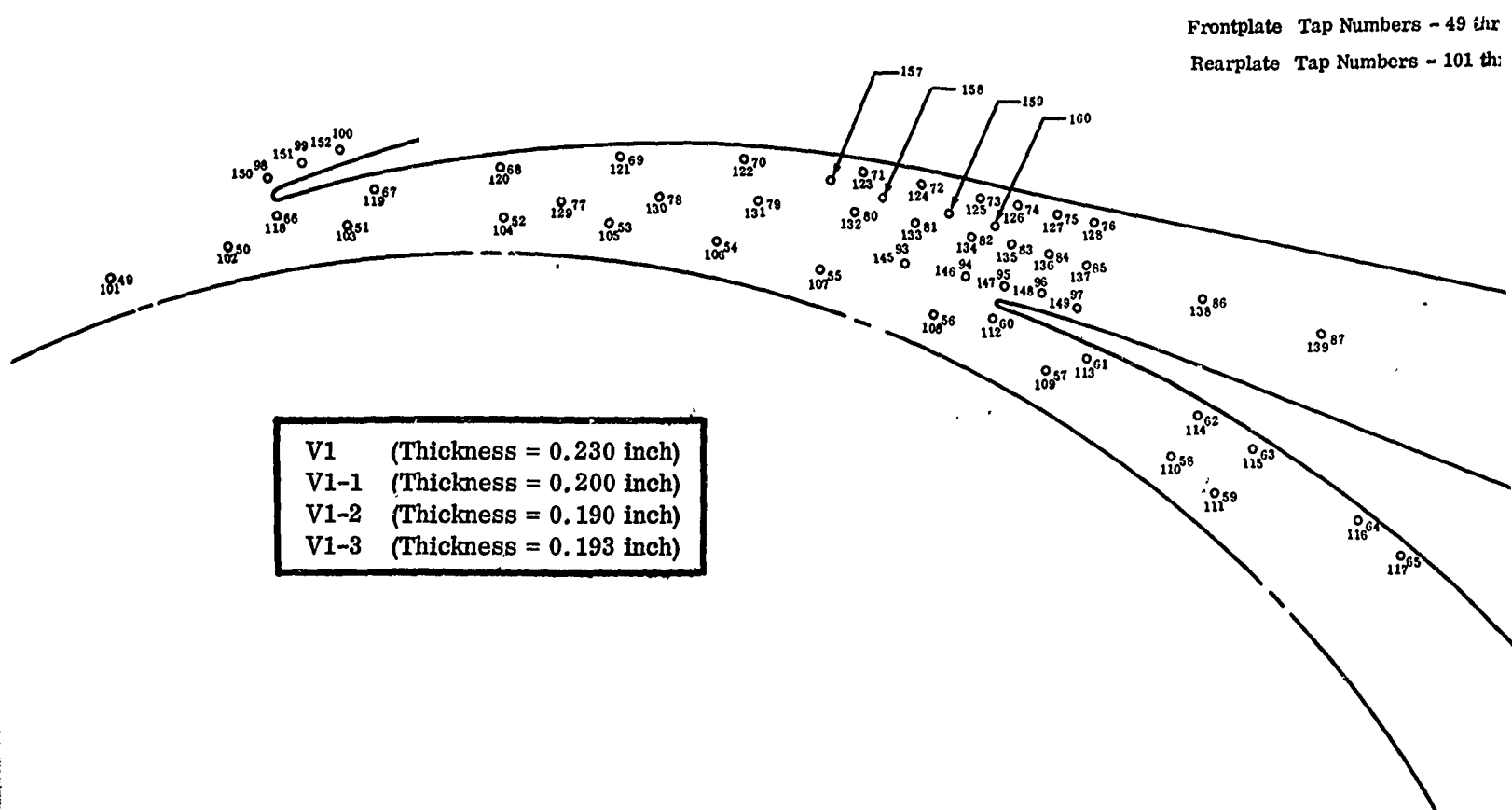
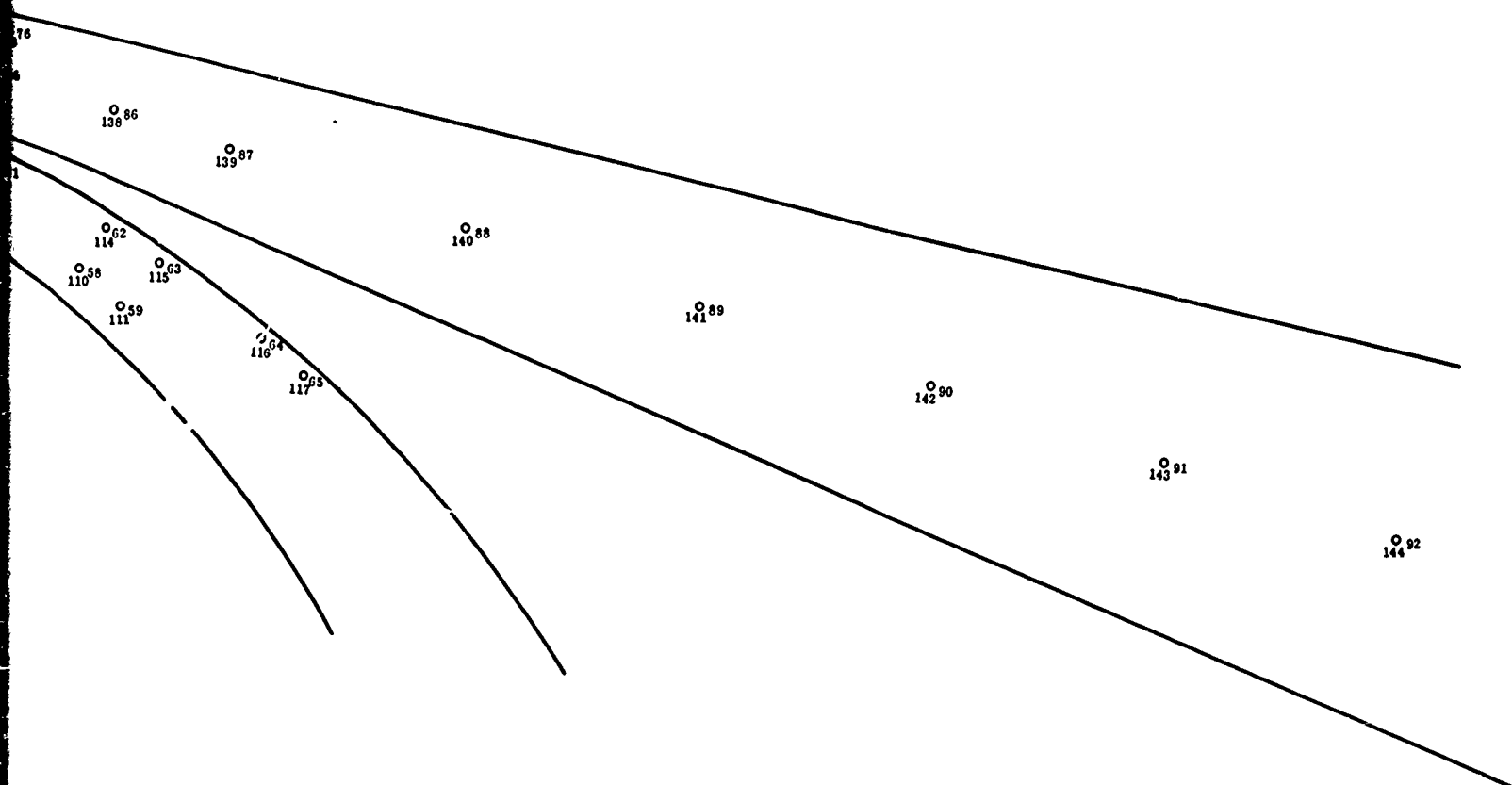


Figure 250. Locations of Static-Pressure Taps with Respect to V1, V1-1, V1-2 and V1-3 Diffuser Vanes.

Frontplate Tap Numbers - 49 thru 100, 157, 158, 159, 160
Rearplate Tap Numbers - 101 thru 152



Corrected Diffuser Data

Static Pressure, P_s/δ (psia)

Test No. 3354, Line 3
Configuration V1-4

Throat Size $\left\{ \begin{array}{l} \text{Total Area} = 0.869 \text{ in.}^2 \\ \text{Depth} = 0.183 \text{ in.} \end{array} \right.$

Speed, $N/\sqrt{\theta} = 50,000 \text{ rpm}$

Airflow, $W_a\sqrt{\theta/\delta} = 1.77 \text{ lb/sec}$

Tap No.	Static Pressure	Tap No.	Static Pressure	Tap No.	Static Pressure	Tap No.	Static Pressure
49	68.2	76	106.6	103	54.4	130	70.2
50	81.9	77	72.8	104	71.7	131	75.3
51	52.7	78	70.4	105	68.4	132	74.3
52	72.4	79	75.5	106	67.4	133	78.4
53	68.0	80	74.6	107	68.3	134	92.4
54	67.9	81	79.1	108	79.4	135	99.7
55	68.3	82	92.6	109	54.0	136	102.8
56	80.9	83	99.6	110	73.1	137	104.7
57	49.4	84	102.8	111	71.6	138	116.1
58	74.0	85	104.9	112	86.2	139	123.1
59	72.2	86	116.0	113	62.8	140	129.4
60	88.9	87	123.1	114	78.7	141	131.4
61	62.4	88	129.4	115	78.7	142	132.0
62	79.7	89	131.4	116	74.7	143	132.5
63	68.6	90	132.2	117	76.7	144	132.7
64	75.0	91	132.5	118	88.8	145	74.6
65	76.3	92	132.6	119	63.0	146	90.5
66	89.6	93	75.2	120	78.6	147	104.3
67	61.2	94	91.0	121	75.7	148	101.4
68	78.9	95	105.0	122	79.0	149	104.0
69	75.8	96	101.5	123	79.1	150	105.5
70	78.9	97	104.5	124	81.7	151	103.3
71	79.3	98	105.6	125	94.1	152	106.1
72	83.4	99	103.0	126	98.4	157	---
73	93.9	100	106.5	127	103.6	158	---
74	99.3	101	68.4	128	106.5	159	---
75	103.1	102	80.9	129	72.9	160	90.0

Corrected Diffuser Data
Static Pressure, P_s/δ (psia)

Test No. 3354, Line 5
Configuration V1-4

Throat Size $\left\{ \begin{array}{l} \text{Total Area} = 0.869 \text{ in.}^2 \\ \text{Depth} = 0.183 \text{ in.} \end{array} \right.$

Speed, $N/\sqrt{\theta} = 50,000 \text{ rpm}$

Airflow, $W_a\sqrt{\theta}/\delta = 1.87 \text{ lb/sec}$

Tap No.	Static Pressure	Tap No.	Static Pressure	Tap No.	Static Pressure	Tap No.	Static Pressure
49	69.2	76	102.0	103	58.4	130	70.1
50	75.6	77	72.7	104	69.7	131	72.5
51	57.8	78	70.3	105	68.6	132	75.5
52	69.7	79	72.7	106	66.5	133	75.2
53	67.7	80	76.0	107	69.6	134	88.2
54	66.4	81	75.8	108	73.8	135	95.3
55	69.4	82	88.6	109	57.6	136	97.6
56	74.6	83	95.5	110	71.3	137	100.3
57	50.2	84	97.8	111	71.8	138	113.2
58	71.5	85	100.6	112	87.4	139	121.1
59	71.7	86	113.2	113	64.9	140	127.6
60	87.4	87	121.2	114	76.4	141	129.5
61	65.9	88	127.7	115	78.6	142	130.1
62	77.7	89	129.6	116	74.5	143	130.7
63	78.8	90	130.3	117	75.3	144	130.8
64	75.1	91	130.6	118	89.7	145	71.6
65	75.1	92	130.7	119	65.9	146	86.7
66	88.2	93	71.8	120	76.1	147	99.7
67	65.0	94	87.1	121	75.2	148	95.3
68	76.8	95	101.3	122	76.2	149	99.8
69	75.7	96	95.3	123	80.2	150	100.2
70	76.2	97	100.3	124	77.8	151	97.3
71	80.5	98	101.3	125	89.4	152	101.6
72	80.0	99	96.7	126	93.8	157	---
73	89.4	100	102.1	127	98.9	158	---
74	95.0	101	69.6	128	102.0	159	---
75	98.3	102	75.9	129	73.0	160	90.0

Corrected Diffuser Data

Static Pressure, P_s/δ (psia)

Test No. 3354, Line 7
Configuration V1-4

Throat Size $\left\{ \begin{array}{l} \text{Total Area} = 0.869 \text{ in.}^2 \\ \text{Depth} = 0.183 \text{ in.} \end{array} \right.$

Speed, $N/\sqrt{\theta} = 50,000 \text{ rpm}$

Airflow, $W_a\sqrt{\theta/\delta} = 1.96 \text{ lb/sec}$

Tap No.	Static Pressure	Tap No.	Static Pressure	Tap No.	Static Pressure	Tap No.	Static Pressure
49	68.1	76	93.0	103	65.8	130	70.9
50	66.7	77	70.6	104	76.7	131	72.4
51	65.1	78	70.8	105	68.7	132	74.4
52	67.3	79	72.4	106	67.3	133	74.9
53	67.5	80	74.7	107	67.9	134	75.2
54	66.7	81	75.6	108	67.0	135	87.1
55	67.4	82	75.2	109	64.6	136	86.7
56	67.0	83	87.7	110	68.8	137	91.0
57	56.8	84	87.1	111	70.1	138	108.1
58	68.8	85	91.6	112	88.9	139	117.0
59	69.9	86	108.3	113	70.5	140	123.5
60	85.4	87	117.2	114	74.1	141	125.2
61	71.0	88	123.6	115	76.8	142	125.6
62	75.7	89	125.3	116	75.0	143	126.4
63	77.5	90	126.0	117	75.8	144	126.5
64	75.8	91	126.4	118	90.3	145	71.4
65	75.9	92	126.5	119	71.8	146	74.6
66	86.0	93	71.5	120	73.2	147	92.1
67	70.5	94	75.4	121	75.5	148	83.0
68	74.3	95	93.9	122	76.8	149	90.5
69	76.3	96	83.1	123	79.0	150	91.9
70	76.9	97	91.0	124	77.2	151	83.3
71	79.4	98	93.0	125	74.0	152	92.5
72	79.7	99	82.4	126	85.3	157	---
73	74.4	100	93.0	127	88.8	158	---
74	87.0	101	68.9	128	93.1	159	---
75	88.1	102	67.1	129	71.3	160	90.1

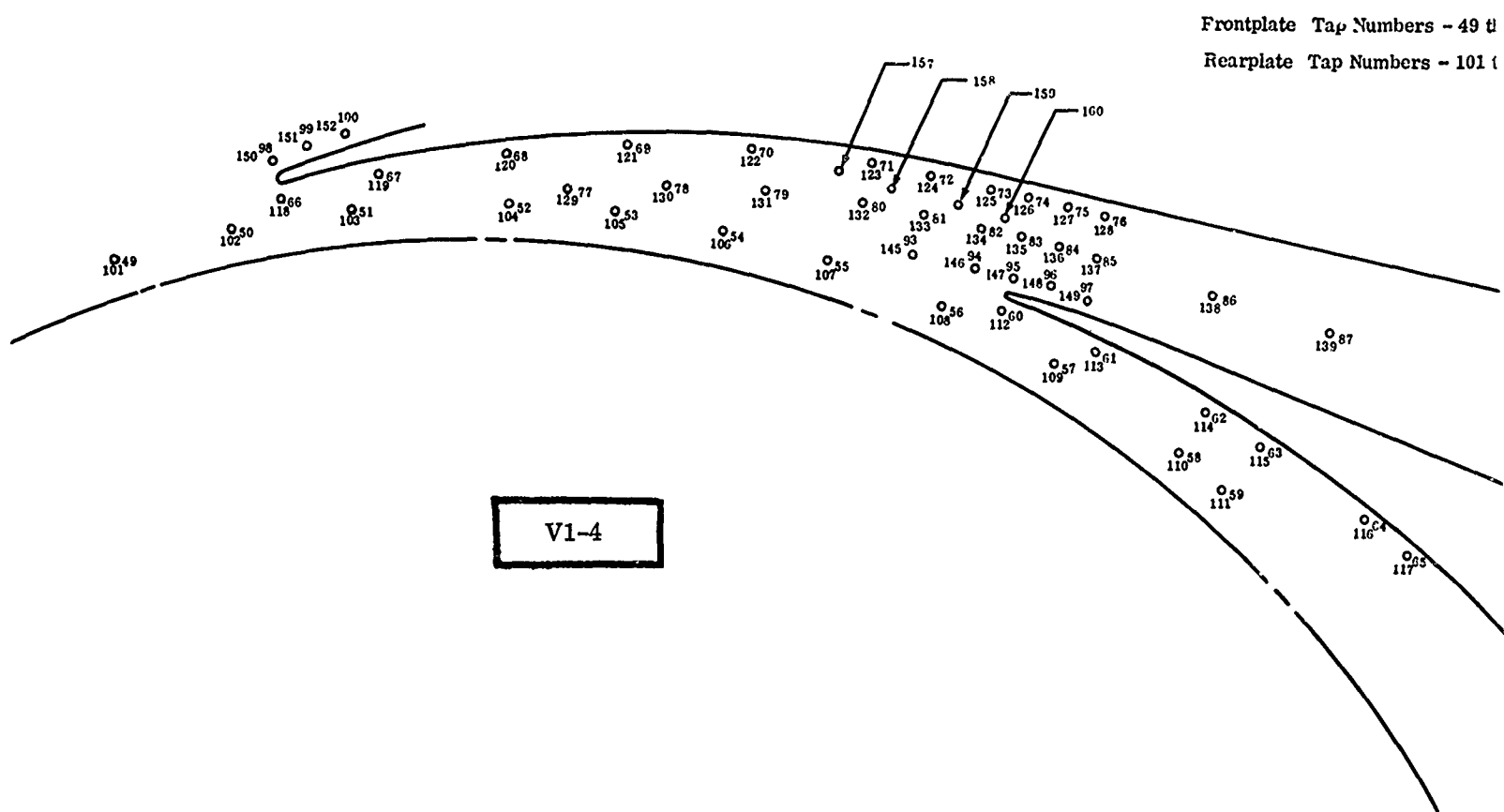
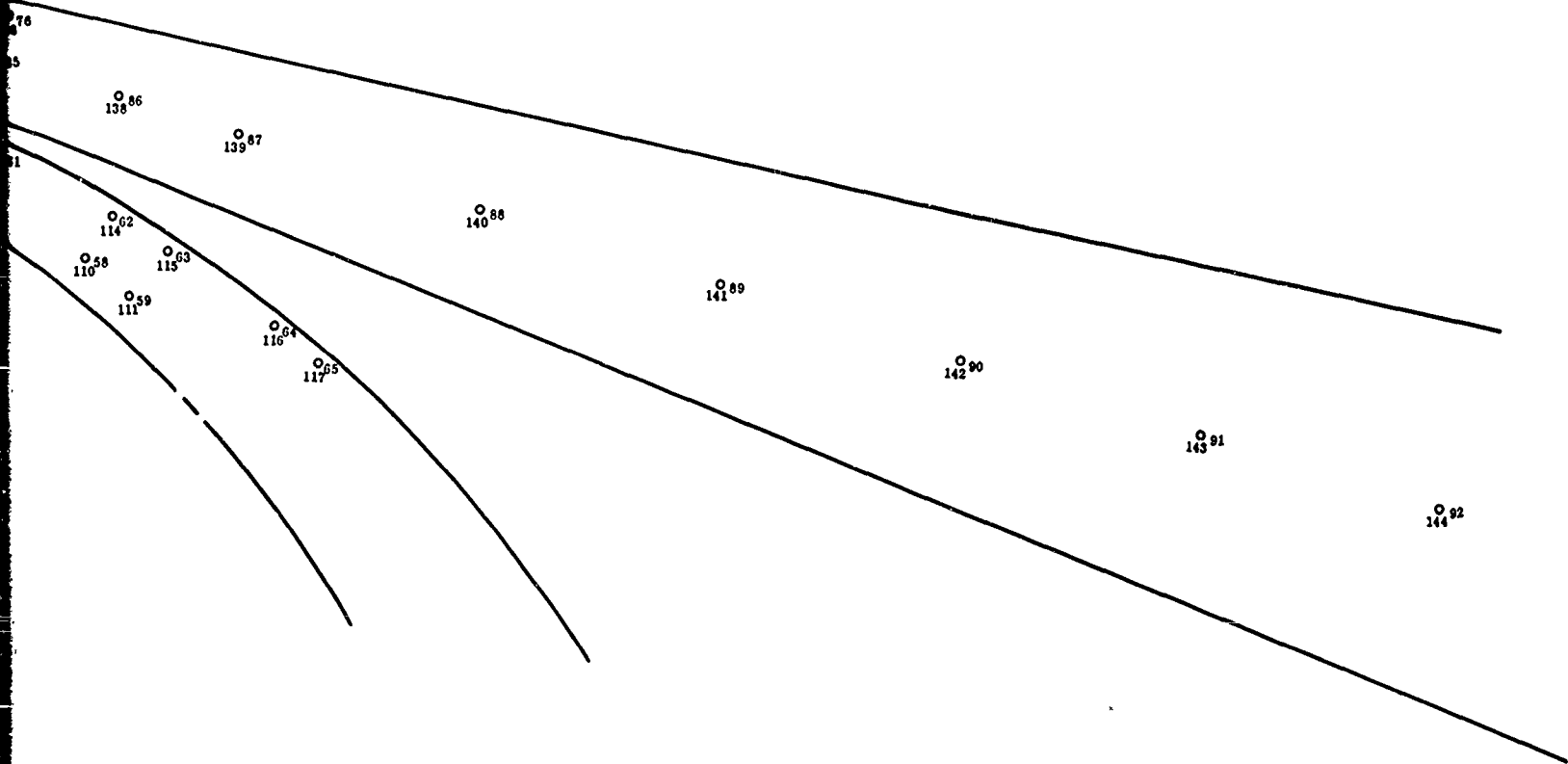


Figure 251. Locations of Static-Pressure Taps with Respect to V1-4 Diffuser Vanes.

Frontplate Tap Numbers - 49 thru 100, 157, 158, 159, 160

Rearplate Tap Numbers - 101 thru 152



Corrected Diffuser Data

Static Pressure, P_s/δ (psia)

Test No. 3355, Line 3
Configuration V1-5

Throat Size $\left\{ \begin{array}{l} \text{Total Area} = 0.909 \text{ in.}^2 \\ \text{Depth} = 0.183 \text{ in.} \end{array} \right.$

Speed, $N/\sqrt{\theta} = 50,000 \text{ rpm}$

Airflow, $W_a\sqrt{\theta}/\delta = 1.81 \text{ lb/sec}$

Tap No.	Static Pressure	Tap No.	Static Pressure	Tap No.	Static Pressure	Tap No.	Static Pressure
49	66.7	76	108.7	103	52.2	130	70.0
50	83.8	77	72.9	104	71.2	131	74.0
51	49.8	78	70.0	105	68.7	132	73.8
52	72.0	79	74.1	106	67.6	133	83.1
53	68.4	80	73.9	107	66.5	134	95.3
54	68.1	81	83.4	108	81.8	135	102.5
55	66.6	82	95.3	109	51.9	136	---
56	83.3	83	102.2	110	72.0	137	107.2
57	46.8	84	105.3	111	71.8	138	117.4
58	73.0	85	107.3	112	85.8	139	123.6
59	72.6	86	117.2	113	60.7	140	130.0
60	88.7	87	123.9	114	77.5	141	132.1
61	60.5	88	130.0	115	78.9	142	---
62	78.3	89	132.1	116	74.5	143	133.3
63	78.5	90	133.1	117	76.5	144	133.6
64	74.5	91	133.4	118	88.9	145	79.3
65	76.0	92	133.6	119	59.0	146	92.9
66	89.7	93	79.8	120	77.9	147	106.9
67	59.1	94	93.3	121	75.8	148	104.4
68	78.1	95	107.3	122	78.1	149	106.6
69	75.8	96	104.3	123	78.9	150	107.5
70	77.8	97	75.3	124	87.0	151	105.6
71	79.1	98	107.5	125	97.1	152	108.0
72	88.1	99	105.2	126	101.1	157	---
73	96.8	100	108.3	127	105.9	158	---
74	101.9	101	67.0	128	108.7	159	---
75	105.4	102	82.8	129	73.2	160	91.9

Corrected Diffuser Data

Static Pressure, P_s/δ (psia)

Test No. 3355, Line 5

Configuration V1-5

Throat Size $\left\{ \begin{array}{l} \text{Total Area} = 0.909 \text{ in.}^2 \\ \text{Depth} = 0.183 \text{ in.} \end{array} \right.$

Speed, $N/\sqrt{\theta} = 50,000 \text{ rpm}$

Airflow, $W_a \sqrt{\theta/\delta} = 1.93 \text{ lb/sec}$

Tap No.	Static Pressure	Tap No.	Static Pressure	Tap No.	Static Pressure	Tap No.	Static Pressure
49	67.8	76	104.0	103	55.6	130	73.4
50	79.2	77	72.8	104	68.7	131	69.8
51	55.0	78	69.7	105	68.9	132	70.8
52	68.7	79	70.8	106	65.7	133	74.6
53	68.1	80	74.8	107	68.7	134	78.8
54	65.7	81	79.3	108	78.4	135	91.1
55	68.4	82	91.4	109	54.9	136	97.9
56	79.2	83	98.0	110	70.2	137	100.6
57	51.6	84	100.6	111	71.8	138	102.7
58	70.3	85	102.8	112	92.1	139	114.5
59	71.8	86	114.4	113	87.2	140	121.6
60	87.1	87	121.9	114	63.3	141	128.4
61	63.8	88	128.4	115	74.7	142	130.5
62	75.9	89	130.6	116	78.7	143	---
63	78.8	90	130.6	117	73.8	144	131.7
64	74.1	91	131.8	118	73.7	145	132.0
65	73.4	92	131.9	119	90.1	146	74.7
66	88.0	93	74.8	120	63.7	147	89.1
67	62.8	94	89.3	121	74.7	148	102.4
68	75.3	95	103.8	122	75.6	149	98.5
69	76.0	96	98.5	123	74.4	150	102.1
70	74.3	97	102.4	124	79.2	151	102.2
71	79.4	98	103.2	125	82.5	152	99.5
72	84.1	99	98.9	126	92.7	157	103.3
73	92.5	100	103.6	127	96.5	158	---
74	97.5	101	68.2	128	101.5	159	---
75	100.8	102	80.1	129	104.2	160	92.0

Corrected Diffuser Data

Static Pressure, P_s/δ (psia)Test No. 3355, Line 7
Configuration V1-5Throat Size $\left\{ \begin{array}{l} \text{Total Area} = 0.909 \text{ in.}^2 \\ \text{Depth} = 0.183 \text{ in.} \end{array} \right.$ Speed, $N/\sqrt{\theta} = 50,000 \text{ rpm}$ Airflow, $W_a\sqrt{\theta}/\delta = 2.04 \text{ lb/sec}$

Tap No.	Static Pressure	Tap No.	Static Pressure	Tap No.	Static Pressure	Tap No.	Static Pressure
49	66.0	76	92.8	103	52.7	130	70.0
50	67.3	77	69.1	104	66.5	131	69.7
51	62.5	78	69.4	105	68.1	132	70.3
52	66.0	79	70.2	106	66.0	133	72.2
53	66.9	80	72.3	107	66.0	134	73.6
54	65.4	81	74.2	108	67.5	135	81.2
55	65.5	82	81.7	109	64.4	136	87.2
56	68.2	83	87.7	110	66.8	137	87.1
57	60.2	84	87.4	111	68.3	138	91.0
58	66.4	85	76.6	112	92.1	139	107.2
59	67.7	86	107.3	113	88.1	140	115.6
60	83.8	87	116.0	114	69.4	141	122.5
61	69.7	88	122.6	115	71.6	142	124.3
62	70.9	89	124.4	116	75.2	143	----
63	75.9	90	125.1	117	73.7	144	125.4
64	74.3	91	125.4	118	73.6	145	125.7
65	73.5	92	125.6	119	90.2	146	70.0
66	84.6	93	69.9	120	70.1	147	80.0
67	68.3	94	80.2	121	71.6	148	92.7
68	72.4	95	94.0	122	74.6	149	83.6
69	75.3	96	83.4	123	74.5	150	90.6
70	74.6	97	90.8	124	76.5	151	91.9
71	77.0	98	92.4	125	76.3	152	83.3
72	78.4	99	82.2	126	81.6	157	91.4
73	81.8	100	91.5	127	85.4	158	----
74	87.0	101	66.8	128	88.9	159	----
75	88.3	102	67.2	129	92.9	160	----
							92.1

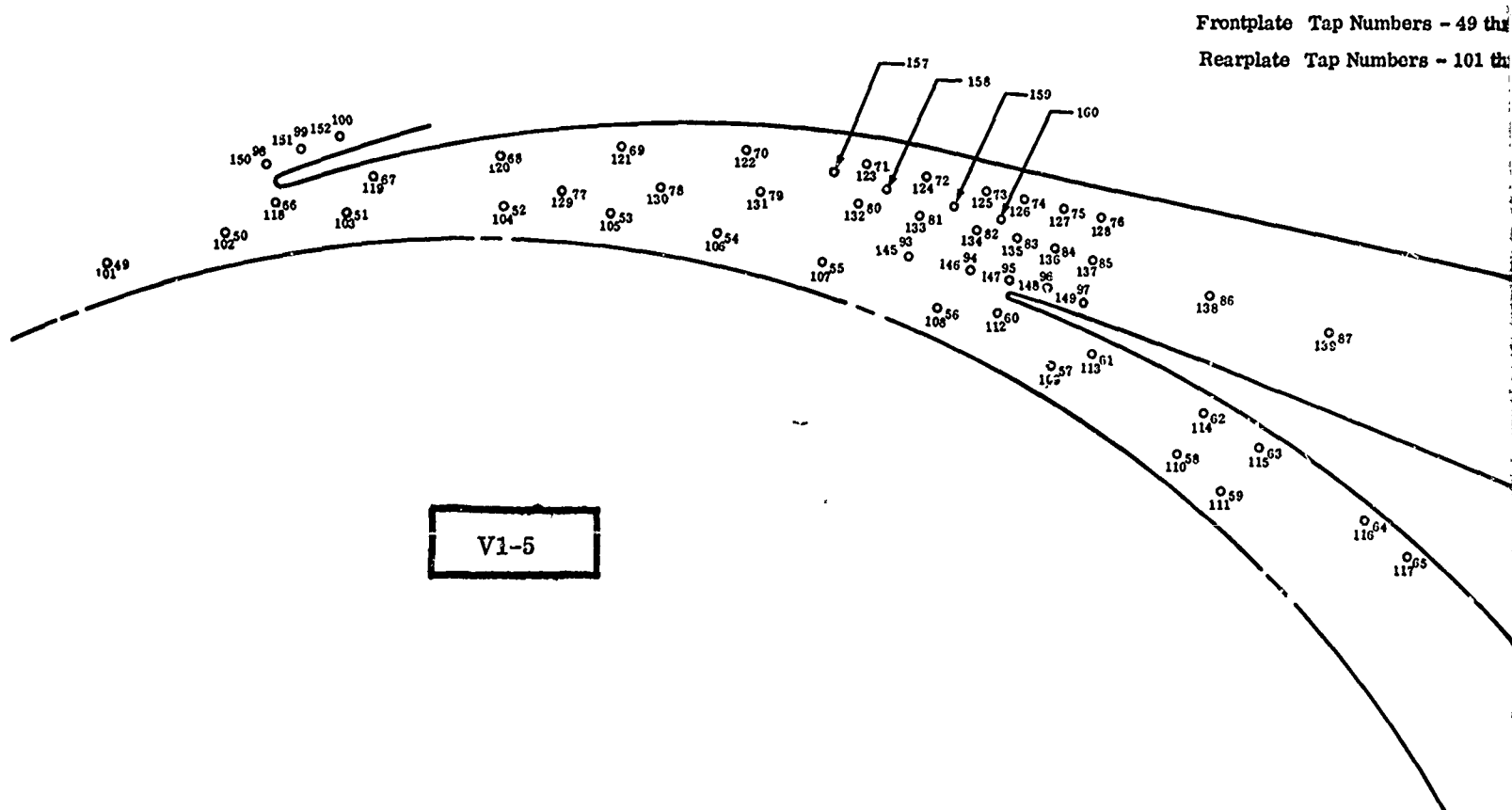
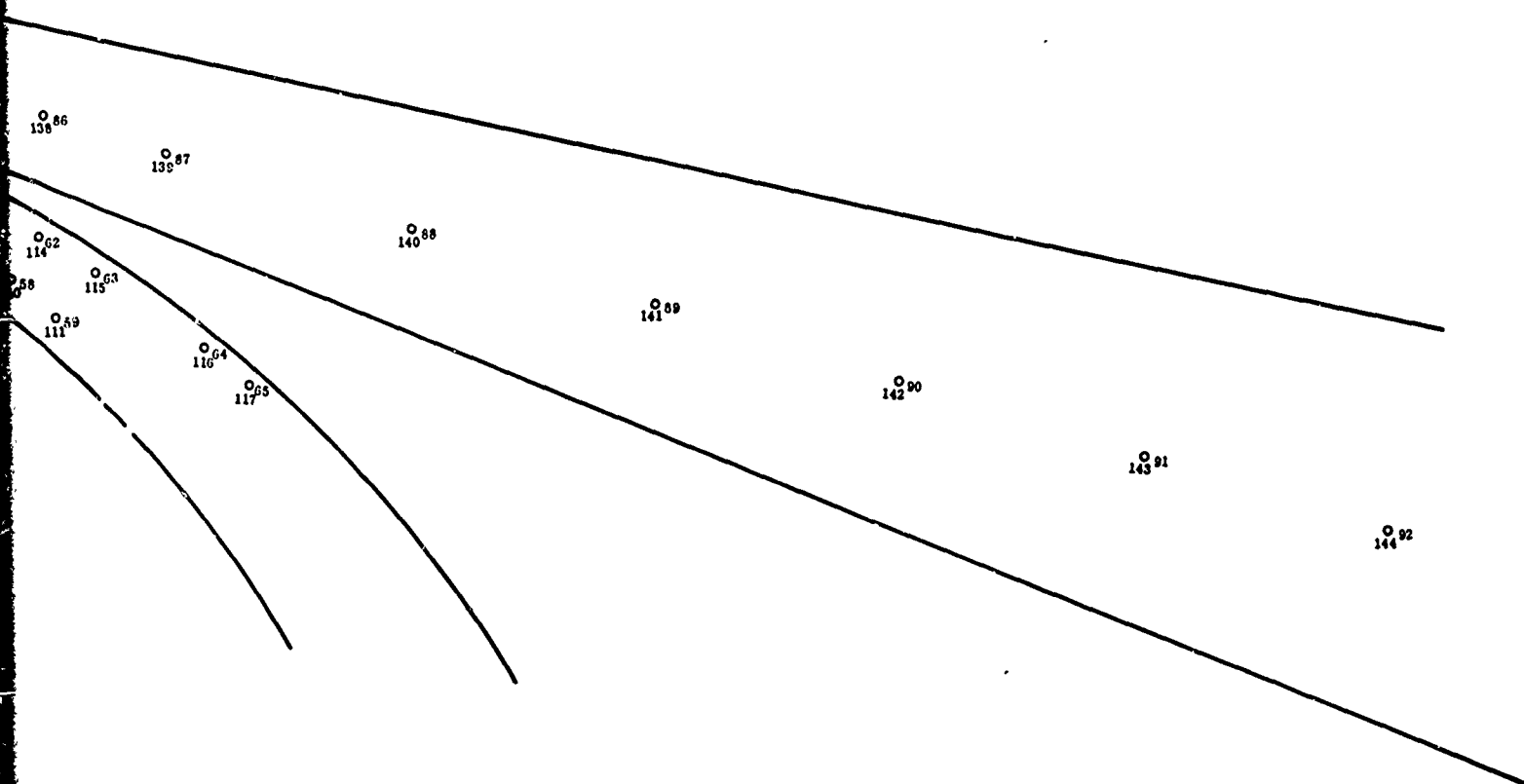


Figure 252. Locations of Static-Pressure Taps with Respect to V1-5 Diffuser Vanes.

Frontplate Tap Numbers - 49 thru 100, 157, 158, 159, 160

Rearplate Tap Numbers - 101 thru 152



Corrected Diffuser Data

Static Pressure, P_s/δ (psia)

Test No. 3356, Line 3
Configuration V1-6

Throat Size $\left\{ \begin{array}{l} \text{Total Area} = 0.946 \text{ in.}^2 \\ \text{Depth} = 0.183 \text{ in.} \end{array} \right.$

Speed, $N/\sqrt{\theta} = 50,000 \text{ rpm}$

Airflow, $W_a\sqrt{\theta/\delta} = 1.88 \text{ lb/sec}$

Tap No.	Static Pressure	Tap No.	Static Pressure	Tap No.	Static Pressure	Tap No.	Static Pressure
49	63.9	76	108.5	103	51.4	130	68.9
50	83.6	77	71.9	104	70.3	131	72.3
51	49.2	78	69.0	105	67.9	132	74.1
52	71.0	79	72.5	106	69.4	133	84.2
53	66.1	80	72.0	107	65.2	134	95.7
54	66.9	81	84.8	108	81.9	135	102.6
55	64.7	82	95.9	109	50.5	136	105.6
56	83.2	83	102.6	110	71.2	137	107.2
57	45.7	84	105.8	111	70.9	138	116.6
58	71.8	85	107.4	112	85.2	139	108.1
59	71.3	86	116.3	113	59.5	140	129.2
60	87.6	87	122.9	114	76.6	141	131.4
61	59.5	88	129.1	115	77.8	142	---
62	77.5	89	131.5	116	73.4	143	132.8
63	77.5	90	132.6	117	75.2	144	133.2
64	73.5	91	133.0	118	88.6	145	80.4
65	74.9	92	133.2	119	60.3	146	93.2
66	88.9	93	80.8	120	76.7	147	106.8
67	59.1	94	93.6	121	74.5	148	104.6
68	77.0	95	107.5	122	76.4	149	106.6
69	74.6	96	104.5	123	79.3	150	107.1
70	76.2	97	107.0	124	88.2	151	105.4
71	79.6	98	107.5	125	97.8	152	107.9
72	89.3	99	104.6	126	101.6	157	---
73	97.6	100	108.2	127	106.0	158	---
74	102.4	101	65.7	128	108.4	159	---
75	105.2	102	82.7	129	72.1	160	---

Corrected Diffuser Data

Static Pressure, P_s/δ (psia)

Test No. 3356, Line 5
Configuration V1-6

Throat Size $\left\{ \begin{array}{l} \text{Total Area} = 0.946 \text{ in.}^2 \\ \text{Depth} = 0.183 \text{ in.} \end{array} \right.$

Speed, $N/\sqrt{\theta} = 50,000 \text{ rpm}$

Airflow, $W_a\sqrt{\theta/\delta} = 1.97 \text{ lb/sec}$

Tap No.	Static Pressure	Tap No.	Static Pressure	Tap No.	Static Pressure	Tap No.	Static Pressure
49	65.2	76	105.2	103	54.1	130	69.1
50	80.1	77	71.5	104	68.1	131	69.8
51	53.5	78	69.0	105	68.2	132	73.7
52	67.9	79	70.0	106	64.9	133	81.2
53	67.6	80	73.9	107	67.0	134	92.7
54	64.8	81	81.9	108	79.6	135	99.3
55	66.3	82	93.2	109	52.9	136	102.2
56	80.2	83	99.6	110	70.0	137	103.8
57	49.7	84	102.3	111	70.7	138	114.6
58	69.9	85	104.1	112	86.5	139	121.4
59	70.6	86	114.3	113	61.7	140	128.2
60	86.2	87	121.7	114	74.5	141	127.0
61	62.1	88	128.2	115	77.4	142	---
62	75.8	89	130.6	116	72.6	143	132.0
63	77.6	90	131.8	117	72.4	144	132.3
64	72.6	91	132.1	118	89.8	145	77.4
65	72.2	92	132.3	119	62.8	146	90.5
66	87.3	93	77.4	120	73.8	147	103.6
67	62.2	94	90.6	121	74.7	148	100.5
68	74.5	95	105.0	122	43.1	149	102.8
69	75.1	96	100.5	123	78.4	150	103.2
70	73.1	97	103.5	124	85.3	151	100.8
71	78.8	98	104.4	125	95.0	152	104.2
72	86.6	99	99.9	126	98.3	157	---
73	94.8	100	104.5	127	103.0	158	---
74	99.1	101	67.0	128	105.3	159	---
75	102.0	102	80.0	129	72.0	160	---

Corrected Diffuser Data

Static Pressure, P_s/δ (psia)

Test No. 3356, Line 7
Configuration V1-6

Throat Size $\left\{ \begin{array}{l} \text{Total Area} = 0.946 \text{ in.}^2 \\ \text{Depth} = 0.183 \text{ in.} \end{array} \right.$

Speed, $N/\sqrt{\theta} = 50,000 \text{ rpm}$

Airflow, $W_a\sqrt{\theta/\delta} = 2.06 \text{ lb/sec}$

Tap No.	Static Pressure	Tap No.	Static Pressure	Tap No.	Static Pressure	Tap No.	Static Pressure
49	63.3	76	96.5	103	60.8	130	68.8
50	72.3	77	68.0	104	65.61	131	68.9
51	59.7	78	68.4	105	67.1	132	71.2
52	65.1	79	68.5	106	64.7	133	75.1
53	66.0	80	71.1	107	64.8	134	85.5
54	64.1	81	75.5	108	72.1	135	90.9
55	63.9	82	85.8	109	61.3	136	92.5
56	72.5	83	91.3	110	66.4	137	94.9
57	56.6	84	92.6	111	67.8	138	108.6
58	65.9	85	95.2	112	87.2	139	116.4
59	67.1	86	108.2	113	67.2	140	123.6
60	82.9	87	116.7	114	71.1	141	125.7
61	67.1	88	123.5	115	74.5	142	---
62	72.4	89	125.9	116	72.2	143	127.0
63	75.0	90	126.8	117	71.8	144	127.3
64	72.7	91	127.1	118	90.1	145	70.8
65	71.7	92	127.3	119	68.2	146	83.6
66	83.9	93	70.7	120	70.7	147	95.5
67	66.3	94	83.5	121	73.4	148	89.3
68	71.3	95	97.0	122	72.8	149	94.0
69	74.0	96	89.5	123	75.3	150	94.9
70	72.8	97	94.2	124	78.5	151	89.5
71	75.7	98	95.6	125	86.7	152	95.2
72	80.3	99	88.4	126	89.6	157	---
73	86.8	100	95.3	127	93.7	158	---
74	90.9	101	65.2	128	96.7	159	---
75	92.5	102	72.4	129	68.9	160	---

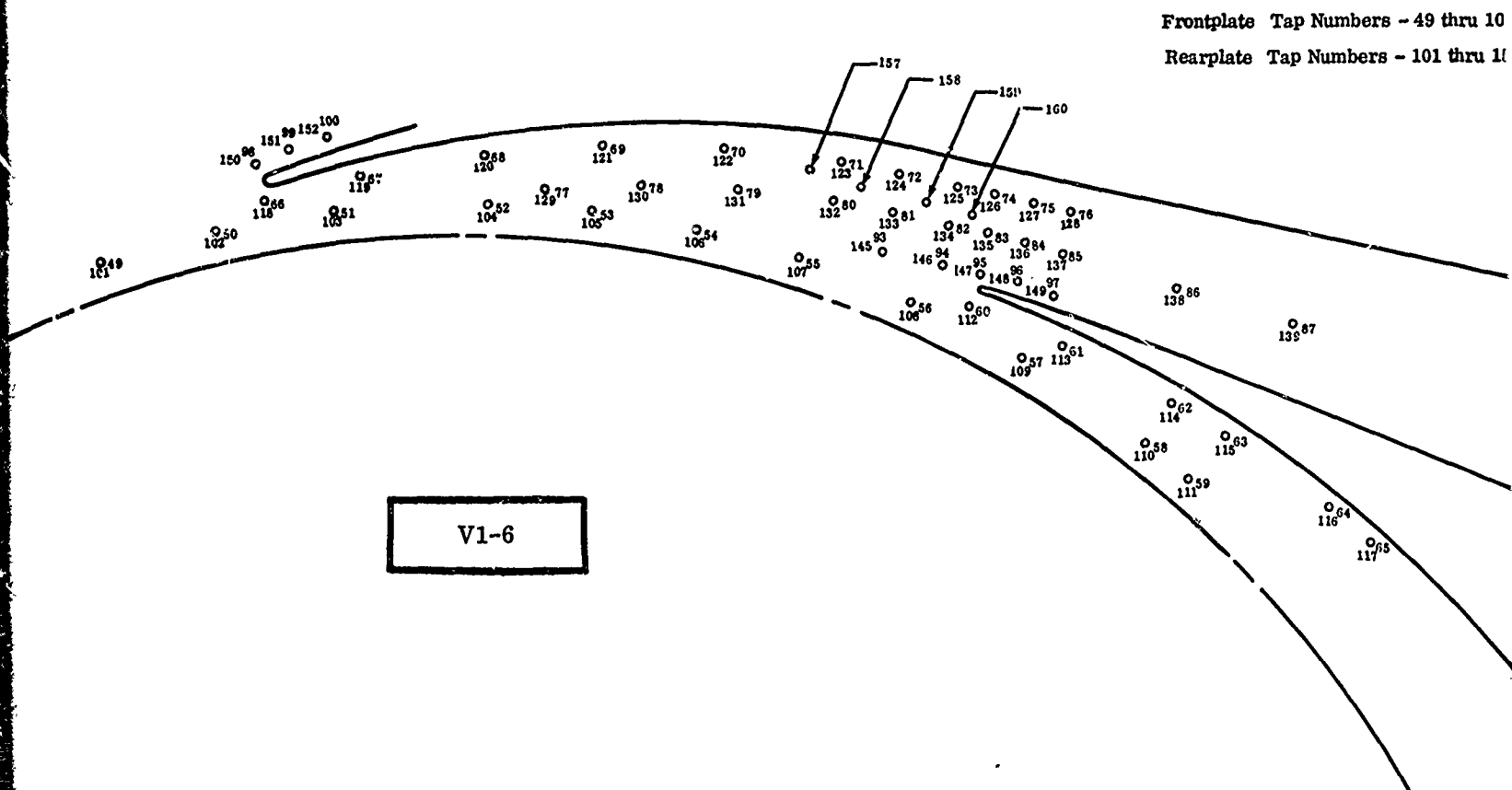


Figure 253. Locations of Static-Pressure Taps with Respect to V1-6 Diffuser Vanes.

00
15
Frontplate Tap Numbers - 49 thru 100, 157, 158, 159, 160

Rearplate Tap Numbers - 101 thru 152

138⁸⁶

138⁸⁷

140⁸⁸

141⁸⁹

142⁹⁰

143⁹¹

144⁹²

114⁶²

110⁵⁸

115⁶³

111⁵⁹

116⁶⁴

117⁶⁵

Corrected Diffuser Data

Static Pressure, P_s/δ (psia)

Test No. 3357, Line 3
Configuration V1-7

Throat Size $\left\{ \begin{array}{l} \text{Total Area} = 0.946 \text{ in.}^2 \\ \text{Depth} = 0.183 \text{ in.} \end{array} \right.$

Speed, $N/\sqrt{\theta} = 50,000 \text{ rpm}$

Airflow, $W_a\sqrt{\theta/\delta} = 1.89 \text{ lb/sec}$

Tap No.	Static Pressure	Tap No.	Static Pressure	Tap No.	Static Pressure	Tap No.	Static Pressure
49	63.7	76	107.5	103	52.6	130	69.1
50	82.6	77	72.3	104	69.5	131	72.7
51	50.7	78	69.2	105	68.3	132	72.1
52	70.0	79	73.0	106	66.5	133	82.7
53	68.0	80	72.4	107	65.3	134	94.6
54	66.7	81	83.5	108	81.0	135	101.4
55	64.8	82	95.0	109	52.6	136	104.5
56	82.1	83	101.6	110	70.0	137	106.3
57	48.9	84	104.5	111	70.7	138	116.2
58	70.4	85	106.6	112	85.4	139	122.7
59	71.0	86	116.2	113	61.3	140	129.0
60	86.9	87	122.9	114	75.1	141	---
61	61.1	88	129.1	115	77.8	142	---
62	76.2	89	131.4	116	73.0	143	131.4
63	77.7	90	131.8	117	74.5	144	131.4
64	73.2	91	131.6	118	89.0	145	79.0
65	74.5	92	131.4	119	61.1	146	92.1
66	88.8	93	79.5	120	76.1	147	105.6
67	60.7	94	92.6	121	75.0	148	103.1
68	76.5	95	106.8	122	76.3	149	105.7
69	75.2	96	103.1	123	77.2	150	106.6
70	76.3	97	106.2	124	86.9	151	104.1
71	77.7	98	106.9	125	96.8	152	106.9
72	88.2	99	103.6	126	100.3	157	71.2
73	96.7	100	107.4	127	105.2	158	77.2
74	101.3	101	65.6	128	107.4	159	---
75	105.0	102	82.0	129	72.4	160	---

Corrected Diffuser Data

Static Pressure, P_s/δ (psia)

Test No. 3357, Line 5
Configuration V1-7

Throat Size $\left\{ \begin{array}{l} \text{Total Area} = 0.946 \text{ in.}^2 \\ \text{Depth} = 0.183 \text{ in.} \end{array} \right.$

Speed, $N/\sqrt{\theta} = 50,000 \text{ rpm}$

Airflow, $W_a\sqrt{\theta/\delta} = 1.98 \text{ lb/sec}$

Tap No.	Static Pressure	Tap No.	Static Pressure	Tap No.	Static Pressure	Tap No.	Static Pressure
49	64.9	76	103.3	103	55.9	130	68.9
50	78.3	77	71.2	104	67.2	131	68.9
51	55.1	78	68.8	105	68.1	132	73.0
52	67.0	79	69.0	106	64.5	133	78.9
53	67.5	80	73.3	107	67.3	134	90.5
54	64.3	81	79.7	108	77.9	135	97.2
55	66.6	82	91.1	109	55.5	136	99.6
56	78.4	83	97.6	110	68.1	137	101.8
57	52.6	84	99.9	111	70.0	138	113.0
58	67.9	85	102.2	112	86.4	139	120.2
59	69.7	86	113.2	113	63.1	140	127.0
60	84.7	87	120.5	114	72.3	141	---
61	63.9	88	127.2	115	76.8	142	---
62	73.7	89	129.5	116	72.4	143	129.8
63	77.2	90	130.1	117	71.8	144	129.9
64	72.9	91	130.0	118	89.7	145	74.8
65	71.9	92	129.9	119	63.8	146	88.4
66	86.2	93	74.8	120	72.4	147	101.5
67	64.1	94	88.6	121	74.3	148	97.6
68	73.2	95	103.2	122	72.4	149	101.2
69	74.9	96	97.8	123	77.5	150	101.6
70	72.5	97	101.5	124	82.8	151	97.9
71	76.6	98	102.4	125	91.8	152	102.0
72	84.5	99	97.3	126	95.9	157	73.3
73	92.6	100	102.4	127	100.7	158	73.3
74	97.0	101	66.9	128	103.2	159	---
75	100.5	102	78.4	129	71.6	160	---

Corrected Diffuser Data

Static Pressure, P_s/δ (psia)Test No. 3357, Line 7
Configuration V1-7Throat Size $\left\{ \begin{array}{l} \text{Total Area} = 0.946 \text{ in.}^2 \\ \text{Depth} = 0.183 \text{ in.} \end{array} \right.$ Speed, $N/\sqrt{\theta} = 50,000 \text{ rpm}$ Airflow, $W_a\sqrt{\theta/\delta} = 2.06 \text{ lb/sec}$

Tap No.	Static Pressure	Tap No.	Static Pressure	Tap No.	Static Pressure	Tap No.	Static Pressure
49	63.0	76	94.4	103	61.9	130	68.7
50	70.3	77	67.0	104	65.2	131	68.6
51	60.7	78	68.2	105	66.7	132	70.6
52	64.5	79	68.3	106	64.5	133	72.7
53	65.7	80	70.6	107	64.4	134	83.4
54	63.9	81	73.2	108	69.1	135	88.6
55	63.7	82	83.8	109	63.3	136	89.7
56	70.0	83	69.7	110	65.4	137	92.7
57	59.2	84	68.8	111	66.7	138	107.1
58	64.8	85	78.0	112	87.0	139	115.2
59	65.9	86	107.1	113	68.2	140	122.2
60	81.8	87	115.5	114	68.1	141	---
61	68.2	88	122.4	115	73.2	142	---
62	71.4	89	124.4	116	72.0	143	125.5
63	73.8	90	125.5	117	71.6	144	125.8
64	72.5	91	125.7	118	89.7	145	68.6
65	71.6	92	125.8	119	68.7	146	81.6
66	83.2	93	68.6	120	70.2	147	93.4
67	67.6	94	81.7	121	73.2	148	86.1
68	70.7	95	94.7	122	72.6	149	91.7
69	73.7	96	86.3	123	74.5	150	93.3
70	72.6	97	92.0	124	76.4	151	86.9
71	75.0	98	93.8	125	84.4	152	93.3
72	78.3	99	86.1	126	87.2	157	---
73	84.5	100	93.4	127	91.1	158	---
74	88.7	101	65.0	128	94.5	159	---
75	90.8	102	70.0	129	68.2	160	---

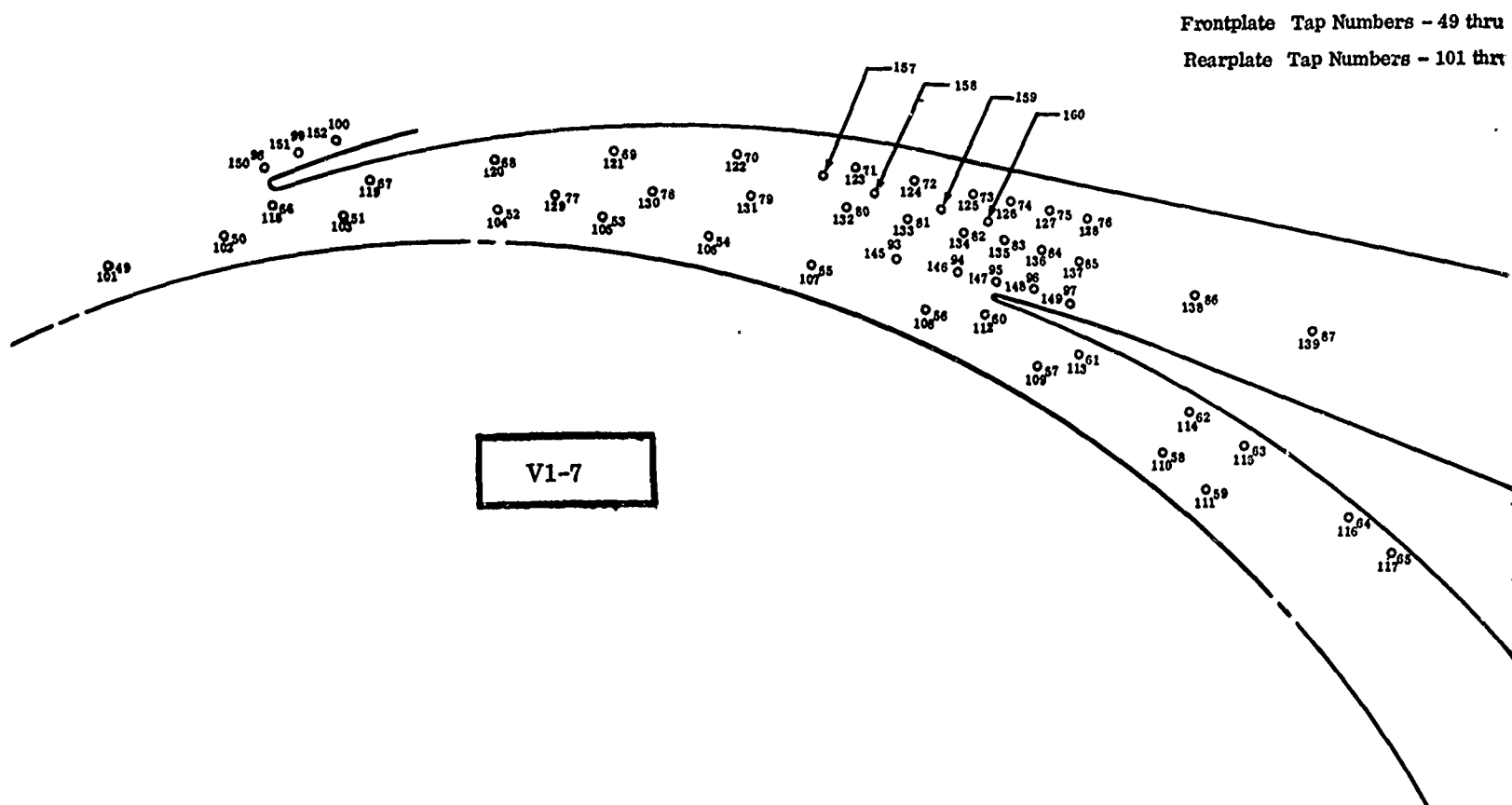
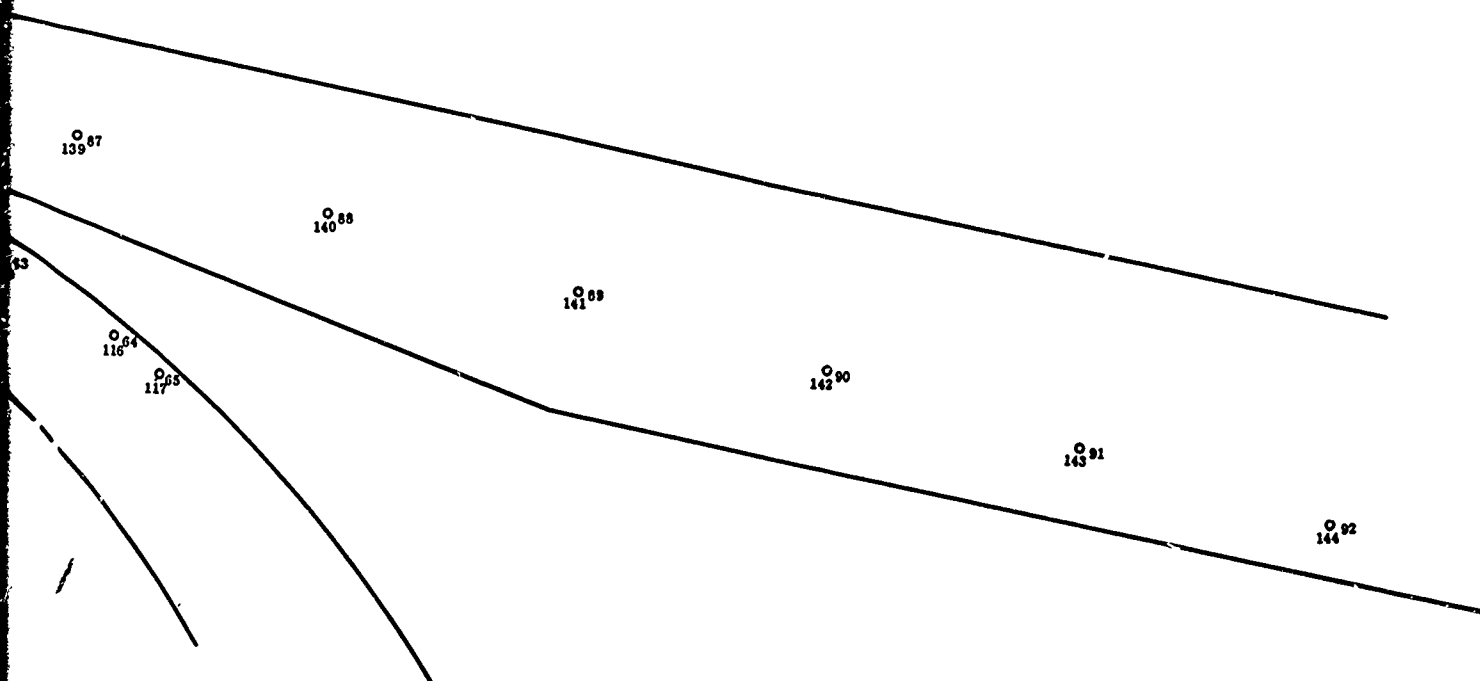


Figure 254. Locations of Static-Pressure Taps with Respect to V1-7 Diffuser Vanes.

ate Tap Numbers - 49 thru 100, 157, 158, 159, 160

ate Tap Numbers - 101 thru 152



Corrected Diffuser Data

Static Pressure, P_s/δ (psia)

Test No. 3358A, Line 3
Configuration V1-8

Throat Size $\left\{ \begin{array}{l} \text{Total Area} = 0.946 \text{ in.}^2 \\ \text{Depth} = 0.183 \text{ in.} \end{array} \right.$

Speed, $N/\sqrt{\theta} = 50,000 \text{ rpm}$

Airflow, $W_a\sqrt{\theta}/\delta = 1.83 \text{ lb/sec}$

Tap No.	Static Pressure	Tap No.	Static Pressure	Tap No.	Static Pressure	Tap No.	Static Pressure
49	64.6	76	110.2	103	48.3	130	69.7
50	85.6	77	72.2	104	70.7	131	71.3
51	44.9	78	69.8	105	67.3	132	76.6
52	72.1	79	71.5	106	66.4	133	86.3
53	67.4	80	76.8	107	64.6	134	97.7
54	66.8	81	86.7	108	82.3	135	104.5
55	64.2	82	97.6	109	50.0	136	108.0
56	84.0	83	104.3	110	70.8	137	109.4
57	44.4	84	107.8	111	70.4	138	115.0
58	71.5	85	109.5	112	84.4	139	118.7
59	71.1	86	114.9	113	58.8	140	123.9
60	87.6	87	119.0	114	77.2	141	---
61	59.0	88	123.9	115	77.8	142	---
62	77.8	89	126.4	116	75.1	143	129.4
63	77.4	90	128.3	117	75.1	144	130.5
64	75.2	91	129.5	118	88.3	145	82.1
65	74.8	92	130.4	119	56.8	146	94.8
66	88.6	93	82.8	120	77.3	147	109.1
67	57.4	94	95.4	121	74.8	148	107.4
68	77.3	95	109.0	122	76.2	149	109.5
69	74.8	96	107.4	123	81.5	150	110.8
70	75.9	97	109.8	124	90.2	151	109.9
71	81.7	98	110.5	125	99.8	152	111.9
72	91.1	99	109.6	126	103.4	157	72.6
73	99.6	100	112.2	127	108.0	158	81.1
74	104.2	101	66.5	128	110.0	159	93.5
75	108.0	102	84.4	129	72.2	160	101.8

Corrected Diffuser Data

Static Pressure, P_s/δ (psia)

Test No. 3358A, Line 5
Configuration V1-8

Throat Size $\left\{ \begin{array}{l} \text{Total Area} = 0.946 \text{ in.}^2 \\ \text{Depth} = 0.183 \text{ in.} \end{array} \right.$

Speed, $N/\sqrt{\theta} = 50,000 \text{ rpm}$

Airflow, $W_a\sqrt{\theta}/\delta = 1.95 \text{ lb/sec}$

Tap No.	Static Pressure	Tap No.	Static Pressure	Tap No.	Static Pressure	Tap No.	Static Pressure
49	63.9	76	105.9	103	52.8	130	69.1
50	81.2	77	72.0	104	68.3	131	71.1
51	51.7	78	69.0	105	67.8	132	72.7
52	68.3	79	71.2	106	64.7	133	81.5
53	67.5	80	72.9	107	65.8	134	93.3
54	64.8	81	82.2	108	79.4	135	100.2
55	65.3	82	93.7	109	53.5	136	103.0
56	80.1	83	100.3	110	69.5	137	105.0
57	50.2	84	103.1	111	70.1	138	111.7
58	69.6	85	105.3	112	71.3	139	116.4
59	70.1	86	111.7	113	62.5	140	122.5
60	86.6	87	116.7	114	74.8	141	---
61	62.8	88	122.5	115	77.5	142	---
62	76.0	89	125.6	116	72.8	143	128.9
63	77.5	90	127.7	117	73.3	144	130.2
64	73.1	91	129.1	118	89.7	145	77.7
65	73.2	92	130.1	119	61.9	146	90.9
66	88.1	93	77.9	120	75.2	147	104.5
67	61.7	94	91.2	121	74.9	148	101.6
68	75.7	95	105.7	122	73.9	149	105.0
69	75.2	96	101.6	123	77.6	150	105.2
70	73.8	97	105.4	124	85.7	151	103.3
71	78.0	98	106.3	125	95.5	152	107.0
72	86.9	99	102.9	126	99.0	157	72.9
73	95.3	100	107.4	127	103.6	158	76.0
74	99.9	101	65.7	128	105.9	159	89.3
75	103.4	102	80.8	129	72.2	160	97.6

Corrected Diffuser Data
Static Pressure, P_s/δ (psia)

Test No. 3358A, Line 7
Configuration V1-8

Throat Size $\left\{ \begin{array}{l} \text{Total Area} = 0.946 \text{ in.}^2 \\ \text{Depth} = 0.183 \text{ in.} \end{array} \right.$

Speed, $N/\sqrt{\theta} = 50,000 \text{ rpm}$

Airflow, $W_a\sqrt{\theta}/\delta = 2.05 \text{ lb/sec}$

Tap No.	Static Pressure	Tap No.	Static Pressure	Tap No.	Static Pressure	Tap No.	Static Pressure
49	62.9	76	96.4	103	59.8	130	68.7
50	73.3	77	68.3	104	65.1	131	68.7
51	58.5	78	68.2	105	66.5	132	71.3
52	64.6	79	68.4	106	64.0	133	74.7
53	65.7	80	71.3	107	64.3	134	85.3
54	63.5	81	75.2	108	71.0	135	90.8
55	63.6	82	85.6	109	61.8	136	92.5
56	71.6	83	91.1	110	65.7	137	95.4
57	57.7	84	92.6	111	67.2	138	104.1
58	65.2	85	95.6	112	87.0	139	109.9
59	66.5	86	104.1	113	67.9	140	117.2
60	82.6	87	110.3	114	70.9	141	---
61	67.7	88	117.3	115	74.5	142	---
62	72.0	89	120.8	116	72.2	143	124.8
63	74.9	90	126.3	117	71.8	144	126.1
64	72.6	91	124.9	118	90.0	145	70.5
65	71.8	92	126.0	119	67.8	146	83.3
66	83.9	93	70.4	120	70.7	147	95.4
67	66.7	94	83.4	121	73.3	148	89.3
68	71.3	95	96.8	122	72.6	149	95.4
69	73.8	96	89.5	123	75.3	150	95.8
70	72.6	97	95.7	124	78.2	151	91.7
71	75.8	98	96.7	125	86.4	152	97.6
72	80.0	99	90.9	126	89.4	157	70.5
73	86.5	100	97.9	127	93.6	158	70.2
74	90.8	101	64.8	128	96.5	159	81.2
75	93.3	102	73.5	129	68.9	160	88.9

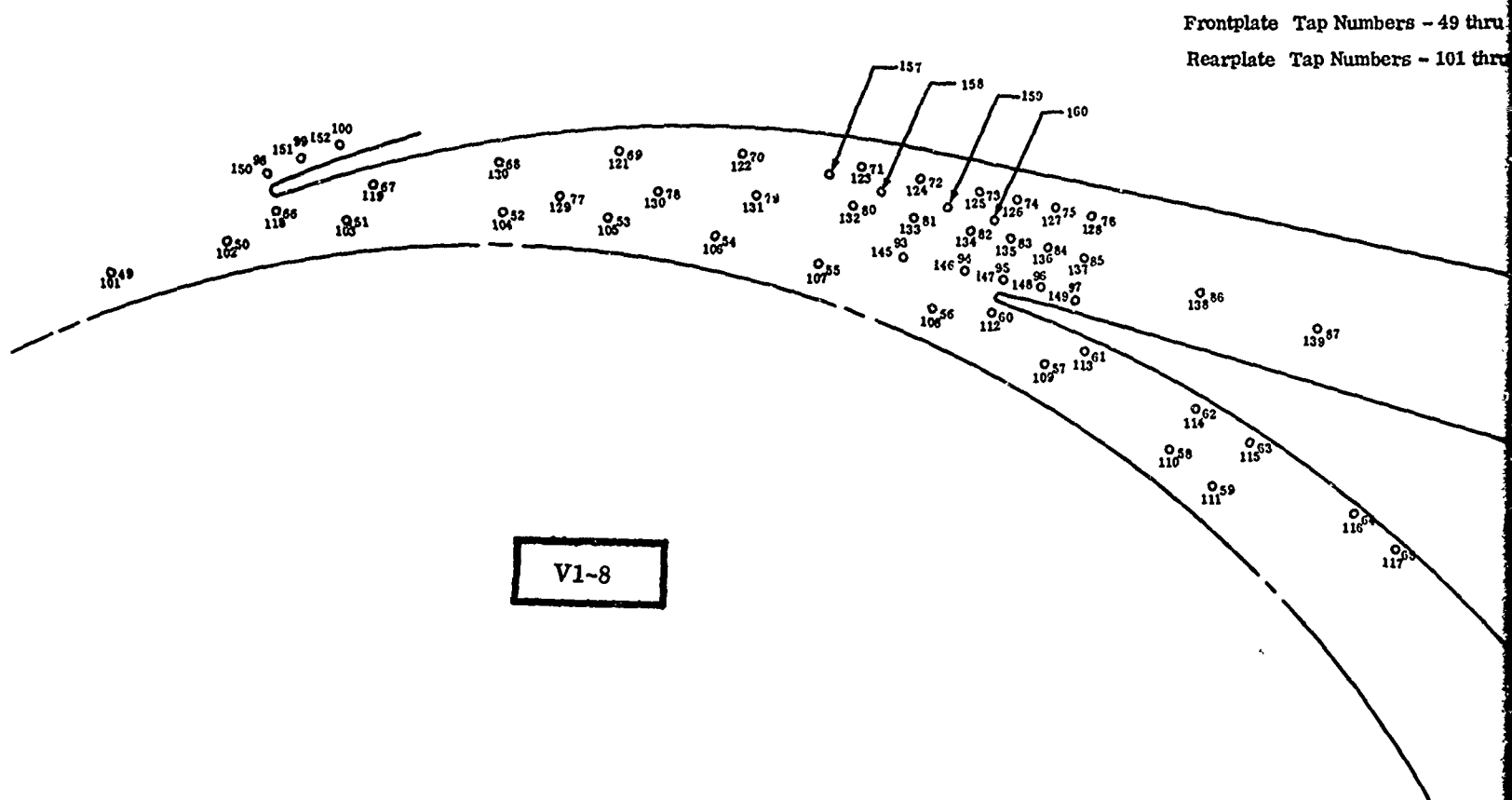
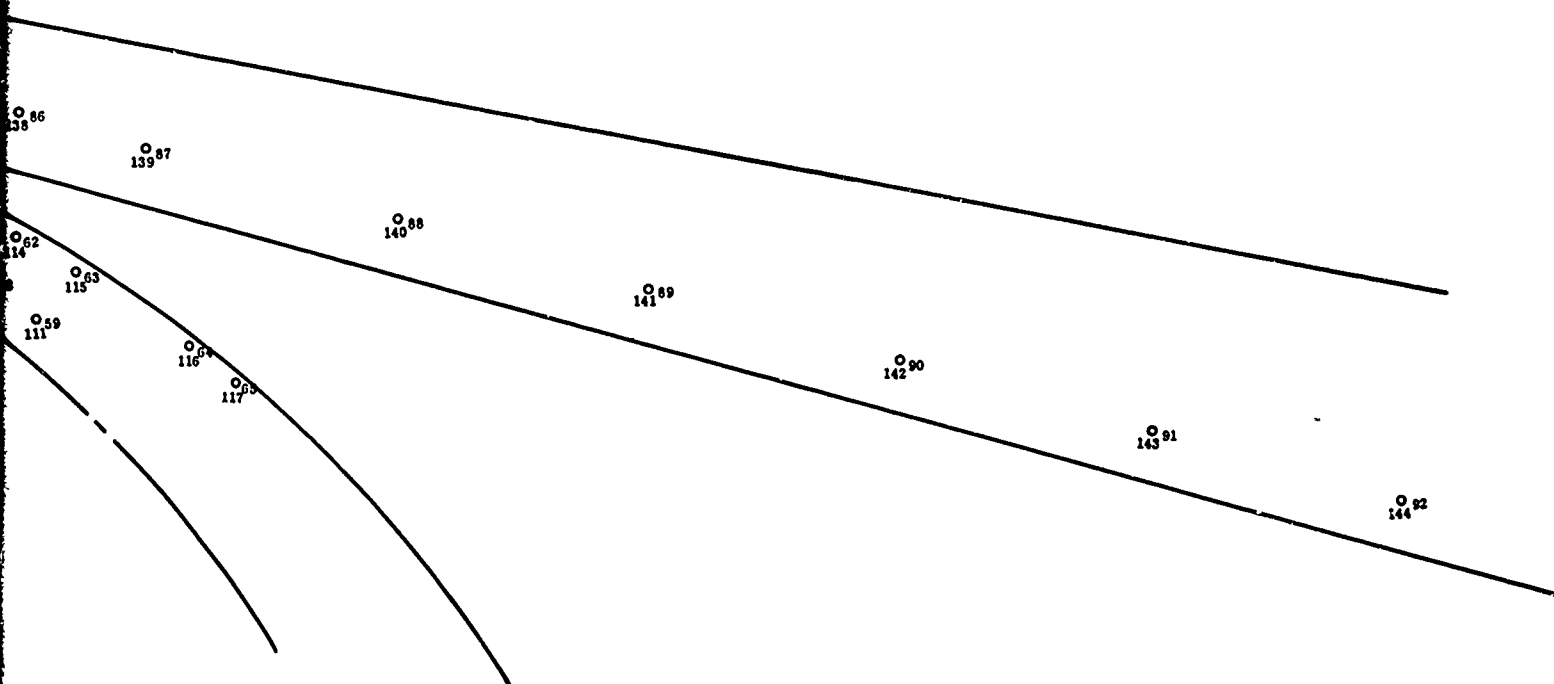


Figure 255. Locations of Static-Pressure Taps with Respect to V1-8 Diffuser Vanes.

Frontplate Tap Numbers - 49 thru 100, 157, 158, 159, 160

Rearplate Tap Numbers - 101 thru 152



Corrected Diffuser Data

Static Pressure, P_s/δ (psia)

Test No. 3359, Line 3
Configuration V1-9

Throat Size $\left\{ \begin{array}{l} \text{Total Area} = 0.946 \text{ in.}^2 \\ \text{Depth} = 0.183 \text{ in.} \end{array} \right.$

Speed, $N/\sqrt{\theta} = 50,000 \text{ rpm}$

Airflow, $W_a\sqrt{\theta/\delta} = 1.92 \text{ lb/sec}$

Tap No.	Static Pressure	Tap No.	Static Pressure	Tap No.	Static Pressure	Tap No.	Static Pressure
49	64.9	76	107.8	103	52.2	130	70.0
50	83.8	77	72.6	104	69.7	131	72.0
51	50.7	78	69.6	105	69.0	132	73.9
52	69.9	79	72.0	106	66.0	133	83.4
53	68.5	80	74.0	107	66.6	134	95.3
54	66.3	81	84.0	108	81.4	135	102.3
55	66.1	82	95.5	109	53.7	136	105.6
56	82.6	83	102.3	110	70.4	137	107.6
57	49.8	84	105.5	111	71.1	138	116.3
58	70.8	85	107.7	112	86.4	139	122.5
59	71.2	86	116.3	113	62.2	140	128.9
60	87.7	87	122.6	114	75.6	141	---
61	62.0	88	128.9	115	78.3	142	---
62	76.6	89	131.8	116	73.7	143	134.1
63	78.0	90	133.3	117	74.6	144	134.9
64	73.8	91	134.3	118	90.2	145	79.6
65	74.3	92	134.8	119	61.0	146	92.8
66	89.2	93	79.8	120	76.5	147	106.7
67	60.6	94	93.0	121	75.8	148	104.6
68	76.7	95	107.6	122	75.0	149	107.9
69	75.9	96	104.6	123	79.0	150	107.9
70	74.6	97	108.1	124	37.6	151	107.5
71	79.2	98	108.6	125	97.5	152	110.0
72	88.7	99	106.1	126	101.2	157	---
73	97.2	100	110.1	127	105.8	158	---
74	101.9	101	66.8	128	107.9	159	---
75	105.6	102	83.1	129	72.9	160	---

Corrected Diffuser Data
Static Pressure, P_s/δ (psia)

Test No. 3359, Line 5
Configuration V1-9

Throat Size $\left\{ \begin{array}{l} \text{Total Area} = 0.946 \text{ in.}^2 \\ \text{Depth} = 0.183 \text{ in.} \end{array} \right.$

Speed, $N/\sqrt{\theta} = 50,000 \text{ rpm}$

Airflow, $W_a\sqrt{\theta}/\delta = 1.99 \text{ lb/sec}$

Tap No.	Static Pressure	Tap No.	Static Pressure	Tap No.	Static Pressure	Tap No.	Static Pressure
49	65.2	76	103.7	103	55.7	130	69.7
50	79.6	77	71.4	104	67.6	131	69.2
51	55.0	78	69.5	105	68.7	132	74.0
52	67.4	79	69.2	106	65.0	133	79.7
53	68.2	80	74.1	107	67.5	134	91.5
54	64.7	81	80.3	108	78.3	135	98.2
55	66.9	82	91.9	109	56.8	136	101.0
56	78.8	83	98.4	110	68.4	137	103.5
57	53.5	84	101.0	111	70.1	138	113.3
58	68.1	85	103.7	112	87.2	139	120.0
59	69.8	86	113.4	113	64.2	140	127.2
60	82.8	87	120.3	114	72.8	141	---
61	64.7	88	127.1	115	77.1	142	---
62	74.0	89	130.3	116	73.2	143	132.9
63	77.2	90	131.9	117	72.7	144	133.7
64	73.6	91	133.0	118	90.7	145	75.5
65	72.6	92	133.6	119	63.8	146	89.3
66	87.0	93	75.3	120	73.2	147	102.6
67	64.2	94	89.2	121	75.2	148	99.3
68	73.8	95	104.1	122	73.1	149	103.9
69	75.6	96	99.4	123	78.5	150	102.8
70	73.0	97	104.2	124	83.7	151	100.6
71	78.9	98	104.1	125	93.5	152	105.4
72	85.1	99	100.0	126	97.0	157	73.9
73	93.3	100	105.8	127	101.5	158	74.4
74	97.9	101	67.1	128	103.8	159	87.4
75	101.1	102	79.5	129	71.8	160	95.6

Corrected Diffuser Data

Static Pressure, P_s/δ (psia)

Test No. 3359, Line 7
Configuration V1-9

Throat Size $\left\{ \begin{array}{l} \text{Total Area} = 0.946 \text{ in.}^2 \\ \text{Depth} = 0.183 \text{ in.} \end{array} \right.$

Speed, $N/\sqrt{\theta} = 50,000 \text{ rpm}$

Airflow, $W_a\sqrt{\theta}/\delta = 2.07 \text{ lb/sec}$

Tap No.	Static Pressure	Tap No.	Static Pressure	Tap No.	Static Pressure	Tap No.	Static Pressure
49	62.9	76	93.1	103	62.4	130	68.7
50	70.1	77	67.1	104	65.2	131	68.6
51	61.2	78	68.2	105	66.5	132	70.3
52	64.5	79	68.3	106	64.6	133	72.0
53	65.6	80	70.3	107	64.3	134	83.0
54	63.9	81	72.6	108	68.4	135	88.2
55	63.5	82	83.3	109	64.1	136	89.4
56	69.4	83	88.7	110	65.4	137	92.8
57	60.2	84	89.5	111	66.6	138	106.0
58	64.9	85	93.1	112	87.1	139	113.8
59	65.8	86	106.1	113	68.7	140	122.0
60	82.0	87	114.1	114	70.2	141	---
61	68.9	88	121.9	115	72.8	142	---
62	71.4	89	125.1	116	72.0	143	128.0
63	73.4	90	126.9	117	71.7	144	128.8
64	72.6	91	128.0	118	90.0	145	68.3
65	71.8	92	128.7	119	69.0	146	81.4
66	83.3	93	68.1	120	70.2	147	93.5
67	68.0	94	81.2	121	73.1	148	86.1
68	55.9	95	94.5	122	72.6	149	93.4
69	73.7	96	86.2	123	74.2	150	93.7
70	72.7	97	93.7	124	75.7	151	87.9
71	74.8	98	93.9	125	83.9	152	95.7
72	77.5	99	87.0	126	86.9	157	69.9
73	84.1	100	95.8	127	90.6	158	---
74	88.2	101	64.8	128	93.2	159	---
75	90.2	102	69.7	129	67.8	160	---

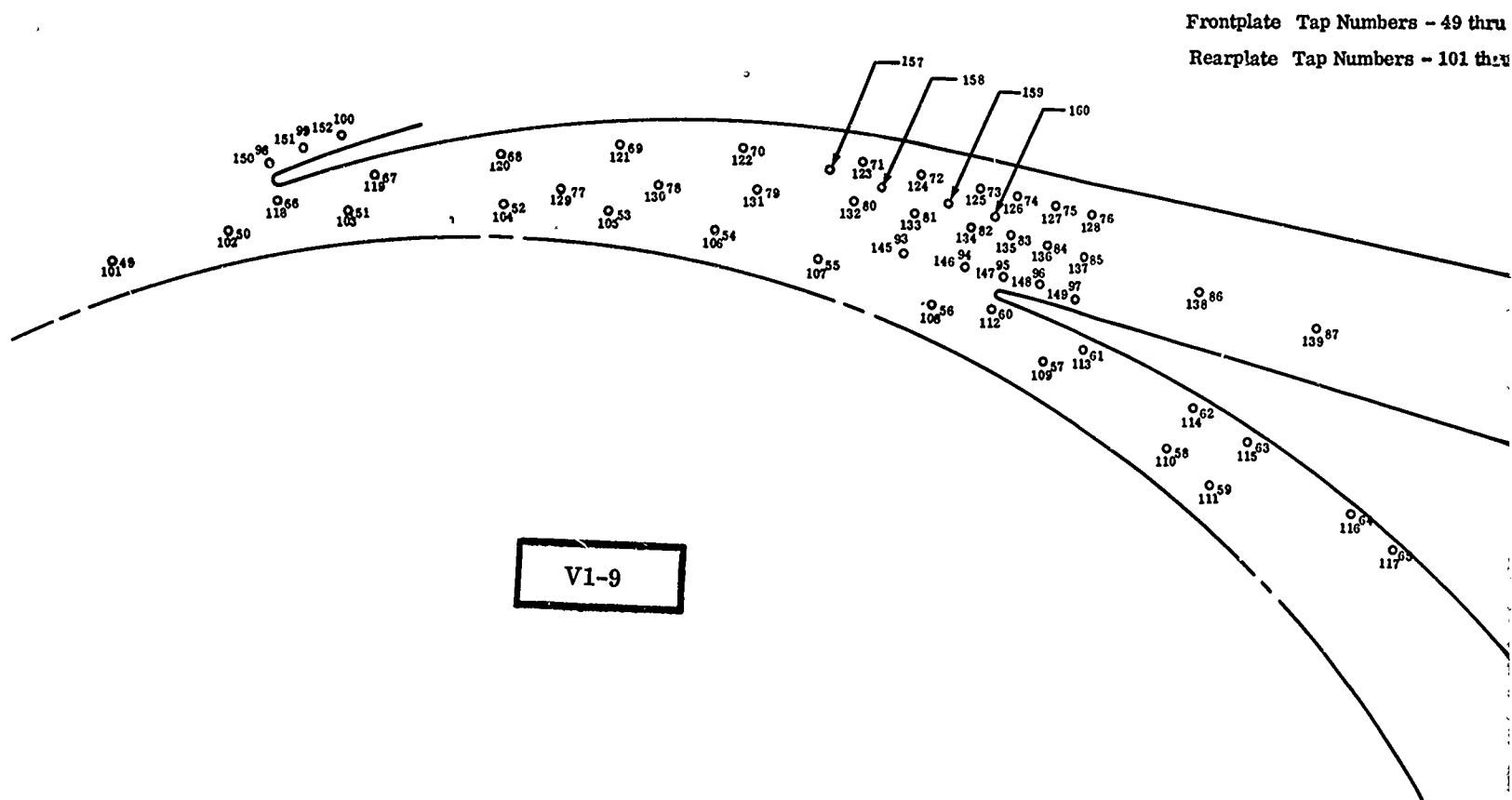
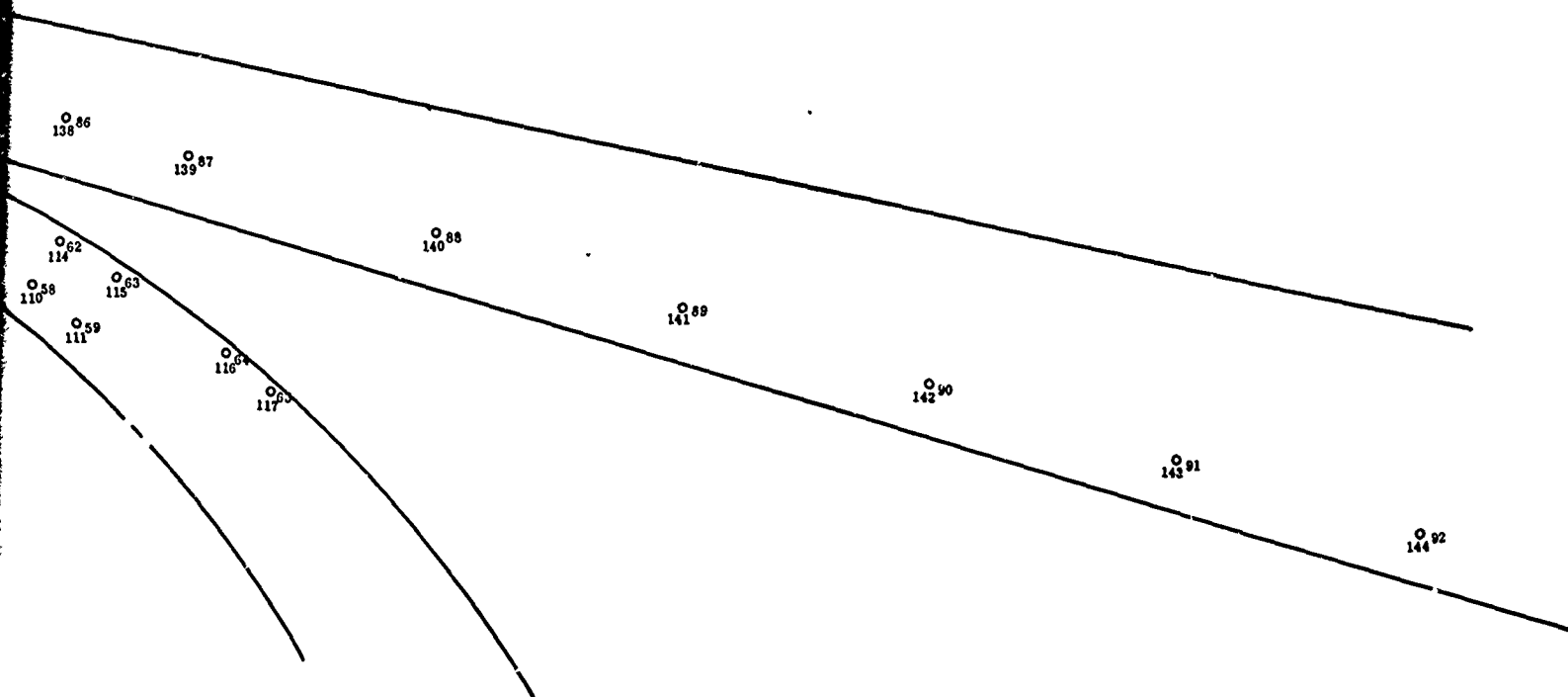


Figure 256. Locations of Static-Pressure Taps with Respect to V1-9 Diffuser Vanes.

Frontplate Tap Numbers - 49 thru 100, 157, 158, 159, 160

Rearplate Tap Numbers - 101 thru 152



Corrected Diffuser Data
Static Pressure, P_s/δ (psia)

Test No. 3360, Line 3
Configuration V1-10

Throat Size $\left\{ \begin{array}{l} \text{Total Area} = 0.946 \text{ in.}^2 \\ \text{Depth} = 0.183 \text{ in.} \end{array} \right.$

Speed, $N/\sqrt{\theta} = 50,000 \text{ rpm}$

Airflow, $W_a\sqrt{\theta}/\delta = 1.92 \text{ lb/sec}$

Tap No.	Static Pressure	Tap No.	Static Pressure	Tap No.	Static Pressure	Tap No.	Static Pressure
49	64.4	76	106.6	103	53.3	130	69.6
50	82.6	77	72.5	104	69.1	131	72.0
51	51.9	78	69.4	105	68.8	132	74.8
52	69.2	79	72.0	106	65.9	133	82.5
53	68.5	80	72.9	107	66.2	134	94.5
54	66.3	81	83.1	108	80.9	135	101.5
55	65.7	82	94.6	109	54.3	136	104.7
56	81.8	83	101.4	110	70.0	137	106.8
57	50.6	84	104.5	111	70.8	138	110.9
58	70.3	85	106.9	112	86.2	139	123.8
59	70.9	86	116.8	113	62.7	140	130.3
60	86.9	87	123.8	114	75.1	141	---
61	62.6	88	130.3	115	78.0	142	---
62	76.0	89	133.0	116	73.5	143	134.8
63	77.8	90	134.2	117	74.3	144	135.2
64	73.5	91	134.8	118	89.9	145	78.7
65	74.0	92	135.1	119	62.1	146	92.0
66	88.7	93	78.9	120	75.7	147	105.8
67	61.5	94	93.2	121	75.6	148	103.6
68	75.9	95	106.9	122	75.0	149	107.2
69	75.7	96	103.5	123	77.8	150	106.4
70	74.7	97	107.4	124	86.7	151	104.9
71	78.0	98	107.2	125	96.7	152	108.7
72	87.8	99	104.3	126	100.4	157	72.6
73	96.3	100	108.9	127	104.9	158	76.7
74	101.0	101	66.2	128	106.8	159	90.4
75	104.6	102	82.1	129	72.8	160	98.9

Corrected Diffuser Data
Static Pressure, P_s/δ (psia)

Test No. 3360, Line 5
Configuration V1-10

Throat Size $\left\{ \begin{array}{l} \text{Total Area} = 0.946 \text{ in.}^2 \\ \text{Depth} = 0.183 \text{ in.} \end{array} \right.$

Speed, $N/\sqrt{\theta} = 50,000$ rpm

Airflow, $W_a\sqrt{\theta}/\delta = 2.00$ lb/sec

Tap No.	Static Pressure	Tap No.	Static Pressure	Tap No.	Static Pressure	Tap No.	Static Pressure
49	65.1	76	103.1	103	56.5	130	69.7
50	68.9	77	71.2	104	67.2	131	69.2
51	55.8	78	69.4	105	68.7	132	73.9
52	67.0	79	69.1	106	65.0	133	79.4
53	68.2	80	73.9	107	67.3	134	91.2
54	64.7	81	80.0	108	78.1	135	97.9
55	66.7	82	91.6	109	57.2	136	100.7
56	78.6	83	98.1	110	68.3	137	103.2
57	53.9	84	100.8	111	70.0	138	114.5
58	68.0	85	103.4	112	87.1	139	122.0
59	69.6	86	114.5	113	64.5	140	129.1
60	85.1	87	122.1	114	72.7	141	
61	65.0	88	129.0	115	77.0	142	
62	73.8	89	131.8	116	73.1	143	133.7
63	77.1	90	133.1	117	72.6	144	134.2
64	73.4	91	133.7	118	90.6	145	75.2
65	72.4	92	134.0	119	64.6	146	89.1
66	86.6	93	75.0	120	72.7	147	102.3
67	64.7	94	89.0	121	75.3	148	99.2
68	73.2	95	103.9	122	73.1	149	103.8
69	75.5	96	99.1	123	68.4	150	102.1
70	72.9	97	104.0	124	83.5	151	99.9
71	78.6	98	103.4	125	93.2	152	104.8
72	84.8	99	99.1	126	96.7	157	73.8
73	93.0	100	105.1	127	101.1	158	74.1
74	97.6	101	67.1	128	103.4	159	87.3
75	100.7	102	79.0	129	71.7	160	95.4

Corrected Diffuser Data
Static Pressure, P_s/δ (psia)

Test No. 3360, Line 7
Configuration V1-10

Throat Size $\left\{ \begin{array}{l} \text{Total Area} = 0.946 \text{ in.}^2 \\ \text{Depth} = 0.183 \text{ in.} \end{array} \right.$

Speed, $N/\sqrt{\theta} = 50,000 \text{ rpm}$

Airflow, $W_a\sqrt{\theta/\delta} = 2.07 \text{ lb/sec}$

Tap No.	Static Pressure	Tap No.	Static Pressure	Tap No.	Static Pressure	Tap No.	Static Pressure
49	63.7	76	94.0	103	62.7	130	68.8
50	71.9	77	67.1	104	65.8	131	68.7
51	61.5	78	68.3	105	67.4	132	70.5
52	65.2	79	68.5	106	65.4	133	72.9
53	66.5	80	70.5	107	65.1	134	83.9
54	64.9	81	73.4	108	70.6	135	89.2
55	64.3	82	84.3	109	64.5	136	90.8
56	71.4	83	89.7	110	66.3	137	94.4
57	60.4	84	90.9	111	67.5	138	108.4
58	65.8	85	94.7	112	87.1	139	116.9
59	66.7	86	108.5	113	68.6	140	124.5
60	82.0	87	117.0	114	70.4	141	
61	68.7	88	124.4	115	73.1	142	
62	71.6	89	127.1	116	72.1	143	128.9
63	73.7	90	128.4	117	71.7	144	129.3
64	72.6	91	128.9	118	90.0	145	69.0
65	71.8	92	129.2	119	68.8	146	82.4
66	83.4	93	68.8	120	70.1	147	94.4
67	67.7	94	82.1	121	73.3	148	87.7
68	70.7	95	95.6	122	72.7	149	95.4
69	73.8	96	87.7	123	74.4	150	94.4
70	72.8	97	95.4	124	76.6	151	88.9
71	74.9	98	94.8	125	84.9	152	97.0
72	78.5	99	87.9	126	87.9	157	70.0
73	85.0	100	97.0	127	91.2	158	69.2
74	89.2	101	65.7	128	94.1	159	79.6
75	91.4	102	71.7	129	67.9	160	87.6

Corrected Diffuser Data

Static Pressure, P_s/δ (psia)

Test No. 3361, Line 3
Configuration V1-10

Throat Size $\left\{ \begin{array}{l} \text{Total Area} = 0.946 \text{ in.}^2 \\ \text{Depth} = 0.183 \text{ in.} \end{array} \right.$

Speed, $N/\sqrt{\theta} = 50,000 \text{ rpm}$

Airflow, $W_a\sqrt{\theta/\delta} = 1.93 \text{ lb/sec}$

Tap No.	Static Pressure	Tap No.	Static Pressure	Tap No.	Static Pressure	Tap No.	Static Pressure
49	65.6	76	108.3	103	53.5	130	69.7
50	82.7	77	72.2	104	69.2	131	71.5
51	52.6	78	69.4	105	69.0	132	73.3
52	69.2	79	71.4	106	65.7	133	82.5
53	68.6	80	73.3	107	66.6	134	94.5
54	65.8	81	83.1	108	80.9	135	101.6
55	66.1	82	94.8	109	54.6	136	106.3
56	81.6	83	101.7	110	69.5	137	108.7
57	52.0	84	106.1	111	70.8	138	118.4
58	70.0	85	108.8	112	87.3	139	125.2
59	70.8	86	118.4	113	62.6	140	131.5
60	86.8	87	125.1	114	74.5	141	
61	62.8	88	131.4	115	78.0	142	
62	75.4	89	134.1	116	73.5	143	135.9
63	77.9	90	135.3	117	74.0	144	136.5
64	73.8	91	136.0	118	90.6	145	78.7
65	73.7	92	136.4	119	61.3	146	91.9
66	88.2	93	78.7	120	75.6	147	104.6
67	63.2	94	92.0	121	75.7	148	106.5
68	75.7	95	106.2	122	74.6	149	109.3
69	75.7	96	106.8	123	78.2	150	105.4
70	74.2	97	109.4	124	87.7	151	107.3
71	78.4	98	106.4	125	96.9	152	110.4
72	87.8	99	107.4	126	101.5	157	74.5
73	96.7	100	110.8	127	106.1	158	80.0
74	101.6	101	66.7	128	108.4	159	90.6
75	105.9	102	82.1	129	72.6	160	99.1

Corrected Diffuser Data
Static Pressure, P_s/δ (psia)

Test No. 3361, Line 5
Configuration V1-10

Throat Size $\left\{ \begin{array}{l} \text{Total Area} = 0.946 \text{ in.}^2 \\ \text{Depth} = 0.183 \text{ in.} \end{array} \right.$

Speed, $N/\sqrt{\theta} = 50,000 \text{ rpm}$

Airflow, $W_a\sqrt{\theta/\delta} = 1.99 \text{ lb/sec}$

Tap No.	Static Pressure	Tap No.	Static Pressure	Tap No.	Static Pressure	Tap No.	Static Pressure
49	65.9	76	75.0	103	56.9	130	70.0
50	78.8	77	52.4	104	67.5	131	69.3
51	56.4	78	51.4	105	68.8	132	73.9
52	67.2	79	51.2	106	65.0	133	79.0
53	68.1	80	54.4	107	67.3	134	81.0
54	64.7	81	58.2	108	77.8	135	97.8
55	66.6	82	66.1	109	57.7	136	102.2
56	78.1	83	70.3	110	67.8	137	105.0
57	55.5	84	73.4	111	69.6	138	116.0
58	67.4	85	75.4	112	88.1	139	123.3
59	69.2	86	82.6	113	64.7	140	130.3
60	61.9	87	87.3	114	72.3	141	
61	48.6	88	92.1	115	76.7	142	
62	54.0	89	94.0	116	73.4	143	135.0
63	56.3	90	94.8	117	72.7	144	135.5
64	54.3	91	95.3	118	91.2	145	74.7
65	53.5	92	95.6	119	63.9	146	88.7
66	62.6	93	54.8	120	93.3	147	101.0
67	49.4	94	64.2	121	75.3	148	102.0
68	54.0	95	73.8	122	73.2	149	105.8
69	55.5	96	73.5	123	78.4	150	100.9
70	53.8	97	76.9	124	84.2	151	102.2
71	57.5	98	73.4	125	93.2	152	106.5
72	61.5	99	73.4	126	97.8	157	75.2
73	67.1	100	76.5	127	102.3	158	77.4
74	70.5	101	67.2	128	104.8	159	87.2
75	73.1	102	78.8	129	71.4	160	95.5

Corrected Diffuser Data

Static Pressure, P_s/δ (psia)

Test No. 3361, Line 7
Configuration V1-10

Throat Size $\left\{ \begin{array}{l} \text{Total Area} = 0.946 \text{ in.}^2 \\ \text{Depth} = 0.183 \text{ in.} \end{array} \right.$

Speed, $N/\sqrt{\theta} = 50,000 \text{ rpm}$

Airflow, $W_a\sqrt{\theta/\delta} = 2.06 \text{ lb/sec}$

Tap No.	Static Pressure	Tap No.	Static Pressure	Tap No.	Static Pressure	Tap No.	Static Pressure
49	63.7	76	96.2	103	62.0	130	68.7
50	70.8	77	66.9	104	65.4	131	68.8
51	61.2	78	63.2	105	66.5	132	70.3
52	64.6	79	68.4	106	64.6	133	72.7
53	65.5	80	70.3	107	64.2	134	83.9
54	64.2	81	73.2	108	69.7	135	89.3
55	63.5	82	84.2	109	64.1	136	92.8
56	70.4	83	89.8	110	65.3	137	96.7
57	61.1	84	93.0	111	66.4	138	110.0
58	64.7	85	97.0	112	87.9	139	118.4
59	65.6	86	110.2	113	68.7	140	125.9
60	82.1	87	118.5	114	70.1	141	
61	68.6	88	125.8	115	72.7	142	
62	71.2	89	128.6	116	72.2	143	103.5
63	73.2	90	129.9	117	71.9	144	130.9
64	72.7	91	130.5	118	90.5	145	68.9
65	71.9	92	130.8	119	68.0	146	82.2
66	82.9	93	68.6	120	70.4	147	93.9
67	69.2	94	81.9	121	73.1	148	91.9
68	70.9	95	94.9	122	72.8	149	97.8
69	73.5	96	92.1	123	74.4	150	94.0
70	72.8	97	97.8	124	77.7	151	92.3
71	74.8	98	94.1	125	85.1	152	99.0
72	78.3	99	92.0	126	89.4	157	71.3
73	85.2	100	99.2	127	93.5	158	73.0
74	89.8	101	65.0	128	96.4	159	79.6
75	93.1	102	70.2	129	67.7	160	87.8

Corrected Diffuser Data

Static Pressure, P_s/δ (psia)

Test No. 3362, Line 3
Configuration V1-10

Throat Size $\left\{ \begin{array}{l} \text{Total Area} = 0.946 \text{ in.}^2 \\ \text{Depth} = 0.183 \text{ in.} \end{array} \right.$

Speed, $N/\sqrt{\theta} = 50,000 \text{ rpm}$

Airflow, $W_a\sqrt{\theta/\delta} = 1.96 \text{ lb/sec}$

Tap No.	Static Pressure	Tap No.	Static Pressure	Tap No.	Static Pressure	Tap No.	Static Pressure
49	65.9	76	109.1	103	53.2	130	69.3
50	82.5	77	71.8	104	68.9	131	70.2
51	52.8	78	69.2	105	68.6	132	73.8
52	68.9	79	70.2	106	65.1	133	71.7
53	68.2	80	74.0	107	67.2	134	93.6
54	65.1	81	82.4	108	80.0	135	100.8
55	66.7	82	94.0	109	55.8	136	106.7
56	80.7	83	101.0	110	69.2	137	109.4
57	54.0	84	106.6	111	70.7	138	119.0
58	69.2	85	109.6	112	87.4	139	125.5
59	70.6	86	119.1	113	63.2	140	131.8
60	86.6	87	125.7	114	73.9	141	---
61	63.7	88	131.9	115	77.8	142	---
62	75.0	89	134.5	116	73.2	143	136.4
63	78.0	90	135.8	117	73.4	144	137.1
64	73.6	91	136.6	118	90.6	145	77.8
65	73.3	92	137.1	119	61.4	146	90.8
66	87.7	93	77.9	120	74.9	147	102.4
67	63.5	94	91.0	121	75.1	148	108.3
68	75.3	95	104.5	122	73.6	149	110.3
69	75.3	96	108.9	123	78.6	150	104.2
70	73.5	97	110.5	124	86.9	151	109.3
71	78.9	98	105.9	125	96.2	152	111.7
72	87.2	99	109.8	126	101.1	157	75.6
73	96.6	100	112.2	127	106.3	158	79.6
74	101.3	101	67.0	128	109.1	159	89.8
75	106.2	102	81.9	129	72.1	160	93.4

Corrected Diffuser Data

Static Pressure, P_s/δ (psia)

Test No. 3362, Line 5
Configuration V1-10

Throat Size $\left\{ \begin{array}{l} \text{Total Area} = 0.946 \text{ in.}^2 \\ \text{Depth} = 0.183 \text{ in.} \end{array} \right.$

Speed, $N/\sqrt{\theta} = 50,000 \text{ rpm}$

Airflow, $W_a\sqrt{\theta}/\delta = 2.01 \text{ lb/sec}$

Tap No.	Static Pressure	Tap No.	Static Pressure	Tap No.	Static Pressure	Tap No.	Static Pressure
49	65.6	76	105.8	103	56.2	130	69.5
50	79.5	77	70.6	104	67.5	131	69.0
51	56.0	78	69.3	105	68.5	132	74.1
52	67.2	79	68.9	106	64.9	133	79.0
53	67.9	80	74.3	107	67.0	134	90.5
54	64.5	81	79.7	108	77.3	135	97.3
55	66.4	82	91.0	109	58.9	136	103.1
56	77.7	83	97.8	110	67.7	137	106.1
57	57.0	84	103.2	111	69.7	138	116.7
58	67.3	85	106.5	112	88.1	139	123.9
59	69.2	86	117.0	113	65.2	140	130.8
60	85.2	87	124.1	114	72.0	141	
61	65.8	88	130.8	115	76.6	142	
62	73.2	89	133.5	116	73.2	143	135.6
63	76.9	90	135.0	117	72.5	144	136.3
64	73.8	91	135.8	118	91.1	145	74.8
65	72.6	92	136.3	119	63.6	146	88.1
66	86.1	93	74.6	120	72.6	147	99.3
67	66.4	94	88.1	121	74.7	148	104.5
68	73.3	95	101.5	122	72.9	149	107.2
69	75.1	96	105.3	123	78.5	150	100.5
70	72.9	97	107.4	124	84.1	151	105.2
71	78.9	98	102.5	125	92.8	152	108.5
72	84.6	99	105.7	126	97.8	157	75.2
73	92.8	100	109.0	127	103.0	158	78.0
74	45.8	101	66.8	128	105.8	159	87.0
75	102.7	102	79.3	129	71.0	160	95.3

Corrected Diffuser Data

Static Pressure, P_s/δ (psia)

Test No. 3362, Line 7
Configuration V1-10

Throat Size $\left\{ \begin{array}{l} \text{Total Area} = 0.946 \text{ in.}^2 \\ \text{Depth} = 0.183 \text{ in.} \end{array} \right.$

Speed, $N/\sqrt{\theta} = 50,000 \text{ rpm}$

Airflow, $W_a\sqrt{\theta}/\delta = 2.07 \text{ lb/sec}$

Tap No.	Static Pressure	Tap No.	Static Pressure	Tap No.	Static Pressure	Tap No.	Static Pressure
49	63.2	76	96.3	103	62.3	130	68.2
50	70.3	77	66.4	104	65.2	131	68.5
51	61.6	78	67.8	105	65.8	132	70.0
52	64.3	79	68.2	106	64.2	133	71.5
53	64.8	80	70.2	107	63.6	134	82.4
54	63.5	81	72.2	108	67.7	135	87.7
55	63.2	82	82.9	109	65.2	136	92.3
56	68.6	83	88.3	110	64.9	137	96.8
57	63.2	84	92.6	111	66.0	138	110.0
58	64.2	85	97.3	112	87.8	139	118.3
59	65.1	86	110.4	113	69.3	140	125.9
60	82.0	87	118.6	114	69.6	141	
61	69.6	88	126.0	115	72.1	142	
62	70.9	89	128.8	116	71.9	143	130.8
63	72.9	90	130.2	117	71.6	144	131.4
64	72.7	91	131.0	118	90.2	145	67.8
65	71.8	92	131.4	119	68.6	146	81.0
66	82.8	93	67.1	120	69.9	147	92.4
67	69.7	94	80.7	121	72.4	148	93.7
68	70.7	95	93.1	122	72.4	149	98.2
69	73.0	96	94.0	123	74.1	150	93.1
70	72.6	97	98.2	124	75.4	151	94.0
71	74.7	98	93.3	125	83.6	152	99.7
72	77.1	99	94.2	126	88.0	157	71.6
73	83.9	100	100.0	127	92.8	158	72.8
74	88.6	101	64.5	128	96.4	159	78.0
75	92.5	102	69.6	129	67.0	160	86.5

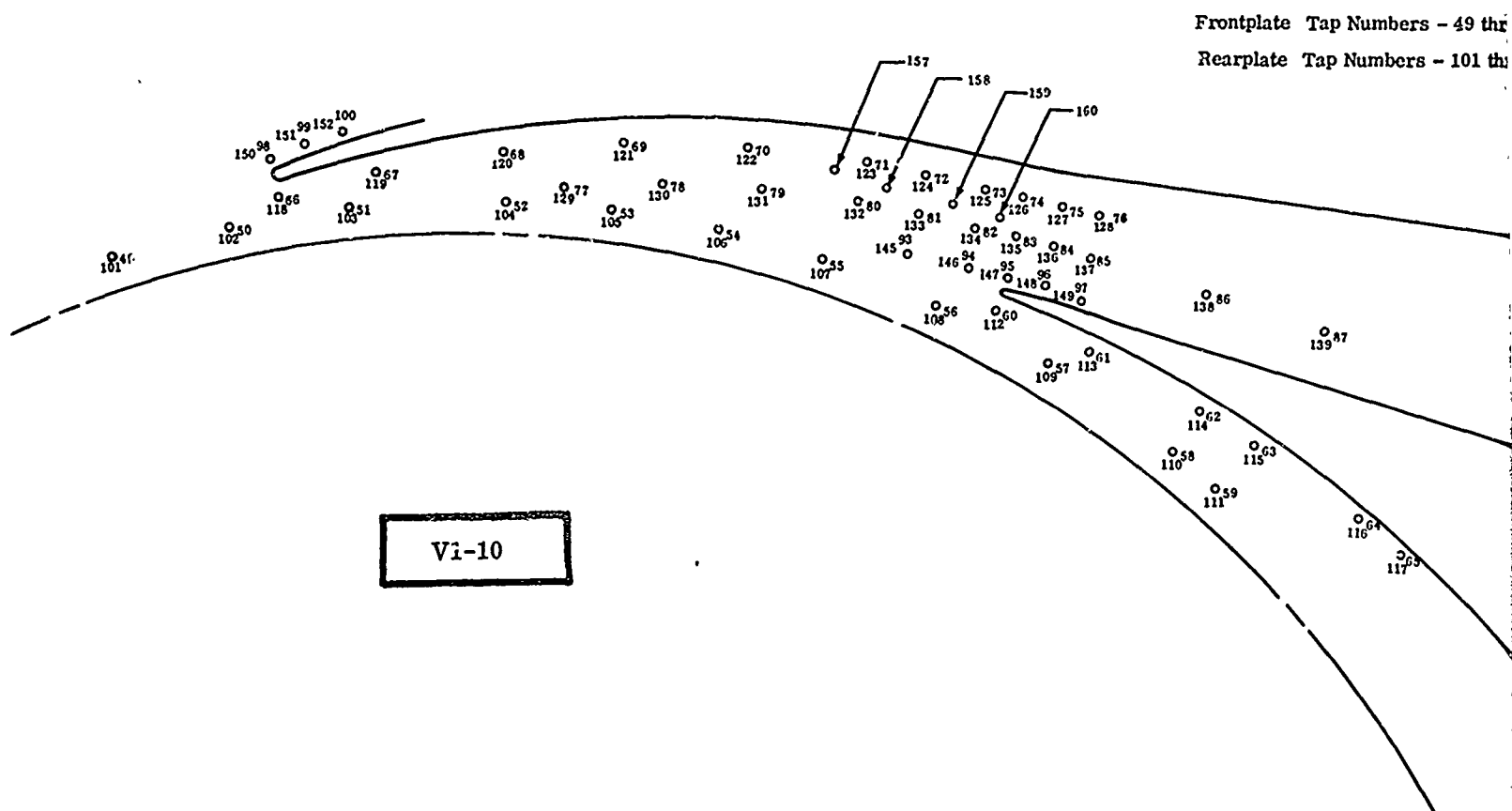
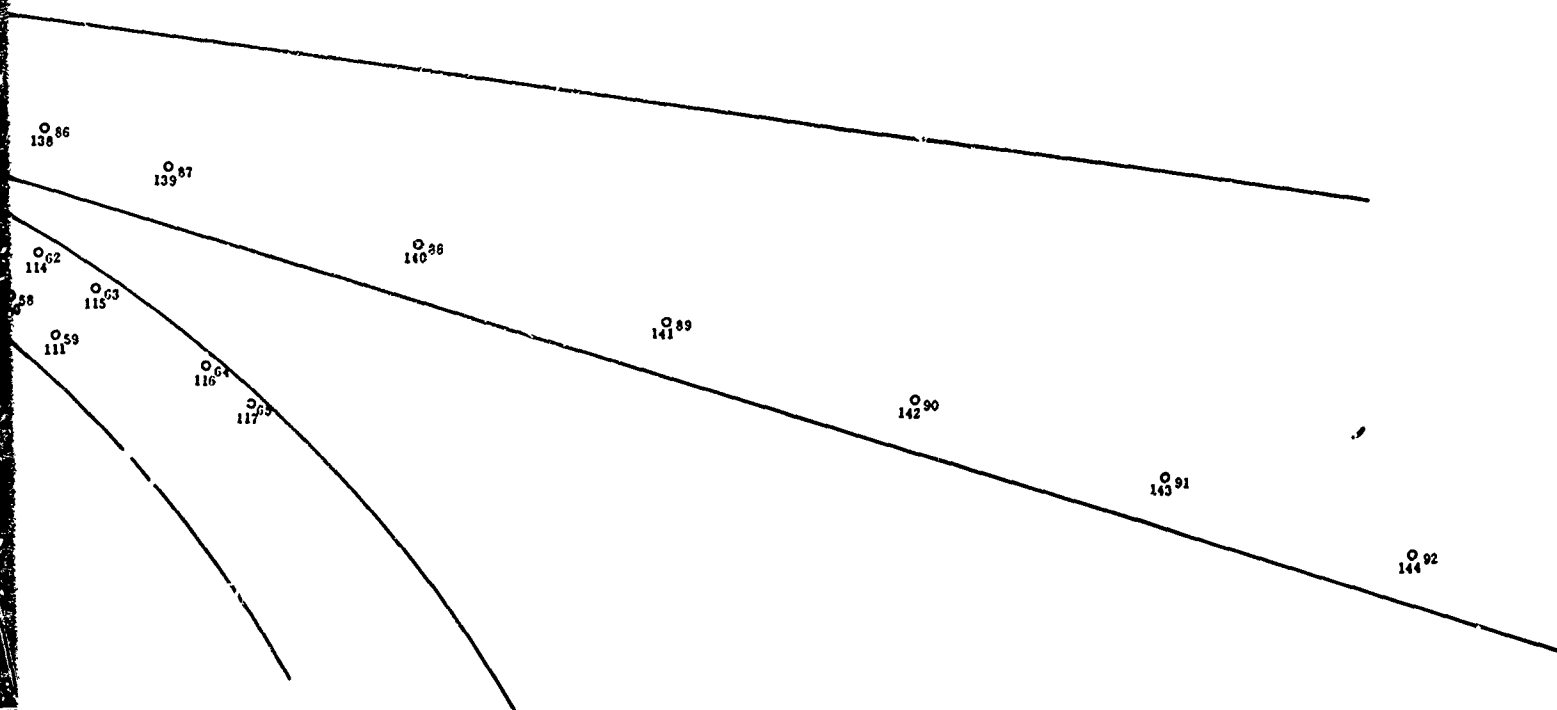


Figure 257. Locations of Static-Pressure Taps with Respect to V1-10 Diffuser Vanes.

Frontplate Tap Numbers - 49 thru 100, 157, 158, 159, 160

Rearplate Tap Numbers - 101 thru 152



Corrected Diffuser Data

Static Pressure, P_s/δ (psia)

Test No. 3363, Line 3
Configuration V1-11

Throat Size $\left\{ \begin{array}{l} \text{Total Area} = 0.946 \text{ in.}^2 \\ \text{Depth} = 0.183 \text{ in.} \end{array} \right.$

Speed, $N/\sqrt{\theta} = 50,000 \text{ rpm}$

Airflow, $W_a\sqrt{\theta}/\delta = 1.98 \text{ lb/sec}$

Tap No.	Static Pressure	Tap No.	Static Pressure	Tap No.	Static Pressure	Tap No.	Static Pressure
49	65.1	76	106.6	103	54.9	130	68.9
50	80.4	77	71.2	104	67.5	131	69.3
51	55.0	78	68.9	105	68.1	132	73.9
52	67.4	79	69.4	106	64.6	133	80.3
53	67.6	80	74.2	107	67.5	134	91.9
54	64.6	81	81.1	108	78.3	135	98.8
55	67.0	82	92.5	109	56.5	136	104.5
56	54.9	83	99.4	110	68.7	137	107.4
57	68.4	84	104.6	111	70.5	138	115.0
58	79.2	85	107.7	112	87.6	139	121.8
59	70.1	86	115.2	113	63.3	140	129.6
60	85.5	87	122.1	114	72.8	141	
61	64.3	88	129.6	115	77.0	142	
62	74.3	89	132.9	116	72.3	143	135.3
63	77.5	90	134.6	117	72.0	144	136.1
64	73.1	91	135.4	118	90.4	145	76.2
65	72.2	92	135.9	119	62.5	146	89.3
66	86.2	93	76.3	120	72.9	147	100.7
67	65.2	94	89.6	121	74.2	148	106.2
68	73.7	95	103.2	122	72.7	149	108.7
69	74.8	96	106.4	123	78.4	150	102.1
70	72.9	97	108.9	124	85.3	151	105.6
71	79.0	98	103.7	125	94.2	152	109.2
72	85.9	99	106.6	126	99.2	157	75.7
73	94.3	100	109.7	127	104.2	158	78.8
74	99.5	101	87.0	128	106.6	159	88.4
75	104.0	102	80.2	129	71.3	160	96.8

Corrected Diffuser Data

Static Pressure, P_s/δ (psia)

Test No. 3363, Line 5

Configuration V1-11

Throat Size $\left\{ \begin{array}{l} \text{Total Area} = 0.346 \text{ in.}^2 \\ \text{Depth} = 0.183 \text{ in.} \end{array} \right.$

Speed, $N/\sqrt{\theta} = 50,000 \text{ rpm}$

Airflow, $W_a\sqrt{\theta/\delta} = 2.01 \text{ lb/sec}$

Tap No.	Static Pressure	Tap No.	Static Pressure	Tap No.	Static Pressure	Tap No.	Static Pressure
49	65.3	76	104.6	103	57.3	130	69.0
50	78.5	77	70.1	104	66.7	131	68.8
51	57.2	78	69.0	105	68.0	132	73.6
52	66.5	79	68.9	106	64.7	133	78.8
53	67.4	80	74.0	107	66.5	134	90.0
54	64.5	81	80.0	108	76.9	135	96.6
55	66.0	82	90.6	109	58.8	136	102.2
56	57.0	83	97.3	110	67.7	137	105.4
57	67.2	84	102.4	111	69.5	138	113.5
58	77.2	85	105.8	112	88.1	139	120.9
59	69.0	86	113.7	113	65.0	140	129.0
60	84.8	87	121.1	114	71.8	141	
61	65.7	88	129.0	115	76.2	142	
62	73.3	89	132.5	116	72.6	143	134.9
63	76.7	90	134.2	117	72.0	144	135.7
64	73.4	91	135.1	118	90.9	145	74.6
65	72.3	92	135.6	119	64.4	146	87.6
66	85.3	93	74.6	120	71.8	147	98.7
67	66.9	94	87.7	121	74.0	148	103.7
68	72.7	95	101.2	122	72.7	149	106.8
69	74.8	96	103.9	123	78.0	150	100.0
70	73.0	97	107.0	124	83.7	151	102.7
71	78.7	98	101.3	125	92.2	152	107.1
72	84.4	99	103.7	126	97.1	157	74.6
73	92.3	100	107.6	127	102.0	158	78.0
74	97.5	101	66.6	128	104.5	159	86.6
75	101.8	102	78.4	129	70.3	160	94.7

Corrected Diffuser Data
Static Pressure, P_s/δ (psia)

Test No. 3363, Line 7
Configuration V1-11

Throat Size $\left\{ \begin{array}{l} \text{Total Area} = 0.946 \text{ in.}^2 \\ \text{Depth} = 0.183 \text{ in.} \end{array} \right.$

Speed, $N/\sqrt{\theta} = 50,000 \text{ rpm}$

Airflow, $W_a\sqrt{\theta}/\delta = 2.06 \text{ lb/sec}$

Tap No.	Static Pressure	Tap No.	Static Pressure	Tap No.	Static Pressure	Tap No.	Static Pressure
49	63.6	76	95.2	103	62.9	130	68.1
50	70.2	77	66.9	104	65.1	131	68.6
51	62.3	78	67.7	105	66.0	132	70.0
52	64.5	79	68.3	106	64.2	133	72.0
53	65.1	80	70.1	107	64.1	134	82.4
54	63.7	81	72.6	108	68.1	135	87.6
55	63.5	82	82.8	109	64.7	136	92.2
56	62.6	83	88.2	110	65.3	137	96.3
57	64.7	84	92.4	111	66.5	138	106.6
58	68.9	85	96.6	112	87.4	139	115.1
59	65.7	86	106.7	113	68.8	140	124.3
60	81.8	87	115.3	114	69.9	141	
61	69.1	88	124.3	115	72.8	142	
62	71.3	89	128.2	116	71.5	143	130.8
63	73.5	90	130.1	117	71.3	144	131.7
64	72.2	91	131.1	118	89.7	145	68.0
65	71.6	92	131.6	119	68.3	146	80.6
66	82.5	93	68.1	120	70.1	147	91.8
67	69.8	94	80.6	121	72.3	148	93.3
68	70.8	95	92.8	122	72.5	149	97.6
69	73.0	96	83.3	123	74.0	150	92.7
70	72.6	97	97.8	124	76.7	151	92.7
71	74.7	98	92.8	125	83.5	152	98.8
72	77.4	99	93.4	126	87.9	157	71.9
73	83.8	100	92.2	127	92.4	158	72.8
74	88.4	101	64.9	128	95.4	159	78.2
75	92.1	102	69.5	129	67.5	160	86.3

Corrected Diffuser Data

Static Pressure, P_s/δ (psia)

Test No. 3364, Line 3
Configuration V1-11

Throat Size $\left\{ \begin{array}{l} \text{Total Area} = 0.946 \text{ in.}^2 \\ \text{Depth} = 0.183 \text{ in.} \end{array} \right.$

Speed, $N/\sqrt{\rho} = 50,000 \text{ rpm}$

Airflow, $W_a\sqrt{\theta/\delta} = 1.96 \text{ lb/sec}$

Tap No.	Static Pressure	Tap No.	Static Pressure	Tap No.	Static Pressure	Tap No.	Static Pressure
49	65.9	76	110.1	103	54.2	130	69.4
50	81.7	77	71.9	104	68.3	131	70.4
51	53.9	78	69.4	105	68.6	132	74.3
52	68.2	79	70.6	106	65.3	133	82.4
53	68.2	80	74.6	107	67.4	134	94.3
54	65.3	81	83.2	108	80.7	135	101.5
55	67.0	82	94.7	109	54.9	136	
56	53.3	83	101.6	110	69.3	137	111.0
57	69.2	84	108.5	111	70.8	138	118.1
58	81.1	85	111.3	112	88.3	139	124.5
59	70.7	86	118.3	113	62.6	140	131.7
60	86.7	87	124.8	114	73.8	141	
61	63.2	88	131.8	115	77.7	142	
62	75.2	89	134.8	116	72.9	143	137.0
63	78.0	90	136.5	117	72.7	144	137.8
64	73.4	91	137.3	118	90.9	145	78.7
65	73.0	92	137.8	119	61.9	146	91.6
66	87.4	93	78.6	120	74.1	147	103.1
67	64.6	94	91.6	121	74.8	148	109.7
68	74.8	95	105.2	122	73.6	149	112.4
69	75.4	96	110.7	123	79.2	150	103.2
70	73.8	97	112.5	124	88.2	151	111.0
71	79.7	98	104.9	125	96.9	152	113.3
72	88.1	99	111.4	126	102.2	157	76.0
73	96.8	100	113.9	127	107.5	158	80.6
74	102.1	101	67.0	128	110.0	159	90.6
75	107.3	102	81.4	129	72.0	160	99.2

Corrected Diffuser Data

Static Pressure, P_s/δ (psia)

Test No. 3364, Line 5
Configuration V1-11

Throat Size $\left\{ \begin{array}{l} \text{Total Area} = 0.946 \text{ in.}^2 \\ \text{Depth} = 0.183 \text{ in.} \end{array} \right.$

Speed, $N/\sqrt{\theta} = 50,000$ rpm

Airflow, $W_a\sqrt{\theta}/\delta = 2.02$ lb/sec

Tap No.	Static Pressure	Tap No.	Static Pressure	Tap No.	Static Pressure	Tap No.	Static Pressure
49	65.2	76	106.9	103	57.7	130	69.1
50	78.4	77	70.2	104	66.9	131	69.1
51	57.1	78	69.1	105	68.0	132	74.0
52	66.6	79	69.2	106	64.9	133	79.8
53	67.3	80	74.3	107	66.7	134	91.1
54	64.6	81	80.6	108	78.0	135	98.0
55	66.2	82	91.6	109	57.9	136	
56	56.2	83	98.4	110	67.8	137	107.9
57	67.3	84	105.1	111	69.6	138	115.6
58	78.1	85	108.2	112	88.4	139	122.6
59	69.1	86	115.8	113	64.5	140	130.3
60	85.1	87	122.9	114	72.0	141	
61	65.3	88	130.4	115	76.3	142	
62	73.4	89	133.7	116	72.6	143	135.9
63	76.9	90	135.4	117	72.1	144	136.6
64	73.4	91	136.3	118	91.1	145	75.9
65	72.6	92	136.8	119	64.6	146	88.7
66	85.5	93	75.6	120	72.0	147	100.0
67	67.3	94	88.6	121	73.9	148	105.9
68	72.9	95	102.1	122	72.9	149	109.4
69	74.8	96	107.1	123	78.5	150	99.2
70	73.2	97	109.5	124	85.5	151	106.7
71	79.1	98	100.6	125	93.5	152	109.7
72	85.5	99	107.1	126	98.9	157	74.9
73	93.6	100	110.3	127	104.0	158	78.8
74	98.9	101	66.5	128	106.9	159	87.7
75	103.8	102	78.3	129	70.4	160	95.9

Corrected Diffuser Data
Static Pressure, P_s/δ (psia)

Test No. 3364, Line 7
Configuration V1-11

Throat Size { Total Area = 0.946 in.²
{ Depth = 0.183 in.

Speed, $N/\sqrt{\theta} = 50,000$ rpm

Airflow, $W_a\sqrt{\theta}/\delta = 2.06$ lb/sec

Tap No.	Static Pressure	Tap No.	Static Pressure	Tap No.	Static Pressure	Tap No.	Static Pressure
49	63.9	76	99.1	103	62.6	130	68.4
50	71.5	77	67.3	104	65.5	131	68.8
51	61.7	78	68.3	105	66.5	132	70.5
52	64.8	79	68.8	106	64.7	133	72.9
53	65.5	80	70.3	107	64.5	134	84.2
54	64.1	81	73.8	108	70.4	135	89.8
55	63.9	82	84.8	109	64.3	136	
56	61.9	83	90.4	110	65.6	137	100.1
57	65.0	84	96.7	111	66.8	138	109.7
58	70.8	85	100.5	112	88.2	139	118.1
59	65.9	86	110.0	113	68.7	140	126.8
60	82.8	87	118.2	114	70.3	141	
61	68.8	88	126.8	115	72.8	142	
62	71.7	89	130.7	116	71.9	143	133.1
63	73.7	90	132.6	117	71.6	144	134.0
64	72.8	91	133.5	118	90.5	145	69.1
65	72.2	92	134.0	119	68.4	146	82.7
66	83.4	93	69.0	120	70.3	147	93.7
67	69.9	94	82.3	121	72.7	148	96.7
68	71.1	95	94.7	122	72.7	149	101.8
69	73.6	96	98.0	123	74.6	150	94.0
70	73.1	97	101.9	124	78.7	151	98.9
71	75.3	98	93.9	125	85.6	152	103.3
72	78.8	99	98.9	126	90.6	157	72.5
73	85.9	100	103.8	127	95.6	158	73.5
74	90.9	101	65.2	128	99.1	159	80.3
75	95.5	102	71.0	129	67.6	160	88.4

Corrected Diffuser Data

Static Pressure, P_s/δ (psia)

Test No. 3365, Line 3
Configuration V1-12

Throat Size $\left\{ \begin{array}{l} \text{Total Area} = 0.946 \text{ in.}^2 \\ \text{Depth} = 0.183 \text{ in.} \end{array} \right.$

Speed, $N/\sqrt{\theta} = 50,000 \text{ rpm}$

Airflow, $W_a\sqrt{\theta}/\delta = 1.95 \text{ lb/sec}$

Tap No.	Static Pressure	Tap No.	Static Pressure	Tap No.	Static Pressure	Tap No.	Static Pressure
49	66.7	76	104.9	103	57.9	130	69.6
50	80.2	77	69.7	104	65.0	131	72.1
51	56.7	78	69.8	105	67.8	132	73.3
52	64.5	79	72.3	106	66.6	133	79.6
53	67.6	80	73.6	107	67.5	134	92.5
54	66.5	81	80.4	108	78.7	135	98.5
55	67.1	82	92.0	109	58.2	136	102.5
56	56.7	83	98.9	110	65.0	137	105.7
57	64.9	84	102.6	111	68.2	138	113.7
58	79.2	85	105.9	112	87.4	139	120.9
59	67.9	86	113.9	113	72.9	140	129.1
60	85.8	87	121.2	114	68.7	141	
61	68.1	88	129.2	115	75.7	142	
62	69.6	89	132.7	116	73.9	143	135.0
63	75.5	90	134.5	117	74.1	144	135.9
64	74.4	91	135.4	118	90.5	145	75.5
65	74.1	92	135.9	119	76.4	146	90.3
66	87.6	93	75.6	120	69.1	147	102.2
67	73.2	94	89.5	121	74.3	148	101.5
68	69.0	95	103.6	122	75.4	149	106.8
69	74.7	96	101.9	123	77.8	150	102.5
70	75.5	97	107.2	124	85.6	151	102.4
71	78.2	98	102.8	125	93.7	152	107.8
72	85.1	99	102.0	126	98.8	157	75.6
73	93.6	100	108.4	127	102.7	158	77.5
74	98.7	101	67.1	128	104.9	159	87.7
75	102.5	102	79.8	129	69.6	160	95.9

Corrected Diffuser Data

Static Pressure, P_s/δ (psia)

Test No. 3365, Line 5
Configuration V1-12

Throat Size $\left\{ \begin{array}{l} \text{Total Area} = 0.946 \text{ in.}^2 \\ \text{Depth} = 0.183 \text{ in.} \end{array} \right.$

Speed, $N/\sqrt{\theta} = 50,000 \text{ rpm}$

Airflow, $W_a\sqrt{\theta/\delta} = 2.02 \text{ lb/sec}$

Tap No.	Static Pressure	Tap No.	Static Pressure	Tap No.	Static Pressure	Tap No.	Static Pressure
49	66.4	76	98.8	103	62.7	130	68.7
50	73.8	77	67.2	104	63.9	131	70.9
51	61.6	78	63.8	105	66.6	132	72.0
52	63.4	79	71.0	106	66.2	133	74.9
53	65.8	80	72.4	107	66.2	134	87.0
54	65.8	81	75.8	108	72.2	135	92.2
55	65.7	82	86.6	109	63.1	136	95.9
56	61.2	83	92.9	110	63.5	137	99.7
57	63.4	84	96.3	111	65.9	138	109.2
58	72.6	85	100.1	112	87.8	139	117.5
59	65.4	86	109.6	113	76.8	140	126.6
60	83.9	87	117.8	114	67.6	141	
61	72.9	88	126.7	115	72.9	142	
62	68.7	89	130.6	116	73.1	143	133.0
63	73.2	90	132.4	117	73.8	144	133.8
64	73.8	91	133.4	118	90.5	145	71.0
65	73.9	92	133.9	119	81.0	146	84.5
66	85.1	93	70.9	120	67.8	147	96.5
67	78.6	94	84.2	121	73.0	148	94.4
68	67.9	95	97.7	122	74.8	149	101.1
69	73.6	96	94.8	123	76.3	150	96.6
70	75.0	97	101.4	124	80.8	151	95.1
71	76.8	98	96.4	125	87.7	152	102.1
72	80.6	99	94.5	126	92.7	157	73.9
73	87.8	100	102.6	127	96.5	158	75.1
74	92.7	101	67.0	128	98.9	159	82.1
75	96.3	102	73.6	129	67.3	160	90.2

Corrected Diffuser Data

Static Pressure, P_s/δ (psia)

Test No. 3365, Line 7
Configuration V1-12

Throat Size $\left\{ \begin{array}{l} \text{Total Area} = 0.946 \text{ in.}^2 \\ \text{Depth} = 0.183 \text{ in.} \end{array} \right.$

Speed, $N/\sqrt{\theta} = 50,000 \text{ rpm}$

Airflow, $W_a\sqrt{\theta/\delta} = 2.06 \text{ lb/sec}$

Tap No.	Static Pressure	Tap No.	Static Pressure	Tap No.	Static Pressure	Tap No.	Static Pressure
49	64.9	76	89.1	103	66.6	130	67.7
50	65.8	77	64.6	104	62.7	131	70.4
51	66.1	78	67.5	105	64.4	132	70.3
52	62.1	79	70.2	106	65.5	133	70.4
53	63.6	80	70.4	107	64.7	134	78.3
54	64.8	81	71.0	108	64.5	135	83.0
55	64.1	82	77.3	109	67.6	136	84.2
56	66.3	83	83.6	110	62.4	137	90.3
57	62.2	84	84.5	111	63.9	138	102.4
58	64.5	85	90.7	112	87.4	139	111.9
59	63.1	86	102.6	113	79.6	140	122.0
60	82.0	87	112.2	114	66.7	141	
61	76.2	88	122.1	115	70.2	142	
62	67.8	89	126.3	116	71.9	143	128.9
63	70.7	90	128.4	117	73.0	144	129.8
64	72.6	91	129.3	118	89.3	145	67.1
65	73.1	92	129.9	119	81.1	146	75.8
66	82.9	93	66.9	120	66.7	147	88.9
67	79.5	94	75.2	121	71.0	148	82.5
68	66.9	95	89.4	122	74.2	149	91.7
69	71.6	96	82.8	123	74.3	150	91.1
70	74.5	97	92.1	124	75.6	151	83.8
71	74.8	98	89.7	125	77.6	152	93.8
72	75.2	99	83.5	126	83.1	157	72.6
73	77.7	100	94.1	127	85.5	158	72.4
74	83.1	101	65.7	128	89.3	159	73.5
75	85.3	102	65.1	129	65.1	160	81.8

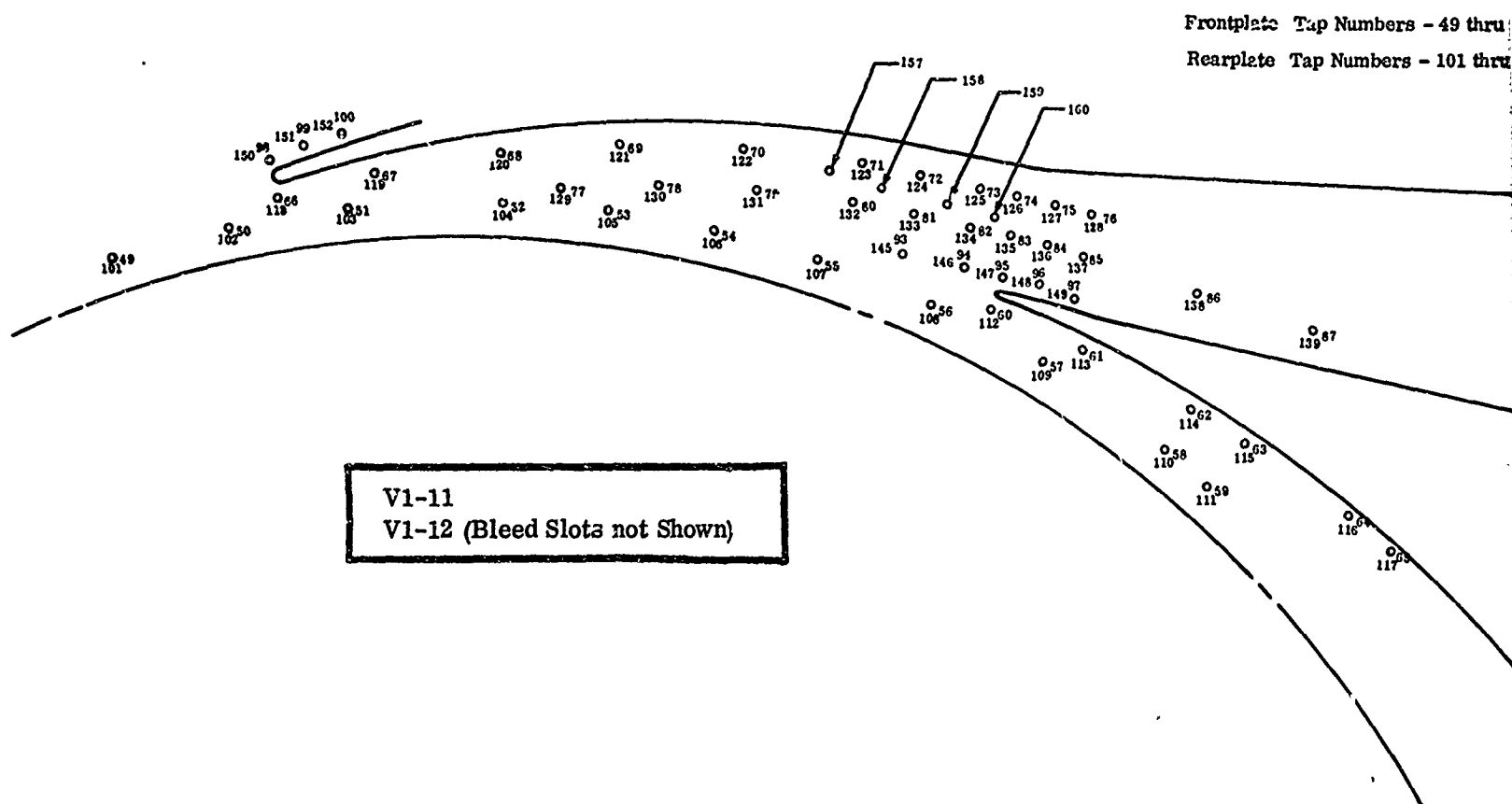
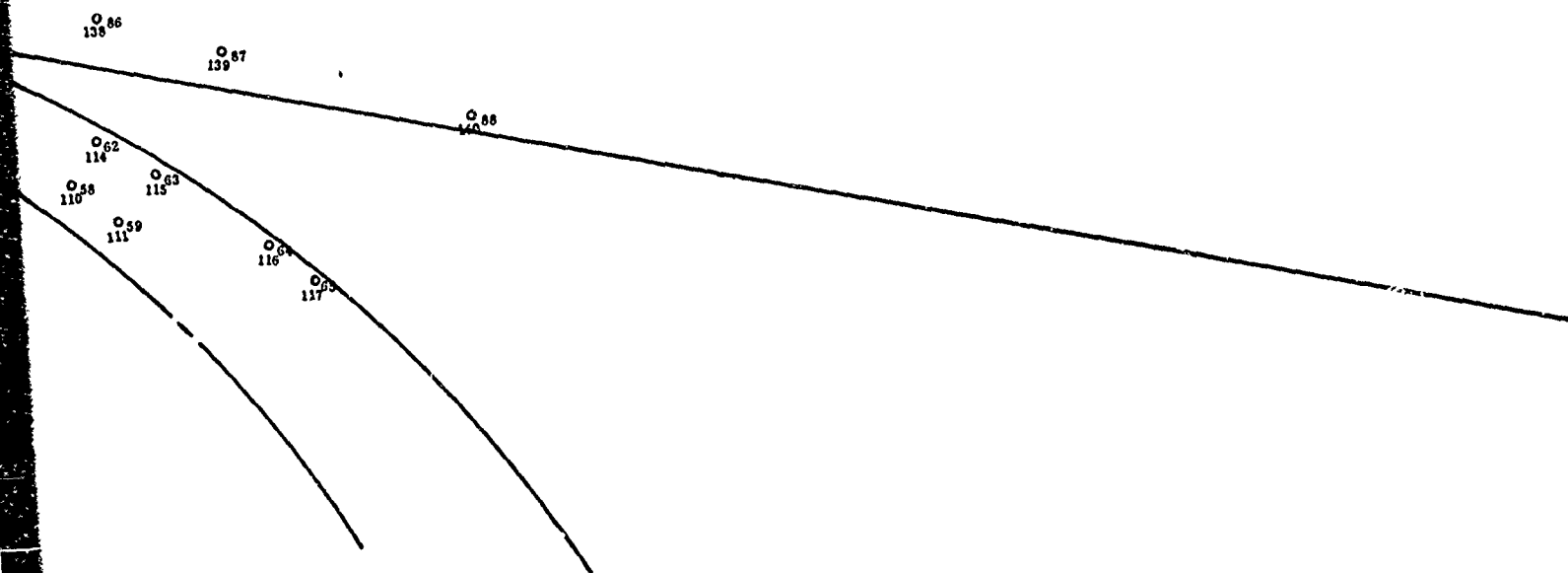


Figure 258. Locations of Static-Pressure Taps with Respect to V1-11 and V1-12 Diffuser Vanes.

Frontplate Tap Numbers - 49 thru 100, 157, 158, 159, 160
Rearplate Tap Numbers - 101 thru 152



Corrected Diffuser Data

Static Pressure, P_s/δ (psia)

Test No. 3366, Line 3
Configuration V2

Throat Size $\left\{ \begin{array}{l} \text{Total Area} = 0.865 \text{ in.}^2 \\ \text{Depth} = 0.203 \text{ in.} \end{array} \right.$

Speed, $N/\sqrt{\theta} = 50,000 \text{ rpm}$

Airflow, $W_a\sqrt{\theta}/\delta = 1.80 \text{ lb/sec}$

Tap No.	Static Pressure	Tap No.	Static Pressure	Tap No.	Static Pressure	Tap No.	Static Pressure
49	70.2	76	108.3	103	54.0	130	71.8
50	75.5	77	74.0	104	73.1	131	75.8
51	51.9	78	71.4	105	69.6	132	76.9
52	73.0	79	75.8	106	68.4	133	73.9
53	69.3	80	76.6	107	70.4	134	92.0
54	68.4	81	73.1	108	76.0	135	98.4
55	69.6	82	90.6	109	54.1	136	102.5
56	51.8	83	97.7	110	73.2	137	107.7
57	73.2	84	101.7	111	72.8	138	120.3
58	76.6	85	107.4	112	87.8	139	126.2
59	72.7	86	120.0	113	61.4	140	131.9
60	91.6	87	126.1	114	78.9	141	
61	60.8	88	131.9	115	80.4	142	
62	79.3	89	133.7	116	77.4	143	134.8
63	80.0	90	134.5	117	79.8	144	135.1
64	77.3	91	134.9	118	88.4	145	70.7
65	78.7	92	135.0	119	63.4	146	89.4
66	89.6	93	70.8	120	79.7	147	103.8
67	62.8	94	90.2	121	77.9	148	101.7
68	79.1	95	103.9	122	80.2	149	108.1
69	77.1	96	101.6	123	82.3	150	103.7
70	79.5	97	108.1	124	75.0	151	103.0
71	81.7	98	103.3	125	91.0	152	108.8
72	74.0	99	102.1	126	97.7	157	79.0
73	90.6	100	109.2	127	101.4	158	77.8
74	97.2	101	70.4	128	108.4	159	74.1
75	100.5	102	75.6	129	74.0	160	94.4

Corrected Diffuser Data
Static Pressure, P_s/δ (psia)

Test No. 3366, Line 5
Configuration V2

Throat Size $\left\{ \begin{array}{l} \text{Total Area} = 0.865 \text{ in.}^2 \\ \text{Depth} = 0.203 \text{ in.} \end{array} \right.$

Speed, $N/\sqrt{\theta} = 50,000 \text{ rpm}$

Airflow, $W_a\sqrt{\theta}/\delta = 1.88 \text{ lb/sec}$

Tap No.	Static Pressure	Tap No.	Static Pressure	Tap No.	Static Pressure	Tap No.	Static Pressure
49	70.0	76	104.9	103	56.1	130	71.4
50	65.3	77	73.4	104	71.7	131	74.0
51	57.2	78	71.0	105	69.3	132	76.7
52	70.7	79	74.3	106	67.9	133	74.2
53	68.3	80	76.8	107	70.5	134	87.3
54	67.2	81	73.9	108	68.0	135	94.2
55	68.9	82	86.6	109	55.8	136	97.8
56	56.5	83	93.9	110	72.3	137	104.1
57	71.2	84	97.2	111	74.4	138	118.0
58	67.9	85	103.9	112	88.7	139	124.1
59	71.2	86	117.8	113	63.8	140	129.9
60	89.7	87	124.1	114	77.5	141	
61	63.8	88	129.9	115	79.7	142	
62	78.6	89	131.7	116	77.0	143	132.7
63	79.9	90	132.5	117	78.9	144	132.9
64	77.2	91	132.8	118	88.7	145	71.1
65	78.0	92	132.8	119	65.6	146	85.1
66	87.4	93	71.2	120	77.9	147	98.9
67	66.1	94	86.4	121	77.0	148	97.2
68	77.9	95	101.1	122	79.0	149	104.7
69	76.7	96	97.1	123	82.4	150	98.4
70	78.5	97	105.0	124	75.3	151	98.2
71	81.8	98	99.9	125	85.3	152	105.2
72	74.5	99	97.1	126	93.8	157	78.8
73	85.0	100	105.8	127	96.8	158	78.3
74	93.2	101	70.9	128	105.2	159	67.2
75	95.8	102	65.9	129	73.7	160	90.9

Corrected Diffuser Data
Static Pressure, P_s/δ (psia)

Test No. 3366, Line 7
Configuration V2

Throat Size $\left\{ \begin{array}{l} \text{Total Area} = 0.865 \text{ in.}^2 \\ \text{Depth} = 0.203 \text{ in.} \end{array} \right.$

Speed, $N/\sqrt{\theta} = 50,000 \text{ rpm}$

Airflow, $W_a\sqrt{\theta/\delta} = 1.95 \text{ lb/sec}$

Tap No.	Static Pressure	Tap No.	Static Pressure	Tap No.	Static Pressure	Tap No.	Static Pressure
49	69.1	76	93.5	103	71.9	130	64.2
50	62.1	77	71.9	104	74.1	131	69.3
51	63.0	78	70.9	105	76.4	132	69.3
52	68.0	79	74.0	106	74.8	133	68.4
53	68.0	80	76.3	107	66.3	134	69.6
54	67.2	81	74.3	108	85.8	135	65.9
55	67.7	82	63.5	109	76.4	136	62.7
56	61.4	83	85.9	110	94.1	137	70.1
57	68.9	84	74.5	111	111.8	138	70.4
58	64.3	85	93.8	112	119.6	139	89.2
59	69.0	86	111.7	113	126.5	140	69.4
60	86.5	87	119.6	114		141	75.7
61	69.4	88	126.3	115		142	78.1
62	76.8	89	128.2	116	129.3	143	77.4
63	78.4	90	128.9	117	129.5	144	79.5
64	77.5	91	129.2	118	71.5	145	88.5
65	78.5	92	129.2	119	66.4	146	71.5
66	83.9	93	71.2	120	90.3	147	75.3
67	71.4	94	64.5	121	78.6	148	77.2
68	75.2	95	94.9	122	94.8	149	79.5
69	77.0	96	77.1	123	83.7	150	82.0
70	79.0	97	95.1	124	83.7	151	76.1
71	81.5	98	92.2	125	96.2	152	65.8
72	75.0	99	81.1	126	78.1	157	84.2
73	64.9	100	96.9	127	78.5	158	76.4
74	83.3	101	70.7	128	67.4	159	94.2
75	75.8	102	63.5	129	75.2	160	73.0

Corrected Diffuser Data

Static Pressure, P_s/δ (psia)

Test No. 3367, Line 3
Configuration V2

Throat Size $\left\{ \begin{array}{l} \text{Total Area} = 0.865 \text{ in.}^2 \\ \text{Depth} = 0.203 \text{ in.} \end{array} \right.$

Speed, $N/\sqrt{\theta} = 50,000 \text{ rpm}$

Airflow, $W_a\sqrt{\theta/\delta} = 1.82 \text{ lb/sec}$

Tap No.	Static Pressure	Tap No.	Static Pressure	Tap No.	Static Pressure	Tap No.	Static Pressure
49	70.0	76	108.3	103	54.3	130	71.6
50	74.6	77	74.2	104	73.0	131	75.6
51	52.7	78	71.5	105	69.5	132	76.9
52	72.8	79	76.0	106	68.5	133	73.7
53	69.0	80	76.9	107	70.5	134	91.9
54	68.3	81	73.8	108	75.7	135	98.2
55	69.5	82	90.8	109	54.3	136	102.4
56	52.5	83	97.8	110	73.5	137	107.6
57	73.3	84	101.8	111	72.8	138	120.2
58	76.0	85	107.5	112	87.3	139	126.1
59	72.7	86	120.2	113	61.8	140	131.8
60	92.1	87	126.1	114	78.9	141	
61	61.3	88	131.9	115	80.4	142	
62	79.7	89	133.7	116	77.5	143	134.8
63	80.3	90	134.6	117	80.1	144	135.1
64	77.6	91	134.9	118	88.2	145	70.6
65	79.1	92	135.1	119	63.0	146	89.4
66	89.8	93	71.0	120	79.5	147	103.6
67	63.4	94	90.4	121	77.6	148	101.5
68	79.1	95	104.3	122	80.2	149	108.0
69	77.2	96	101.6	123	82.3	150	103.5
70	80.0	97	108.2	124	74.9	151	103.2
71	81.9	98	103.9	125	90.9	152	109.0
72	74.2	99	102.4	126	97.5	157	79.0
73	90.7	100	109.7	127	101.2	158	77.8
74	97.3	101	70.3	128	108.3	159	73.8
75	100.6	102	75.4	129	73.8	160	94.3

Corrected Diffuser Data

Static Pressure, P_s/δ (psia)

Test No. 3367, Line 5
Configuration V2

Throat Size $\left\{ \begin{array}{l} \text{Total Area} = 0.865 \text{ in.}^2 \\ \text{Depth} = 0.203 \text{ in.} \end{array} \right.$

Speed, $N/\sqrt{\theta} = 50,000 \text{ rpm}$

Airflow, $W_a\sqrt{\theta/\delta} = 1.88 \text{ lb/sec}$

Tap No.	Static Pressure	Tap No.	Static Pressure	Tap No.	Static Pressure	Tap No.	Static Pressure
49	70.0	76	104.5	103	57.3	130	71.5
50	64.4	77	73.5	104	71.3	131	74.1
51	58.3	78	71.0	105	69.4	132	77.0
52	70.2	79	74.4	106	68.1	133	74.3
53	68.3	80	77.0	107	70.7	134	86.3
54	67.3	81	74.5	108	67.2	135	93.7
55	69.0	82	85.5	109	56.8	136	97.1
56	57.5	83	93.5	110	72.4	137	103.8
57	71.2	84	96.5	111	72.4	138	117.9
58	66.9	85	103.6	112	88.9	139	124.1
59	71.3	86	117.8	113	64.6	140	129.9
60	89.9	87	124.1	114	77.6	141	
61	64.5	88	129.9	115	79.8	142	
62	78.7	89	131.7	116	77.3	143	132.6
63	80.1	90	132.4	117	79.3	144	132.8
64	77.5	91	132.7	118	88.8	145	71.3
65	78.2	92	132.8	119	65.9	146	84.2
66	87.4	93	71.3	120	77.5	147	98.5
67	67.0	94	85.5	121	77.1	148	96.5
68	77.3	95	101.0	122	79.2	149	104.3
69	76.8	96	96.4	123	82.6	150	97.9
70	78.9	97	104.4	124	75.5	151	98.0
71	82.0	98	100.1	125	83.9	152	105.3
72	74.8	99	96.7	126	93.4	157	78.9
73	83.7	100	91.0	127	96.1	158	78.5
74	92.8	101	70.9	128	104.9	159	67.2
75	95.0	102	65.3	129	73.8	160	90.3

Corrected Diffuser Data

Static Pressure, P_s/δ (psia)

Test No. 3367, Line 7
Configuration V2

Throat Size $\left\{ \begin{array}{l} \text{Total Area} = 0.865 \text{ in.}^2 \\ \text{Depth} = 0.203 \text{ in.} \end{array} \right.$

Speed, $N/\sqrt{\theta} = 50,000 \text{ rpm}$

Airflow, $W_a\sqrt{\theta}/\delta = 1.94 \text{ lb/sec}$

Tap No.	Static Pressure	Tap No.	Static Pressure	Tap No.	Static Pressure	Tap No.	Static Pressure
49	69.1	76	96.2	103	64.2	130	71.6
50	62.0	77	72.0	104	69.4	131	74.1
51	62.9	78	57.2	105	69.2	132	76.5
52	68.2	79	74.1	106	68.4	133	74.5
53	67.9	80	76.5	107	69.9	134	67.0
54	67.2	81	74.7	108	65.7	135	86.2
55	67.9	82	64.0	109	62.9	136	83.3
56	61.5	83	86.4	110	70.5	137	96.0
57	69.2	84	82.4	111	70.6	138	112.8
58	64.2	85	95.8	112	88.9	139	120.2
59	69.4	86	112.9	113	69.2	140	126.7
60	87.0	87	120.3	114	75.9	141	
61	69.2	88	126.6	115	78.2	142	
62	77.1	89	128.5	116	77.4	143	129.4
63	78.6	90	129.2	117	79.5	144	129.5
64	77.8	91	129.5	118	88.0	145	71.4
65	78.6	92	129.5	119	70.4	146	68.0
66	84.6	93	71.3	120	75.4	147	90.8
67	71.1	94	65.9	121	76.9	148	84.0
68	75.3	95	95.5	122	79.4	149	96.7
69	76.9	96	84.1	123	82.1	150	89.4
70	79.2	97	97.0	124	75.8	151	87.8
71	81.6	98	93.5	125	66.2	152	98.1
72	75.0	99	86.5	126	84.8	157	78.2
73	65.5	100	98.8	127	81.9	158	78.4
74	84.2	101	70.6	128	96.7	159	67.3
75	81.0	102	63.4	129	72.7	160	67.3

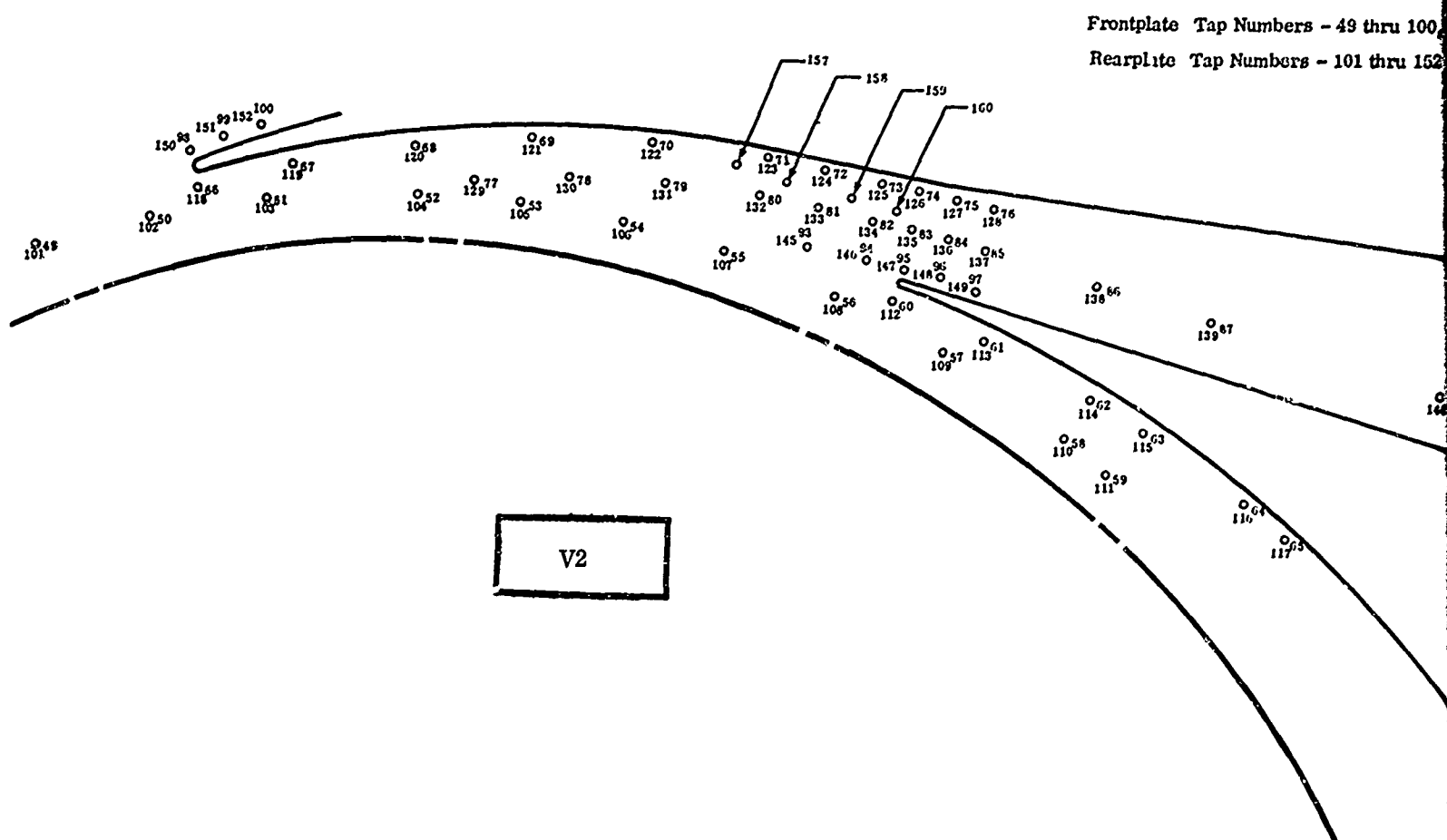
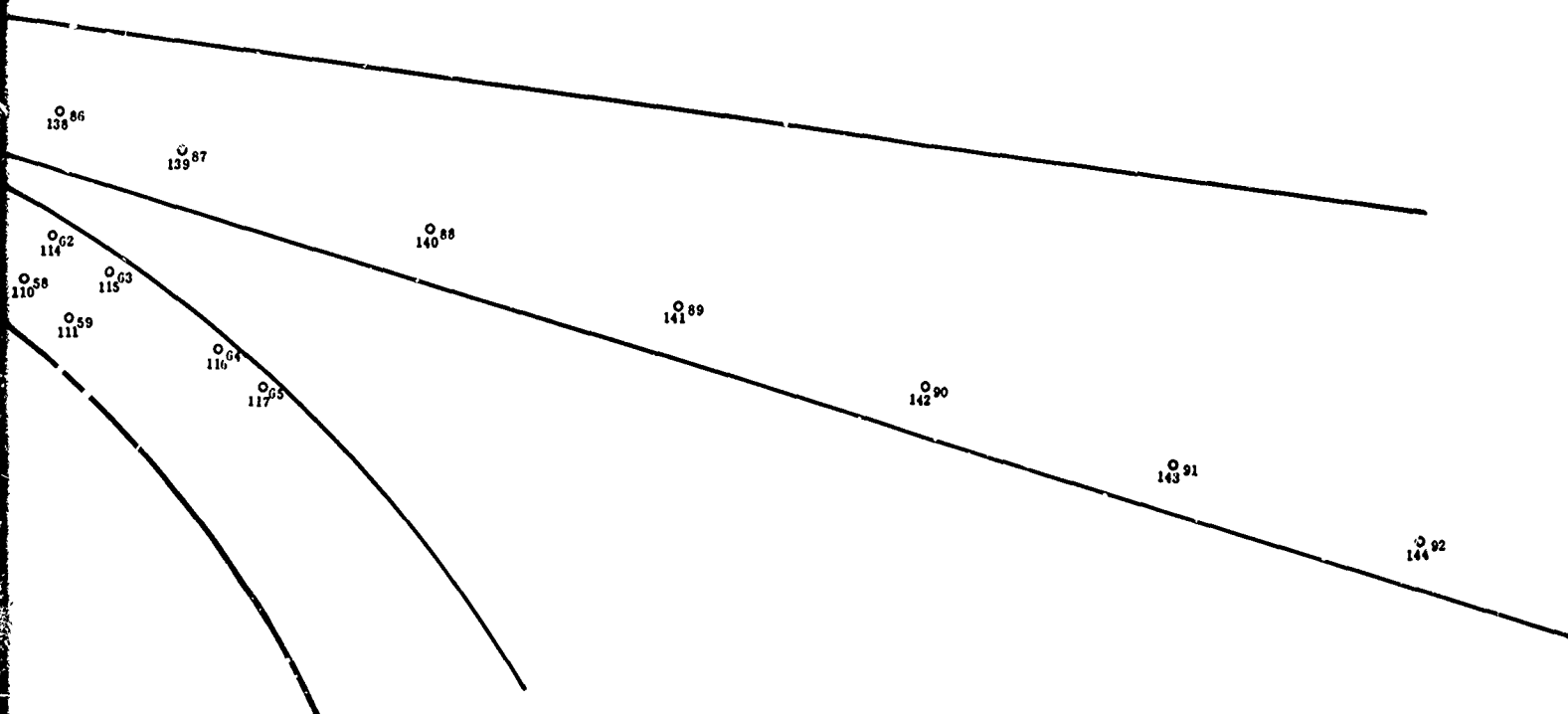


Figure 259. Locations of Static-Pressure Taps with Respect to V2 Diffuser Vanes.

Frontplate Tap Numbers - 49 thru 100, 157, 158, 159, 160

Rearplate Tap Numbers - 101 thru 152



037182A.1340

Corrected Diffuser Data

Static Pressure, P_s/δ (psia)Test No. 3368, Line 5
Configuration V2-1Throat Size $\left\{ \begin{array}{l} \text{Total Area} = 0.956 \text{ in.}^2 \\ \text{Depth} = 0.203 \text{ in.} \end{array} \right.$ Speed, $N/\sqrt{\theta} = 50,000 \text{ rpm}$ Airflow, $W_a\sqrt{\theta}/\delta = 2.03 \text{ lb/sec}$

Tap No.	Static Pressure	Tap No.	Static Pressure	Tap No.	Static Pressure	Tap No.	Static Pressure
49	67.4	76	104.0	103	53.4	130	70.0
50	72.2	77	71.5	104	67.9	131	69.8
51	55.9	78	69.4	105	69.1	132	74.0
52	66.6	79	70.0	106	65.4	133	74.0
53	67.7	80	74.4	107	67.4	134	88.2
54	64.3	81	74.6	108	74.6	135	93.7
55	65.8	82	88.1	109	54.6	136	97.4
56	74.3	83	94.5	110	68.5	137	103.0
57	56.2	84	97.5	111	70.8	138	116.2
58	67.1	85	103.6	112	88.4	139	122.8
59	69.5	86	117.0	113	62.6	140	129.0
60	85.0	87	123.5	114	72.6	141	
61	62.7	88	129.6	115	77.3	142	
62	74.3	89	131.8	116	73.4	143	132.4
63	78.4	90	132.7	117	74.2	144	132.7
64	74.6	91	133.2	118	89.4	145	70.9
65	74.1	92	133.3	119	62.9	146	86.4
66	84.0	93	70.6	120	72.8	147	98.1
67	64.2	94	86.8	121	75.7	148	96.7
68	73.1	95	101.5	122	74.4	149	103.8
69	76.3	96	97.1	123	78.8	150	97.7
70	74.9	97	104.1	124	78.8	151	98.1
71	79.0	98	101.2	125	88.5	152	104.7
72	78.0	99	97.5	126	93.5	157	75.2
73	88.3	100	105.7	127	96.2	158	76.5
74	93.3	101	68.8	128	103.8	159	79.4
75	95.9	102	73.3	129	71.9	160	91.3

037182A.1340

UNCLASSIFIED

Corrected Diffuser Data

Static Pressure, P_s/δ (psia)

Test No. 3368, Line 7
Configuration V2-1

Throat Size $\left\{ \begin{array}{l} \text{Total Area} = 0.950 \text{ in.}^2 \\ \text{Depth} = 0.203 \text{ in.} \end{array} \right.$

Speed, $N/\sqrt{\theta} = 50,000 \text{ rpm}$

Airflow, $W_a\sqrt{\theta/\delta} = 2.11 \text{ lb/sec}$

Tap No.	Static Pressure	Tap No.	Static Pressure	Tap No.	Static Pressure	Tap No.	Static Pressure
49	65.6	76	95.3	103	61.7	130	70.2
50	64.2	77	68.1	104	66.4	131	70.7
51	63.3	78	69.1	105	67.9	132	72.3
52	65.0	79	70.3	106	66.0	133	72.0
53	66.3	80	72.1	107	65.9	134	75.9
54	64.5	81	72.2	108	65.6	135	85.1
55	64.1	82	73.4	109	63.7	136	83.3
56	64.8	83	85.6	110	66.4	137	94.8
57	61.1	84	82.3	111	67.9	138	111.3
58	65.3	85	94.9	112	89.5	139	119.2
59	66.6	86	111.6	113	68.8	140	125.7
60	82.4	87	119.1	114	71.6	141	
61	68.2	88	125.6	115	74.8	142	
62	72.7	89	127.7	116	73.8	143	128.9
63	75.6	90	128.6	117	74.7	144	129.2
64	74.4	91	129.0	118	89.6	145	69.1
65	74.3	92	129.1	119	68.3	146	75.0
66	81.3	93	68.3	120	71.6	147	41.9
67	68.2	94	75.3	121	75.1	148	83.4
68	71.5	95	94.3	122	75.2	149	95.8
69	75.4	96	83.0	123	77.1	150	90.4
70	75.6	97	95.7	124	76.7	151	87.0
71	77.1	98	93.0	125	71.7	152	97.5
72	75.6	99	85.4	126	84.6	157	73.9
73	71.6	100	97.9	127	81.0	158	74.6
74	83.9	101	67.0	128	95.6	159	70.8
75	80.4	102	65.9	129	69.1	160	83.7

UNCLASSIFIED

UNCLASSIFIED

UNCLAS

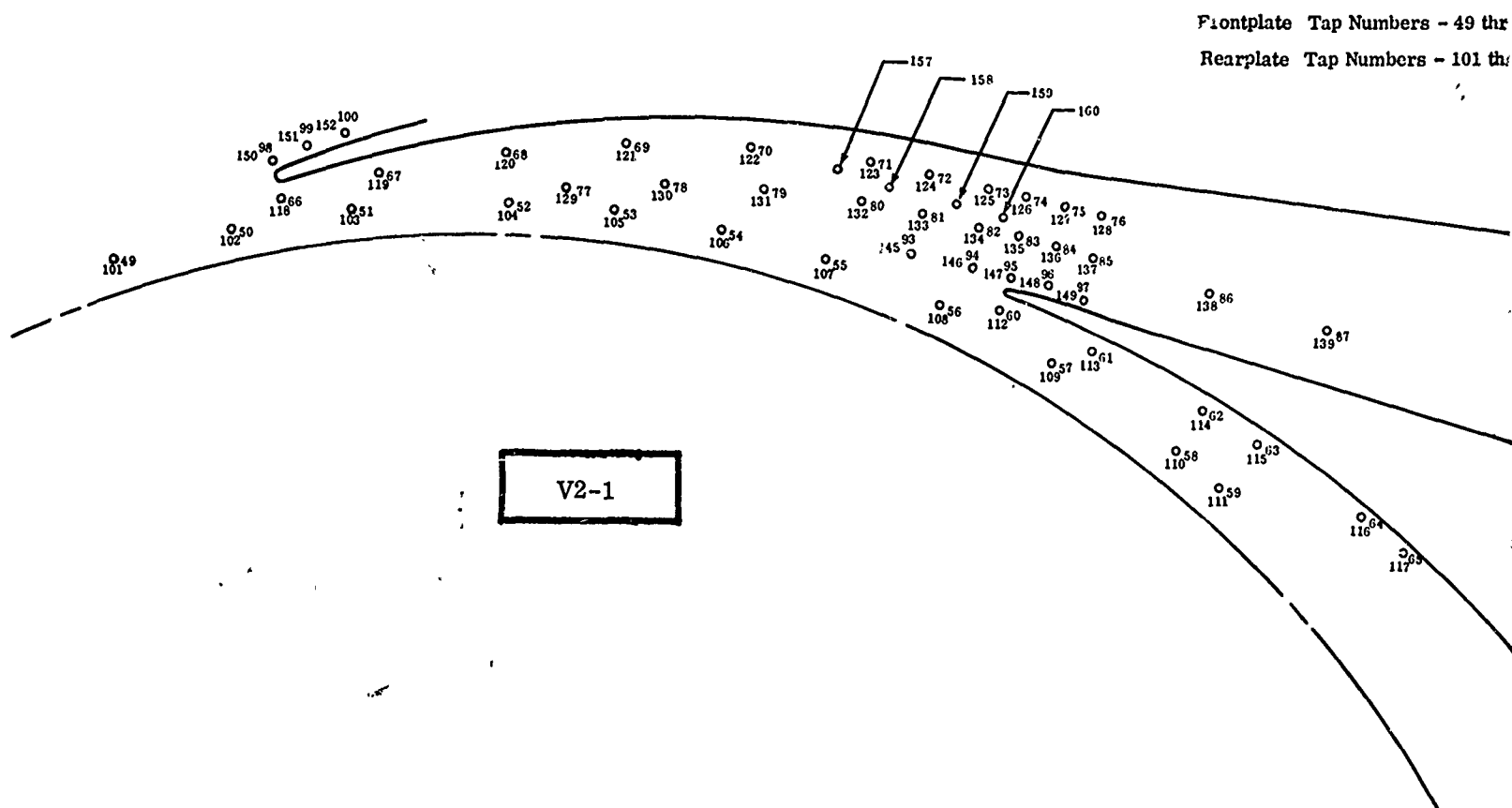


Figure 260. Locations of Static-Pressure Taps with Respect to V2-1 Diffuser Vanes.

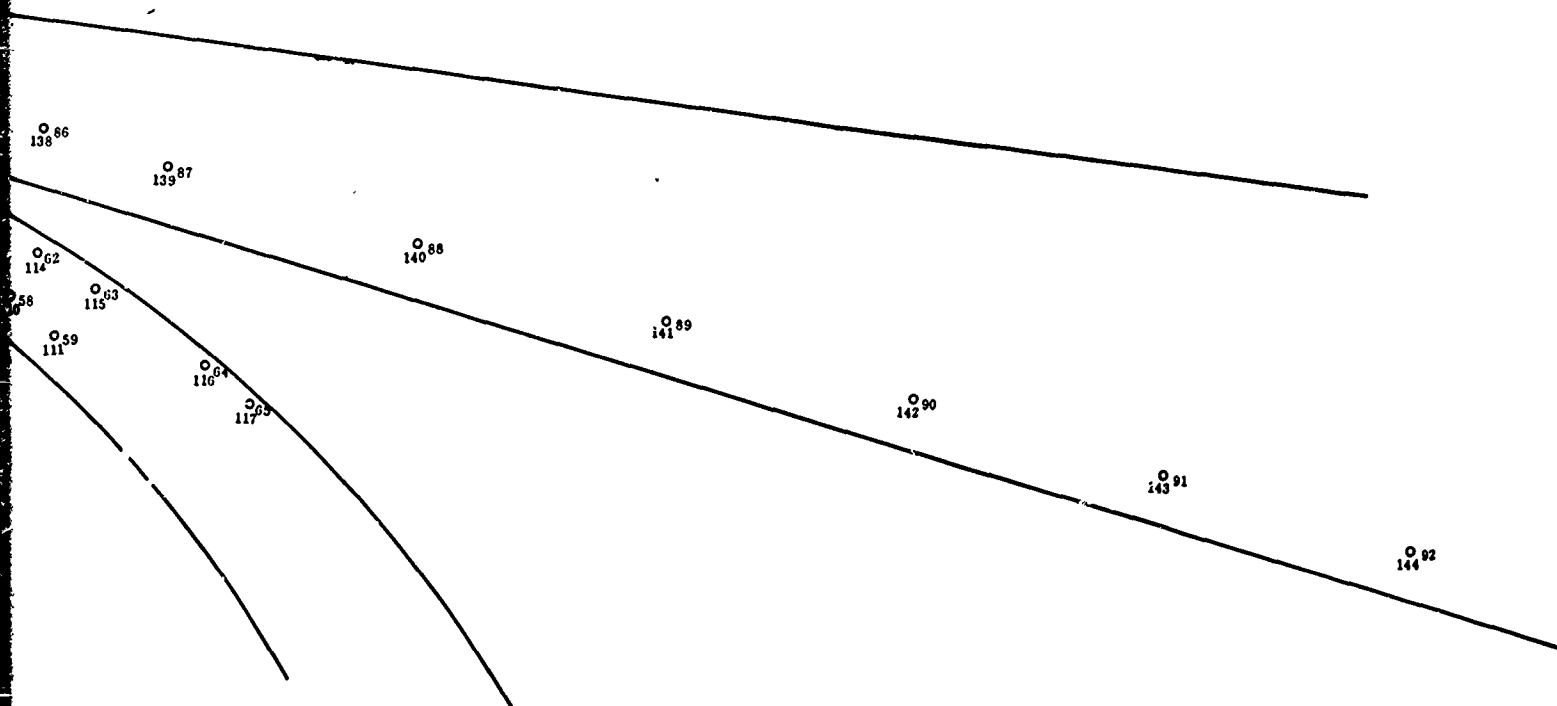
UNCLASSIFIED

UNCLAS

UNCLASSIFIED

Frontplate Tap Numbers - 49 thru 100, 157, 158, 159, 160

Rearplate Tap Numbers - 101 thru 152



UNCLASSIFIED

UNCLASSIFIED

Corrected Diffuser Data

Static Pressure, P_s/δ (psia)

Test No. 3369, Line 3
Configuration V2-2

Throat Size { Total Area = 0.862 in.²
Depth = 0.158 in.

Speed, $N/\sqrt{\theta} = 50,000$ rpm

Airflow, $W_a\sqrt{\theta}/\delta = 1.86$ lb/sec

Tap No.	Static Pressure	Tap No.	Static Pressure	Tap No.	Static Pressure	Tap No.	Static Pressure
49	66.4	76	101.3	103	60.7	130	69.6
50	76.6	77	69.7	104	68.9	131	70.0
51	59.3	78	68.6	105	68.3	132	73.4
52	67.5	79	69.5	106	65.8	133	79.9
53	66.9	80	74.4	107	66.8	134	89.5
54	64.5	81	80.1	108	77.4	135	92.6
55	65.4	82	88.9	109	63.9	136	95.3
56	76.9	83	93.0	110	68.8	137	100.8
57	61.4	84	95.0	111	70.3	138	113.4
58	67.6	85	101.0	112	92.4	139	120.1
59	68.9	86	113.6	113	69.5	140	126.6
60	85.0	87	119.9	114	72.8	141	
61	69.4	88	126.5	115	76.3	142	
62	73.8	89	129.3	116	73.1	143	131.7
63	76.8	90	130.9	117	73.0	144	132.3
64	73.5	91	131.7	118	93.1	145	76.6
65	72.5	92	132.2	119	64.5	146	87.6
66	84.2	93	75.2	120	73.5	147	99.6
67	68.4	94	86.6	121	74.3	148	93.7
68	73.4	95	99.7	122	73.4	149	101.8
69	74.5	96	93.4	123	78.8	150	98.9
70	73.7	97	101.0	124	85.0	151	96.3
71	78.9	98	99.4	125	90.6	152	103.3
72	84.2	99	95.0	126	92.2	157	74.4
73	90.2	100	103.4	127	95.5	158	79.5
74	92.0	101	67.4	128	101.6	159	85.6
75	94.9	102	77.9	129	70.5	160	91.0

UNCLASSIFIED

UNCLASSIFIED

Corrected Diffuser Data

Static Pressure, P_s/δ (psia)

Test No. 3369, Line 5
Configuration V2-2

Throat Size $\left\{ \begin{array}{l} \text{Total Area} = 0.862 \text{ in.}^2 \\ \text{Depth} = 0.158 \text{ in.} \end{array} \right.$

Speed, $N/\sqrt{\theta} = 50,000 \text{ rpm}$

Airflow, $W_a\sqrt{\theta/\delta} = 1.89 \text{ lb/sec}$

Tap No.	Static Pressure	Tap No.	Static Pressure	Tap No.	Static Pressure	Tap No.	Static Pressure
49	66.3	76	99.7	103	63.2	130	69.9
50	75.7	77	68.9	104	68.5	131	70.2
51	61.6	78	68.9	105	68.3	132	73.3
52	67.1	79	69.7	106	66.4	133	78.9
53	66.9	80	73.0	107	66.2	134	88.3
54	65.0	81	79.1	108	76.2	135	90.6
55	64.7	82	87.7	109	66.7	136	92.7
56	76.0	83	91.1	110	68.5	137	98.9
57	63.9	84	92.6	111	69.5	138	112.4
58	67.2	85	99.3	112	92.5	139	119.4
59	68.2	86	112.8	113	71.1	140	126.2
60	84.9	87	119.4	114	72.4	141	
61	70.9	88	126.2	115	75.4	142	
62	73.4	89	129.1	116	73.4	143	131.3
63	76.1	90	130.6	117	73.3	144	131.9
64	73.9	91	131.4	118	93.0	145	75.9
65	72.9	92	131.9	119	66.0	146	86.4
66	84.0	93	74.4	120	72.9	147	98.5
67	69.9	94	85.5	121	74.3	148	91.4
68	72.8	95	98.1	122	73.7	149	99.9
69	74.5	96	91.1	123	77.5	150	97.6
70	74.2	97	99.4	124	83.8	151	94.4
71	77.8	98	97.9	125	89.0	152	101.9
72	83.2	99	93.1	126	90.1	157	73.6
73	88.8	100	102.2	127	93.0	158	78.4
74	90.0	101	67.3	128	99.8	159	84.5
75	92.6	102	77.0	129	69.6	160	89.5

UNCLASSIFIED

UNCLASSIFIED

Corrected Diffuser Data

Static Pressure, P_s/δ (psia)

Test No. 3369, Line 7
Configuration V2-2

Throat Size $\left\{ \begin{array}{l} \text{Total Area} = 0.862 \text{ in.}^2 \\ \text{Depth} = 0.158 \text{ in.} \end{array} \right.$

Speed, $N/\sqrt{\theta} = 50,000 \text{ rpm}$

Airflow, $W_a\sqrt{\theta/\delta} = 1.92 \text{ lb/sec}$

Tap No.	Static Pressure	Tap No.	Static Pressure	Tap No.	Static Pressure	Tap No.	Static Pressure
49	65.4	76	94.1	103	70.7	130	69.9
50	72.6	77	67.8	104	67.9	131	70.6
51	67.7	78	68.8	105	67.3	132	71.6
52	66.4	79	70.0	106	66.7	133	76.2
53	65.9	80	71.1	107	65.5	134	85.4
54	65.1	81	76.3	108	73.4	135	85.9
55	63.9	82	84.4	109	70.9	136	82.0
56	73.7	83	86.0	110	67.8	137	93.6
57	67.4	84	81.2	111	68.1	138	108.9
58	66.4	85	93.8	112	92.2	139	116.5
59	66.8	86	109.1	113	72.6	140	123.7
60	84.0	87	116.4	114	72.1	141	
61	72.4	88	123.6	115	74.0	142	
62	72.9	89	126.6	116	73.6	143	129.0
63	74.4	90	128.2	117	73.8	144	129.5
64	73.9	91	129.0	118	52.2	145	73.3
65	73.3	92	129.4	119	68.1	146	83.7
66	83.1	93	71.7	120	72.5	147	96.3
67	71.9	94	82.7	121	73.9	148	81.8
68	72.2	95	94.9	122	74.4	149	94.9
69	74.0	96	81.0	123	75.6	150	94.3
70	74.7	97	94.2	124	81.2	151	87.9
71	75.7	98	93.3	125	85.5	152	97.7
72	80.3	99	86.3	126	84.5	157	72.6
73	85.1	100	97.7	127	82.9	158	75.2
74	84.1	101	66.5	128	94.4	159	81.3
75	82.1	102	73.6	129	68.6	160	85.4

UNCLASSIFIED

UNCLASSIFIED

UNCLAS

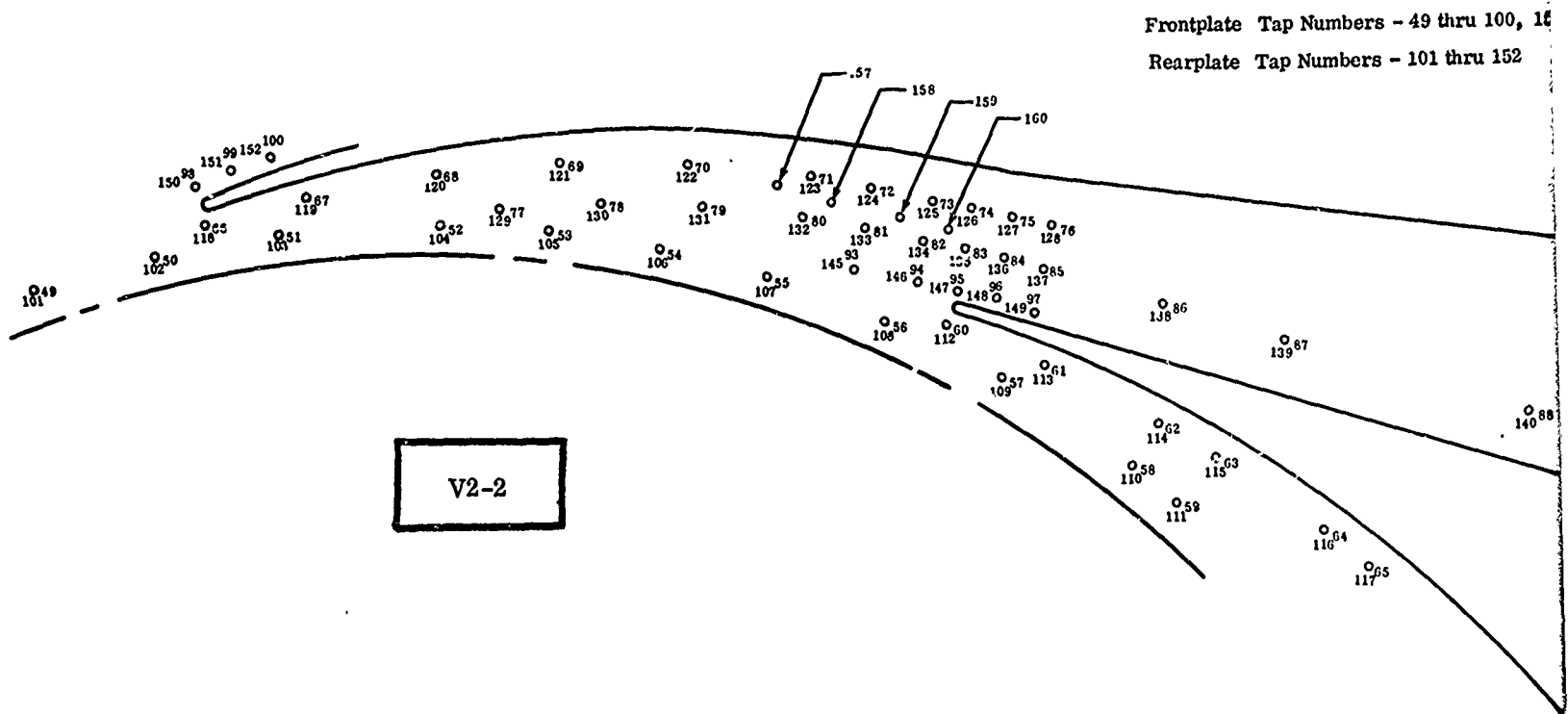


Figure 261. Locations of Static-Pressure Taps with Respect to V2-2 Diffuser Vanes.

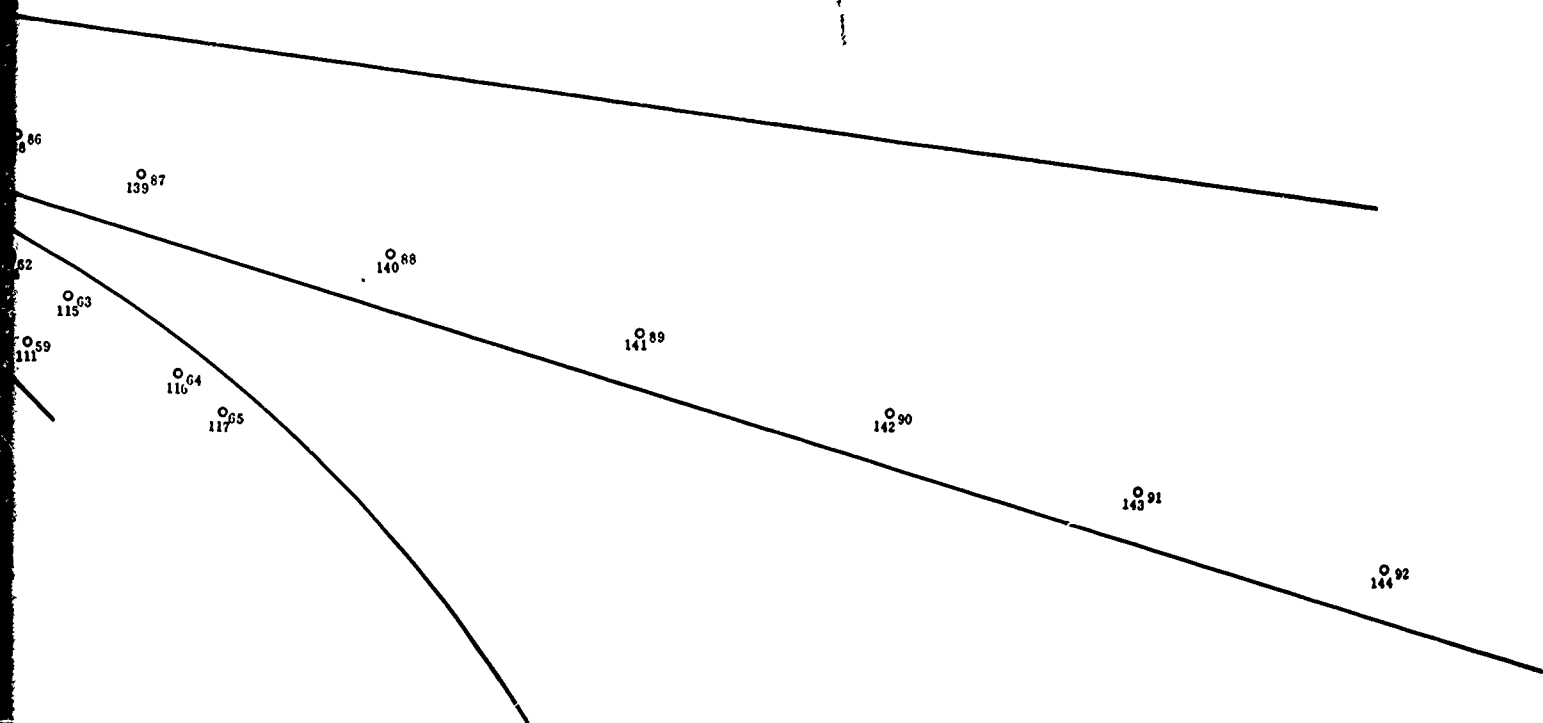
UNCLASSIFIED

UNC

UNCLASSIFIED

Frontplate Tap Numbers - 49 thru 100, 157, 158, 159, 160

Rearplate Tap Numbers - 101 thru 152



UNCLASSIFIED

Unclassified

Security Classification

DOCUMENT CONTROL DATA - R & D		
(Security classification of title, body of abstract and indexing annotation must be entered when the overall report is classified)		
1. ORIGINATING ACTIVITY (Corporate author) The Boeing Company Seattle, Washington		2a. RESEARCH AND DEVELOPMENT ACTIVITY UNCLASSIFIED 2b. GROUP 3B
3. REPORT TITLE DESIGN AND DEVELOPMENT OF SMALL, SINGLE-STAGE CENTRIFUGAL COMPRESSOR (U)		
4. DESCRIPTIVE NOTES (Type of report and inclusive dates)		
5. AUTHOR(S) (First name, middle initial, last name) Welliver, Albertus D. Acurio, John		
6. REPORT DATE September 1967	7a. TOTAL NO. OF PAGES 447	7b. NO. OF REFS 10
8a. CONTRACT OR GRANT NO. DA 44-177-AMC-173(T)	8b. ORIGINATOR'S REPORT NUMBER(S) USAAVLABS Technical Report 67-47 ✓	
b. PROJECT NO. 1M121401D14413	9a. OTHER REPORT NO(S) (Any other numbers that may be assigned this report) DA-3434	
10. DISTRIBUTION STATEMENT In addition to security requirements which apply to this document and must be met, each transmittal outside the Department of Defense must have prior approval of U. S. Army Aviation Materiel Laboratories, Fort Eustis, Virginia 23604.		
11. SUPPLEMENTARY NOTES	12. SPONSORING MILITARY ACTIVITY U. S. Army Aviation Materiel Laboratories Fort Eustis, Virginia	
13. ABSTRACT (U) The purpose of the work was to define, by analysis and experimental evaluation, the design criteria and performance characteristics of the high-pressure-ratio, single-stage centrifugal compressor. The overall performance target was a pressure ratio of 10:1 at an adiabatic efficiency of 80 percent at an airflow of 2 pounds per second. The research was expected to lead to development of advanced technologies applicable to small gas turbine engines. The potential advances identified were: <ol style="list-style-type: none"> (1) Doubling of current power to weight ratio, (2) Reducing full and part load fuel consumption, and (3) Minimizing cost per horsepower. <p>To illustrate the advances possible, two types of thermodynamic cycles (simple and regenerative) were studied. It was shown that a compressor meeting the above targets would provide an opportunity for reducing specific fuel consumptions to 0.49 pound per horsepower per hour (simple cycle) and 0.38 pound per horsepower per hour (regenerative).</p> <p>This report presents the design and test results of a single-stage, high-pressure-ratio (10:1) centrifugal compressor. Impeller and diffuser modifications are discussed, including diffuser throat boundary-layer bleed.</p>		

DD FORM 1473

REPLACES DD FORM 1473, 1 JAN 64, WHICH IS OBSOLETE FOR ARMY USE.

Unclassified

Security Classification

Unclassified

Security Classification

14. KEY WORDS	LINK A		LINK B		LINK C	
	ROLE	WT	ROLE	WT	ROLE	WT
Centrifugal Impeller Vane Diffuser High-Pressure-Ratio, Single-Stage Compressor Impeller-Exit Mixing Loss Inducer Nose Shape Diffuser Entry Shock Two-Dimensional Channel Diffuser Boundary-Layer Bleed						

Unclassified

Security Classification